The evolution of the Eyjafjoll volcanic system, southern Iceland.

Susan C. Loughlin

The evolution of the Eyjafjöll volcanic system, southern Iceland.

by

Susan C. Loughlin

A thesis submitted in partial fulfilment of the requirements for the degree of Doctor of Philosophy

Department of Geological Sciences

University of Durham

August 1995

This thesis is dedicated

to my Mum and Dad.

DECLARATION

I declare that this thesis, which I submit for the degree of Doctor of Philosophy at the University of Durham, is my own work and is not substantially the same as any which has previously been submitted for a degree at this or another university.

S.C. Loughlin

S.C. Loughlin

University of Durham

Department of Geological Sciences
August 1995

ABSTRACT

The evolution of the Eyjafjoll volcanic system, southern Iceland.

S.C Loughlin, University of Durham, 1995.

The Eyjafjöll volcanic system is a central volcano which has been constructed above the anomalously thick crust of the Eastern Volcanic Zone in southern Iceland. The volcano has been active for the last 800Ka (Kristjansson *et al.*, 1988) and has been constructed through six glacial and six interglacial periods.

Volcanic activity during the glacial periods produced a variety of unusual cogenetic deposits consisting of lava, hyaloclastite and volcaniclastic lithofacies. Nine commonly occurring 'lithofacies associations' have been described and interpreted, showing that the form of the subglacial deposits varied depending upon the thickness of the ice, the subglacial topography, the eruption rate and the viscosity of the lava. Most of the subglacial volcanism at Eyjafjöll occurred beneath temperate ice up to 400m thick, the thickest ice tending to occur in valley-confined glaciers extending from the summit ice cap. Volcanism beneath valley-confined glaciers formed distinctive deposits which, after retreat of the glacier, commonly underwent marginal erosion and topographic inversion, a process which is diagnostic of valley-confined subglacial volcanism on a polygenetic volcano.

The Eyjafjoll volcanic system has an anomalous E-W orientation in a NE-SW orientated rift zone and is linked along E-W fissures to the nearby volcano, Katla.

Transitional alkali basalt to hawaiite compositions at Eyjafjöll were generated by the fractional crystallisation of olivine, clinopyroxene, plagioclase, Ti-magnetite and ilmenite, all of which are observed mineral phases in lavas and gabbroic xenoliths. Mugearite to trachyte compositions involve the addition of apatite to the fractionating assemblage. Fractionation took place in interconnected crustal magma chambers of varying depth and oxygen fugacity. Ankaramites are high-MgO lavas erupted directly from the base of the crust during the early stages of the growth of the volcano. They do not represent an average parental composition for the basalts.

Trace element ratios suggest a common parental source material for all lavas at the Eyjafjöll volcanic system. All lavas are LREE-enriched and may be produced by small (~4%) degrees of melting in a melting column of restricted depth extending to the spinel-garnet lherzolite transition zone. Small variations in trace element ratios may be explained by segregation of instantaneous melts from this column. Highly differentiated, high FeTi basalts may have differentiated from high Fe mantle melts which underwent substantial olivine fractionation prior to eruption. These basalts are enriched in certain incompatible trace elements suggesting that they may have assimilated some crustal material.

ACKNOWLEDGEMENTS

I would like to thank the following individuals for their help and support during the production of this thesis:

- Firstly my very sincere thanks to Dr. Henry Emeleus for taking over the role as supervisor for this project at short notice and for continuing to give me help and advice after his retirement.
- Thanks also to Dr. Bob Holdsworth for supervising me over the last year.
- In Iceland, Dr. Kristjan Saemundsson introduced me to my field area and helped with various logistical problems, shipping and transport throughout the project. Dr. Sveinn Jakobsson also gave me much practical advice. I am very grateful for their help.
- Didi, Gretar, Anna, Sigurjon, Oscar and Anna-Sigga at Seljavellir deserve a special mention for their wonderful hospitality and friendship over the last four years. The generosity and support of the family helped to make my fieldwork a thoroughly enjoyable time.
- Thanks to Dr. Geoff Robson and Bill Pace for giving me an opportunity to accompany them during their study of Eldgja and the surrounding area. I learned a lot in their company, about geology and Iceland.
- I am particularly grateful to my field assistants Roger, Nicola, Steve and Fiona for coming and spending time in Iceland with me. Their help and company was greatly appreciated.
- Back in Durham, my special thanks to David for helping me with all the final stages in the production of the thesis.
- Many other people at Durham have helped me with my work during the last few years, especially Kate, Sarah, Vicky, Jon Bole, Charlotte, Jon, Affonso, Sally and Paul.
- Special thanks to Ron Hardy for helping with sample preparation and XRF; to Dr. A. Peckett for assistance and training on the microprobe; to Julie, George and Ron for numerous thin sections; to Karen for advice on Coreldraw; Alan and Jerry for photography and Dave Asbery for introducing me to the Lada.
- Thanks to Kim Jarvis and the staff at Royal Holloway for their help and advice on the ICP and to Tim Hopkins at Manchester for helping with the microprobe.
- Thanks to Paul, Jon, Si, Michelle, Pete, Billy and Jennie for being excellent housemates and to Zoe, Jane, Neil, Angus, Ziad, Jo, Wayne, Alun, Roberto, Alwyn and the rest of the postgrads and postdocs for lots of laughs over the last few years.
- Last, but not least, thanks to all my friends outside Durham.

CONTENTS

CHAPTER 4 FIELDWORK

CHAPTER 5 PETROGRAPHY AND MINERAL CHEMISTRY

CHAPTER 6 GEOCHEMISTRY AND PETROGENESIS

CHAPTER 7 CONCLUSIONS

REFERENCES

APPENDICES

BACK POCKET

MAP M1
MAP M2

CHAPTER 1
INTRODUCTION

1.1 INTRODUCTION

Iceland is part of the North Atlantic Tertiary Province which includes Eastern and Western Greenland, the Faeroe Islands and the British Tertiary Igneous Provinces of N Ireland and Scotland (Figure 1.1). This region underwent substantial extension prior to the Tertiary, which involved the opening of the Labrador sea between Greenland and North America (~92Ma). The arrival of a mantle plume at ~60Ma lead to ridge jumping and the initiation of rifting between Greenland and Europe (Hill, 1991). Contemporaneous eruption of voluminous flood basalts occurred throughout the North Atlantic Tertiary Province at this time (e.g. White *et al.*, 1987). The proposed track of the mantle plume from ~50Ma to its present location in East Iceland is shown in Figure 1.1 (Lawver and Muller, 1994).

The Iceland plateau formed as a result of the interaction of the North Atlantic mantle plume and the slowly spreading Mid-Atlantic Ridge, giving rise to melts 200-250°C hotter than average (Sleep, 1990) and excessive magma production (McKenzie, 1984). The oldest *exposed* Tertiary basalts in Iceland are 16 Ma and outcrop in the far northwest, although much older basalts undoubtably occur deeper in the volcanic pile (Palmason & Saemundsson, 1974).

1.2 STRATIGRAPHY OF ICELAND

The volcanic products of Iceland may be divided into four stratigraphic subdivisions. These divisions are based predominantly on climatic evidence from inter-lava sediments and on palaeomagnetic reversal patterns, supported by absolute age data (Saemundsson, 1979). The Tertiary of Iceland includes all rocks older than 3.1Ma. The Plio-Pleistocene lasted from 0.7-3.1Ma (corresponding to the Matuyama and Gauss geomagnetic epochs), the Upper Pleistocene corresponds to the current Brunhes geomagnetic epoch and the Postglacial covers the last 9000 to 13000 years (Saemundsson, 1979), (Figure 1.2).

The Iceland crust is composed of up to 6.5km of extrusives. The Tertiary lavas form broad plateaus of gently dipping sheet lavas with occasional evolved hypabyssal remains of eroded central volcanoes. Of the exposed Tertiary rocks, 80-85% are basaltic and about 10% are acidic or intermediate, volcanic sediments constitute the remaining 5-10%. The Quaternary contains similar proportions of acid and basic rocks but considerably more of the Quaternary pile is composed of fragmentary subglacial hyaloclastites and reworked volcanic sediments (Saemundsson, 1979). The lava pile

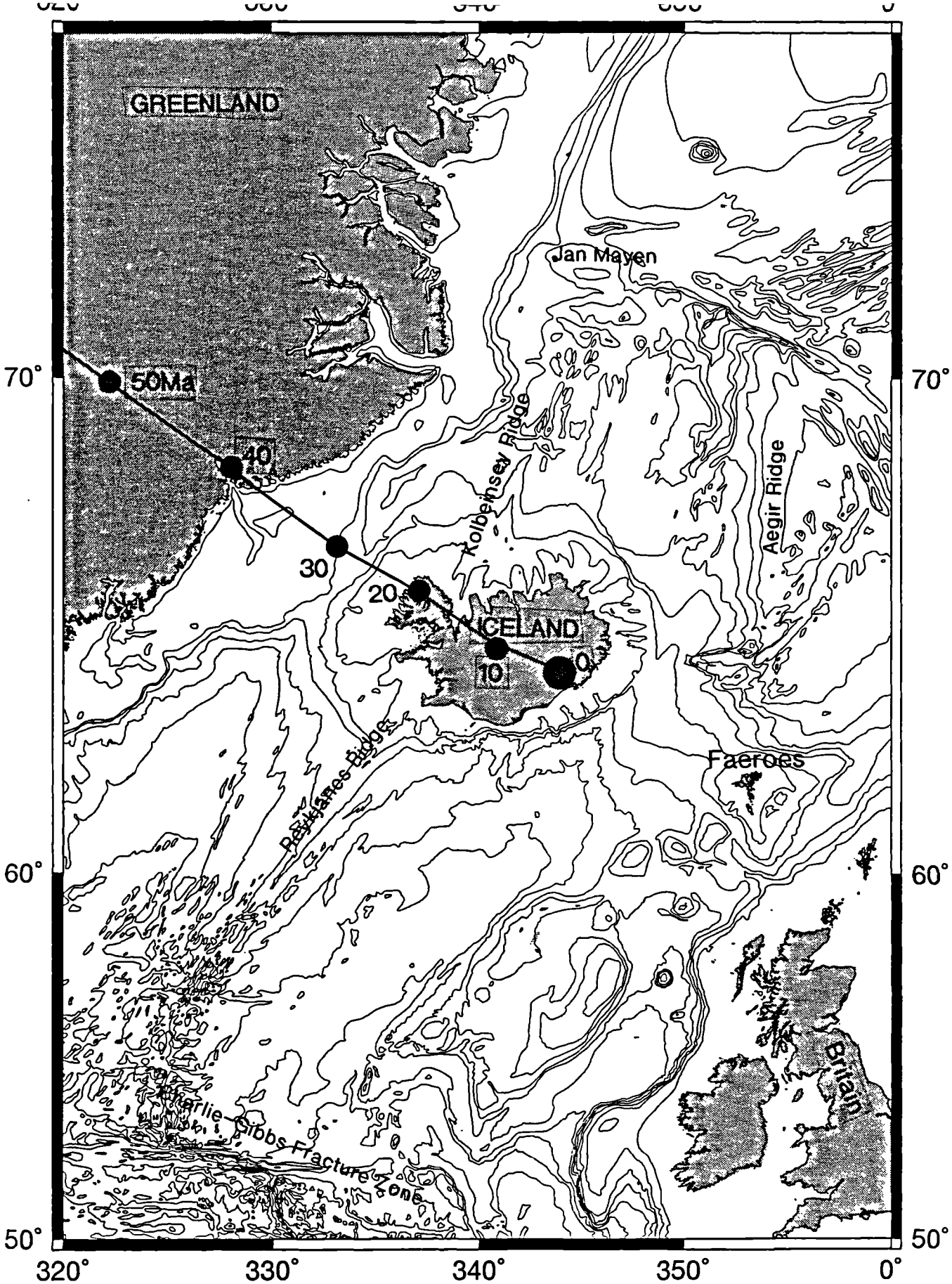

Figure 1.1 *Bathymetric map of the N. Atlantic region showing Iceland in relation to the Mid-Atlantic ridge and the trace of the Iceland hotspot over the last 50Ma (Lawver and Muller, 1994). The diagram was constructed using GMT (Wessel and Smith, 1991) with data from the GEBCO digital atlas (IOC, IHO and BODC, 1994). Contours are at 0, 200m, 500m and at 500m intervals thereafter. Diagram courtesy of Dr. C. Peirce.*

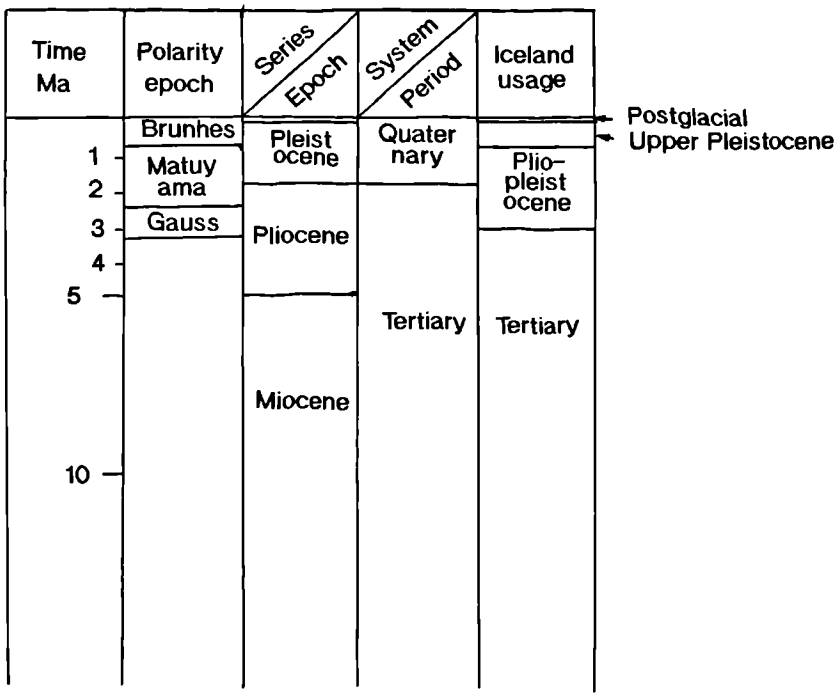

Figure 1.2 *Stratigraphic time table based on La Breque et al., (1977) with the modified version commonly used in Iceland (Saemundsson, 1979).*

dips towards the central part of Iceland at 0-10°, individual volcanic units also thicken down dip. This suggests that the lavas were tilted during their formation at the axial rift zones as a result of subsidence associated with extension and the loading of the crust by the lava pile (*Ibid*).

1.3 TECTONIC STRUCTURE OF ICELAND

1.3.1 NEOVOLCANIC ZONES

Postglacial volcanic activity in Iceland is confined to discrete volcanic zones known collectively as the ***Neovolcanic Zones*** (Figure 1.3).

The Western Volcanic Zone (WVZ) is the onland extension of the Mid-Atlantic (Reykjanes) Ridge and runs northwest from Reykjanes to Langjokull. The Northern Volcanic Zone (NVZ) also marks the plate boundary and runs from Vatnajokull north-northwest to Tjornes on the north coast. These are the ***Axial Rift Zones*** (Figure 1.3), characterised by relatively thin crust (8-10km) (Palmason, 1971; Gebrande *et al*, 1980), high heat flow (up to 160°/km) (Palmason, 1973; Palmason *et al*, 1979) and well-developed tensional features (Saemundsson, 1979).

By contrast, off-axis volcanic zones or ***Flank Zones*** are situated on older, thicker crust (20-30km), (Palmason, 1971); heat flow is lower (Palmason, 1973), and tensional features are poorly developed (Saemundsson, 1978). The Eastern Volcanic Zone (EVZ) runs southwest from Vatnajokull to Vestmannaeyjar off the south coast. It

changes in character from an axial rift zone in the north, to a flank zone in the south. It has been suggested that the EVZ is a southwards propagating rift whose tip is currently beneath Vestmannaeyjar. The Snaefellsnes Volcanic Zone (SVZ) and the Oraefajokull Volcanic Zone (OVZ) are also flank zones. Jan Mayen, an island north of Iceland (Figure 1.1), is believed to be an analogue of an Iceland flank zone, since it formed off the Mid-Atlantic Ridge (Saemundsson, 1986).

The neovolcanic zones are linked by areas of intense seismic activity which may be comparable with transform fault zones on the ocean floor. The Tjornes Fracture Zone (TFZ) in northern Iceland connects the NVZ with the submarine Kolbeinsey Ridge which is offset to the west (Figure 1.3). The South Iceland Seismic Zone (SISZ) appears to connect the WVZ and the EVZ. The SISZ has rotated faults in the WVZ from a NE trend to a N-S orientation (Figure 1.3). This effect could be achieved by the sinistral rotation of crustal blocks (Foulger *et al.*, 1992). The SISZ may also be responsible for a localised E-W tectonic fabric observed in the NE-SW oriented EVZ.

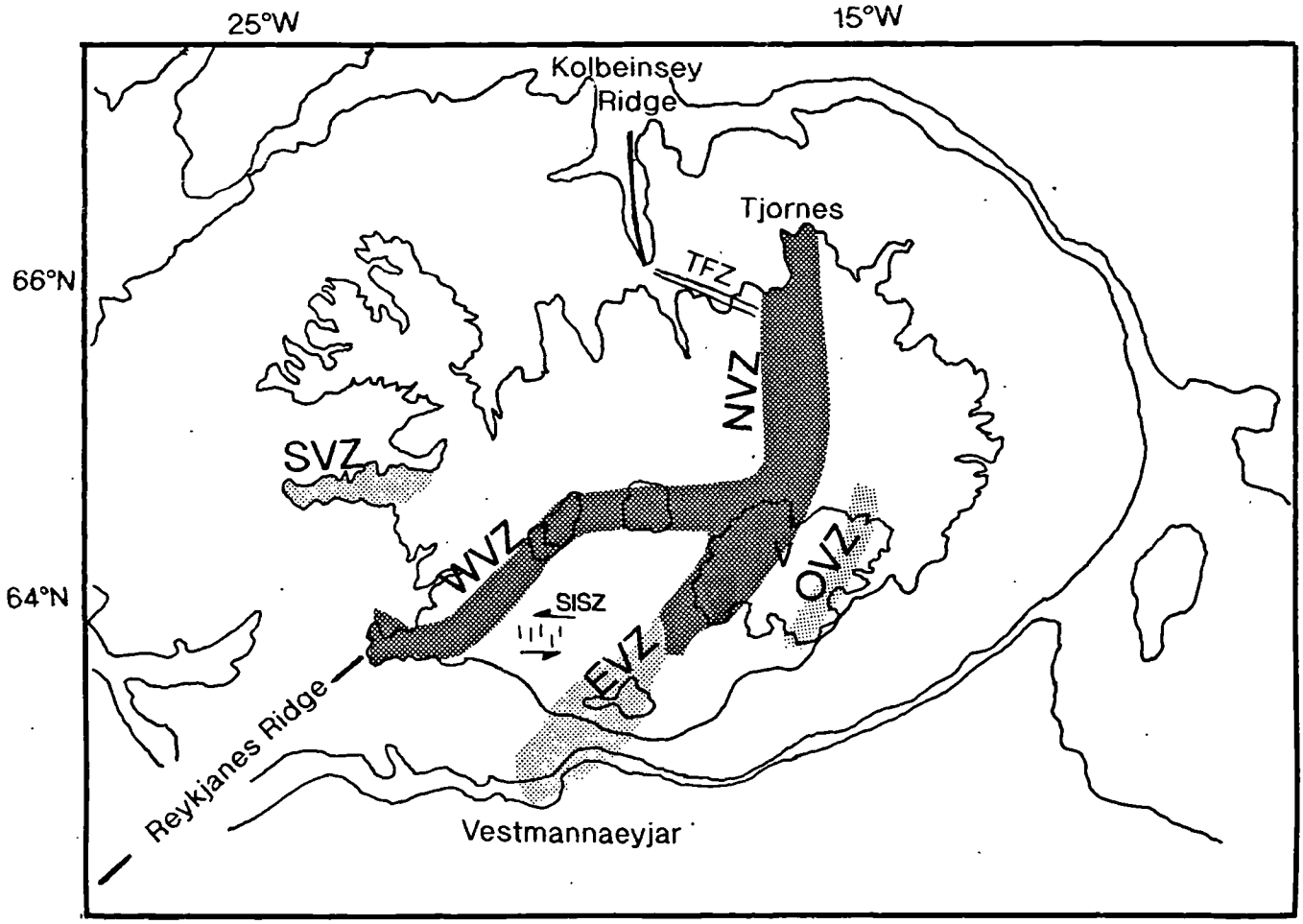

Figure 1.3 *Map of Iceland showing the neovolcanic zones. The hatched zones (WVZ and NVZ) are the axial rift zones, the stippled zones (EVZ, SVZ and OVZ) are off-axis flank zones. SISZ = South Iceland Seismic Zone, TFZ = Tjornes Fracture Zone, V = Vatnajokull, L = Langjokull. Based on Jakobsson, 1979b.*

1.3.2 VOLCANIC SYSTEMS

The neovolcanic zones are made up of discrete ***volcanic systems*** (Jakobsson,1979a, 1979b; Saemundsson, 1979). A volcanic system is a lenticular unit composed typically of a fissure swarm and a central volcano (Figure 1.4). Volcanic systems tend to form an en-echelon arrangement where there is non-orthogonal spreading, this is particularly pronounced on the WVZ. Fissure swarms may be between 10km and 100km long and have variable trends, a central volcano usually attains the same width as the associated fissure swarm (Saemundsson, 1979). Central volcanoes are sites of copious basaltic volcanism but are also characterised by the presence of acid and intermediate lavas and typically a central caldera, indicating the presence of a shallow crustal magma chamber (Walker, 1963). A high proportion of intrusive sheets in the core of central volcanoes increases the geothermal gradient, giving rise to temporary hydrothermal convection cells. These metamorphose the core rocks to well above the zeolite facies metamorphism seen at deep levels in the lava pile elsewhere in Iceland (Saemundssson, 1979).

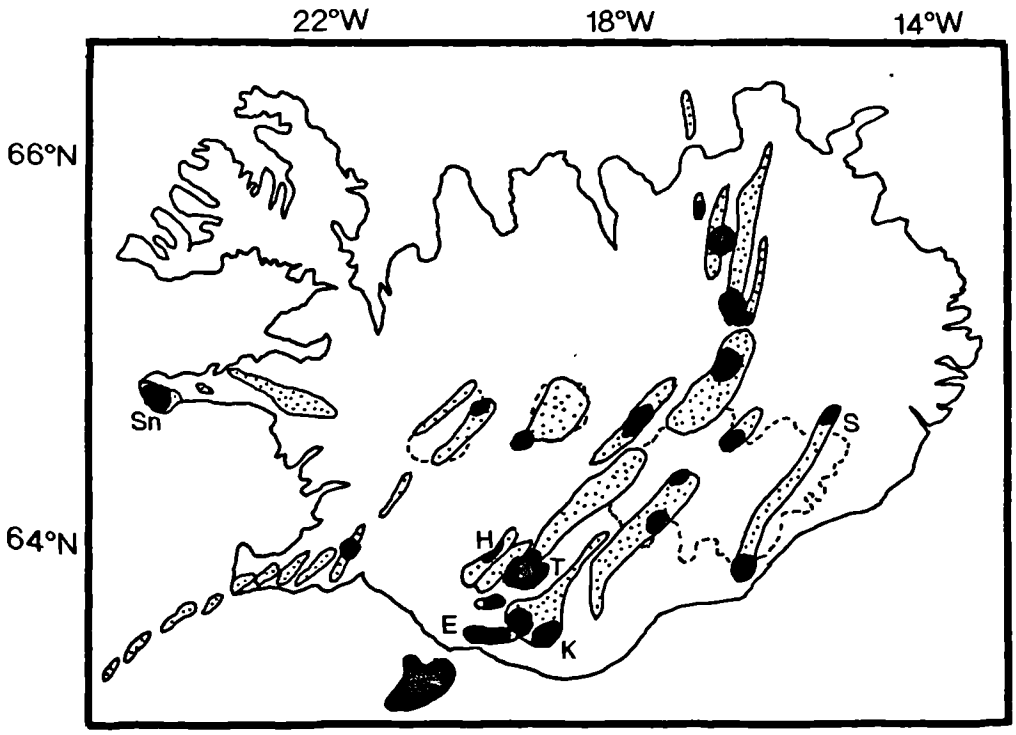

Figure 1.4 *Map showing the volcanic systems within the neovolcanic zones. The stippled areas represent fissure swarms, the black areas are central volcanoes; E = Eyjafjöll volcanic system, K = Katla, T = Torfajökull, H = Hekla, S = Snaefell, Sn = Snaefellsjökull. Based on Jakobsson, 1979b.*

Central volcanoes of flank zones that have been studied in some detail include Torfajökull (McGarvie, 1984; McGarvie *et al.*, 1990; Macdonald *et al.*, 1990), Snaefellsjökull (Sigurdsson, 1970a; 1970b) and Snaefell (Hards, in press), (Figure 1.4). Tertiary central volcanoes have been described by several authors e.g Breiddalur (Walker, 1963), Thingmuli (Carmichael, 1964, 1967) and Austurhorn (Furman *et al.*, 1992a, 1992b). These volcanoes are typically highly dissected, allowing the study of shallow level intrusions.

1.3.3 RIDGE JUMPS

It has been proposed that the EVZ is actually replacing the WVZ in response to the relative eastward migration of the mantle plume (Einarsson, 1991). This process of ***ridge jump*** over 100-200km may have occurred repeatedly throughout Iceland's history, possibly every 6-8Ma (Helgason, 1984). Helgason also proposes that small-scale ridge jumps of 20-40km may occur more frequently, i.e every 2Ma. This theory may explain why there is a variable depth to seismic layer 3 across Iceland (2-11km) as this depth would be constant if steady symmetric spreading occurs. It also helps to explain the excessive width of Iceland, which is 40% wider than expected from a single spreading boundary (Schilling *et al.*, 1982; Helgason, 1985).

The NVZ probably jumped to its present location from a position north of the WVZ (Figure 1.3). Evidence for this includes the fact that the Tjornes Fracture Zone formed about 4Ma, at the same time as the unconformable lavas of the NVZ (Saemundsson, 1974). Also, the remains of transform fault scars can be found where the old rift zone was located (Saemundsson, 1974).

Extinct Tertiary central volcanoes such as Austerhorn in south eastern Iceland may have formed in propagating rift zones similar to the EVZ (Furman *et al.*, 1992b). Some of these extinct volcanic centres actually form linear arrays suggesting that they formed along the same rift zone (Saemundsson, pers. comm.).

1.4 ERUPTIVE TYPES

Recent volcanic activity in Iceland tends to produce either ***fissure*** eruptions or ***shield*** eruptions.

Fissure eruptions are of variable volume, but typically produce between 1 and 13.5km^3 of eruptive material (Jakobsson, 1979b). As an exception, the Laki eruption of 1783-1785 produced 14.7 $\pm$ 1.0km^3 of basalt (Thordarson & Self, 1992). The form of a fissure eruption depends on the environment of deposition, composition of the lava and the duration of volcanic activity. Subaerial fissures are recognised by strings of cinder and spatter cones, whereas subglacial fissure eruptions form elongate, steep-sided ridges of hyaloclastite deposits known as 'tindas'. Aa flows erupted from the fissures of the

axial rift zones are typically composed of olivine-poor tholeiites suggesting that these lavas originated from shallow magma chambers (Saemundsson, 1979).

Shield volcanoes develop around a single, central vent from which monogenetic pahoehoe flows consisting of numerous thin flow units are erupted (Saemundsson, 1979). The volume of eruptive products may vary from 1-17km^3 (Jakobsson, 1979a; Saemundsson, 1992). Shield eruptions on the axial rift zones are frequently composed of olivine tholeiites, suggesting that they are in a superheated state and from a deeper source than fissure eruptions (Saemundsson, 1979; C.Walker, 1992). Subaerial shield volcanoes are dome-shaped, they have low-angle slopes probably due to low effusion rates (Walker, 1971). Subglacial shield eruptions form flat-topped, steep-sided table mountains known as 'tuyas'.

Central volcanoes exhibit both fissure and shield eruptions. Fissures may follow the regional trend or have a radial component, whilst shield eruptions may occur on the flanks of the central volcano. The form of an eruptive unit on a central volcano depends upon the pre-existing topography and whether the vent was in a subaerial, subaqueous or subglacial environment.

1.5 CLIMATE CHANGES

The nature of the topography in Iceland and the form of volcanic edifices is strongly dependent on climate and on glacial periods in particular. Erosion is rapid between glacial periods, particularly of the soft hyaloclastite lithologies, resulting in the formation of deep, steep-sided river gorges.

The first tillites in Iceland appear at the beginning of the Plio-Pleistocene, inter-stratified with subaerial lavas in the southwest and northeast of Iceland. The rest of the Plio-Pleistocene and the Upper Pleistocene is characterised by glacial and interglacial periods. There is a particularly high proportion of subglacial rocks relative to subaerial rocks in the Upper Pleistocene of southwest and central Iceland (Saemundsson, 1979). Einarsson and Albertsson (1988) have found evidence of at least four glacial periods since 0.7Ma at Tjornes in northern Iceland.

Although there is evidence that thick ice sheets covered much of Iceland at the maximum of the last glaciation (about 20,000 BP), it seems that alpine-style glaciation occurred in the highlands so that ridges and nunataks may have been free of ice (Bjornsson, 1988). The extent of the glaciers was tremendous. End moraines have been found 130km off the coast of west Iceland at a depth of 150-250m (Einarsson & Albertsson, 1988). During the glacial retreat, some re-advances occurred corresponding to the Older Dryas (12ka BP) and Younger Dryas (11-10ka BP). Hjartarson and Ingolfsson (1988) dated shells found near Reykjavik and found that S.W.Iceland was still heavily glaciated at 9000 BP. They proposed that this would also have affected southern Iceland as a result of its exposed position. Shortly after glacial retreat in

southern Iceland, the sealevel rose to flood the lowlands. The subsequent isostatic and eustatic readjustment was very rapid and by about 8ka BP sealevel had fallen to 20m lower than it is today (Einarsson & Albertsson, 1988). This is probably a typical sequence of events following a glaciation.

1.6 GEOLOGY OF THE EASTERN VOLCANIC ZONE

The EVZ show structural, petrological and geochemical variations along its length (Meyer *et al.*, 1985). The northern EVZ is dominated by well-developed fissures erupting olivine tholeiites and tholeiites; the crust is about 8-10km thick (Meyer *et al.*, 1985) and in all respects resembles an axial rift zone (section 1.3.1). The central and southern parts of the EVZ show features typical of flank zones, with thickened crust (20-30km), (Palmason, 1971) and little evidence of rifting (Saemundsson, 1978). The central EVZ is dominated by large central volcanoes erupting transitional alkali basalts, intermediate and acid rocks. At the southern tip of the EVZ (Vestmannaeyjar) the crust is up to 30km thick (Palmason, 1971) and alkali basalts to mugearites are erupted.

1.6.1 VOLCANIC SYSTEMS OF THE EASTERN VOLCANIC ZONE

Individual volcanic systems of the central and southern EVZ include Torfajökull, Hekla, Tindfjöll, Katla, Eyjafjöll and Vestmannaeyjar (Figure 1.5).

Torfajökull is dominated by peralkaline rhyolites and postglacial subalkaline rhyolites (McGarvie, 1984). The production of such large volumes of evolved lavas would have required ponding and fractional crystallisation of transitional basalt within a large, shallow crustal magma chamber (Macdonald *et al.*, 1990). The fractionating magma chamber was replenished by, and underwent mixing with tholeiitic basalts which were fed laterally into the system from the Veidivotn rift zone to the north (McGarvie *et al.*, 1990).

Recent eruptions of andesites, dacites and rhyolites from Hekla have occurred along a summit fissure system showing a slight radial component (Takada, 1994). Each eruptive cycle is initiated by acidic rocks, but eruptive material becomes more basic during the course of an eruption (Baldridge *et al.*, 1973). There is no summit caldera and it is thought that Hekla is fed from a deep, zoned magma chamber.

Katla is a large seismically active volcano dominated by Fe-Ti rich transitional alkali basalts (Meyer *et al.*, 1985), small volumes of rhyolite are also documented (Robson, 1956, Carswell, 1983). Katla appears to have two seismically active centres (Einarsson, 1991), the easternmost of which lies above a circular magma chamber which is 5km in diameter and 1km thick (Gudmundsson *et al.*, 1994).

Tindfjallajökull is the source of the Thorsmörk Ignimbrite (Jorgensen, 1980). The large summit caldera predates the ignimbrite, but may have undergone further

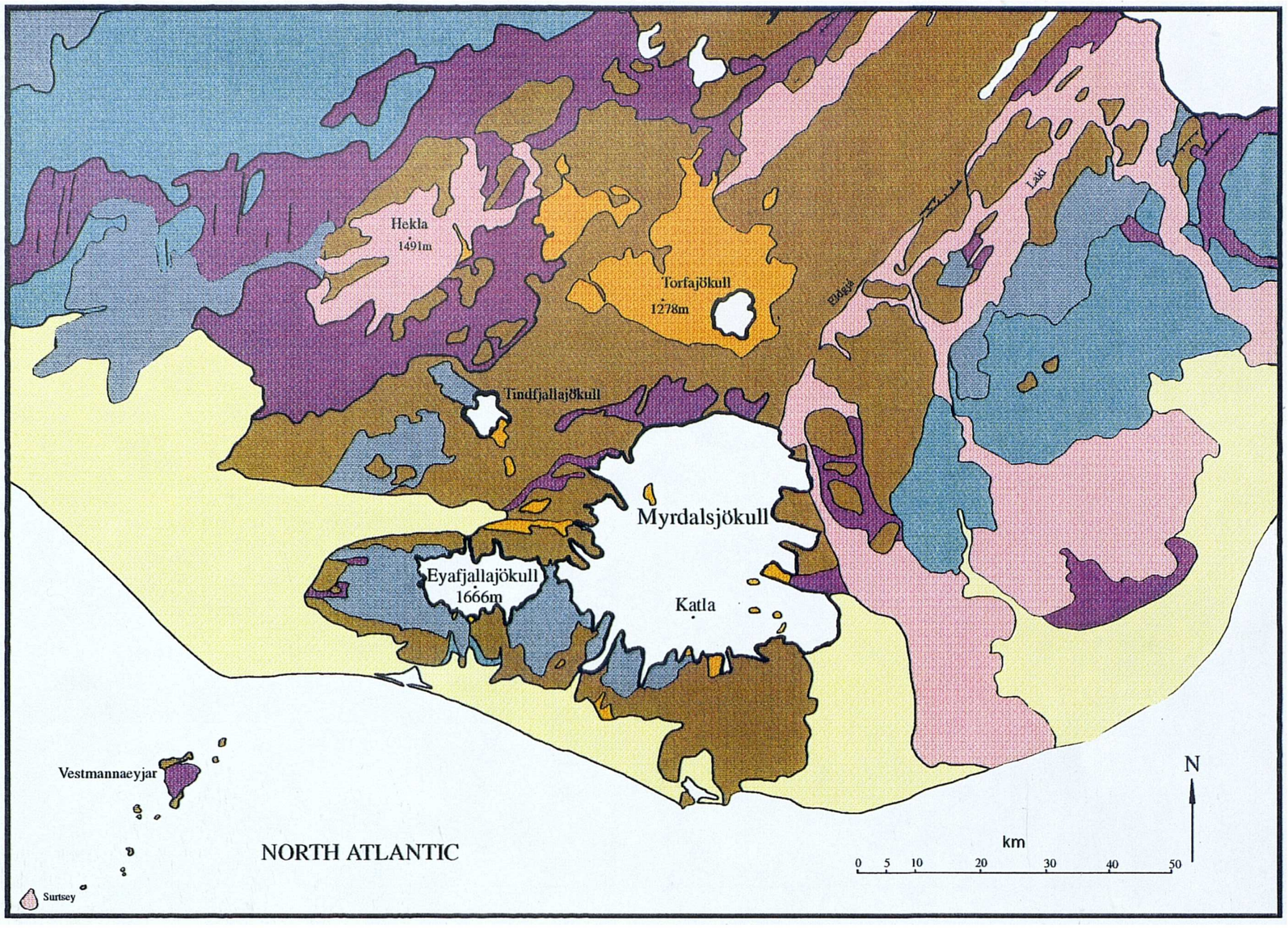

Figure 1.3 Geological Map of the Eastern Volcanic Zone, Iceland.

Legend

- Holocene sediments (sandur).
- Postglacial basic and intermediate lavas, younger than 1100 years.
- Postglacial basic and intermediate lavas, older than 1100 years.
- Pleistocene acid extrusives.
- Upper Pleistocene, basic and intermediate interglacial lavas and intercalated sediments.
- Upper Pleistocene, basic and intermediate hyaloclastites, pillow lavas and associated sediments.
- Upper Pliocene and lower Pleistocene, basic and intermediate extrusive rocks with intercalated sediments.

Based upon: Jóhannesson, H and Saemundsson, K., 1989: Geological Map of Iceland. 1:500,000. Bedrock Geology. Icelandic Museum of Natural History and Iceland Geodetic Survey, Reykjavik (1st ed.)

collapse on eruption. All of the volcanic systems except Tindfjöll have been active in Postglacial times. The orientation of the Tindfjöll and Eyjafjöll volcanic systems (E-W) is at a sharp angle to the regional NE-SW trend. This E-W trend may be caused by a sinistral transform zone, the presence of which is suggested by the SISZ (see section 1.1.2).

Lavas from the Heimaey central volcano in the Vestmanaeyjar have evolved to intermediate compositions (Jakobsson *et al.*, 1973). Trace element and isotope data suggest that the influence of the mantle plume is minimal here (Kurz *et al.*, 1985; Meyer *et al.*, 1985).

1.6.2 GEOCHEMICAL VARIATION

Iceland has at least two different potential magma source compositions: a) undepleted mantle plume material and b) depleted MORB-source mantle. The geochemistry of basalts along the Reykjanes Ridge becomes progressively more enriched towards Iceland apparently corresponding to an increase in the degree of melting (Schilling *et al.*, 1982). Icelandic basalts have incompatible trace element ratios reflecting a higher abundance of the more incompatible elements relative to Atlantic mid-ocean-ridge-basalt (MORB). Therefore, high degree melts are expected to have enriched trace element and isotope signatures. However, high MgO basalts from the axial rift zones have depleted trace and isotope signatures relative to lower MgO basalts. This apparent decoupling of major and trace element behaviour has been explained by Elliot *et al.* (1991), who suggest that incremental melts from different depths in the melting column may be segregated and erupted independently. Melts derived from shallow mantle are relatively depleted whereas melts from deeper mantle are enriched. Basalts have variable Rare Earth Element (REE) trends which may be flat, representing mixing throughout the melting column, to light rare earth element (LREE) depleted, representing mixing of shallower melts. Further variations in isotopic and trace element data of Icelandic basalts indicate that there may be some heterogeneity in the source region (e.g. Wood *et al.*, 1979; Wood, 1981).

The northern part of the EVZ is similar to an axial rift zone; magma supply rates are correspondingly high and lead to the eruption of tholeiite*s* and olivine tholeiites (Meyer *et al.*, 1985). Basalts from the northern EVZ show REE patterns similar to basalts of the axial rift zones, which are flat to LREE-depleted. This may signify melting and mixing throughout a range of depths (Elliot *et al.*, 1991), (Figure 1.6). Modelling by Meyer *et al.* (1985) suggests that incremental melting of a spinel lherzolite source can generate compositions similar to those observed.

In the extreme south of the EVZ, at Vestmannaeyjar the crust is particularly thick (30km) and alkali basalts are erupted (Figure 1.6). The mantle plume influence on the geochemistry of alkali basalts is minimal, as indicated by low $^{3}He/^{4}He$ ratios (Kurz

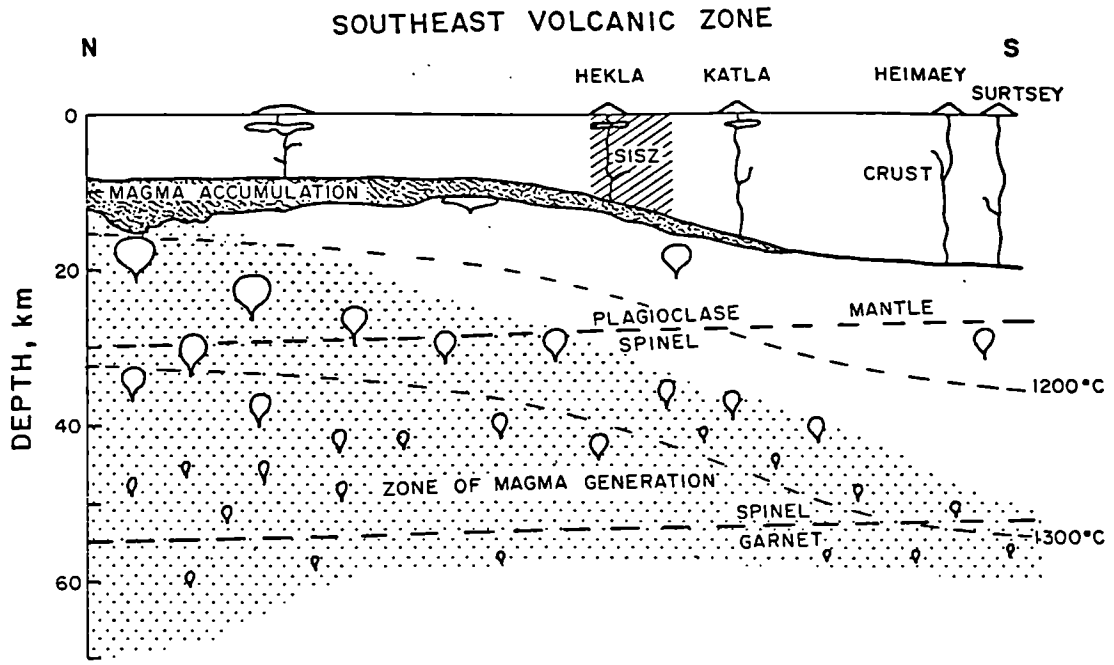

Figure 1.6 *A model of magma generation along the EVZ from Meyer et al., (1985). The crustal thickness is based on seismic data (Palmason, 1971; Angenheister et al., 1980), the magma accumulation layer is based on magnetotelluric data (Hermance et al., 1975; Beblo and Bjornsson, 1980) and contains 10-20% melt. Isotherms are based on geothermal gradients caculated by Palmason (1973) and Palmason, et al., (1979).*

et al.,1985). The moderately LREE-enriched alkali basalts may be derived by small degrees of melting in the spinel - garnet lherzolite transition zone (Meyer *et al.*, 1985).

In the central Hekla-Katla region of the EVZ (Figure 1.6), it has been suggested that moderate degrees of mantle melting cause ponding at the base of the crust since magma supply rates exceed eruption rates (Meyer *et al.*, 1985). The presence of a zone of partial melt at 8-10km depth is also indicated by seismic (e.g Palmason, 1971; Zverev *et al.*, 1980) and magnetotelluric data (e.g Eysteinsson & Hermance, 1985). Uniformly LILE-enriched transitional alkali basalts are erupted in this area, their uniformity suggesting either uniform melting conditions or ponding in large subcrustal magma reservoirs (Meyer *et al.*, 1985). Enrichment in LREE may be explained by small degrees of melting of a source which is sufficiently deep to contain some stable garnet (Meyer *et al.*, 1985). Isotopic and trace element evidence (e.g $^{3}He/^{4}He$ ratios) suggests a substantial mantle plume component in the source of the central EVZ (Kurz *et al.*, 1985; Meyer *et al.*, 1985).

It has been suggested that crustal assimilation plays an important role in the petrogenesis of Iceland rocks, particularly of alkali basalts (Oskarsson, *et al.*, 1982, 1985; Steinthorsson *et al.*, 1985). These workers suggest that mixing of partial melts from a hydrated, amphibolitised lower crust with mantle derived tholeiites can produce alkali basalts and other compositionally diverse magma types. Meyer *et al.* (1985) have shown (see above) that alkali basalts can be derived by small degrees of melting in the spinel-garnet lherzolite transition zone and that crustal assimilation is not necessary. Nevertheless, gabbroic xenoliths have been found in lavas from Tindfjoll and Heimaey which have reacted with the host magma to produce pargasitic hornblende and/or kaersutite (Jakobsson *et al.*, 1973; Larsen, 1979). Such small-degree melts (<10%) are enriched in K_2O and other incompatible elements and may contaminate basalt magmas rising slowly through the lower crust (Larsen, 1979) .

1.6.3 THE EYJAFJALLAJÖKULL VOLCANO

The Eyjafjallajökull central volcano (or the Eyjafjöll volcanic system), (Figures 1.4 and 1.7) is a large, east-west orientated complex reaching a height of 1666m and covering an area of about 400km^2; it has been active for over 0.78Ma (Kristjansson *et al.*, 1988). It is bounded to the south and west by extensive coastal sandur deposits and to the north by the broad, meandering river system of Markarfljöt (Figure 4.1, a detailed location map, is shown on page 82). An icecap covers the summit down to an altitude of about 1000m. The northern and southern flanks of the volcano are highly dissected by glacial valleys and deep river gorges which expose old lavas in the core of the volcano. The southern margin of the complex is sharply defined by old, wave-cut cliffs up to 700m high. The base of these cliffs is almost 100m above present sea-level. Isostatic and eustatic readjustments at the end of the last glacial period (and possibly the one before) are probably responsible for this uplift (see section 1.4). The western flanks of the volcano slope gently down to the sandur and to the east, a high plateau (the Fimmvorduhals Pass) joins Eyjafjallajökull to Myrdalsjokull, the glacier which covers the large, active neighbouring volcano Katla. The last eruption (of mainly acid tephra) occurred between 1821 and 1823 from the central crater. As this event ended, an eruption at neighbouring Katla began.

Previous work in the area includes two MSc theses (Wiese, 1992; Arney, 1974) both of which concentrated on geochemical aspects of the volcano's evolution. Wiese (1992) analysed 57 rocks for major and trace elements, 4 samples for Helium isotopes and did K/Ar dating on 27 samples. Both Wiese and Arney concluded that fractional crystallisation was the dominant differentiation process at Eyjafjöll. Wiese (1992) also found evidence of magma mixing and rare high-pressure crystallisation. Jonsson (1990) produced a map of Eyjafjöll outlining the extent of glacial and interglacial lithologies (Figure 1.7). Kristjansson *et al.*, (1988) found the Brunhes-Matuyama boundary (~0.7Ma) towards the base of a sequence at Nupakot (S. Eyjafjöll) using

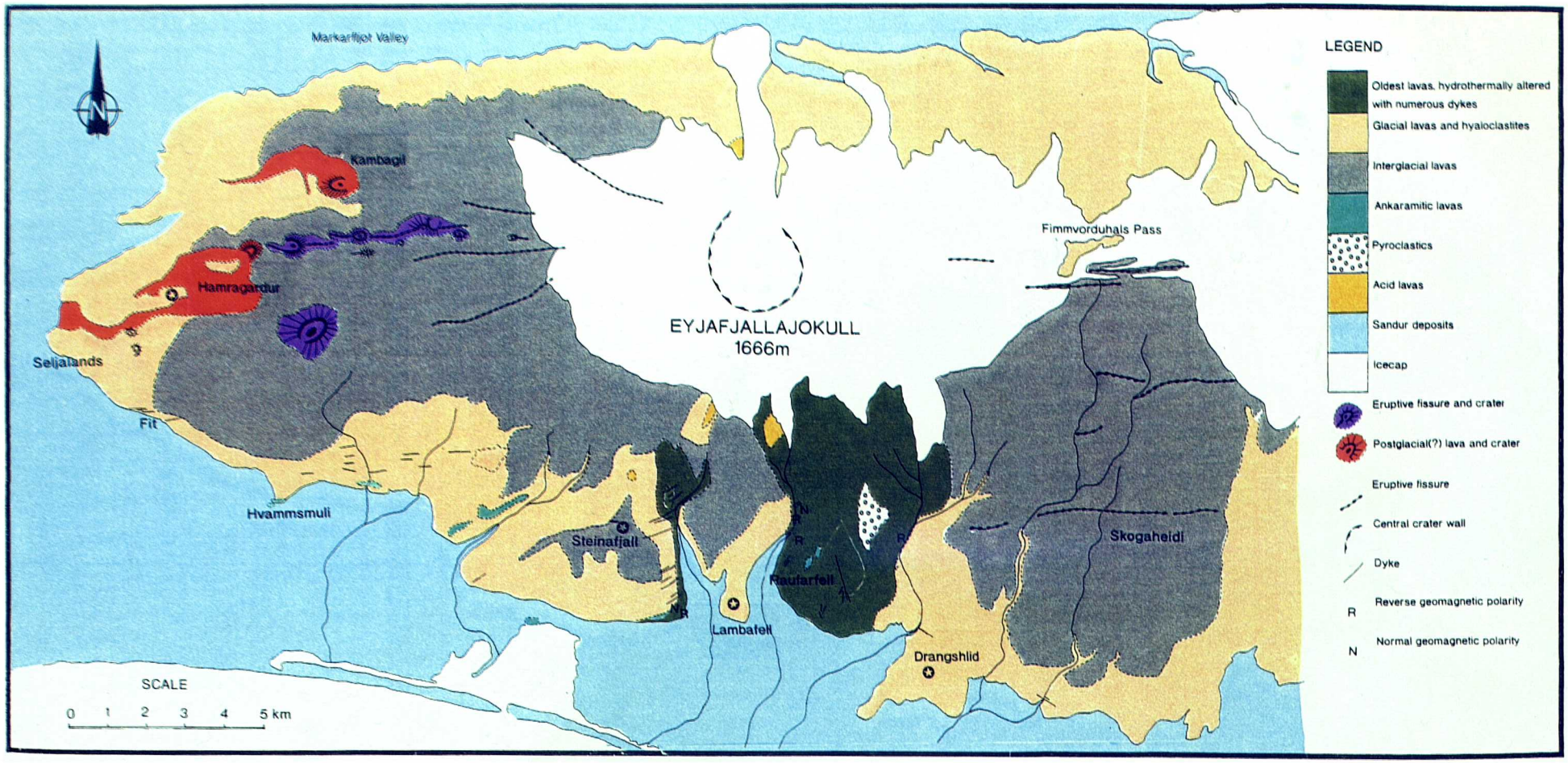

FIGURE 1.7 Map of the Eyjafjoll volcanic system, partly based on a map by Jonsson (1988)

palaeomagnetism. They described the vertical sequence above the boundary and suggested that nine alternations between subaerial and subglacial, or subaqueous conditions had since occurred. A system of E-W fissures links Eyjafjöll to Katla. The products of these fissures were studied and described by Carswell (1983) who suggested that they were subglacial deposits. He studied the chemistry of these deposits and proposed that there was a trend towards more alkalic compositions. Jakobsson (1979) sampled some recent lavas from Eyjafjoll in a study of the postglacial petrology of the EVZ and found that they were dominantly 'transitional basaltic andesites' (2-4.5% MgO). He suggested that the icecap covers four eruption centres and that Eyjafjöll has been active during the last two glacial periods and the last interglacial. Sigurdsson (1970a) sampled three evolved lavas from the volcano including two quartz trachytes and one benmoreite. The Hvammsmuli ankaramite which crops out near the roadside south of the volcano was studied in detail by Steinthorsson (1964) who suggested that the ankaramites represent a suite of sills.

During the last glaciation, a thick glacier formed in the Markarfljöt valley to the north of Eyjafjöll. Northward dipping lodgement tills cover the steep lower slopes on the north side of Eyjafjöll, marking the glacier margins. There are two relatively recent subaerial lavas on the western flanks of the volcano named the Kambagil and Hamragarder flows (Figure 1.7). Both erupted from the western end of the fissure system. Kjartansson (1958, 1970) believed that they were erupted 10,000-11000 years ago. Johannesson (1985) showed that the Kambagil flow is covered in ground and terminal moraine from 325m down to sea level. It was therefore overridden by the Markarfljöt glacier at least 12,000 years ago. The Hamragarder flow extends down to Seljalandsfoss. It lies on a striated surface and on conglomerates. The striations run roughly north-south (Section 2.2) suggesting that it was the Markarfljöt glacier that formed them and not the advancing/retreating Eyjafjallajokull ice cap. It is therefore substantially younger than the Kambagil flow, 11,000 years old at the most (Johannesson, 1985). A more detailed assessment of the palaeoclimate during the growth of the volcano will be undertaken in chapter three.

1.7 AIMS OF THE PROJECT

This study aims to shed some light on the volcanological and petrogenetic processes involved in the construction of an Icelandic central volcano.

Three field seasons amounting to 22 weeks were spent mapping and sampling. The stratigraphy is very complex in places, many of the volcanic units are subglacial in origin and an understanding of their formation and deposition processes was needed before the stratigraphy could be determined. Chapter 2 gives an introduction to the terminology and products of volcanic eruptions in Iceland. A model for subglacial volcanism is given in Chapter 3 and a general stratigraphy and palaeoenvironmental

reconstruction are presented in Chapter 4. Chapter 5 contains the results of a petrological study and the implications for magmatic processes. Overall, 250 samples were analysed for trace elements, 150 samples were analysed for major elements and a further 40 were analysed for REE. These data and their petrogenetic implications are discussed in Chapter 6. The final conclusions reached in this thesis are presented in Chapter 7.

There are two appendices. Appendix A contains details of mineral chemistry obtained from microprobe analysis. Appendix B contains the methods used to obtain the geochemical whole-rock data, an assessment of error and all the whole-rock data.

Two geological maps based on fieldwork, may be found in the back pocket of the thesis.

1.8 SUMMARY

The Eyjafjallajökull central volcano (or Eyjafjöll volcanic system) lies on the Eastern Volcanic Zone, a southward-propagating flank zone in southern Iceland. The volcano has an anomalous E-W orientation that may be influenced by the South Iceland Seismic Zone. Some of the oldest lavas have been dated at 0.78Ma (Kristjansson *et al.*, 1988), these are alkaline basalts; the latest activity was acidic and occurred between 1821 and 1823 from the summit crater. Compositionally, lavas are dominated by transitional alkali basalts however, a range of compositions from ankaramite to quartz trachyte has been documented. Subglacial and subaqueous lithologies are common but complex, reflecting a broad range of flow mechanisms and modes of deposition.

CHAPTER 2
VOLCANOLOGY AND TERMINOLOGY IN ICELAND

2.1 INTRODUCTION

The eruptive environment in Iceland is strongly dependent on climate and on the extent and thickness of ice cover. The Eyjafjallajökull volcano is dominated by complex volcanic and sedimentary assemblages related to subglacial volcanism; their variety suggests a diverse range of subglacial eruptive environments and depositional processes. Subaerial lavas and tephra are also common and even submarine deposits occur towards the base of the volcano.

This chapter will briefly describe the eruption types seen at Eyjafjöll, their products and terminology.

2.2 SUBAERIAL VOLCANISM

2.2.1 INTRODUCTION

Subaerial basaltic volcanoes are distinct from all other volcano types because the volume of coherent lavas far exceeds the volume of volcaniclastics. This is because basic magmas usually have lower volatile contents and are typically fluidal and mobile allowing rapid release of volatiles (Cas and Wright, 1988). Basaltic flows are typically voluminous compared to more silica-rich lavas. The latter are viscous and form short thick flows or domes during effusive eruptions. During explosive eruptions, silicic magmas are fragmented and form pyroclastic falls, flows or surges.

Subaerial basalt lavas tend to be black with a reddened, clinkery breccia base and may show lava drips. Flows may be columnar, massive, platy or blocky and often lie on a palaeosol, or on fluvial sediments (e.g. Emeleus, 1985). They are typically associated with cinders, scoria and spatter.

Silicic lavas are typically pale in colour, or glassy and black. They are commonly associated with ash deposits containing pale grey pumice and ash.

2.2.2 LAVAS

Subaerial basic lavas are typically either pahoehoe, aa or block flows. Pahoehoe flows are smooth with undulating or ropy surface textures, whilst aa flows are rough and blocky in appearance. Block lavas have a fragmental top and front, but individual fragments are smooth polyhedral blocks. The type of flow formed depends primarily on the viscosity of the lava and hence its composition and temperature; eruption rate is also important (Walker, 1971). Flows may change from pahoehoe to aa with distance from the vent (Hall, 1987). The lavas on Eyjafjöll are typically exposed in vertical sequences,

so surface textures are not always clear. Exposed lava flows have often been glaciated so that distinctive surface textures may have been removed.

Thin columnar basalt lavas often develop two tiers of columnar jointing where cooling has advanced from the lower and upper surfaces towards the centre. A single tier of columnar-jointed rock in which the columns formed perpendicular to the boundaries in this way, is termed a colonnade (Tomkeieff, 1940). Thicker lava flows may contain a tier which shows curved or fanning columns known as the entablature (Tomkeieff, 1940). Many columnar basalt lavas consist of two or more tiers of jointing where a basal colonnade is topped by a substantial thickness of entablature and occasionally an upper colonnade (Tomkeieff, 1940). This basic structure has been described at the Giant's Causeway (Tomkeieff, 1940; Spry, 1962) and at the Columbia River Plateau (Mackin, 1961; Long & Wood, 1986).

The colonnade forms by contraction cooling of a tabular geometry in which two solidification fronts migrate towards the centre of the body from the contact surfaces (Jaeger, 1961). The principle tensile stress directions are parallel to isothermal surfaces, i.e. the contact surfaces and promote cracking perpendicular to the flow contacts. The cracking front propagates inwards, following the solidification front and dividing the rock into prismatic columns (Ryan & Sammis, 1978; DeGraff & Aydin, 1987; Budkewitsch & Robin, 1994). Crack advance is incremental due to cyclic release of tensile stress as a result of cooling and each crack 'segment' forms a transverse band across the columnar joint face (Figure 2.1).

Spry (1962) described the twisted columns of the entablature at the Giants Causeway as resulting from stress induced by movement of the still fluid interior of a partially solidified lava. The entablature of lava flows in Iceland may include radiating columns (Figure 2.2), but there are many examples of a cube-jointed and hackly entablature (Icel. kubbaberg) suggesting a slightly different origin. Saemundsson (1970) described some two-tiered interglacial lava flows at Hreppur, in northern Iceland, with such an entablature. These lavas had flowed along river valleys and Saemundsson (*Ibid*) proposed that they may have temporarily dammed the rivers which later flooded out over the top of the still partially molten lava. The surface of these aa flows had already solidified before flooding occurred, so he suggested that flooding accelerated the cooling of the lava and caused extreme thermal stresses to build up within the partially solidified interior causing the hackly jointing. The glassy texture of such rocks strongly suggests aqueous chilling as does the grading of some entablature into pillow lava and hyaloclastite (Saemundsson, 1970). Long & Wood (1986) suggested that similar features in the Columbia River Basalts also formed following flooding. They found that heavy rainfall is generally insufficient to form the entablature and that flooding by 'deranged drainage' is necessary. The water infiltration front must move down through the lava just behind the solidification front in order to produce a thick, quenched, hackly flow interior. Sigvaldason (1968) and Walker & Blake (1966) have both reported lava

flows with lower colonnade and upper hackly entablature that were emplaced subglacially. Both occur in association with pillow lavas and hyaloclastite. Saemundsson (1970) pointed out that generalisations on the formation of kubbaberg in Iceland must be avoided, since it can form by either post-emplacement flooding or by flowing/erupting into a subaqueous environment.

Columnar jointing also develops in evolved lavas and ignimbrites. Trachyte lavas high on the Eyjafjallajökull volcano have broad columns up to 80cm in diameter.

Figure 2.1 *Columnar lavas at Eyjafjöll [690 497*] showing cracks which have formed by inwards propagation of the cooling front (Budkewitsch & Robin, 1994).*

* Grid references in this thesis refer to the 'Defense Mapping Agency Hydrographic/Topographic Center/Iceland Geodetic Survey map of Eyjafjallajokull, 1990. Scale 1:50,000.

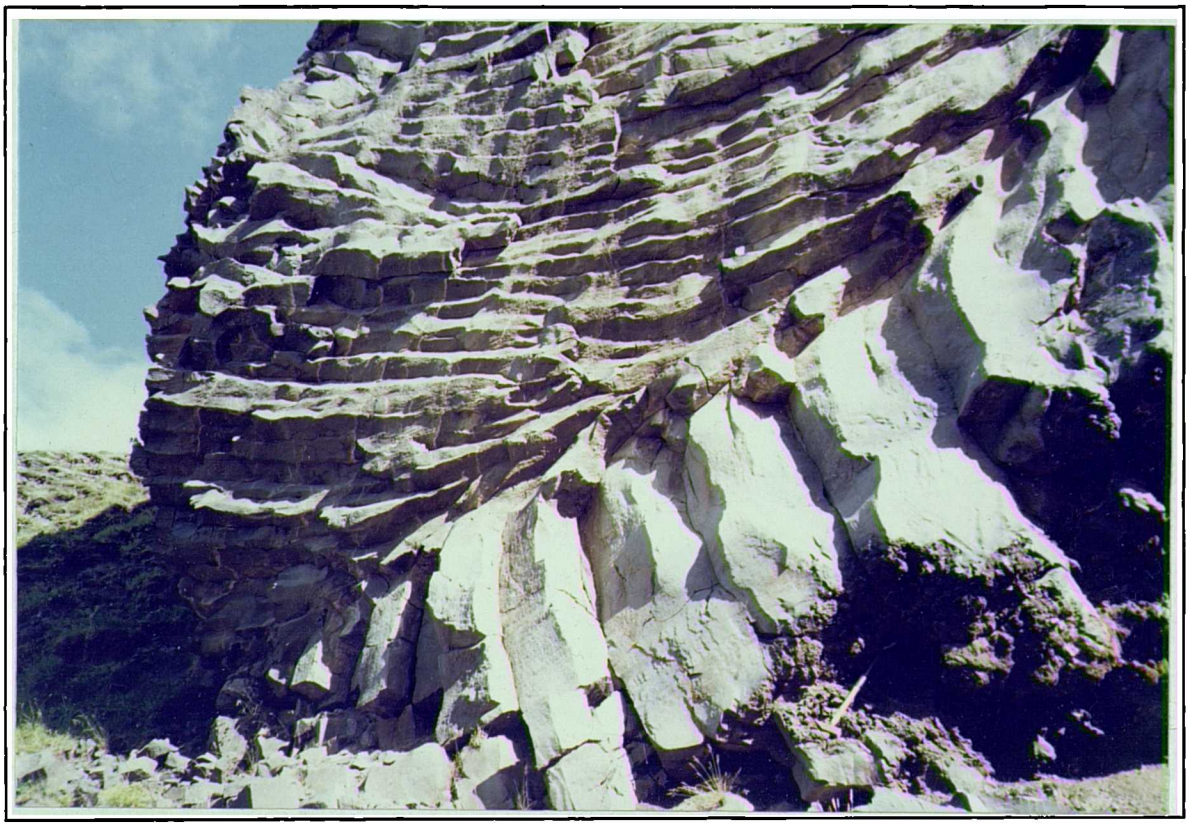

Figure 2.2 *Radiating and fanning columnar lavas at Eyjafjöll [602 494].*

Platy or laminate-textured lava flows are typically of intermediate composition and may be caused by flow alignment of groundmass and phenocryst plagioclase.

Lavas erupted on Eyjafjöll during the last interglacial period cover most of the upper western and southern flanks of the volcano (Jacobsson, 1979b), most are porphyritic fissure eruptions. They erupted from vents along E-W oriented and radial fissures, now defined by strings of cinder and spatter cones (Figure 1.7). The extent of subaerial lava flows is dictated by the topography and columnar jointing is well-developed in places, probably due to ponding of the lava in topographic lows. The flows were all glaciated by the advancing icecap during the last glaciation. Inter-lava sediment is sparse with thin layers of clinkery breccia dividing most of the subaerial flows.

2.2.3 PYROCLASTIC ROCKS

A *pyroclast* is any fragment released in the course of a volcanic eruption or explosion. Pyroclasts over 64mm in diameter are termed **bombs** (or blocks), those between 64mm and 2mm are known as **lapilli** and fragments less than 2mm in diameter are known as **ash** (Cas and Wright, 1988). All pyroclastic deposits may be described as **tephra** (Self and Sparks, 1981)

Pyroclastic rocks can include juvenile fragments (bombs, spatter, scoria, glass shards), crystals and lithic fragments.

Recent fissures to the east and west of the central crater all erupted subaerially forming strings of cinder and spatter cones (Figure 1.7). Large bombs up to 1 metre in

Figure 2.3 *A basalt bomb on the flanks of Arnagilshryggur crater, Eyjafjöll [561 567]. (Photo courtesy of Miss V.Hards).*

Figure 2.4 *A volcanic agglomerate on Raufarfell [712 489] containing hydrothermally-altered clasts (pale green) with vesicular and non-vesicular fragments of a highly pyroxene-phyric lava. The matrix is composed of glass and rock fragments in a zeolite cement.*

length are relatively common (Figure 2.3). Cinders and ash can be found close to subaerial vents throughout the stratigraphic sequence. Crystal-lithic tuffs occur high on the volcano associated with trachyte lavas. These are thick acid deposits, relatively rare in Iceland, although trachytes, rhyolites and ignimbrites have been previously documented (e.g Thorarinsson, 1969; Jorgenson, 1980). Volcanic near-vent agglomerates occur to the east of Raufarfell which contain a variety of clasts including hydrothermally-altered, highly pyroxene-phyric bombs and blocks (Figure 2.4).

2.3 SUBAQUEOUS VOLCANISM

2.3.1 INTRODUCTION

Submarine, subglacial and lacustrine eruptions all occur in subaqueous environments. The processes and products of magma-water interactions depend largely upon the volatile content of a magma, its viscosity (and hence its composition) and hydrostatic pressure (e.g. Jones, 1969a; Allen, 1980; Kokelaar, 1986).

In shallow subaqueous environments, volcaniclastics are predominant over effusive deposits and are formed by a variety of processes:

1) **magmatic explosivity**, the explosive release of magmatic volatiles.

2) **contact-surface steam explosivity**, the explosive expansion and contraction of steam at the magma-water contact.

3) **bulk interaction steam explosivity**, the explosive expansion of steam after water has been trapped or enclosed by magma (Kokelaar, 1986).

Volcanoes formed in deep water are dominated by effusive pillow and sheet lavas because high hydrostatic pressure in deep water inhibits the explosive release of volatiles which is a major clast-forming process (Kokelaar, 1986). Similarly, eruptions under thick ice are dominated initially by pillow lavas (Jones, 1970; Sigvaldason, 1968). The depth at which magmatic explosivity begins depends on the juvenile volatile content of a magma. Moore & Schilling (1973) and Kokelaar (1986) concluded that it is up to 200m for tholeiitic magmas and Kokelaar (1986) suggested water depths up to 1km for alkalic magmas. Walker (1974) showed that at water depths below 1km, gas exsolution from lava is very unlikely. Allen (1980) looked at the transition from effusive pillow lavas to explosive hyalotuffs at the base of subglacial volcanoes in Iceland and suggested that explosive activity begins at depths of about 200m below the presumed ice surface. Moore & Fiske (1969) and Jones (1970) suggested that explosive basaltic volcanism can begin at water depths of 100m.

Kokelaar (1986) pointed out that the formation of clastic deposits is not simply dependant on the exsolution of magmatic volatiles and that magmatic explosivity is subordinate to steam explosivity as a clast-forming process at shallow depths.

2.3.2 PRODUCTS OF SUBAQUEOUS VOLCANISM

Subaqueous volcanism results in a variety of clastic and effusive products. The terminology used in this thesis to describe these products is as follows:

2.3.2.1 HYALOCLASTITE

Hyaloclastite forms as a result of the *non-explosive* quenching and granulation of magma when it is exposed to water (Rittman, 1962; Honnorez, 1961; Nayadu, 1962; Carlisle, 1963; Honnorez & Kirst, 1975; Kokelaar, 1986). It can occur at any water depth but may be replaced by steam explosivity at shallow depths (Kokelaar, 1986). A hyaloclastite deposit is typically composed of abundant blocky and angular, non-vesicular, clasts of brown glass (sideromelane) or black glass (tachylite), (Macdonald, 1972). Clasts are of sand size and above with planar edges (Figure 2.5).

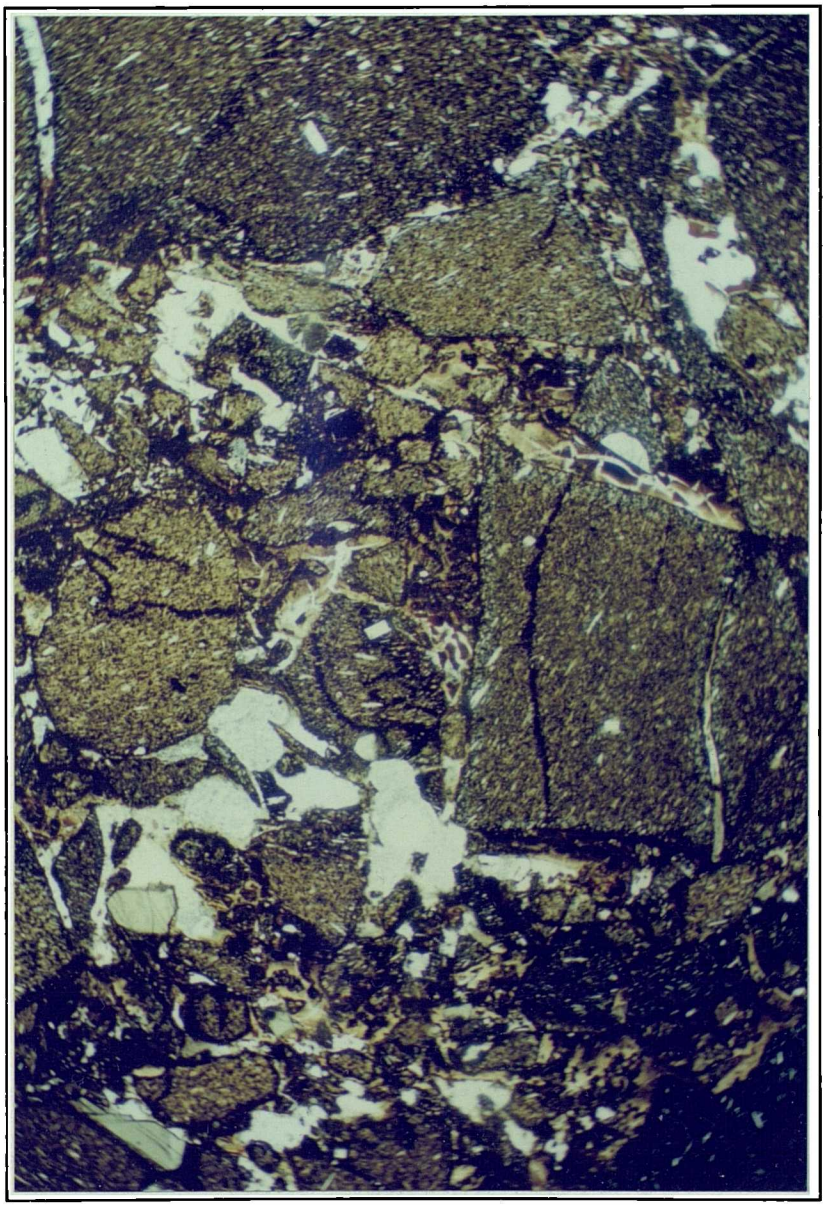

Figure 2.5 *Angular clasts of hyaloclastite fragmenting from the base of a ponded lava flow [685 492]. This lava probably ponded in a subglacial environment (Figure 3.19). Field of view 12 x 7.2mm. Sample number 518.*

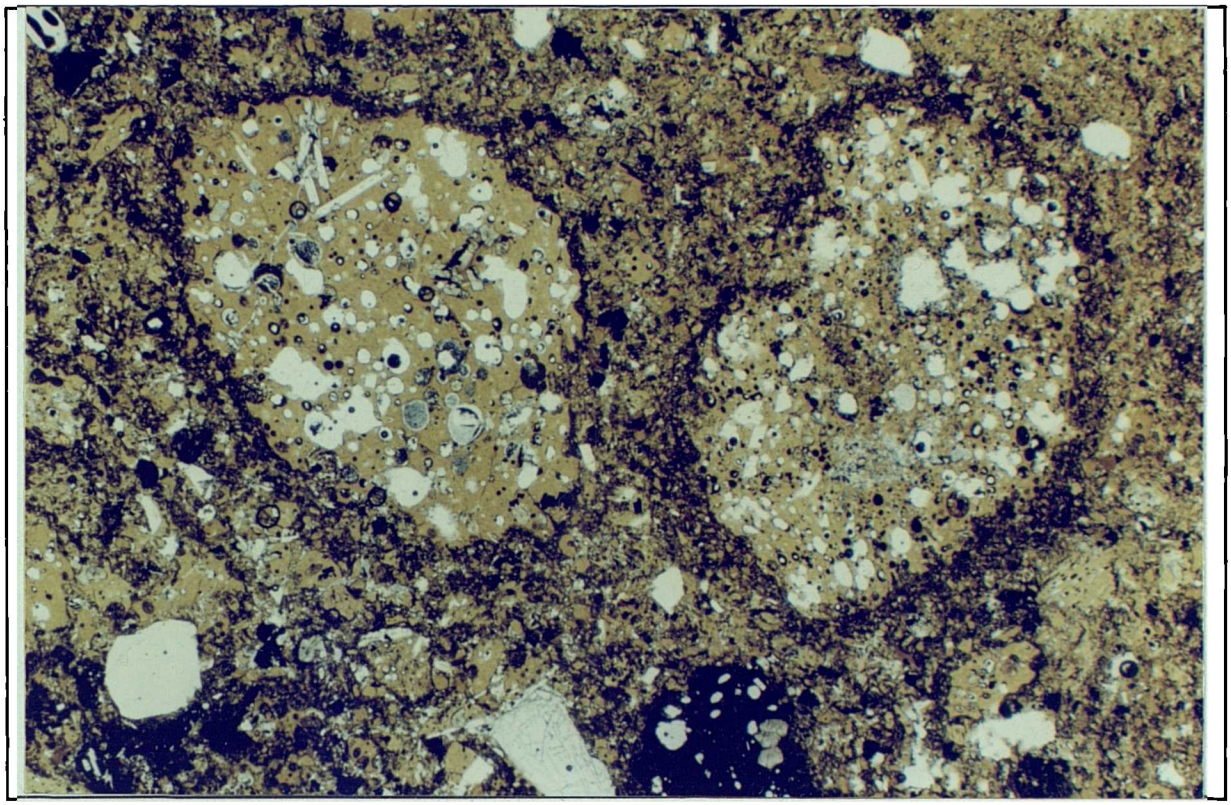

Figure 2.6 *Armoured lapilli in a massive deposit of hyalotuff on Fagrafell [704 479]. Clast shapes suggest that vesicles did not play a major role in fragmentation, steam explosivity was probably more important. Field of view 6 x 3.7mm. Sample number 600.*

2.3.2.2 HYALOTUFF

Hyalotuffs form as a result of the ***explosive*** interaction between magmas and water (Honnorez & Kirst, 1975). They form in any environment where water is in contact with magma and explosive activity is not suppressed, e.g. shallow water (< 200m for basaltic rocks-section 2.2). They are composed of angular glass lapilli with few planar edges and numerous corners and inflections formed by exploding vesicles and/or steam explosions. If these lapilli are propelled into a subaerial environment they may develop a coating of ash (armoured lapilli) and may be subsequently deposited in a subaerial or subaqueous environment (Figures 2.6 and 4.23).

2.3.2.3 PILLOW LAVAS

The early effusive stage of a deep, subaqueous eruption may create pillow lavas or sheet lava flows. Pillow lavas form during eruptions of relatively low effusion rate (Ballard *et al.*, 1979) and advance by budding of subaqueous lava tubes (Moore *et al.*, 1973). Isolated pillows form by a spalling-off process whereby a chilled skin of basalt is inflated by magma and develops a glassy rind. However, apparently discrete pillows may be cross sections of lava tubes. The pillows typically pile up around a vent with little interpillow sediment or fragmental material present. With steepening slopes, the pile may eventually become unstable resulting in slumping, mass flow and the

formation of pillow breccias. Most pillow breccias are monolithologic and contain variable proportions of lithic pillow fragments, glassy rind fragments and hyaloclastite.

2.3.2.4 SHEET LAVA FLOWS

Sheet flows form during eruptions with high effusion rates and are analagous to subaerial, unchannelled pahoehoe lavas (e.g Ballard *et al.*, 1979). They are usually massive with vertical or partly radial columnar jointing. The upper and lower surfaces may show a variety of textures including pillowy, brecciated, hackly, smooth or lobate (Cas & Wright, 1987). Examples on Iceland have been described by Sigvaldasson (1968), Jones (1969a) and Bergh & Sigvaldasson (1991).

2.4 SUBGLACIAL VOLCANISM

2.4.1 INTRODUCTION

Volcanic eruptions that occur under ice are essentially subaqueous, but show specific features diagnostic of their subglacial origin. These features will be described briefly in this section and a more detailed analysis of subglacial volcanism is presented in Chapter 3.

Steep-sided hyaloclastite ridges ('tindas' - formed during fissure eruptions) and table mountains ('tuyas' - formed during shield eruptions, section 1.4) develop in englacial water reservoirs as a result of melting of the overlying ice sheet. They contain a continuum of lithologies from a central feeder zone, grading laterally and vertically away through pillow lavas, pillow breccias, hyaloclastite breccias and hyalotuff (Figure 2.7), (e.g Noe-Nygaard, 1940; Mathews, 1947; Jones, 1968). This assemblage was known collectively as 'palagonite tuff' (Icel. 'moberg') for many years, but it is now known as the ***hyaloclastite formation***. The hyaloclastite formation in Iceland is now widely accepted to have a subglacial origin (e.g. Mathews, 1947; Saemundsson, 1967; Jones, 1968).

There is abundant evidence for a subaqueous environment during the formation of subglacial edifices. The pervasive palagonitisation of hyaloclastite may be a result of the warm water-saturated conditions (Jakobsson, 1978). Pillow lavas form near the vent as they do on the sea floor. Associated lavas frequently have thick entablatures indicative of water saturation (Long & Wood, 1986; Saemundsson, 1970) and associated sediments are all water-lain (Long & Wood, 1986).

The subglacial table mountains (tuyas) of Iceland are typically dominated by hyaloclastite and massive deposits of explosive hyalotuff (Jones 1780, Figure 2.7). If the volcano breaks the surface of the ice, subaerial capping lavas or cinder cones may form thus giving a rough estimate of the ice thickness (Jones, 1970). The basal pillow lavas of several table mountains have been found to be between 100m and about 200m below the presumed ice surface (e.g. Jones, 1970; Sigvaldasson, 1968) suggesting that

subaqueous volcanism is effusive above certain hydrostatic pressures (section 2.2). Jones (1969a) found a correlation between the vesicularity of pillow basalts from table mountains and presumed water depth but highly vesicular basalts can occur at great water depths (Luyendyk *et al.*, 1979). This suggests that hydrostatic pressure simply *inhibits* magmatic explosive, clast forming processes.

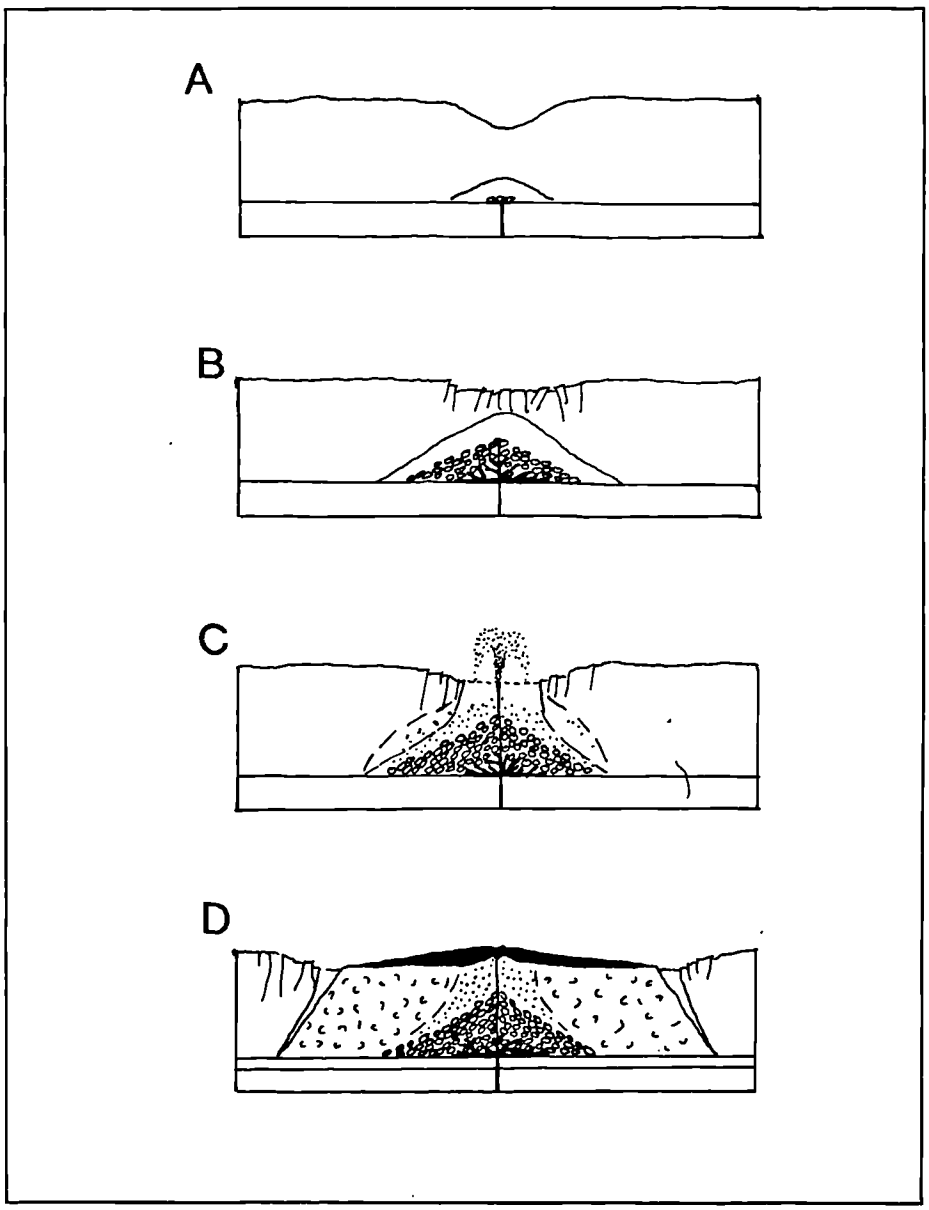

Figure 2.7 *Simplified version of Jones' 1969b model for the growth of a tuya.*

A. Magmatic heat causes melting of ice sheet above vent and forms a meltwater vault into which lava erupts. Assuming the ice is at least 200m thick (section 2.3.1) the eruption is effusive.

B. A steep-sided pile of pillow lavas develops in the vault, fed by a central feeder zone.

C. The roof of the vault collapses to form an englacial lake. Volcanism becomes explosive and thick hyalotuff deposits accumulate over the pillow lavas.

D. Explosive activity is replaced by subaerial effusive activity as lavas flow from the vent over deltas of hyaloclastite breccias (flow foot breccias). The deltas form by progradation of the pillow-hyaloclastite complex from the vent into the englacial lake.

The former presence of ice may only be appreciated when it has laterally confined the growing hyaloclastite pile forming steep-sided tindas or tuyas (Walker & Blake, 1966), or, when a hyaloclastite unit lies directly on glacial deposits. The association of striated bedrock and tillites (and occasional subaerial lavas) with assemblages of hyaloclastite and hyalotuff is considered to be evidence of a subglacial rather than submarine origin (e.g. Walker & Blake, 1966; Carswell, 1983).

2.4.2 THE PRODUCTS OF SUBGLACIAL VOLCANISM

Subglacial eruptions are effectively subaqueous so products of magma-water interaction are the same as described in section 2.3. Nevertheless, during subglacial eruptions the confining ice causes complex interactions between meltwater, ice, lava, pre-existing volcanic and clastic deposits and the topography (Nielson, 1936). Variable proportions of lava, pillow lava, hyaloclastite, pillow breccias, hyalotuff and glacio-fluvial sediments are produced. The general features of these and related subglacial lithologies are described below.

2.4.2.1 HYALOCLASTITE

Primary hyaloclastites typically form *in-situ* from granulating margins of pillows and lavas. Hyaloclastite is also common in the interstices of pillow breccias. Due to the topography at Eyjafjöll, lava bodies may actually have been flowing downslope in subglacial volcanic debris flows as granulation occurred (see chapter 3). Spallation and granulation is continuous during movement of the lava body and much of the hyaloclastite is removed by meltwater. At Eyjafjöll, hyaloclastite (section 2.3) often occurs in secondary deposits, redeposited by meltwater or slumping. The vitric fragments rapidly change to the orange-brown alteration product termed palagonite, giving the deposits a distinctive appearance.

2.4.2.2 HYALOTUFF

Thick deposits of primary hyalotuff (>200m) probably formed where subglacial meltwater ponded in an englacial lake (see section 2.5) resulting in voluminous *in-situ* phreatomagmatic activity during the emergent phase of an eruption. Jones' model for the growth of a tuya (Figure 2.7) shows how the early effusive products may be mantled by tuffs. These are in turn overlain by dipping hyaloclastite breccias representing the foreset beds of a delta complex formed during progradation of effusive lavas and breccias from the emerged vent into the englacial lake. The tuffs may also show evidence of redeposition by a variety of mass flow processes (Smellie & Skilling, 1994). Localised reworking due to the movement of meltwater is common and much hyalotuff is transported well away fom the eruption site by meltwater to be redeposited on coastal sandur (Maizels, 1989, 1990). Hyalotuff has the same distinctive orange-brown colour as hyaloclastite due to palagonitisation of the glass fragments.

2.4.2.3 PILLOW LAVAS

Pillow lavas are round or elongate bodies of lava that contain little or no interpillow sediment. They vary in size from tens of centimetres to megapillows several metres across; megapillows were probably feeders to the flow front. There are only a few examples of true pillow lavas at Eyjafjöll (e.g. Fit, Figure 3.7). Jones (1970) described units of lava which had a similar internal structure to pillows, but had a ragged outline and were enclosed in a breccia of hyaloclastite and lithic and vitric fragments. He termed this lithology ***para-pillow lava*** suggesting that it forms when lava apophyses fail to inflate. This may occur if a lava body is on a slope and flows too fast or if it detaches from its feeder zone, or if the magma supply wanes.

Pseudo-pillow lavas consist of massive lavas penetrated by fissures along which water entered causing intensive prismatic jointing (Walker, 1994; Watanabe & Katsui, 1976). The result is a mass of irregularly-shaped blocks of prismatically-jointed rock which may superficially resemble pillows but which have not undergone inflation and are not feeders to the flow front. Figure 4.5 shows a unit containing pillow buds (<0.5m in diameter) and irregularly sized and shaped prismatic jointed lava blocks which may be pseudopillows.

2.4.2.4 PILLOW AND HYALOCLASTITE BRECCIAS

Most pillows observed at Eyjafjöll tend to be fragmental constituents of pillow and hyaloclastite breccias. Breccias are common due mainly to the steep topography, which leads to instabilities in subglacial deposits and encourages mass movement. Pillow breccias are very varied in their appearance. Jones (1970) divided them into two major types: ***orthobreccias*** which are texturally homogeneous in appearance with little or no matrix and ***parabreccias*** which contain angular clasts in a finer grained matrix; this difference relates to the flow processes by which they were emplaced (see section 3.6.2). A continuum of lithologies between the pillow breccias and hyaloclastite breccias is developed. Definitions and general descriptions of the dominant breccia types are given below:

Pillow Breccia: This is made up almost entirely of pillow fragments and glassy rind fragments and tends to occur at the margin of pillow lavas. The lithic pillow fragments are typically wedge-shaped showing that they were fragmented after the development of the radial joints. Glassy rind fragments are curved and often associated with poorly developed glassy pillow fragments. Hyaloclastite is present in small quantities as a result of the cooling-contraction granulation of pillow fragments.

Pillow-hyaloclastite breccia: This is basically pillow breccia that is dominated by a matrix of hyaloclastite and/or hyalotuff (e.g. Figure 3.9). Pillows are often isolated or broken by mass movement during and after the 'spalling off' process from feeders and

are incorporated into the surrounding hyaloclastite. This is typically the constituent of 'flow foot breccias' found as aprons around the margins of subglacial edifices.

Hyaloclastite breccia: This term covers all breccias that are dominated by hyaloclastite and angular lithic fragments (e.g. Figure 3.7). These fragments are typically 1 - 20cm in size with no glassy margins or rinds, although pillows and pillow fragments may form a small proportion of the deposit. These deposits probably formed from heavily jointed lava bodies that disintegrated during mass flow.

Lobate basalt hyaloclastite breccia: The lava bodies (see above) are still mostly intact in this facies and form fingers, sheets and isolated lobes of cube-jointed basalt within a matrix of hyaloclastite (Bergh & Sigvaldason, 1991; e.g. Figure 3.15). The proportion of hyaloclastite is variable from <10% to over 90%. Units with these features are often associated with a basal cube-jointed sheet lava which is clearly seen feeding the lobes and fingers from below. These units often form on steep slopes during collapse and flow of sheets and blobs of lava in an enclosing mass of hyaloclastite. Jones (1970) suggested that para-pillow lava may form in association with these irregular and often chaotic deposits.

2.5 PALAGONITISATION AND SECONDARY ALTERATION

Palagonitisation is the hydration and alteration of pale brown sideromelane glass to a yellow-brown glassy material known as palagonite (Peacock & Fuller, 1928, Macdonald, 1972). Palagonite is largely composed of smectite clay and may be fibrous or gel-like and isotropic (Jakobsson & Moore, 1986). Considerable element mobility is also associated with palagonitisation, generally with depletion in Si, Al, Ca, Na and enrichment in K and H_2O relative to the parent sideromelane (Cas & Wright, 1988; Furnes, 1984; Jakobsson & Moore, 1986); Fe, Ti and Mg are also mobile. All hyaloclastite and hyalotuff deposits exposed at the Eyjafjöll volcano have been palagonitised to some extent. Research based on the tephra on Surtsey has shown that the extent and rate of palagonitisation is temperature dependant. At 120°C virtually all glass is altered to palagonite; at 80°C 75% to 80% of glass is altered and at temperatures close to 40°C about 5% of glass is altered (Jakobsson & Moore, 1986). This process can occur very slowly at normal surface temperatures, but in areas of increased heat flow where temperatures of 40°C - 100°C can be sustained, palagonitisation may occur within about one year. The cause of hydrothermal anomalies sufficient to alter surface tephra at Surtsey was intrusion of feeder dykes (Moore, 1965; Jakobsson & Moore, 1986).

Palagonitisation is usually accompanied by precipitation of secondary minerals such as zeolites, calcite and opaline silica (Jakobsson, 1978) and weathering products

such as goethite (Figure 2.8). Together these minerals serve to cement hyaloclastite and hyalotuff deposits. Subglacial deposits are typically water-saturated and emplaced at high temperatures, providing ideal conditions for the precipitation of secondary minerals.

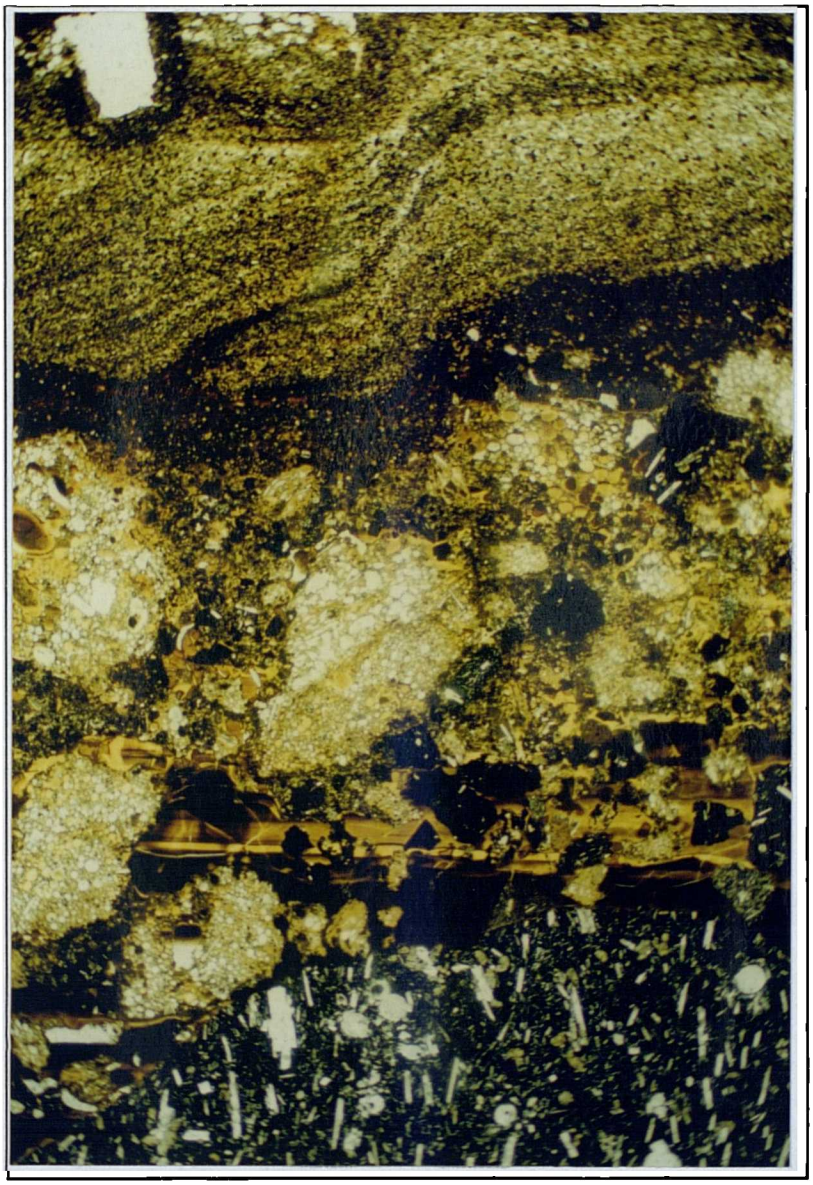

Figure 2.8 *The top of a hyaloclastite breccia from Skogaheidi [755480] showing reworked hyalotuff cemented by banded goethite. Such minerals are precipitated by warm, circulating fluids. Field of view 12 x 7.2mm.*

2.6 GLACIAL DEPOSITS

As a result of the ubiquitous basaltic source rock in Iceland, sediments with very different depositional environments (e.g. glacial, glacio-fluvial, mass flow) may look very similar (Geirsdottir, 1991). It is crucial that the correct genetic interpretation of

sediments associated with probable subglacial deposits is made before palaeoenvironmental or climatic models are constructed.

Lodgement till is formed by the direct deposition of debris from a thin basal regelation layer in active glacial ice by pressure melting, it undergoes deformation as a result of the shear imposed by the ice (Boulton, 1972). A lodgement tillite often has the following features:

a) A glacially striated/polished substratum.

b) Poorly or non-sorted sediments containing a wide range of particle sizes.

c) Sediments are massive, non-stratified, often foliated or fissile due to shearing and have a distinctive grey rock flour matrix.

d) Clasts are subangular to subrounded and are often striated or faceted.

The presence of a lodgement tillite and/or striated bedrock proves only that a glacier was once in the vicinity. It does not reveal the thickness or extent of the ice (Geirsdottir, 1991) and it is only indicative of a regional glaciation if it can be correlated with other glacial horizons on a regional scale (Geirsdottir, 1991). Many of the lodgement tillites at Eyjafjöll were deposited by Alpine valley glaciers which may have been present during interglacial periods. Major glaciations have only been inferred in this study where there is evidence that substantial thicknesses of ice (>100m) may have extended down to the present sea level.

Figure 2.9 *Glacial diamictites intercalated with finely laminated silts of lacustrine origin near Laugara [688 504]. These rocks were probably deposited in a glacial lake at the tip of a valley glacier.*

Till-like sediments which do not show the specific features of lodgement till are here termed ***diamictites*** (diamicts if unconsolidated) and defined as poorly sorted, matrix supported clastic sediments containing large clasts in a fine-grained matrix. These deposits may contain striated clasts and may lie on a striated/polished bedrock but this is not sufficient evidence for a glacial association (Eyles *et al.*, 1983). They could also be flow till, melt-out till or mass-flow deposits (See section 2.7). ***Flow tills*** are composed of glacial debris released supraglacially (on the ice surface) which is subsequently redeposited in a subaerial environment. Flow tills tend to be derived from debris in the upper part of the englacial (within ice) load as opposed to lodgement tills which are derived from the lower part (Boulton, 1972). ***Melt-out tills*** are released directly from slowly melting debris-rich stagnant ice which is buried beneath supraglacial sediments. Melt-out tills may preserve some of the original englacial structure.

Lacustrine sediments may be intercalated with tills and diamictites deposited near the ice margin (Figure 2.9).

2.7 CLASTIC SEDIMENTS

Volcanic and non-volcanic sediments described in this chapter have been transported and deposited by a variety of flow processes most of which are related to catastrophic flooding events (i.e. jokulhlaups). The properties of the flow and features of the deposits generally relate to the sediment concentration in a fluid-sediment mix. At different stages during a jokulhlaup the sediment concentration and flow characteristics change (Maizels, 1989). The criteria used for distinguishing these processes and the terminology used in this thesis is summarised below. Table 2.1 shows a simplified version of a model produced by Maizels (1989) based on sandur deposits on the south coast of Iceland.

Normal stream flow

This is dominated by the grain by grain deposition of sediment from traction currents. The sediment concentration is generally low and as a result the fluid-sediment mix is cohesionless with a low yield strength. Turbulent flow supports and transports the sediment load so that deposition is typically in fluid bedforms such as cross-bedding and horizontal-bedding.

Debris flows

Debris flows are water-saturated, viscous flows (non-Newtonian fluids) with very high sediment concentration (>80%) and a yield strength. Features typical of debris flows include: a) poor sorting, b) lack of internal stratification, c) matrix support of the largest clasts, d) a tendency to flow in pulses and occasionally e) inverse grading at the base of the flow.

Debris flows move with laminar motion, they come to rest *en masse* when the shear stress of the fluid-sediment mixture decreases below the yield strength. On steep slopes internal shear stresses may be sufficient to keep the entire flow in motion but as the flow slows on gentler slopes, internal shear stresses decrease below the critical yield stress and the mass of debris stops abruptly. However, thick flows may maintain a high shear stress at the base or sides of the flow and this basal part will flow in a laminar fashion carrying the rigid overlying mass until reduced shear stresses cause deposition. Such flows approximate Bingham substances in which the yield strength must be exceeded before flow will take place. A velocity profile across a channel containing a Bingham substance shows that at the channel sides and base are zones of high shear stress where laminar flow occurs, however in the centre of the channel the yield strength is not exceeded and the substance has solid-like behaviour and moves as a plug. This type of flow is known as plug flow.

Dispersive pressure in non-cohesive debris flows can produce inverse grading (e.g Bagnold 1956, Schmincke 1967, Lowe 1982). The dispersive stress is greatest close to the shear surface and large particles are able to exert a greater stress than smaller ones thus enabling them to move upwards. Inverse grading throughout a deposit is not observed in volcanic debris flows at Eyjafjöll. In most deposits, large fragments occur above the base as a result of the high density (buoyancy) and high matrix strength of the fluid. Often a thin basal layer of sand-sized material (<15cm) occurs at the base of volcanic debris flows at Eyjafjoll, this is a common feature of lahars and other pyroclastic flows (Sparks, 1976).

Hyperconcentrated grain flow

These hyperconcentrated flood flows contain 40-80% solids. They are turbulent, although dispersive pressure is also important because of the high sediment concentration (Beverage & Culbertson, 1964). Hyperconcentrated grain flow deposits show some features suggesting rapid deposition from high concentration suspension and some by traction currents; they are therefore intermediate between debris flow and stream flow (Beveridge & Culbertson, 1964; Smith, 1986). Deposits are typically poorly-sorted, clast-supported, structureless deposits. Sand-dominated deposits may be horizontally-bedded and graded beds with a massive lower part and horizontally-bedded upper part may also occur (Smith, 1986).

CHARACTERISTICS OF FLUID-SEDIMENT MIX

LAMINAR ← → TURBULENT

100% ← HIGH ← 70% SEDIMENT CONCENTRATION 40% → LOW → 0%

NON-NEWTONIAN ← BINGHAM NEWTONIAN → FLUIDAL

COHESIVE ← → COHESIONLESS

VISCOUS, HIGH YIELD STRENGTH ← → NON-VISCOUS, LOW YIELD STRENGTH

FLOW TYPE

DEBRIS FLOWS ← → HYPERCONCENTRATED GRAIN FLOWS → FLUID FLOWS

DOMINANT CLAST SUPPORT MECHANISM

BUOYANCY, YIELD STRENGTH ← → DISPERSIVE STRESS ← → TURBULENCE

MORPHOLOGY OF DEPOSIT (LOBES AND SHEETS)

MASSIVE STRUCTURELESS NONGRADED POORLY SORTED ANGULAR CLASTS	MASSIVE STRUCTURELESS NONGRADED WELL SORTED	CRUDELY BEDDED IMBRICATED INVERSELY GRADED	FLUID BEDFORMS CLAST SUPPORTED ROUNDED CLASTS NORMAL GRADING

Table 2.1. *Table simplified from Maizels (1989) shows the different types of sedimentary structure which may be formed during flood flows of different sediment concentrations.*

2.8 SUMMARY

The products of subglacial and shallow subaqueous eruptions include hyalotuff, hyaloclastite, pillow lavas and pillow breccias. These products may be redeposited by slumping, mass flow and debris flow leading to the formation of breccias and other chaotic deposits. Flooding associated with subglacial eruptions (jokulhlaups) may carry fine-grained volcaniclastics great distances in sheet flows and hyperconcentrated grain flows.

Subglacial eruptions may be distinguished from shallow submarine eruptions in the following ways:

- Monogenetic subglacial eruptions form steep-sided flat-topped piles of hyaloclastite, hyalotuff and pillow lavas.
- They commonly lie directly on polished or striated surfaces.
- Deposits may be topographically-confined.
- Intense palagonitisation suggests saturation with warm water.

CHAPTER 3
PRODUCTS OF SUBGLACIAL VOLCANISM

3.1 INTRODUCTION

Subglacial, monogenetic volcanoes in Iceland form steep-sided, flat-topped tuyas (shield eruptions) or tindas (fissure eruptions) as described in section 2.4.1. The deposits of these distinctive volcanoes are typically ponded within an englacial lake enclosed by thick ice (eg Jones, 1970; Skilling, 1994). In contrast, polygenetic central volcanos are constructed over a much longer time period (<1Ma Saemundsson, 1979) through both glacial and interglacial periods. The extent and thickness of ice cover on a large polygenetic volcano can be very variable, but will typically be dominated by a summit icecap and Alpine-style valley-confined glaciers which will wax and wane with climatic changes. Active volcanic vents are usually high up on the flanks or near the summit of a central volcano. At the onset of an eruption, meltwater will either pond at the base of the glacier, flush through subglacial passages, or flow along the margins of valley glaciers and over the glacier surface depending amongst other things on the thickness of the ice and the sub-glacier topography. Volcaniclastics and lava may build up around the vent eventually becoming unstable and forming debris flows, avalanches and other mass gravity flows which tend to follow the path taken by the meltwater.

This chapter provides the first detailed account of the subglacial products of a polygenetic volcano. Studies on glacial hydrology during subglacial volcanic eruptions will be reviewed and combined with lithofacies analysis, mapping and succession analysis to interpret outcrops at Eyjafjöll. Specific problems which will be addressed include:

a) what factors predispose meltwater and subglacial volcanics to flow in sheets or tunnels;

b) how mode of deposition changes throughout an eruption from the early catastrophic release of meltwater and sediment to the later stages of rapidly waning meltwater and sediment supply; and,

c) how lava and tephra interact with ice and meltwater during their eruption, transportation and deposition;

3.2 HYDRODYNAMIC MODELS OF GLACIERS

To comprehend the processes of subglacial transport and deposition during a subglacial volcanic eruption, an understanding of the hydrology of glaciers is necessary.

3.2.1 TEMPERATE ICE

At present, the climate in Iceland results in 'temperate' or 'wet-based' glaciers. Temperate ice differs from polar ice in that it lies close to its pressure melting point so that there is abundant basal meltwater and it may slide over the bedrock. The basal ice of a temperate glacier is typically loaded with debris incorporated during pressure melting and refreezing (Leeder, 1988).

Basal meltwater is supplied by:

a) basal pressure melting;

b) geothermal heat from subglacial eruptions or permanent geothermal areas; and

c) surface (supraglacial) meltwater that has drained through arborescent ice tunnels, moulins and veins to the glacier base (Shreve, 1972; Nye, 1976; Bjornsson, 1988). All subglacial meltwater will then tend to follow valleys and depressions in the subglacial topography.

Meltwater may flow along the bedrock-glacier interface in a variety of ways:

a) in tunnels cutting up into the ice (Rothliesburger tunnels, Rothliesburger, 1972);

b) in channels cutting down into the sediment or bedrock at the base of the glacier (Nye channels, Nye, 1976); or c) in sheets between the ice and the substrait (e.g Shoemaker, 1992). There have been several papers discussing the stability of subglacial sheet flows relative to tunnels (e.g Nye, 1976; Bjornsson, 1975; Shoemaker, 1992; Shreve, 1972; Weertman & Birchfield, 1983). Nye's model (1976), which is supported by most authors, suggests that water flowing in a sheet is unstable and tends to become channelised. This is because any variation in thickness of the water sheet will result in heterogeneous heat production (due to turbulence and friction) and melting, and ultimately flow localisation. Larger passages will then tend to increase in size at the expense of smaller ones because they contain comparitively more heat relative to the wall area (Rothliesburger, 1972; Shreve, 1972). To sustain these subglacial passages, the rate of melting of the ice must equal or exceed the rate of closing by plastic deformation. Therefore, if the flow rate and/or turbulence of the meltwater decreases, the tunnels will begin to close (Nye, 1976). Weertman and Birchfield (1983) accept Nye's theory, but suggest that channels have a maximum separation beyond which they have a tendency to collapse and reform as a sheet, especially if the volume of meltwater is waning. They propose that a sheet of water either reaches stability with areas of varying thickness or a cyclic sequence of events from sheet to channelled flow develops.

Supraglacial and englacial meltwater is already channelised in moulins and veins before it reaches the glacier bed and so tends to remain channelised, whereas meltwater

derived from increased melting of the glacier base will have a tendency to flow, at least initially, as a sheet (Weertman & Birch, 1983).

3.2.1.1 ERUPTIONS UNDER THICK TEMPERATE ICE (>100m)

As described in section 2.4.1 the hydrostatic pressure and therefore the thickness of ice above a vent affects the magmatic explosivity of an eruption. The ice thicknesss also affects the glacier hydrology during an eruption. Bjornsson (1988) and Nye (1976) have developed models to explain the occurrence of jökulhlaups in Iceland, particularly at Grimsvotn where the ice is between 200 and 300m thick.

Before a subglacial volcanic eruption, magmatic heat will cause localised melting at the base of the glacier. This meltwater can initially escape continuously along the bedrock-glacier interface, widening and adding to the pre-existing system of anastamosing tunnels or sheets (section 3.3.1, Nye, 1976; Bjornsson, 1988).

A depression will eventually form on the ice surface above the vent reflecting the initial loss of volume below. This will then direct englacial and subglacial meltwater *towards* the vent as the surface slope of glaciers is ten times more efficient at directing englacial and subglacial water than the slope of the bedrock (Bjornsson, 1975; Nye, 1976).

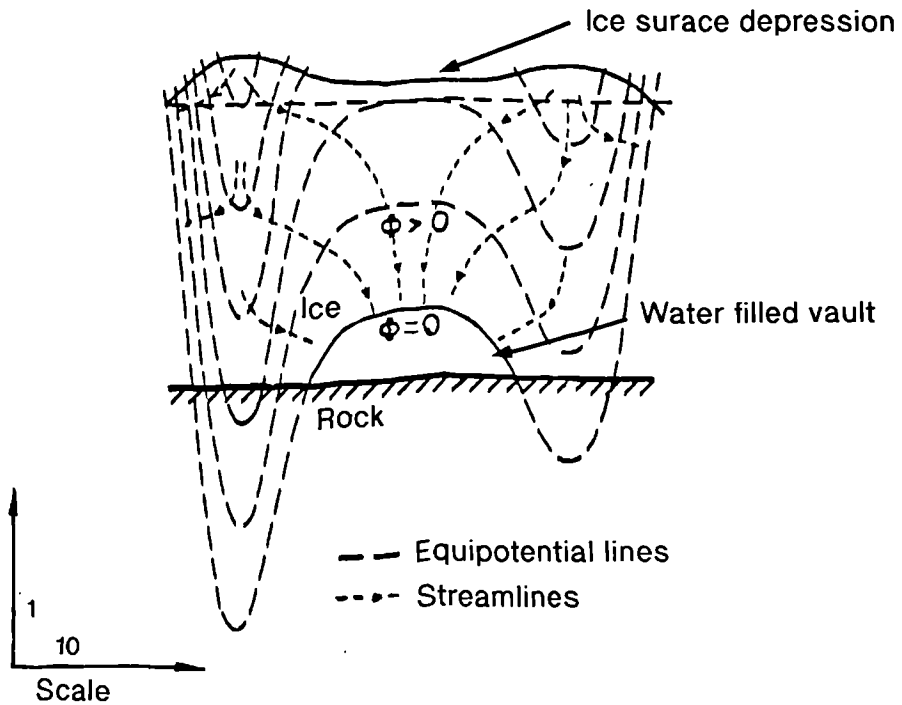

Figure 3.1 *Diagram to show the relationship between the glacier surface and the shape of the subglacial water vault (Bjornsson, 1975).*

Overburden pressure is now higher on the bed around the vent than over the vent itself thus trapping water and forming a vault (Bjornsson, 1975, 1988), (Figure 3.1). The products of an ensuing eruption are then erupted directly into water; they have no clear escape route and may pond subglacially within the vault (Bjornsson, 1975, 1988; Smellie, 1993).

If heat transfer from the magma is incomplete, then the volume of magma would eventually exceed the free space and the cupola would rise upwards briefly 'floating' the glacier (Bjornsson, 1988) and giving rise to a jökulhlaup charged with volcaniclastics. After this jökulhlaup, the subglacial tunnels may reseal again as the pressure over the vent is released, Bjornsson (1975) suggests that rather than one catastrophic jökulhlaup, several may occur during one long eruption, this may explain the pulses of sediments observed by Maizels (1988) in the sandur deposits, see section 3.3.1.

Bjornsson (1975) deduced from observations of jökulhlaups at Katla and Grimsvotn that a subglacial water reservoir must have been released during each event. Katla in particular, produced catastrophic floods that reached a discharge of 100-200m^3/s in a few hours. Bjornsson considered this too short a time for the volcanic eruption to melt sufficient ice. Thorarinsson (1965) noted that heat from Grimsvotn was sufficient to produce a surface depression many years before or after an eruption. These observations suggest that at the beginning of a volcanic eruption under thick ice (>100m Smellie *et al.* 1993; Smellie and Skilling, 1994) a water filled cavity will exist, even if the vent is on a topographic high.

3.2.1.2 ERUPTIONS UNDER THIN TEMPERATE ICE (<100m)

Smellie *et al.* (1993) pointed out that a glacier less than 100m thick may be composed of mostly snow and firn since the firn-ice transition occurs at 50-70m below the surface of a typical glacier. Snow and firn are permeable compared to ice so meltwater and volcanic debris may escape continuously from the vent area in subglacial tunnels, sheets and along the flanks of valley glaciers (Shreve, 1972), or perhaps over the glacier surface as observed at Katla in 1918 (Jonsson, 1982). Ponding under such thin ice may occur briefly around the vent (Smellie *et al.*, 1993), but, hydrostatic pressure at the base of the vault would rapidly reach that at the base of the surrounding ice and the thin glacier ice would be rafted as the meltwater escaped.

The ice above the vent may melt completely allowing subaerial lava flows to form. Tephra deposited on the glacier surface around the vent will increase supraglacial melting, surface meltwater and tephra will ultimately be incorporated in the subglacial meltwater.

3.2.2 POLAR ICE

Polar ice is frozen to the bedrock and impermeable suggesting that subglacial ponding of meltwater and volcanic products is likely to occur and drainage would be poor to

non-existent. A vault will probably form in the same way as described above, but because the ice is frozen to the bedrock, the initial meltwater will not be able to escape (Smellie and Skilling, 1994). Where sequences are dominated by ponded lithologies (eg tuyas and tindas) and deposits from flowing water are lacking, eruption under polar ice is likely.

3.3 LITHOFACIES DESCRIPTIONS

3.3.1 PREVIOUS WORK

There have been several papers describing the formation of subglacial monogenetic volcanoes (eg Noe-Nygaard, 1940; Matthews, 1947; Jones, 1968; Skilling, 1994). However, until recently the complex interplay of topography and the products of subglacial eruptions on polygenetic volcanoes had only been studied by a few authors.

Walker and Blake (1966) described a thick 'palagonite breccia mass' at Dalsheidi, southern Iceland which lies on a glacially scoured palaeovalley floor. They interpreted this as a valley-confined subglacial eruption in which a lava flowed through an englacial tunnel at the base of the valley. Carswell (1983) described the thick hyaloclastite and hyalotuff deposits west of Solheimajökull and inferred from the intercalated glacial deposits that they were formed during subglacial fissure eruptions.

Recent authors have described and interpreted deposits in more detail using lithofacies analysis. Multiple flows of very similar lithology to the deposits at Dalsheidi were described by Bergh & Sigvaldason (1991) in southern Iceland. These flows differed from those at Dalsheidi in that they are not topographically confined, forming instead extensive sheetlike deposits intercalated with sediments. These hyaloclastite-lava-sediment assemblages were interpreted as mass flow deposits emplaced on a distal submarine shelf.

Smellie *et al.* (1993) used lithofacies and succession analysis to interpret proximal, valley-confined volcanogenic sequences at Mount Pinafore in Antarctica. These sequences are again similar to the deposits at Dalsheidi and include heterogeneous masses of lava and hyaloclastite and complex associations of volcaniclastic material reflecting deposition from flowing water. Smellie *et al.* (1993) suggested that these deposits must have formed under thin, temperate ice sheets (100-150m). Smellie and Skilling (1994) also suggested that deposition of sequences at Mount Pinafore occurred in subglacial tunnels in a manner similar to esker formation. Their lithofacies codes are based partly on the existing systems of Eyles et al. (1983) and Miall (1977), which describe glacial and fluvial deposits respectively and they have added hyaloclastite and lava lithofacies. Smellie & Skilling (1994) and Skilling (1994) also described Brown Bluff volcano in Antarctica whose deposits ponded in an englacial lake enclosed by thick ice (>400m). The lithofacies system devised by Skilling (1994) is perhaps the most comprehensive. He has divided the lithofacies into four main groups:

lava; previously unlithified hyaloclastite; previously unlithified hyalotuff and previously lithified conglomerate. Each is then further sub-divided into 17 lithofacies based on grainsize, structure etc.

Additional information about the processes involved in subglacial eruptions may be obtained by studying the distal sandur deposits emplaced by the volcanically-induced jökulhlaups that accompany each eruption. Maizels (1988) studied the Skogasandur and Myrdalssandur sediments on the south coast of Iceland. She demonstrated that the sandur are outwash deposits which are composed almost entirely of stacked jökulhlaup deposits with only thin horizons of braided river sediments. The sediment load is dominated by fresh, black, juvenile volcaniclastics indicating that volcanic eruptions do trigger jökulhlaups.

Jonsson (1982) studied sandur deposits produced during the 1918 eruption of Katla. The sediment concentration of these flood deposits was sufficient for hyperconcentrated grain flow (i.e. at least 40%; section 2.7), but boulders of 4m diameter and ice blocks up to 40m across were transported, suggesting that sediment concentration may have exceeded 40% (Jonsson, 1982; Maizels, 1993). Jonsson (1982) describes 8m thick deposits of tephra (0.5-4mm) showing inverse grading with coarser clasts up to 1m in size at the surface of the deposit. These he interpreted as volcanic debris flows formed during the jökulhlaup which accompanied the eruption. Maizels (1993) estimated that the jökulhlaup produced during this 20 hour eruption of Katla reached flow rates of $1\text{-}2\text{x}10^6$ m^3 s^{-1} and deposited $2.2km^3$ of pumice on the sandur.

Maizels (1989, 1993) found that the dominant sediment sequence in a distal jökulhlaup flood deposit begins with a lower massive, poorly sorted, non-graded to inversely-graded deposit indicative of hyperconcentrated fluid-sediment mixtures. This grades up into thin, planar cross-bedded and horizontally-bedded fluid deposits. This sequence represents an initial sediment-rich flood surge followed by flow deceleration, sediment depletion and the development of turbulent traction currents and reworking. The vertical increase in fluidal flow features is often repeated and may be due to several possible processes:

a) renewed volcanic activity;

b) the release of temporary sediment blockages;

c) reactivation of a more proximal surge front; or

d) the multiphase arrival of the surge at a distal site.

3.3.2 LITHOFACIES DESCRIPTIONS AT EYJAFJÖLL

3.3.2.1 INTRODUCTION

The stratigraphy at Eyjafjöll is dominated by complex proximal assemblages of lava, *in-situ* and redeposited hyaloclastite and volcaniclastic sediments emplaced in subaqueous conditions. Subaerial lithofacies, including lava and volcaniclastics redeposited by traction currents probably account for less than one third of the volume of the volcano.

Thick assemblages of *genetically-related* lava, hyaloclastite breccias and reworked hyaloclastite and hyalotuff can be observed. Certain of these assemblages show very distinctive structures. Field observations suggest the existence of a number of such assemblages which occur repeatedly both spatially and temporally at Eyjafjoll. Understanding the processes involved during deposition of these assemblages can help to constrain their environment of deposition, this in turn helps to constrain the stratigraphy.

Nine distinctive proximal lithofacies associations are described, each representing a different mode of deposition in a different environment. Each association commonly shows repetition within a single succession suggesting successive phases of a single volcanic event. The lithofacies associations are commonly palagonitised, suggesting warm water-saturated conditions during transport and deposition (section 2.4.1) and they are frequently intercalated with diamictites suggesting that deposition occurred during or soon after glacial conditions. The constituent lithofacies are rarely *in-situ* and have been redeposited by a variety of processes including debris-flow and normal stream flow. Despite a subglacial eruption environment, some assemblages were probably deposited in subaerial or submarine conditions. Distal deposits are dominated by redeposited volcaniclastics and lack lava and in-situ hyaloclastite.

The lithofacies which make up each assemblage may be described individually (see Table 3.1) and the mode of transport and environment of deposition of each can be deduced. Each lithofacies association is then described in terms of its constituent lithofacies in section 3.3.3 and is summarised in Table 3.2 (page 72).

Lithofacies at Eyjafjöll are described using the following criteria. Diamictites are described using a simplified version of the lithofacies code used by Eyles *et al.* (1983) . Secondary volcaniclastics (hyalotuff, hyaloclastite) redeposited by meltwater are divided up by grainsize and described using a system based on that of Miall (1977) and also that of Maizels (1993) for glacio-fluvial sediments. These sediments are usually palagonitised and may be cemented by zeolites and other secondary minerals. Hyaloclastite breccias are divided on the basis of structure and clast type in a manner similar to that used by Bergh and Sigvaldason (1989). Hyaloclastite breccias are defined as secondary deposits showing in-situ pillow/lobe spallation from feeder bodies and/or in-situ granulation and brecciation of pillow/lobe margins. There is little evidence of chilled *glassy* contacts between the matrix material and feeders implying that the deposit was emplaced hot. *In-situ* hyaloclastite is rare at Eyjafjoll except as thin veneers around lavas or pillows.

There are five lava lithofacies, each defined on the basis of structure. A summary of the lithofacies, their descriptions and tentative interpretations is given below and in Table 3.1.

3.3.2.2 GLACIAL LITHOFACIES

DIAMICTITE (Dmm, Dcm, Dmm(s); see Table 3.1)

Description

Lithofacies Dmm (Figure 3.2) forms beds up to 6m thick the boundaries of which are sharp and well-defined. The beds are polymict, poorly-sorted, massive and matrix-supported with rounded to subangular clasts. The percentage volume of clasts may vary from 10% to 80% and they may be vesicular, non-vesicular, glassy and crystalline and show a variety of petrographic types and degrees of weathering. Some deposits may be dominated by primary monogenetic clasts which are angular and fresh compared to other clasts. Some clasts may be striated and the unit may lie on a striated or polished bedrock. The matrix is composed of silt to sand-sized fragments of the same material as the clasts and may also contain hyalotuff and hyaloclastite fragments. Lithofacies Dmm is rarely laterally extensive, deposits are commonly lobe-shaped or channelled.

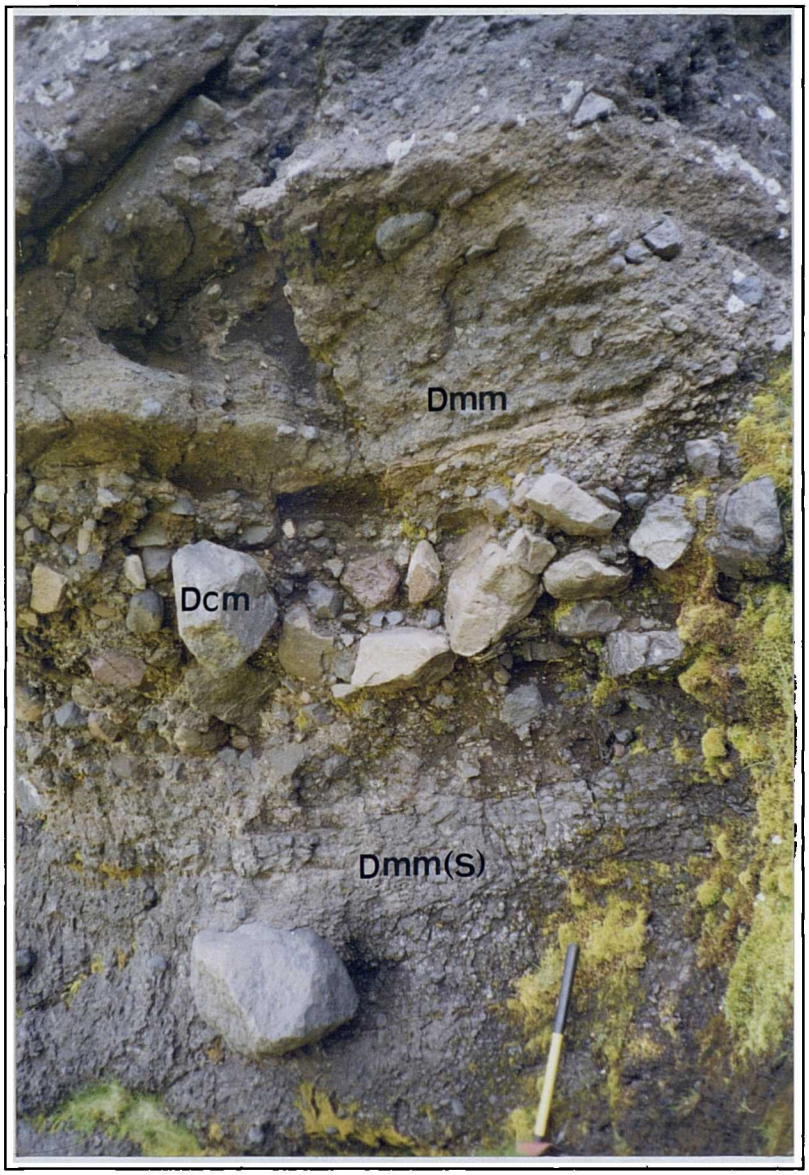

Figure 3.2 *Shows a basal lodgement till (Dmm(s)) containing striated clasts overlain by a thin layer of inversely-graded meltout till (Dcm) and a thick debris flow (Dmm). Near Laugara [689 506].*

Lithofacies	Code	Description	Interpretation
DIAMICTITE Heterolithic	Dmm	Matrix-supported, massive, poorly sorted, rounded to sub-angular polymict clasts <1m diameter, <70vol.%; sharp bed boundaries, beds <6m thick; matrix of silt to coarse sand includes palagonitised glass shards and lapilli, lithic fragments and crystals.	Melt-out tills, flow tills or debris flows derived from glacial and volcanic material. If a large proportion of clasts are monogenetic, debris flow may have been triggered by a volcanic eruption.
	Dcm	Clast-supported, massive, poorly-sorted, rounded to subangular polymict clasts; beds <2m thick; matrix of sand to gravel sized lithic fragments.	Meltout till or flow till.
	Dmm(s)	Matrix-supported, massive, poorly to moderately sorted; as Dmm but outsize clasts are rare. Shearing may be intense.	Lodgement till, shearing due to movement of overlying ice.

Lithofacies	Code	Description	Interpretation
GRAVEL 8-256mm Monomict	Gms	Massive, matrix-supported beds <10m thick; poorly sorted, angular to sub-rounded, vesicular and poorly vesicular lithic clasts, some scoriaceous material. Matrix of palagonitised glass shards and fine-grained scoriaceous fragments.	Subaqueous deposition of subaerial pyroclasts and hyaloclastite in volcanically-induced debris flow deposits, slumping of near-vent tephra or other gravity mass flow.
	Gm	Massive or crudely-bedded, poorly sorted, clast-supported. Clasts sub-rounded to angular lithics, pillow fragments, crystals. Matrix similar. Beds <1.5m thick.	Rapid deposition from suspension or coarse hyperconcentrated flood flow deposits.
GRANULES 2-8mm Monomict	GRm	Massive, well-sorted, beds 5cm-1m thick, vesicular to non-vesicular palagonitised glass shards, may be some scoria., sharp contacts, fills hollows etc.	Primary lapilli tuff (?), examples with weak bedding may be reworked.
	GRh	Horizontal beds <5cm thick of vesicular to non-vesicular palagonitised glass shards, lithics and crystals. Bed contacts may be gradational, units may be laterally extensive <150m.	Reworked hyaloclastite and/or tephra, deposition by traction currents; laterally extensive units may be sheetflood deposits.
	GRt	Large scale trough cross-bedded vesicular to poorly vesicular palagonitised glass shards, lithics and crystals, outsize clasts common (pillow fragments), gravelly units are also common.	Channel-confined deposition from high velocity currents, cross set size indicates high sediment suspension load and a substantial water depth.
	GRp	Large or small scale planar cross-bedded vesicular to poorly vesicular palagonitised glass shards, lithics and crystals, gravel clasts are common; beds < 2m thick. Foresets dip<20.	Deposition from traction currents (small scale bedforms) or currents of high suspension load and high velocity (large scale bedforms).
	GRl	Very low angle cross-bedding (<15), pebbly beds mostly phreatomagmatic tephra (hyalotuff).	Transitional dune to upper bed deposits.
SAND 0.063-2mm	Sm	Massive, well-sorted, beds 5-60cm thick, diffuse planar lamination, grains dominated by pyroclasts or hyalotuff.	Airfall tephra, homogenised planar-bedded sands.

Table 3.1 *Lithofacies descriptions at Eyjafjöll.*

Lithofacies	Code	Description	Interpretation
LAVA	Ls	Simple flows, margins are blocky, lobate or pillowy; 0.5-50m thick. May be blocky, columnar, massive, may be gradational with Lk.	Coherent lavas, may be topographically confined, lie on wet sediments, majority are subaerial.
	Lc	Compound flows, massive or columnar, commonly with reddened surfaces intercalated with cinders or thin lenses of reworked hyaloclastite.	Subaerial compound lavas, lenses of reworked hyaloclastite occur in transitional subaerial/subaqueous environments.
	Lk	Cube-jointed and hackly-jointed lava (Icel. kubbaberg), may form isolated lobes or thick entablature.	Water-saturated, fragmentary lava. May be subaqueous, flooded in a river valley or subglacial.
	Lp	Pillow lavas, irregularly shaped radially-jointed pseudo-pillows, ragged para-pillows; < 30% interstitial hyaloclastite.	Subaqueous (subglacial) margins of lava flows, feeder zones etc.
	Lb	Clast-supported coarse autoclastic breccia, poorly sorted angular lithic blocks in coarse sand-gravel matrix. May contain radially-jointed 'globes'. Gradational upslope with Lp and/or Lk.	Autoclastic breccias, formed by gravitational collapse of Lp or Lk.
Hyaloclastite and hyaloclastite breccia	Bhm	Massive, matrix-supported, poorly-sorted, angular to sub-angular clasts of basalt and basalt pillows, some jigsaw-fit clasts and lava lobes. Closely associated with Ls or Lp. Matrix of palagonitised glass shards and crystals.	Forms during interaction of lava with water and ice. In-situ envelope of hyaloclastite around lava bodies, or distal volcanically-induced debris flow.
	Bpm	Same as Bhm, however, clasts dominated by round, elongate or ragged pillows.	As Bhm, but occurs in close proximity to feeder lava bodies. May be due to slumping or collapse.
	Bhs	Matrix-supported, bedded hyaloclastite breccia. May be large or small scale bedforms. Matrix material is more abundant than in Bhm.	Resedimented hyaloclastite breccia, debris avalanches, debris flows and grain flows; found downslope from Bhm.

Table 3.1 *(continued). Lithofacies descriptions at Eyjafjöll.*

Lithofacies Dcm (Figure 3.2) is massive and clast-supported. Clast size is <1.5m, beds are <2m thick and typically laterally discontinuous, often forming lenses within sequences of glacial rocks.
Lithofacies Dmm(s) (Figure 3.2) is sheared, is typically grey, but may also be pinkish and contains a large proportion of finer grained fragments. Rare outsized, striated and rounded clasts occur. Bed boundaries are sharply defined, this lithofacies commonly lies on striated surfaces defining the base of former glacial valleys. Beds are rarely more than 1.5m thick although they are commonly laterally extensive.

Interpretation
Lithofacies Dmm is the commonest diamictite type at Eyjafjoll. Matrix-supported diamictites may be flow tills, melt-out tills (see section 2.6) or remobilised glacial deposits laid down by debris flow processes. If there is a large primary volcanic clast population, debris flows may have been triggered by a volcanic eruption or landslips. Geirsdottir (1991) and Eyles *et al* (1983) both state that the presence of striated clasts and a glaciated bedrock are *not* diagnostic of a glacial association.
Lithofacies Dcm may be a flow till or meltout till (section 2.6).
Lithofacies Dmm(s) shows features of lodgement till deposited at the base of a glacier as it is sheared by the movement of the overlying ice. The rare pinkish appearance of these deposits is due to the presence of tephra (ash, spatter, cinder) in the matrix, in which case subaerial rocks must have made up a proportion of the glacial bedrock.

3.3.2.3 VOLCANICLASTIC LITHOFACIES

GRAVEL 8-256mm

(Gms, Gm)

Description
Lithofacies Gms forms massive, matrix-supported beds typically <2m thick, but occasionally up to 10m thick. Bed boundaries are sharp and non-erosive. Clasts include vesicular to non-vesicular lithic and vitric fragments. In some cases reddened scoria fragments are abundant. The matrix is composed of sand to silt size vitric, lithic and occasionally scoriaceous material, the latter giving the rock a red-pink appearance. There may be inverse grading. Deposits may be palagonitised and/or zeolitised, clay pore-fillings are also common.
Lithofacies Gm (e.g. Figure 3.3) is massive or crudely bedded, clast-supported gravel. Clasts are reasonably well-sorted, angular to subrounded and otherwise as lithofacies Gms, although scoriaceous material is rare. Material is commonly monogenetic. There may be normal grading and outsize angular clasts occur. The gravels may be openwork or have a matrix of sand/silt. Beds are up to 1.5m thick, monomict and may be laterally continuous for up to 200m.

Figure 3.3 *Massive, clast-supported lithofacies Gm overlain by horizontally-bedded lithofacies GRh. This combination represents an initial flood surge of high sediment concentration, followed by sheet floods of lower sediment concentration. The volcaniclastic sequence is overlain by a subaerial basalt lava flow (lithofacies Ls).*

Interpretation

Lithofacies Gms is massive, matrix-supported and non-erosive indicating that sediments were deposited rapidly from high density mass flows. The large volume of juvenile clasts in these monomict deposits indicates that the debris flow is volcanically-induced. These deposits contain a large proportion of hyalotuff suggesting eruption and deposition in a subaqueous environment. Some deposits contain a high proportion of scoriaceous material and armoured lapilli, suggesting subaqueous deposition of subaerial pyroclasts which are then resedimented by slumping of oversteepened tephra near the vent or in gravity-induced mass flows. The pervasive palagonitisation of these deposits is due to saturation by warm water; older deposits near hydrothermal areas may also be zeolitised.

Lithofacies Gm probably represents rapid sedimentation from coarse, hyperconcentrated flood flow deposits. It is commonly overlain by horizontally-bedded lithofacies GRh. Flood flow deposits are more fluid than debris flows (they may in some cases represent the more distal, residual, diluted deposits of debris flows). The well-sorted nature of the deposits suggests that these are distal deposits, the common monogenetic nature suggests that these are volcanically induced flood flow deposits.

GRANULE 2-8mm

(GRm, GRh, GRt, GRp, GRl)

Description

Lithofacies GRm forms sharply defined, well-sorted, massive, clast and matrix supported beds 0.1 to 1.0 m thick (Figure 3.4). The base of the deposit may be erosive. Deposits are typically dominated by either hyalotuff or scoriaceous material but may also include armoured lapilli. Scoraceous material gives the rock a pink appearance. The beds often drape over or fill hollows in pre-existing topography. Thin, sheet-like deposits (< 0.5m) may occur at the base of thick hyaloclastite breccias or lavas, or erosively overlie diamictite lithofacies. Faint laminations may occur in the deposit.

Figure 3.4 *Lithofacies GRm, a massive unit dominated by scoria. Glassy fragments are largely palagonitised suggesting that they may have been deposited in a subaqueous environment. Overlain by subaerially deposited cinder, blocks and scoria.*

Lithofacies GRh forms planar, horizontally-bedded units of hyalotuff and hyaloclastite up to 1.5m but usually <1m thick (Figure 3.3). Beds are roughly 1-10cm thick and may include some small-scale cross-bedding. This lithofacies is commonly closely associated with lithofacies Gm and forms laterally extensive sheet-like deposits. The tephra are commonly monogenetic and may have an open framework, the gaps may be filled by banded palagonite, zeolites or clays and outsize clasts are rare.

Lithofacies GRt forms monomict, large-scale trough cross-beds composed of hyalotuff, hyaloclastite and lithics with some outsized clasts (usually pillows or pillow fragments), (Figure 3.12). Beds may be composed of dominantly sand-sized material or gravel. Occasional beds contain outsize clasts which are usually isolated pillows. Trough cross beds are up to 2.5m in height with variable wavelength between 3 and 10m.

Lithofacies GRp forms monomict, planar cross-bedded hyalotuffs, with foresets dipping <20°, overlain by planar strata which merge downflow into the foresets (e.g Figure 3.5). Bed boundaries are sharp and beds are <1.5m thick. Such units tend to have a lenticular shape but not all outcrops are well enough exposed to determine their overall shape. Lithic clasts (<0.5m) may be abundant and isolated bodies of lava several metres across with pillowed margins may also be closely associated with these deposits. These lithic units are all genetically-related. This lithofacies is common at high levels in the stratigraphy and is frequently associated with deposits showing soft-sediment deformation (e.g. Raufarfell summit).

Lithofacies GRl forms monomict, low angle cross-beds (foresets dip <15°), cross sets are up to 1m thick. This lithofacies is rare, where it occurs it lies on top of channelled, genetically-related hyaloclastite breccia. Outsize clasts are uncommon and hyalotuff is the dominant component of this lithofacies. The lateral extent of this lithofacies appears to be limited, exposure is not sufficient at any outcrop to deduce the overall shape of the deposit.

Interpretation

Lithofacies GRm represents the subaqueous deposition of both subaqeously and subaerially erupted hyalotuffs and pyroclasts. The massive appearance of some deposits may represent rapid deposition from slumping or debris flows. Deposits with an erosive base may be laid down by turbidity currents. Deposits dominated by scoriaceous material may have formed as subaerial or subaqeous fall deposits.

Lithofacies GRh represents high flow regime, shallow sheet flows characterised by high traction and suspension loads which are typical of a waning flood surge. Occassional small-scale cross-beds indicate that the the thin horizontal beds are water-lain and not air fall deposits. Rarely, in places where the beds are not monomict, or at the top of fluvial successions, individual beds may represent air-fall tephra.

Lithofacies GRt represents channel-confined flow of traction currents in which the trough cross-beds formed as migrating dunes. The size of the cross sets indicates the high sediment suspension load of the current and a substantial depth to the water. Flow must have been of high velocity to carry abundant gravel-sized particles and occasional outsize clasts. This lithofacies was probably created during flood conditions.

Lithofacies GRp represents deposition from currents of high suspension load and high velocity in the dune to upper stage plane bed transition. Deposition of this lithofacies from suspension rather than grain flow is suggested by the presence of clasts within the

foresets and the low angle of the foresets. As current strength increases, deposition from suspension and the counter-current circulation in the lee of the bedform become more important (Roe, 1987) leading to a reduction in the foreset dip. This lithofacies represents deposition in flood conditions. The close association of sediments showing soft sediment deposition also indicates rapid deposition.

Figure 3.5 *Planar cross-bedded granules (lithofacies GRp) containing outsize clasts of basalt pillows, summit of Raufarfell [704 491].*

SAND 0.063-2mm

(Sm)

Description

Lithofacies Sm forms massive or faintly laminated, well-sorted beds up to 60cm thick commonly intercalated between lava flows. This lithofacies may be composed of variable proportions of the following: vesicular glass shards, hyaloclastite, lapilli, scoria and lithic fragments, however most fragments are monogenetic. Some examples are dominated by monogenetic lapilli and scoria they tend to be pink in colour and are commonly massive with little palagonitisation (Figure 3.18). More commonly lithofacies Sm is a palagonitised deposit which is dominated by vesicular glass shards. Such deposits may occur as thin laminated lenses (<10cm thick) filling voids in hyaloclastite breccias (Figure 2.8).

Interpretation

Lithofacies Sm represents a variety of deposits. The pink, poorly palagonitised deposits are probably primary air-fall tuffs, these are typically preserved beneath subaerial lavas. Such deposits may also occur beneath thick mass-flow deposits of hyaloclastite breccia (Figure 3.18), this suggests a marginal glacial environment of deposition, perhaps near the snout of a valley-confined glacier. The most common deposits of this lithofacies represent volcaniclastics (especially vesicular hyalotuff) redeposited by hyperconcentrated streamflow and/or traction currents.

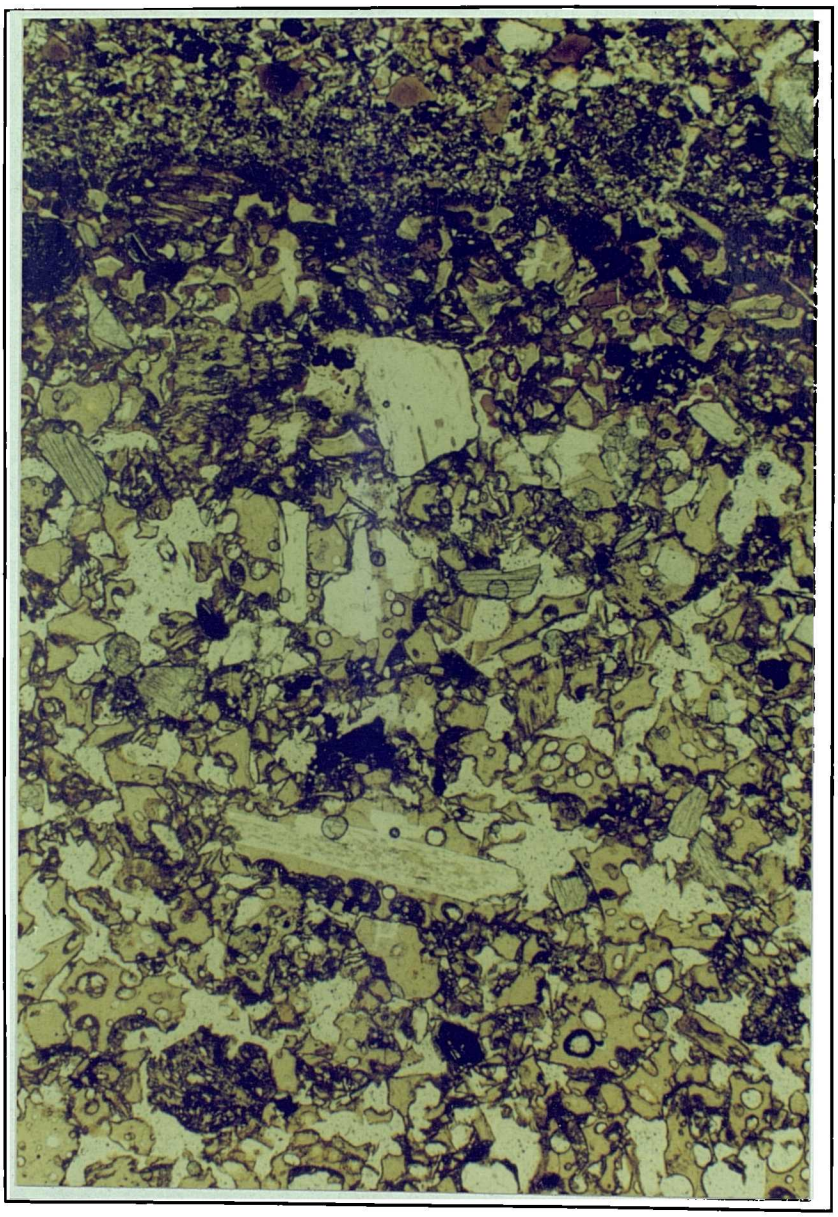

Figure 3.6 Redeposited glass shards and crystals (lithofacies Sm) from the summit of Raufarfell [706 494]. Field of view 6 x 3.7 mm.

3.3.2.4 LAVA AND HYALOCLASTITE BRECCIA LITHOFACIES

LAVA

(Ls, Lc, Lk, Lb, Lp)

Description

Lithofacies Ls consists of simple basaltic lava which may be massive, blocky, platy or columnar, these lava bodies may form extensive, lobate flows typically <8m thick and several hundred metres broad (Figure 3.3), or channelled flows up to 40m thick, but only up to 50m wide which are confined to palaeovalleys (stream valleys) and are elongate in the flow direction. These are common on the eastern and south-eastern slopes of Steinafjall, and further west on the hillside between Fit and Hvammsmuli (location map - page 82).

Lithofacies Lc is made of compound basaltic flows which may be subaerial or transitional between subaerial and subaqueous. Thin individual flows <1.5m thick are separated by either cinders or hyaloclastite and may be massive, blocky or columnar. Compound lavas described in this thesis all erupted from a single vent, the flows spread from the point source downslope in a generally lobate shape.

Lithofacies Lk consists of cube-jointed or hackly-jointed lava (kubbaberg). This lithofacies corresponds to the 'entablature' of thick or ponded lava flows (section 2.2.2) and may reach thicknesses of <20m. However it may also occur as isolated lobes or blocks within hyaloclastite breccia lithofacies and as feeders fingering upwards into hyaloclastite breccias or sediments from a basal lava flow/sill (Figure 3.20).

Lithofacies Lp includes pillow flows (e.g. Figure 3.7), ragged para-pillow lavas, irregularly shaped radially-jointed pseudopillow lavas (Figure 4.5) and isolated, radially jointed 'globes' of lava (Figure 3.8). Such 'globes' appear to develop on steep slopes where they break away from their feeders during gravitational collapse or avalanching to form isolated bodies. Lithofacies Lp may contain up to 30% hyaloclastite. The pillow flow in Figure 3.7 is laterally extensive <2km, however, most other pillow flows are of limited lateral extent and several are channelled.

Lithofacies Lb (Figure 3.8) consists of blocks of fragmented Lk, Lp or Ls with little or no matrix material (orthobreccia). The deposit has a texturally homogenous appearance and may be well-sorted to poorly-sorted. Clasts may be up to 50cm in diameter.

Interpretation

Lithofacies Ls represents subaerial flows or subaqueous flows that have been insulated sufficiently to allow them to cool slowly. Columnar flows usually require a degree of ponding, so these flows may be topographically confined.

Lithofacies Lc represents compound flows which may be divided by cinders when they are subaerial, or by planar-bedded lenses of hyaloclastite. In some cases, cinders *and*

Figure 3.7 *Pillow lavas (lithofacies Lp) near Fit [520 525].*

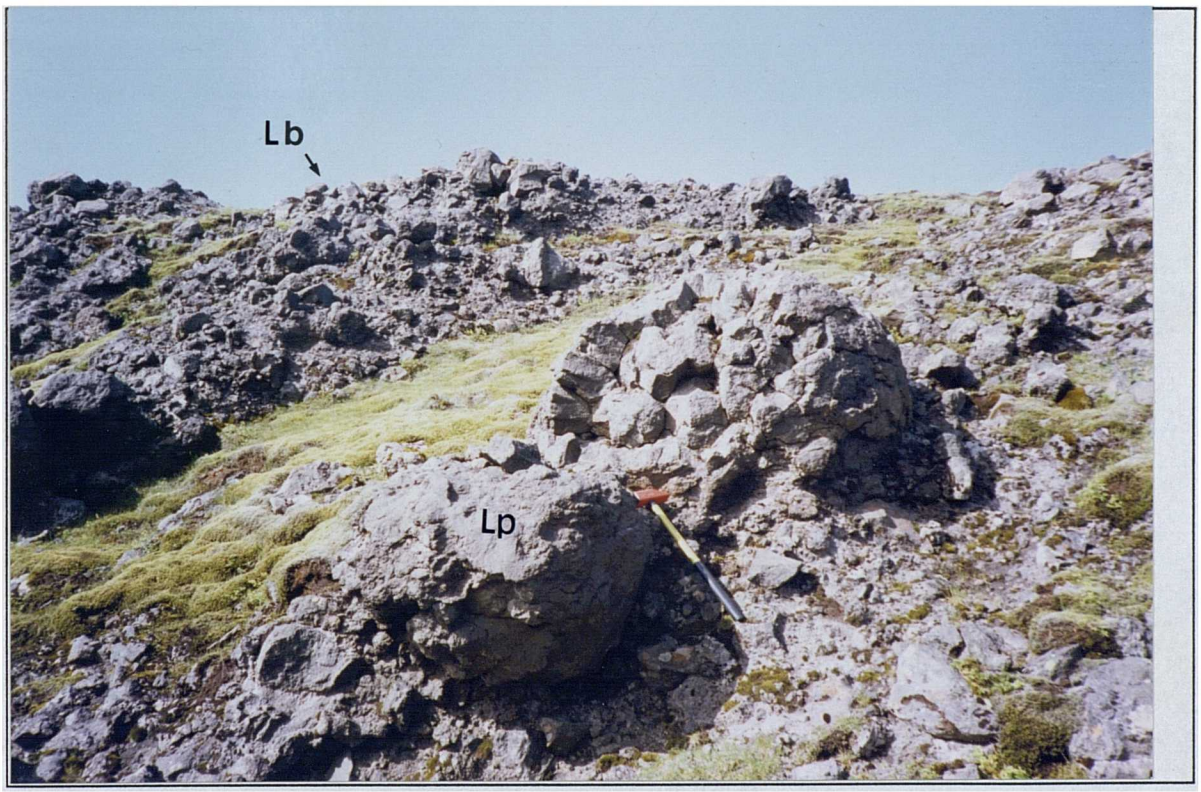

Figure 3.8 *Basalt 'globes' (lithofacies Lp) and autoclastic breccia (lithofacies Lb) on Lambafellsheidi [681 465].*

hyaloclastite occur, suggesting that the deposits are transitional between subaerial and subaqueous environments and some reworking of the volcaniclastics has occurred.
Lithofacies Lk typically forms by flooding of partially solidified ponded lava (see section 2.1). Lobate lava forms within hyaloclastite are again water-saturated, but not ponded. They are frozen in place showing spallation and interfingering with surrounding hyaloclastite breccia deposits.
Lithofacies Lp represents subaqueous pillow lavas formed as degassed lava flowed into the sea. Ragged subaqueous para-pillows formed during disintegration of lavas on steep slopes, 'globes' may also form by the collapse of water-saturated lava. Pseudopillows represent water-saturated massive lavas.
Lithofacies Lb represents secondary deposits of fragmented lava bodies. These are essentially autoclastic deposits which occur downslope from the parent deposit (usually Lp or Ls). The intermediate deposits contain coherent bodies of radially-jointed lava (globes) in a matrix of angular fragments and hyaloclastite. These deposits lack glassy margins suggesting that they were emplaced hot.

HYALOCLASTITE BRECCIA

(Bhm, Bpm, Bhs)

Description

Lithofacies Bhm is a massive, matrix-supported palagonitised deposit (Figure 3.11). Clasts are poorly sorted, angular to sub-angular fragments of basalt and basalt pillows <20cm in size. There are few glassy chilled contacts between pillows/feeders and the matrix; angular fragments which fit together like a jigsaw are common. There may be large bodies and lobes of cube-jointed lava spalling and brecciating *in-situ* within the deposit. The matrix is poorly sorted and composed of sideromelane shards and lapilli which have been palagonitised. Zeolite cements are common. Dewatering structures or inverse grading may also be present.
Lithofacies Bhs comprises poorly-sorted, fining-upwards, matrix and clast-supported deposits with outsize blocks of pillows and pillow fragments. Upper, finer-grained sections of the deposit show large-scale cross-bedding (Figure 3.20), cross-bedded sets may be <30m thick, with foresets dipping <20°. This lithofacies is voluminous and typically valley-confined, it may extend for several kilometres in length and width. Clasts are vitric to lithic, angular and poorly vesicular. Isolated, massive bodies of cube-jointed basalt are more common than pillows.
Lithofacies Bpm (pillow hyaloclastite breccia) is massive, matrix to clast-supported and poorly sorted (Figure 3.9). Deposits are densely packed with either vesicular ragged para-pillows or radially-jointed pillows and angular pillow fragments. Isolated blocks and lobes of lava may also occur within the hyaloclastite breccia which have detached from feeder zones nearer the source. The matrix is composed of palagonitised sideromelane shards and lapilli. Zeolite cement is common.

Interpretation

Lithofacies Bhm is monomict, massive, poorly sorted and matrix-supported indicating that sediments were dumped rapidly from high density flows, i.e in a volcaniclastic debris flow. The high flow concentration allows floating of large clasts in a finer-grained matrix. The large volume of juvenile clasts indicates that this is volcanically induced. These deposits contain a large proportion of pillow fragments, hyaloclastite and hyalotuff suggesting eruption and fragmentation in a subaqueous environment. The pervasive palagonitisation may be due to saturation by warm water and the lack of chilled contacts is due to emplacement of the deposit while it is still hot. The lack of exotic clasts (i.e. pebbles or clasts not genetically related) suggests that this deposit was emplaced as a non-erosive debris flow, or that loose material was flushed away ahead of the debris flow by an initial flooding event. Inverse grading towards the base of the unit is typical of non-cohesive debris flows whilst the normal grading towards the top may be due to the waning flow and/or reworking. Fragmentation and auto-brecciation occurs as the deposit moves away from the vent.

Lithofacies Bhs represents progradation of a hyaloclastite complex into a body of meltwater. Large scale cross-beds imply deposition from high velocity currents of high sediment suspension load.

Lithofacies Bpm (Figure 3.9) represents a debris flow deposit with a more rapid lava discharge rate than BHm; feeders within the deposit produce lobes and pillows.

Figure 3.9 *Pillow hyaloclastite breccia (Bpm) containing densely-packed vesicular pillows and cut by an inclined sheet near the base of Raufarfell [698 476].*

3.4 LITHOFACIES ASSOCIATIONS

Each proximal volcanic assemblage may be described in terms of its constituent lithofacies all of which are genetically related. The resulting 'lithofacies association' then defines the characteristics of that particular assemblage.

Nine distinctive lithofacies associations are described and can be divided into two groups:

1) lithofacies associations A to G which require mass flow processes during their formation; and

2) lithofacies associations H and J which are formed by ponding processes.

Lithofacies associations A to D are particularly common in relatively flat-lying successions. The lava lithologies of these associations are intruded into their cogenetic volcaniclastics during transport. Lithofacies associations E and F represent topographically-confined eruption products. Lithofacies association G represents a simple hyaloclastite breccia mass flow which may have variable substraits. Lithofacies association H requires ponding of lava between ice and the topography and lithofacies association J requires ponding of volcaniclastics beneath a thick ice sheet and perhaps within an englacial lake.

The nine lithofacies associations are described below together with an interpretation as to how they were formed. Diagrammatic representations of each association are given in Figure 3.10 A-K and photographs of specific examples are given in Figures. 3.11 -3.21.

3.4.1 LITHOFACIES ASSOCIATION 'A'

Hyaloclastite and pillow breccias with lavas lying conformably on resedimented, syn-eruptive volcaniclastics.

Lithofacies Ls, Bhm, Gm, GRh/GRp.

e.g Nupakot [658 475].

DESCRIPTION

This association may vary from only 4-5m thick to over 20m thick (Figure 3.11).

The thin, basal unit of massive to crudely-bedded monomict gravel (Gm) is up to 1m thick. The overlying lava (Ls) lies conformably on top with some minor pillowing and brecciation due to reaction with the underlying wet sediments.

The lava unit (Ls) is composed of discontinuous blobs to sheet-like masses of lava with sharp to diffuse contacts with the underlying sediments. The lava base may be blocky or slightly pillowy. The lava bodies are usually blocky or crudely columnar jointed and typically discontinuous laterally (rarely broader than 20m), but elongate in the flow direction (up to 50m). The lava may contain pods of hyaloclastite breccia, whilst isolated lava bodies may occur in the overlying breccia. The upper surface of the

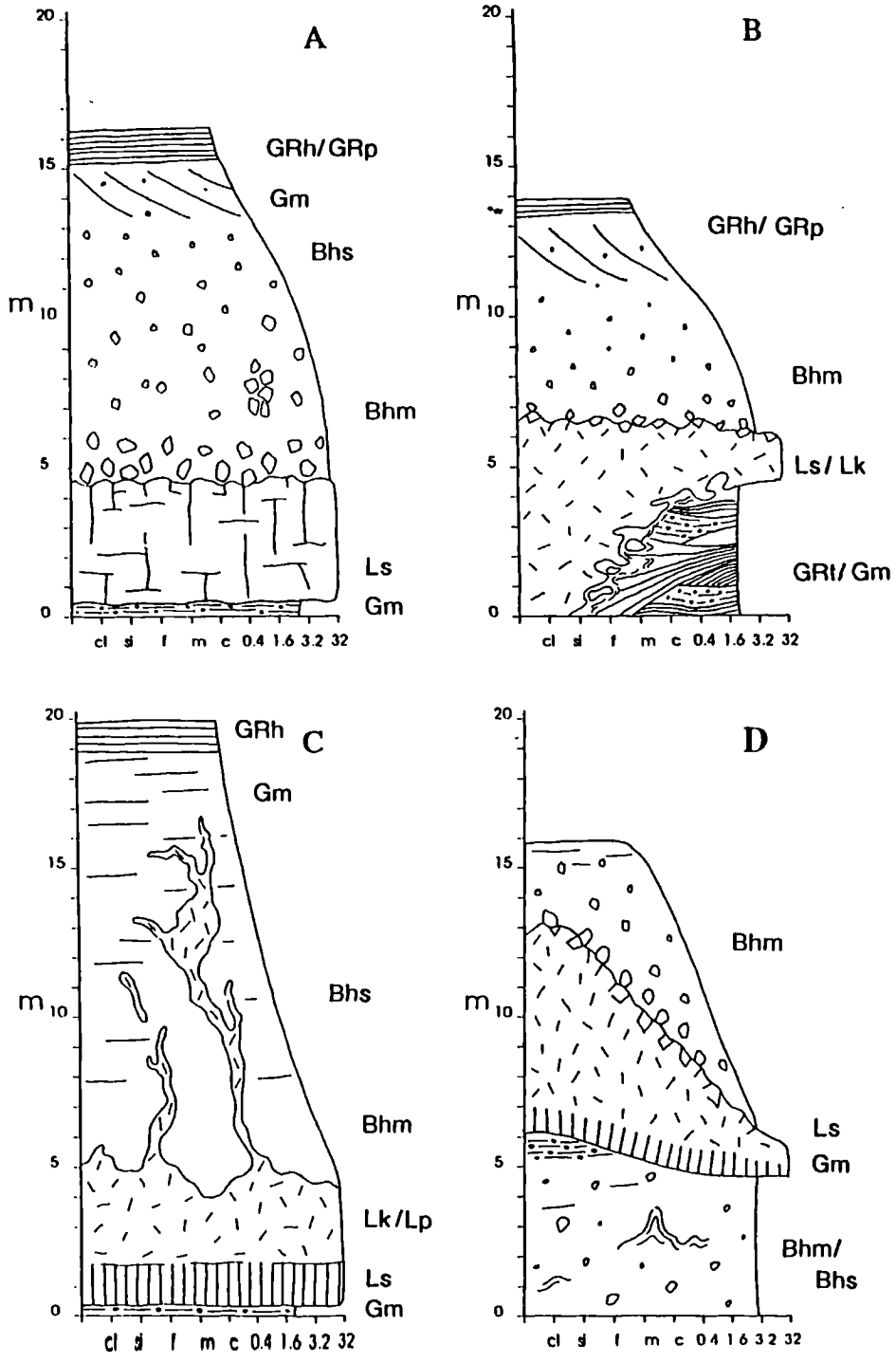

Fig. 3.10
COMMON LITHOFACIES ASSOCIATIONS AT EYJAFJOLL

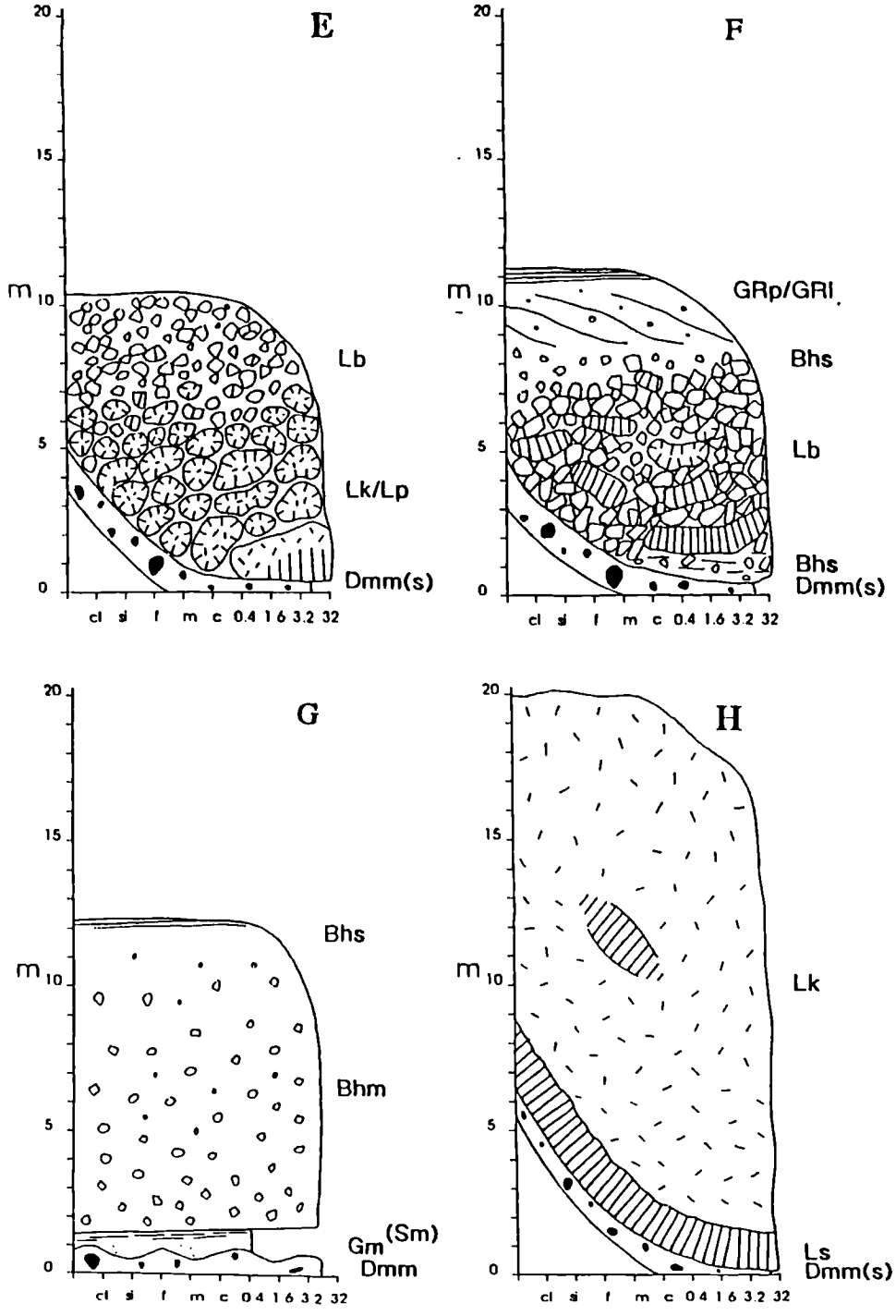

Fig. 3.10 (cont'd)
COMMON LITHOFACIES ASSOCIATIONS AT EYJAFJOLL

lava may be blocky with poorly developed pillows which spall off into the breccia unit above.

The hyaloclastite breccia (Bhm) is typically massive, matrix-supported and poorly sorted. It may incorporate fragments from the blocky upper surface of the lava. In associations where the lava is absent, the breccia may have a conformable or erosive basal contact with the underlying sediments. The upper part of the hyaloclastite breccia typically shows faint stratification.

The uppermost lithofacies of the association consists of 1-2m of cross-bedded gravel (GRp) occasionally grading up into laminated or planar-bedded granules (GRp).

The sequence at Nupakot consists of a stack of two to three of these associations.

INTERPRETATION

The lowest gravelly unit (Gm) represents deposition from hyperconcentrated grain flows which produce sheet-like, clast-supported massive and horizontally-bedded sediments. The sediments are dominantly composed of hyalotuff presumably derived from the early, explosive subaqueous eruption.

The lava and associated hyaloclastite breccia follows the same path as the early turbulent meltwater. The blocky, jointed margins of the lava (aa lava?) break up and become incorporated in the surrounding hyaloclastite breccia and in places, the lava envelopes blocks of hyaloclastite breccia. However, despite such interaction during flow, the contact between the two lithologies is often sharp. This suggests that although the two lithologies have clearly flowed and interacted together, they were not necessarily deposited simultaneously and there may have been some late-stage relative motion of the hyaloclastite breccia relative to the underlying lava. The massive nature of the breccia suggests rapid deposition without sorting from a non-cohesive debris-type flow containing discrete bodies of lava which cool after deposition to form radially-jointed blocks.

Cross-bedding and a reduction in clast size in the upper part of the breccia (Gm, GRh, GRp) reflect the waning flow at the end of a flooding event. The uppermost horizontally-bedded gravels and granules (GRh, GRp) represent reworking of the finer-grained hyaloclastite by traction currents. This late-stage reworking is due to shallow, running water in a subglacial or subaerial environment.

The deposits do not appear to be laterally confined or channelled. They are nevertheless thick and vertically stacked, implying that large volumes of material were deposited very rapidly. It is suggested that deposition occurred at, or very near, the ice margin in either open subglacial channels or on the glacio-fluvial outwash plain. The pulses of activity are due either to separate volcanic events or to different 'surge fronts' reaching the glacial margin at different times. Alternatively, successive surges may have taken different flood pathways across the glacial outwash plain in a similar manner to pulses on the sandur (Maizels, 1992). Blockages within subglacial conduits would lead

to ponding and freezing of the lava; the overlying hyaloclastite breccia may then be reactivated if the channel reopens.

DISTRIBUTION

This lithofacies association is very common in layer cake successions around the core of the volcano. It is a relatively proximal deposit, forming as a result of both summit and flank eruptions. It is particularly common on western Steinafjall (Nupakot).

Figure 3.11 *Looking east, at a vertical stack of lithofacies association A near Nupakot [658 475].*

3.4.2 LITHOFACIES ASSOCIATION 'B'

Lava and hyaloclastite breccia cutting trough cross-bedded volcaniclastics.
Lithofacies GRt, GRm, Ls, Lk, Bhm, GRh, GRp.
e.g Seljaland [509 535], Hvammsmuli [560 505].

DESCRIPTION

The association at Seljaland (Figure 3.12) can only be seen in cross-section. It consists of large-scale trough cross-bedded tephra granules (cross-bed sets <2m high) and clast-supported gravels (GRt, Gm) containing angular basalt clasts (<5cm) cut by a lava body (Ls, Lk) at least 15m in diameter, which grades upwards into a genetically related hyaloclastite breccia (Bhm). Aligned clasts in the bedded sediments indicate a palaeoflow direction towards the SSW. Isolated basalt pillows and lobes in the sediment appear to have spalled off, or be protrusions from, the main lava body, they lack glassy margins indicating that they were emplaced at high temperature. Lava lobes and fingers project from the lava into the bedded sediments (GRt, Gm) over a 2m thick contact zone in which the sediments are massive or chaotically bedded. Each lava body is surrounded by a thin halo of massive sand only a few centimetres thick. The contact between these deformed sediments and the trough cross-bedded sediments is sharp. The entire association is at least 50m in width and 10m in height. Pillows and basalt lobes spall off the upper, irregular surface of the lava into the overlying massive, matrix-supported hyaloclastite breccia (Bhm), the margins of which also truncate the bedded sediments (GRt, Gm). Clast size within the hyaloclastite breccia decreases upwards.

The deposit at Hvammsmuli is more laterally extensive, i.e. >100m in width (Figure 4.19). A laterally extensive cube-jointed and brecciated lava body grades upwards into hyaloclastite breccia (Bhm) and has sharply truncated early bedded sediments (GRt, Gm) which are now preserved as lenses at the base and margins of the deposit. Most of the sediments are deformed into tight folds or show chaotic bedding. The contact zone between the sediments and lava is similar to that described above. In contrast to the Seljalands flow, this deposit is well-exposed on three sides and can be seen to flow downslope at about 5° in a SSW direction.

INTERPRETATION

Trough cross-bedded sediments (GRt) suggest deposition in channels, although the base of such a channel is not exposed at Seljalands. The size of the cross beds at Seljalands implies large scale bedforms (dunes) which formed in deep water (up to 5m) during a period of high flow strength. Such conditions must have occurred during a flooding event. The Seljalands deposit appears to show the lava cutting into the sediment as a narrow finger-like projection whereas the Hvammsmuli deposit (a larger volume eruption?) has formed a sheet-like 'intrusion'.

The lava at Seljalands is pervasively jointed (Lk) with pillowed margins and

grades upwards into cogenetic hyaloclastite breccia (Bhm) suggesting that on deposition it was water saturated. The hyaloclastite breccia (Bhm) is massive and was clearly interacting with the lava at the time of its deposition. The massive sands surrounding the lava body and the truncation of bedding suggest that it replaced the wet sediments partly by the process of fluidisation (Kokelaar, 1982).

The lava body at Hvammsmuli is sheet-like and its jointed and brecciated nature suggests that it erupted and flowed in a subaqueous environment before deposition in a channel originally occupied by cross-bedded and horizontally-bedded volcaniclastic sediments. Lenses of sediments preserved beneath and at the margins of the lava show folding and distortion of bedding, this may have occurred prior to the emplacement of the lava as a result of the partial collapse of liquified bedforms.

At both localities, clasts in the sediments petrographically resemble the main lava body suggesting that the sediments and later lava are genetically related. If this is so, the eruption environment and depositional processes must have changed during an eruption event. A tentative sequence of events may proceed as follows: Early explosive phreatomagmatic activity probably coincides with a jokulhlaup during which a large volume of meltwater transports tephra away from the vent area. This material is deposited on flood plains surrounding the volcano (e.g. GRt, Gm). As the eruption proceeds, subglacial tunnels increase in size due to water turbulence and the vent area may even become semi-emergent due to melting or collapse of the overlying ice sheet.

Figure 3.12 *Lithofacies association B at Hofsar [507 535].The exposed face is about 8 metres high.*

Later stage activity then becomes more effusive and lavas follow the subglacial tunnels opened by the meltwater. Interaction between the flowing lava, meltwater, the ice walls and roof produces very large quantities of hyaloclastite (Smellie et al. 1993, Walker and Blake, 1966). This envelope of hyaloclastite continues to interact with the lava as it moves *en masse* downslope. This particular lithofacies association is emplaced in a distal environment, probably at the break of slope between the growing volcanic edifice and the surrounding flood plains. Deposition is near the ice margin. The example from Seljalands may represent deposition from anastamosing subglacial tunnels whereas the Hvammsmuli example may represent deposition from sheet-like subglacial channels.

DISTRIBUTION

This lithofacies association occurs predominantly around the periphery of the volcanic cone. This reflects the requirement of a break in slope in its formation. Most examples are the result of flank eruptions.

3.4.3 LITHOFACIES ASSOCIATION 'C'

Basal sheet lava and hyaloclastite with feeders intruding overlying resedimented syn-eruptive volcaniclastics.

Lithofacies Ls, Lk, Lp, Bhm, Bhs, Gm, GRh.

e.g Holtsnupur [610 483], nr. Hvammur [557 511], Fit [520 525].

DESCRIPTION

This whole association may vary in thickness from 5 to 40m, although deposits in all areas have a very similar structure (Figure 3.13). These deposits have only been observed on the south margin of the volcano. There may be a thin, discontinuous basal unit of massive or planar-bedded gravels (Gm) or diamictite up to 0.5m thick but more commonly, the lava rests directly on a glacially scoured substrait.

The lava (Ls) base is often sharp, though it may be blocky with poorly developed pillows and lobes. The lava body typically has well developed vertical columns which become cube-jointed near to its upper surface (Lk). The upper surface is irregular, with flame structures, fingers and lobes of hackly lava protruding into a mantle of *in-situ* hyaloclastite (Bhm), redeposited hyaloclastite (Bhs) and volcaniclastic sediments (Gm). Budding and spalling from these apophyses creates an abundance of isolated lava bodies in the lower part of the hyaloclastite. The basal lava forms a sheet which may be several tens of metres or hundreds of metres in breadth, thinning towards its margins.

The *in-situ* hyaloclastite (Bhm) is gradational upwards with redeposited hyaloclastite (Bhs) and massive and redeposited volcaniclastic gravels. Cross-bedded gravels may occur locally, but horizontally-bedded, clast-supported gravels and granules (Gm, GRh) are most common. Basalt lobes and feeders attached to the basal lava may

intrude these uppermost stratified units. The basal lava and overlying volcaniclastics are genetically related and so originated from the same eruptive event.

The minimum volume of the deposit at Holtsnupur is 0.6km^3. The deposit at Fit is much thinner in comparison and although not exposed in three dimensions is probably much smaller in volume. Despite the variation in volume of these deposits, the processes forming them are probably very similar.

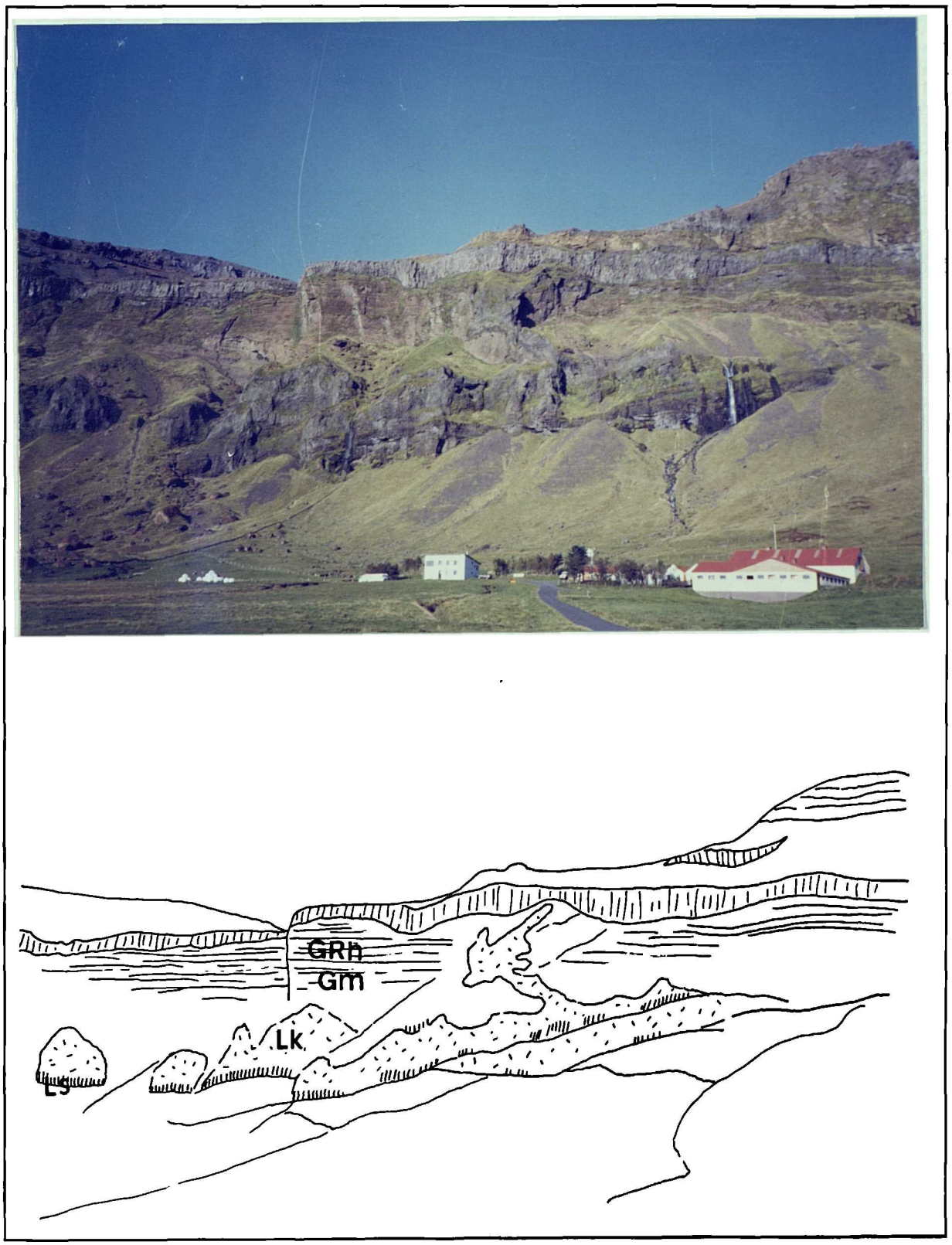

Figure 3.13 *Looking north towards lithofacies association C at Varmahlid [623 478].*

INTERPRETATION

The occurrence of large volumes of hyaloclastite and reworked volcaniclastic sediments suggests a subaqueous origin for this material. Volcaniclastic sediments might normally be expected to be carried by meltwater to the distal flood plain environment, however in this case, such sediments accumulated in gently sloping to flat-based palaeo-valleys and in broad channels in a more proximal environment. The common occurrence of a glacially scoured base lacking soils or weathering and the topographically-confined nature of these deposits suggests that this association was emplaced beneath a valley-confined glacier. The presence of some basal gravels may indicate deposition near the ice margin, perhaps where the glacial valley emerges onto the surrounding flood plain.

The volcaniclastics are more strongly bedded towards the top of thicker deposits and essentially massive in lower parts. This may be caused by rapid '*en masse*' deposition of the sediments which might cause partial fluidisation of upper parts of the sediment, decreasing the concentration of water-sediment mixtures and allowing deposition of tractional bedforms. The basal lava feeds the overlying mantle of hyaloclastite and was clearly water-saturated at the time of its deposition, the lavas and overlying volcaniclastics were therefore deposited almost contemporaneously. This lithofacies association is very similar to, but on a much smaller scale than, the mass-flow deposits of Bergh and Sigvaldason (1991). It is proposed that this association formed beneath valley-confined glaciers (large volume deposits) or in subglacial channels (small volume deposits) where the slope is gentle and the basal lava is laterally restricted thus forming thick ponded sheets which resist rapid cooling. Rapid extrusion rates would aid this process. Normally, such large volumes of volcaniclastic sediments would be transported away from the vent area by meltwater; presumably, thick ice and a gentle gradient allowed for the proximal deposition of the sediments.

DISTRIBUTION

This distinctive lithofacies association is common in successions younger than 600Ka which are dominated by topographically-confined deposits. The voluminous example in Figure 3.13 was deposited in the distal region of a deep palaeovalley extending south from the central vent region. Smaller volume examples occur mostly to the east and west of the volcano where they were probably fed by flank eruptions.

3.4.4 LITHOFACIES ASSOCIATION 'D'

Cube-jointed lava 'tubes' lying on thick resedimented volcaniclastics and hyaloclastite breccias.

Lithofacies Bhm, Gm, Ls, Lk.

e.g. Raufarfell [703 478], Lambafellsheidi [688 504], Nupakotsdalur [658 510].

DESCRIPTION

This association is typically up to 15m thick and occurs in proximal areas. It is characterised by elongate lava tubes' (Ls, Lk) lying upon equally elongate and laterally discontinuous redeposited volcaniclastic lithofacies (Bhs, Gm). Several such associations of similar petrography and chemistry (i.e. same eruption event) are typically aligned and interleaved, together they may extend laterally for several hundred metres. In some examples the lava 'tubes' feed large ponded lava bodies further downslope.

At Raufarfell (Figure 3.14), the lower unit is a thick, massive or locally stratified redeposited hyaloclastite breccia (Bhs). There may be dewatering structures and localised chaotic bedding. The top metre or so of this unit may consist of planar cross-bedded or horizontally-bedded redeposited volcaniclastics (Gm), which are capped by the sharp base of a lava unit (Ls). The lava tubes are triangular in cross-section; their surfaces are blocky rather than pillowy. They have well-developed columns arranged perpendicular to the lava surface and an internal entablature (Lk). Massive hyaloclastite breccia (Bhm) may form a mantle over the lava but is typically only 1-2m thick above the apex of the lava tube.

At Lambafellsheidi, linear ridges up to 200m long and 20m wide are formed by the lava tubes which splay out downslope like fingers. The lavas are again roughly triangular in cross-section. Some ridges are stacked one on top of another. Much of the surrounding hyaloclastite has been removed by subsequent glaciation but there is still evidence of massive hyaloclastite breccias horizontally-bedded volcaniclastics intercalated between the lava bodies. The lava tubes slope up to about 20° and feed the thick ponded lavas of lithofacies association G which occur downslope. The lava is intermediate in composition and is cube-jointed, although patches of columnar jointing occur.

The Nupakotsdalur deposits are inaccessible, but the distinctive cross-section of the lava tubes is clearly visible.

INTERPRETATION

The lower, redeposited hyaloclastite breccias (Bhs) show chaotic bedding and dewatering structures in places suggesting *en masse* deposition. Slump structures may also have formed after melting of ice walls of a subglacial glacial tunnel or ice blocks incorporated in the breccias. The upper stratified parts of the hyaloclastite breccia point to a reduced volume of sediment in the meltwater following deposition of the debris flow. Bedding may be horizontal or cross-bedded implying deposition from traction currents with perhaps dunes migrating downstream.

The distinctive cross-sectional shape of the lava tube may reflect the shape of a subglacial Rothliesburger-type tunnel (section 3.3.1). These tunnels form when turbulent meltwater cuts up into the overlying ice and any reduction in flow rate or

turbulence of the meltwater results in the closing of the passage. Esker formation is proposed to occur in R-tunnels (Bannerjee & McDonald, 1975). Sediment accumulation occurs at the floor of the tunnel reducing its cross section causing increased pressure and turbulence of the water which then cuts upwards into the ice. In this way, thick sediments can be deposited in tunnels which only ever contained relatively shallow water (McDonald & Vincent, 1972). Experimental work by McDonald and Vincent (*ibid*) has shown that water depth in a tunnel may be 2 to 10 times dune height. The dune height is about 80cm in Figure 3.15, whilst the overlying lava and breccia sheath is about 6m thick. This is consistent with formation in a subglacial tunnel.

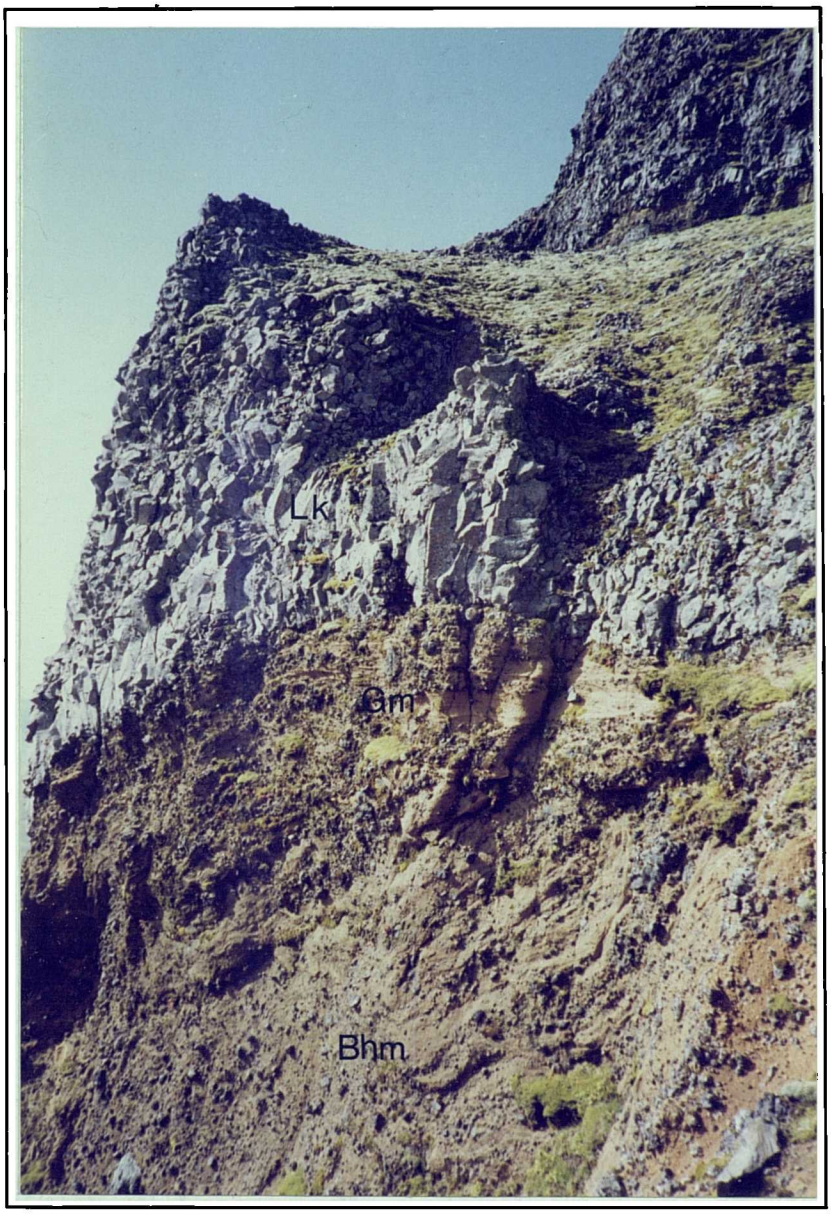

Figure 3.14 *Lithofacies association D at Raufarfell [703 478]. The lava unit is 5m thick at its thickest point.*

Smellie & Skilling (1992) suggested this mechanism for deposition of volcaniclastic assemblages at Mt Pinafore, Antarctica.

The lava tubes are insulated from the ice by the surrounding breccia sheath allowing the lava to cool slowly and develop columnar or cube jointing (kubbaberg, Lk).

These lava bodies may form blockages in the subglacial tunnels forcing subsequent meltwater to take different pathways and forming a system of anastamosing tunnels as occurs during normal esker deposition (Banerjee & McDonald, 1975). Such blockages may cause different 'surge' events at the glacial margin. Such a process may explain the interleaving of such deposits (e.g. at Lambafellsheidi), where channels may have been continuously shifting.

DISTRIBUTION

This lithofacies association tends to be very localised and may develop laterally and downslope into other forms e.g. lithofacies associations C or H. It is a proximal near-vent deposit which occurs only at higher levels in the stratigraphy. It may result from summit or flank eruptions.

3.4.5 LITHOFACIES ASSOCIATION 'E'

Topographically-confined basalt lobe/pillow/feeder zone with interstitial hyaloclastite.
Lithofacies Dmm (s), Lk/Lp, Lb.
e.g. Midskalagil [617 519].

DESCRIPTION

This association is valley-confined and forms lobes that are elongate in the flow direction (Figure 3.15).

The basal unit is typically a diamictite (e.g. Dmm(s)) which defines the outline of a palaeo-valley. Lodgement tillites may reach angles of dip up to 50° defining steep-sided palaeovalleys.

The lava lithofacies directly overlie the diamictite with a sharp, non-erosive contact. The lava may be coherent in places with crude columnar jointing (Lk). However, the greater part, if not all, of the unit is composed of radially-jointed basalt lobes/feeders and pseudo-pillows (Lp) in a matrix of *in-situ* hyaloclastite. The palaeo-valley at Midskalagil was steep-sided and narrow, up to 200m across and 30m deep. Other similar deposits lie in palaeovalleys of similar proportions high on the flanks of the volcano.

INTERPRETATION

This association clearly represents valley-confined deposition. The sharp contact between the lodgement till and the lava suggests that any loose material was flushed down the valley by meltwater before the main lava body was deposited. The lava unit comprises a mass of feeders, lobes and pillows in a hyaloclastite matrix which feed the brecciating flow front further down the slope. There is no evidence of free flowing water in the upper part of the deposit so it must have been hot and well insulated from the ice. The lack of large volumes of phreatomagmatic tephra suggests that the ice may have

been relatively thin, nevertheless, the presence of basal tillite, lack of other sediments and the evidence that large amounts of water were involved suggests a subglacial origin and subglacial emplacement for this association. Since the lava does not form a coherent sheet, the extrusion rate of such an eruption may have been relatively low.

Figure 3.15 *Lithofacies association E at Midskalagil [617 519]. The basal diamictite (Dmm) defines a palaeovalley side.*

DISTRIBUTION

This lithofacies association is found on the upper western and southwestern flanks of the volcano and probably formed during small volume subglacial eruptions from radial and E-W fissures. This is a proximal, near vent deposit. Downslope and under the influence of gravity, the lava unit appears to break up and brecciate. It loses the fine hyaloclastite matrix, which is removed by meltwater, the brecciated blocks may then be remobilised in debris flows and ultimately form autoclastic breccias such as lithofacies association F.

3.4.6 LITHOFACIES ASSOCIATION 'F'

Topographically-confined autoclastic breccia, pillows/blocky lava clasts, minimal interstitial hyaloclastite.

Lithofacies Dmm(s), Lb, GRp, GRl.

e.g. Seljaland [509 546].

DESCRIPTION

A good example of this lithofacies example occurs on the south bank of the Seljalandsá stream (Figure 3.16). The flow has a lensoid cross-section and the base lies on a gently curving palaeovalley bottom. There is ~1m of massive, poorly-sorted, clast-supported

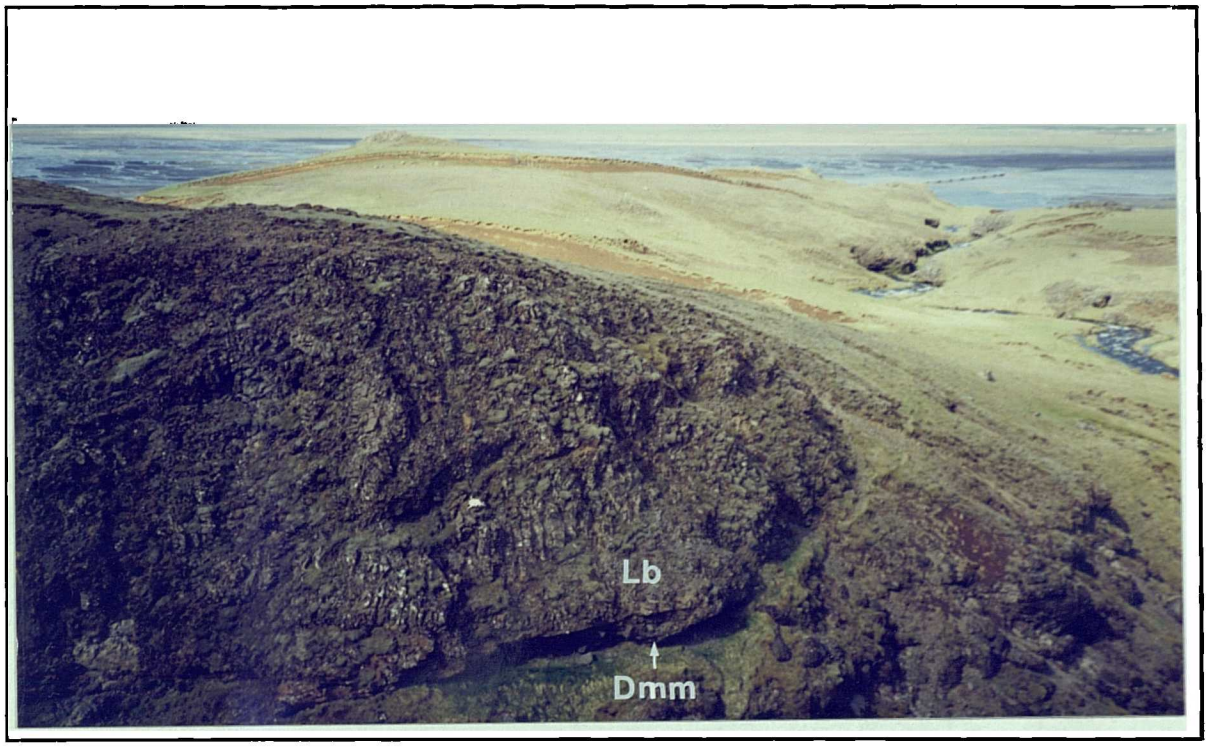

Figure 3.16 *Looking south west at lithofacies association F near Seljaland [509 546]. The deposit is ~10m thick and the stream flows along the northern margin.*

diamictite at the base (Dmm(s)), containing subangular to rounded clasts up to 40cm in diameter and there is local reworking of silts in the sandy matrix. The deposit itself is a chaotic mixture of irregularly columnar lava, broken columns, radial-jointed 'pillows' and fragments of pillow in a sparse matrix of vitric sands, silts, and crystals (plagioclase, olivine and pyroxene). The clasts and blocks show no evidence of marginal quenching. The deposit lies directly on the basal conglomerate and is locally capped by low angle cross-bedded sands and gravels (GRp/GRl).

INTERPRETATION

The basal conglomerate is a melt-out till as it lacks the shear texture of lodgement till and is clast-supported. The chaotic appearance of the deposit is probably due to the brecciation, granulation and collapse of pillows, jointed lava blocks and lobes as they flowed downslope. The lack of sandy sediments in this unit, suggests that this was not a depositional area, i.e. the flood water carried finer sediments away down slope. The clasts formed by autobrecciation and collapse not by quenching as is the case with hyaloclastite. The uppermost cross-bedded sediments were deposited during the late stages of the event by the waning, low sediment concentration, turbulent meltwater. The

eruption certainly originated in a subaqueous (subglacial) environment judging by the quantity of pillow lavas and hyaloclastite. The width to height ratio and lensoid cross-section of the deposit, suggest that it was confined on deposition, probably in subglacial to emergent channels near to the margin of the icecap.

DISTRIBUTION

This lithofacies association occurs near breaks of slope on the periphery of the volcano. It is a medial deposit, reflecting the gravitational collapse of proximal deposits. It is common in younger successions (<600Ka).

3.4.7 LITHOFACIES ASSOCIATION 'G'

Massive redeposited hyaloclastite breccia commonly overlying thin layers of redeposited volcaniclastics, or with a thin basal sand layer.

Lithofacies Dmm, Gm, Sm, Bhm.

e.g. Fit [524 526], Hvammsmuli [561 503], Moldnupur [602 495].

DESCRIPTION

The underlying unit of this lithofacies association is typically diamictite (Dmm) but on rare occasions may be lava (Figure 3.18). At Fit, the diamictite is typically 0.5 to 1m thick (Figure 3.17). This is overlain by the erosive base of a thin gravel unit (Gm) (<50cm) dominated by palagonitised volcanic lapilli, lithic fragments and crystals. The gravels show some evidence of faint laminations. The contact with the overlying breccia

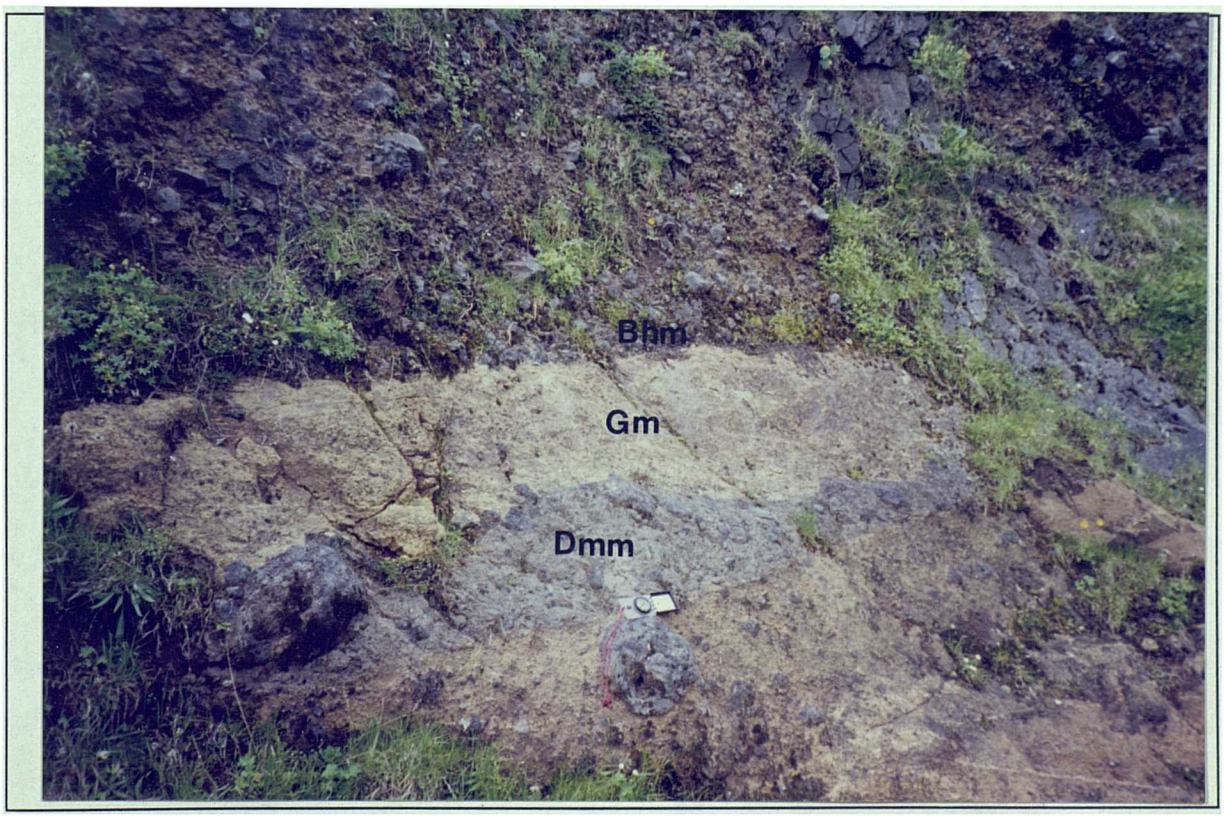

Figure 3.17 *Lithofacies association G at Fit [524 526]*

(Bhm) is sharp. The hyaloclastite breccia unit is a coarse, monomict, blocky debris flow which may or may not be genetically related to the underlying gravels. At Hvammsmuli (Figure 3.18), the gravels are overlain by a thin layer of volcanic ash and scoria (Sm) which has a diffuse contact with the overlying hyaloclastite breccia (Figure 3.18). At other localities the hyaloclastite breccia may rest directly on the substrait.

INTERPRETATION

The erosive palagonitised gravels (Gm) at Fit (Figure 3.17) were probably emplaced by high concentration, erosive flood flows which may have been induced by collapse of unstable heaps of tephra near the vent. The overlying hyaloclastite breccia was emplaced soon afterwards by mass flow processes but it is not clear if it is a product of the same eruptive event as the gravels. At other localities the two lithofacies are certainly related to the same eruptive event and the basal layer may be formed during late stage depositional processes of the hyaloclastite breccia (volcanic debris flow - section 2.7).

Non-erosive massive ash deposits (Sm) may be subaerially or subaqueously deposited. The pink sands at Hvammsmuli (Figure 3.18) show no sign of palagonitisation and so they were probably subaerially deposited. Where palagonitised sands occur, they may represent tephra formed in the initial phreatomagmatic explosive stage of an eruption which are deposited by suspension in shallow water. Overlying hyaloclastite breccia (Bhm) serves to preserve the finer-grained underlying sediments. At Hvammsmuli, the overlying hyaloclastite breccia appears to have loaded the thin sand layer indicating that they were deposited in rapid succession.

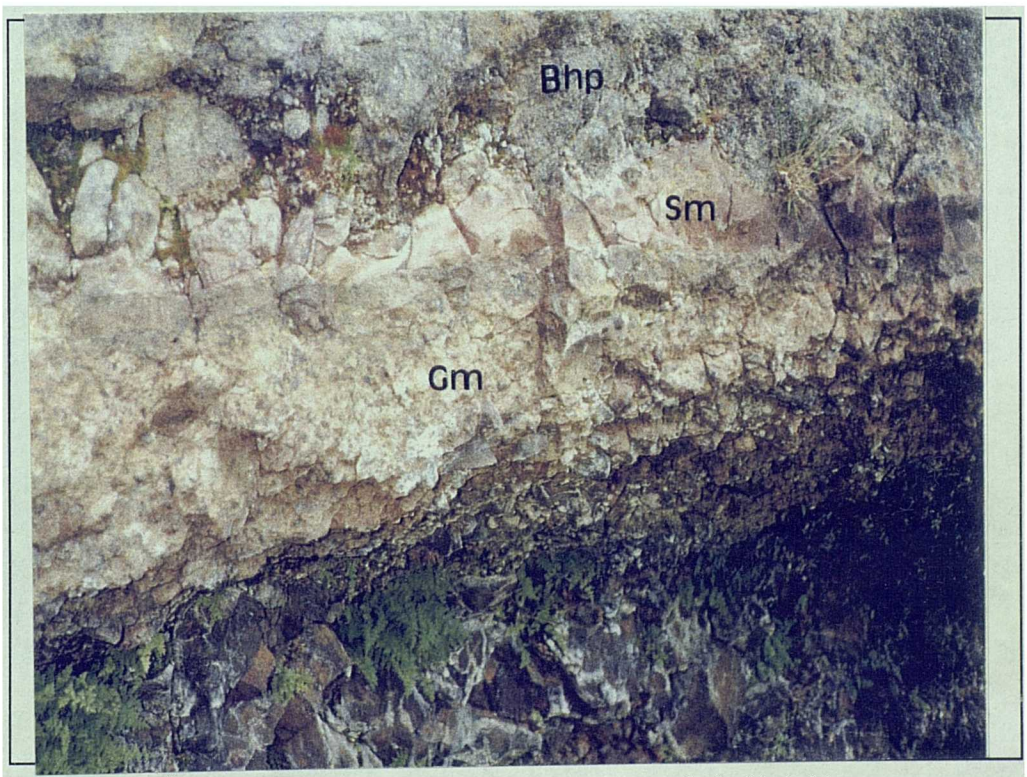

Figure 3.18 *Lithofacies association G at Hvammsmuli [561 503].*

This lithofacies association may represent deposits formed near the periphery of an ice cap or glacier where abundant water enables mass flow processes to occur and localised deposits of tephra and other fine grained volcaniclastics are preserved. Deposits lacking a basal unit of volcaniclastics may have formed wholly within subglacial conduits.

DISTRIBUTION

Massive redeposited hyaloclastite is very abundant and represents deposition in a water-saturated probably subglacial environment. The occurrence of a thin bed of redeposited volcaniclastics (e.g Gm, Sm) beneath a thick hyaloclastite breccia is common at several localities and represents deposition in semi-emergent environments in more distal locations.

3.4.8 LITHOFACIES ASSOCIATION 'H'

Lavas with very thick entablature and thin basal colonnade which crop out on valley sides.

Lithofacies Dmm(s), Ls, Lk.

e.g. 'Svarthamrar' at Seljavellir [685 494] and Holtsheidi [618 496].

DESCRIPTION

This association is composed of dominantly lava lithofacies. It occurs in only a few places at Eyjafjoll, but its mode of deposition has important consequences.

'Svarthamrar' (black cliffs) at Seljavellir (Figure 3.19) formed on glacial valleysides sloping at up to 40°. They are fed by lava tubes on higher, gentler slopes forming lithofacies asssociation F. At the base of the association, a thin (0.5m) basal veneer of hyaloclastite lies on 2m of diamictite (Figure 2.5), small-scale pillow buds spall into the hyaloclastite from the overlying lava The lower 0.5-2m of the lava lithofacies Ls is composed of well-developed columns up to 0.5m wide which are perpendicular to the basal topography (colonnade). Above this is up to 60m of hackly and cube-jointed lava (entablature, lithofacies Lk). There may be thin, discontinuous horizons of columnar basalt within the entablature.

At Holtsheidi, the lavas are very similar in structure and lie on a steep valley side (about 30°) but the source for this unit has not been identified (Figure 4.14).

INTERPRETATION

To form such a thick entablature a vast quantity of water is required (section 2.2.1). This may be supplied by flooding. The lava has ponded on a steep valley side, not on the valley floor and must therefore be supported laterally. Ice is the only viable support mechanism, this lava has therefore flowed into the sides of a valley glacier. The

preserved lava was intruded between the basal topography and the ice but more lava may have flowed onto the ice surface.

Lava is not an effective heat conductor once its surface is chilled so only just enough ice to accommodate the lava would melt (Bjornsson, 1985). The lava may originally have been erupted in a subaerial environment and flowed into the sides of a valley-confined glacier, e.g. the Holtsheidi lavas (Figure 4.14). Alternatively, the lava could have flowed through subglacial tunnels and sheets on gentle slopes before ponding at the steep base of the section as is the case at Seljavellir. Smellie (1993) observed lavas very similar to those at Seljavellir in Antarctica and also considered them to be ponded subglacial lavas.

Figure 3.19 *Looking north at a strike section of lithofacies association H at Seljavellir [685 494]. The cliffs are at least 80m in height and flowed downslope towards the observer.*

DISTRIBUTION

There are only two very good examples of this lithofacies association, each occurs on the steep sides of a glacial valley (e.g Figure 4.6). These lavas formed during localised eruptions of high effusion rate.

3.4.9 LITHOFACIES ASSOCIATION 'J'

Thick, massive and fore-set bedded hyaloclastite breccias and syn-eruptive resedimented volcaniclastics.

Lithofacies Lk/Lp, Bhm, Gm, GRh, Ls.

e.g. Skogaheidi [725 480], Holtsdalur [625 504].

DESCRIPTION

The Skogaheidi association can reach thicknesses of <75m (Figure 3.20) and may also be laterally extensive although the margins are sharply defined by palaeo-valley sides. The main body of the association is composed of thick, massive or cross-bedded units of hyaloclastite breccia (Bhm). Towards the base of the unit there may be isolated pillows, ragged blocky lobes, feeders of lava and irregular patches of hyaloclastite breccia (Bhs) and hyalotuff. The upper sands and gravels include cross-bedded and horizontally-bedded tephra (Gm/GRh) and basalt fragments. In places, this association is capped by a thin sequence of subaerial lavas. These are the lateral equivalents of the deposits described by Carswell (1983) near Solheimajökull, 6km to the east.

The Holtsdalur deposits (Figure 4.13) are dominated by hyaloclastite and hyalotuff which is crudely bedded (Bhs). Deposits are up to at least 150m thick and the proportion of basalt lobes and feeders appears to be less than at Skogaheidi. These deposits are valley confined and lie on diamictite horizons which dip steeply eastwards (Figure 4.13). The total volume of the Holtsá deposit is at least 0.9km^3.

Figure 3.20 *Looking south east down Kaldaklifsgil gorge, west of Skogaheidi. Lithofacies association J is exposed in the gorge sides. The gorge is at least 100m deep.*

INTERPRETATION

These deposits are similar to typical tuya and tinda deposits (e.g. Jones, 1968, Smellie *et al.*,1993; Smellie and Skilling, 1994). They erupted into a subglacial vault under thick ice. At Eyjafjöll these deposits appear to have accumulated beneath valley-confined flat-bottomed or gently-sloping glaciers. Hyaloclastite, pillow lavas, hyalotuff etc build up around the vent then are redeposited by grain flow on foresets. Post-depositional slumping may also occur. The thick, massive deposits (<150m) at Holtsá may have

LITHOFACIES ASSOCIATION	DESCRIPTION	DEPOSITION ENVIRONMENT	COMMENTS
A	Hyaloclastite (& pillow) breccias with lavas lying conformably on resedimented, syn-eruptive volcaniclastics	Broad subglacial and glacio-fluvial channels near the ice margin, medial deposit.	Resedimented volcaniclastics represent hyperconcentrated flood flow, lavas and breccias are mass flows.
B	Lava and hyaloclastite (& pillow) breccias cutting trough cross-bedded volcaniclastics	In channels at the break of an ice-covered slope e.g alluvial fans or beneath a glacier spreading across a fluvial plain, medial to distal deposit.	Bedded volcaniclastics represent channelled flood flow, breccias are mass-flow deposits.
C	Basal sheet lava and hyaloclastite with feeders intruding overlying resedimented syn-eruptive volcaniclastics	Ponding beneath thick, broad temperate glacier with flat or gently sloping base, medial deposit.	Lavas intruded and ponded between initial phreatomagmatic deposits and topography.
D	Cube jointed lava 'tubes' lying on thick resedimented volcaniclastics and hyaloclastite breccias.	Pre-existing subglacial tunnels and channels, proximal deposit.	Similar to esker formation in Rothliesberger tunnels.
E	Topographically-confined basalt lobe/pillow/feeder zone with interstitial hyaloclastite	Subglacial, in topographic channels and valleys beneath thinning temperate ice, proximal deposit.	
F	Topographically-confined autoclastic breccia, pillows/ blocky lava clasts, minimal interstitial hyaloclastite	Subglacial pre-existing channel/ valleys near temperate ice margin, medial to distal deposit.	
G	Massive hyaloclastite breccia commonly overlying thin layers of redeposited volcaniclastics	Shallow subaqueous/subglacial environment, widespread proximal deposit.	Some volcaniclastics may represent dilution at snout of a volcani-clastic debris flow.
H	Lavas with very thick entablature and thin basal colonnade which crop out on valley sides	Ponded between topography and temperate valley-confined glacier.	
J	Thick, massive and fore-set bedded hyaloclatite breccias and syn-eruptive resedimented volcaniclastics	Subglacial, beneath thick, flat or gently sloping valley-confined glaciers, proximal to medial deposit.	Equivalent of tuya or tinda deposits.

Table 3.2. Summary table of lithofacies associations.

formed under polar ice or very thick temperate ice. The thinner deposits (<100m) at Skogar which show large-scale planar cross-bedding are probably formed under thick temperate ice. The subaerial capping lavas at Skogar indicate that the uppermost subglacial deposits must eventually have breached the ice surface.

DISTRIBUTION

This lithofacies association is found at two localities where extensive glacial erosion has created deep flat-based, steep-sided valleys. These deposits are proximal and form as a result of large-scale summit or flank eruptions.

3.5 DISCUSSION

3.5.1 SHEET FLOWS AND TUNNEL FLOWS

At least six of the described lithofacies associations (B, C, D, E, F and G; Table 3.2) contain units which suggest that following a subglacial eruption, volcaniclastics and lava may flow in subglacial conduits opened by large volumes of turbulent meltwater (jökulhlaup).

Factors contributing to the development of sheet flows include a large volume eruption, a high rate of discharge (Bergh & Sigvaldasson, 1985), a broad source area (i.e. a fissure source) and a relatively flat topography. Large scale deposits of this kind are rare at Eyjafjoll, presumably due to a scarcity of large scale eruptions and the uncommon occurrence of large flat-lying ice sheets conducive to their development. Most sheet-like deposits were deposited in a distal site on the volcano or at the base of deeply incised valleys. Lithofacies association C, which develops at a variety of scales, and at several different localities (e.g. Figure 3.21) indicates that sheet flow occurred both beneath thick, flat-based valley glaciers and beneath the distal, gently-sloping, thin margins of the volcano's icecap.

Lithofacies associations A and B are sheet-like and occur repeatedly in vertical successions on the western and southwestern flanks of the volcano. Such associations are intercalated with subaerial lavas and successsions rarely dip at more than 10°. These lithofacies associations are dominated by palagonitised volcaniclastics (hyaloclastite breccia, hyalotuff, etc) reflecting both their subaqueous origin, hot emplacement and saturation by warm water. The lavas are blocky and laterally discontinuous, suggesting that they may have higher viscosity than lavas of lithofacies associations C. It is proposed that both lithofacies associations erupted in a subglacial environment and were deposited by decelerating debris flows and sediment-charged flood flows in a distal, possibly semi-emergent glacial environment. The extent of reworking is highly variable. Deposits dominated by hyaloclastite breccia and with minimal reworking (e.g. lithofacies association G) were probably deposited in marginal areas away from major flood paths, perhaps within subglacial channels, whereas deposits dominated by

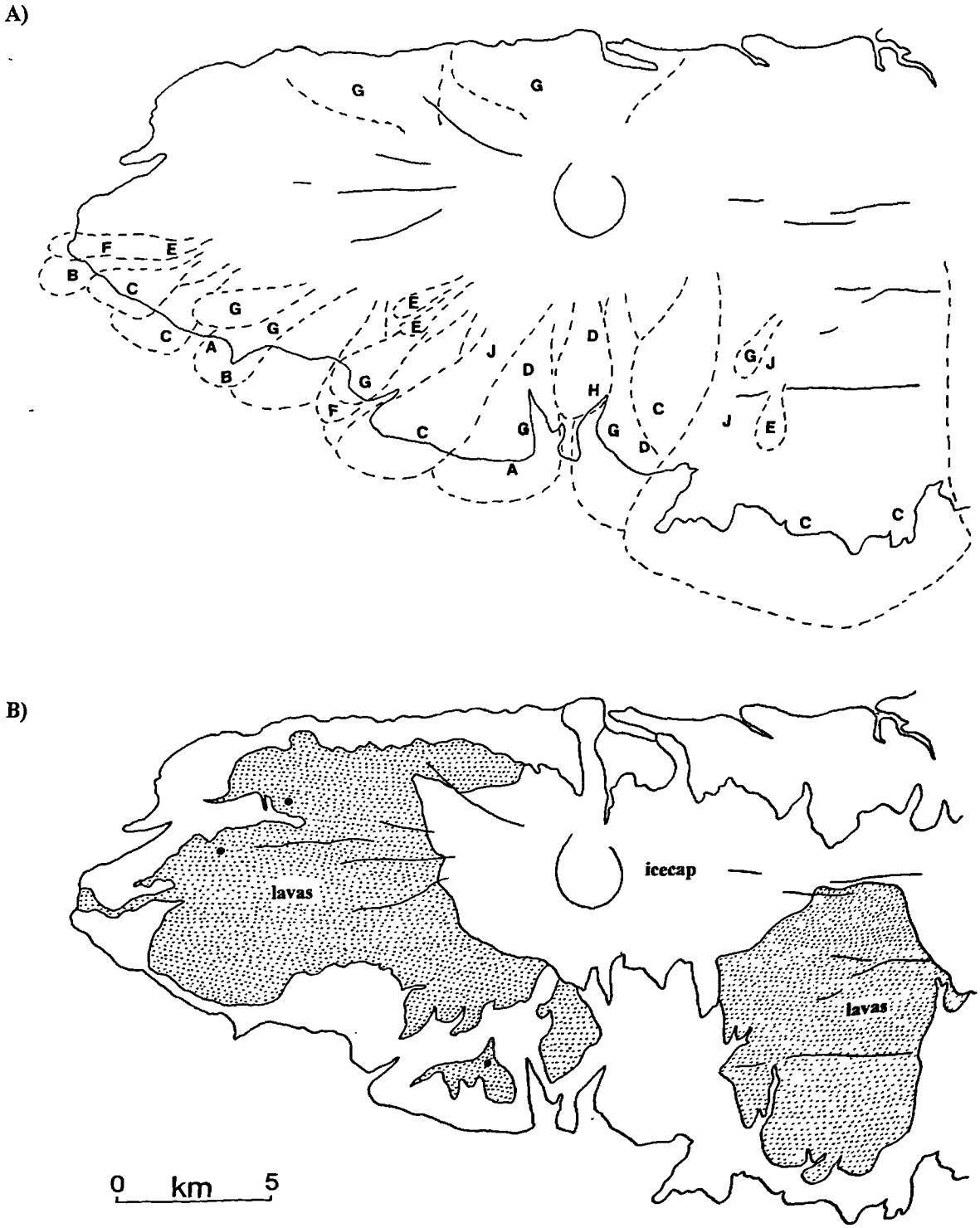

Figure 3.21 Diagrams to show the hypothetical distribution of lithofacies associations at the Eyjafjallajokull volcano during glacial and interglacial periods. The present position of the caldera and fissures are shown.

A) Glacial period: Lithofacies associations D, E, G and J are commonly proximal whereas A, B, C and F are medial deposits.

B) Interglacial period/present: Subaerial lavas erupted mainly from radial and E-W fissures extend over the gently sloping upper flanks of the volcano. In more distal and dissected parts of the volcano, lavas follow valleys and gullies (Jonsson, 1988; see also Figure 1.7).

horizontally bedded hyalotuffs and hyaloclastite were deposited in the flood path, in a more distal environment, perhaps on a glacial fan. An advancing and retreating ice cap or valley glacier extending down the gentle sloping flanks of the volcano, could have been responsible for these deposits. Both sheet flows and channelled flows occurred, suggesting that flood pathways rapidly changed in size, shape and position in response to the passage of jökulhlaups and volcanic debris.

Lithofacies association J is a broad category covering tuya and tinda type deposits. The Skogar deposits are valley-confined, thick and sheet-like, they are similar to deposits described by Jones (1969), Smellie and Skilling (1994) and Skilling (1994). However, rather than radiating dips around a central vent, deposits in the study area have a unidirectional, downslope dip away from a fissure source. The Holtsdalur deposits are even thicker but unfortunately the source area is unknown. The Skogar and Holtsdalur deposits both formed during the middle stages of volcano growth and required thick, extensive valley-confined ice sheets with a relatively flat-bottomed topography. The mature nature of the glacial valley (i.e. with a flat base and steep sides) provides evidence that these preserved subglacial deposits formed during the later stages of a glaciation event. As the volcano grew, topographically-confined deposits, dominated by mass flow and redeposition by running water, became more common.

Lithofacies association D, has also been interpreted as subglacial but in this case deposition is in tunnels. It is proposed that these eruptions had a lower discharge rate and were smaller volume eruptions than the previous examples, they are also more common on slopes. Meltwater may have been unable to sustain sheet flow, perhaps the vent was a point source and melting and magma supply was concentrated from this point. Lava flowed into tunnels opened by the meltwater, effectively turning them into lava tubes feeding lava bodies further downslope. For example, the Lambafellsheidi lava tubes (lithofacies association D) feed the 'Svarthamrar' cliffs at Seljavellir (lithofacies association H, Figure 3.21). These impressive overhanging cliffs formed as lava supplied through the discrete, subglacial tunnels ponded between steep valley sides and a thick, valley-confined glacier. The 'tubes' at Raufarfell are on gentler slopes and may be more distal deposits where flow rates are reduced and lava has frozen *in situ*, blocking the subglacial tunnels. These deposits must have formed beneath relatively thick temperate ice because if the ice was much thinner than 100m, the lava would have flowed over its surface.

Lithofacies associations E and F are topographically-confined subglacial deposits. During transport, these lava-dominated assemblages presumably followed pre-existing conduits down valleys, gullies and depressions in the subglacial topography. They are relatively small-volume eruptions unlikely to develop into sheet flows. Lithofacies association E is entirely proximal and confined to the upper slopes of the volcano, lithofacies association F includes more distal deposits which have undergone auto-brecciation as a result of gravitational collapse (Figure 3.21).

3.5.2 MODE OF TRANSPORT AND DEPOSITION

Lithofacies associations A, B, D, E, F and G are dominated by gravity mass flow processes.

Debris flow deposition was largely responsible for the coarse-grained, hot masses of hyaloclastite breccia found in lithofacies associations A and G. Debris flows may be induced by eruption or by gravitational collapse of unstable piles of near vent material. These deposits rarely incorporate exotic clasts although the bases of such deposits are unconformable. This may be due to the initial flood surge (or jökulhlaup) which flushes away loose debris in hyperconcentrated flood flows and cuts channels into which the volcanic debris is later deposited.

Those deposits which are fed by a basal lava such as A and C are gravity mass flows, in which interaction of the basal lava and overlying volcaniclastics occurs throughout transport. The intrusion of upper reworked volcaniclastics by the basal lava suggests that interaction between the two lithologies continues whilst the upper parts of the deposit are reworked. Such reworking is by hyperconcentrated grain flow. Subsequent meltwater drainage probably occurred at the margins of the deposit, or in localised channels as evidence of late stage traction currents is minimal.

Distal deposits, dominated by reworked volcaniclastics, are transported by hyperconcentrated flood flow, sheet flows and traction currents. Typically, deposits show a thin lower horizontally stratified unit, a massive middle unit and an upper horizontally and/or cross-stratified unit. This commonly repeated sequence, from massive to well-stratified lithologies is also observed in sandur sediments (e.g. Maizels 1989, 1992). The massive unit represents deposition at the peak of a high density flood surge, later fluid bedforms represent deposition in the waning stages of the flood when sediment concentration is lowered.

3.5.3 EFFECT OF TOPOGRAPHY

Steep slopes increase the instability of water-saturated debris resulting in landslides and debris flows. Deposits preserved on slopes are usually dominated by lava and hyaloclastite lithologies, finer grained volcaniclastics are transported away in suspension by rapidly flowing meltwater.

There are several occurrences at Eyjafjoll of coherent lava flows being transformed downslope into chaotic hyaloclastite breccia deposits (Figure 4.6). This appears to occur when lava on gentle upper slopes suddenly flows down into a steep-sided valley. The chaotic hyaloclastite deposits were clearly water saturated on deposition, although upslope the lavas may be subaerial. The simplest explanation for this is that the lower valleys contained thin glaciers into which the lava flowed. Such deposits may form during interglacial periods.

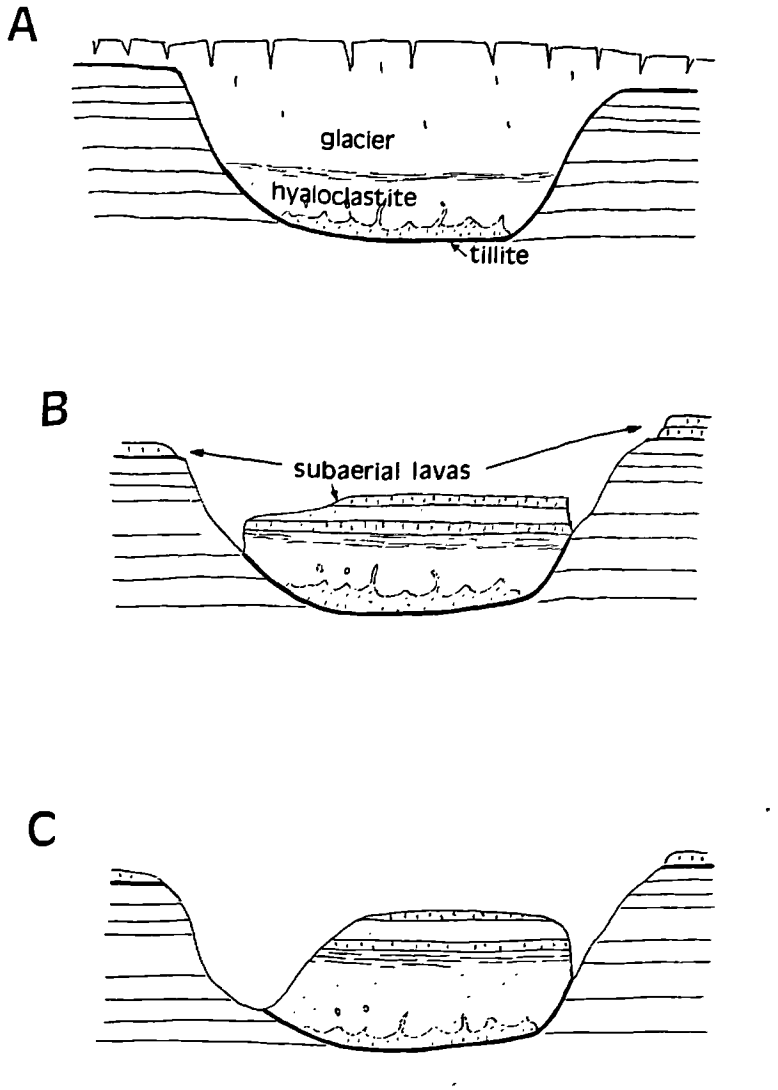

Figure 3.22 *A schematic diagram showing the sequence of events leading to topographic inversion and the appearance of apparent gaps in the stratigraphy. Each view is a cross section of a glacial valley roughly 10km from the central vent of the volcano.*

A. In the later stages of a glaciation an extensive ice sheet covers most of the volcano but is particularly thick in glaciated valleys radiating out from the centre of the volcano. The thick black line represents tillite deposited by the ice sheet. Volcanic activity near the central crater produces mass flows of volcanic material (e.g. lithofacies association C) which is channelled into the valley and deposited on the valley floor.

B. As the ice receeds, subaerial lavas may fill the valley, covering earlier subglacial deposits and thus preserving them. Meltwater flows along the valley margins cutting deep gorges into the soft underlying volcanic material. Flank eruptions may produce lava flows on the higher plateaux producing apparent gaps in a layer-cake stratigraphy. Thin tillite or hyaloclastite horizons within the 'gap' suggest the former presence of ice.

C. Further erosion and perhaps the renewed advance of valley-confined glaciers deepens and widens the gorges.

3.5.4 PRESERVATION OF SUBGLACIAL DEPOSITS

Many of the described subglacial deposits were probably formed during glacial retreat in the same way as eskers and other glacial deposits (Banerjee & McDonald, 1973). If these soft clastic lithologies were deposited during glacial advance they would rapidly be eroded and incorporated in the glacier sediment load. Some till horizons at Eyjafjöll contain a considerable proportion of glass (<40%, but see Geirsdottir, 1993) which may have been incorporated in this way. If a subglacial eruption occurs beneath ice during deglaciation, the ice that is melted may not be replaced. Later lavas may then erupt or flow under substantially thinned or even completely melted ice. Preserved subglacial successions are nearly always capped by subaerial lavas which cover substantial areas of the volcano during interglacial periods (Figure 3.21).

Many deposits at Eyjafjöll, particularly on the south side of the volcano, have been interpreted as valley-confined, subglacial mass flows. These successions now form positive topographic features, bounded by deep glacial valleys indicating that topographic inversion has occurred (Figure 3.22). This appears to be a diagnostic feature in the volcanological development of a polygenetic volcano dominated by subglacial lithologies. The process of inversion can be observed developing at several scales, streams will develop at the margins of a single lava flow (e.g. Figure 3.16) or at the margins of a broad valley-fill deposit capped by lava. These streams rapidly cut into underlying soft clastic material and form deep gorges at the valley margins. The formation of deep gullies at valley margins is currently taking place between the thick subglacial deposits of Skogaheidi and Raufarfell, (Figure 3.20). Most gorges at Eyjafjöll have formed between valley-fill deposits and valley margins and thus stratigraphy can rarely be followed across a gorge or a glacial valley. The valley-confined subglacial deposit described by Walker & Blake (1966) at Dalsheidi, has also undergone topographic inversion following continued erosion along its margins. Wiese (1992) noted an apparent 'gap' in the stratigraphy at Steinafjall. She proposed that since thin tillite occurs in this gap, it corresponds to a glacial period. It appears that during such a period deposition simply occurred elsewhere. The thick, subglacial valley-confined deposits of western Steinafjall (lithofacies association C - Figure 3.13) were probably emplaced during this glacial period.

3.6 SUMMARY

- The complex deposits of lava, hyaloclastite breccia, hyalotuff and other clastic sediments at Eyjafjöll may be described and classified using lithofacies and sequence analysis. Proximal deposits can be described in terms of their cogenetic constituent lithofacies and then defined as one of nine 'lithofacies associations'.

- Field observations suggest that each 'lithofacies association' occurs in a specific environment, so that the peculiarities of the structure of each deposit reflects differing conditions of transport, deposition, magma volume, magma viscosity, eruption rate, thickness of the ice and the subglacial topography. Most lithofacies associations at Eyjafjoll were deposited beneath or at the margins of temperate ice sheets.

- Proximal sheet flows develop during eruptions of high discharge rate. Lava intrudes between the topography and initial phreatomagmatic deposits and is of low viscosity.

- Proximal tunnel flows develop during eruptions of lower discharge rate, slopes may be steep and lava viscosity is low. Cooling of such deposits is rapid, leading to the blocking of subglacial conduits.

- Laterally extensive subglacial deposits formed beneath extensive summit ice sheets. Laterally discontinuous, topographically-confined subglacial deposits formed beneath temperate valley glaciers.

- Distal glacio-fluvial deposits of subglacial origin at Eyjafjoll are dominated by resedimented volcaniclastics and are found predominantly on the low western slopes of the volcano.

- Subglacial deposits are rapidly eroded so preservation is enhanced when they are capped by subaerial lavas. Subsequent marginal erosion of valley-confined deposits may ultimately result in topographic inversion. This is a diagnostic feature of polygenetic volcanoes which have developed during several glacial and interglacial periods.

CHAPTER 4
FIELDWORK

4.1 INTRODUCTION

In this chapter, field observation, mapping and lithofacies and succession analysis are combined to deduce the stratigraphy of specific sections of the volcano. This information is also used to produce palaeo-reconstructions of the volcano's growth history. The orientation and distribution of intrusive rocks is used to deduce how the local stress field has changed during different eruptive phases.

4.1.1 MAPPING AND MARKER HORIZONS

Jón Jónsson (1989) produced a geological map of the entire Eyjafjallajökull volcano which suggests that most of the lower slopes are composed of hyaloclastite containing feeders and intrusions of basalt, whilst the upper slopes are covered by more recent intraglacial and postglacial lavas (Figure 1.7). A more detailed mapping and petrological study of the postglacial and intraglacial lavas was carried out by Jakobsson (1979b.) who noted that the majority of these lavas were of intermediate (rather than basic or acid) composition.

In this study, mapping was focused on small, complex areas in the older successions to the south of the volcano which were mapped on a scale of 1:40,000 (Maps M1 and M2, back pocket).

Eruption units are distinguished on the basis of a) percentage and type of phenocrysts, b) whole-rock geochemistry, c) the size, shape and percentage of vesicles, d) the occurrence of lithofacies associations as described in chapter 3 and sometimes e) the degree of weathering or hydrothermal alteration.

The three-dimensional geology at Eyjafjöll is far more complex than it at first appears, particularly in the highly dissected areas to the north and south of the summit crater. The lateral extent of both subglacial and subaerial deposits in these areas is limited due to deposition in valleys, gullies and depressions in the palaeo-topography. Glaciation has smoothed the topography making the field relationships in these areas difficult to resolve.

The mapping technique employed in all areas of the volcano involved initial detailed vertical succession logging at several localities. Distinctive eruption units and/or marker horizons allowed lateral correlation between sections (e.g see Figures 4.3, 4.9 and 4.20). Some marker horizons or eruption units may be so distinctive that they can be observed from a distance (using binoculars) and this is especially useful on the steep, ancient sea cliffs on the south margin of Eyjafjöll. The most reliable marker horizons for larger scale correlations are thick lodgement tills (1-3m) which define glacial erosion horizons. These were deposited by valley-confined glaciers and have

dipping margins (<50°) that delimit the palaeovalley in which they formed. These glacial horizons are very distinctive, cutting sharply through the underlying stratigraphy and are usually conformably overlain by thick, extensive subglacial lithologies.

The Brunhes-Matuyama boundary is also a useful marker horizon in the southern section of the volcano. Lavas beneath this horizon are reversely-magnetised, whereas those above are normally-magnetised.

Where possible, the stratigraphic successions were divided into Groups. Each Group contains a number of eruption units which show similar mineralogy and geochemistry. The Groups are divided by distinct unconformites that are often defined by diamictites.

4.1.2 SAMPLING

Some subglacial hyaloclastite breccias and lavas near the core of the Eyjafjallajökull volcano have undergone intense hydrothermal alteration, so rock samples were always collected from the fresh interior of lavas and pillows wherever possible. Despite localised hydrothermal alteration, most lavas at Eyjafjöll are very fresh, with weathered crusts rarely exceeding 3mm in thickness.

Sampling was particularly thorough in the dissected sectors immediately south and southwest of the central crater since exposure is particularly good here. Elsewhere, only major lavas or hyaloclastite breccias were sampled. The strategy adopted was to sample several vertical sections, often following streams or rivers, then link the stratigraphy between sections.

Nearly 600 samples were collected, from which 262 selected samples were used for geochemical analysis. Most samples are porphyritic; even 'aphyric' samples usually contain some microphenocrysts (as noted by both Jacobsson, 1979b and Carswell, 1983).

4.1.3 K-Ar AND PALAEOMAGNETIC DATING

Kristjansson *et al.* (1988) located the Brunhes-Matuyama (B-M) boundary near the base of the Nupakôt section at Eyjafjöll using palaeomagnetic data (Figure 4.9). The boundary may also be located near the base of Raufarfell, in Kaldaklifsgil (Jonsson, 1988) and in the Laugará gorge (Figure 4.3). Using K-Ar dating, Kristjansson *et al.* (1988) dated a lava (NU2) several flows below the B-M boundary at Nupakôt, at 780±30Ka (Figure 4.9). The B-M boundary at Eyjafjöll occurs in sections near the core of the volcano which expose some of the stratigraphically oldest lavas suggesting that the oldest lavas at Eyjafjöll are not much older than about 0.78Ma. Wiese (1992) calculated K-Ar ages for a number of lavas at Eyjafjöll and confirmed that unit 'NU2' of Kristjansson *et al.* (1988) has an age of 809±50Ka.

Some of Wiese's dates have been used in this thesis to check relative ages of eruption units and stratigraphic groups deduced during fieldwork (Table 4.1 and Table

4.2: p.119). Generally fieldwork is consistent with these dates. As noted in chapter 2, apparent time gaps in the stratigraphy of Wiese (1992) occur during glacial periods. During glaciations little volcanic material is preserved *in situ*, however, it appears that subglacial valley-confined deposits are commonly preserved. The products of subglacial valley-confined volcanism may represent material erupted during the apparent time gaps. Topographic inversion of such deposits may mean that the 'missing' time period of a vertical succession is represented by the deposits of an adjacent hillside.

Area	**Sample numbers this study.**	**Sample numbers Wiese 1992.**	**K/Ar date Wiese 1992.**
LAMBAFELLSHEIDI	SCL 140 SCL 75-83 SCL 2,3	Ey 24 Ey31 Ey 22, 23	31±28 Ka 54±15 Ka 87±16 Ka
STEINAFJALL	SCL 278,279 SCL 237 SCL 98	Ey 7, 9, 11 Ey 6 Kristjansson *et al.(1988)* *NU2*	706±11 Ka 722±33 Ka 780±30 Ka
FJELL (FELLSHAUS)	SCL 58	Ey27	116±20 Ka
SKOGAHEIDI	SCL 66, 67	Ey 45, 46 STF 5, Ey21	18±16 Ka 118±34 Ka
ASOLFSSKALAEGG	SCL 509	Ey 50	129±20 Ka
HVAMMSMULI	SCL 43, 74 SCL 44-50 SCL 52-54 SCL 60	Ey 1 Ey19 Ey20 Ey52	587±31 Ka 589±37 Ka 619±26 Ka 349±19 Ka

Table 4.1 *K-ar dates of Eyjafjöll samples by Wiese (1992) and Kristjansson et al. (1988). Grid references are shown for each sample in Appendix B.*

4.2 FIELDWORK

The volcano has been divided into five sections; these sections, place names and the location of vertical logs and cross sections are shown on Figure 4.1. Within each section distinctive stratigraphic groups will be described along with other features of interest. Within each section deposits are described in order of relative age. A summary of each section will review the points of particular importance.

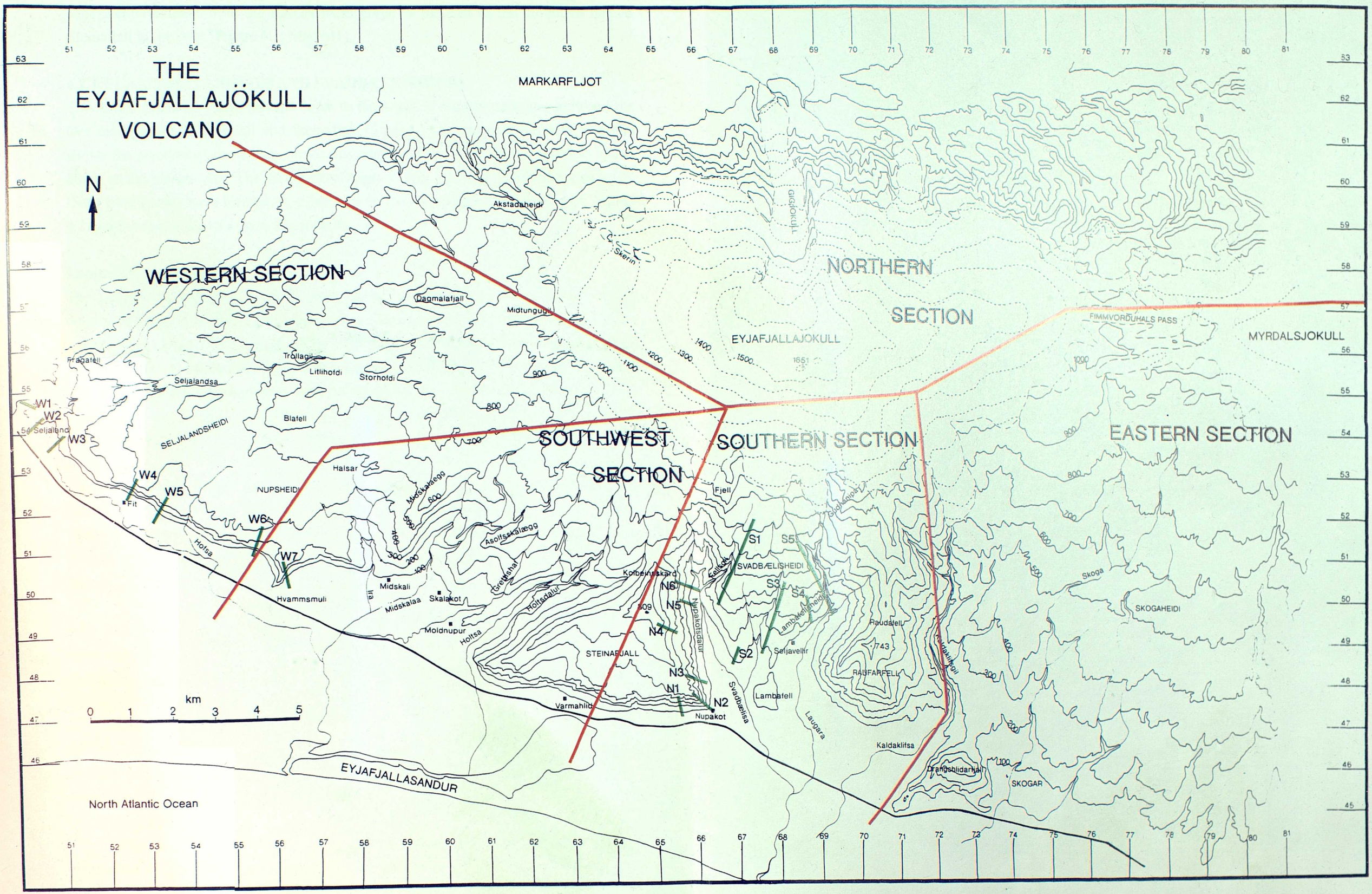

Figure 4.1 *Map of the Eyjaföll volcanic system showing place names and locations of lithostratigraphic profiles (Figures 4.3, 4.9 and 4.20).*

4.2.1 SOUTHERN SECTION

This section extends from the Kaldaklifsgil gorge in the east to the mountain named Steinafjall in the west (Figure 4.1; Map M1).

4.2.1.1 LAMBAFELLSHEIDI AND SVADBAELISHEIDI

This broad glaciated valley sweeps down to the south of the central crater between the two mountains of Raufarfell and Steinafjall (Figure 4.1). Terminal moraine at 600m shows the position of the icecap earlier this century which has since receded to above 800m at the present day. The valley base slopes gently down from 800m to sea level. Deep river gorges have formed on either side of the valley (Laugará to the east, Figure 4.2 and Svadbaelisá to the west, Figure 4.6).

Laugará (La) Group

The Laugará Group (profile S5, Figures 4.1 and 4.3) is comprised of basalts which outcrop in the lower 300m of Laugará gorge. These are the oldest rocks exposed in the volcano's core (Figure 4.2, Figure 4.24a). This Group was erupted during the Matuyama polarity epoch so most of the basalts are reversely magnetised. They comprise at least four thick (<75m) heterogeneous units of hyaloclastite, hyaloclastite breccia, pillow breccia and cube-jointed (on a centimetre to decimetre scale) or hackly-jointed basalt. The rocks are propylitised to at least zeolite facies by hydrothermal activity. Pore space in the hyaloclastite and vesicles and cavities in the lava are filled with secondary minerals such as zeolites (mordenite, phillipsite, chabazite and thompsonite) and calcite. Lavas are Ne-Hy normative and contain 10-20 vol% phenocrysts of olivine, clinopyroxene and plagioclase. The rocks have a green-brown colour but are stained red (hematite) at the margins of the numerous intrusive sheets (Figure 4.24). Despite their chaotic field appearance, the Laugará eruptive units are roughly flat-lying (Figure 4.2).

At the base of the Laugará gorge, 150m west of the old swimming pool (Figure 4.2), a heavily altered, fragmentary deposit contains numerous rounded gabbroic xenoliths . It is unclear to which group, if any, this deposit is related. It is cut by several populations of dykes so is probably closest in age to the Laugará Group. These xenoliths are described in section 5.4.

The Laugará Group outcrops continuously from the Laugará gorge and around the base of Raufarfell from sea-level to a height of roughly 300m. At Nupakôt, on the southeastern tip of Steinafjall, a short sequence of thin porphyritic basalts occurs with chemistry similar to that of the Laugará Group and is here termed Laugara subgroup La2 (e.g. Figure 4.24a).

The lowest lavas in this short sequence are Ne-normative and reversely magnetised. These are subaerial lavas with intercalated sediment (mostly hyaloclastite) suggesting a different eruption environment (more distal) or perhaps a different vent to those at the Laugará gorge.

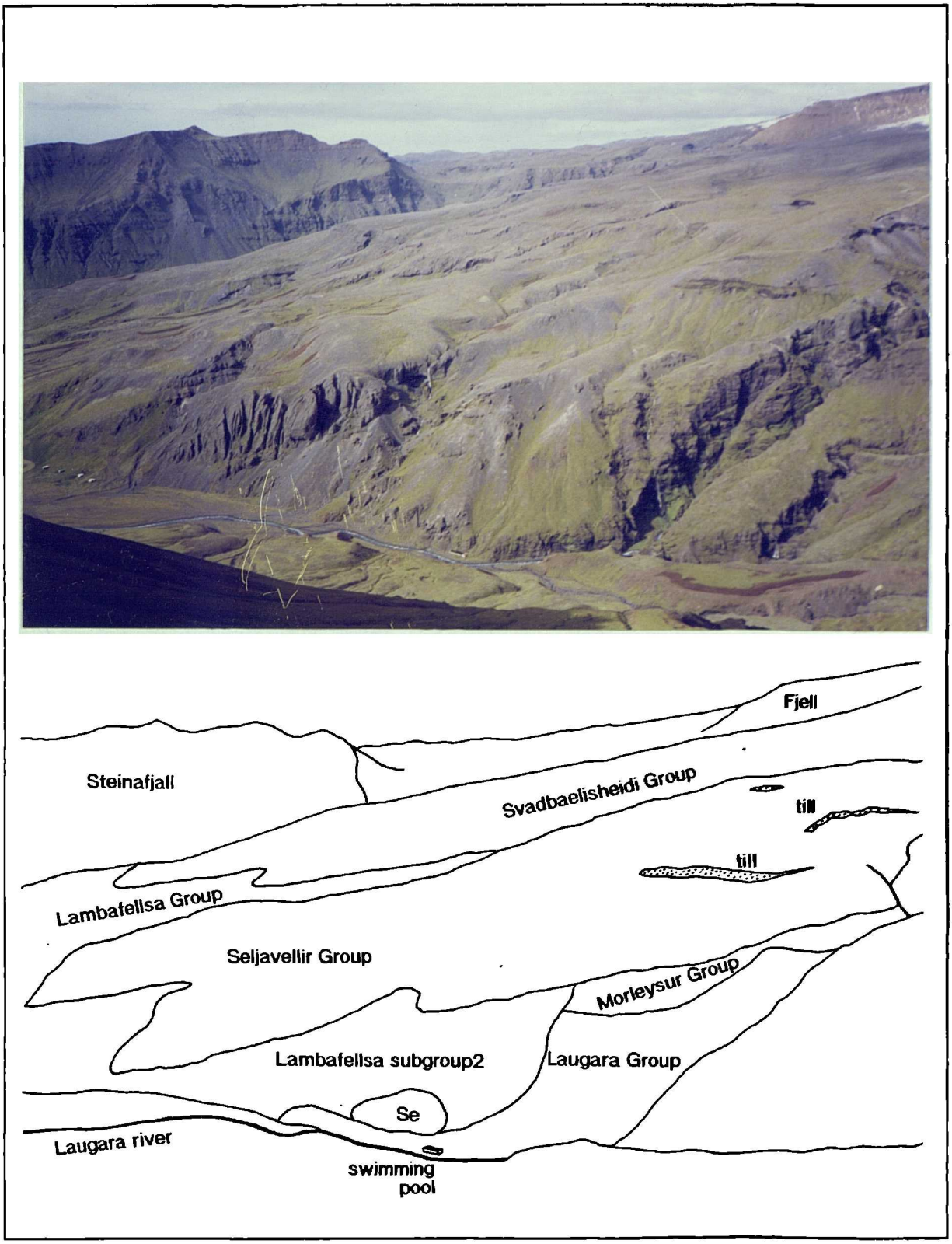

Figure 4.2 *Looking northwest across Lambafellsheidi and Svadbaelisheidi with the base of the Laugará gorge and the Laugará river in the foreground.*

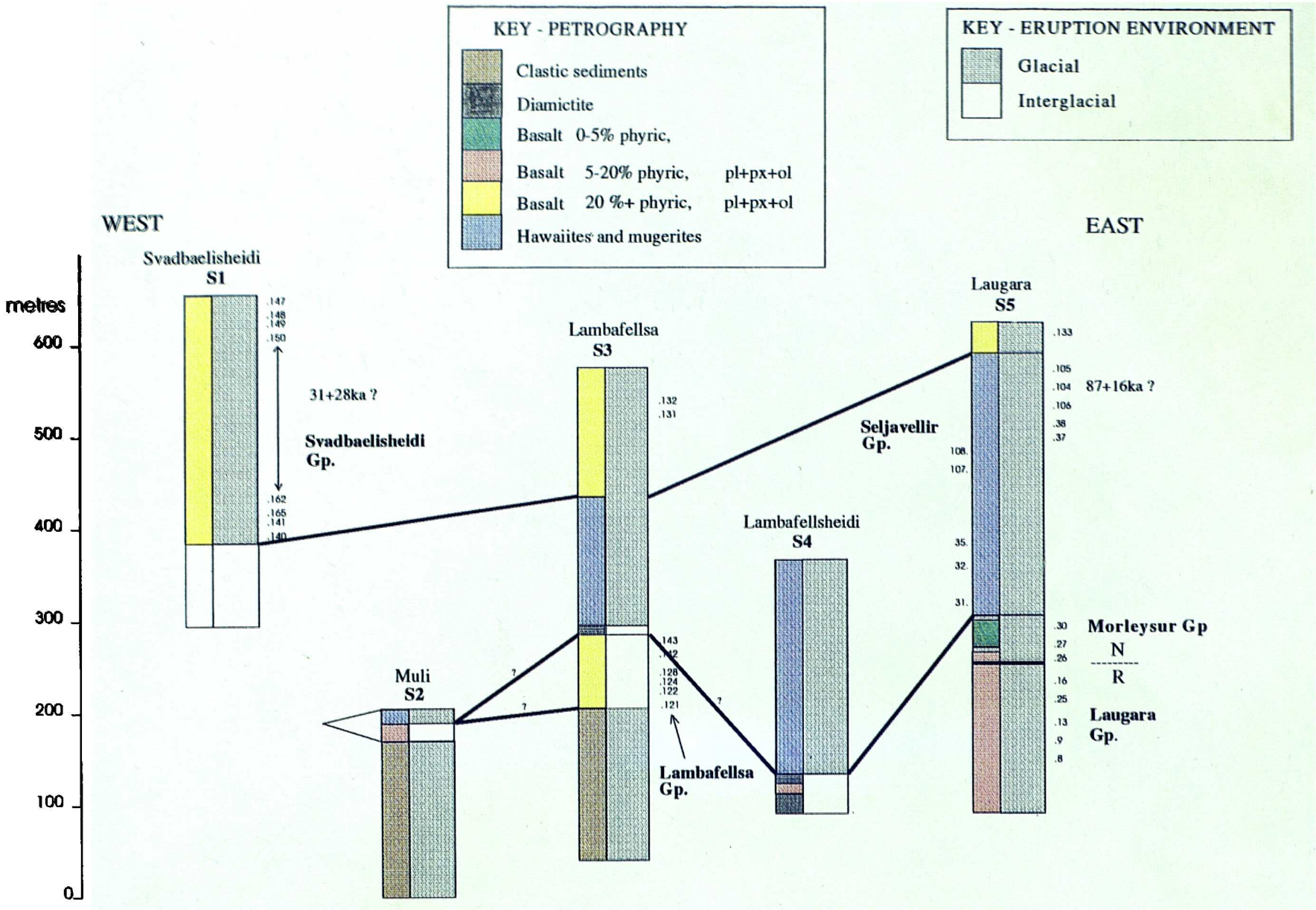

Figure 4.3 Profiles of Lambafellsheidi and Svadbaelisheidi with sample numbers to right of column, Brunhes/Matuyama boundary (N/R) and K/Ar dates (Wiese, 1992). For profile locations see Figure 4.1. These sections are projected onto a vertical plane so do not represent true thicknesses. Bold tie lines divide stratigraphic groups.

Morleysur (Mo) Group

Above the Laugará Group (above 300m) is a normally-magnetised, 15m thick sequence of hydrothermally altered hyaloclastite and a lava which are here termed the Morleysur Group (profile S5, Figures 4.1 and 4.3). The Morleysur Group lies unconformably on the Laugará Group (Figure 4.2). The lower lava (sample 26) is 5m thick and porphyritic wheras the coherent, dark, fine grained, aphyric lava (sample 27) is 2m thick. Both are more evolved than lavas of the Laugara Group and are anomalously rich in iron. This short sequence is unconformably overlain by valley-filling evolved basalts, hawaiites and mugearites (the Seljavellir and Lambafellsá Groups,

Lambafellsá (Ll) Group

The Lambafellsa Group (profile S3, Figures 4.1 and 4.3) comprises five thin, columnar, subaerial basaltic lavas with pillowy margins each intercalated with up to 15m of horizontally-bedded sediments. The lavas dip towards the southwest, presumably following the axis of a shallow palaeovalley. They contain up to 20% phenocrysts of plagioclase, pyroxene and olivine. This subaerial succession is unconformably overlain by both the Seljavellir Group and a thick, debris flow which is part of the Svadbaelisheidi Group (Figure 4.2, Figure 4.24a).

Lambafellsá (L2) Subgroup 2

On the lower slopes above Seljavellir, a 2m thick lava with pinkish weathering lies over at least 50m of deformed gravels and sands which are probably glacial outwash deposits (profile S4, Figures 4.1 and 4.3). The lava is columnar jointed, up to 2m thick, porphyritic and contains glomerophyric clusters of plagioclase, clinopyroxene and olivine up to 2cm in size. This lava appears to be related to the Lambafellsá Group containing columnar lavas intercalated with outwash sediments. Up to 6m of diamictite overlies this lava, it thins eastwards and is overlain by the Seljavellir Group (Figure 4.3).

Glacial outwash deposits

The Lambafellsá Group overlies a sequence of thick, horizontally-bedded volcaniclastics and reworked glacial material exposed in the lower reaches of the Lambafellsá stream (see Map M1, Figure 4.24a). There is a high glass content indicating that many of the sediments were probably syn-eruptional. These sediments are probably glacial outwash deposits and as they are palagonitised they must have been saturated with warm water during and after deposition.

Seljavellir (Se) Group

The gravels and sands, lava and diamictite on the lower slopes above Seljavellir are directly overlain by the Seljavellir Group (profiles S1 to S5, Figures 4.1 and 4.3). The

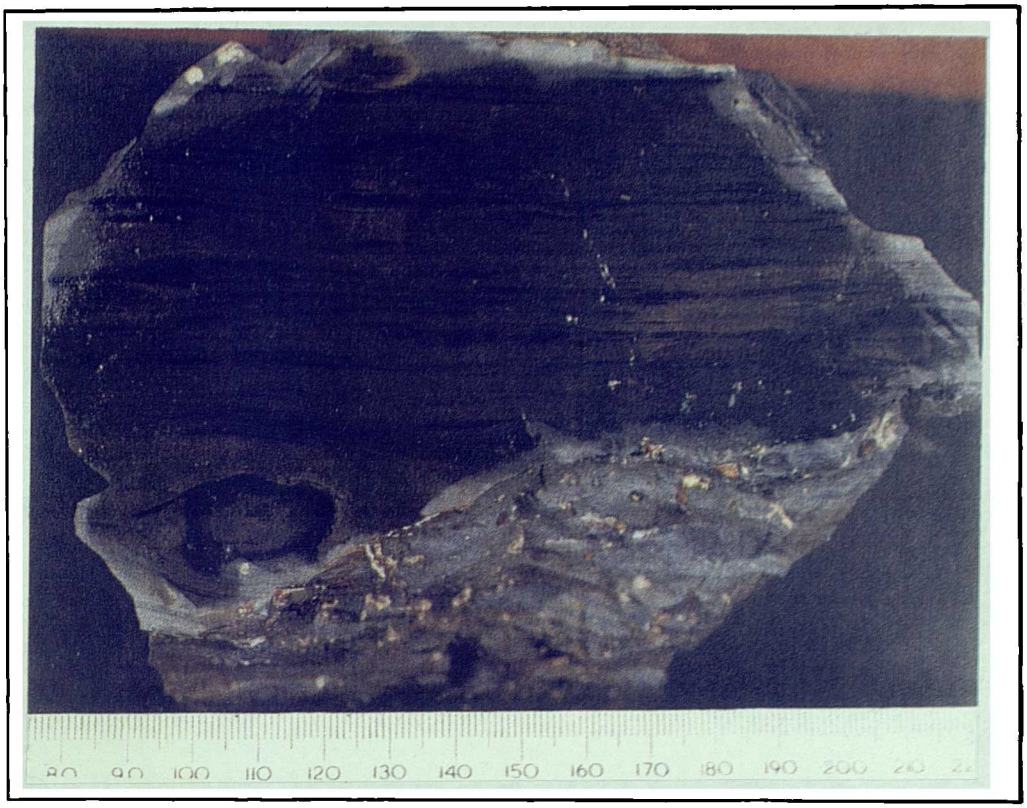

Figure 4.4 *Flow-banded hawaiite (sample 33-[6905 5035]) from the Seljavellir Group.*

Seljavellir Group consists of thick, evolved basalts which form the overhanging cliffs (lithofacies association H - Figure 4.24a) at Seljavellir (Figures 4.2 and 3.20). On higher slopes, these lavas form highly jointed 'tubes' of lava with a lozenge cross-section intercalated with hyaloclastite breccia (lithofacies association D). However, near sea-level, just above Seljavellir, the lavas lie on the steeply-dipping valley sides and form overhanging cliffs with a thin basal colonnade and a very thick entablature (lithofacies association H). Thick volcaniclastic and glacial deposits associated with these lavas are exposed on the hillside above the overhanging cliffs (Lambafellsheidi) and in the Laugará gorge between 400m and 500m altitude. The Seljavellir Group is not very extensive and only a few isolated outcrops (e.g. at Muli, sample 184) occur west of Lambafellsheidi.

The lavas of the Seljavellir Group are either flow-banded hawaiites (Figure 4.4), or laminar-textured mugearites.

Wiese (1992) dated columnar-jointed lavas which are probably members of the Seljavellir Group at 87±16Ka. An Alpine-style valley-confined glacier filled the valley at the time of their eruption extending from the icecap down to sea-level.

Lambafell

This small, isolated hill (Figure 4.1) has a distinct chemistry and all the features of a subglacial shield eruption. It is steep-sided, flat-topped and composed of hyaloclastite breccia and hyalotuff; some lavas occur on and near its summit, i.e. between 140m and 160m. It has a total volume of about 1km^3 and lies only 50m above the present sea

level. Wiese (1992) dated a lava from Lambafell at 54±15Ka, therefore glacial ice was at least 100m thick over Lambafell at this time.

Svaðbaelisheidi (Sv) Group

The Svadbaelisheidi Group (profiles S1,S3,S5, Figures 4.1 and 4.3)) is characterised by its numerous, large plagioclase phenocrysts which may occupy up to 30% of the rock; minor olivine also occurs. The group dips at about 20° to the south and southwest and outcrops on the Svaðbaelisheidi slopes between 700 and 150m above sealevel (Figure 4.2). Lavas on the higher slopes form thick, columnar flows; downslope and lower in the succession, thin compound lavas intercalated with horizontally-bedded volcaniclastics are dominant (Figure 3.3, Figure 4.24a). Above Nupakôtsdalur, the Svadbaelisheidi Group is exposed on the sides of Fellsgil gorge, where a thick basal unit of pillow lavas and radially-jointed feeder lobes occurs at an altitude of about 400m (Figure 4.5). The lavas here overlie glacial sediments. Further downslope, the Svadbaelisheidi Group becomes a tongue of chaotic palagonitised debris (Figure 4.6). This group is clearly transitional between a subaerial and subaqueous depositional environment. The upper slopes appear to have been subaerial however the lower slopes of Nupakôtsdalur were subaqueous. These lavas either flowed into a fjord-like environment during a period of very high sea level or into a thin valley-confined glacier. Field relationships show that these plagioclase-rich lavas formed *after* the evolved Seljavellir Group.

A debris flow exposed in the banks of the Lambafellsa river, above Lambafellsheidi, contains a variety of clasts including vesicular, aphyric fragments,

Figure 4.5 *Looking northeast into Fellsgil at pillows and irregularly-shaped pseudopillows at the base of the transitional subaerial-subaqueous Svaðbaelisheidi Group [667 505]. The Svadbaelisheidi Group overlies glacial sediments.*

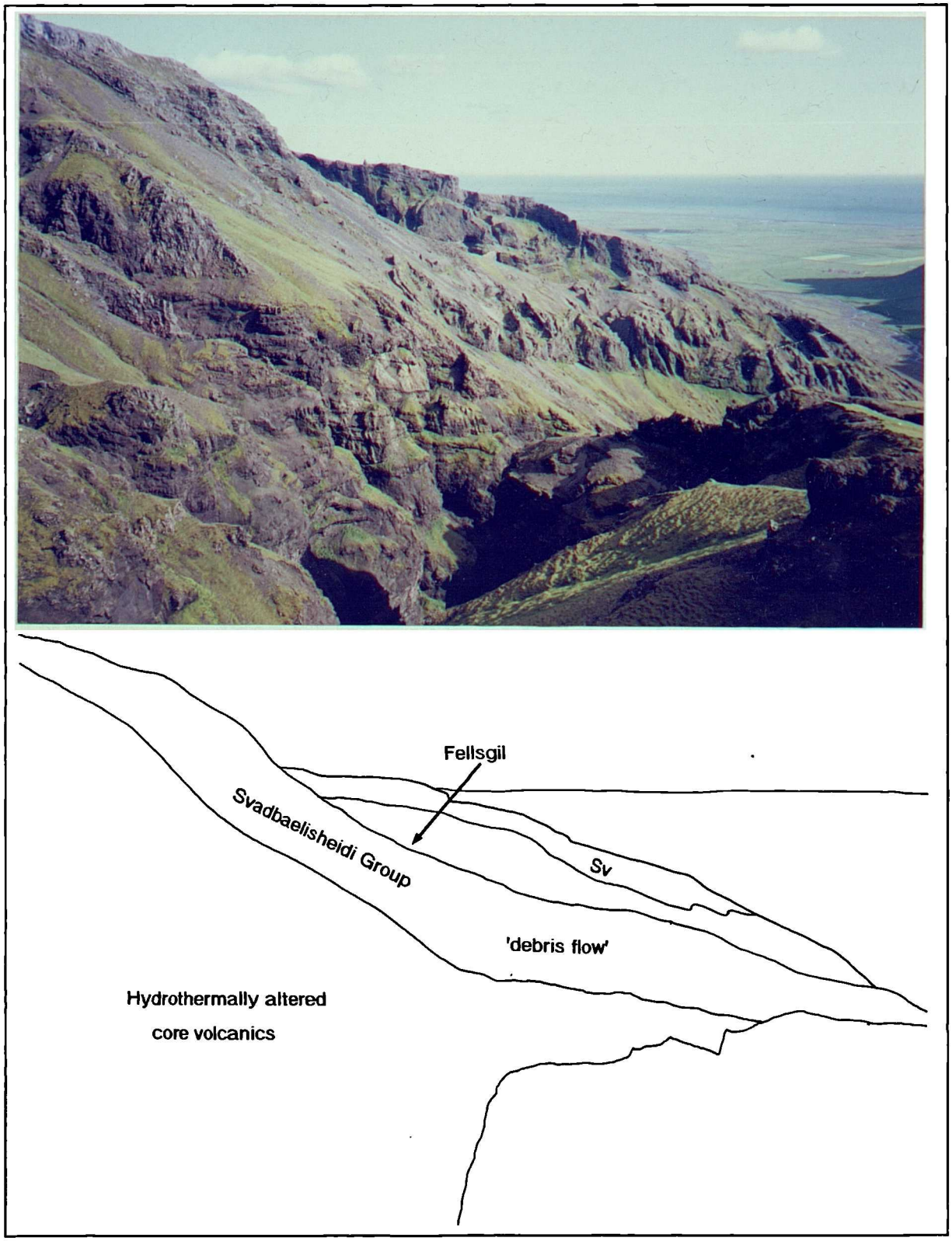

Figure 4.6 *Looking south from the core of the volcano into Nupakotsdalur. The foreground is composed of hydrothermally-altered lavas of the Nupakotsdalur Group which are cut by numerous intrusive sheets. The Svadbaelisheidi Group can be seen on the ridges on either side of Fellsgil gorge. Water-saturated lavas from this group have formed a debris flow in the centre of the photograph.*

highly porphyritic lavas and pumice-like clasts as well as a high proportion of vitric fragments (Figure 4.7). The debris flow dips southwest at 25° and also contains floating blocks of grey diamictite up to 10m long and 2m thick. Upstream, this debris flow is intimately associated with plagioclase-phyric hyaloclastite breccia, feeder dykes and lobes, suggesting that the debris flow was syn-eruptional with the Svadbaelisheidi Group. Inverse grading and fluid escape structures can be observed, suggesting rapid emplacement.

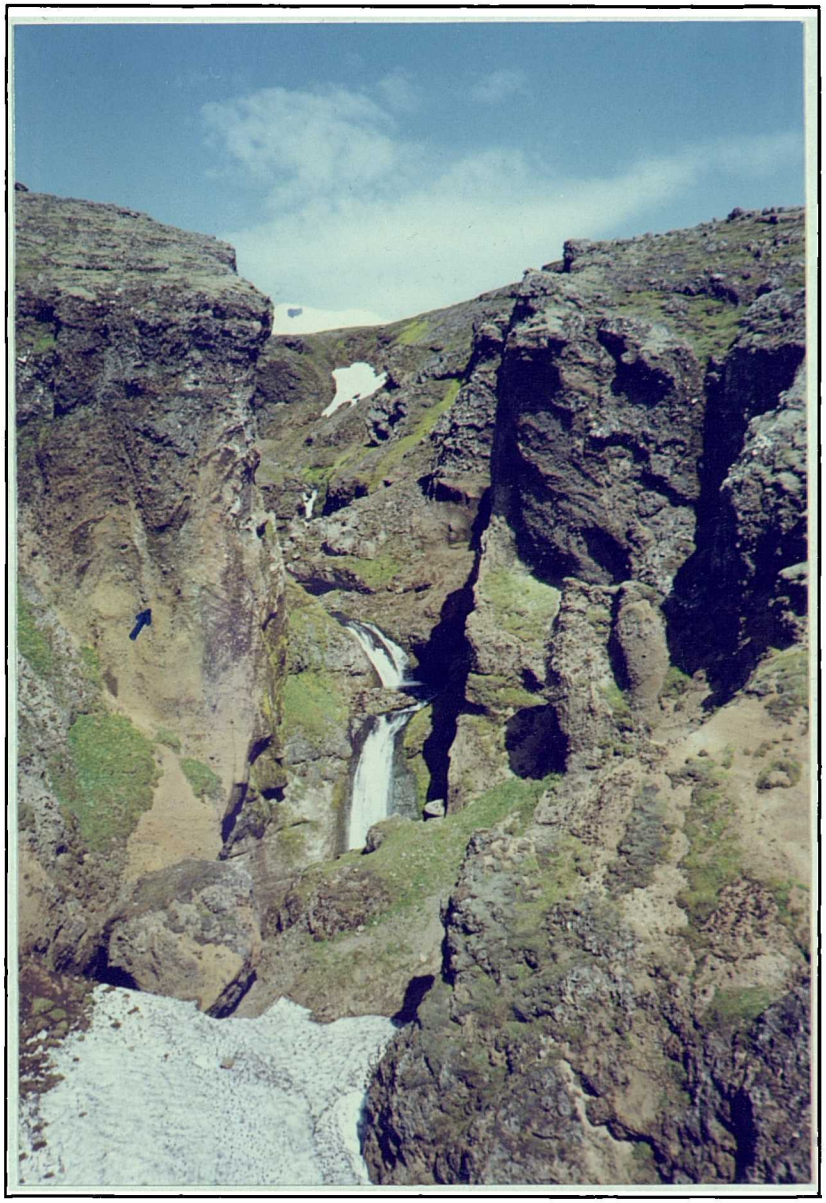

Figure 4.7 *Looking north at a syn-eruptional debris flow with water escape structures (arrowed), inverse grading and basalt feeders in Lambafellsá river at [681 507]*

Laugará trachyte

At the top of the Laugará river, right at the glacier margin, an outcrop of mixed lava occurs (Map M1). The host rock is quartz trachyte (sample 578) weathering reddish-pink and containing up to 40% of angular to rounded blue-grey mafic inclusions. The inclusions are from <1cm up to 75cm in diameter, the smaller clasts tending to be more rounded. Due to the abundance of loose glacial material in this area, field relationships

are difficult to distinguish. The deposit lies above evolved basalts which are probably members of the Seljavellir Group.

Loose fragments of another acid rock are found here (sample 579). Preferential weathering has given the rock the appearance of being an emulsion of dark round blebs in a pale matrix.

Fjell

Fjell, is a steep-sided NNE-SSW orientated ridge stretching south from the icecap (Figures 4.1, 4.2 and 4.8). It is dominantly composed of hydrothermally altered material cut by numerous intrusive sheets. On the eastern side of Fjell, thick eastward dipping ash deposits underlie a columnar trachyte flow which clings precipitously to the slope (Figure 4.8). It is possible that this flow filled a palaeovalley prior to recent glacial erosion. There are Fe-Ti basalt dykes cutting through the trachyte to feed more lavas above. These lavas appear to form a delta-type feature which thickens to the east. This succession is older than the Lambafellsa, Seljavellir and Svadbaelisheidi Groups, but younger than the Laugara Group. Wiese (1992) dated FeTi basalts from the summit of Fjell at 116±20Ka, although the precise field locality of these lavas is not clear.

Figure 4.8 *Looking east towards Fjell ridge showing the red trachyte flow overlain by eastward-dipping columnar Fe-Ti basalts [669 529]. Gullies in the trachyte show the position of numerous Fe-Ti basalt dykes feeding the overlying lavas.*

4.2.1.2 NUPAKOTSDALUR AND EASTERN STEINAFJALL

Nupakôt (Nu) Group

The Nupakôt Group includes the oldest exposed lavas in Nupakôtsdalur, the glacial valley between Svadbaelisheidi and Steinafjall (profile N6, Figures 4.1 and 4.9, Map M1). The lavas are porphyritic basalts with up to 20 vol% phenocrysts of olivine, clinopyroxene and plagioclase. The massive and columnar, discontinuous lavas are exposed at the stream junction at [659 505]. These lavas probably correlate with 20m of thin plagioclase-pyroxene phyric lavas, hyaloclastite breccia and reworked sediments (lithofacies asociation A) exposed at the Nupakôt section further to the south (profiles N1 and N2, Figures 4.1, 4.9, 4.10, 4.24a). Here, the base of the Nupakôt Group is marked by a discontinuous lens of massive redeposited hyaloclastite breccia overlain by grey diamictite and a thick unit of planar-bedded and cross-bedded volcaniclastics (Figure 4.10). This wedge of sedimentary material thickens to the south east and the planar-bedding is strongly suggestive of outwash/sheetflood deposits.

Nupakôtsdalur (Nd) Group

The Nupakôtsdalur Group is a distinctive and extensive Group (profiles N1 to N6, Figures 4.1, 4.9, 4.24a). The following is a description of the succession at profile N6 (Figures 4.1 and 4.9). The Nupakôt Group is overlain by up to 10m of highly porphyritic (<50%), massive, green-brown pillow hyaloclastite breccia containing aligned pillows and lobes comprising the basal units of the Nupakôtsdalur Group. Clinopyroxene phenocrysts up to 3cm across are common. A 2m thick matrix-supported diamictite containing rounded clasts up to 20cm in diameter interrupts the sequence of porphyritic basalts. Above the diamictite are further thick deposits (<40m) of highly px-ol-pl phyric (<40 vol%) clastic material, probably originally hyalotuff, containing discontinuous lenses of lava. The unit is heavily weathered, green-brown in colour and zeolitised. Above this is a further 20m of highly porphyritic, zeolitised pillow breccia, hyaloclastite and lava which in places has a distinctive crimson colour (Figure 4.11). One discontinuous lava sheet within this unit shows flow differentiation of phenocrysts suggesting that it was emplaced by laminar flow.

A highly porphyritic hyalotuff deposit in the valley bottom at [659 506] contains numerous gabbroic xenoliths with varying textures and modal mineralogy. Some clasts are angular, some rounded and most are no bigger than 12cm in diameter. There are patches of felsic material up to 1.5m across with diffuse margins within the tuff. The unit also contains skeletal clinopyroxene crystals up to 4cm in length (see section 5.4).

The Nupakotsdalur Group is cut by numerous inclined sheets. Nearer the core of the volcano the sheets are numerous and many appear to dip at a very low angle (Figure 4.6). However, on the western slopes of Nupakôtsdalur, most sheets trend roughly NE-SW and several are highly evolved (e.g. D169, D189, D213).

The Nupakôtsdalur group can be traced southwards to the Nupakôt section

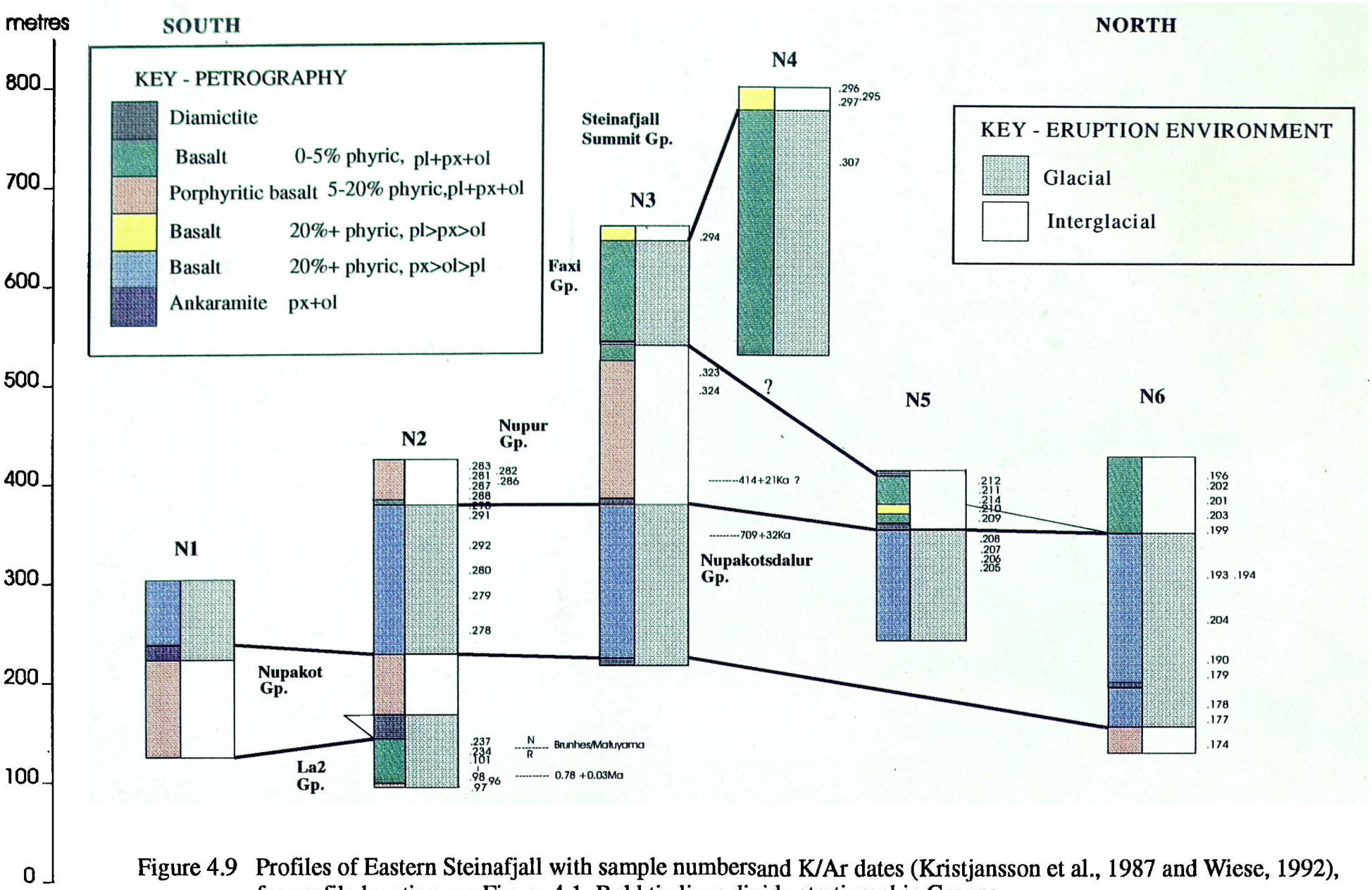

Figure 4.9 Profiles of Eastern Steinafjall with sample numbersand K/Ar dates (Kristjansson et al., 1987 and Wiese, 1992), for profile location see Figure 4.1. Bold tie lines divide stratigraphic Groups.

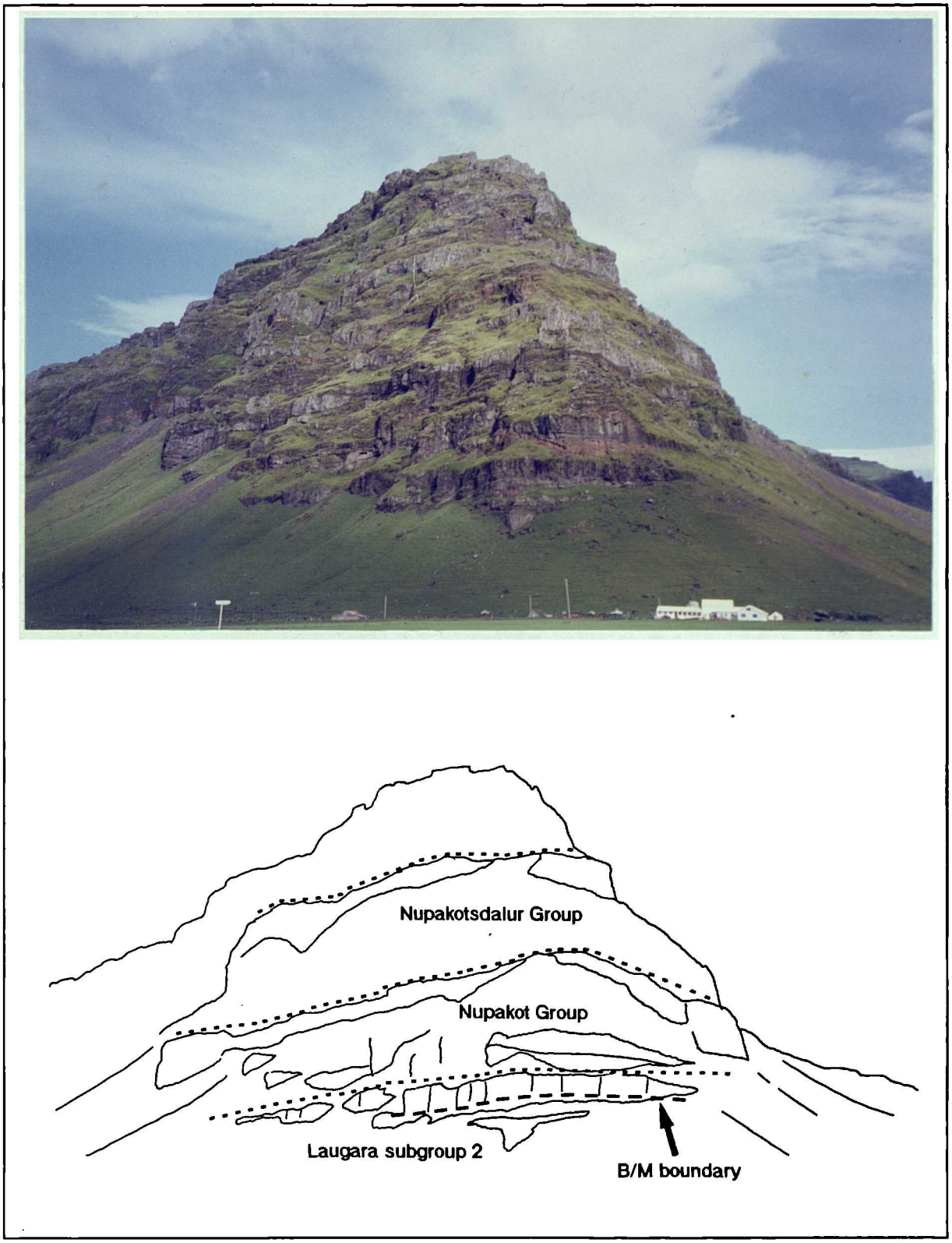

Figure 4.10 *Looking northwest at the Nupakôt section (profile N2: Figure 4.9) showing the Brunhes-Matuyama boundary (Kristjansson et al., 1988), the La2 subgroup, the Nupakôt Group and the Nupakôtsdalur Group.*

where the lavas are lensoid, crudely columnar, up to 40m thick and enveloped by volcaniclastic material. Wiese (1992) dated lavas within this group at 709±32Ka and 706±11Ka. The Nupakôtsdalur Group formed in subaqueous to subaerial conditions in

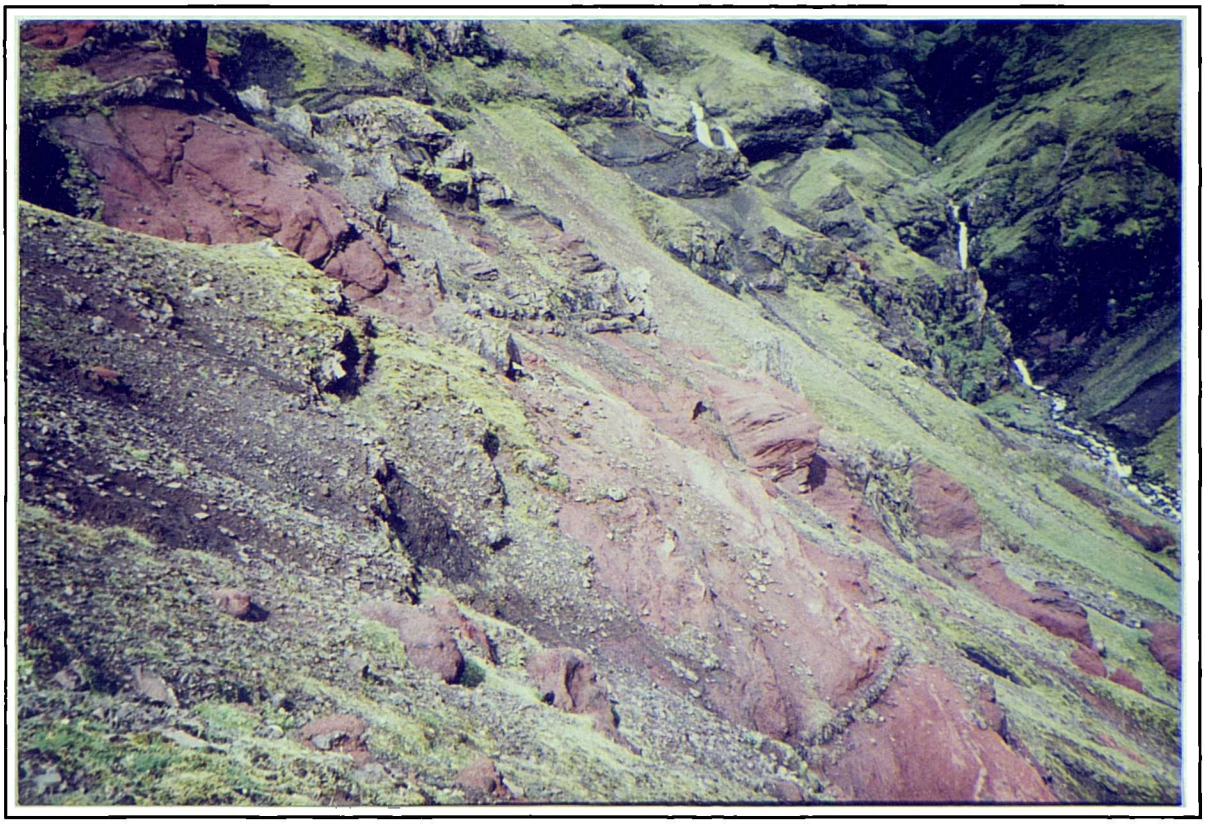

Figure 4.11 *Looking north at the lower reddened deposits of the Nupakôtsdalur Group (profile N6, Figures 4.1 and 4.9) [658 505]. The deposits shown in the photograph are approximately 100m thick.*

which the early stages of the eruption were dominated by phreatomagmatic activity whilst later or more distal stages of the eruption (at Nupakôt) may have been subaerial. The Nupakôtsdalur Group can be traced around the head of Nupakôtsdalur and into the deep gorge (Fellsgil) to the east of Nupakôtsdalur.

Basalt lavas

The Nupakôtsdalur Group is capped by a distinct weathered horizon (~20cm thick) above which lies a sequence of about 20m of hyaloclastite breccias and pillow breccias of largely aphyric basalts. These lavas are laterally discontinuous and occur above the Nupakôtsdalur Group in profiles 'N5' and 'N6' (Figures 4.1 and 4.9). They have variable chemistry, the lowest flows being particularly rich in iron and titanium. The top of the sequence is sharp, the evolved basalts are capped by a sheer face of redeposited hyalotuff with crude bedding (Faxi Group?) which is not represented on the profiles and is cut by subvertical, thin, sinuous dykes.

Nupur (Nr) Group

About one kilometer north of Nupakôt, a steep gully passes all the way to the summit of Steinafjall. In this gully, above the Nupakôtsdalur Group, is a major unconformity and a discontinuous horizon of diamictite (profiles N2 and N3, Figures 4.1 and 4.9). A

sequence of irregularly shaped lavas (lenses and sheets) with large volumes of intercalated redeposited volcaniclastics overlies the unconformity and is termed the Nupur Group (Figures 4.9, 4.10, 4.24a and Map M1). The lavas are almost all plagioclase and pyroxene-phyric, with 15% being the maximum proportion of phenocrysts. These *may* be the lavas dated by Wiese (1992) at 414±21Ka, unfortunately the precise location of the dated lavas is not clear. Two very thick, columnar lavas appear to flow down at an angle of about 10° to the north (samples 323 & 324).

The Nupur Group is overlain by 6m of diamictite on the north side of the gully, but elsewhere is directly overlain by the base of a massive hyaloclastite breccia. The Nupur Group appears to be largely subaerial, the lavas are discontinuous and may have erupted from vents at or near Steinafjall.

Faxi (Fa) Group

The hyaloclastite breccias overlying the Nupur Group are here termed the Faxi Group (profiles N3 and N4, Figures 4.1, 4.9, 4.24a, Maps M1 and M2). The Faxi Group overlies the Nupur Group lavas along the eastern slopes of Steinafjall and thickens to the north above Nupakotsdalur. Beneath the summit of Steinafjall, it almost certainly thickens westwards and is part of the thick deposits which make up western Steinafjall. Above the farm of Varmahlid on the south side of Steinafjall, a distinct, westward-dipping unconformity truncates the the thick lavas of the Nupakôt sequence (Figure 4.12). It appears that this unconformity marks the base of the Faxi Group. Below this horizon and to the east (Nupakôt), Steinafjall is dominated by a succession of thin lavas and intercalated reworked volcaniclastics (Figure 4.10); above this horizon and to the west, thick deposits of hyalotuff and hyaloclastite are dominant (including lithofacies association C, Figure 4.24a) indicating deposition in a subglacial environment. This unconformable contact appears to mark the eastern margin of a large, southwesterly trending palaeovalley which at one time contained a glacier.

The deposits of western Steinafjall are thus younger than the Nupakôtsdalur Group and the Nupur Group (Figure 4.24a), it is proposed that these subglacial deposits fill a time gap found by Wiese (1992) in the eastern Steinafjall stratigraphy. This is an example of topographic inversion where only one margin of the glacial valley deposits has been subsequently eroded. This western eroded margin is now a glacial valley itself, known as Holtsdalur (Map M2).

The occurrence of volcanic assemblages such as lithofacies association C and the present altitude of the deposits suggests that the Faxi Group was erupted in a subglacial environment. The thick, volcaniclastic assemblages are nevertheless intercalated with subaerial lavas suggesting that the ice margin may have retreated, or alternatively, that late stages of an eruption became subaerial due to the volume of ice melted. The presence of these subaerial lavas has ensured the preservation of the underlying clastic deposits.

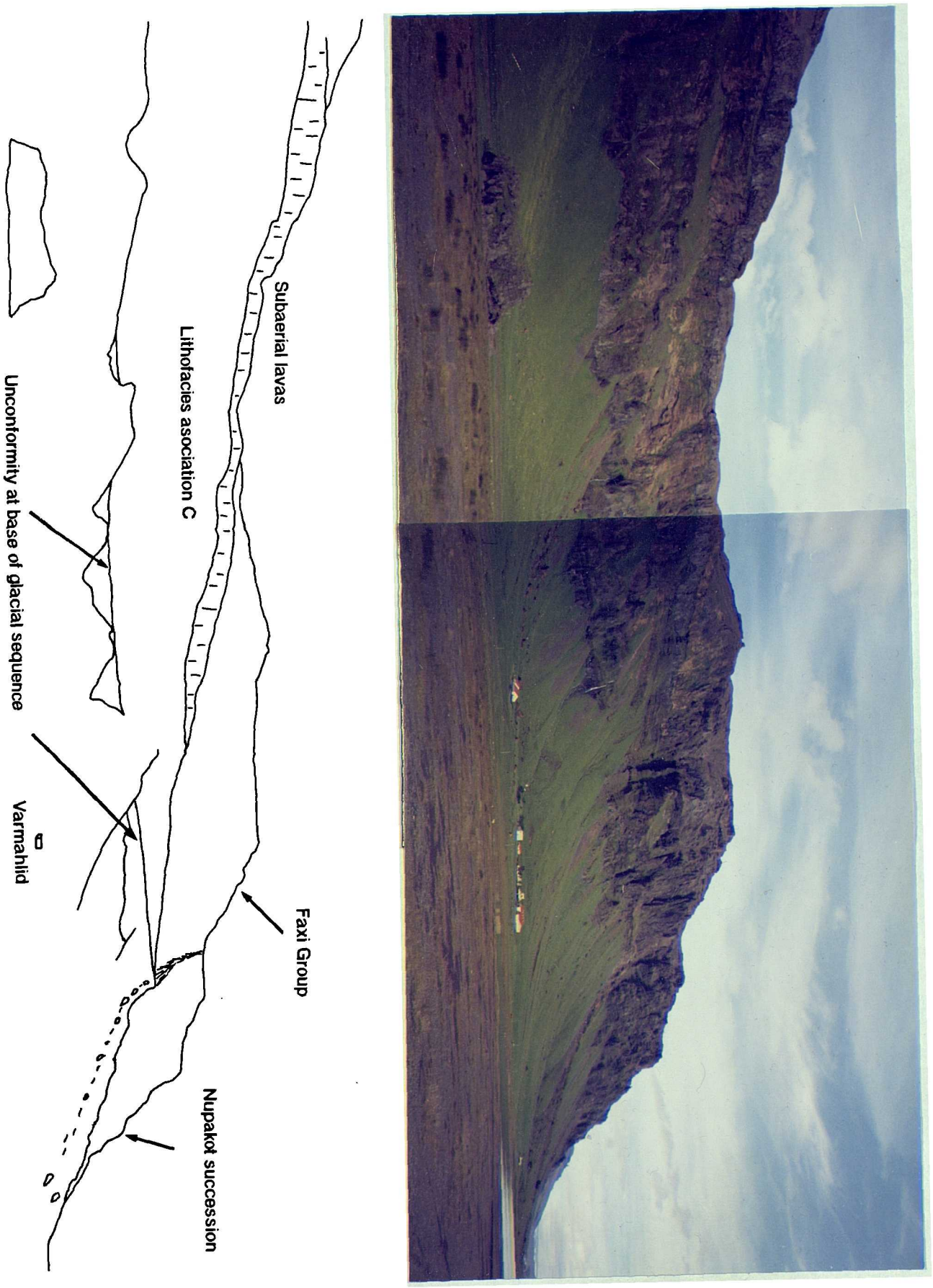

Figure 4.12 *Looking northeast at the unconformity above Varmahlid [630 477]. This unconformity marks the eastern margin of a (glaciated) palaeovalley, the western margin of which is exposed in Holtsdalur (Figure 4.13).*

Steinafjall Summit (Sg) Group

The summit of Steinafjall itself is a scoria cone composed of highly porphyritic (<30%) plagioclase and pyroxene phyric lava, which also contains several glomerophyric clusters (profiles N3 and N4, Figures 4.1 and 4.9, Maps M1 and M2). East of the summit of Steinafjall, is a porphyritic compound lava which has flowed down into Nupakôtsdalur. The lavas are coherent at the top of the slope, but the lowermost lavas become cube-jointed and hackly-jointed as if they have flowed into water/ice at about 300m altitude. These lavas appear to be fed by fissures with a ENE-WSW orientation. Lavas at the top of the Nupakot succession are also highly porphyritic.

These successions show that *at least* three major glaciations occurred during the formation of Steinafjall and Nupakotsdalur. Table 4.3 (p.120) arranges the stratigraphic Groups in age using some of the K-Ar dates of Wiese (1992) as a guide.

4.2.1.3 RAUFARFELL AND RAUDAFELL

The entire volcanic pile of which Raufarfell is composed can be divided into three major parts: a) lower plagioclase-pyroxene-olivine phyric massive breccias and lavas (**Laugará Group**), b) a sequence of redeposited hyalotuff and hyaloclastite intercalated with aphyric or sparsely phyric basalts (**Raufarfell (Rf) Group**), and c) the uppermost plagioclase and plagioclase-pyroxene phyric lavas intercalated with redeposited hyalotuff and hyaloclastite (**Raudafell (Rd) Group**), (Figure 4.24a, Map M1). There are also sparse outcrops of intermediate rocks on the summit fed by radial dykes.

The lower lavas on the western and southern slopes of Raufarfell are petrographically and chemically similar to the Laugará basalts, i.e. plagioclase-pyroxene-olivine phyric. Much of this lower sequence is composed of massive, altered pillow hyaloclastite breccias of green-brown colour, with discontinuous sheets and lenses of massive, columnar and/or pillowy lava (Figure 3.9). They are reversely magnetised (Jonsson, 1988), but are not as heavily altered as the basalts in and around Laugará gorge. Although these basalts contain a high proportion of intrusive sheets, they are not as abundant as in the core of the volcano and the sheets also tend to be thicker (<1.5m). This group of lavas and hyaloclastite is up to 300m thick on the south side of Raufarfell and the top is marked by a distinct unconformity. The Raufarfell and Raudafell Groups are distinctive as they are dominated by yellow-orange, horizontally-bedded hyalotuff, intercalated with sheets and lenses of lava; they are clearly exposed on the south side of the mountain however the western and northern slopes are steep, covered in scree and poorly exposed. Clearly these tuffs have a subaqueous origin and were deposited mainly by running water. There is a lack of coarse-grained polymict sediments. The Raufarfell Group is composed of aphyric and sparsely porphyritic lavas which are both subaerial and subaqueous, interspersed with bands of reworked hyalotuff, hyaloclastite or cinders. These sequences were probably deposited near the margin of a glacier. There appears to be more coherent lava to the east and more

hyalotuff/hyaloclastite to the west. Lithofacies associations A and C occur here presenting some evidence for glacio-fluvial and subglacial tunnel deposition. A 2m thick horizon of diamictite separates the Raufarfell Group from the Raudafell Group of plagioclase-phyric basalts and plagioclase-pyroxene phyric basalts. The Raudafell Group again shows more coherent lava to the east and on the summit of Raufarfell; along the ridges and upper western flanks of the mountain thick clastic assemblages of hyalotuff and hyaloclastite closely associated with hyaloclastite breccias and diamictite occur, often with chaotic bedding. These deposits have the appearance of glacial deposits in which the chaotic bedding may be due to shearing caused by movement of ice or melting of ice blocks incorporated in the sediments. There are also horizons of reworked, cross-bedded hyalotuff containing isolated pillows and lava blocks (Figure 3.5).

The northwestern slopes of Raufarfell are poorly exposed but at 300m and above, steeply dipping sheets of lava outcrop on the hillside. Their strike and dip vary from 008/45W and 180/76W on western slopes to 030/60W on the northwestern slopes. These sheets are all of different mineralogy, from ankaramite and plagioclase-pyroxene phyric lavas to aphyric lavas and yet they occur at the same orientation within metres of one another. There is no evidence of chilling at the sheet margins. It is proposed that these lavas erupted from a vent near the summit of Raufarfell and flowed down steep valley sides, hence the variable strike.

4.2.2 SOUTHWESTERN SECTION

This section extends from Steinafjall in the east to Hvammsmuli in the west. A reconnaissance map of part of the area (M2) may be found in the back pocket.

4.2.2.1 HOLTSDALUR

This glaciated valley contains the river Holtsá which runs to the west side of Steinafjall. The western flanks of Steinafjall are composed of thick (<50m), reworked hyalotuff/hyaloclastite breccia deposits with thin, intercalated lavas (Faxi Group - Figure 4.24a). These deposits dip at about 15° to the SSW and form thick sheets (<75m) which can be traced round the west and north sides of Steinafjall. To the north of Steinafjall, tributaries to the Holtsá have cut deep gorges through thick basal tuff deposits (lithofacies association J). On the east bank of the Holtsá river a 4m thick diamictite horizon crops out dipping at about 30° to the east *beneath* these thick tuff deposits (Figure 4.13).This horizon defines the western margin of a glacial palaeovalley in which the thick, massive tuffs and breccias of Western Steinafjall were deposited during a glacial period. The eastern margin of the palaeovalley is exposed in the cliffs above Varmahlid. The thick deposits exposed in the Holtsa gorges may represent early volcanics formed beneath thick ice. The reworked deposits of which the upper parts of western Steinafjalll are composed may represent volcanics and lavas deposited during

Figure 4.13 *Looking northeast into the upper parts of Holtsdalur. The eastward dipping diamictite horizon (X - X') marks the western margin of a palaeovalley within which much of western Steinafjall was deposited. The diamictite is up to 4m thick. Steinafjall summit is indicated by an arrow.*

thinning of the same valley glacier towards the close of the glacial period.

Cropping out on the west side of Steinafjall is a very thick ponded lava flow which has a thin columnar base 1-2m thick and an entablature up to 100m thick (Figure 4.14). This flow clings to the valley side, its columnar base dipping at about 40° to the SE. Evidence suggests that this lava has flowed from the upper levels of Steinafjall down into the sides of a glacier occupying Holtsdalur where it has 'frozen' (lithofacies association H). This must have occurred during the last glacial period.

Kolbeinsskard Trachyte

At the very top of Holtsdalur (at Kolbeinsskard), immediately north of the summit of Steinafjall is an outcrop of trachyte (sample 566) lying on a saddle. The outcrop is reddened by weathering and shows flow banding and folding (Figure 4.15). Sparse, small clasts (<6cm) of vesicular, more mafic lava occur within the trachyte and thin mafic dykes (<40cm thick) cut the outcrop with a strike of 060°. The age of this trachyte is difficult to assess, its highly eroded nature and isolated position suggest that it has been subjected to glaciation, but it is probably no older than the last interglacial period.

Figure 4.14 *Looking east from Midskalaegg to Steinafjall. The gorge to the bottom left is the Midskalaa gorge, the valley in the middle distance is Holtsdalur.*

Figure 4.15 *Looking west at the flow banded trachyte at Kolbeinsskard, north of Steinafjall [649 510].*

4.2.2.2 ASOLFSSKALAEGG

This is the area between Holtsdalur to the southeast and Midskalaegg to the northwest (Figures 4.14 and 4.24a). Asolfsskalaegg itself is a hill and ridge surrounded by gentle glaciated slopes. The geology here is complex and field relationships were difficult to distinguish as a result of poor exposure.

Moldnupur (Md) Group

The lowest outcrops in this area occur in the Grettishaf stream valley to the southeast of Asolfsskalaegg. The lavas and sediments exposed are here termed the Moldnupur Group (Map M2, Figure 4.24a). The basal lava is dense, fine-grained and blue-green with microphenocrysts of pyroxene and plagioclase; it weathers to a pink crust. Above this is a discontinuous unit of sparsely porphyritic lava (<2% phenocrysts) which grades into hyaloclastite breccia in places. The nature of the contact between this and the basal lava is unclear. The upper 30cm of this deposit is a glass-rich gravel with fragments < 30mm in size and cemented by brown and yellow banded palagonite. This is overlain by a discontinuous layer of conglomerate up to 30cm thick containing rounded and striated blocks <25cm in size of the same sparsely porphyritic lava set in a gravelly matrix. This grades upwards into the brecciated and pillowy base of the overlying porphyritic lava. Where there is no basal conglomerate, this porphyritic lava (10% phenocrysts) intrudes

down into the glass-rich top of the lower hyaloclastite breccia in lobes. The lava is discontinuous and occurs within thick, massive hyaloclastite breccias. It is overlain by 30-40cm of horizontally-bedded sands and gravels followed by 4m of matrix-supported diamictite showing normal grading and supporting boulders up to 2m across. The diamictite clasts include aphyric to porphyritic types.

Just 50m to the east of this succession is a similar but more complex stack of deposits. At the base of this succession, beneath the Moldnupur Group a lens of plagioclase-phyric basalt occurs which is vesicular and reddened and probably subaerial. This lava has a glacially polished surface with striations aligned E-W and it is overlain by till. The till is 3m thick and in its uppermost 60cm, contains glassy fragments and appears pink. It has an irregular contact with the overlying hyaloclastite pillow breccia (base of the Moldnupur Group) into which it intrudes as flame structures and sedimentary dykes. Clasts from the diamict are also entrained in the base of the hyaloclastite pillow breccia. The breccia is sparsely porphyritic and corresponds to the sparsely porphyritic deposit by the Grettishaf stream. It is unconformably overlain to the east by a lens of coarse conglomerate/boulder bed which corresponds to the diamict in the Grettishaf stream section. This sequence appears to form the oldest deposits in this area. It is probable that these deposits are older than the Western Steinafjall subglacial deposits but poor exposure means that there is no field evidence for such a hypothesis.

All the eruption units and clastic deposits in the Moldnupur Group dip at about 20° to the ESE. Deposition probably occurred in a palaeovalley judging by the large quantity of diamictite and other clastic lithologies. Most lavas are coherent suggesting that the valley was subaerial.

Grettishaf (Gr) Group

The diamictite overlying the Moldnupur Group is overlain conformably by a 15cm thick unit of massive red-brown gravel containing angular lithic and hyaloclastite fragments (lithofacies association G) at GR [605 495](Figure 4.24a). This grades up into an ankaramite lava flow containing up to 40% by volume phenocrysts of olivine and pyroxene in equal proportions (sample 498). The gravels may have been tephra deposits homogenised by deposition of the thick overlying (water saturated?) lava. The ankaramite lava is blocky to pillowy with little associated hyaloclastite breccia, it dips at about 10° to the south west. However, 1km to the north, on the western valley sides of Holtsdalur, the ankaramite is at least 50m thick. It is composed of fragmentary deposits near its base and several thin vesicular ankaramitic flows near its upper contact. The ankaramite is overlain by a discontinuous, massive, aphyric, laminar-textured lava which weathers to red-pink (sample 500). These two lava types make up the Gretishaf Group.

The Grettishaf Group is unconformably overlain by <0.5m of conglomerate containing ankaramite, aphyric and sparsely phyric cobbles.

Skalakot (St) Group

The plagioclase/pyroxene phyric pillow breccias and thin (0.5-2m thick) vesicular lavas of the Skalakot Group cover much of the hillside (Map M2, Figure 4.24a). Where exposed, the base lies on the conglomerate overlying the Gretishaf Group. The lavas and breccias of the Skalakot Group contain <30% by volume phenocrysts of plagioclase and pyroxene in the proportions 9:1; phenocrysts are <7mm in size. They are overlain by 1m of eastward-dipping diamictite which was deposited during the last glacial period and covers the western slopes of Holtsdalur. These lavas were therefore deposited at least before the onset of the last glacial period, probably during the last interglacial period. Plagioclase-phyric lavas occur widely in this area, but glaciation and poor exposure make the mapping of field relationships very difficult.

The lower southern slopes of the Asolfsskalaegg ridge are poorly exposed. A sequence of eight thin plagioclase-phyric lavas occurs towards its base capped by a thin diamictite containing numerous plagioclase-phyric clasts. These lavas are also believed to belong to the Skalakot Group (see Map M2).

Basalts of unknown affinity

The Skalakot Group is overlain on the Asolfsskalaegg ridge by a series of dark grey, aphyric to sparsely porphyritic lavas and hyaloclastite breccias. The ridge top is composed of plagioclase and pyroxene phyric hyaloclastite breccia, dipping 20° to the south. This unit *overlies* the massive basal hyaloclastite breccia of the Asolfsskalaegg Group.

Asolfsskalaegg (As) Group

The top of the Asolfsskalaegg ridge is largely composed of a 50-70m thick succession of thin (<2m), vesicular, highly porphyritic basalts (Figure 4.24a) containing 40-60% phenocrysts of pyroxene (<20mm) and olivine (<10mm) with minor plagioclase (<8mm). These lavas are dated by Wiese at 129+20Ka, i.e. they erupted during the last interglacial period. The lower 10m of the succession is dominated by hyaloclastite breccias. The lavas have a purple-brown weathered surface and look initially like ankaramites.

Midskalaa Gorge

West of Asolfsskalaegg, the Midskalaá river enters a deep gorge cut into thick deposits of hyalotuff and hyaloclastite breccia thought to be subglacial deposits. The gorge is cut by several E-W ankaramitic and porphyritic basalt dykes. Northwest of Asolfsskalaegg, the river cuts through a succession of small, valley-confined subglacial flows each with a base of diamictite (lithofacies association E, Figure 4.24a). The flows vary from massive lavas with lobate pillowy margins to flows of hyaloclastite breccia. The petrology of each flow is distinctive, from 60% by volume phenocrysts of plagioclase,

pyroxene and olivine to aphyric. These deposits are older than the Asolfsskalaegg and Skalakot Groups.

Correlation of deposits in this area is difficult due to poor exposure and glaciation. It is clear however, that ankaramites and highly porphyritic olivine and pyroxene-rich lavas are intercalated with a sequence of dominantly plagioclase-phyric lavas showing that these highly olivine and pyroxene phyric deposits, the true ankaramites in particular, are not confined to the basal parts of the succession.

4.2.2.3 MIDSKALAEGG AND HALSAR

Between Asolfsskalaegg and the next major headland to the west, Hvammsmuli, is a ridge known as Midskalaegg (Figures 4.1 and 4.24a), composed of thin, discontinuous sheets and lenses of lava intercalated with redeposited palagonitised volcaniclastics. The Irá stream flows along the western side of Midskalaegg to the coast. The lowest 100m of this section is exposed between the Irá and Midskali farm at [583 506] and includes horizontally-bedded sands and gravels, diamictites and reworked hyaloclastite and hyaloclastite breccias, with intercalated diverse lavas. The basal unit is composed of about 4m of highly altered and zeolitised hyaloclastite pillow breccia which is massive with reworked horizons towards the top. It contains <20% phenocrysts of dominantly plagioclase with pyroxene and olivine. This is overlain by up to 7m of sediments, the basal units are cross-bedded sands and gravels with pebble lags, overlain by 1.5m of horizontally-bedded sands then a succession of thin graded sand and gravel beds < 20cm thick and then at least 1m of massive matrix-supported gravels. Clasts in these sediments are all highly zeolitised, altered basalts with phenocryst of plagioclase, pyroxene and olivine in varying abundancies. The sediments are overlain by another cube-jointed, zeolitised lava flow. There follows a series of lavas each < 3m thick intercalated with up to 2m of horizontally-bedded hyaloclastite, cinders or diamictite. These are all highly altered and each has distinctive properties; they are all massive and vesicular. Ankaramites occur towards the top of this sequence. There are three subaerial flows, separated by horizons of cinders, the largest is 4m thick. These *may* correlate with the subaerial ankaramites of the Grettishaf Group and the ankaramites at Hvammsmuli.

The ankaramites are overlain by thick (<70m) hyaloclastite breccia and hyalotuff deposits which are exposed in the Ira gorge along with a multiple sinuous dyke striking roughly at 070° (Figure 4.16). The dykes cut the entire hyaloclastite breccia including the upper 2-3m of stratified sands. It is unclear if the dyke is a feeder for this deposit. However, as the dyke contains 50% phenocrysts, by volume, (in which plagioclase is the most abundant followed by pyroxene and olivine), whilst the breccia contains only <10% microphenocrysts (of plagioclase and pyroxene), the two are probably unrelated. East of the stream, Midskalaegg rises up to a height of 713m. It is composed of a

Figure 4.16 *A multiple dyke with strike 070°cuts the Irá stream [583 507]. The band of orange, reworked hyalotuff at the top of the gorge is 2m thick (arrowed).*

stacked sequence of reworked hyalotuffs, hylaoclastite and thin lava flows. The eastern side of Midskalaegg is a steep, almost vertical drop down into Midskalaá. Dykes cut the sequence trending E-W to SW-WSW, the beds in the stacked volcanic sequence dip at 10° to the NW.

Following the Irá up to Halsar at [582 533], a sequence of at least ten lavas, which form broad sheet flows over much of the upper flanks of the volcano, is exposed. These lavas are highly porphyritic and vesicular, although the exact proportion of phenocrysts varies between 25% and 75%; the phenocrysts are plagioclase, pyroxene and olivine in decreasing order of relative abundance. Cognate gabbroic nodules are common in these highly porphyritic lavas. The lavas erupted from radial fisssures high on the volcano's flanks during an ice-free period. They have glaciated surfaces but are very fresh. It is proposed that these lavas erupted during the last interglacial period (Table 4.2)

4.2.2.4 HVAMMSMULI

Hvammsmuli Ankaramite

At Hvammsmuli, there is an extensive outcrop of ankaramite previously described by Steinthorsson (1968), (Figure 4.19 and profile W2, Figure 4.20). The major part of this locality is composed of massive, pale grey, granular to subophitic, porphyritic (<40%) ankaramite containing phenocrysts of olivine, pyroxene, magnetite and rare plagioclase.

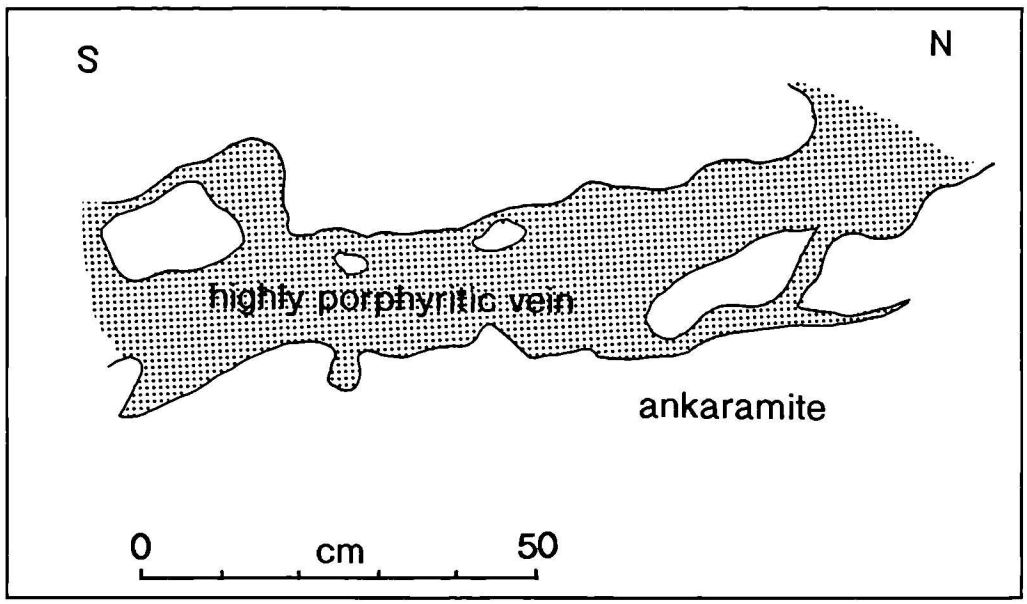

Figure 4.17 *Field sketch of intrusive phenocryst-rich veins in the Hvammsmuli ankaramite.*

Figure 4.18 *A sample of the subaerial ankaramite lava (sample 43) which overlies the Hvammsmuli ankaramite at [558 504].*

The ankaramite has been dated at 587±31ka by Wiese (1992), so although these rocks occur at the base of this succession they are not the oldest rocks at Eyjafjöll. The ankaramite is intruded by a 'dyke' of highly vesicular 'frothy' material (<1.5m wide) containing smaller phenocrysts. This intrusive body has rather diffuse sinuous margins accompanied by margin parallel joints in the country rock and there is no chilling. There are xenoliths of aphyric lava within the ankaramite. Some of these clasts are lensoid and aligned (Steinthorson 1968), they are fine grained with a laminate texture. Thin (<5cm) intrusive veins of highly porphyritic (<90%) material cut through the ankaramite,

incorporating clasts (Figure 4.17). These outcrops are overlain by at least 2m of bedded red and grey cinders and ash containing a large proportion of olivine and pyroxene phenocrysts, but no plagioclase. There is a thin, reddened lava flow associated with these cinders (Figure 4.18) which has the same chemical signature as the underlying ankaramite. The entire complex is over 50m thick and covers an area 300x400m. Steinthorsson interpreted this ankaramite outcrop as a sill complex. In this study, petrological evidence suggests that this was a lava lake (Chapter 5).

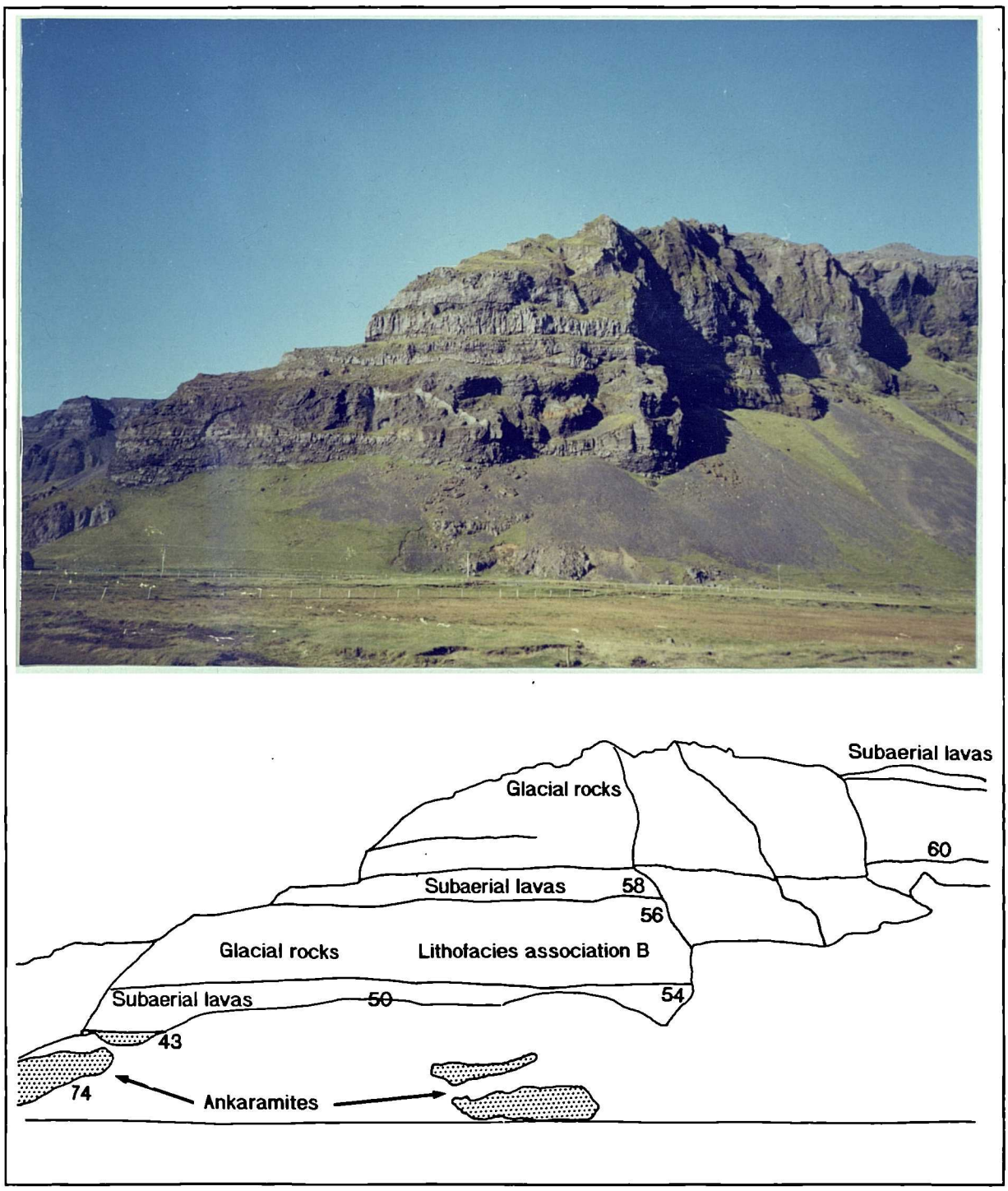

Figure 4.19 *The Hvammsmuli sequence, showing the basal ankaramites and selected sample numbers in the overlying succession.*

Hvammsmuli (Hv) Group

Above the ankaramitic cinders is a succession of six vesicular, olivine-rich subaerial lava flows each up to 3m thick ('G1' on profile W7, Figures 4.1 and 4.20). Wiese (1991) dated one of the uppermost lavas of this group at 589±37Ka, similar to the basal ankaramite. These lavas are fine-grained with phenocrysts of olivine, pyroxene and microphenocrysts of plagioclase in an intergranular groundmass and each lava has a rubbly or scoriaceous surface. The upper three lavas of this Group are up to 4m thick. The Hvammsmuli Group is unconformably overlain by a thick deposit of hyaloclastite and pillowy, brecciated lava, which has cut through bedded deposits of hyalotuff (lithofacies association B - Figure 4.18; G2 - Figure 4.20). Clearly there is a sharp change in eruption environment from subaerial to subaqueous/subglacial at this point. Above this unit are several more sheet-like lavas representing deposition in an ice free environment (G3 & G4 - Figure 4.20), then more hyaloclastite breccia deposits (lithofacies association C) which can be traced laterally, especially westwards, for some distance (G5 - Figure 4.20). These deposits have been dated by Wiese (1992) at 349±19Ka. Above this subglacial unit lie highly porphyritic subaerial lavas which were deposited during the last interglacial period.

In summary, since the deposition of the Hvammsmuli ankaramite during an interglacial at 589±37ka (Wiese, 1992), at least three glacial periods have affected the Hvammsmuli area. During the first glacial period, lavas were deposited in a shallow NE-SW trending valley (G2) which followed the present line of the Hvammsmuli promontary. During the second glacial period (349±19Ka, Wiese, 1992), sheet-like hyaloclastites were deposited that can be traced laterally (especially to the west - Figure 4.20 - G5) for some distance. During the third glacial period, ice advanced over the uppermost subaerial lavas, this corresponds to the last glacial which peaked at ~110Ka. It will be seen in the next section that overall there have been at least four glacial events which have affected the west and southwest of the Eyjafjöll volcanic system.

4.2.3 WESTERN SECTION

From Hvammsmuli to Seljalands at the western tip of the Eyjafjöll volcanic system, a continuous cliff exposure of stacked sheetlike westerly-dipping deposits separated by distinct unconformites occurs (Figures 4.19 and profiles W1 to W7, Figure 4.20). These deposits include compound and simple lavas, hyaloclastite breccias and redeposited volcaniclastics. The deposits overlap towards the west (Figure 4.19), the youngest, westernmost lavas being around 10Ka. Deposits exposed at Hvammsmuli (either 'G4' or 'G5'on profile W7, Figure 4.20) are at least 350Ka (Wiese 1992).

4.2.3.1 NUPSHEIDI AND SELJALANDSHEIDI

Seljaland section (profile W1, Figures 4.20, 4.20a). Stratigraphic unit G9 - At Seljaland, there are 50m of massive sands and gravel at the base of the sequence, these

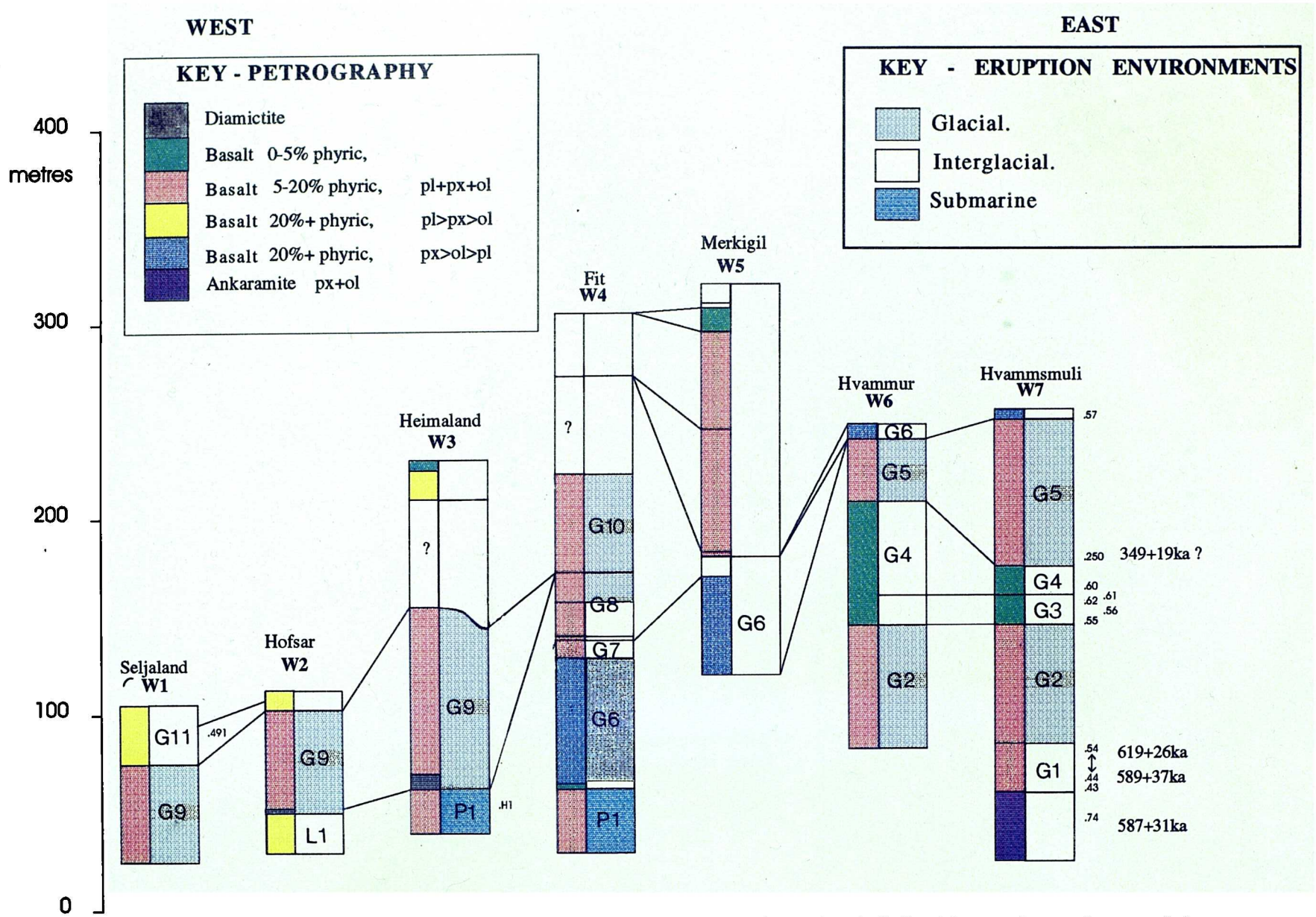

Figure 4.20 Profiles along the south west coastline of Eyjafjoll with sample numbers to right, of column and K/Ar dates (Wiese, 1992). For profile locations see Figure 4.1.

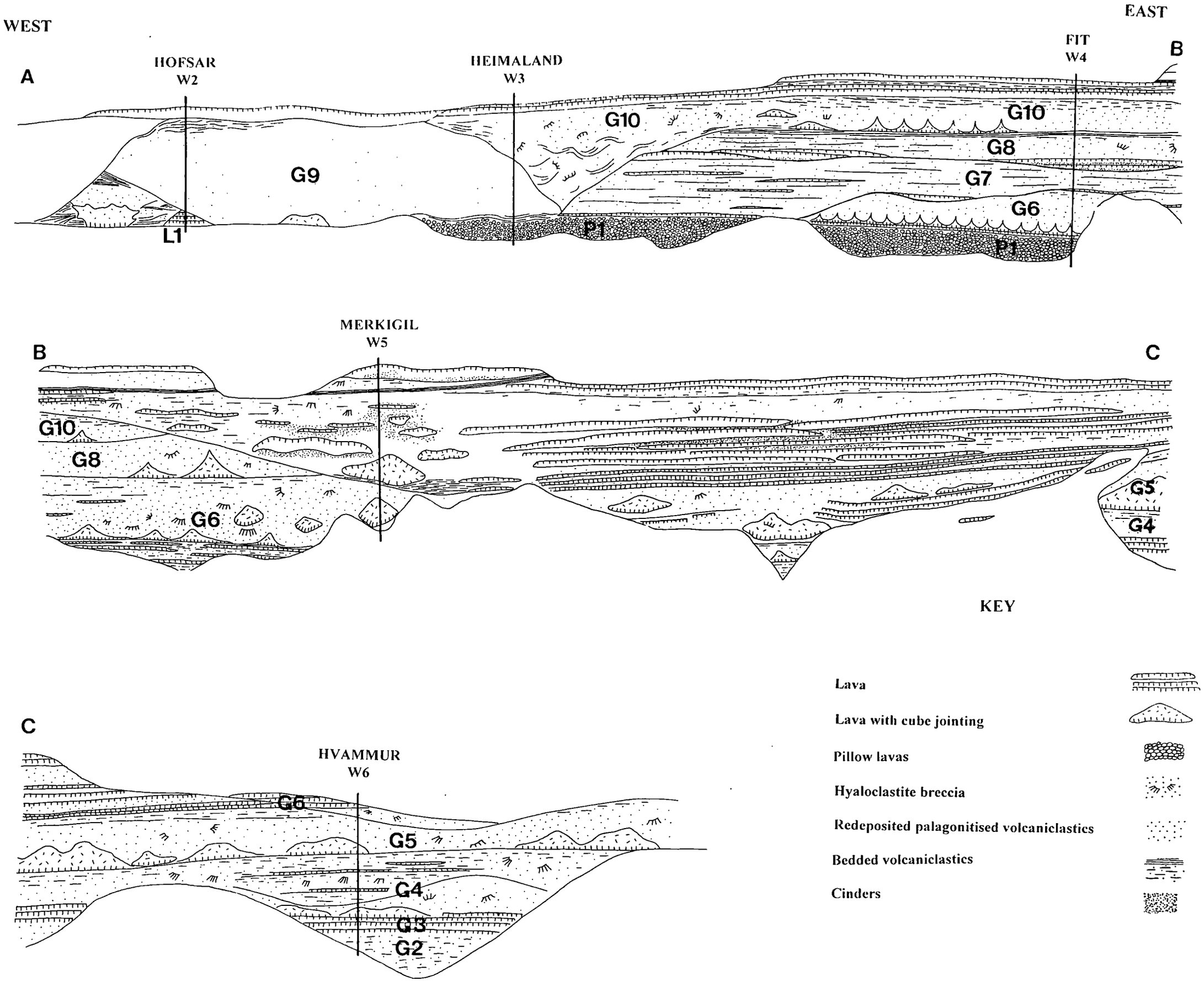

Figure 4.20a Simplified sketch (not to scale) showing the relationships between units described in the profiles shown on Figure 4.20. For location of profiles see Figure 4.1.

are overlain by 10m of horizontally-bedded sands at the top of which is a palaeosoil horizon. These are distal glacio-fluvial sediments deposited during a volcanically induced flood (jökulhaup).

Stratigraphic unit G11 - Above the glacio-fluvial sediments are three to four porphyritic basalt lava flows which outcrop in the Fagrafell quarry just 1km to the north [513 560]. These lavas are massive, vesicular and contain 40% by volume phenocrysts of plagioclase, pyroxene and olivine up to 8mm in length; glomerophyric clusters of plagioclase and pyroxene are common. The uppermost lava is thickest (<10m) and contains proportionately more plagioclase than the lower lavas. The lower lavas have been dated at 76±45Ka and the upper lava at 82±21Ka (Wiese, 1992). The upper lava is columnar, of variable thickness and phenocryst rich. It has a striated upper surface, the striations indicating glacier movement from north to south, i.e. from the Markarfljot valley, not from the summit of the volcano. The youngest lava in the area at ~10Ka is the subaerial 'Hamragardur lava' (Figure 1.7) which lies on the glaciated lower lavas.

Hofsar section (profile W2, Figures 4.20, 4.20a).

Stratigraphic unit L1 - A 15m sequence of channel-confined subaerial lavas, with blocky bases and tops, overlain by 5m of cinders containing lava blocks up to 2m in diameter. A vesicular 2m thick feldspar-rich subaerial lava overlain by 0.5m of poorly sorted, gravel derived from the lava caps the unit.

A 0.5m thick, grey diamictite, glass-poor towards its base, more abundant glass fragments towards its top,divides unit L1 from unit G9.

Stratigraphic unit G9 comprises thick (<60m), redeposited volcaniclastics, deposited in broad, distal channels. There is up to 30% glass in the matrix, the remaining 70% is composed of basalt fragments, upper parts of the deposits are reworked. These deposits are derived from subglacial eruptions which occurred not in the last glacial period, but the one prior to that.

Stratigraphic unit G11 - Subaerial lavas lie above the thick volcaniclastic deposits, some of which correlate with the lava at Seljaland (profile W1, Figure 4.20).

Heimaland section (profile W3, Figures 4.20, 4.20a).

Stratigraphic unit P1 - A thick (<20m) basal unit of pillow extends as far as the Fit section (profile W4, Figure 4.20). The pillows are up to four metres across, are closely packed and interpillow hyaloclastite is scarce. There does not appear to be a strong orientation of the long axes suggesting deposition on a shallow slope (Walker, 1994). Some of the pillows are partially drained, but are still complete indicating a minimal vertical stress suggesting that they were not formed in deep water. The upper parts of the unit contain large irregularly shaped lobes of radially jointed lava. This unit may have formed as a lava poured from the land into the sea. Thorarinsson (1966) observed lava flows from Surtsey entering the sea and forming pillow lavas rather than explosive (littoral) deposits. Studies have shown that only a few metres of open flow is required for a highly fluid basaltic magma to expel most of its volatiles and hence form pillow

lavas in shallow subaqeous environments (Sigvaldasson & Elison 1966). The pillow lavas are overlain by about 10m of conglomerates and glacial sediments. These sediments provide the base to the same channelled redeposited volcaniclastics (unit G9) described at Hofsar (profile W3, Figures 4.20, 4.20a).

Fit Section (profile W4, Figures 4.20, 4.20a).

Stratigraphic unit P1 - Pillows at the base of the Fit section correlate with those at Heimaland (profile W3, Figures 4.20, 4.20a, 4.21).

Stratigraphic unit G6 - Unit P1 is overlain by 2m of columnar lava which grades up into 40m of cube-jointed lava and hyaloclastite breccia (lithofacies association C; Figure 4.20, 4.20a). There is then an unconformity marked by 0.5m of diamictite and 0.5m of gravels. This is overlain by discontinuous, vesicular subaerial lavas (G7) up to 7m thick which contain sparse phenocrysts of plagioclase and pyroxene and are intercalated to the west with bedded hyaloclastite, this may be a shallow marine/tidal succesion.

Stratigraphic unit G8 comprises a lower sequence of subaerial lavas and cinders deposited in channels and topographic lows (Figure 4.21). These are overlain by redeposited palagonitised volcaniclastics. The overlying unit G10, comprises massive redeposited volcaniclastics with hyaloclastite breccia in the form of lithofacies association C (Figure 4.21). To the east this unit becomes chaotic, it clearly filled an incised topography by en masse deposition and slumping (Figure 4.20a).

The Fit section shows evidence for deposition during submarine conditions, at least one glacial period and at least two subaerial periods.

Merkigil section (profile W5, Figures 4.20, 4.20a).

The Merkigil section is dominated by thick lavas, fluvial sediments and cinders. Unlike the other sections in this area, there are no thick deposits dominated by hyaloclastite breccia or hyalotuff, suggesting that this section is composed of dominantly subaerial lithologies. There are units of brecciated lava and hyaloclastite up to 15m thick, intercalated with fluvial sediments but these are small in volume. Lavas are thick, but laterally discontinuous suggesting a degree of lateral topographic confinement. Cinders and scoriaceous material are abundant in the middle of the sequence suggesting that there may have been a vent in this area at the time of their eruption. A 2m thick dyke cuts the cinders and lower lavas, it is columnar jointed and strikes at 070^{o} with a 60^{o} dip to the south. The uppermost stratigraphic unit at Merkigil is a distinctive, highly px-ol-pl porphyritic lava.

Hvammur section (profile W6, Figures 4.20, 4.20a).

The Hvammur section exposes lavas and sediments deposited during two glacial and two interglacial events (Figures 4.20, 4.20a). The Hvammur section correlates well with the nearby Hvammsmuli section, although the interglacial lavas deposited prior to 349$\pm$19Ka are thicker and are intercalated with sediments. It appears that these subaerial lavas were deposited in a valley or channel, the Hvammur section revealing their

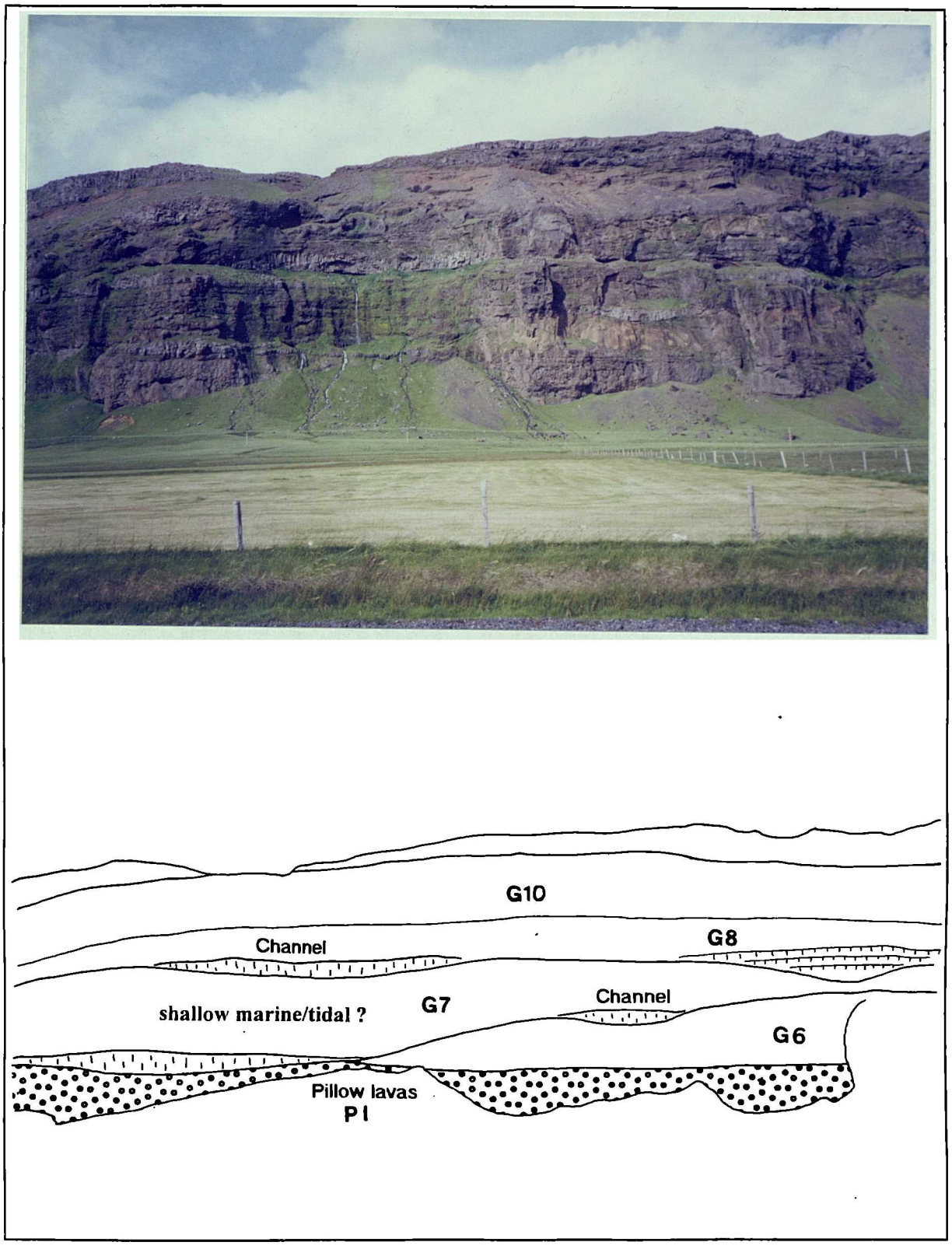

Figure 4.21 *The Fit profile in the western section of the Eyjafjöll volcanic system, showing channelled deposits and the westward younging succession.*

greatest thickness.

In summary, this series of sections provides evidence that at least four glacial events have affected the west and south west of the Eyjafjöll volcanic system since

~600Ka. The glacial periods correspond to deposition of units G2, G5 and G8-10 (Figure 4.20) and the last glacial. Lava and hyaloclastite assemblages provide evidence that eruptions occurred in subaqueous conditions. The deposits dip to the west and southwest and many are channel or valley-confined suggesting that deposition was not submarine. The basal pillows at Heimaland and Fit were deposited in shallow submarine conditions.

4.2.3.2 WESTERN SLOPES

The upper, western slopes of the volcano are dominated by the lavas erupted from radial fissures during the last glacial and the post-glacial period. These lavas are laterally extensive and generally of intermediate composition. All the lavas are porphyritic, the lavas with most abundant phenocrysts tend to contain glomerophyric clusters of clinopyroxene and plagioclase. This area was not studied in great detail but the most extensive lavas were sampled. Many of the evolved lavas lie on very highly px-pl-ol phyric lavas (<50 vol%) which contain large clinopyroxene phenocrysts (<15mm). These distinctive lavas have been described at Halsar (section 4.2.2.3), Merkigil (section 4.2.3.1) and Akstadaheidi (section 4.2.4.2), they were probably erupted during the last interglacial or early in the last glacial period.

4.2.4 NORTHERN SECTION

The northern side of Eyjafjöll appears to be composed of entirely hyaloclastite lithologies (Jonsson, 1990). However, on closer inspection it can be seen that the northern slopes are draped with steeply-dipping hyaloclastite lithologies which have truncated an underlying layercake stratigraphy (Figure 4.22). Such features were caused by the presence of thick valley glaciers in the Markarfljot valley, north of Eyjafjoll, during glacial periods. Only two successions were traversed in the northern area due to time constraints.

4.2.4.1 INNSTUHNAUSAR (GIGJÖKULL)

A traverse up the western margin of Gigjökull shows that cube-jointed and hackly-jointed lavas dip steeply into the Markarfljöt valley, truncating underlying lavas and sediments (stratigraphic unit N2, Figure 4.22). These deposits are similar to those of the Svaðbaelisheidi Group which flow steeply down the sides of valley-confined glaciers (Figure 4.6). They are more coherent on higher slopes, but are dominated by breccias and hyaloclastite on lower slopes.

The earliest lavas at Gigjökull are a succession of flat-lying subaerial lavas and cinders which can be traced along the northern slopes, to the east, for 2-3km (stratigraphic unit S1, Figure 4.22). Lava flows are up to 8m thick, blocky with poorly developed columns and pink-grey weathering. They contain <15% phenocrysts of plagioclase, pyroxene and olivine and small gabbroic nodules. The subaerial lavas are

overlain by 50m of subglacial hyaloclastite breccia containing small, sparse phenocrysts of plagioclase and pyroxene (stratigraphic unit N1, Figure 4.22). The subglacial assemblage can be seen, in the gorge, to lie flat on the lavas. However, it then truncates the lavas of unit S1 and flows steeply down to the Markarfljöt valley floor (Figure 4.22). A further 40m thick succession of thin (1m) subaerial lavas intercalated with ash and cinders overlies glacial unit N1. These subaerial lavas (stratigraphic unit S2, Figure 4.22) are, in turn, truncated by an overlying 20m thick subglacial deposit containing up to 25% phenocrysts dominated by plagioclase (stratigraphic unit N2, Figures 4.22 and 4.23). This deposit is massive and fragmentary and has flowed downslope to lie on top of the earlier subglacial deposit in the valley bottom. The very top of this deposit is cut

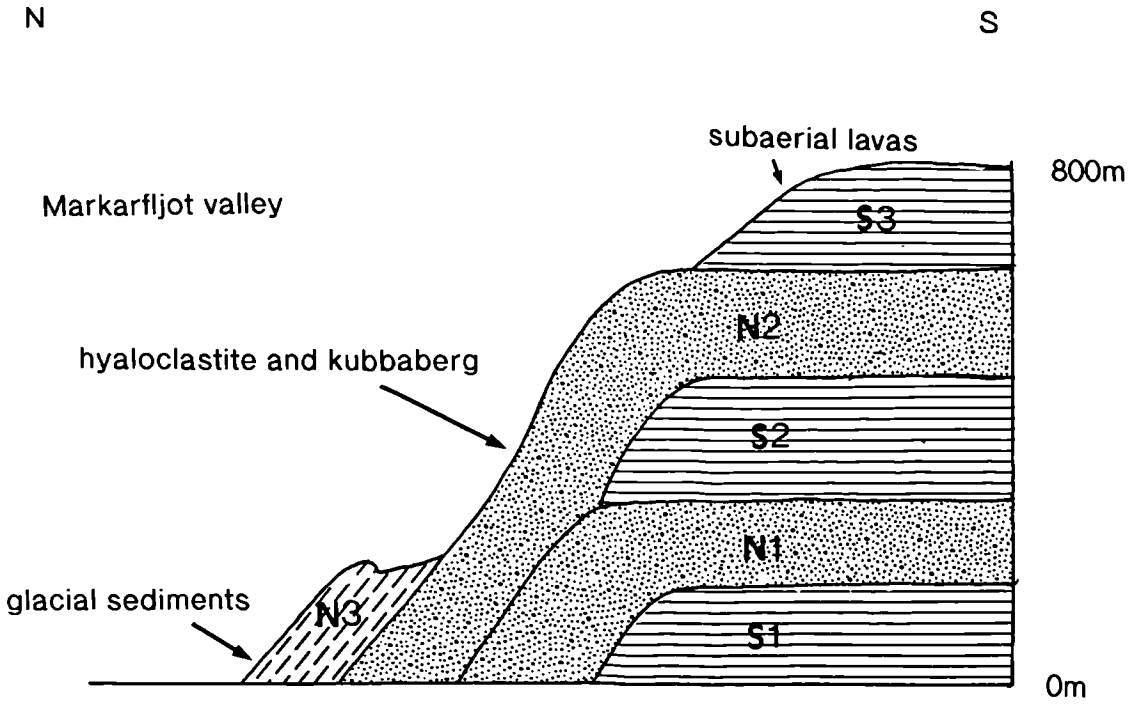

Figure 4.22 *Idealised sketch cross-section of the geology of the Gigjökull area. Deposits relating to three major glacial events may be discerned and are labelled 1, 2, and 3, in order of decreasing relative age.*

by a boulder bed/diamictite (060/30N) that marks the base of a sequence of highly evolved subaerial lavas (stratigraphic unit S3, Figure 4.22). The lower 2-3 flows are glassy with numerous plagioclase phenocrysts, these are overlain by greenish, platy trachyte lavas containing plagioclase, pyroxene (ferrohedenbergite) and olivine (fayalite).

A lodgement tillite exposed on the western margins of the Gigjökull glacier at about 450m altitude indicates the route of the glacier in recent times, striations are aligned towards 295° and the tillite dips at 39° in this direction. Tillites deposited at the base of the Gigjökull succession overlie all the described lithologies representing the last glaciation event (stratigraphic unit N3, Figure 4.22). The Gigjökull succession

Figure 4.23 *Looking east, across Gigjökull, at the layer-cake stratigraphy beneath steeply dipping sheet lavas and hyaloclastite breccias.*

4.2.4.2 AKSTADAHEIDI

The sides of the Akstadaá stream valley expose a very similar structure to that at Gigjökull; sheetlike, subglacial deposits which have flowed over earlier flatlying deposits into the Markarfljöt valley. At the ice margin at the top of the Akstadaá stream, several small outcrops of intermediate lava occur. Some lie on dark aphyric vesicular lavas whilst another lies on a glaciated porphyritic basalt containing <60% phenocrysts of olivine, pyroxene and plagioclase. The lavas have a laminate texture so are probably mugearites which were erupted during the late stages of the last glacial period or the early part of the postglacial.

It is proposed that the Markarfljöt glacier has consistently eroded the northern side of Eyjafjöll, creating very steep slopes. Each time a glacier occupied the Markarfljot valley, the products of any eruption on Eyjafjöll would be forced to flow out onto the glacier, or, to cut down between the steep topography and the ice. Evidence for latter has been observed at other parts of the volcano e.g. the Svadbaelisheidi Group (Figure 4.6) and the Steinafjall Summit Group. When this process is repeated during more than one glacial period, a vertical succession comprising of flat-lying subaerial lavas intercalated with draped glacial deposits which extend almost to the present sea-level is created (Figure 4.22).

4.2.5 EASTERN SECTION

It is unclear to which volcanic system volcanic deposits in this area belong. Carswell (1983) suggested that lavas from both the Eyjafjallajökull and Katla volcanoes occur. For this reason, the area was not studied in very great detail.

4.2.5.1 SKOGAHEIDI

Carswell (1983) described in detail thick deposits in this area and surmised that they are subglacial, topographically-confined deposits probably fed by E-W fissures. The Kaldaklifsgil gorge on the western margin of Skogaheidi exposes the thick deposits of hyaloclastite breccia and hyalotuff of which Skogaheidi is composed (dominantly lithofacies association J - Figures 3.20, 4.24a). These deposits will be referred to as the **Skogaheidi (Sk) Group**. The gorge has formed along the unconformity between the old, topographic high of Raufarfell, partly composed of Laugará Group basalts, and the younger subglacial valley-fill deposits of Skogaheidi. Traces of a basal tillite are exposed on the eastern slopes of Raufarfell which dip steeply eastwards beneath the thick deposits of Skogaheidi. The topographic high which forms the eastern-most margin of the Skogaheidi deposits is Jökulgil, a ridge near Solheimajökull (Carswell, 1983). Skogaheidi is composed of successive eruptive units each composed of massive hyaloclastite breccia and hyalotuff grading upwards into reworked hyaloclastite and hyalotuff. Two such units, each roughly 50m thick, are exposed in Kaldaklifsgil, these are probably amongst the oldest deposits in this area. The thick subglacial units are capped by a thin succession of subaerial lavas dated by Wiese (1992) at 118±34Ka. The interglacial lavas are then overlain by channelised subglacial eruption units with a basal diamictite and a lensoid cross section. Such deposits frequently contain lenses of reworked sediments and are cemented by palagonite and goethite (the latter reflecting the Fe-rich nature of the lavas) suggesting that late stage warm fluids were abundant during deposition. These lavas are anomously FeTi rich and probably erupted from the Katla volcanic system. The Skogaheidi Group represents deposition during two glacial periods and the intervening interglacial period.

Interglacial lavas

Overlying the Skogaheidi Group is a succession of laterally discontinuous subaerial basalt lavas up to 10m thick. Their discontinuity is caused by glaciation and many outcrops are capped by <1m of diamictite. The lavas are sparsely porphyritic and were erupted from east-west fissures where spatter cones are still preserved. Recent (postglacial) activity has occurred along E-W fissures on the Fimmvorduhals Pass where spatter cones are also evident. These lavas are of intermediate composition and form thick columnar-jointed tubes of porphyritic lava.

In summary, the first subglacial deposits of the Skogaheidi Group represent deposition beneath thick ice (lithofacies association J). Following an interglacial period

(118±34Ka Wiese, 1992), deposition occurred in channels beneath thin temperate ice during the early stages of the last glacial period. (Similar channelled deposits are exposed all along the southwest margins of the volcano (Figures 4.19 and 4.20). The subaerial lavas were emplaced during a temporary ice retreat at 18±16Ka (Wiese, 1992), and were subsequently smoothed by readvancing ice.

Drangshlid

Drangshlid is a distinctive monogenetic eruption centre to the south of the volcano near Skogar. Beds of hyaloclastite and hyalo-tuff dip steeply away from the vent. They are typically thick (<3m), massive and laminated containing angular to sub-rounded vesicular vitric clasts supported in a vitric mud matrix (Figure 4.24). The nature of the clasts suggests that steam explosivity was more important than magmatic explosivity during their formation since vesicles are intact. Some units contain sparse lithic clasts (mostly pillow fragments) up to 20cm in diameter. The scarcity of effusive volcanics and the lack of evidence for lateral confinement (by ice) suggest a shallow submarine origin for Drangshlid. The very steep slopes of the edifice and its water saturated nature would have made it quite unstable. Continuous slumping and sliding of the water saturated tephra produced an apron of secondary deposits around the vent. The pile probably grew above sea level but the lava would continue to react with the water saturated tephra forming hyaloclastite breccias and in places poorly developed pillows. Some lava and hyaloclastite has tumbled down the south west slopes creating the rather chaotic and discontinuous deposits observed there.

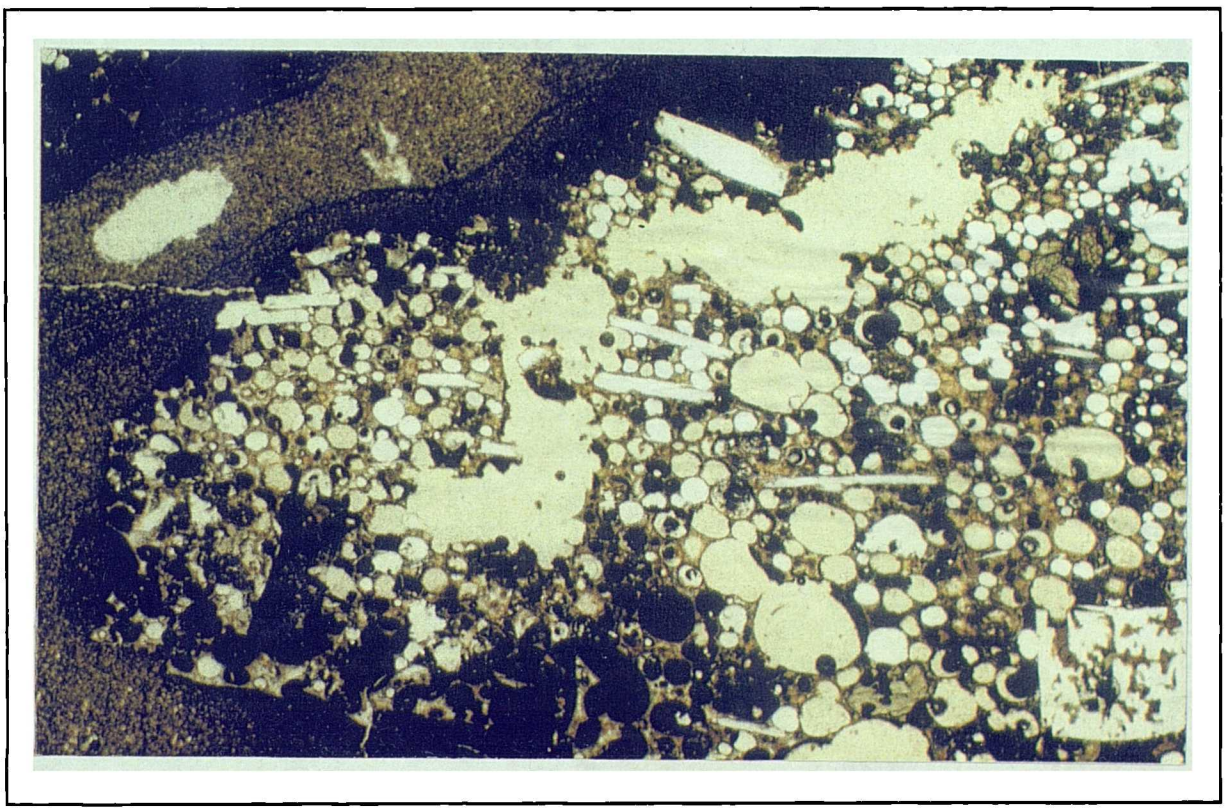

Figure 4.24 *Photomicrograph of a lapilli fragment in a vitric mud groundmass, from Drangshlid. Field of view 12 x 7.2 mm.*

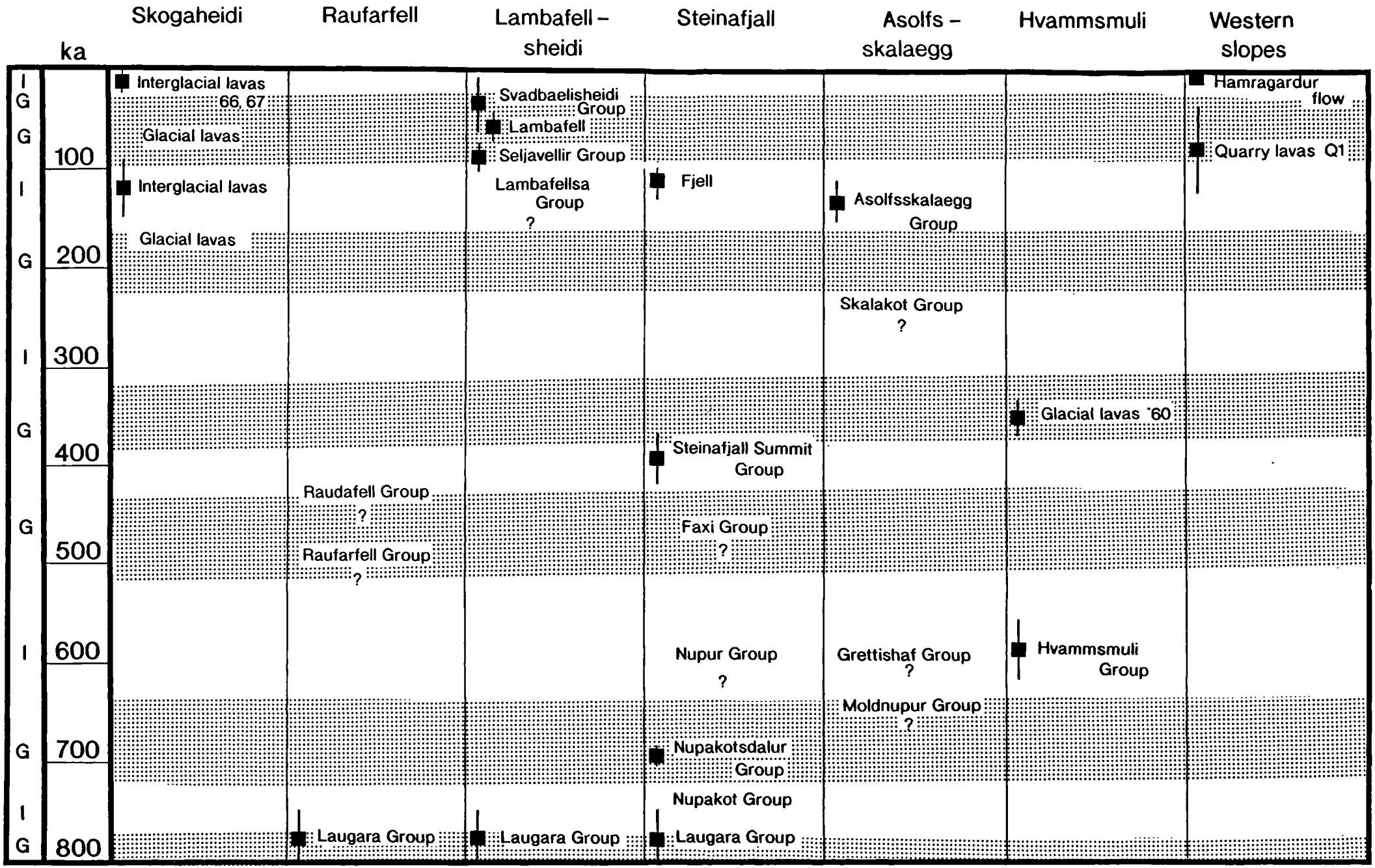

Table 4.2 *Chart showing the age of the stratigraphic Groups described in this thesis, using the K-Ar dates of Wiese (1992); (error bars are shown). The proposed positions of the other stratigraphic Groups, eruption units and individual lavas are shown based on field evidence. This chart suggests that there have been up to six major glacial events during the construction of the volcano (shaded bars on the chart).*

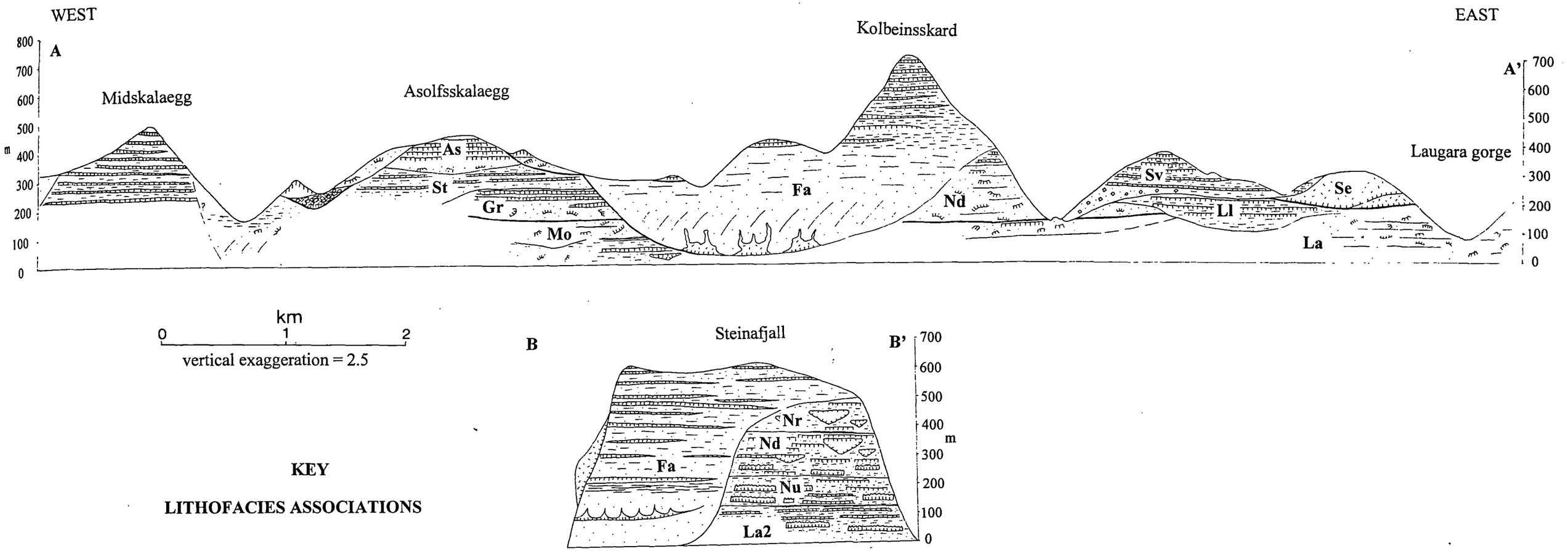

Figure 4.24a East-west sections through proximal deposits at Eyjafjoll showing relationships between lithostratigraphic units. The distribution of lithofacies associations described in Chapter 3 is also shown in comparison with subaerial and transitional subaerial-subaqueous lithofacies associations. The position of each section (A-A', B-B', C-C') is shown on Figure 4.1.

Drangshlid is over 400m in height, this suggests that sea level was at some time several hundred metres higher than it is today. The K-Ar data of Wiese (1992) show that capping lavas on subglacial deposits at Skogaheidi are 118±34 Ka. These deposits onlap the lower slopes of Drangshlid so it has an age of at least 100 Ka. Assuming sea level rises briefly after a glaciation (Section 1.2) it seems likely that Drangshlid may have formed shortly after a major glaciation.

4.2.6 STRATIGRAPHIC SUMMARY

Using some of the K-Ar dates of Wiese (1992), combined with field relationships deduced in this study, the relative ages of the stratigraphic Groups may be elucidated (Table 4.2). This corrolation shows that the Eyjafjöll volcanic system may have undergone at least six glacial periods and six interglacial periods since 800Ka. The glacial periods appear to last roughly 100Ka before giving way to an interglacial period.

It is very difficult to assess if these glacial periods correlate with regional events. One method of doing this is to assume that during such regional glacial periods, thick, valley-confined glaciers would extend to at least present sea-level. However, it must be borne in mind that such glaciers only developed during the mid to late stages of the growth of the volcano. The northern part of the volcano provides evidence of three major glacial events (Figure 4.22). During each event, a glacier occupied the Markarfljot valley. The southern part of the volcano also provides evidence for at least three major glacial events (1, last glacial, forming the glacial valley of Holtsdalur; 2, deposition of the lower Skogaheidi Group; and 3, deposition of the Faxi Group, western Steinafjall), as well as evidence for three other glacial events which were not so extensive.

The periodicity of these proposed glacial and interglacial periods is in general agreement with time scales predicted by stable isotope work on marine sediments (Johnson, 1982; Shackleton and Opdyke, 1973).

A summary of the relationships between proximal stratigraphic units is shown in Figure 4.24a. Most of the stratigraphic units were erupted from the summit area, radial fissures or NE-SW fissures passing through the summit area. Some lavas in the Nupakotsdalur and Nupur Groups appear to flow radially away from a vent site in the vicinity of Steinafjall mountain. Since there is a small vent on Steinafjall summit at present it is possible that some of the units on eastern Steinafjall are the result of flank eruptions in this area. Western Steinafjall (Faxi Group) is composed of material derived from summit eruptions or near summit radial fissure eruptions. Distal stratigraphic units are shown in Figure 4.20a, the majority of these units result from eruptions along E-W or radial fissures.

4.3 INTRUSIVES

The term 'inclined sheet' applies to a discordant, usually discontinuous intrusion associated with a central volcano. These sheets commonly dip inwards towards the volcanic centre (the 'cone sheets' of Bailey *et al.*, 1924), but may also be vertical ('ring dykes') or dip outwards. Dykes are also abundant in the cores of central volcanoes, but they are typically subvertical. In this study, the term 'sheet' includes vertical and inclined sheet intrusions as well as concordant sills.

Inward-dipping inclined sheets associated with central volcanoes have an average dip of 45° (Gautneb *et al.*, 1989), but may have a steeper dip in the core of the volcano and a gentler dip further away (Billings, 1972). Models of magma chamber evolution and caldera collapse mechanisms predict that inward-dipping inclined tensional fractures will occur during periods of high magmatic pressure (e.g. Roberts, 1970). Lava may consequently erupt from these fractures or along pre-existing regional fractures. Caldera collapse resulting from contraction of the magma body or periods of low magmatic pressure may result in outward-dipping faults (e.g. Anderson, 1936; Robson & Barr, 1965; Phillips, 1974; Druitt & Sparks, 1984; Komuro, 1987). Outward-dipping faults are usually much less common than inward-dipping faults, but have been described by several authors (Richey, 1932a; Mori & McKee, 1987).

Spherical or prolate ellipsoid magma chambers subjected to excess magmatic pressure exert a tensile stress which reaches a maximum above the centre of the chamber (Gudmundsson, 1988). These stress conditions usually result in the formation of radial fractures (eg Koide and Battachaji 1975); this may be demonstrated experimentally (eg. Komuro 1987).

4.3.1 DISTRIBUTION OF INTRUSIVES

In total, 142 sheets were described and measured (Figure 4.25 and Figure 4.26). A brief summary of observations is presented below.

4.3.1.1 SOUTH SECTION

Due to the highly dissected nature of the southern part of the volcano, numerous sheets are exposed here. The gorges cut deep into the core of the volcano where intrusive sheets may comprise at least 60% of the exposed rocks. Gabbros and/or granophyres have been described from the cores of several Icelandic Tertiary central volcanoes (e.g Walker, 1963; Furman *et al.*, 1992), but none are exposed at Eyjafjöll. Nevertheless, volcaniclastic deposits near the base of both the Laugara and Nupakotsdalur Groups contain gabbroic xenoliths, suggesting that there may have been partially or wholly crystalline magma bodies near the surface in this area,prior to ~700 Ka.

At the base of the Laugará gorge, there are many inclined sheets dipping at a low angle (<50°) to the south, away from the core of the volcano (Figure 4.27). In the gorge

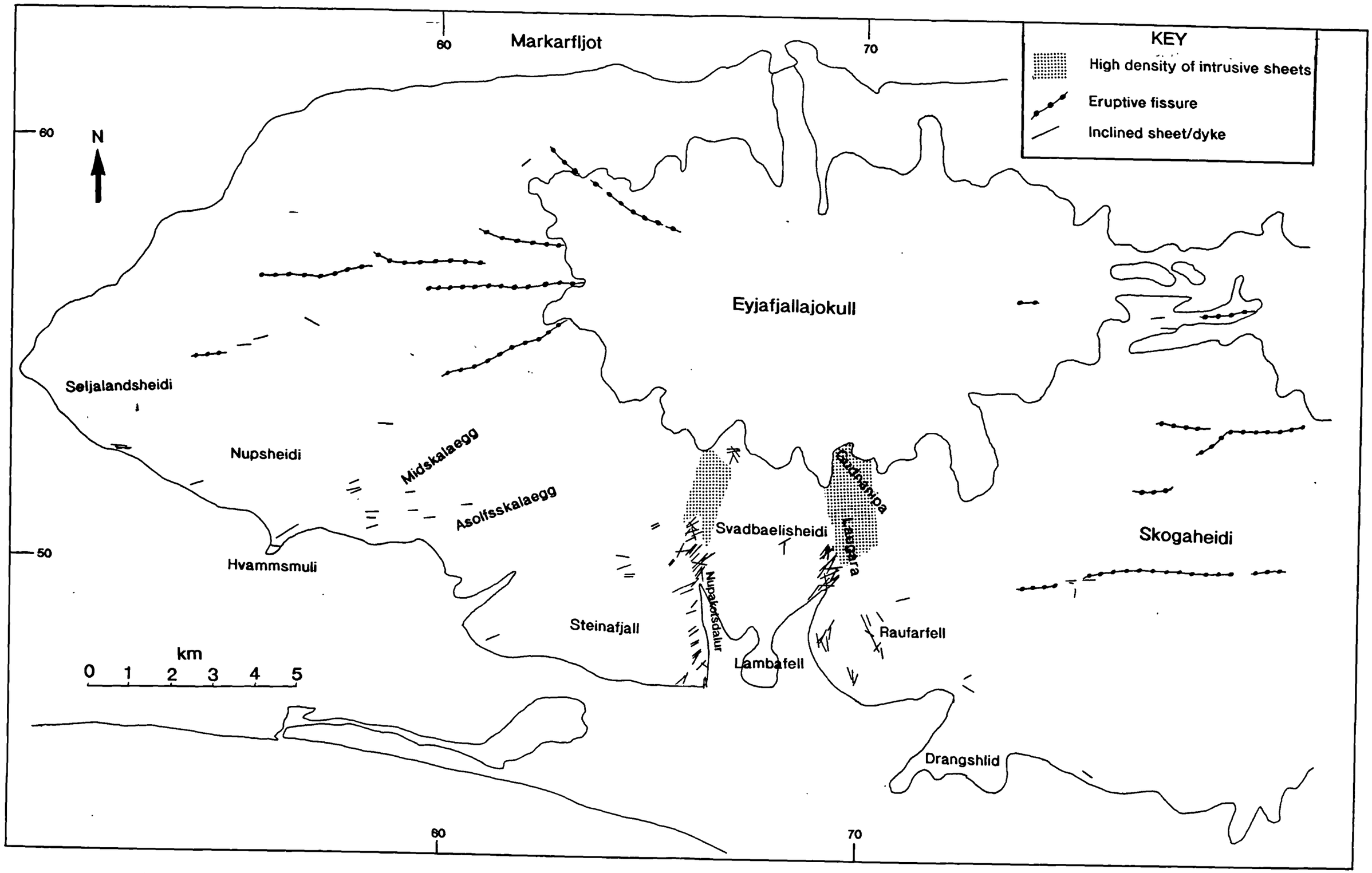

Figure 4.25 *Map of the Eyjafjöll volcanic system showing fissure eruptions and the orientations of intrusive sheets.*

and on the mountainsides east of the gorge, conjugate sheets can be seen, one set dipping towards, one set away from the volcano; there are also numerous sheets of other orientations. The conjugate sheets appear to have a roughly NE-SW strike. Many sheets are slightly sinuous and the dip of a single sheet may vary from 45° to 90°; in such cases both strike and dip were measured by sighting from a distance. Sheets range in width from 20cm to 1.5m, but the majority (90%) are between 50cm and 1m. This is similar to observations at Hafnarfjall volcano in S.W.Iceland where 80% of dykes are less than 1.2m thick (Gautneb *et al.*, 1989). The majority of dykes can only be traced for up to 10 or 20m along strike, but the conjugate sets of dykes are straighter and laterally more persistent than other sheets and can be traced for up to 150m. Glassy or fine-grained margins are very common and some develop jointing perpendicular to the dyke margins. Vesicles are frequently flow-banded, with a central zone of spherical vesicles and marginal pipe vesicles inclined in the flow direction. The vesicles often host amygdales as a result of the migration of hydrothermal fluids through the porous, vesicular parts of the dyke. A small proportion of the outward-dipping sheets contain pipe vesicles showing flow to the south, i.e. from a higher to a lower structural level. However, lineations on an outcrop scale do not necessarily reflect large scale movements (Takada, 1988) and these pipe vesicles may simply show a local or late-stage movement of magma. Higher up the Laugara gorge and closer to the core of the volcano, sheets become more numerous. Offsets may be seen in many of the sheets. Cross-cutting relationships are complex and there are many generations of sheets outcropping in the Laugara gorge. At the base of the section, an outward-dipping sheet (sample D1, showing flow to the south) is cut by a steeper, thinner outward-dipping sheet (sample D6). Moving up section, nearer the core of the volcano, inward-dipping sheets become more abundant. The conjugate sheets also show variable cross-cutting relationships.

In the Laugará gorge, the country rock (Laugará Group) is generally more primitive than the intrusive sheets; elsewhere, rare primitive sheets (e.g. ankaramites) cut more evolved lavas. There are examples of primitive dykes cutting more evolved dykes at the Laugará gorge (e.g. sample D18 cuts D19). Some individual sheets in this area have highly distinctive chemistry (eg sample D19 has very high P_2O_5) setting them apart from other sheets of similar strike. The chemistry of the sheets will be investigated in more detail in Chapter 6.

High on the mountain sides of Gudnanipa, above the glacier and above the upper reaches of the Laugará, numerous inclined sheets have an apparent dip of about 45° into the core of the volcano. These sheets are not exposed elsewhere.

The Svadbaelisá gorge also hosts numerous inclined sheets (Figure 4.25). Higher up and closer to the volcano, the sheets are abundant and have various orientations (Figure 4.6). However, in the Nupakotsdalur valley, within the Nupakotsdalur Group, the majority of sheets are oriented NE-SW and are within 10°-20° of vertical. These

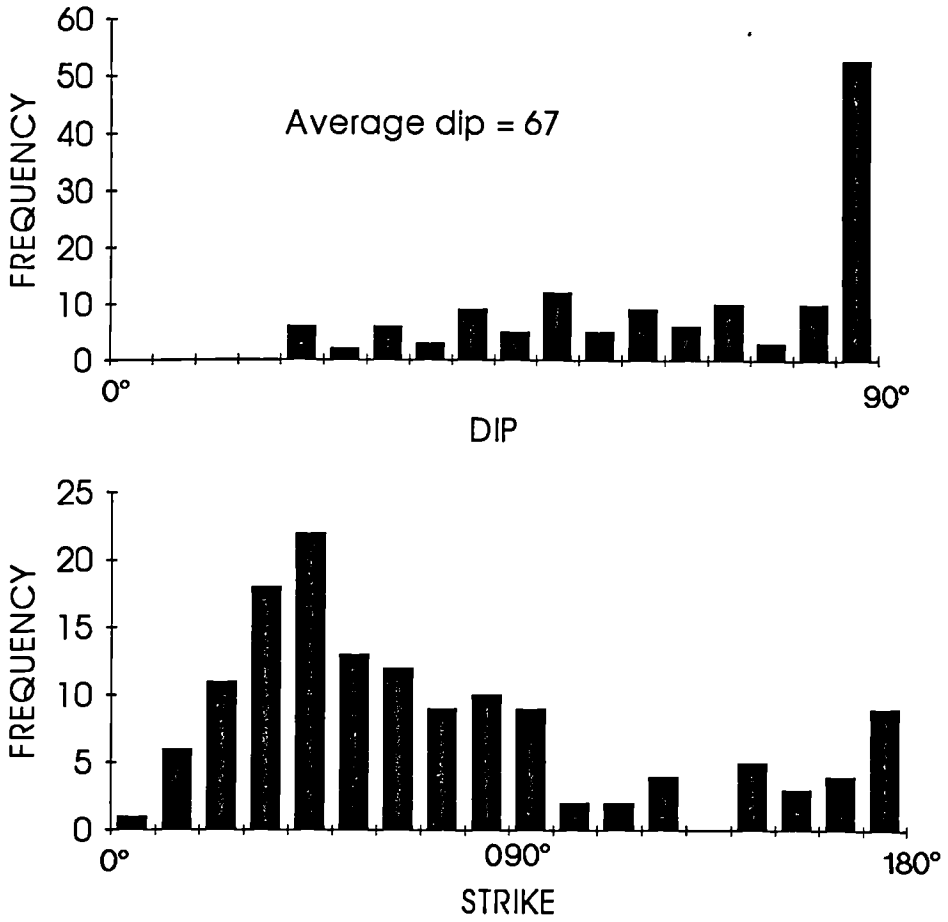

Figure 4.26 a) *Histogram showing the dip of sheets measured at Eyjafjöll (n=118).* **b)** *Histogram showing the strike of sheets measured at Eyjafjöll (n=118).*

sheets are not so volumetrically abundant as those higher up the gorges or in Laugará. Some of these sheets extend almost to the summit of Steinafjall to the west. Cross-cutting relationships are relatively rare compared to sheets at Laugara, the majority of sheets being subparallel. Sheets are from 10cm to 70cm wide. Two exceptions are about 1.5m wide, these are compositionally highly evolved. After consideration of the density structure of the Iceland crust and the density of acid and basic magmas, Gudmundsson (1987b) proposed that the overpressure of acid magma would be higher than the overpressure of a basaltic magma at the surface. Consequently, acid sheets are likely to be thicker than basic sheets from the same shallow magma chamber. Gautneb *et al.* (1989) found a relationship between thickness and dip suggesting that thicker sheets tend to have steeper dips. This relationship holds true at Eyjafjöll where the few sheets >1m in thickness are close to vertical.

Nupakotsdalur valley sheets often show vesicular banding as at Laugará and highly porphyritic sills show flow differentiation of olivine and pyroxene. Chilled, glassy margins are ubiquitous on dykes and inclined sheets but are lacking in the highly porphyritic sills. These appear to have been intruded into massive fragmentary subglacial deposits of similar mineralogy, probably whilst the deposits were still warm and unconsolidated; they have ragged margins with no evidence of chilling.

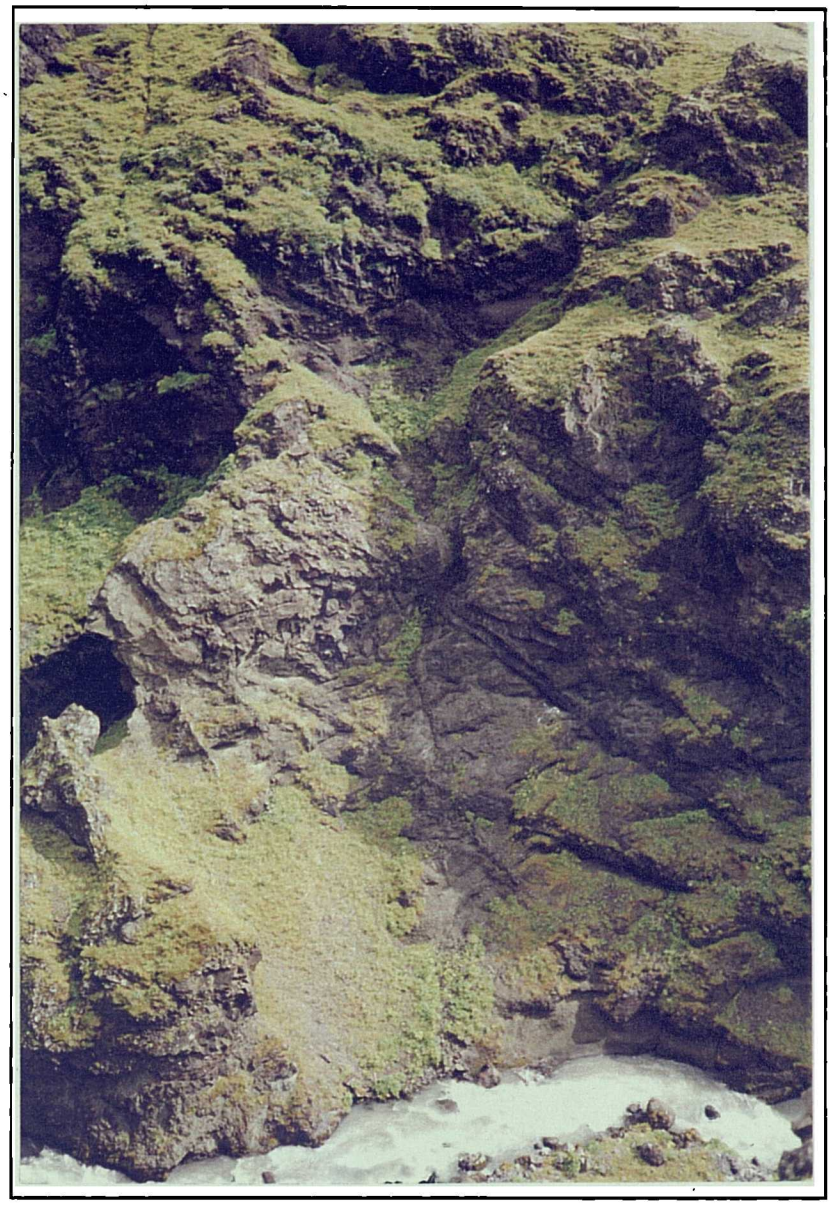

Figure 4.27 *Looking east into the lower reaches of the Laugará gorge showing the numerous outward-dipping sheets. The gorge is 150m deep here, sheets are up to 2m wide.*

Some feeder dykes within the hyaloclastite lithologies are en-echelon (Figure 4.28).

Several sheets exposed on and near the summit of Raufarfell can be followed along strike for several hundred metres. They trend towards the central crater and appear to be radial dykes. They are close to vertical, less than 1m in width and cut the highest stratigraphic levels of Raufarfell. Sheets in the lowest parts of Raufarfell are thicker (up to 1.75m) and have variable strikes (Figure 3.9). These sheets are hydrothermally altered with glassy chilled margins and are slightly sinuous.

4.3.1.2 SOUTHWEST SECTION

Sheets are exposed in the Irá and Midskalaá gorges in the southwest section. Much of the upper slopes are covered by recent lavas so no sheets are exposed. Sheets are typically thin (<1m) and slightly sinuous but laterally continuous for at least several hundred metres. They represent only a limited range of compositional types from ankaramitic to basaltic; no evolved sheets were sampled. The great majority of sheets in

Figure 4.28 *An eastward dipping dyke with en-echelon apophyses in Nupakotsdalur valley. The dyke is 60cm thick and has intruded hyaloclastite breccia.*

the southwest section (~80%) are oriented between E-W and NE-SW, the latter representing radial sheets.

4.3.1.3 WEST SECTION

Large areas of the western slopes of the Eyjafjöll volcanic system are covered by recent lavas. These lavas are fed from radial fissures which are marked by aligned cinder and spatter cones. The fissures show offsets and sharp changes in strike direction along their length (Figure 4.25) but most tend towards an E-W orientation. This fissure pattern may be due to the effect of a regional E-W non-magmatic stress system superimposed on a local (radial) magmatic stress system (Nakamura, 1977). Sparse sheets are exposed in the cliff sections along the western margins of the volcano, these are, on average, orientated WSW-ENE.

4.3.1.4 NORTH SECTION

Only rare sheets were observed in the north section and most outcropped in inaccessible gorges and gullies. Since the Gigjökull area is only 3-4km north of the central crater, it is surprising that the gorges here do not expose a high density of intrusives, as observed in the Laugará and Svadbaelisá gorges which are 6-7km south of the central crater. There is no apparent high temperature area to the north of the crater either. The central crater marks the present position of a shallow crustal magma chamber suggesting that the magma chamber has migrated towards the north. Alternatively, there may be another magma chamber, or magma chambers beneath the southern part of the volcano.

4.3.1.5 EAST SECTION

On Skogaheidi, only few sheets are exposed, amongst these are feeders that have produced E-W aligned spatter cones. These sheets are only 0.5m thick, some are offset to a more southwesterly strike, perhaps coinciding with faults trending at roughly 070°. The E-W feeder dykes on the Fimmvorduhals Pass are 0.5-1.0m thick and are sinuous. Rare sheets from lower in the stratigraphy have a strike of about 125°, these may be radial sheets. Some feeder lobes and intrusions in subglacial deposits have strikes of roughly ENE-SSW.

4.3.1.6 COMPOSITE AND MULTIPLY-INTRUDED DYKES

Composite dykes are common in the central volcanoes of Eastern Iceland (Walker, 1963; Furman, 1992b) but only one was identified at Eyjafjöll, GR[663 498], reflecting the relative paucity of exposed acid lavas.

Multiply intruded dykes are common and are exposed in several gorges (eg Nupakotsdalur and Irá). They are all basic, near vertical and intrude massive hyalotuff or hyaloclastite lithologies (Figure 4.29 and 4.16). Multiply intruded dykes often taper away vertically and nearly all strike approximately E-W to ENE WSW.

4.3.2 DISCUSSION

In common with other central volcanoes, the occurrence of a summit caldera, acid and intermediate rocks, hydrothermal alteration and numerous inclined sheets in the core, suggests that Eyjafjöll is partly fed by a shallow, crustal magma chamber. Based on seismic evidence, Einarsson (1978) has proposed that the central volcanoes Krafla and Askja have shallow magma chambers, the tops of which are at a depth of between 3 and 7km beneath the surface. Brandsdottir (1994) and Gudmundsson *et al.* (1994) have used seismic methods to show that a magma chamber beneath Katla is 5km across, at least 1km in height and at a depth of 3km.

4.3.2.1 RADIAL AND E-W SHEETS

The occurrence of radial sheets at Eyjafjöll suggests that the central magma chamber has undergone inflation and tumescence. Lavas erupted from these radial fissures are up to at least 100Ka in age. During this time period, voluminous sheet basalts, hawaiites and mugearites were erupted from radial fissures to the east and west of the volcano. Radial sheets are not evenly distributed, but are concentrated to the east and west of the volcano indicating that a regional E-W stress regime was concurrent with the local, magmatic radial stress regime. It is not clear why there is an E-W stress regime in this area. It may be related to the proximity of the SISZ which is an E-W zone of deformation connecting the EVZ with the WVZ (Ward, 1971; Saemundsson, 1979).

During the last glacial period, E-W fissures which link Eyjafjöll and Katla

Figure 4.29 *An east-west striking, multiply-intruded dyke in Svadbaelisa river gorge [658 508].*

erupted lavas of distinctive high Fe-Ti chemistry typical of Katla lavas (Carswell, 1983; Meyer *et al.,* 1985), suggesting that these fissures may be fed by a chamber beneath Katla rather than Eyjafjöll. However, there are also E-W fissures at Fimmvorduhals Pass which have erupted evolved basalts of the Eyjafjöll system. It is unclear if the magmatic plumbing system of the two volcanoes is linked at depth, but it seems very likely.

4.3.2.2 NE-SW SHEETS

There is evidence for only a few radial sheets in the south section of the volcano, these outcrop on Raufarfell summit. Apart from sparse radial dykes and the numerous inclined sheets exposed within the core of the volcano, there is a population of near-vertical NE-SW sheets exposed in the south section (Figure 4.25). These sheets, which are oriented parallel to the regional stress field are spatially concentrated around the Nupakotsdalur valley and the Laugara Gorge, i.e. the core of the volcano. These sheets differ widely in age and chemistry suggesting either that they are tapping different sources or that they

belong to a long-lived fissure system connected to an evolving magma chamber. The trachyte sheets are compositionally quite different to trachyte lavas exposed on the upper flanks of the volcano, they do not contain mafic inclusions and appear to have been emplaced separately, suggesting that they are from a different source. According to Gudmundsson (1989) a sill-like magma chamber will produce near vertical sheets that follow the regional stress field. Both Walker (1963) and Furman *et al.* (1992) suggest that the crustal structure beneath a central volcano consists of several sill-like magma bodies at different depths. Sill-like magma chambers may represent the early stages in the formation of large shallow crustal magma chambers (Gudmundsson, 1986, 1987a; Walker, 1963). If such a structure exists beneath the core of the Eyjfjoll volcanic system, it could explain the abundance of NE-SW oriented sheets of differing age and composition.

Gudmundsson (1995) suggests that with increasing distance from a magma chamber, inclined sheets will tend to follow the regional rather than the magmatic stress field. Consequently, in upper crustal levels, above a deep magma chamber, the magmatic stress system has a smaller effect and inclined sheets may become almost vertical. Nevertheless, Gudmundsson (1995) proposes that only inclined sheets with a strike approximately perpendicular to the regional minimum compressive stress are likely to penetrate the upper levels of the crust, other sheets will die out at deeper levels. Therefore, there may be an evolving magma chamber of considerable size beneath the southern part of the volcano which might produce NE-SW oriented sheets rather than inclined or radial sheets.

4.3.2.3 CONE SHEETS/INCLINED SHEETS

Although the core of the volcano is exposed, numerous concentric, inward-dipping inclined sheets which are observed in other central volcanoes (Gautneb *et al.*, 1989) are not seen. Most sheets exposed in the lower part of the Laugara gorge (~40%) actually dip outwards, away from the volcano (Figure 4.24). Outward-dipping fractures may form during contraction of a magma body. Only at Gudnanipa, which is very close to the summit caldera (Figure 4.25), are numerous inward-dipping sheets exposed which may be cone sheets.

4.4 SUMMARY

- Fieldwork at the Eyjafjöll volcanic system has shown that the volcano is composed of intercalated subaerial, subglacial and submarine deposits. A stratigraphy has been constructed and this suggests that the volcano has been built up during six glacial and six interglacial periods.

- The oldest rocks of the Eyjafjöll volcanic system outcrop in the core of the volcano; they are at least 780Ka in age (Kristjansson *et al.*, 1988).

- The youngest exposed lavas occur at the western end of the radial fissure system. The stratigraphy suggests an overall westward progression of volcanic activity during the last 300Ka.

- Ankaramites are restricted to the older part of the volcanic succession and trachytes are restricted to the upper parts of the succession suggesting that the volcano is becoming chemically more evolved with time.

- The topographic inversion of valley-confined subglacial deposits is occurring at several localities. The ages of such valley-confined deposits may fill the apparent time gaps found in vertical successions by K-Ar dating (Wiese, 1992).

- The north side of the Eyjafjöll volcanic system is draped with hyaloclastite lithologies which intruded between the steep slopes of Eyjafjöll and a glacier occupying the Markarfljot valley. Beneath these deposits, there is a typical layer-cake stratigraphy.

- Numerous inclined sheets of varying orientation are exposed in the core of the volcano. In the Laugara gorge, 7km south of the summit crater, roughly 20% of sheets dip outwards away from the volcano whereas at Gudnanipa, 4km south of the summit, there appears to be a much greater density of inward-dipping sheets.

- Sheets exposed at Eyjafjöll typically fall into three categories relating to three concurrent stress regimes:
  1) radial (magmatic);
  2) E-W; and
  3) NE-SW (regional).

  The core of the volcano is dominated by inclined sheets and NE-SW orientated sheets.

- NE-SW sheets represent basalt to trachyte compositions and may be fed by a deep, evolving magma chamber or several independently evolving sill-like magma chambers.

CHAPTER 5
PETROGRAPHY AND MINERAL CHEMISTRY

5.1 INTRODUCTION

Most of the previous work on the Eyjafjöll volcanic system has been of a petrologic nature. Steinthorsson (1964) produced a detailed petrological study of the Hvammsmuli ankaramite, on the south side of Eyjafjöll, which he interpreted as a sill complex. Sigurdsson (1970) briefly described two quartz trachytes and a benmoreite from Eyjafjöll and found that they correspond to the mildly alkalic differentiates of transitional or alkalic provinces. Jakobsson (1979b) studied 20 recent lavas from the upper slopes of Eyjafjöll, 17 were intermediate lavas ('basaltic andesites'), there were also 2 basalts and one acid lava. Carswell (1983) described the petrography of lavas in the Solheimajokull area, he found that the stratigraphically lowest lavas were ankaramites. Arney (1978) and Wiese (1992) both gave petrographic descriptions of a range of samples collected for geochemical analysis. In this study, outcrops of ankaramite, intermediate lavas and felsic lavas have been found which will help in understanding the magmatic processes taking place at the Eyjafjöll volcanic system.

5.2 CLASSIFICATION AND NOMENCLATURE

The postglacial lavas of the Eastern Volcanic Zone are composed of three types of basic rock: alkali olivine basalts, tholeiitic basalts and transitional alkali basalts (Jakobsson, 1979b). Alkali olivine basalts and tholeiites fall in two distinct fields on a total alkalies versus silica diagram (e.g Tilley, 1950; Macdonald and Katsura, 1964; Miyashiro, 1978), they also form separate trends on an AFM diagram (Irvine and Baragar, 1972). Transitional alkali basalts, as their name implies, may fall in the alkali field in one diagram and the tholeiite field on another; according to Jakobsson (1979) all the transitional alkali basalts of the EVZ are Hy-normative. Figures 5.1 and 5.2 show that the basic rocks of the Eyjafjöll volcanic system are dominated by transitional alkali basalts, although several alkali olivine basalts and rare tholeiites also occur.

The transitional alkali basalts of the EVZ also contain substantial amounts of Fe_2O_2T and TiO_2 (Jakobsson, 1979b; Meyer *et al,* 1985). High Fe-Ti basalts are defined by Melson (1976) as containing more than 12 wt% Fe_2O_3T and more than 2 wt% TiO_2, most of the transitional alkali basalts at Eyjafjöll may thus be described as 'high Fe-Ti transitional alkali basalts' (Figure 5.3). The transitional alkali basalts also show similarities to the ferrobasalts of the Galapagos, which are defined by McBirney and Williams (1969) as having more than 12 or 13 wt% Fe_2O_3T and less than 6% MgO. In this study, the rocks of the Eyjafjöll volcanic system have been classified according to

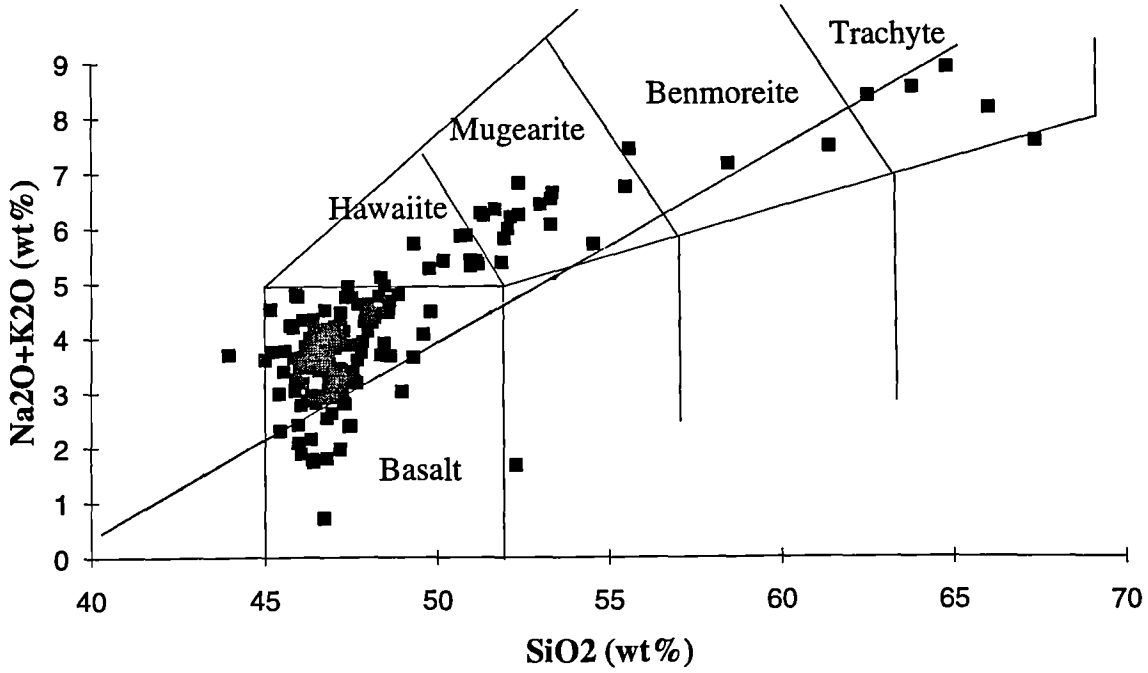

Figure 5.1 *Total Alkalis versus Silica (TAS) diagram showing the Hawaiian dividing line of Macdonald (1968).*

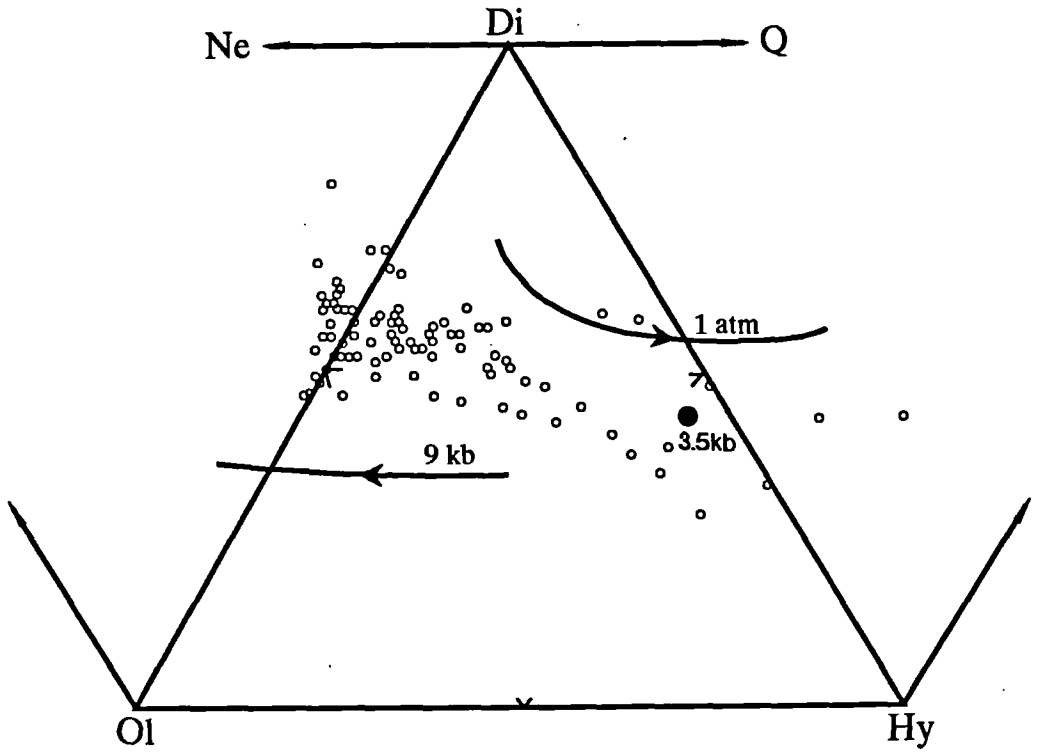

Figure 5.2 *CIPW normative diagram for selected basalts, 1 atm and 9kb cotectic curves from Thompson et al.(1983), 3.5kb 'Martindale basalt' from Helz (1980).*

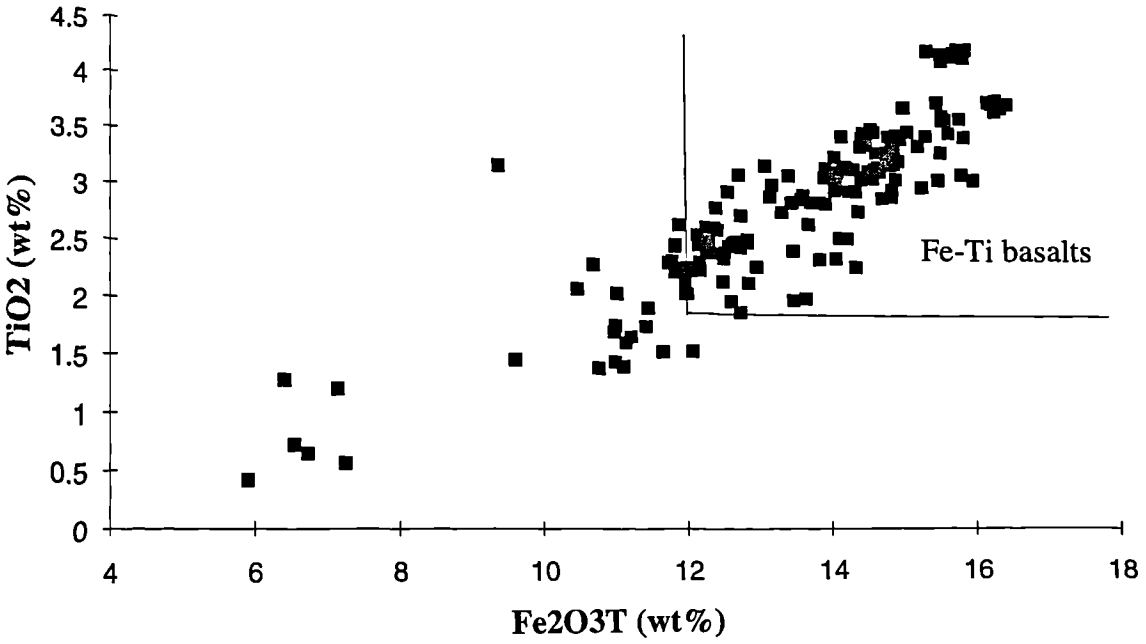

Figure 5.3 *Fe_2O_3T versus TiO_2 for all whole rock data showing the FeTi basalt field according to Melson (1976).*

the I.U.G.S classification scheme (Le Bas *et al.*, 1986; Le Maitre *et al.*, 1989; Le Bas and Streckeisen, 1991). When plotted on a total alkali versus silica (TAS) diagram (Figure 5.1), data points fall in the basalt, hawaiite, mugearite, benmoreite and trachyte fields; most data points plot above the dividing lines of Macdonald and Katsura (1964) and Miyashiro (1978). The original definitions of hawaiite and mugearite (Iddings, 1909) define these rocks in terms of normative plagioclase content; in this study, these names apply simply to the field in which the rocks fall on a TAS diagram.

Jakobsson (1979b) described the transitional series at Eyjafjöll as ankaramites (>15 wt% MgO), transitional alkali basalts (4.5-8 wt% MgO) and basaltic andesites (2-4.5 wt% MgO). In this study, the rocks he classified as 'basaltic andesites' fall in the fields of basalt, hawaiite and mugearite.

Ankaramites are a variety of picritic basalt. Picritic basalts are defined by Macdonald and Katsura (1964) as containing more than 25% normative olivine, they may be divided into two types: oceanite, which is a member of the tholeiitic series and ankaramite, which is a member of the transitional alkali series. Oceanite contains very abundant phenocrysts of olivine whereas ankaramite contains abundant phenocrysts of olivine and clinopyroxene, the picritic basalts at Eyjafjöll are of the ankaramite type. According to Macdonald and Katsura (1964) a true ankaramite must contain less than 30% modal feldspar.

5.3 MAIN LITHOLOGIES

5.3.1 ANKARAMITES

There are numerous lavas rich in olivine and clinopyroxene phenocrysts at Eyjafjöll, however, the term 'ankaramite' is reserved for those rocks which appear to lack plagioclase phenocrysts and have less than 30% modal plagioclase. In thin section, rare plagioclase phenocrysts or microphenocrysts can occasionally be found. There is a population of px-ol-pl phyric basalts which can contain up to 40% phenocrysts. These basalts have been termed ankaramites by several authors but they contain over 30% modal plagioclase. Table 5.1 shows a comparison of modal mineralogy for selected true ankaramites and selected px-ol-pl phyric basalts.

Table 5.1 *Table showing the modal mineralogy of selected ankaramites and px-ol-pl phyric basalts.*

SAMPLE NO.	Pyroxene	Olivine	Plagioclase	Magnetite
Ankaramites				
43	43	32	16	9
74	20	47	30	3
501	46	24	26	4
502	46	18	27	9
Px-ol-pl phyric basalts				
190	36	15	37	12
279	32	22	41	5

True ankaramites occur at Hvammsmuli (samples 74 & 43), Ira (390), Arnarklettur, Gretishaf (498, 501 & 502), Raufarfell (524) and Nupakot (251). The extent of the 'true' ankaramites is much greater than previously realised. It is also clear that they are not confined to the base of the succession as is the case at Solheimajökull (Carswell, 1983).

In most of the ankaramites at Eyjafjöll, olivine and diopsidic augite phenocrysts occupy between 10 and 25% of the whole rock (Figure 5.4 A). The two phenocryst types usually occur in sub-equal proportions. Samples 43, 501 and 502 contain abundant irregularly shaped vesicles, these ankaramites all lie directly on non-vesicular ankaramites which show no other apparent differences.

5.3.1.1 OLIVINE

Olivine phenocrysts form euhedral, embayed and subhedral crystals, all of which may coexist in one rock (Figure 5.4 A, B & C). Olivine core compositions in ankaramites typically fall between Fo_{81-90} and olivine rim compositions fall between Fo_{77-84}, however, the Hvammsmuli ankaramite (sample 74) is slightly more differentiated, core

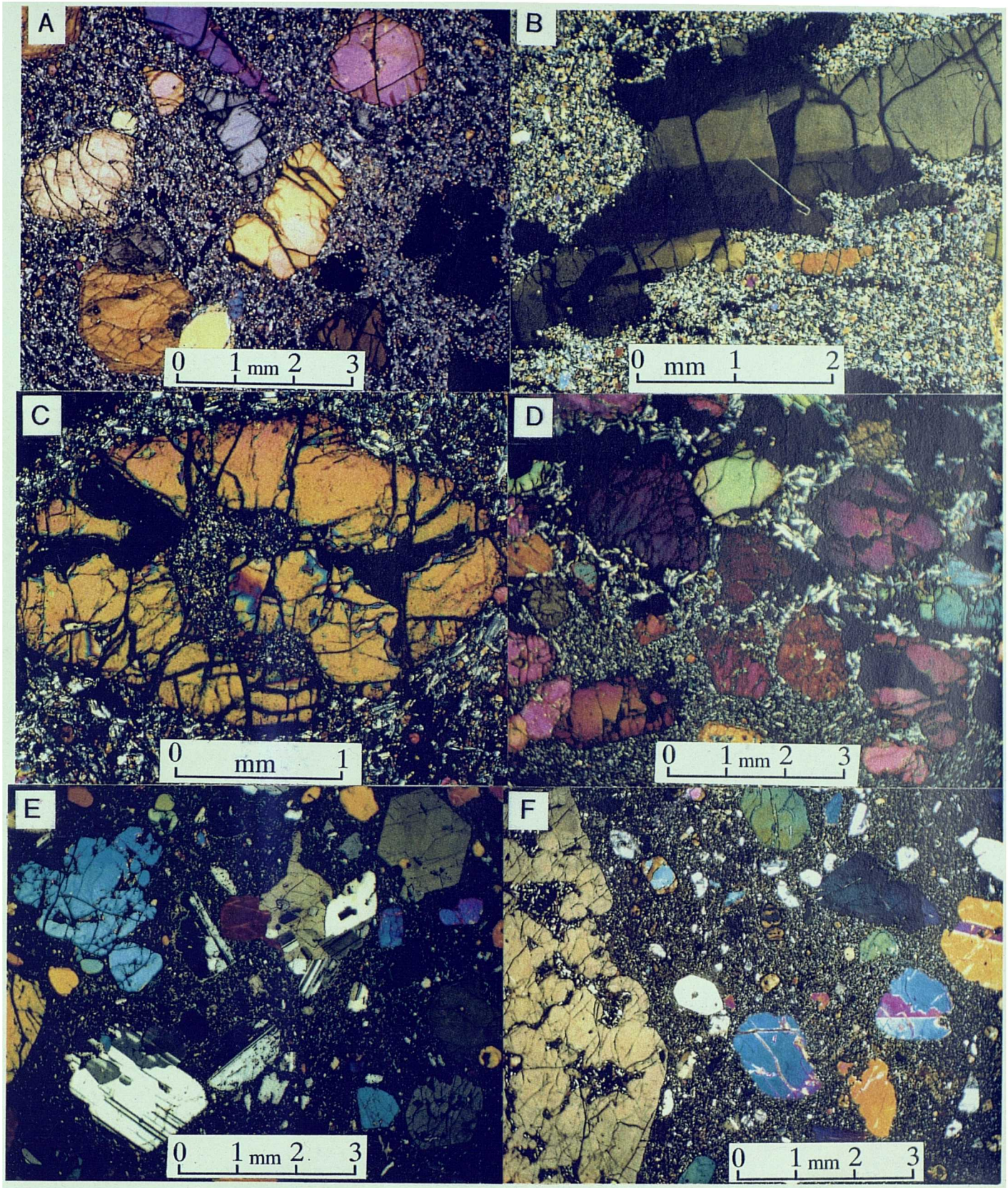

Figure 5.4 A: *Sample 74 (Hvammsmuli ankaramite) showing euhedral and subhedral olivine phenocrysts, clinopyroxene phenocrysts with sieve-textured margins and Ti-magnetite phenocrysts with poikilitic rims. Groundmass is granular and contains feathery Ti-magnetite.* **B:** *A strained, kink-banded, subhedral olivine phenocryst in sample 74.* **C:** *Hvammsmuli ankaramite adjacent to a highly porphyritic vein, showing granular clinopyroxene occupying an embayment in an olivine. Groundmass is intergranular and subophitic.* **D:** *Contact between a highly porphyritic vein (sample 74B) and host rock. The vein contains olivine, clinopyroxene and plagioclase phenocrysts in an evolved plagioclase-rich groundmass.* **E:** *Porphyritic basalt (sample 279 - Nupakotsdalur Group) showing co-existence of euhedral and resorbed phenocrysts of clinopyroxene and plagioclase, subhedral olivine and occasional gabbroic xenoliths.* **F:** *Porphyritic basalt (sample 190 - Nupakotsdalur Group) showing the margin of a primitive, skeletal clinopyroxene coexisting with resorbed, evolved clinopyroxene, partially altered olivine and resorbed and euhedral plagioclase.*

compositions are in the range Fo_{76-84}, rim compositions are between Fo_{72-79} and groundmass olivines are Fo_{69} (Figures 5.4 A-D).

Euhedral phenocrysts (<6mm) are commonly zoned to more Fa-rich compositions at the rim, indicated by higher order polarisation colours and a stronger brown colour. Curving fractures around the rim may be a response to the compositional zoning (Moore & Evans, 1967). Some euhedral phenocrysts, especially in the Hvammsmuli ankaramite (sample 74) are slightly rounded, suggesting resorption. Euhedral olivines typically show a range of Fo contents in a single sample, for example, in sample 43 the most primitive and the most evolved olivines are euhedral (Fo_{81} and Fo_{90}).

Subhedral olivine phenocrysts form large irregular crystals (<12mm) which at first appearance look like clusters of smaller euhedral olivines. The core compositions of these large, subhedral olivines is relatively constant in all samples at around Fo_{84}. The subhedral phenocrysts do not show strong zoning, but strain-banding is very common (Figure 5.4 B); euhedral olivines are rarely strain-banded. The co-existence of euhedral, undeformed olivine and large subhedral, strain-banded olivine of similar composition has been noted in picrites from Mauna Loa and Kilauea (Wilkinson & Hensel, 1988), Kilauea Iki lava lake (Helz, 1980; 1987) and in tholeiites from Mauna Kea (Frey *et al.*, 1991). Wilkinson & Hensel (1988) interpreted the strain-banded crystals as cognate minerals deformed as they were forced through narrow conduits in pressurised magma. In contrast, Helz (1987) interpreted strain-banded olivines as xenocrysts torn from ultramafic cumulates by relatively evolved magmas. Some olivines, especially euhedral phenocrysts, contain inclusions of dark brown chrome spinel. The relatively constant composition of strain-banded phenocrysts in different lavas suggests that a cumulate origin is the most likely scenario.

5.3.1.2 CLINOPYROXENE

Most ankaramite lavas contain euhedral, subhedral and resorbed (rounded) phenocrysts of diopsidic augite up to 8mm in size (Figure 5.4 A). Core compositions are in the range $Wo_{41}En_{51}Fs_6$ to $Wo_{44}En_{44}Fs_{12}$, and rim compositions are in the range $Wo_{44}En_{49}Fs_7$ to $Wo_{44}En_{45}Fs_{11}$. Zoning to more Fe and Ti-rich margins may be detected by a change in colour to darker brown, this only affects the euhedral clinopyroxenes. Several clinopyroxene phenocrysts show slight reverse zoning towards the margin (e.g. $Wo_{44}En_{44}Fs_{12}$ core to rim $Wo_{45}En_{45}Fs_{10}$, sample 43). Some ankaramites (e.g sample 251 in the Nupakotsdalur Group) contain large skeletal augites up to 4cm in size which commonly coexist with smaller, resorbed diopsidic augites of a more evolved composition. These are similar to those described at Jan Mayen by Maaloe *et al.* (1986). The diopsidic augite phenocrysts of the Hvammsmuli ankaramite (sample 74) have rounded, resorbed cores and a discontinuous rim marked by a distinct line of tiny melt

inclusions (Figure 5.4 A). The rim itself shows sieve texture and subophitic overgrowth with the plagioclase laths of the groundmass.

Sparse microphenocrysts of Ti-magnetite occur in the ankaramites, these are typically equant crystals less than 1mm in size. The Hvammsmuli ankaramite contains microphenocrysts up to 2mm in size with homogenous cores and poikilitic rims (Figure 5.4 A).

All ankaramite lavas, except the Hvammsmuli ankaramite, have a very fine-grained groundmass dominated by plagioclase and clinopyroxene with varying amounts of olivine and iron oxides, the texture is typically subophitic or intergranular. The ankaramite at Hvammsmuli shows a variety of different groundmass textures including granular, intergranular and subophitic. Groundmass olivines in ankaramites are rounded suggesting that they crystallised first, plagioclase forms laths or stubby tabular crystals, clinopyroxene forms small equant grains and ilmenite forms acicular crystals. Ti-magnetite forms an abundant, granular groundmass phase in most ankaramites and elongate, feathery crystals in the Hvammsmuli ankaramite (Figure 5.4 A).

5.3.1.3 THE HVAMMSMULI ANKARAMITE - A LAVA LAKE?

The Hvammsmuli ankaramite is clearly distinctive from other ankaramites in several respects (Figures 5.4 A-D). The Hvammsmuli area is composed of several isolated outcrops which altogether cover an area of roughly 400 x 400m. The ankaramite is at least 45m thick. Steinthorsson (1964) documented several different types of ankaramite based on phenocryst content and groundmass textures, including aphyric ankaramite (Figure 5.5). The granular-intergranular type described above is the most abundant and forms most of the exposure. Steinthorsson (1964) also noted the presence of xenoliths and intrusive veins and bands within the Hvammsmuli ankaramite. Elongate, aphyric xenoliths are 15-30cm long with a rounded end and a sharp end, these lie parallel to non-porphyritic bands which dip at about 30° to the southwest. The bands are thin, aphyric planes, folded in cross-section and containing aligned plagioclase laths. Steinthorsson (ibid) also noted a columnar basalt xenolith lying parallel to these bodies, it shows a degree of fusion at its margins. There is also a composite xenolith, 0.5 x 1m in size, half of which is composed of porphyritic ankaramite and half of non-porphyritic basic lava. Late-stage highly porphyritic veins also cut much of the complex. Based on the parallelism of the inclusions and bands, Steinthorsson (1964) interpreted the Hvammsmuli area as a sill complex.

A highly vesicular, 'frothy' rock forms a dyke-like intrusion in a southern outcrop (Figure 5.5) and also caps the quarry outcrop, this clearly contained abundant volatiles and is now heavily weathered. Above this is a grassy slope which separates the ankaramite from the lava succession above. Although no upper contact is exposed, the lowest eruptive unit of the overlying sequence has almost exactly the same whole-rock composition as the underlying ankaramite (sample 74).

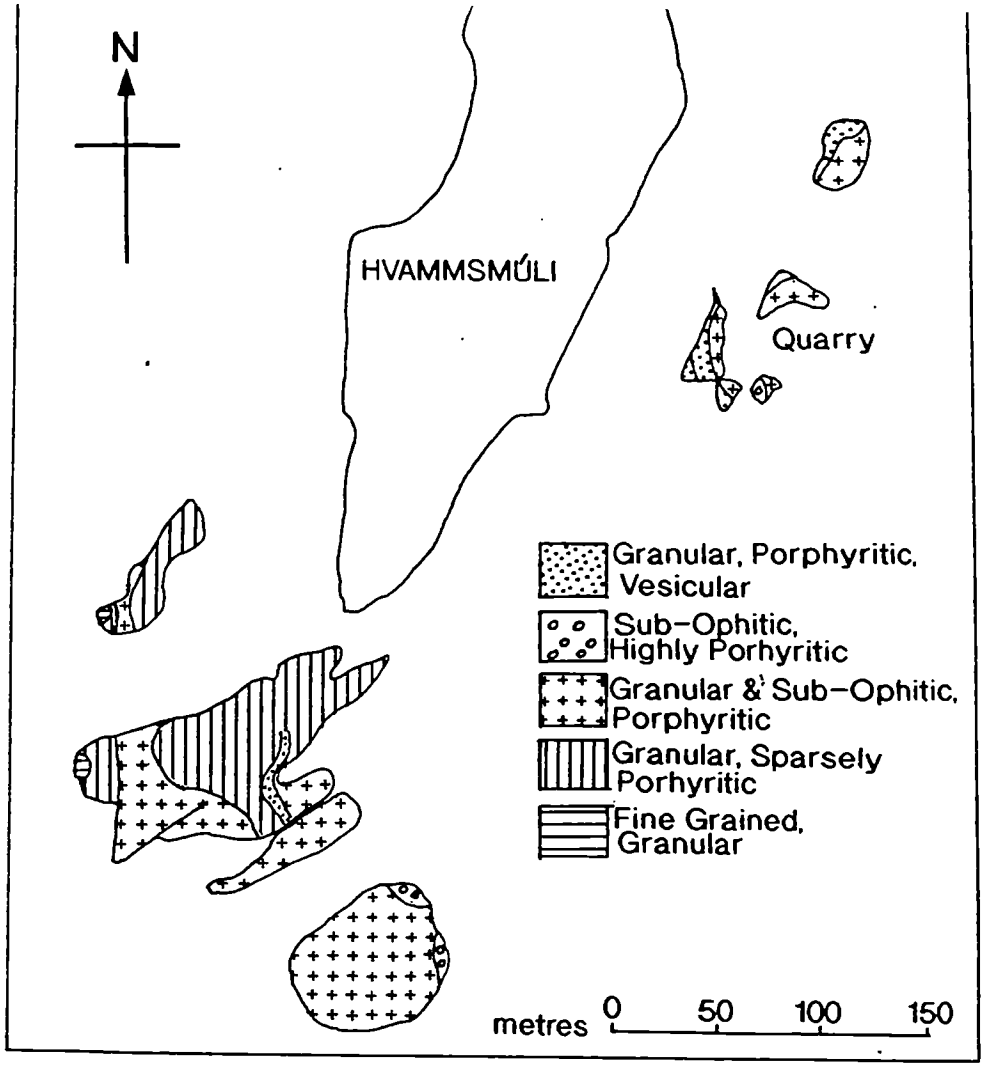

Figure 5.5 *Sketch map of the Hvammsmuli ankaramite outcrops from Steinthorsson (1964).*

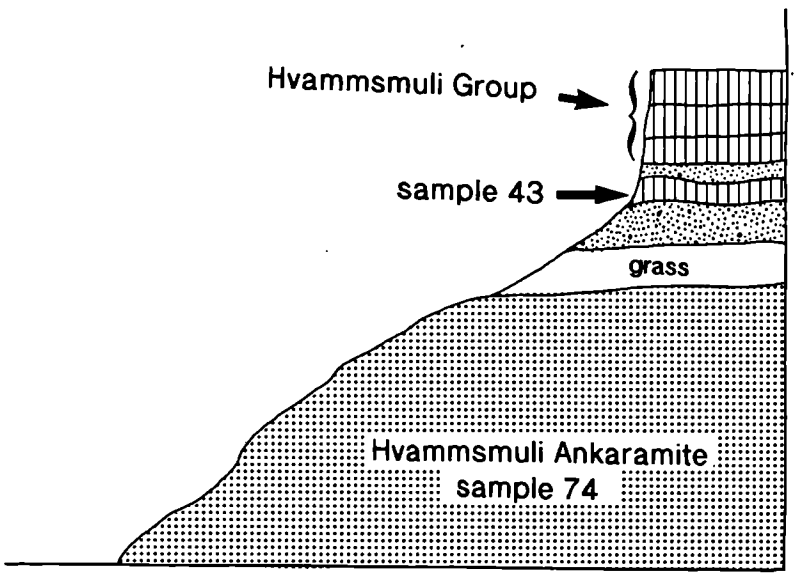

Figure 5.6 *Schematic cross-section of the Hvammsmuli area. See also Figure 4.17.*

This unit (sample 43 - Figure 5.6) is a deposit of reddened, weathered, bedded ash and cinders and a thin (<0.5m), vesicular lava flow. The lava contains phenocrysts of olivine and clinopyroxene with only slight zoning in a very fine-grained groundmass, it contains sparse, euhedral olivines of Fo_{81-90} composition. This lava is clearly related to the Hvammsmuli ankaramite, however, it's subaerial nature suggests that it is not part of a sill complex.

The highly porphyritic veins which intrusively cut the Hvammsmuli ankaramite contain at least 60% phenocrysts (Figure 5.4 D). They are rarely thicker than 6cm. The phenocryst proportions are: diopsidic augite (55%), olivine (40%) and, in contrast to the host rock, (5%) plagioclase phenocrysts. The olivine phenocrysts are commonly subhedral and strain-banded, core compositions are between Fo_{66-84} and rim compositions are between Fo_{65-71}. It is possible that in this case strain banding is imparted to the phenocrysts during intrusion into the vein in a similar manner to that envisaged by Wilkinson and Hensel (1988). Pyroxene phenocrysts are subhedral with margins subophitically enclosing groundmass. Plagioclase phenocrysts have resorbed cores (An_{82-87}) which often contain glass and rectangular opaque inclusions aligned within the crystal structure, mantles (An_{65-68}) show strong oscillatory zoning and may also contain numerous inclusions. A distinct rim (An_{52-65}) may show subophitic intergrowth with the groundmass and/or resorption along twin planes. The groundmass is composed of aligned to stellate plagioclase laths 4 or 5 times larger than in the host groundmass (<0.5mm) but of a similar composition (An_{68}) with sparse, intergranular clinopyroxene, rounded olivines and blocky magnetite. In places, especially between clinopyroxene phenocrysts, the groundmass is composed wholly of plagioclase. In other parts of the vein there is only a single thickness of plagioclase laths between phenocrysts, the phenocrysts show partial alignment to the vein margins.

The host ankaramite near these intrusive veins shows some unusual characteristics. Stringers and elongate patches of pure plagioclase occur in the groundmass which are similar to the larger plagioclase-rich bands described by Steinthorsson (1964). The groundmass mineral proportions and textures are variable over small distances (cms). Intergranular and subophitic textures are common, in places plagioclase is the most abundant groundmass phas. However,. elsewhere (particularly in olivine phenocryst embayments), small, granular pyroxenes are the most abundant groundmass phase (Figure 5.4 C). Phenocrysts of pyroxene are commonly surrounded by zones of pure groundmass plagioclase up to 0.3mm thick, suggesting diffusion as a mechanism for growth of the pyroxene rim. Such evidence for diffusion is more likely in stagnant magma (McBirney, 1993)

The great variety of petrographic features at Hvammsmuli requires some explanation. Although it was not studied in great detail, it is proposed in this study that Hvammsmuli may have been the site of a small, topographically-confined lava lake. The exposure shows that the ankaramite has a limited lateral extent but is about 45m thick

suggesting that ponding has occurred. The granular-intergranular texture of the Hvammsmuli ankaramite may have been caused by relatively slow cooling and perhaps movement of the crystallising groundmass (Steinthorsson, 1964). The margins of the complex tend to have subophitic texture and are finer-grained, perhaps as a result of more rapid, *in-situ* cooling. Stringers and bands of plagioclase-rich material may form by segregation or flow differentiation, or, by the rise of residual, differentiated liquid from a crystal mush at the base of the lake (Helz *et al.*, 1989). Alternatively, they may have formed during diffusive processes. The phenocryst-rich veins contain plagioclase phenocrysts, olivine and clinopyroxene phenocrysts of similar composition to the host rock and an evolved plagioclase-rich groundmass. The veins cut through the host rock when it was partially solidified. These veins are similar to the 'vertical-olivine-rich-bodies' described by Helz *et al.* (1989) at Kilauea Iki lava lake, Hawaii, however the latter are described as diapirs, not veins. The vesicular, volatile-rich body may have formed as a diapir-like body (Helz *et al.*, 1989). This material may subsequently have ponded beneath a crust at the top of the lake. Subsequent lavas (i.e.sample 43) flowed over the surface crust of the lava lake. Alae lava lake in Hawaii was only 13.7m thick and solidified completely within a year (Helz *et al.*, 1989), a similar time scale may apply to a lava lake at Hvammsmuli which was not much thicker. Only a detailed geochemical study of the Hvammsmuli exposures will be able to discuss this theory in more depth.

5.3.2 BASALTS

The majority of the Eyjafjöll basalts are Hy normative. The few Ne-normative lavas are also the stratigraphically oldest lavas (Laugara Group, Laugara subgroup 2 and members of the Nupakotsdalur Group and Hvammsmuli Group). Basalts vary a great deal in mineralogy, phenocryst proportions and texture. Most basalts contain phenocryst assemblages of either plagioclase + augite, or, plagioclase + augite + olivine.

Basalts have been divided into four main types:

1) aphyric basalts (<5% phenocrysts),
2) Fe-Ti basalts (>4% TiO2),
3) highly porphyritic basalts (>20% phenocrysts), and
4) weakly to moderately porphyritic basalts (5-20% phenocrysts).

Types 1 and 2 are not mutually exclusive, in fact most Fe-Ti basalts contain < 5% phenocrysts.

5.3.2.1 APHYRIC BASALTS

Aphyric basalts are not common, reflecting the scarcity of superheated liquids reaching the surface in the Eyjafjöll volcanic system. Aphyric and sparsely-phyric basalts tend to be either high in MgO (>5%) or contain >3.5% TiO2. The most primitive aphyric basalt lava contains 7% MgO (sample 206, Nupakotsdalur Group).

5.3.2.2 FeTi BASALTS

FeTi basalts are small in volume and confined to only a handful of localities. Basalts with particularly high Fe_2O_3T and TiO_2 are exposed over most of the upper slopes at Skogaheidi, to the east of the volcano. TiO_2 content is over 4%, very similar to basalts of the Katla system (Carswell, 1983; Meyer. *et al* 1985). Later lavas, erupted from the E-W fissures which cross Skogaheidi have reduced TiO_2 and Fe_2O_3T contents in comparison (e.g. samples 65 and 68; TiO_2 = 3.72-3.73). Other basalts containing high Fe_2O_3T and >4% TiO_2 are small in volume and localised in extent, but clearly belong to the Eyjafjoll volcanic system, they occur at Drangshlid, Nupakotsdalur and Fjell. At Fjell, Fe-Ti rich basalt dykes cut the Fjell trachyte and feed overlying Fe-Ti rich basalt lavas. These lavas contain small, sparse phenocrysts of plagioclase, often with a resorbed core containing inclusions, a mantle showing oscillatory zoning and a resorbed rim. Rare clinopyroxene microphenocrysts also show signs of resorption. Occasionally glomerophyric clusters of stellate plagioclase with sector-zoned augite and skeletal microphenocrysts of Fe-oxides occur. Tiny Fe-oxides are abundant in the groundmass together with plagioclase laths, which often show flow alignment. Samples 404 and 406 from Drangshlid show mixing between different basalt magmas. Rounded inclusions of cryptocrystalline material containing stubby plagioclase, augite and apatite crystals may be found in a host rock with an intergranular and intersertal groundmass of plagioclase,

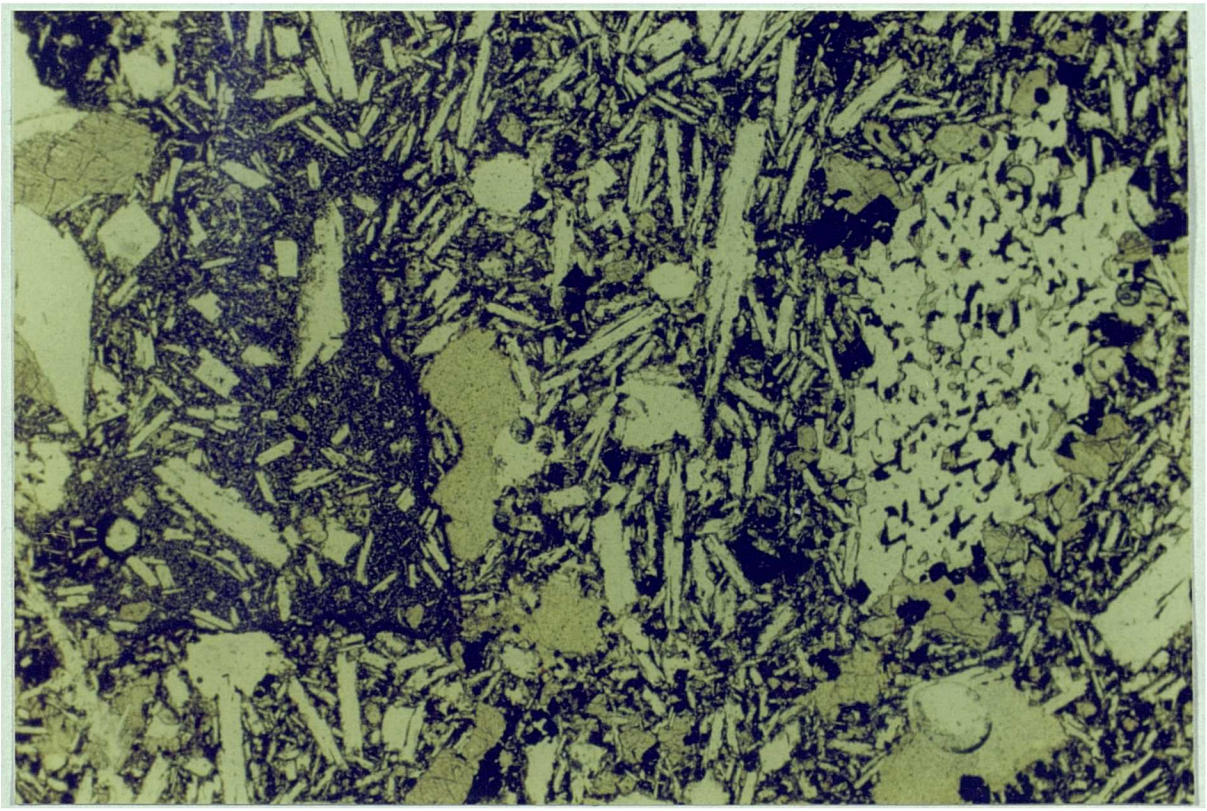

Figure 5.7 *Sample 406 from Drangshlid, an FeTi basalt containing basalt inclusions. Field of view 3 x 1.9 mm.*

augite, apatite and glass. The cryptocrystalline inclusions contain numerous tiny Fe-oxides in the groundmass and the margins of the inclusion are marked by a thin band of Fe-oxides (Figure 5.7). The host lava contains sparse phenocrysts of plagioclase and augite with stellate clusters of subophitic plagioclase and sector-zoned augite. The abundant evidence for disequilibrium in these high Fe-Ti basalts may be caused by mixing of different magmas as observed in samples 404 and 406, and/or by incorporation of phenocrysts from conduit or magma chamber walls. Liquid immiscibility may also have played a role in the generation of these basalts.

5.3.2.3 HIGHLY PORPHYRITIC BASALTS

A very distinctive group of porphyritic basalts contains between 20 and 60% phenocrysts of clinopyroxene (<12mmm, rarely <4cm), plagioclase (<10mm) and olivine (<9mm). The numerous phenocrysts occur in varying proportions from lava to lava, even within a genetically-related sequence. Typically, in order of abundance, the phenocryst phases are px-ol-pl or pl-px-ol. The px-ol-pl phyric basalts are more common towards the base of the succession, the modal abundances of two such basalts from the Nupakotsdalur Group are shown in Table 5.1. The pl-px-ol phyric basalts are common on the upper slopes of the volcano, the phenocrysts occasionally comprising up to 60% of the whole rock.

Taking sample 190 from the Nupakotsdalur Group as an example of a px-ol-pl phyric basalt (Figure 5.4 F), it shows abundant evidence of disequilibrium, with co-existing euhedral, skeletal and resorbed phenocrysts. Large, skeletal clinopyroxenes (core - $Wo_{45-46}En_{47-44}Fs_{7-9}$) coexist with smaller euhedral phenocrysts (core - $Wo_{45-46}En_{44-41}Fs_{11-13}$) suggesting that they formed during supercooling of a primitive liquid, perhaps during replenishment of an evolving magma chamber. These skeletal phenocrysts are up to 4cm in length, with well-defined crystal faces. The groundmass enclosed by the megacryst is coarser-grained but otherwise similar to the host lava, however, fans of quench plagioclase can be seen growing from the megacryst margins into these pockets of basaltic groundmass. A phenocryst of olivine has been enclosed by one skeletal clinopyroxene. It is proposed that the skeletal form of these megacrysts is caused by rapid crystallisation as opposed to resorption. The groundmass clinopyroxene has a relatively primitive composition of $Wo_{46}En_{46}Fs_{8}$. Euhedral plagioclase phenocrysts (An_{79-80}) co-exist with sieve-textured phenocrysts (An_{38}) and resorbed, zoned phenocrysts (core - An_{80-81}, mantle - An_{60-63}, rim - An_{72}). Olivine phenocrysts have a relatively restricted compositional range of Fo_{75-80}.

Sample 345 occurs near the top of a sequence of highly pl-px-ol phyric basalts at Halsar. This particular basalt contains a high proportion of plagioclase phenocrysts, many of which contain numerous glass inclusions. The olivine core compositions show a limited range of Fo_{74-79}. Plagioclase phenocryst core compositions are limited to

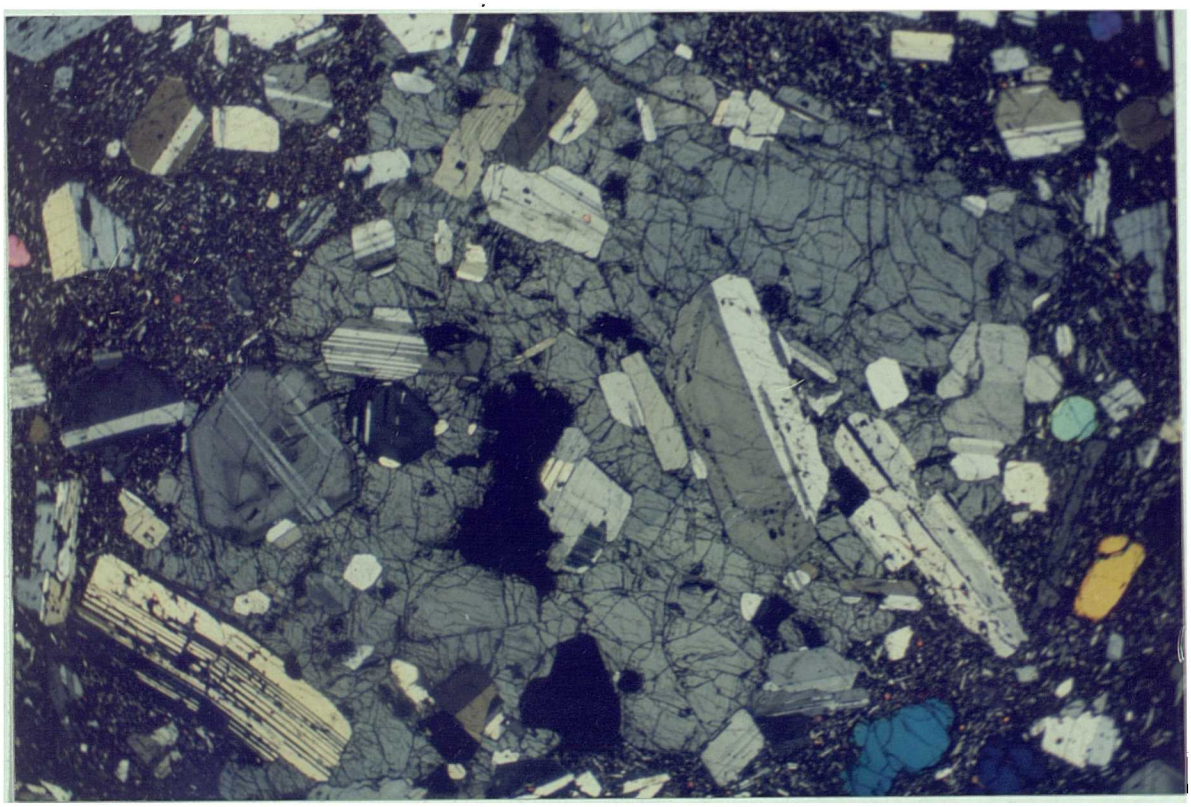

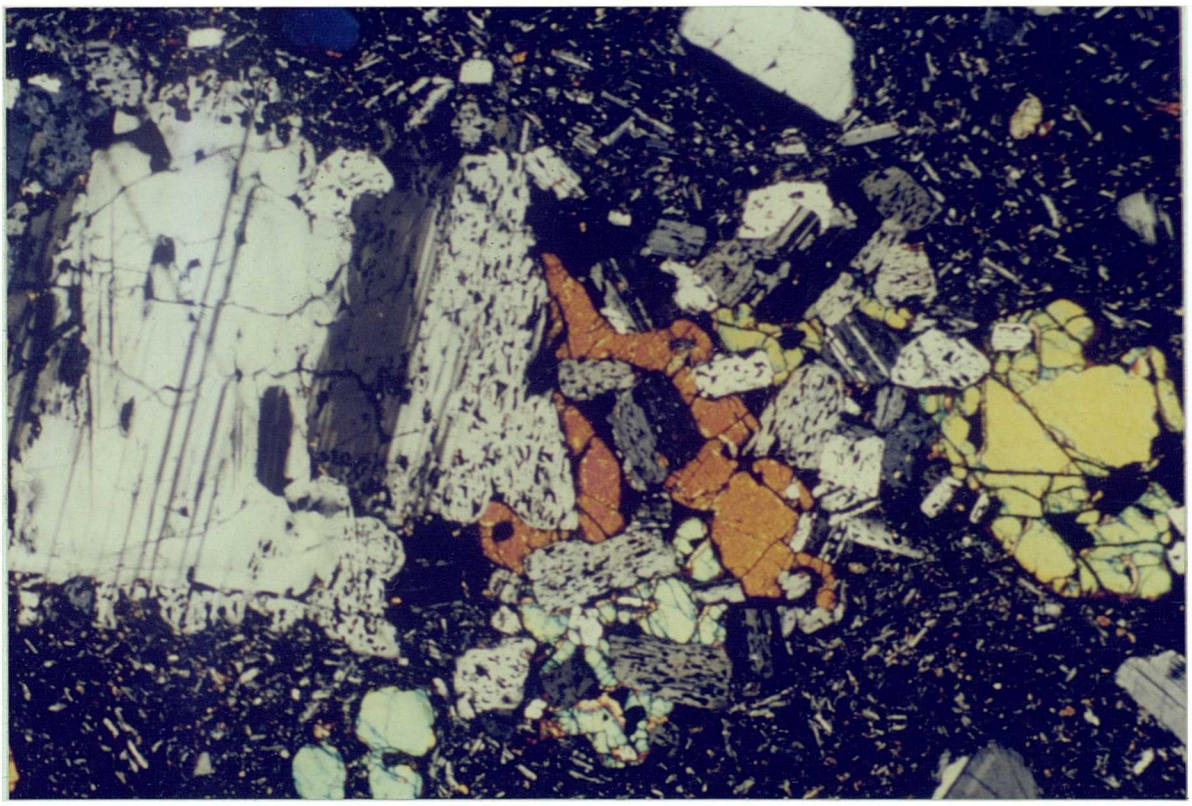

Figure 5.8 a) *A large clinopyroxene crystal poikilitically enclosing zoned, euhedral and slightly rounded plagioclase phenocrysts. Sample 345, a highly porphyritic basalt. Field of view 12 x 7.2 mm.* **b)** *A xenolith composed of resorbed plagioclase with intergranular clinopyroxene, from sample 345, a highly porphyritic basalt. Field of view 6 x 3.7 mm.*

An_{76-81}, whereas plagioclase phenocryst rims and groundmass compositions have a range of An_{49-66}.This basalt also contains numerous crystal aggregates showing different textures. These include large clinopyroxenes (<10mm) with poikilitic plagioclase phenocrysts and rare magnetite microphenocrysts (Figure 5.8a), and clusters of sieve-textured plagioclase with intergranular clinopyroxene (Figure 5.8b). The latter show evidence of resorption at the margins suggesting that they may be xenoliths.

These highly porphyritic basalts all have high MgO contents between 7% and 12%, this is directly as a result of the accumulation of phenocrysts.

5.3.2.4 WEAKLY TO MODERATELY PORPHYRITIC BASALTS

This description again covers a variety of petrological types. Weakly to moderately porphyritic basalts from some of the major stratigraphic Groups are described below.

The Laugará Group basalts are moderately porphyritic (10-20 vol% phenocrysts). Olivine phenocrysts containing chromite have compositions of Fo_{89-90}, a second population of olivine phenocrysts falls in the range Fo_{75-80}. Some clinopyroxene phenocrysts are embayed but it is not clear if this is due to resorption or not. Crystal aggregates are common in these lavas; rounded plagioclase aggregates which appear to have nucleated on single olivine crystals are particularly abundant.

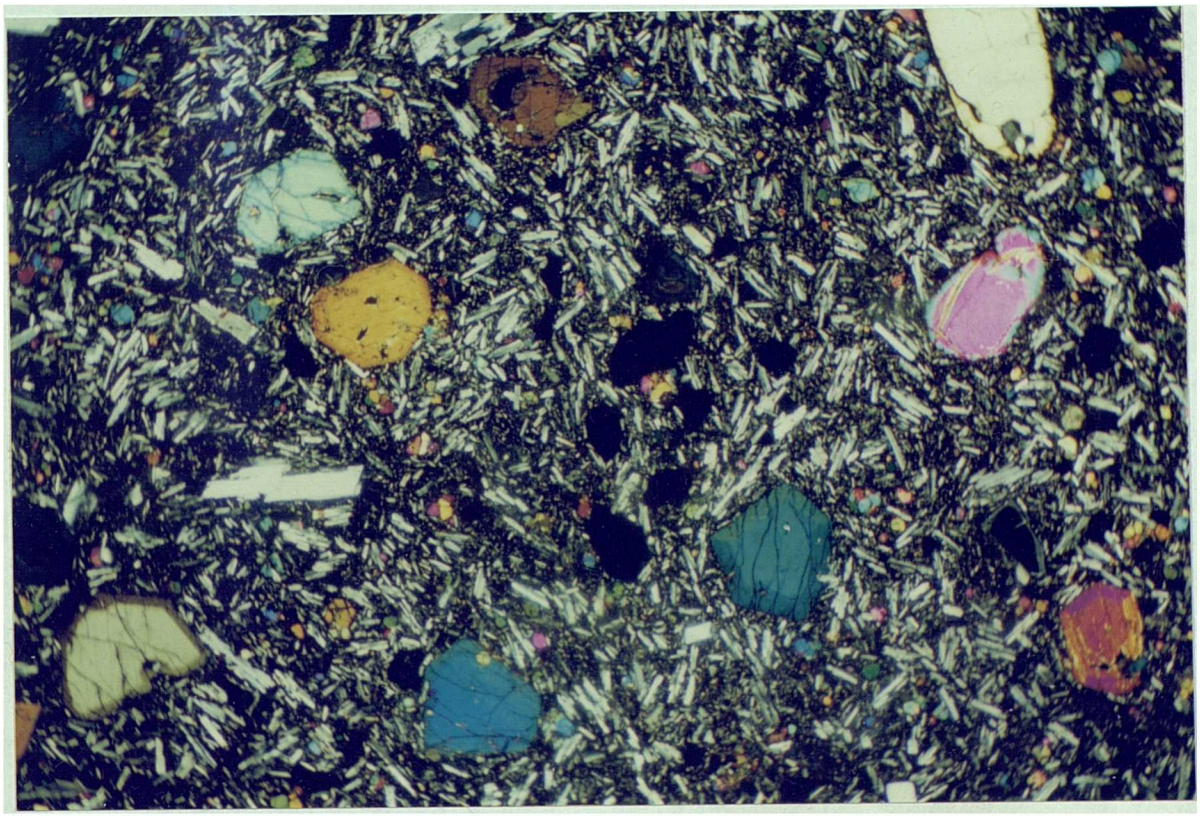

Figure 5.9 *Sample 44, a member of the Hvammsmuli Group, showing olivine (top right) and clinopyroxene (bottom left) phenocrysts with distinct rims. The clinopyroxene at the bottom right shows sector-zoning within the outer rim. Field of view 12 x 7.2 mm.*

Basalts of the Svadbaelisheidi Group are unusual because they contain abundant phenocrysts (5-20 vol%) of plagioclase and olivine; clinopyroxene phenocrysts are rare. Groundmass olivine is abundant in the later lavas from this group (Fo_{63-69}) but virtually absent from the lower lavas. Isolated olivines in the groundmass are highly evolved e.g. Fo_{36}. The euhedral olivine phenocrysts have core compositions between Fo_{73-80}. They are commonly zoned to more Fe-rich rims and are rarely larger than 3mm in length. Plagioclase phenocrysts are larger (<5mm) and also show evidence of zoning (An_{74-82}), groundmass plagioclase compositions are in the range An_{64-70}.

Another distinctive basalt sequence is the Hvammsmuli Group, which compositionally includes two sub-groups of basalts. The lower subgroup lies directly over the Hvammsmuli ankaramites, it contains numerous clinopyroxene and olivine phenocrysts up to 4mm in size. The clinopyroxenes show homogenous euhedral or rounded cores with an oscillatory-zoned mantle. Sector-zoning in the phenocrysts is common (Figure 5.9). The olivines are euhedral and show zoning to Fe-rich rims. There are sparse plagioclase microphenocrysts containing glass inclusions. The intergranular groundmass contains plagioclase laths, Fe-oxides and abundant euhedral olivine and clinopyroxene crystals.

5.3.3 HAWAIITES AND MUGEARITES

Hawaiites and mugearites are low magnesium, evolved basalts which may be distinguished from less differentiated basalts by the presence of groundmass andesine and/or oligoclase and the distinctive sub-trachytic texture of the groundmass. At Eyjafjöll, mugearites may develop distinctive contact-parallel platy jointing, both hawaiites and mugearites weather to a pale grey and may show flow banding.

Most of the postglacial lavas mapped by Jakobsson (1979b) are of hawaiite or mugearite composition (originally termed 'basaltic andesite'), they erupted from radial fissures to the west of the volcano and now cover large areas on the upper flanks of the volcano. Hawaiites and mugearites also occur at Fimmvorduhals, on Lambafellsheidi (the Seljavellir Group), at the summit of Raufarfell and above Asolfsskalaegg. Altogether however, they only amount to ~0.3km^3 in volume. All the lavas appear to have erupted from radial fissures during the last glacial period and the early stages of the postglacial period.

The petrography of these lavas is highly variable, including aphyric to at least 15% phyric. Phenocryst phases include plagioclase, clinopyroxene, olivine and Ti-magnetite. In each lava, at least two populations of plagioclase typically occur, for example, sample 270 (Fimmvorduhals Pass) contains phenocryst cores of An_{23-38} and An_{50-61} and contains groundmass plagioclase of An_{23-26}.

The Seljavellir Group includes flow-banded lavas with phenocrysts of oligoclase, labradorite (<6mm), augite (<8mm), olivine (<5mm) and Ti-magnetite, and platy-jointed lavas with only sparse microphenocrysts (<2%). The phenocryst phases in

the flow-banded lavas form rare clusters of macrophenocrysts up to 3cm in diameter, some of these may be xenoliths. Euhedral and tabular sodic plagioclase may coexist with resorbed and strongly-zoned calcic plagioclase megacrysts An_{70-79}. Most clinopyroxene phenocrysts show zoning and/or resorption. Sparse olivines are also slightly resorbed, with core compositions between Fo_{74} and Fo_{82} and rim compositions between Fo_{74} and Fo_{77}. The flow-banding is caused by clots and streaks of darker coloured material in the groundmass. This material is very fine-grained, it may contain a higher proportion of opaques than the host groundmass which is composed of aligned plagioclase laths, opaques and chlorite (after clinopyroxene?). These bands may represent mixing of basic magmas with differing oxygen fugacities. The non flow-banded lavas often have a slightly coarser-grained, patchy or heterogeneous groundmass dominated by sub-trachytic textured plagioclase laths. The bimodal plagioclase and heterogeneous groundmass textures in some of these lavas suggests that magma mixing may have occurred. Even the lavas which appear homogenous contain phenocrysts which are clearly not in equilibrium with the host lava (Figure 5.10).

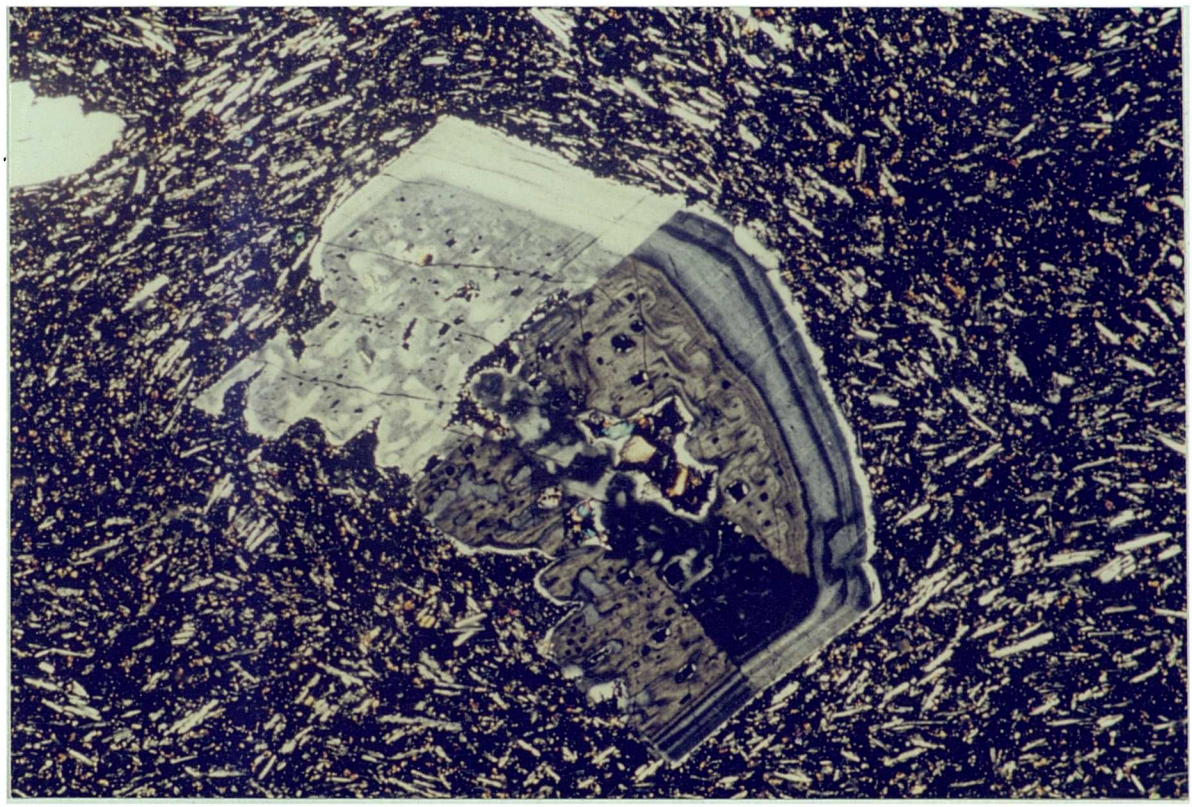

Figure 5.10 *A broken plagioclase phenocryst from sample 30, a hawaiite of the Seljavellir Group, showing a skeletal core, an oscillatory-zoned mantle and a resorbed rim. Field of view 3 x 1.9 mm.*

5.3.4 FELSIC LAVAS (BENMOREITE AND TRACHYTE)

5.3.4.1 BENMOREITES

Only one sample of benmoreite were collected at Eyjafjöll, it is a NE-SW striking dyke from Nupakotsdalur.

Sample 189 contains glomeroporphyritic clusters of zoned plagioclase and rounded clinopyroxene in a trachytic groundmass. Clinopyroxene phenocrysts have the composition $Wo_{42}En_{28}Fs_{30}$ and plagioclase phenocryst core compositions are between An_{26-32}.

5.3.4.2 TRACHYTE

Glacial moraine on the Eyjafjallajokull volcano contains fragments of varied evolved lavas, indicating that they do occur in some abundance on the volcano. In this study, *in-situ* outcrops of felsic lavas (trachytes) were discovered at only four localities. No rhyolite lavas were found, the most evolved trachyte contains 68% SiO_2. The outcrops are typically small in extent and occur high in the stratigraphic sequence, all are above 600m.

To the north of the volcano, on the western slopes above Gigjokull, a greenish, platy, trachyte lava dips towards the north. There is an abundance of glassy, feldspar-phyric loose fragments here suggesting that there are more evolved lavas further upslope. The lavas at this locality contain up to 15% euhedral phenocrysts of ferrohedenbergite ($Wo_{41}En_{16}Fs_{43}$ to$Wo_{43}En_{18}Fs_{39}$), fayalite (Fo_{7-12}) and alkali feldspar (Or_{3-6}). The mafic phases frequently enclose equant microphenocrysts of magnetite. The very fine-grained groundmass contains laths of aligned feldspar, with accessory hornblende, apatite and zoisite. No inclusions or xenoliths were found.

The most evolved lava found in this study (sample 582) is a trachyte which outcrops on the east side of Fjell, south of the summit crater, at a height of 950m (Figure 4.8). This lava is glassy, it weathers to a pink-red colour, it is at least 20m thick and is cut by mafic Fe-Ti rich basalt dykes. The base of the lava is crudely columnar and steeply dipping. The lava contains sparse euhedral phenocrysts of alkali feldspar (Or_{7-19}), ferrohedenbergite ($Wo_{44}En_5Fs_{50}$), small altered fayalite phenocrysts (Fo_{2-4}) and microphenocrysts of equant Fe-oxides. The phenocrysts often form clusters, the mafic phases frequently enclosing the Fe-oxides. The groundmass is composed of very fine feldspar laths and partly devitrified pale brown glass, showing flow banding. The different bands are laterally continuous and show slight differences in grain size suggesting that the bands represent laminar flow of a lava rather than a recrystallised ignimbrite.

The rest of the felsic lavas encountered in this study contain abundant basic and/or intermediate inclusions. The Laugara trachyte (samples 576, 577, 578) contains <30% basic and intermediate inclusions (Figure 5.11 A, B, C, D). The groundmass of this lava is composed of very fine-grained feldspar, clinopyroxene and opaques, it is

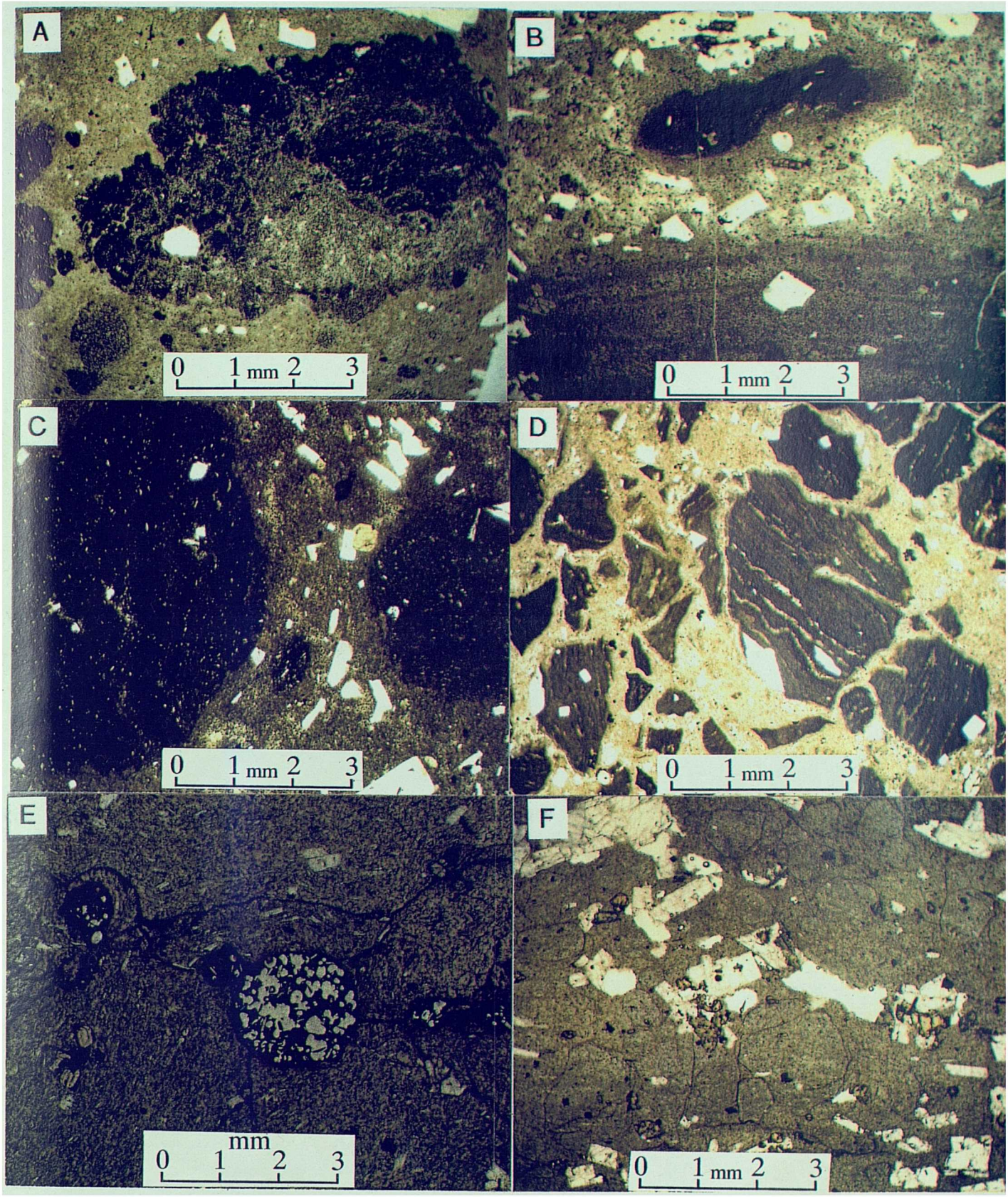

Figure 5.11 A: *Sample 578 (upper parts of the Laugara trachyte) showing a mafic inclusion with cuspate margins in a porphyritic, trachyte host.* **B:** *Sample 577 (lower parts of the Laugara trachyte) showing a mafic band and inclusion in the hedenbergite-fayalite-oligoclase phyric host. Some phenocrysts have been entrained and partially resorbed by the mafic magma.* **C:** *Intermediate inclusions in sample 578 (Laugara trachyte) with diffuse margins, note the patchy groundmass.* **D:** *Jigsaw fragments of evolved rock in trachyte host (base of Kolbeinsskard trachyte).* **E:** *Glassy, vesicular basic inclusions in sample 566.* **F:** *Loose sample 579 with phenocrysts of oligoclase (o), fayalite (f), hedenbergite (h) and Fe-oxides (ox). The rock shows perlitic cracking.*

heterogeneous in appearance with pale and dark patches. Phenocrysts of oligoclase are strongly zoned, some are euhedral and some show resorption. Ferrohedenbergite ($Wo_{44}En_{20}Fs_{36}$) and fayalite phenocrysts also show resorption. Inclusions vary in size and shape, the largest are up to 60cm across and tend to have sharper, more angular contacts than smaller inclusions (>2cm) which are more rounded, often with cuspate or diffuse margins (Figure 5.11 A). Rounded intermediate inclusions (<2cm) frequently have diffuse as opposed to cuspate margins. These inclusions show flow banding of glassy bands containing numerous tiny Fe oxides and bands containing plagioclase laths. Sparse phenocrysts of plagioclase feldspar and Ti-magnetite occur. Bands of mafic magma occur towards the base of the trachyte, they appear to have entrained phenocrysts from the evolved host (Figure 5.11 B). Basalt inclusions are usually non-vesicular and tend to have very few phenocrysts compared to the host trachyte. Some small, round basalt inclusions are highly vesicular. This lava has clearly undergone a complex mixing history involving mixing with both basaltic and intermediate melt compositions. The nature of the contacts between the inclusions and the host suggests that the inclusions were incorporated as magmatic blobs (Bacon, 1986).

The fourth trachyte outcrop occurs at Kolbeinsskard, north of Steinafjall (Figure 4.15). The outcrop is small in size (10x10m), it is flow-banded and cut by basic dykes. Most of the outcrop is composed of a very fine groundmass of aligned feldspars and Fe-oxides (pilotaxitic texture). Sparse phenocrysts of plagioclase, microcline and anorthoclase show zoning and resorption, glomerophyric clusters of zoned ferrohedenbergite, alkali feldspar and Fe-oxides are also resorbed. There are rare vesicular, basic inclusions in this trachyte from 1-10mm in diameter (Figure 5.11E), these contain strongly zoned plagioclase phenocrysts with resorbed cores and small alkali feldspar phenocrysts showing sieve texture and a rim of plagioclase. The groundmass contains plagioclase and pyroxene with intergranular texture and numerous acicular ilmenite crystals. The fine-grained host trachyte fills cavities and vesicles in the inclusions and margins are cuspate and irregular. At the base of the outcrop is a discontinuous zone of highly deformed trachyte up to 0.5m thick. This zone is glassy and flow-banded showing hyalopilitic texture. Small (<5mm), rounded, mafic inclusions with skeletal feldspars and numerous skeletal and acicular Fe-oxides also occur in this zone. Also found at the base of the outcrop is a breccia containing numerous clasts <1cm in size (Figure 5.11 D). The clasts are flow-banded and contain sparse phenocrysts of euhedral alkali feldspar. They are thus of fairly evolved composition. Clasts have diffuse margins and are randomly arranged in the host. However some can clearly be pieced together as a jigsaw, suggesting that these fragments were formed by thermal shock and were not transported far. The host trachyte is highly evolved and was evidently very fluid, forming thin veins between the jigsaw fragments.

A loose sample (579) was collected from the glacial moraine above the Laugara stream. It is a trachyte very similar in appearance and petrology to sample 534 at Gigjokull. Sample 579 contains oligoclase, anorthoclase (An_{9-12}, Or_{20}), fayalite and hedenbergite. Perlitic cracks have given it a spotted appearance due to preferential weathering (Figure 5.11F).Samples from two trachyte dykes (samples D169 and D213) were also collected from Nupakotsdalur and W. Steinafjall respectively. Sample 169 is highly altered. It contains stumpy groundmass plagioclase with abundant secondary calcite. Sample 213 is also heavily altered. Euhedral plagioclase phenocrysts and sparse clinopyroxene occur in a hyalophitic groundmass.

5.4 GABBROIC NODULES AND XENOLITHS

Many of the rocks from the Eyjafjöll volcanic system contain megacrysts, xenoliths and/or show glomeroporphyritic texture. Distinguishing glomerophyric clusters from xenoliths may be difficult in some cases, although xenoliths are usually composed of crystals of very different composition to the host rock and may have corroded margins.

5.4.1 GLOMEROPHYRIC CLUSTERS

Glomerophyric clusters are common in all lavas which contain phenocrysts. Several basalt lavas and dykes contain only radiating clusters of plagioclase, subophitically enclosed in clinopyroxene up to 4mm in size, single phenocrysts are rare. These clusters are all roughly the same size and composition and are numerous. Similar glomerophyric clusters were described at Hengill (C.Walker, 1992).

Evolved basalts (50-52% SiO_2, e.g members of the Seljavellir Group) contain clusters of euhedral clinopyroxene, olivine and tabular plagioclase, these are typically less than 5mm across.

Many basalt lavas contain stellate clusters of plagioclase and sector-zoned augite up to 1mm in size formed during quenching of the groundmass.

The porphyritic basalts (>15% phyric) contain clusters of plagioclase and clinopyroxene which are rarely more than 15mm in size. These clusters are very numerous and due to a lack of reaction with the host lava and the similarity of phenocrysts in the clusters and the lava, it is assumed that they are glomerophyric clusters (e.g. Figure 5.8a).

5.4.2 GABBROIC XENOLITHS

All the xenoliths identified during this study contained an assemblage of either: a) plagioclase + clinopyroxene + olivine, b) plagioclase + olivine, or c) plagioclase + clinopyroxene + Fe-oxides. Olivine is usually a minor component of the xenoliths, plagioclase and clinopyroxene being the most abundant. Fresh olivine was found in only

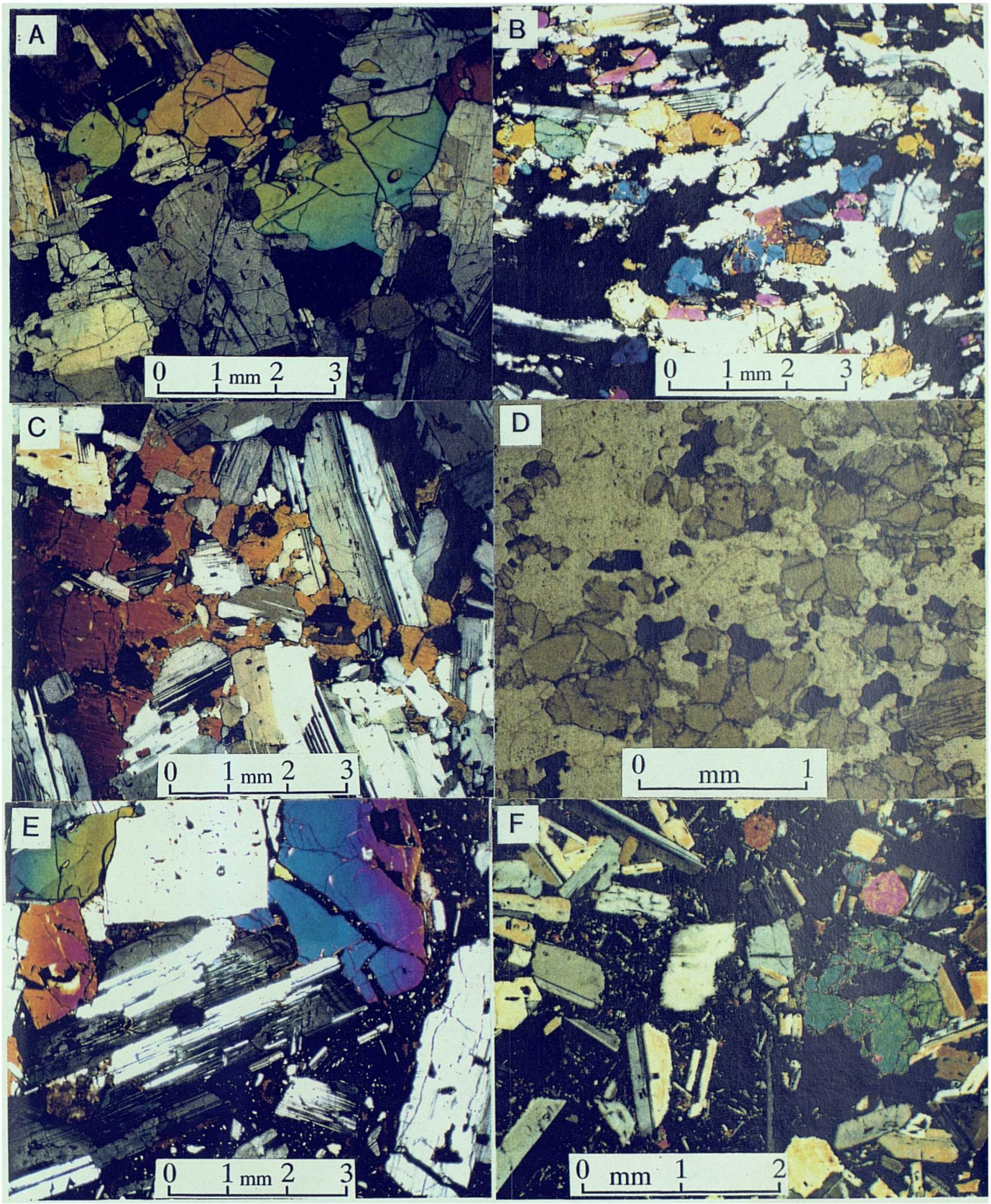

Figure 5.12 *Gabbroic xenoliths found at Nupakotsdalur (A - D), Seljavellir (E) and Seljalands (F).* **A:** *Sample N1 showing plagioclase with anhedral clinopyroxene.* **B:** *Sample N2 showing plagioclase with kinked twin planes, intergranular clinopyroxene and Fe-oxides (all black area). The plagioclase crystals have resorbed margins.* **C:** *Sample N3 showing plagioclase with devitrified glass inclusion poiklitically enclosed by clinopyroxene.* **D:** *Sample N4, a very fine-grained gabbro containing plagioclase, clinopyroxene and Fe-oxides with equilibrated texture.* **E:** *Sample S2 showing strongly-zoned plagioclase phenocrysts and intergranular clinopyroxene in a glassy host.* **F:** *Sample Q1, an open-textured xenolith. Plagioclase and olivine form a framework of crystals; the groundmass is vesicular within the xenolith and contains plagioclasė laths, granular clinopyroxene and quench olivine. The host basalt contains plagioclase and clinopyroxene phenocrysts; olivine phenocrysts are rare.*

one recent xenolith. Xenoliths in a single lava may show a variety of textures and compositions. There are two localities which show an impressive number of xenoliths, both are in the southern section. One occurs within the Nupakotsdalur Group and it is believed that the other is associated with the Laugara Group (near the old swimming pool).

5.4.2.1 NUPAKOTSDALUR XENOLITHS

The outcrop in Nupakotsdalur contains at least five textural varieties of gabbroic xenolith, these have been numbered N1 to N5. The xenoliths collected range in size from 2x3x4cm to 7x5x4cm. The most leucocratic xenoliths (e.g. type N1) are rounded. Each xenolith is described briefly below:

N1: Euhedral pseudomorphs after olivine enclosed in a mosaic of partially equilibrated, anhedral plagioclase and clinopyroxene. Modal mineralogy: Plagioclase 70%, clinopyroxene 25%, olivine < 5%. Some plagioclase shows zoning, although the compositional range is small (cores An_{69-74}). Olivines are pseudomorphed by serpentine and Fe-oxides (Figure 5.12 A).

N2: Plagioclase and clinopyroxene orthocumulate with laminate texture and intercumulus Fe-oxides. Plagioclase rims are resorbed and twin planes are kinked (Figure 5.12 B). Plagioclase core compositions are in the range An_{61-64} and augites are close to $Wo_{42}En_{41}$ Fs_{15}.

N3: Plagioclase poikilitically enclosed by clinopyroxene. Plagioclase crystals are broken, subhedral and resorbed and of widely varying size and shape (<12mm). Larger phenocrysts may contain devitrified glass inclusions (Figure 5.12 C).

N4: Fine-grained plagioclase-clinopyroxene-Fe oxide gabbro with granular texture. Plagioclase and clinopyroxene crystals enclose some Fe-oxides. Rare larger plagioclase crystals (<1mm) show signs of resorbtion (Figure 5.12 D).

N5: Strongly zoned, euhedral to subhedral plagioclase with intergranular clinopyroxene and Fe-oxides, also sparse pseudomorphs after olivine.

These xenoliths match a variety of gabbroic textures found in gabbro intrusions. The fine-grained N4 is probably from the rapidly chilled margins of an intrusion. Sample N2 may represent crystallisation at the base or on the walls of a solidifying magma chamber. However, the rest of the xenoliths are dominated by plagioclase and generally lacking in olivine or Fe-oxides, they probably formed in the higher levels of a magma chamber. At this field locality irregularly-shaped patches of plagioclase-rich material over a metre in size were observed in the host lava. The margins of the material were diffuse. These patches were not sampled but may represent 'crystal mush' torn from the roof or walls of a solidifying magma chamber. The host magma would have been a relatively primitive porphyritic basalt, containing olivine, clinopyroxene and plagioclase phenocrysts. The pyroxenes may reach 4cm in length, some are clearly

skeletal, others are euhedral. Olivine and plagioclase phenocrysts rarely exceed 1cm in size. The host lava has entrained these xenoliths during its ascent to the surface, presumably from a partially-solidified magma chamber. The high crystal content of the host magma will have made it reasonably viscous, despite its primitive composition, enabling it to carry these large xenoliths. Furman *et al.*(1992a) encountered a dyke at Austurhorn which contained xenoliths representing the entire spectrum of gabbroic types seen in the nearby Hvannesfjall gabbro.

5.4.2.2 LAUGARA XENOLITHS

Near the old swimming pool on the banks of the Laugará river, a glassy host rock containing less than 15% plagioclase phenocrysts contains both rounded gabbroic xenoliths up to 12cm in size (S1, S2 & S4) and rounded clots of very highly plagioclase-porphyritic material up to 20cm in size (sample 519). Xenoliths include plagioclase orthocumulates with intercumulus clinopyroxene and plagioclase poikilitically enclosed by a single clinopyroxene crystal. Plagioclase crystals vary in size up to 12mm. They show complex zoning, often with a resorbed core containing devitrified glass inclusions, an oscillatory-zoned mantle and a rim. Rare, small, resorbed plagioclase crystals are found poikilitically enclosed in pseudomorphs after olivine which in turn may be enclosed by clinopyroxene and Fe oxides.

A sample of the highly porphyritic material contains about 60% phenocrysts in the proportions ~90% plagioclase, <5% olivine and <5% clinopyroxene. The olivine is pseudomorphed by serpentine and iddingsite, the pyroxenes are small (<1mm) and resorbed. The plagioclase phenocrysts vary greatly in size up to a maximum of 12mm, zoning is complex with resorbed cores, oscillatory-zoned mantles often with signs of resorption and a ragged partially resorbed rim. Plagioclase phenocrysts are euhedral to subhedral, larger phenocrysts tend to contain numerous glass inclusions. Aggregates of plagioclase, clinopyroxene, olivine (pseudomorphs) and Ti-magnetite up to 1cm in size are abundant in these rocks.

The composition of plagioclase is similar in the host lava, the porphyritic material and the xenoliths, the plagioclase phenocrysts also have similar zoning patterns. This suggests that all the material may be related. The host magma may have entrained some crystal mush and phenocrysts from the magma chamber roof and walls during eruption. The scarcity of olivine in the host rock or the xenoliths suggests that they both originated from the upper parts of a magma chamber.

Lavas of the Laugará Group (which appear to overlie the xenolith-rich deposit) contain highly resorbed xenoliths of plagioclase adcumulate which often have a single pseudomorph after olivine as a core. These xenoliths are rounded and up to 12mm across.

5.4.2.3 OTHER XENOLITHS

An unusual xenolith was found in lavas exposed in the Katarnes quarry, west of Fragafell. Sample Q1 is 8x5x2cm in size and is composed solely of plagioclase (<4mm) and olivine (<3mm) (Figure 5.12 F). Olivine is euhedral to subhedral, and golden in colour, plagioclase is euhedral to subhedral with zoned rims. The xenolith has an open texture, interstitial areas are filled by a basaltic groundmass with plagioclase laths, intergranular clinopyroxene and skeletal olivine. The host basalt is sparsely vesicular, but within the xenolith, vesicles are numerous. The host basalt is porphyritic, containing up to 10 vol% plagioclase phenocrysts and up to 5% pyroxene and sparse olivine. Small glomerophyric clusters of plagioclase and pyroxene up to 2cm in size are common in the lava. The xenolith is very fresh and unaltered, reflecting its recent age. The host basalts are older than the Hamragardur flow, which lies directly on their glacially polished upper surface, but not much older, as they have followed a similar topography. Wiese (1992) has dated lavas in this area, which are presumably the same ones, at 82 $\pm$ 20Ka, giving them a similar age to the more evolved Seljavellir Group in the southern section of the volcano.

Sample 74 is highly porphyritic but crystal aggregates of any kind are rare in ankaramites. The only example found is a xenolith composed entirely of clinopyroxene. The clinopyroxene crystals are equant, some are rounded in shape, they are small (<0.5mm) and contain numerous tiny inclusions. The xenolith is about 5mm across.

No acid xenoliths were found in any of the rock types at Eyjafjoll.

5.5 MINERAL CHEMISTRY

5.5.1 OLIVINE

Olivine phenocrysts are found in many of the Eyjafjöll lavas. Forsteritic olivine is present in substantial amounts in ankaramites and porphyritic basalts. Forsteritic olivine is also particularly abundant in basalts of the Hvammsmuli Group and the Laugara Group where it occurs both as a phenocryst and a groundmass phase. There are nevertheless many basalt lavas in which olivine is absent. Fayalite is a ubiquitous phase in the trachytes (Figure 5.11 B, E, F), where it forms elongate euhedral crystals up to 2mm in size. The most Fe-rich olivine (Fo_3) occurs in the most evolved trachyte, sample 582.

Olivines are usually cracked and show signs of alteration along the cracks (Figure 5.4 F). Pseudomorphs after olivine are particularly common in the hydrothermally altered rocks near the core of the volcano. Alteration products of olivine include serpentinite, talc, chlorite, clays and iddingsite.

The most Mg-rich olivine (Fo_{90}) occurs in an ankaramite lava at Hvammsmuli (sample 43). It is a euhedral phenocryst with a rim of Fo_{89}. This phenocryst may have crystallised from a mantle melt.

Using the equation:

$K^{(D)} = (FeO^*/MgO)_{ol} / (FeO^*/MgO)_{liq}$ (Where FeO^* is total iron)

and assuming that $K^{(D)} = 0.3$ (Roeder & Emslie, 1970), this phenocryst formed in equilibrium with a liquid having an FeO^*/MgO ratio of 0.63-0.65. The more Fe-rich olivine phenocrysts found in the same sample (Fo_{81-89}), would have been in equilibrium with liquids having FeO^*/MgO ratios of 0.71-1.32. This variety of liquid compositions suggests that either a primitive magma has mixed with a more evolved magma, accumulation of phenocrysts has occurred or that crystal fractionation has caused compositional changes in the magma. No basalts at Eyjafjöll have such low FeO^*/MgO except the highly px-ol-pl phyric basalts which are not liquid compositions. The Laugara Group has the lowest FeO^*/MgO ratio at 1.7.

A sample of the Hvammsmuli ankaramite (sample 74) which is phenocryst-free (Jakobsson, 1979b) has a FeO/MgO ratio of 0.86. This suggests that a relatively primitive ankaramite liquid has entrained phenocrysts which are both more primitive and more evolved than itself prior to eruption, this may occur in a convecting magma chamber. Very primitive olivines were not found in sample 74, (the main body of the Hvammsmuli ankaramite), the majority of olivine phenocrysts are more evolved (Fo_{73-84}).

To calculate the MgO content of the parental magma, the last temperature of equilibration of a rock must be known. Wiese (1992) obtained a temperature of 1229 °C using coexisting magnetite and ilmenite in the Hvammsmuli ankaramite. Unfortunately, no suitable coexisting crystals were found in this study which did not show signs of disequilibrium. Re-equilibration of Fe-oxides is rapid after extrusion (McBirney, 1993), so if the Hvammsmuli ankaramite did crystallise in a small lava lake, re-equilibration of these phases is almost inevitable. Nevertheless, using the temperature calculated by Wiese (1992) the calculated MgO content for the ankaramite is only 7%, which is clearly not a parental melt. However, it may reflect the composition of the crystallising liquid in the lava lake.

Equilibrium and disequilibrium in a rock can be assessed by plotting olivine compositions versus Mg# of the whole rock. The Mg# gives a measure of differentiation of the whole rock. If a rock is in perfect equilibrium, groundmass and phenocryst compositions should all be the same. Equilibrium olivine compositions were calculated using the computer modelling program TRACE3 (Nielsen, 1988). Figure 5.13 shows a relatively good correlation between Mg# and olivine compositions, showing that there is a clear tendency towards more Fe-rich olivine as basalts undergo differentiation. Olivine core compositions in the basalts tend to be within a small range for each sample, however, they do not all approximate to the equilibrium composition. Some samples contain two populations of olivine, more Mg-rich olivines are probably xenocrysts.

---

* Mg# is defined on page 157.

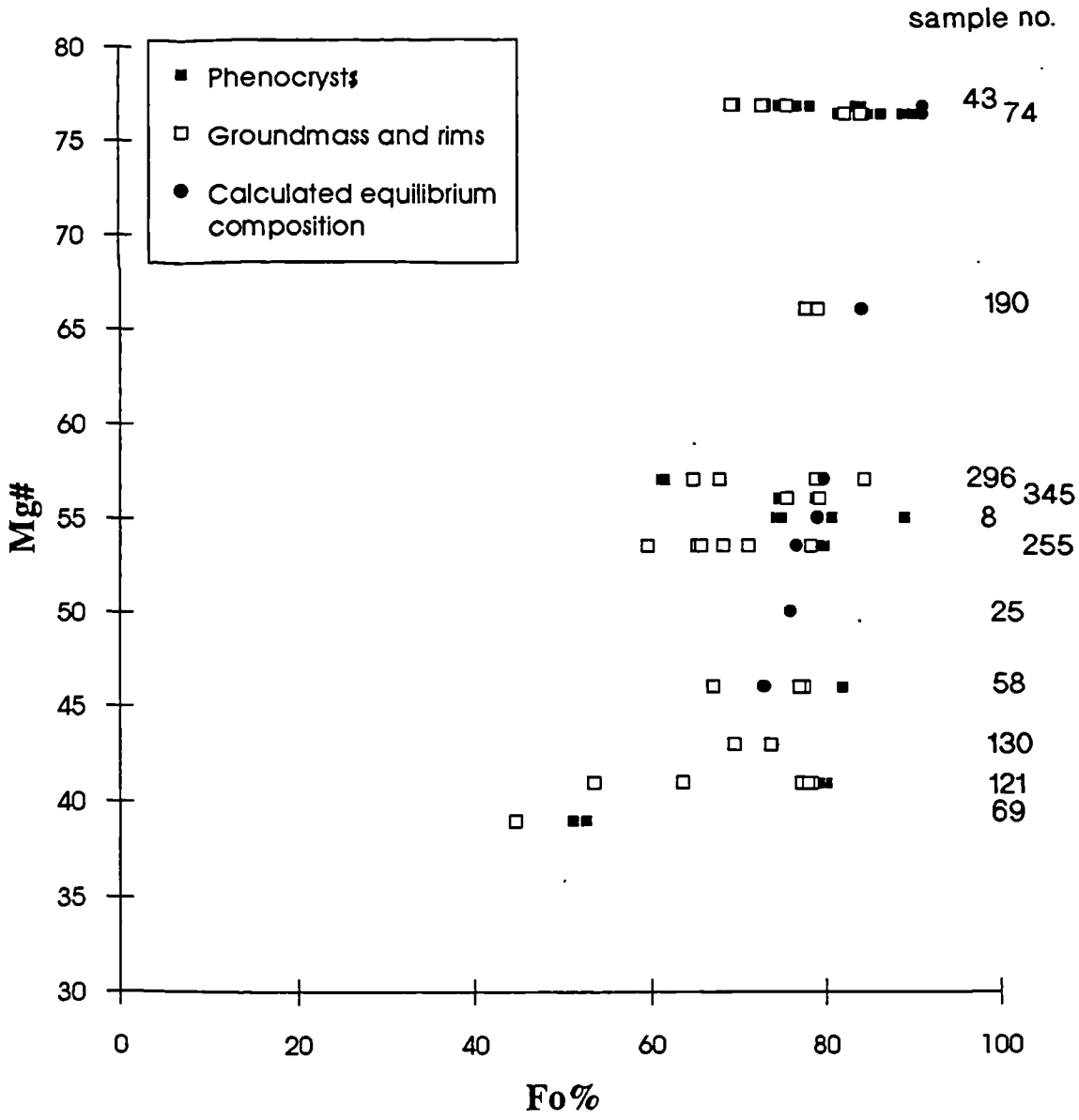

Figure 5.13 *Plot of Mg# (whole rock) versus Fo% of olivine phenocrysts for selected samples.*

$$Mg\# = 100 \times \frac{(MgO/40)}{(MgO/40) + 0.85(FeO^*/72)}$$

(FeO^* = total iron, $Fe_2O_3/FeO = 1.5$)

Sample 74, the Hvammsmuli ankaramite, shows a great variety of olivine core compositions, most of them less magnesian than the calculated equilibrium composition, These may be xenocrysts, but, another explanation is that the olivines were undergoing re-equilibration towards more Fe-rich compositions during closed-system differentiation of the cooling lava lake. This process was described in the Makaopuhi lava lake in Hawaii by Moore & Evans (1968). Re-equilibration occurred during crystallisation of the groundmass and later subsolidus cooling from 1000°C to 800°C.

MnO contents in olivines are usually below detection limits, however, MgO-rich olivines in the highly olivine and clinopyroxene-phyric vein that cuts the Hvammsmuli ankaramite contain 0.15-0.54% MnO. This may reflect a tendency for Mn to be taken up by olivine in the absence of Fe-oxides. Fe-rich olivines in the trachytes contain up to 2.25% MnO.

The majority of olivines contain between 0.14-0.45% CaO, which is typical for extrusive basic rocks (Simkin & Smith, 1970). There are three basalt groundmass olivines wich contain over 0.5 wt% CaO and over 25 wt% Fe_2O_3T. Two occur in samples 130 and 131, dykes feeding the Svadbaelisheidi Group and one occurs in sample 58 in the Hvammsmuli sequence.

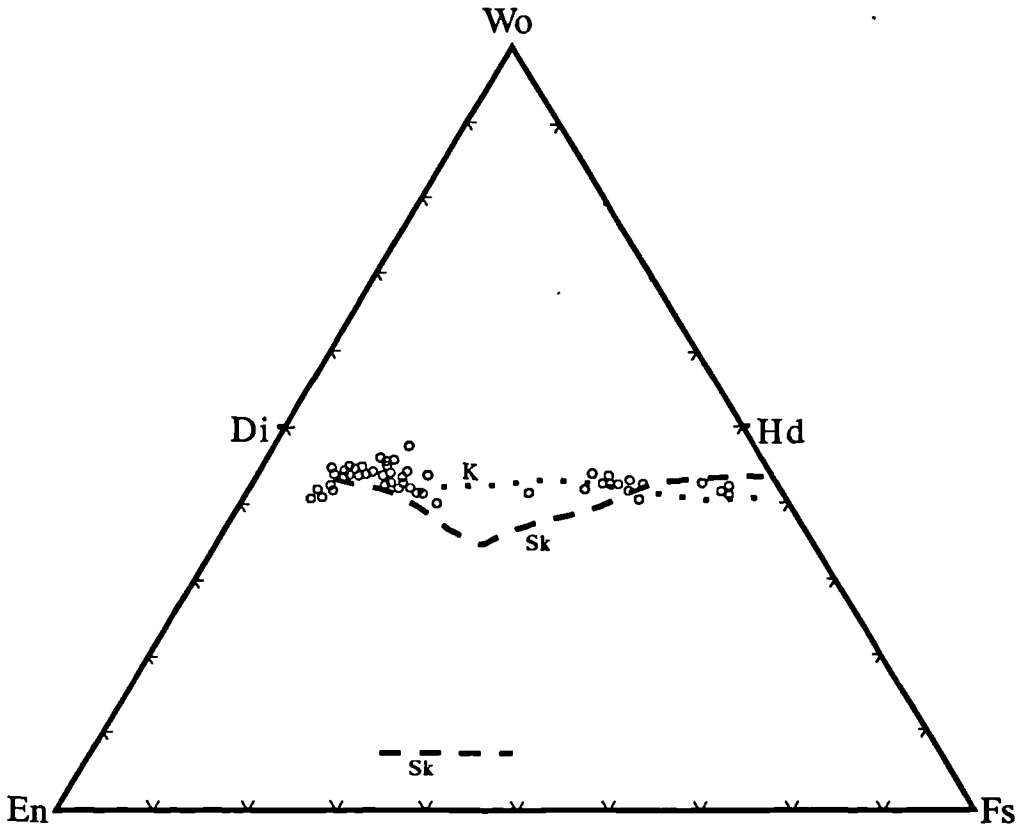

Figure 5.14 *Wo-Fs-En diagram showing selected compositions of clinopyroxenes from the Eyjafjöll volcanic system. The dashed line shows the Skaergaard trend (Wager and Brown, 1967) and the dotted line shows the Kiglapait trend (Morse, 1980).*

5.5.2 CLINOPYROXENE

Clinopyroxenes at Eyjafjöll show an alkalic trend at a roughly constant Wo content from $Wo_{41}En_{51}Fs_6$ to $Wo_{43}En_5Fs_{50}$ (Figure 5.14). This trend is similar to that at Austurhorn (Furman, 1992) and Kiglapait (Morse, 1980). There is a compositional gap between the augites and the hedenbergites; rare clinopyroxenes which fall within this gap (~$Wo_{42}En_{28}Fs_{30}$), are from intermediate dykes (e.g. samples 169, 189 and 213). The gap between clinopyroxenes of the most evolved trachyte ($Wo_{43}En_5Fs_{50}$ - sample 582) and clinopyroxenes of the other trachytes (~$Wo_{43}En_{20}Fs_{40}$ - samples 534, 566, 579) may reflect a sampling bias.

Clinopyroxene is present as a phenocryst, and as a groundmass phase in almost all Eyjaföjll rocks, the only exception being sparsely porphyritic (<5%) intermediate lavas in which only plagioclase is a phenocryst phase. Microphenocrysts of clinopyroxene frequently show sector zoning and subophitically enclose plagiclase laths. This may reflect rapid cooling.

Rare, primitive clinopyroxenes found in the ankaramites and porphyritic basalts fall within the diopside and endiopside fields of Poldervaart & Hess, (1951). These phenocrysts are large (<11mm) and tend to be rounded. They show chemical zoning especially in TiO_2 (0.58-0.85) and Al_2O_3 (2.42-4.45) both of which show a decrease towards the rim. Each phenocryst is rich in Cr_2O_3 (0.39-1.20) which also shows an increase in concentration towards the crystal rims. A similar feature was noted in clinopyroxenes of the Maelifell picrite (Hardardottir, 1985), however, the Cr_2O_3 content of the crystal cores was also much higher (>1.0). Hardardottir interpreted these Cr-Al endiopsides as having crystallised at pressures greater than 10 kbars as inferred by the experiments of Bender et al. (1978) on basalts from the Famous area. The Eyjafjöll endiopsides may also reflect crystallisation at moderate pressures.

Assuming that:

$K^{(D)} = (FeO^*/MgO)_{cpx} / (FeO^*/MgO)_{liq}$

and

$K^{(D)}_{cpx/liq} = 0.23$ (Grove & Bryan, 1983),

an Mg-rich clinopyroxene from sample 43 was in equilibrium with a liquid having FeO^*/MgO of 1.2. This is a more evolved liquid composition than that which equilibrated with Fo_{90} from the same sample. This may reflect the later crystallisation of clinopyroxene.

The liquid with which the gabbroic xenolith N2 from Nupakotsdalur was in equilibrium with may also be calculated. These clinopyroxenes were in equilibrium with a liquid having Fe^*O/MgO of 2.85-2.9. Liquids of this composition are common in the stratigraphic pile, the lavas of the Laugara subgroup 3 at Nupakot are one example. These lie below the Nupakotsdalur Group so may well be related to the xenoliths. The

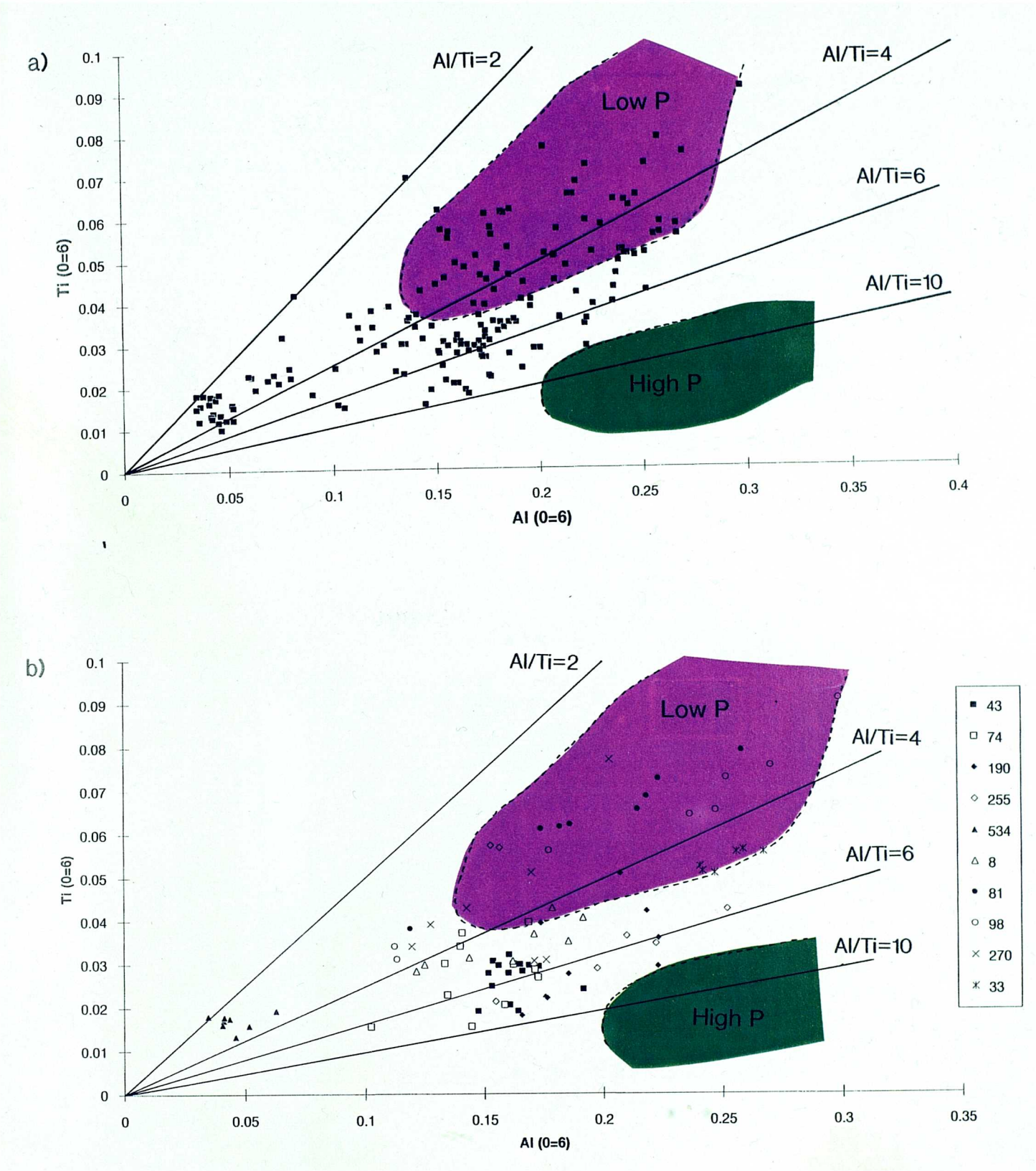

Figure 4.15 *a) Ti versus Al (O=6) for clinopyroxenes, high and low pressure fields from Thy 1991a. b) Ti versus Al (O=6) for clinopyroxenes in selected samples. For sample locations see Appendix B.*

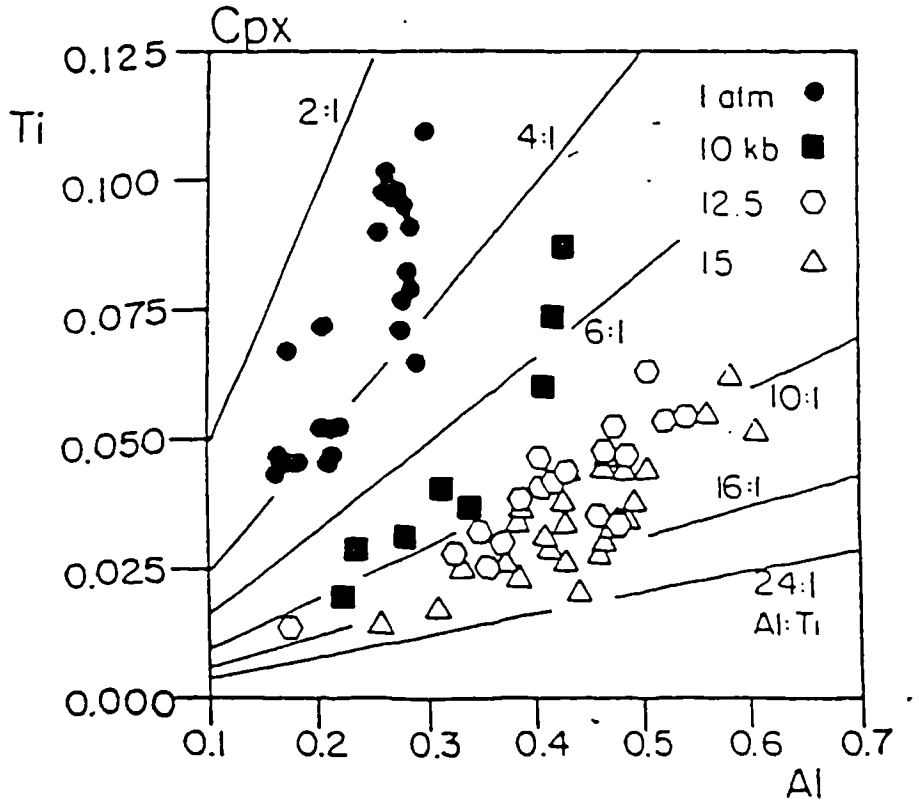

Figure 5.16 *Clinopyroxene experimental data from crystalliation experiments on a Surtsey basalt (Thy, 1991a).*

Laugara Group itself has a much lower FeO^* /MgO ratio. The xenoliths are certainly more evolved than the host rock.

Sample S2 (Figure 5.12 E) contains clinopyroxene slightly more Fe-rich and Ca-rich than the Nupakotsdalur xenoliths ($Wo_{43}En_{40}Fs_{16}$). Based on the FeO^* and MgO contents of the clinopyroxene (FeO^* = 9.3-9.4, MgO = 13.98-14.06), it was in equilibrium with a liquid of FeO^*/MgO = 2.75-2.80. This is very similar to the xenoliths from the Nupakotsdalur Group. These xenoliths are again more evolved than the host rock. The Laugara and Nupakotsdalur Groups may have entrained the xenoliths from the same magma chamber at a similar time.

Groundmass and phenocryst clinopyroxene show a range of Al/Ti ratios from 2 (the atomic ratio) to 10, reflecting the addition of a tschermakitic component (Figure 5.15a). This is achieved by substitutions such as $(Mg, Fe)^{VI} + Si^{IV} = Al^{VI} + Al^{IV}$ and $(Mg, Fe)^{VI} + Si^{IV} = (Fe^{3+}, Cr)^{VI} + Al^{IV}$. The Ti content of the clinopyroxenes is due to the substitution $(Mg, Fe)^{VI} + 2Si^{IV} = Ti^{VI} + 2Al^{IV}$. The evolved lavas contain the lowest contents of Al and the ankaramites and basalts contain the highest contents of Al (i.e a higher tschermakitic component) (Figure 5.15b). This may reflect the higher crystallisation temperatures of these more primitive rocks (Larsen et al., 1989). Herzberg & Chapman (1976) showed that a Tschermakite component in clinopyroxene in a spinel lherzolite assemblage was more soluble at higher temperatures and was uninfluenced by pressure. Nevertheless, Thy (1991a) conducted 1 atmosphere and high pressure (10, 12.5 and 15 kbars) crystallisation experiments on a Surtsey basalt sample

and found that the compositions of clinopyroxenes crystallised at high pressures had higher Al/Ti ratios than clinopyroxenes crystallised at 1 atmosphere pressure (Figure 5.16).

Clinopyroxenes from the ankaramites and porphyritic basalts at Eyjaföjll have Al/Ti ratios which approach 10, comparing this to Thy's experimental results, crystallisation appears to have occurred under moderate pressures of up to 10 kbars.
The presence of only olivine and clinopyroxene in ankaramites also suggests that the ankaramites form at sufficient depths to inhibit plagioclase crystallisation.

5.5.3 PLAGIOCLASE

Plagioclase is an abundant phenocryst phase in all porphyritic lavas at Eyjafjöll. In some basalts plagioclase phenocrysts may occupy up to 40% of the rock; even 'aphyric' lavas typically contain sparse microphenocrysts of plagioclase. Plagioclase compositions show an increase in Or% with differentiation (Figure 5.17).

All plagioclase phenocrysts show compositional zoning to some degree. Zoning may be normal, reverse, oscillatory or a complex combination of these three types. Phenocrysts are typically composed of a core region, a mantle and a rim (Figure 5.15). Cores are frequently rounded or embayed at their margins suggesting resorption in the magma reservoir.

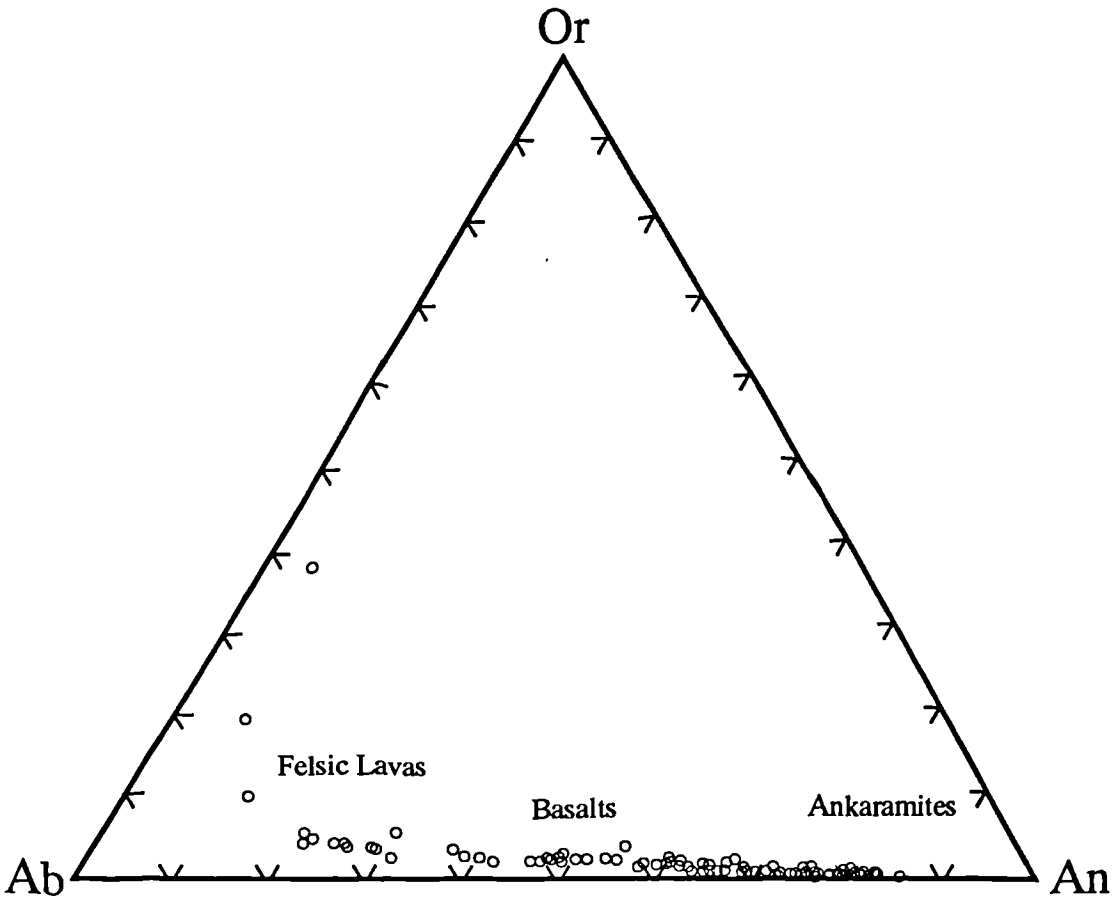

Figure 5.17 *Compositions of plagioclase phenocryst cores showing an increase in Or% with differentiation.*

Resorption may occur during replenishment of an evolving magma reservoir with hot primitive liquid, this would cause superheating and resorption of evolved phenocrysts. In contrast, the primitive magma would undergo supercooling as it is injected into the magma reservoir, this may lead to skeletal phenocrysts. The contact between the mantle and the rim may be sharp, or gradational, zoning is always to more evolved compositions (normal zoning).

Phenocrysts in one rock may show two or even three populations of plagioclase each showing different types of zoning, crystal shape and composition (Figure 5.4 E). This is an indication that mixing has occurred.

Plagioclase phenocryst cores have a very consistent composition in basalts and ankaramites (An_{75-85}), however groundmass compositions are more variable due to differing degrees of differentiation. The more calcic plagioclase phenocrysts are typically large and show complex zoning, often with resorbed cores containing glass inclusions. Similar crystals are also found in abundance in gabbroic xenoliths (Figure 5.12 A, B, E). The plagioclase cores probably formed as hot, primitive magma was injected into a differentiating magma chamber; supercooling would cause imperfect skeletal growth of plagioclase (Kuo & Kirkpatrick, 1982). Liquid trapped within the crystal structure ultimately forms glass inclusions. The oscillatory zoning observed in the mantle may be due to mixing in the replenished, convecting magma chamber and the rims formed during transport of the magma to the surface and cooling of the lava (Kuo & Kirkpatrick, 1982). Similar plagioclase phenocrysts have been described from Iceland (e.g. Makipaa, 1978; Walker, 1992), the Mid Atlantic Ridge (Kuo and Kirkpatrick, 1982) and Greenland (Larson et al., 1989). The form of these phenocrysts presents evidence that open system magma chamber processes have occurred.

Many basalts contain bimodal plagioclase, typically An_{55-65} and An_{75-85}. This suggests that some degree of accumulation of phenocrysts has occurred as indicated by the abundance of phenocrysts in many basalts.

Some highly px-ol-pl phyric basalts which are otherwise fairly primitive contain plagioclase of very low An content. For example, sample 190 (Nupakotsdalur Group) contains small, sparse phenocrysts of An_{33} showing sieve texture and a thin outer rim. Sample 251 (Nupakotsdalur Group) an ankaramite, contains groundmass plagioclase trapped within the crystal structure of skeletal clinopyroxenes which have fractionated to An_{55} and An_9.

When plagioclase compositions are plotted versus Mg# as an indicator of differentiation, the basalts and ankaramites show a slight but clear tendency to lower An values with increased differentiation (Figure 5.18). Equilibrium values of plagioclase were calculated using TRACE3 (Nielsen, 1988), they do not show a good trend and many samples clearly contain phenocrysts which are out of equilibrium with the host rock. This diagram presents more evidence that open-system magma chamber processes have occurred.

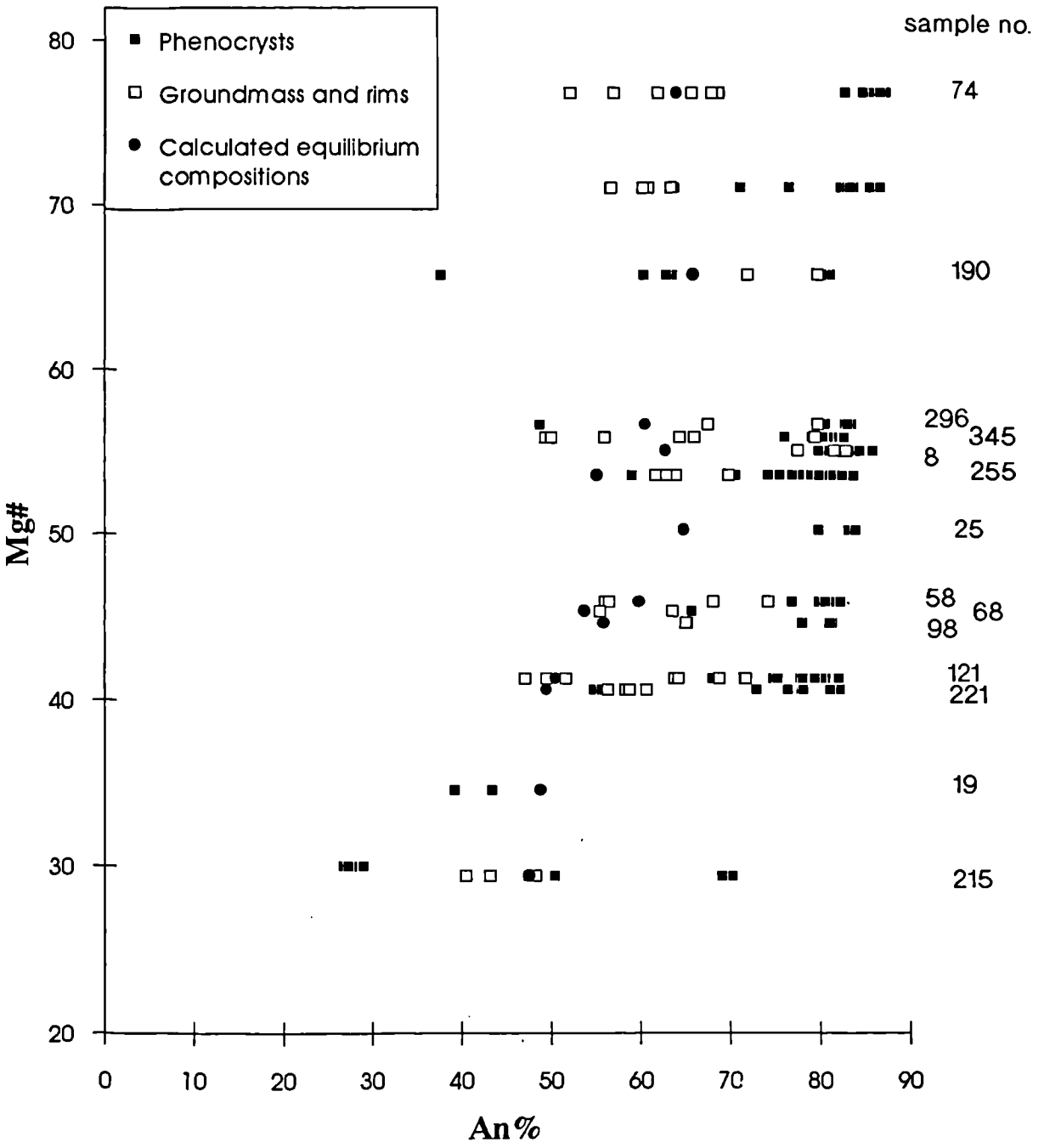

Figure 5.18 *Mg# (whole rock) versus An% of plagioclase phenocrysts for selected samples.*

5.5.4 ALKALI FELDSPAR

Alkali feldspar occurs in the most evolved trachytes at Eyjafjöll. Oligoclase phenocrysts in the trachytes (An_{18-27}) contain up to 11% orthoclase. Anorthoclase forms euhedral, tabular phenocrysts in sample 582 of variable composition (Figure 5.17).

5.5.5 CHROME SPINEL

Chrome spinel forms small, opaque to red-brown, equant crystals usually enclosed within olivine or diopsidic augite. Chrome spinel was found within olivines and diopsidic augites in the Hvammsmuli Group (samples 74 and 43), in some olivines in the porphyritic basalts of the Nupakotsdalur Group and in pseudomorphs after olivine in the Laugara Group. These lavas are all relatively primitive with high Mg and Cr contents. The enclosing crystals tend to be highly magnesian. The compositions of these chromites are shown in Table 5.2.

Table 5.2 *Compositions of selected chromites from the Eyjafjoll volcanic system.*

Sample no.	**345**	**190**	**190**	**8**	**8**
SiO_2	0.18	0.275	2.957	0.285	0.281
TiO_2	4.30	9.64	9.71	1.65	1.51
Cr_2O_3	11.74	24.58	22.21	44.10	46.24
Al_2O_3	32.41	5.19	4.80	13.60	15.17
FeO*	39.09	52.12	51.09	31.85	20.80
MgO	9.11	5.39	6.07	6.32	13.59
Total	97.36	97.85	98.44	98.44	97.99

5.5.6 Ti-MAGNETITE AND ILMENITE

Ti-magnetite occurs as a groundmass phase in all except the glassy rocks. Groundmass crystals may be equant and granular, skeletal or elongate and poikilitic. Microphenocrysts are usually blocky, equant and occasionally poikilitic. The abundance of magnetite reflects the high TiO_2 content of the Eyjafjöll lavas in general. Ilmenite is not as abundant as Ti-magnetite and the majority of rocks contain much more Ti-magnetite than ilmenite. One exception is the P_2O_5-rich dyke (sample 19) at Laugara which contains ilmenite almost exclusively. Ilmenite usually forms elongate needle-like or bladed crystals in the groundmass. The trachytes tend to contain more ilmenite than Ti-magnetite. Coexisting domains of Ti-magnetite and ilmenite suitable for calculating temperature and oxygen fugacity were not found in this study as signs of disequilibrium are common. Wiese (1992) used an ankaramite sample from Hvammsmuli and a Holocene flow from Seljalandsheidi and got temperatures of 1129°C and 916°C respectively. Oxygen fugacities were between the QFM and NNO buffers. Crystallisation along the NNO buffer was proposed at Austurhorn (Furman *et al.*, 1992). This represents relatively high oxygen fugacity. Compositions of Ti magnetite and

ilmenite from selected samples are presented in Appendix A.

5.5.7 RESIDUAL GLASSES

Most of the trachytes contain a proportion of glass in the groundmass representing the residual crystallisation products. These analyses may be found in Appendix B. They are of rhyolite composition (SiO_2>70%), however they show some variation in the abundance of other elements.

5.5.8 AMPHIBOLE AND MICA

Jakobsson (1978) noted the occurrence of primary amphibole in several of the flows on the western slopes of the volcano. In his 398-Midskalaheidi lava, which extends from the ice cap along a radial fissure towards Midskalaegg, amphibole occurs as a groundmass phase and in gabbroic nodules, which are common in the lava. Jakobsson (1978) also found primary amphibole in vugs in the groundmass of the 401-Sker lava and the 306-Hofdi lava. Amphibole also occurred in reaction zones in gabbroic nodules found in the latter lava. These lavas were not studied extensively in this study. However, amphibole, particularly rich in Al_2O_3, was noted in sample 25 of the Laugara Group. Amphibole was also found in the groundmass of sample 256,

	SAMPLE 25 microphenocryst	**SAMPLE 25** microphenocryst	**SAMPLE 256** groundmass
SiO_2	52.2	47.9	52.2
TiO_2	0.9	0.9	1.2
Al_2O_3	17.2	22.5	10.9
FeO*	5.5	3.8	7.1
MgO	6.9	4.9	10.0
CaO	14.3	16.5	17.8
NaO	3.2	2.1	2.2
Total	100.2	98.6	101.5

Table 5.1 *Compositions of primary amphiboles found at the Eyjafjoll volcanic system.*

a lava at Fimmvorduhals. The compositions of two amphibole microphenocryst from sample 25 and a groundmass amphibole from sample 256 are shown in Table 5.1. The majority of lavas in the Laugara Group are Ne-normative and thus may be classed as alkali basalts.

Secondary mica was noted in the brecciated rock at the base of the Kolbeinsskard trachyte. It is the only occurrence of mica.

5.6 SUMMARY

- Lavas of the Eyjafjöll volcanic system span a broad compositional spectrum from ankaramite to trachyte.

- Olivine, clinopyroxene, plagioclase, Ti-magnetite and ilmenite are observed as phenocrysts in basalts and hawaiites and as mineral phases in gabbroic xenoliths, suggesting that they comprise the fractionating assemblage for basalt to hawaiite compositions.

- Mugearites to trachytes contain phenocrysts of plagioclase, alkali feldspar, iron oxides and clinopyroxene suggesting that these mineral phases are involved in the fractionation of more evolved rock types.

- Many lavas are porphyritic suggesting long periods of cooling in crustal magma chambers. The scarcity of aphyric lavas suggests that few superheated magmas reach the surface in this area

- There is abundant evidence that magma mixing has occurred at Eyjafjöll. Mixing is often between magmas of extreme compositions, suggesting that fractional crystallisation is interrupted by infrequent replenishment.

- Some of the trachytes show extensive mixing with intermediate and basaltic magmas, suggesting that basic and acid compositions co-existed in a stratified magma chamber.

- The Hvammsmuli ankaramite represents the remains of a lava lake which ponded and cooled slowly.

- Ankaramites are common towards the base of the stratigraphic sequence but do not occur in higher in the sequence, whereas highly px-pl-ol phyric lavas are abundant in recent successions.

CHAPTER 6
GEOCHEMISTRY AND PETROGENESIS

6.1 INTRODUCTION

In this chapter, the geochemistry of whole-rock and glass samples from the Eyjafjöll volcanic system will be presented. Data will be used to determine how primary mantle melts are generated in this area and how these melts are affected by crustal magmatic processes before eruption. Some of the ideas and evidence presented in Chapter 5 will be enlarged upon to produce an overall magmatic model for the Eyjafjöll volcanic system.

Geochemical analysis was carried out on 262 whole rock samples, these included 217 lavas and 45 intrusive sheets. Analysis of the whole rocks for major element oxides and trace elements took place on the Durham University XRF spectrometer, a subset of 40 samples was analysed for rare-earth elements and selected trace elements on the ICP-AES at Egham. An additional 25 glass samples were analysed for major elements only, using the Durham University electron microprobe.

The full data set, sample preparation methods and analytical procedures are described in Appendix 3, together with precision errors (2σ) calculated using replicate analyses on internal monitors and International Reference Materials (IRM).

6.1.1 IGNEOUS PROCESSES

Primary magmas are generated by partial melting of the mantle, a process which is induced by increased temperatures, decompression, or the addition of volatiles which decrease the melting point of the source material. The composition of the partial melt relates to the source composition and the degree and type of melting (Rollinson, 1992).

Fundamental processes which may affect this primary melt before its eruption or intrusion near the surface include: 1) fractional crystallisation, 2) magma mixing and 3) crustal assimilation. The geochemical effect of each of these processes on the bulk composition of the residual liquid must be identified in order to understand the magmatic history of a suite of samples. When a rock is solidified at, or near the surface, it may be affected by hydrothermal alteration and surface rocks will undergo weathering. The geochemical affects of these processes must also be identified before the whole-rock geochemistry is interpreted.

The geochemical signature left by both melting and crystallisation processes is caused by the differential partitioning of elements between crystals and melt. *Incompatible elements* are partitioned into the melt and *compatible elements* are partitioned into suitable crystals. The degree of compatibility shown by an element for a particular mineral phase is described by its distribution coefficient K_D (K_D = concentration of element in solid/ concentration of element in liquid; Arth, 1976).

Mineral phases which are important in mantle melting processes beneath Iceland are olivine, orthopyroxene, clinopyroxene, spinel and at sufficient depths, garnet. Based on petrographic examination, the mineral phases involved in basalt fractionation are: chrome-spinel, olivine, clinopyroxene, plagioclase feldspar, Ti-magnetite and ilmenite. At high degrees of fractional crystallisation, alkali feldspar, apatite, hornblende and zircon may also be fractionating phases (Furman *et al.*, 1992a). Tables 6.1 and 6.2 show which elements are compatible with which mineral phases.

Table 6.1 *The compatible major element oxides and the mineral phases into which they are preferentially partitioned.*

MgO -	olivine (forsterite), clinopyroxene (augite)
Fe_2O_3T-	olivine (fayalite), clinopyroxene (hedenbergite), Ti-magnetite, ilmenite
Al_2O_3 -	feldspar, spinel
CaO -	feldspar, clinopyroxene
TiO_2 -	Ti-magnetite
P_2O_5 -	apatite

Table 6.2 *The major phases involved in the melting and crystallisation of a dry basaltic system and their compatible trace elements.*

garnet	Y, heavy REE (HREE)
spinel	Co, Ni
orthopyroxene	Sc, Co, Ni, V
clinopyroxene	Sc, Co, Ni, V
olivine	Ni, Co
chrome-spinel	Cr
plagioclase	Sr, Eu
Ti-magnetite	V

6.1.2 PRESENTATION OF GEOCHEMICAL DATA

6.1.2.1 VARIATION DIAGRAMS

The purpose of a variation diagram is to show how the concentration of a chosen trace element or oxide varies during the evolution of the parental melt. In this study, several different fractionation indices have been used.

MgO is a well-established index of basalt fractional crystallisation, it shows good correlation with other major element oxides as they are enriched or depleted in

residual liquids (e.g. Figure 6.2). Recent studies of Torfajökull in the EVZ (Macdonald *et al.*, 1989; McGarvie *et al.*, 1989) and Austurhorn in southeast Iceland (Furman *et al.*, 1992a) have all used MgO as a differentiation index. However, very evolved rocks such as trachyte contain so little MgO that analytical errors become significant (Cox *et al.*, 1979). Another problem concerning the Eyjafjöll samples is that the ankaramites and porphyritic basalts are partly accumulative and so produce greatly increased MgO contents, this decreases the size of the basalt field on a diagram.

SiO_2 is a poor index for basalts because it only begins to increase when Ti-magnetite starts to crystallise, so most of the fractional crystallisation of basalts occurs at roughly constant SiO_2. It is, however, a good index for intermediate and acid compositions (e.g. Figure 6.5).

Elements that are incompatible over the observed range of rock compositions and are unaffected by secondary alteration, may serve as good fractionation indices. These criteria are satisfied by La and Zr, for which most samples have been analysed. The great advantage of such an index is that the basalt field is not confined within a small range. Furman *et al.* (1992a) also used La as a fractionation index, thus comparisons can easily be drawn between the two areas.

The magnesium-iron ratio can be useful for studying the early stages of basalt fractional crystallisation because it falls steadily when only ferromagnesian minerals are forming. However, the later crystallisation of Ti-magnetite, which is an important feature of the Eyjafjöll sequence, can cause the index to become unreliable (Cox *et al.*, 1979).

Fractional crystallisation is best studied using variation diagrams. Plotting compatible elements versus a suitable differentiation index shows how the composition of a fractionating magma changes during fractional crystallisation (*liquid line of descent).* Inflections in the data trends show at what point during the evolution of the magma different mineral phases began to crystallise. If a single batch of magma has evolved and a sequence of progressively more evolved compositions has erupted and been sampled, a variation diagram will show a single liquid line of descent. Deviations from the liquid line of descent may be caused by phenocryst accumulation or loss. Parallel liquid lines of descent may represent different parental magmas evolving in a similar manner.

6.1.2.2 MANTLE-NORMALISED MULTI-ELEMENT PLOTS

These diagrams present a range of elements which are incompatible with respect to primordial or primary mantle compositions (e.g. Figure 6.18). The elements are arranged in order of decreasing incompatibility and abundances of each element are normalised to primordial mantle compositions (Sun and McDonough, 1992). These diagrams show clearly the scatter of certain elements affected by hydrothermal alteration (e.g. 6.18a). They may also show peaks or troughs at P, Ti and K caused by addition or

removal of apatite, Ti-magnetite and K-feldspar respectively. The fractional crystallisation of more evolved lavas can be investigated this way (e.g. Figure 6.18d).

6.1.2.3 CHONDRITE-NORMALISED REE PLOTS

The normalising composition used in this study is chondrite C1 (Sun and McDonough, 1989). The REE are incompatible during the fractional crystallisation of a basaltic magma, with the exception of Eu, which is compatible with plagioclase feldspar. Consequently, during fractional crystallisation, the relative abundance of all the REE in the residual melt increases, resulting in parallel profiles (e.g. Figure 6.7). During extreme fractional crystallisation, the ratios between the LREE and MREE may be slightly increased.

The overall shape of the REE profiles relates to partial melting processes. At small degrees of melting, the incompatible LREE are preferentially partitioned into the melt giving a profile which dips down towards the HREE. As the degree of melting increases, the profile may flatten out, approaching the source composition. The degree of enrichment or depletion of LREE relative to HREE may be assessed using a ratio such as $[La/Yb]_n$ (subscript n denotes that these are normalised values). Values above one may be described as enriched in LREE. Extreme depletion of HREE, especially Yb, may indicate the presence of garnet in the source material.

6.1.2.4 INCOMPATIBLE ELEMENT RATIO PLOTS

Incompatible elements including selected major, trace and REE, can be used to deduce the characteristics of the source composition and the melting processes which occurred. The most incompatible elements include light REE's (LREE's), Zr, Nb, and Ba. Ba, La, Ce and P are particularly incompatible during the melting of a mantle source containing garnet, olivine, pyroxene or plagioclase (Furman *et al.*, 1992a). Ratios of such incompatible elements in basalts at Eyjafjöll may also reflect their ratios in the mantle source region, with different ratios indicating that more than one source is involved in the petrogenesis of the magmas.

6.1.3 RIFT ZONE PETROGENESIS - A SUMMARY

There are two opposing theories concerning the origin of the various basalt types found in the Iceland volcanic zones:

One model suggests that the differences between mafic rocks (tholeiites to alkali basalts) are caused by different depths and degrees of melting of a mantle source (e.g Sigurdsson, 1970; Jakobsson, 1972, Meyer *et al.*, 1985; Macdonald *et al.*, 1990; Elliot *et al.*, 1991).

The alternative model proposes that a mantle-derived olivine tholeiite interacts with crustal melts formed during the breakdown of amphibolite facies assemblages at the base of the subsiding crust (Oskarsson *et al.*, 1982; 1985; Sigmarsson *et al.*, 1991).

As the hydrated crustal rocks cross their solidus, partial silicic melts are formed. Late-stage melts from the same assemblage form from the breakdown of kaersutitic amphibole and apatite. These melts are ne-normative and high in Ti, Fe, P and Zr. Mixing between the various melts forms the variety of mafic rocks found at the surface.

Iceland has a thick crust in comparison to normal oceanic crust due to the excessively high temperatures and high degree of melting induced by the mantle plume. Since the plume is enriched, high degrees of melting in such circumstances might be expected to produce high MgO magmas with an enriched signature. However, Elliot *et al.* (1991) have found that the most MgO-rich Icelandic basalts from the axial rift zones have depleted signatures. They have explained this phenomena in terms of a dynamic melting column in which instantaneous melts from different depths mix and are extracted. The geochemical signature of the magma gives a 'point depth average' for the depth of extraction. Melts segregated from the shallow mantle tend to have depleted signatures since partial melts have already been extracted from this depth, whereas melts from deeper in the melting column have more enriched signatures. Fe_2O_3T is a function of the mean depth of partial melting (Elliot *et al.*, 1991), therefore, shallow depleted melts have a relatively low Fe_2O_3T whereas deeper, enriched melts have higher Fe_2O_3T.

A comprehensive study of the petrological and geochemical variation in basalts from the neovolcanic zones of Iceland was carried out by Meyer *et al.* (1985). They found that alkali basalts from Vestmannaeyjar, at the southern tip of the Eastern Volcanic Zone (EVZ), were moderately LREE-enriched whereas transitional alkali basalts from the 'Hekla-Katla' region of the EVZ were highly LREE-enriched. Tholeiites from the axial rift zones show flat to LREE-depleted patterns. Modelling showed that the axial rift zone patterns could be matched by dynamic melting of a spinel lherzolite source, that is to say, the addition of incremental melts from a melt column (Langmuir *et al.*, 1977) extending down to the spinel lherzolite stability field. A spinel lherzolite source could not produce the LREE-enriched patterns of the alkali basalts, even at very small degrees of melting. However, if melting took place at greater depths, so that small amounts of garnet became stable, then LREE-enriched patterns could be reproduced. The modelling of Meyer *et al.* (1985) showed that up to 6% melting of a source near the spinel-garnet lhezolite transition zone was required to produce the Vestmannaeyjar basalts, whereas the Hekla-Katla area underwent smaller degrees of melting of a similar source to produce more LREE-enriched magmas.

Recent work by Macdonald *et al.* (1990) at Torfajökull also suggests that different mantle melting events are sufficient to explain the differences between tholeiite and transitional alkali basalts. At Torfajökull, the Veidivotn tholeiitic rift system meets the Torfajökull volcanic system, which is dominated by transitional basalts, intermediate rocks and rhyolites. Macdonald *et al.* (1990) showed that the tholeiite and transitional basalts were derived from a similar mantle source composition,

but that the transitional basalts were formed in the garnet stability field whereas tholeiites were formed in the spinel stability field.

Further corroboration for the first model alsó comes from work done by Furman *et al.* (1992a) at Austurhorn, which shows that Qz-normative basalts may be formed simply by fractional crystallisation and that the addition of a silicic melt, as proposed by Oskarsson *et al.* (1982), is not required.

Slight variations in the isotopic data of Iceland basalts may be accounted for by envisaging a veined or heterogeneous mantle (Wood, 1979; Wood *et al.*, 1979, Schilling *et al.*, 1982); alternatively, different degrees of crustal contamination may have occurred (Meyer *et al.*, 1985).

The Eyjafjallajökull volcano has high $^{3}He/^{4}He$ (18-19 x atmospheric - Wiese, 1991) as do all volcanoes from the central EVZ, indicating an enriched mantle plume input. Wiese (1992) found that four lavas from Eyjafjöll of differing age and chemistry had very consistent $^{3}He/^{4}He$, such constant values suggest that all basalts generated throughout the history of the volcano had a similar enriched source. If crustal contamination was an important process, smaller and more variable $^{3}He/^{4}He$ would be expected. The central EVZ is also enriched in $^{87}Sr/^{86}Sr$, $^{206}Pb/^{204}Pb$, $^{207}Pb/^{204}Pb$, $^{208}Pb/^{204}Pb$ and depleted in $^{143}Nd/^{144}Nd$ compared to axial rift zones (Meyer *et al.*, 1985).

Data and modelling in this chapter will provide further evidence that crustal assimilation is not essential in the petrogenesis of transitional and mildly alkaline basalts and that most variation can be explained in terms of mantle melting processes.

6.2 ALTERATION AND ELEMENT MOBILITY

Most of the samples collected at Eyjafjöll were extremely fresh. During loss on ignition (LOI), in which samples were heated to 800°C to remove H_2O, many samples actually gained weight due to the oxidation of iron. However, in the core of the volcano some samples have been exposed to hydrothermal alteration. Dykes and hyaloclastite breccias are particularly affected and contain zeolites, calcite and other secondary minerals. The consequences of this alteration must therefore be taken into account before the geochemical data are interpreted in terms of magmatic processes.

There have been many studies based upon element mobility in basalts caused by hydrothermal alteration (e.g. Wood *et al.*, 1976; Mottl and Holland, 1978; Humphris and Thompson, 1978; Humphris *et al.*, 1978 and Gibson *et al.*, 1982). In this study, Zr, Nb, Y and LREE were found to be immobile since they show a high degree of correlation with eachother. Rb, Ba, Sr, K_2O, Na_2O, CaO, SiO_2 and Fe_2O_3T all showed some degree of scatter in hydrothermally altered rocks. Several dykes and lavas from the core of the volcano and glassy sample 582, the Fjell trachyte, show a substantial loss of Rb and K_2O. Sample 94, a dyke from the Laugara area, was clearly hydrothermally

altered and contained zeolites which could not all be picked out before analysis. This dyke shows a loss of Na_2O, Al_2O_3, CaO, Rb and an increase in SiO_2 and Ba. Sr is particularly high in sample 239, a dyke at Nupakot, this is due to the occurrence of epidote in this rock (Humphris and Thompson, 1978). Samples 213 and 189, both evolved dykes, show mobility of K and Al; sample 213 also shows mobilisation of Fe and sample 189 shows mobilisation of Na. Two basic dykes, sample 92 from Laugara and sample 52 from Hvammsmuli, show mobility of Fe. The Hvammsmuli dyke is epidotised and shows secondary iron oxides lining vesicles, the Laugara dyke contains a large amount of calcium which also fills vesicles.

These altered samples (most of which are dykes) were not plotted on diagrams including the affected elements.

Glass is readily affected by hydrothermal alteration (Wood *et al.*, 1976), this is readily seen in the glass data (Figure 6.5), where K_2O, Na_2O, Al_2O_3 and Fe_2O_3T all show scatter. Wood *et al.*, (ibid) also found that the LREEs are mobile during the alteration of glass.

6.3 OXYGEN FUGACITY

The differentiation of basalt to intermediate and acid compositions requires enrichment of the residual liquid in SiO_2. This enrichment can be achieved by crystallisation of Ti-magnetite. The temperatures at which mineral phases such as Ti-magnetite and ilmenite reach the liquidus are strongly controlled by the oxygen fugacity (fO_2) of the magma (Lapin *et al.*, 1985). The higher the fO_2 of an initial basalt, the more likely fractionation to Qz-normative compositions will be since magnetite crystallisation occurs earlier at high fO_2. There is also some indication that magnetite crystallisation temperatures increase with alkalinity (Lapin *et al.*, 1985). In magmas of low fO_2 there is only limited crystallisation of magnetite and ilmenite, resulting in enrichment of Fe_2O_3T and TiO_2 at roughly constant SiO_2.

Processes which can influence oxygen fugacity in the near-surface environment include:

1) outgassing and the loss of volatiles,

2) reaction of magma with fluids from crustal rocks, and

3) magma contamination by crustal rocks of differing oxidation states (Lapin *et al.*, 1985).

Unfortunately no quantitative estimates of fO_2 were obtained in this study since coexisting magnetite and ilmenite were rarely in equilibrium. Wiese (1992) calculated the oxygen fugacity of a Holocene flow from Seljalandsheidi to be close to the QFM buffer. Furman *et al.* (1992a) showed that gabbros and pillows from Austurhorn have oxygen fugacity values between the QFM and NNO buffers.

6.4 MAJOR ELEMENT VARIATION AT EYJAFJOLL

When the data are plotted on the Total Alkali Silica (TAS) diagram, used in the classification of the Eyjafjöll rocks (Figure 6.1), they tend to form three clusters: one centred in the basalt field; one centred in the mugearite field including high Si hawaiites; and one centred on the trachyte field. Evolved compositions with between 53 and 63 wt% SiO_2 are rare and there is an apparent compositional gap between 56 and 61 wt% SiO_2. This gap is not due to sampling bias, since all identified acid and intermediate lavas and intrusions were sampled. There is no doubt that lavas and intrusives within this 'gap' are rare and small in volume.

Macdonald *et al.* (1990) found that intermediate rocks are also rare at Torfajökull, but there is no significant compositional gap. A compositional gap was noted by Furman *et al.* (1992a) at Austurhorn, which occurred between 54 - 62 wt% SiO_2.

Normative compositions of Eyjafjöll basalts plot between the 1atm and 9kbar cotectics of Thompson *et al.* (1983) and below the 'Martindale basalt' of Helz (1980) which differentiated at 3.5kbar (Figure 5.2). This suggests that differentiation of most of the basalts occurred at moderate pressures close to or even above 3.5kbars. The ankaramites plot closest to the 9kbar cotectic which supports evidence presented in Chapter 5 that the ankaramites crystallised at high pressures.

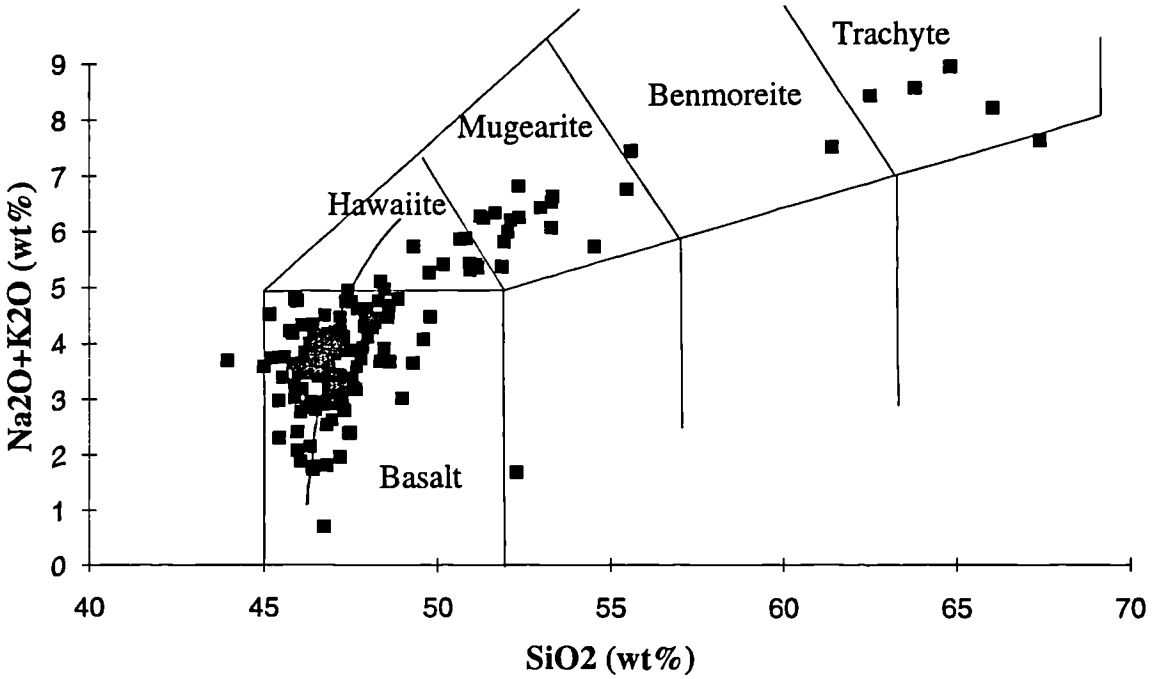

Figure 6.1 *Total alkalis versus silica diagram showing whole rock data from Eyjafjoll. The solid line represents the alkalic trend from Vestmannaeyjar (Furman et al., 1992a).*

The major elements show broad, coherent trends when plotted against MgO as a differentiation index, but there is a degree of scatter. Some of the scatter, particularly of alkalis, is due to hydrothermal alteration as discussed in section 6.2, the rest of the scatter may be explained in terms of magmatic processes.

6.4.1 BASALTS TO MUGEARITES (2.5 - 8 wt% MgO)

The most primitive aphyric basalt contains only 6.9 wt% MgO, this reflects the scarcity of primitive magmas reaching the surface at Eyjafjöll. Those samples with higher MgO contain abundant phenocrysts of clinopyroxene and olivine. The proportion of plagioclase phenocrysts increases as the MgO content falls.

The trends between ~2.5 wt% MgO and ~8 wt% MgO show curves and inflections consistent with fractional crystallisation.

SiO_2, K_2O and Na_2O increase as MgO decreases, whereas CaO shows a rapid decrease with MgO as it is removed in plagioclase feldspar.

Maximum TiO_2 and Fe_2O_3T occur at about 5% MgO; with falling MgO, TiO_2 and Fe_2O_3T are reduced, signifying the onset of Ti-magnetite crystallisation. Both iron and titanium show a broad spread of values at ~5 wt% MgO suggesting that different batches of magma existed which may have had different oxygen fugacities. There is a cluster of lavas and a sheet on Skogaheidi with exceptionally high TiO_2 (4.5 wt%). The very high TiO_2 is unlike any other lavas analysed from Eyjafjöll. Such high TiO_2 rocks have been documented from Katla (Meyer *et al.* 1985; Carswell, 1983), suggesting that Katla may be the source of these lavas.

Phosphorus abundances steadily increase from 0.2 wt% at 8 wt% MgO to 0.8 wt% at 4 wt% MgO at which point it decreases, as apatite begins to crystallise. However, there are several samples which show particularly abundant P_2O_5. A Laugara dyke (sample 19) contains 1.6 wt% P_2O_5 and samples 404 and 406 from Drangshlid, the monogenetic tuff cone to the south of the volcano, contain 1.35 and 1.18 wt% P_2O_5 respectively. Other samples which contain anomalously high P_2O_5 include lavas from Lambafell (the small shield to the south of the volcano) and some members of the Seljavellir Group (mugearites and hawaiites). No apatite phenocrysts were found in any of these samples suggesting that crystal accumulation is not responsible for elevated P_2O_5 concentrations, but apatite is a groundmass phase in samples 19, 404 and 406.

Al_2O_3 concentrations are roughly constant for most basalts at 13 - 16 wt%, although some basalts show evidence for accumulation of plagioclase phenocrysts. Those samples with over 17 wt% Al_2O_3 include 234 and 236 (members of the Laugara subgroup La2 at Nupakot) and 490 (member of the Laugara Group at Raufarfell). These lavas are up to 40% phyric and contain abundant, rounded aggregates and phenocrysts of plagioclase with sparse pyroxene phenocrysts. One other rock of particularly high Al_2O_3 is sample 345, a highly pl-px-ol phyric basalt from Halsar (section 5.3.2.3), plagioclase phenocrysts occupy at least 30% of the rock.

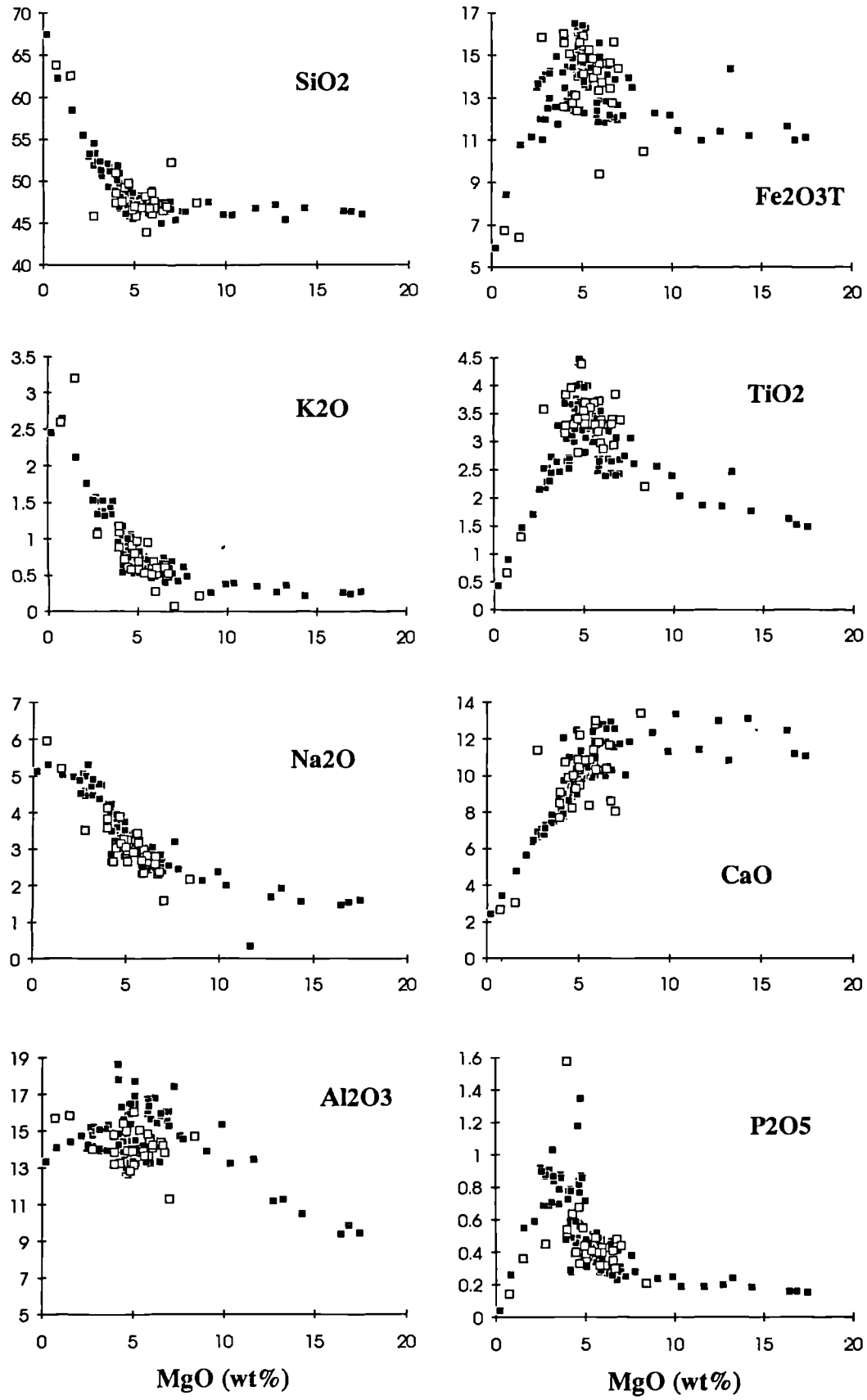

Figure 6.2 *Plots of major elements (wt%) versus MgO (wt%) for whole rock data. Closed squares are lavas, open squares are inclined sheets.*

The whole rock compositions of intrusive sheets have also been plotted on Figure 6.2 and show that most basalt lava compositions (apart from the highly plagioclase-phyric lavas) are represented by intrusive sheet compositions.

6.4.2 ANKARAMITES TO HIGHLY Px-Ol-Pl PHYRIC BASALTS (8-18 wt% MgO)

The rocks with over 8% MgO include ankaramites and px-ol-pl phyric basalts with over 20% phenocrysts. These rocks are unlikely to be liquid compositions. Despite the obviously primitive nature of some phenocrysts (e.g. Fo_{90}), the high MgO contents of these rocks are at least partly the result of olivine and clinopyroxene accumulation. Very high CaO is predominantly due to the accumulation of clinopyroxene although some rocks at the more 'evolved' end of the range may have accumulated plagioclase. TiO_2 and Al_2O_3 increase with decreasing MgO since they are incompatible with olivine and clinopyroxene. However, one of the highly porphyritic basalts with ~10 wt% MgO contains accumulative plagioclase and has anomalously high Al_2O_3.

One px-ol-pl phyric lava shows increased Fe_2O_3 and TiO_2. This is sample 509 (representative of the Asolfsskalaegg Group), which contains abundant acicular and granular Fe-oxides in the groundmass and large quantities of secondary Fe-oxides. This lava only erupted 129±20 Ka (Wiese, 1992), so extreme alteration is unlikely, the abundance of Fe-rich minerals suggests that this lava represents a magma enriched in Fe_2O_3 and TiO_2.

Abundances of SiO_2, K_2O, Na_2O and P_2O_5 are consistently low for this group of rocks, although Na_2O appears to show a slight increase with decreasing MgO. The rapidly decreasing CaO/Al_2O_3 of ankaramites with increasing degree of differentiation (Figure 6.3) again indicates that plagioclase was not being removed from this range of compositions.

Jakobsson (1979b) analysed a phenocryst-free part of the Hvammsmuli ankaramite, from which the phenocrysts had apparently been removed by flow differentiation. This composition has ~9 wt% MgO. Using this as a starting composition, the addition of up to 15% clinopyroxene and up to 25% olivine can explain even the most MgO-rich ankaramites (Figure 6.4).

The highly porphyritic rock samples appear to form a spectrum of compositions between two endmembers: ankaramite and transitional alkali basalt. It is proposed that this variation is partly due to the accumulation of phenocrysts, partly due to mixing and partly due to fractional crystallisation. It was shown in chapter 5 that the highly porphyritic, high MgO basalts (particularly of the Nupakôtsdalur Group) show abundant petrological evidence for mixing between a primitive ankaramite composition and a basalt composition. The Nupakôtsdalur Group shows a spectrum of compositions from ankaramites to highly porphyritic basalts containing variable proportions of olivine,

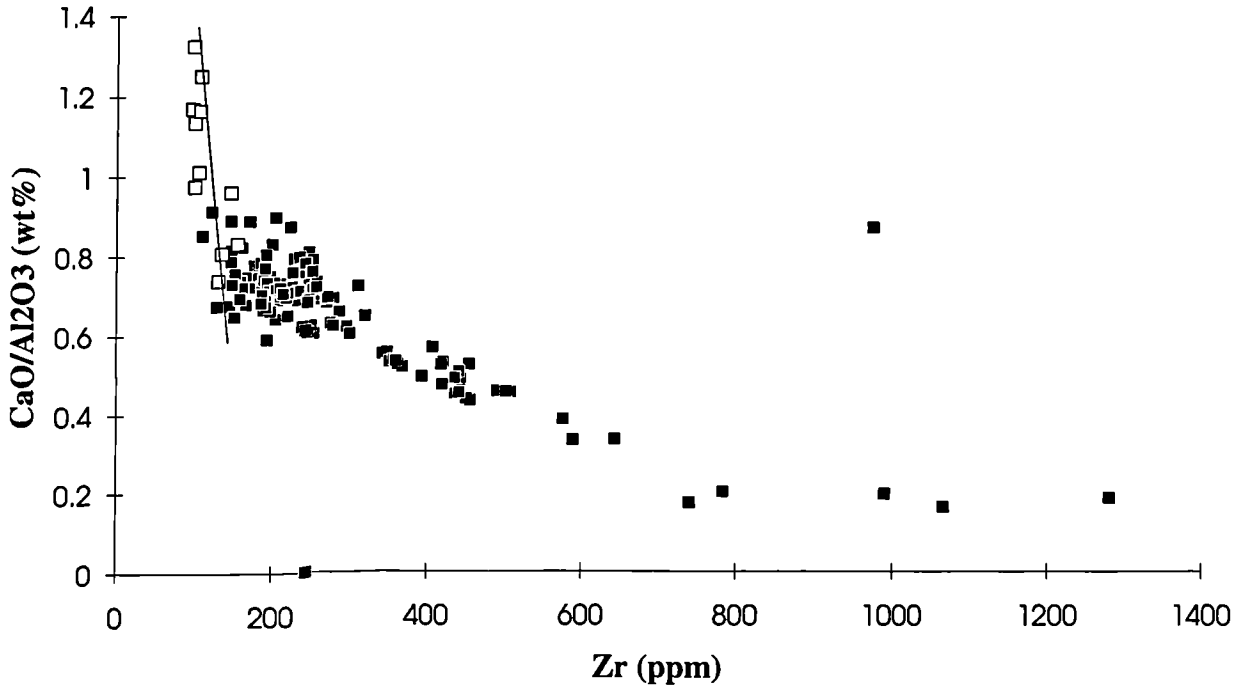

Figure 6.3 *Plot of CaO/Al_2O_3 versus Zr ppm; open squares represent ankaramites and highly pl-ol-px phyric basalts*

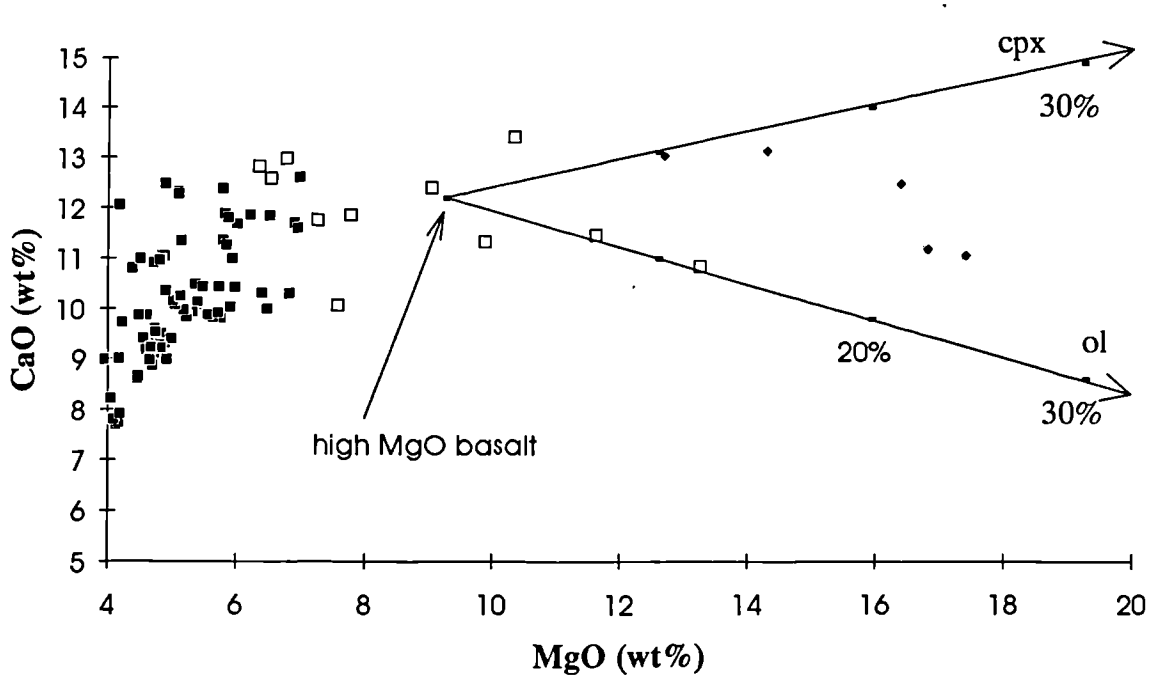

Figure 6.4 *Modelling the addition of clinopyroxene and olivine to an aphyric, high MgO basalt composition (NON 654, Jacobsson, 1979). Closed squares are basalts, open squares are highly px-Ol-pl phyric basalts and closed diamonds are ankaramites. The addition of 15% clinopyroxene and 25% olivine may account for even the most MgO-rich ankaramite, but see Figure 6.5.*

clinopyroxene and plagioclase phenocrysts. These lavas erupted in close succession suggesting that they originated from the same magma reservoir (see Figure 6.20).

6.4.3 BENMOREITE TO TRACHYTES (<2.5 wt% MgO)

These samples show increasing abundances of SiO_2, K_2O and Na_2O with decreasing MgO. Abundances of Fe_2O_3T, TiO_2, CaO and P_2O_5 correlate positively with MgO, whereas Al_2O_3 stays relatively constant.

The only benmoreite (sample 189 - 61wt% SiO_2), is a vertical NE-SW orientated intrusive sheet with no apparent extrusive equivalent. Trachyte sheets which occur in close proximity and in the same orientation as the previous example also lack extrusive equivalents. The trachyte lavas sampled from the upper slopes of the volcano have no intrusive equivalents and each has a distinctive field appearance, i.e. the Laugara trachyte contains numerous large basic inclusions (e.g 5.11A); the Kolbeinsskard trachyte contains small, vesicular basalt fragments (5.11D) and the Fjell trachyte is very glassy with flow-banding and no inclusions. Each trachyte also appears to be emplaced separately, there is no central conduit or fissure linking the outcrops. This evidence suggests that each trachyte was generated independently, perhaps in different magma chambers.

6.4.4 GLASS DATA

Glass data includes basalt pillow margins and hyaloclastite fragments, and interstitial glass within trachyte samples (Figure 6.5). The high MgO sample is a glass from the chilled margin of an ankaramite feeder indicating that the accumulation of olivine and clinopyroxene phenocrysts is not solely responsible for the high MgO of ankaramites. Another interesting feature of this glass is that it contains high CaO and low Al_2O_3, as do the ankaramite whole rocks. This suggests that the high CaO/Al_2O_3 of the ankaramites is a primary feature and is not caused by the accumulation of clinopyroxene. The basalt and trachyte glasses show relatively coherent trends for TiO_2, Fe_2O_3T and MgO. CaO and Al_2O_3 show some degree of scatter and Na_2O, K_2O and MnO show a very high degree of scatter due to alteration.

Intermediate compositions shown on Figure 6.5 represent hybrid glass from the Kolbeinsskard trachyte (sample 566) and the Laugara trachyte (sample 578), (see section 5.3.4.2). Element mobility may also be caused by the juxtaposition of trachyte and basalt. Experimental work has shown that K diffuses rapidly into the basalt when rhyolite and basalt liquids are in contact (e.g. Watson, 1982; Watson and Jurewicz, 1984). Other elements may be similarly affected.

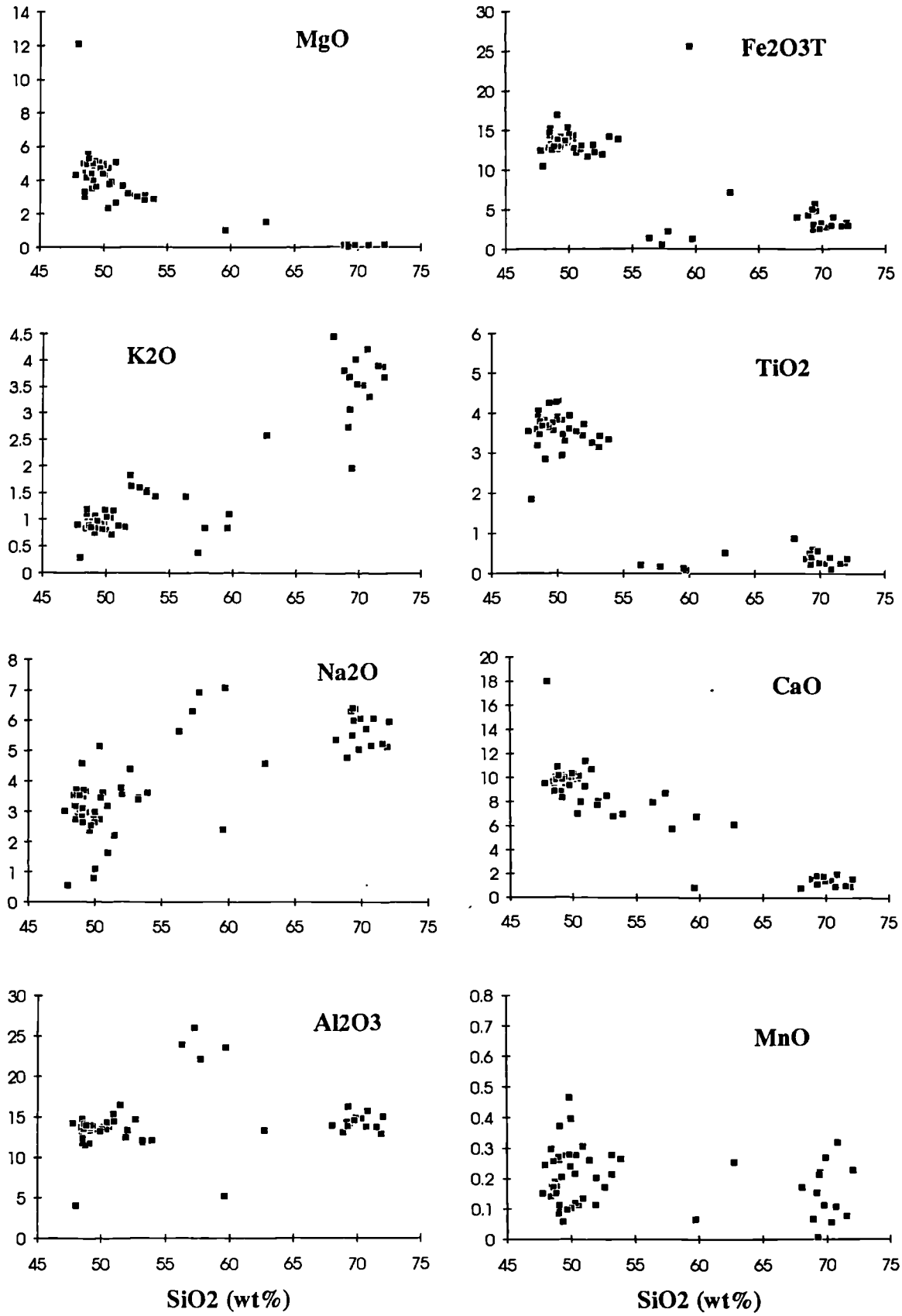

Figure 6.5 *Plots of major elements (wt%) versus SiO_2 (wt%) for glass samples.*

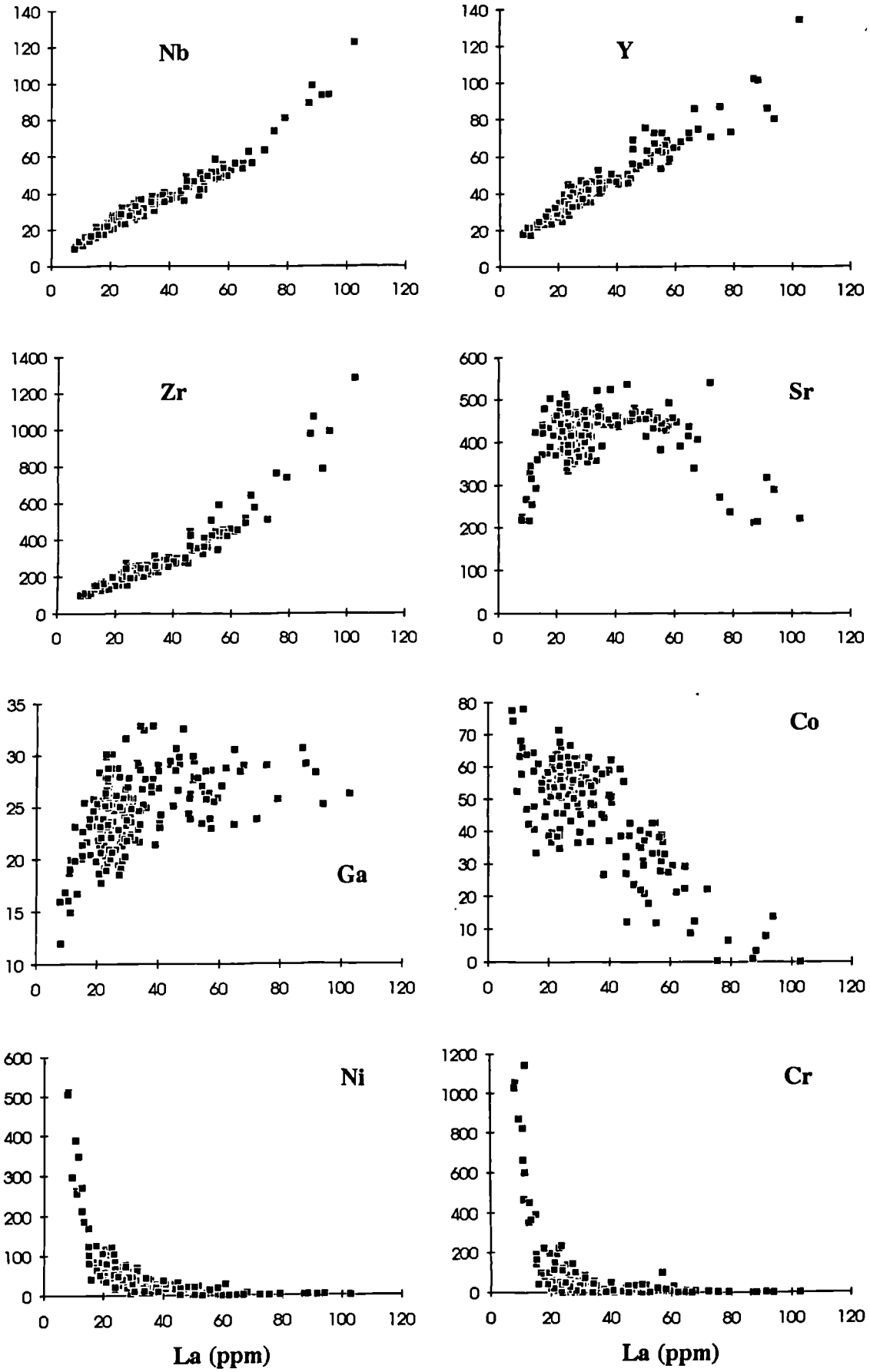

Figure 6.6 *Plots of trace elements (ppm) versus La (ppm) for whole rock data.*

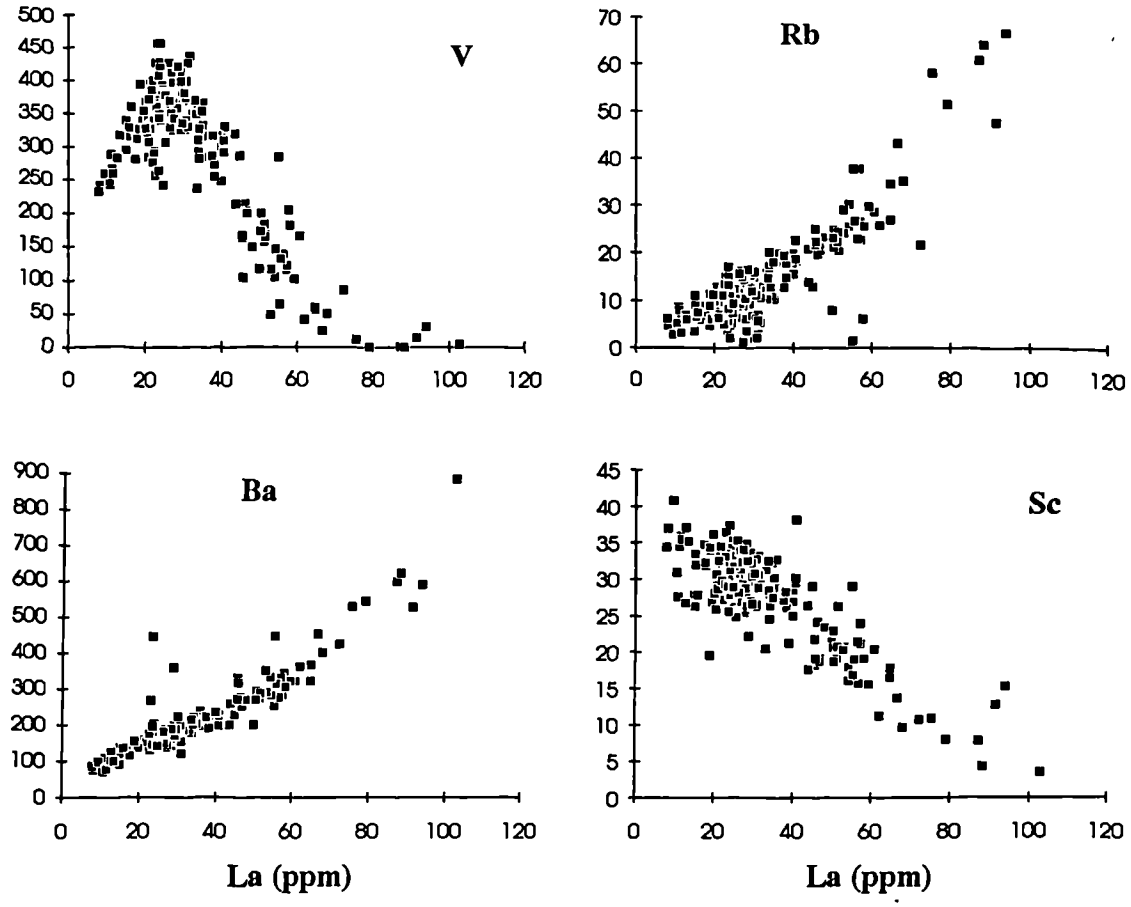

Figure 6.6 *(continued).*

6.5 TRACE ELEMENT VARIATION AT EYJAFJOLL

The incompatible trace elements La, Th, Zr, Nb, Y and Ba show positive correlations with each other for both basic and felsic compositions (Figure 6.6). Rb shows a weak positive correlation with La and a degree of scatter which may be attributed to hydrothermal alteration. Some scatter at more evolved compositions is evident for each element except Nb. No zircon was found in any of these trachytes and therefore Zr behaves as an incompatible element throughout the differentiation of the sampled rocks. Ni is abundant in samples containing olivine phenocrysts and shows steep, negative trends when plotted versus La. Cr shows a similar trend since chrome spinel inclusions are occasionally found in olivine and rarely, in clinopyroxene phenocrysts. In more evolved rocks, the concentrations of Cr and Ni are below detection limits. The abundance of Sr in ankaramites is particularly low, for basalts to mugearites the abundance remains relatively constant. For more evolved rocks, Sr shows a negative correlation with La, suggesting the extensive removal of plagioclase feldspar. V shows an initial steep positive correlation with La followed by a steep negative trend, the

inflection occurring at about 25 ppm La, this is consistent with removal of V in Ti-magnetite at about 5 wt% MgO. The compatible element Sc shows a broad negative correlation with La from primitive to more evolved compositions, which is consistent with the removal of clinopyroxene.

To test quantitively whether fractional crystallisation is the major process affecting the Eyjafjöll samples, modelling will be presented in section 6.4.1.

6.5.1 REE VARIATION

All the Eyjafjöll rocks are enriched in LREE relative to chondrite C1 (Sun and McDonough, 1989), (Figure 6.7). The patterns are broadly uniform for all samples regardless of age, or locality. A study of basalts from Hekla and Katla also show uniformly LREE-enriched trends (Meyer *et al.*, 1985). These workers suggested that these trends represent either mixing and homogenisation in a magma reservoir, or uniform melting conditions. The relatively parallel nature of the REE patterns from ankaramite to trachyte suggest that fractional crystallisation is of major importance in the generation of these rocks. Mixing of magmas at different stages of this differentiation process would also produce parallel patterns. It seems therefore, that the Eyjafjöll lavas may be generated from a single LREE-enriched parental basalt. However, there are subtle variations between the samples which must be explained.

The Eu anomaly in the most evolved sample (582-Fjell trachyte) signifies a high degree of plagioclase fractionation. In MORB basalts the Eu anomaly develops at a much earlier stage in the differentiation since olivine and plagioclase are the first minerals to crystallise. At Eyjafjöll, plagioclase only joins the crystallising assemblage after the extensive crystallisation of olivine and clinopyroxene.

The trachytes have high $[La/Sm]_n$ values (2.55) compared to the very constant value of 1.5 - 2.3 for the basalts (Figure 6.8a). This is caused by the highly incompatible nature of La relative to Sm after high degrees of fractional crystallisation.

Values of $[Ce/Yb]_n$ for Eyjafjöll basalts range between 3.4 and 6.3, the lowest value belongs to an ankaramite, the lowest value for an aphyric basalt is 3.6 (Figure 6.8b). This compares to transitional mafic rocks from Torfajökull which have a range of 4.5 to 7.0 (Macdonald *et al.*, 1990) and Austurhorn 2.5 to 4.9 (Furman *et al.*, 1992a). Most of the felsic rocks at Eyjafjöll have ratios of 4.4 - 4.6 suggesting that fractional crystallisation has not strongly affected the ratio.

The basalts with the highest $[Ce/Yb]_n$ have REE patterns which cross those of the other basalts (Figure 6.9). These are samples 69 (Skogaheidi), 82 (Lambafell) and 406 (Drangshlid). Other samples with high $[Ce/Yb]_n$ ratios include sample 307 from a shield eruption at the summit of Steinafjall, the FeTi basaltic dykes cutting the Fjell trachyte (sample 583) and sample 169, a trachyte dyke from Nupakotsdalur. These samples all occur to the south and the east of the Eyjafjöll volcanic system and as stated

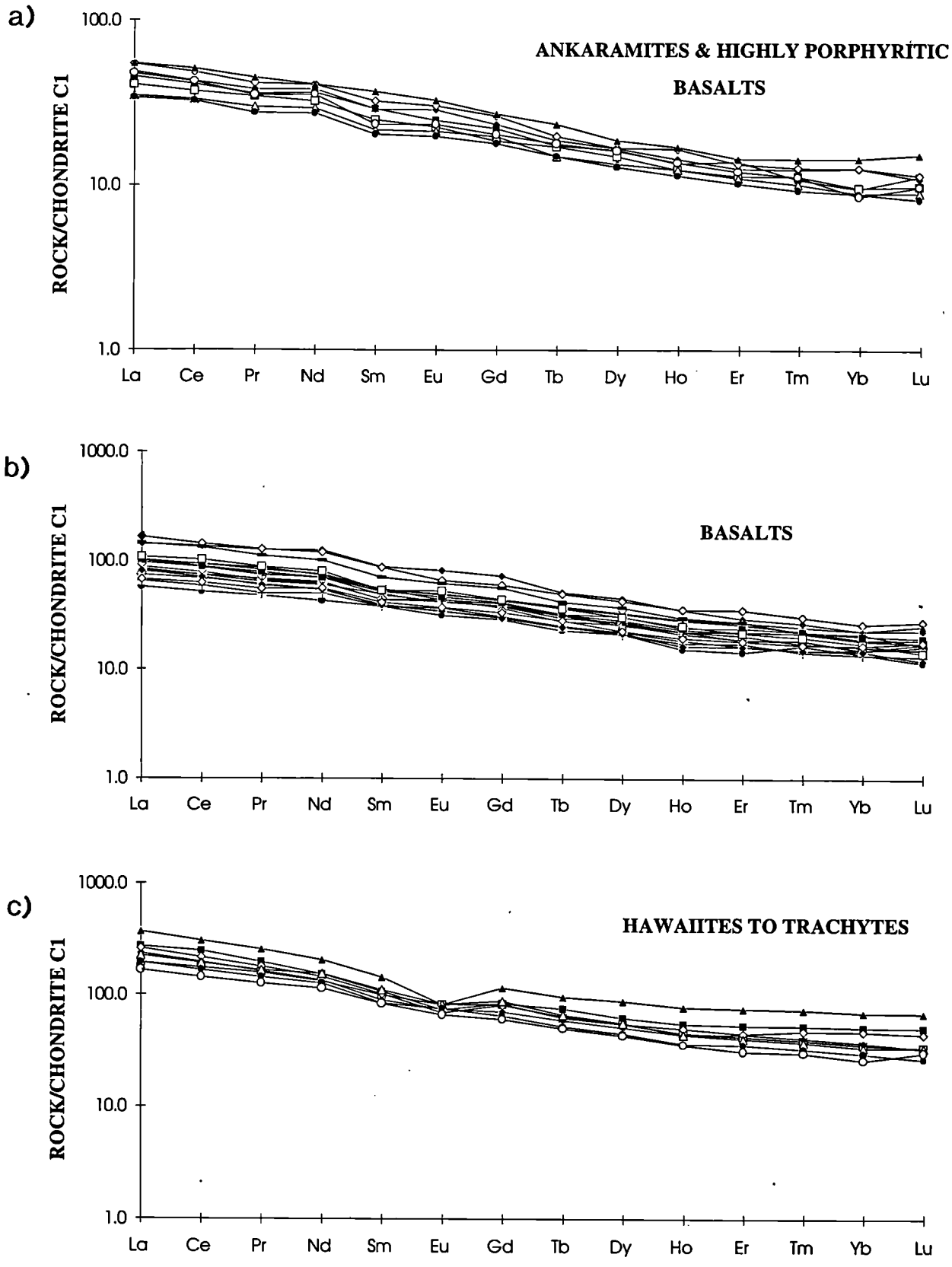

Figure 6.7 a) *Rare earth element (REE) data for ankaramites and highly px-ol-pl phyric lavas normalised to chondrite C1 (Sun and McDonough, 1989).* **b)** *REE data for basalts normalised to chondrite C1.* **c)** *REE data for hawaiites, mugearites, benmoreite and trachyte, normalised to C1 chondrite.*

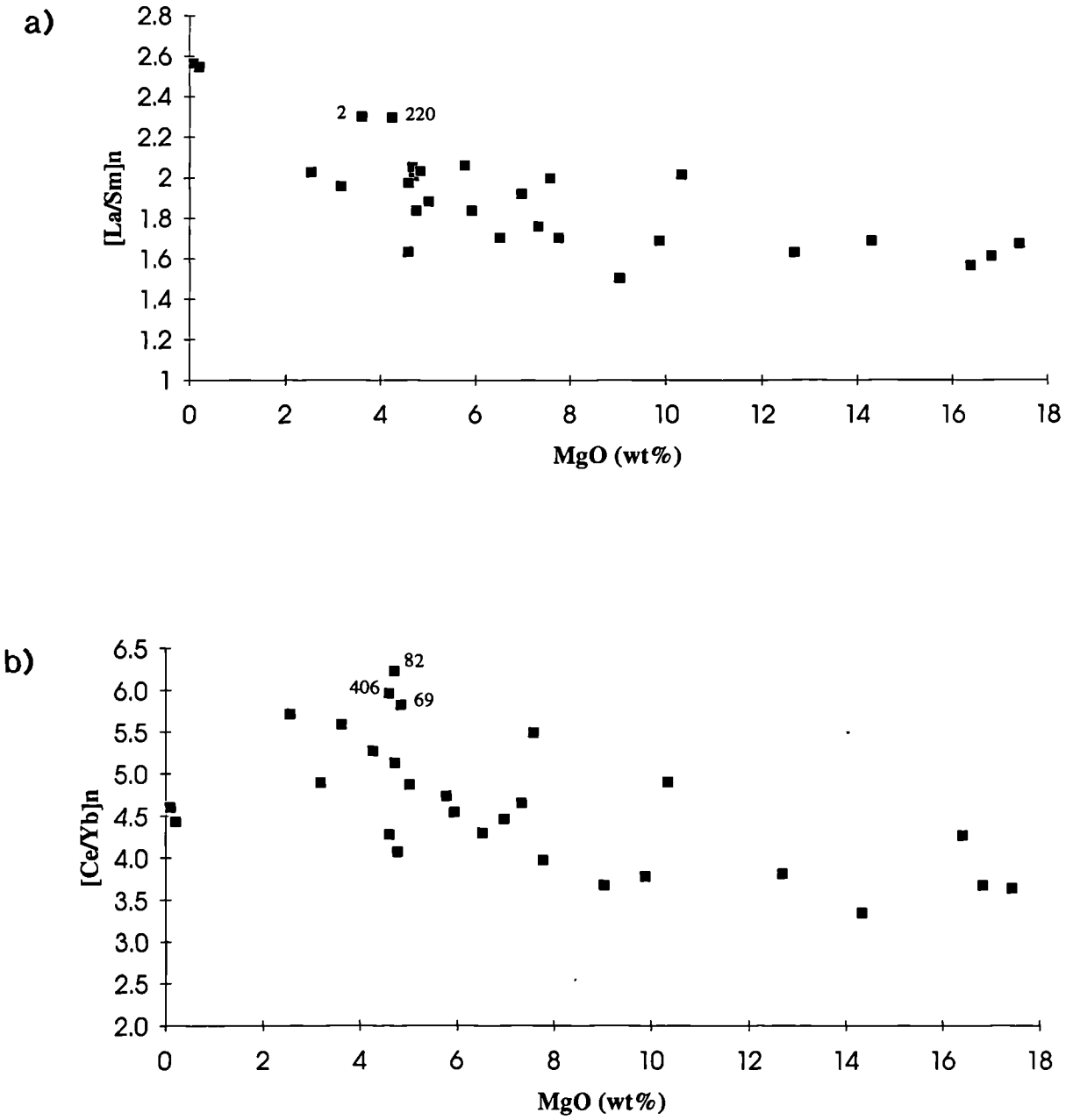

Figure 6.8 a) *La/Sm normalised to C1 chondrite, plotted versus MgO (wt%).***b)** *Ce/Yb normalised to C1 chondrite, plotted versus MgO (wt%).*

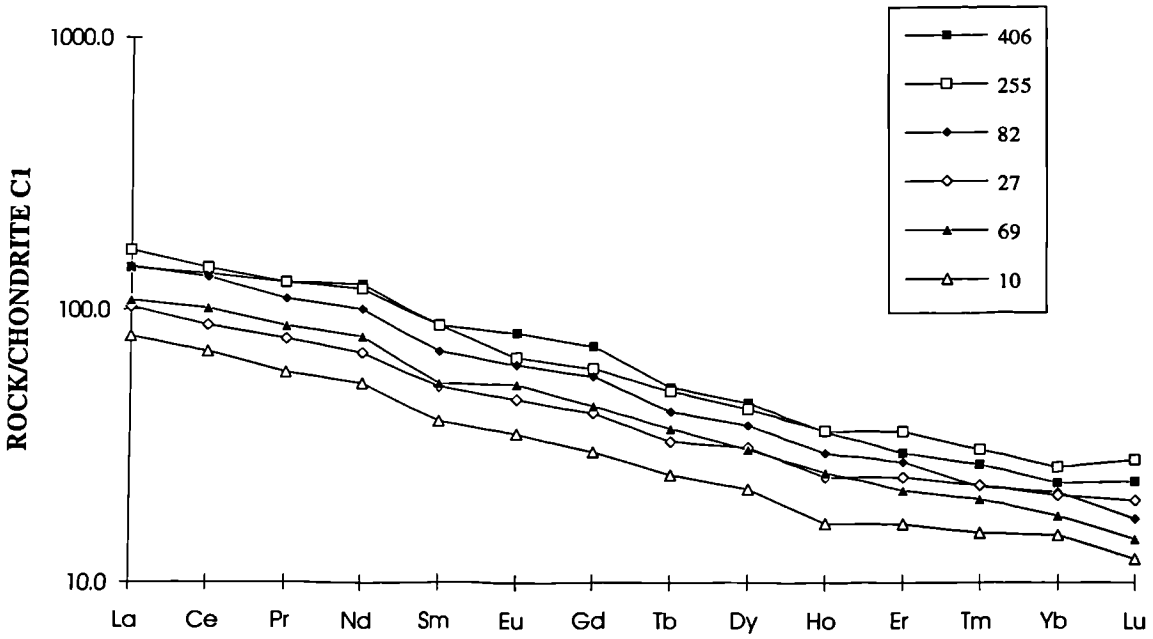

Figure 6.9 *REE patterns of six selected lavas: Sample 10 (Laugara Group), sample 69 (Skogaheidi), sample 27 (Morleysur Group), sample 82 (Lambafell), sample 255 (Fimmvorduhals Pass) and sample 406 (Drangshlid). The open symbols represent almost parallel patterns, the closed symbols represent steeper trends. Note that sample 406 is slightly enriched in middle REE.*

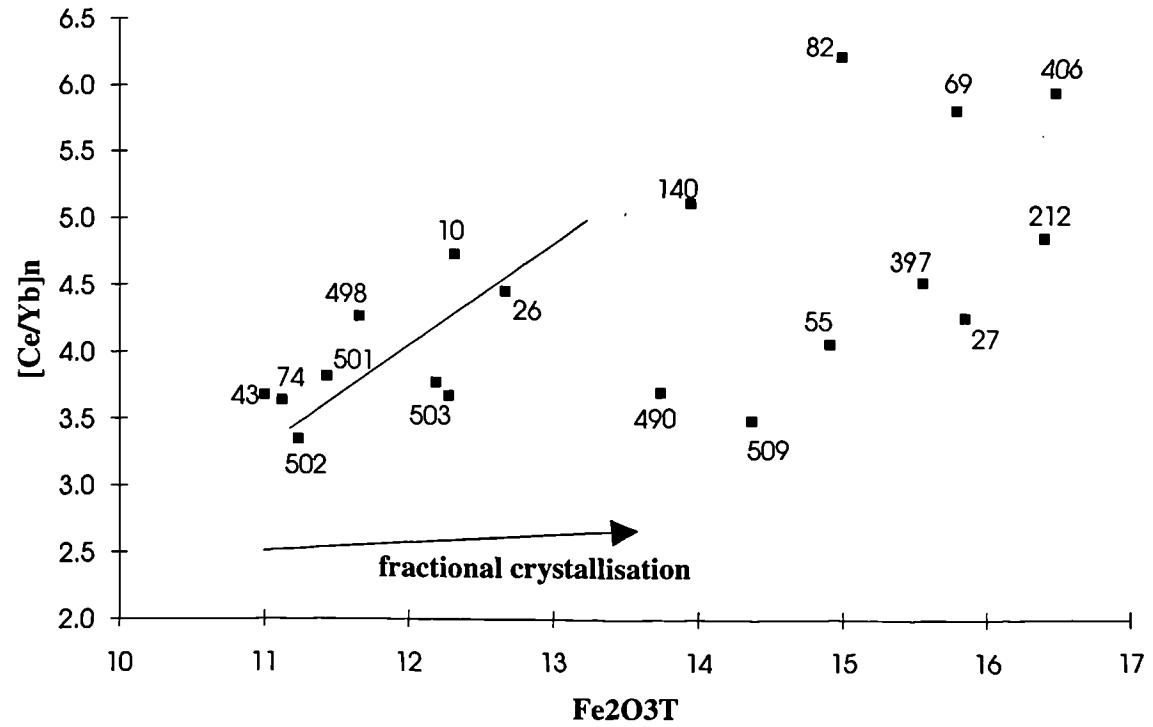

Figure 6.10 *Ce/Yb normalised to C1 chondrite, plotted versus Fe_2O_3T (wt%)*

earlier, sample 69 may actually belong to the Katla volcanic system. The samples are all evolved and contain moderate to high abundances of Fe and Ti.

Very small degrees of melting of a source containing garnet can cause steeply-dipping HREE-depleted patterns, since HREE and Y are retained in garnet.

Plotting $[Ce/Yb]_n$ versus Fe_2O_3T for basalts and ankaramites shows a distinct positive correlation (Figure 6.10). This appears to suggest that the ankaramites, which have low Fe_2O_3T and low Ce/Yb, represent mantle melts which have segregated at shallow depths at relatively high degrees of melting (<6%). Lavas with the highest Fe_2O_3T also have the highest Ce/Yb (i.e. samples 82, 404, 406, 69), suggesting that these may be melts segregated by smaller degrees of melting or, they are generated deeper in the mantle. The majority of basalts appear to have fractionated from parental melts which are intermediate between these two endmembers.

6.5.2 INCOMPATIBLE TRACE ELEMENT RATIOS

Basalts at Eyjafjoll have a range of Zr/Y ratios between 5 and 7, (Figure 6.11a), this is slightly lower than transitional basalts at Torfajökull which have a range of 6.4 - 8.4 (MacDonald *et al.*, 1990). By contrast, tholeiites at Torfajökull have a range of 3.4 to 4.0 indicating that Y was retained in the source of the transitional basalts but not in the source of the tholeiites. The spread of values at Eyjafjöll suggests that Y and HREEs were retained in the source to different degrees for different magmas. This suggests that melting occurred at different depths, as predicted by the modelling. The increasing Zr/Y in the more evolved basalts, hawaiites and mugearites suggest that Y is more compatible in the crystallising assemblage than Zr. As the increase occurs between 4-5wt% MgO it is proposed that Y shows a degree of compatibility for Ti-magnetite.

The majority of basalts show Ba/La ratios of between 4.5 and 7 (Figure 6.11b). The ankaramites contain particularly high Ba/La (6.5-10.6) which overlaps the basalt range. There appears to be a slight increase in Ba/La with differentiation (felsic lavas Ba/La = 5.75-8.5). The highest Ba/La for a basalt is sample 206 which has a Ba/La of 9, the lowest Ba/La for a basalt is for Lambafell (4.5), (sample 82).

Ba/La shows a broad range of values in both basalts and felsic rocks. nevertheless, it appears to show a slight decreasing trend through the basalt-mugearite sequence and an increase with differentiation in the felsic lavas. Likewise, the ratio La/Nb shows a broad increase through the basalt-mugearite sequence and a decrease with differentiation in the felsic rocks. These ratios suggest that Ba is less compatible and Nb is more compatible than La in the crystallising assemblage of basalt (clinopyroxene, plagioclase, magnetite). In the felsic rocks this is reversed and La is more compatible than Ba and less compatible than Nb.

The ankaramites also have high Zr/Nb (6.9-10.8) which overlaps the basalt range (5.9-8.8).

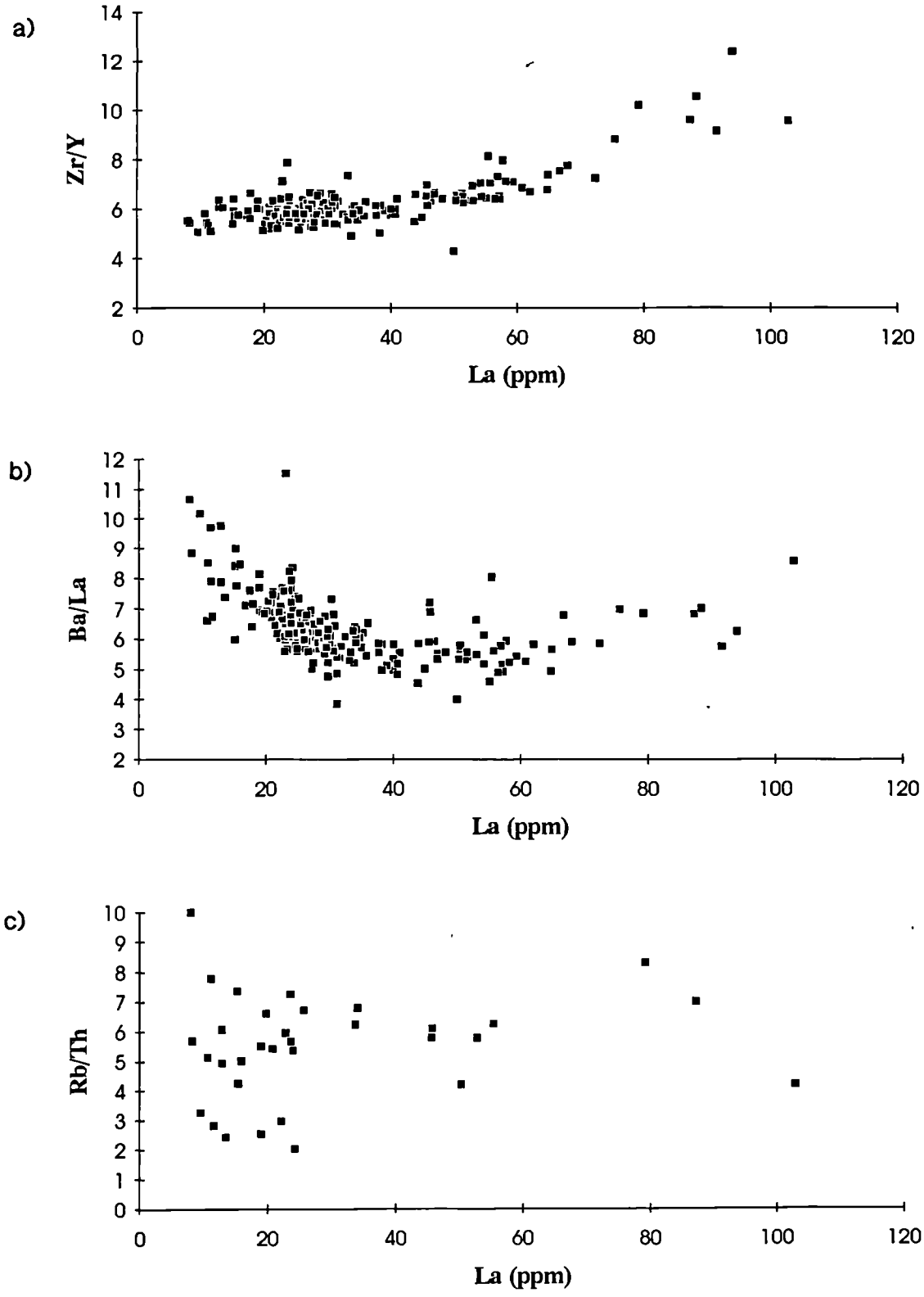

Figure 6.11 a) *Zr/Y plotted versus La (ppm).* **b)** *Ba/La plotted versus La (ppm).* **c)** *Rb/Th plotted versus La (ppm).*

Rb/Th ratios are between 2.04 and 7.80 for basalts and felsic rocks (Figure 6.11c). The lowest ratios belong to members of the high Fe series which have high abundances of Th and other incompatible elements. The Hvammsmuli ankaramite (sample 74) has an anomalously high Rb/Th ratio of 10.

6.6 STRATIGRAPHIC VARIATION

There is clearly a great variation in geochemical compositions at Eyjafjöll. As mentioned in chapter 4, the most evolved compositions occur later in the stratigraphic sequence, and more primitive compositions tend to occur earlier in the stratigraphic sequence. Three sections which show typical geochemical trends are described below.

6.6.1 LAUGARA

Plotting lava compositions which outcrop alongside the Laugara River, each stratigraphic Group consists of several lavas which appear to represent a 'batch' of magma with almost constant chemistry (Figure 6.12a). Each subsequent batch tends towards a more evolved composition. Members of the Laugara Group (La) contain varying abundances of compatible elements reflecting different abundances of phenocrysts such as olivine. The two lavas which comprise the Morleysur Group are Fe-Ti rich and more evolved than the Laugara Group.

The Seljavellir Group (Se) contains two compositional populations, one group is Fe- rich (>13 wt%) and the other is Fe-poor (< 13 wt%), (Figure 6.12a). It is difficult to assess the order of eruption of individual lavas in the Seljavellir Group which may, in part, account for the scatter on Figure 6.12a. However, one short sequence clearly shows subglacial Fe-poor mugearites overlain by diamictites then Fe-rich mugearites. This suggests that the Fe-poor basalts erupted first, there was then a period of inactivity and glacial deposition before the Fe-rich lavas were erupted. As well as geochemical differences, the two trends have different and distinctive petrological features (Figure 5.3.3). It is probable that they have distinct parental magmas and/or evolved under different oxygen fugacities. This suggests evolution either in separate magma chambers or perhaps in a stratified chamber with layers of differing oxygen fugacity.

The Laugara trachyte occurs higher in this sequence, it is unclear if the trachyte lies upon the Seljavellir Group or not. The trachyte has high Zr and low Sr.

The Svadbaelisheid Group (Sv), which outcrops to the west of this section and is not included on Figure 6.12a, is composed of basalts which are younger than the intermediate rocks of the Seljavellir Group. These basalts contain olivine and are thus not evolved. This provides some evidence that magmatic heat was still available at ~30Ka, when the Svadbaelisheidi Group was erupted.

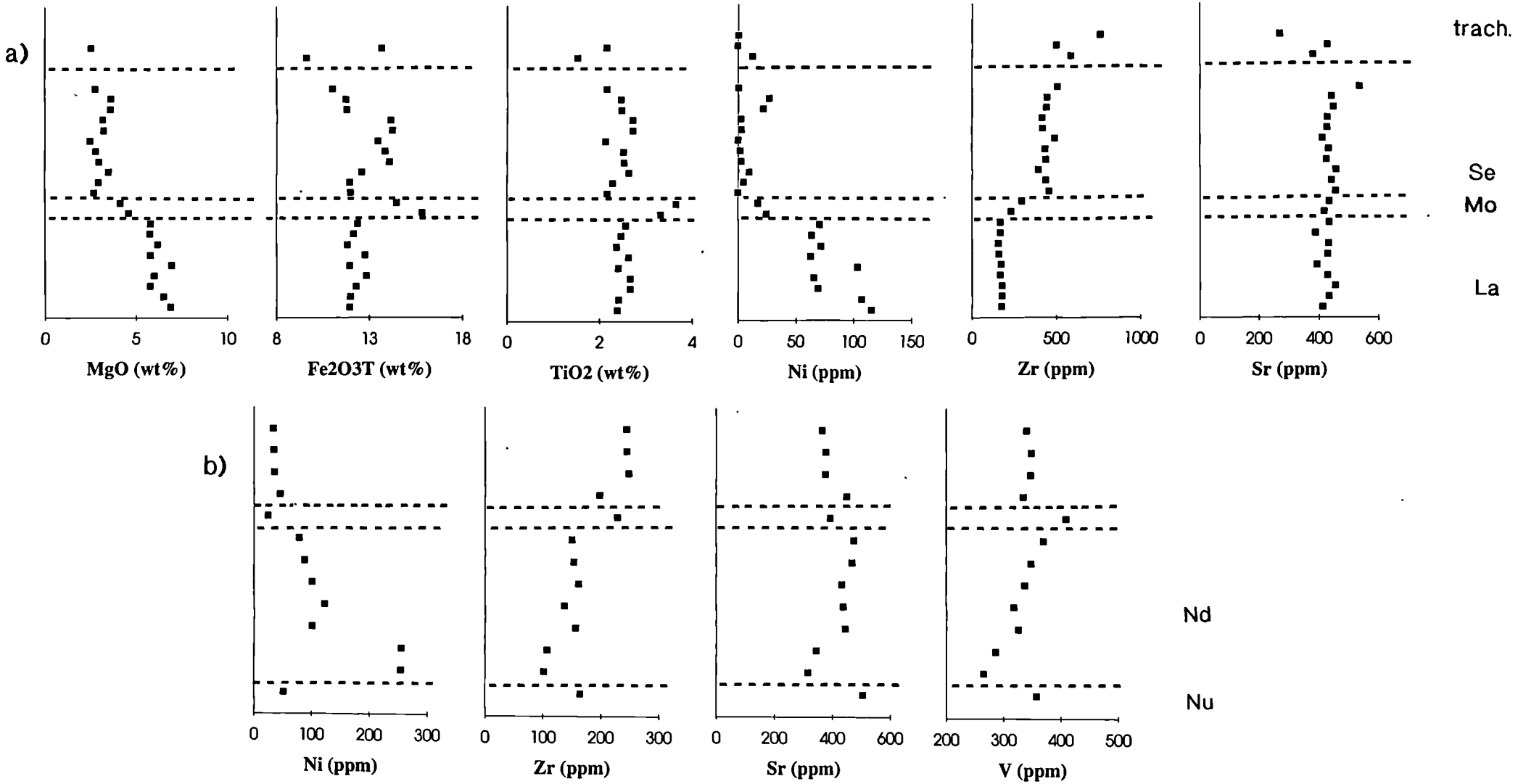

Figure 6.12 a) *Variation of selected major and trace elements within the Laugara river section, (La - Laugara Group; Mo - Morleysur Group; Se - Seljavellir Group; trach - Laugara trachyte).* **b)** *Variation of selected trace elements within the Nupakotsdalur section, (Nu - Nupakot Group; Nd - Nupakotsdalur group).*

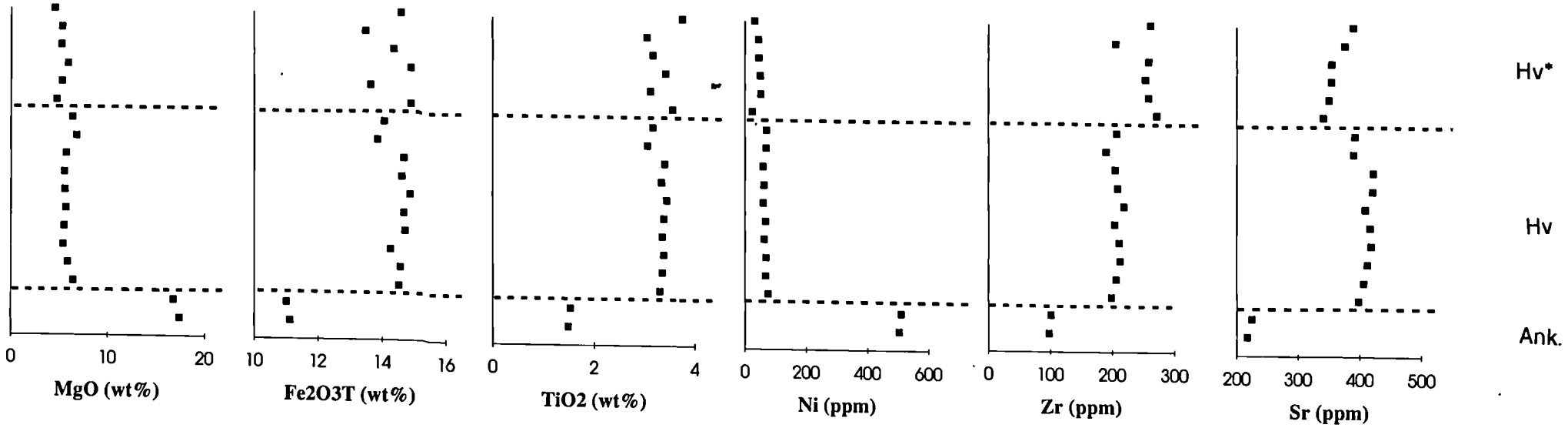

Figure 6.12 *(continued).* **c)** *Variation of selected major and trace element data for the Hvammsmuli section, (Ank - samples 74 and 43; Hv - Hvammsmuli Group; Hv* - evolved basalts).*

6.6.2 NUPAKOTSDALUR

Figure 6.12b shows a section through part of the stratigraphic pile at Nupakotsdalur which includes several stratigraphic groups. The basal Nupakot Group is overlain by the more primitive Nupakotsdalur Group (Nd) which shows evidence for the replenishment of an evolving basaltic magma chamber by a primitive magma (section 5.3.2.3 and Figure 6.20). This is overlain by Fe-Ti rich basalts which thicken towards the south (these FeTi basalts are referred to as Nd* on Figures 6.13 to 6.15). The FeTi basalts are in turn overlain by more evolved basalts.

6.6.3 HVAMMSMULI

The compositional variation in the stratigraphic succession at Hvammsmuli also shows a trend towards more evolved compositions (Figure 6.12c). The Hvammsmuli section consists of three groups: the basal Hvammsmuli ankaramite, the Hvammsmuli Group (Hv) and an upper slightly more evolved group (referred to as Hv* on Figures 6.13 to 6.15). The uppermost subglacial unit was not included in this study, but it is known that above this lie highly pl-px-ol phyric basalts (sample 57) which are more primitive than the underlying basalts.

6.6.4 STRATIGRAPHIC CONSTRAINTS ON THE MAGMATIC PLUMBING SYSTEM

The lava sequences provide evidence that batches of magma generally became progressively more evolved with time. Occasionally primitive lavas (e.g. Svadbaelisheidi Group, Asolfsskalaegg Group) are intercalated between more evolved lavas, but this is not a common occurrence. Batches of Fe-Ti basalt also occur intercalated between basalts of lower FeTi contents. The eruption of such distinct batches of magma indicates that there was not a single, central homogenous magma chamber. In contrast there may have been several smaller magma chambers fractionating independently and supplying discrete batches of magma to the surface.

When selected stratigraphic Groups and lavas are plotted on variation diagrams there appear to be several liquid lines of descent (Figures 6.13 to 6.15). Each trend may represent fractionation of a distinct parental magma and/or differentiation under different oxygen fugacities. The Seljavellir Group contains Fe-rich lavas and Fe-poor lavas which have erupted almost contemporaneously. Since the Fe-poor lavas erupted earlier, this may reflect emptying of a zoned magma chamber. An alternative is that this stratigraphic Group includes magmas from two different magma chambers which may have been evolving under different oxygen fugacities.

To fractionate as far as trachyte compositions, the magma chamber(s) must be able to cool and differentiate over long time periods with minimal replenishment. As previously suggested in section 6.2.2.3, the Eyjafjöll trachytes are unlikely to have erupted from a large homogenous central magma chamber. Since the trachytes which

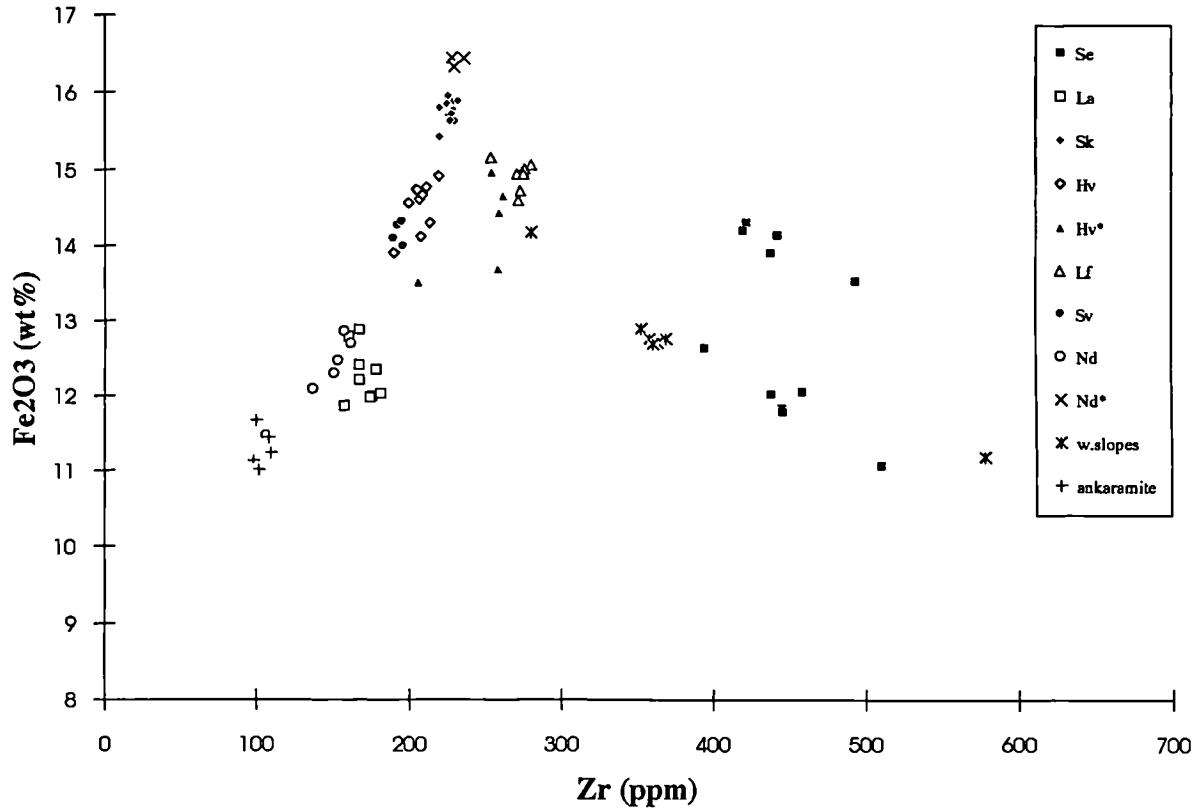

Figure 6.13 *Selected stratigraphic Groups and lavas plotted on a Fe_2O_3T (wt%) versus Zr (ppm) variation diagram. Se (Seljavellir Group), La (Laugara Group), Sk (Skaogaheidi high FeTi basalts), Hv (Hvammsmuli Group), Hv* (upper sequence at Hvammsmuli), Lf (Lambafell), Sv (Svadbaelisheidi Group), Nd (Nupakotsdalur Group), Nd* (high FeTi-basalts above Nd), w. slopes (hawaiites and mugearites from intraglacial, radial fissures), ankaramite (all samples).*

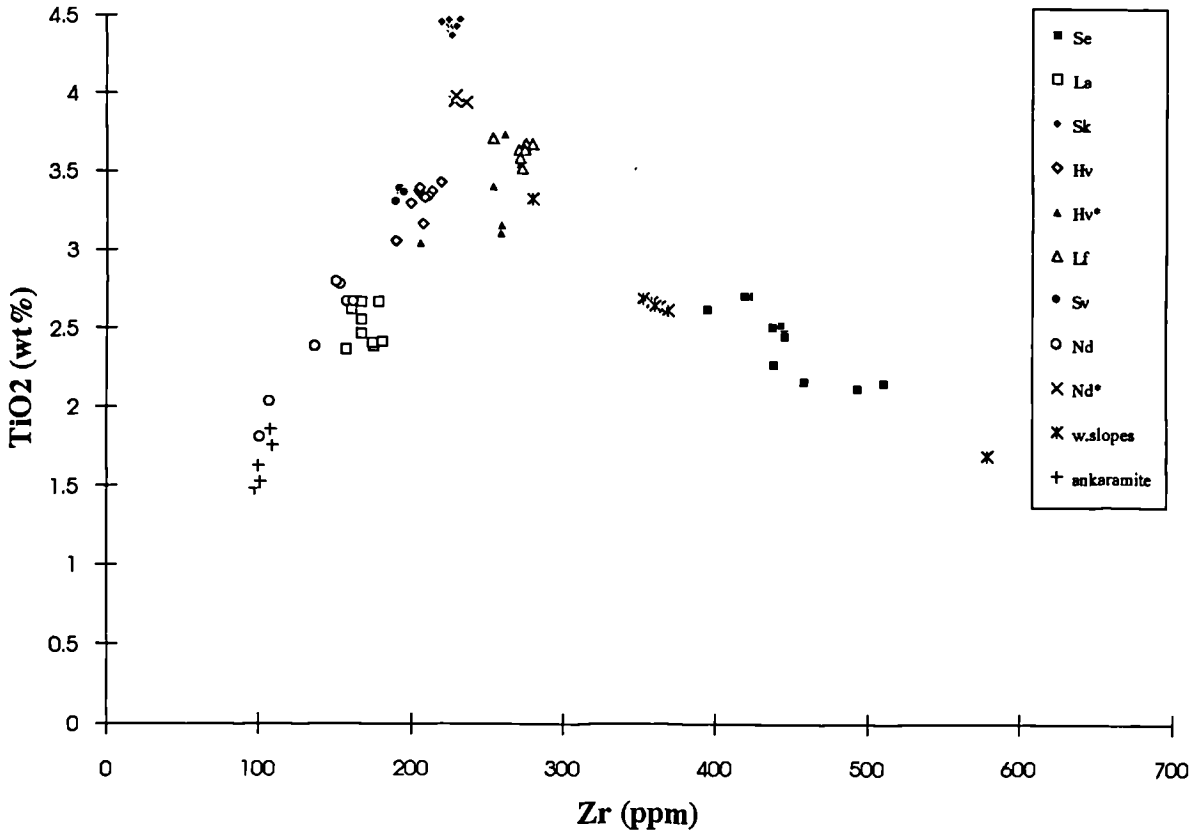

Figure 6.14 *TiO2 (wt%) plotted against Zr (ppm) for selected stratigraphic groups and lavas. For key explanation see Figure 6.13.*

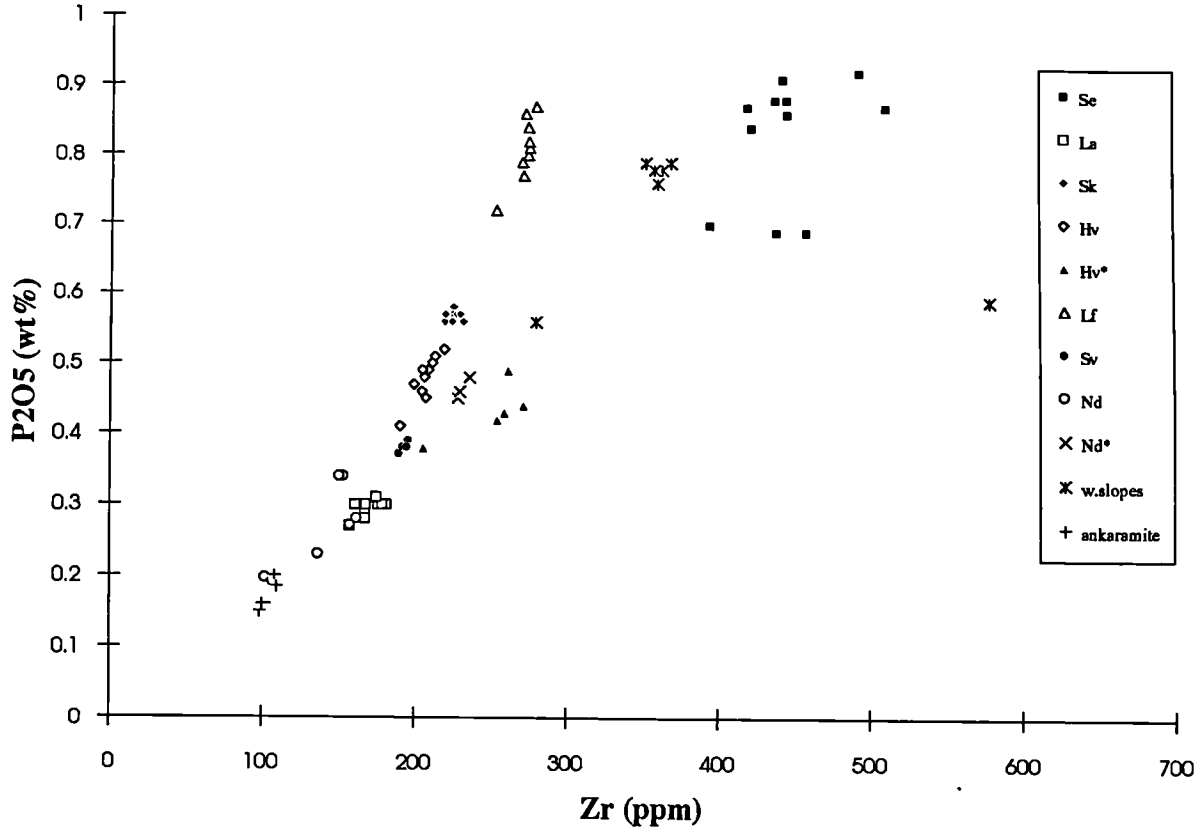

Figure 6.15 *P_2O_5 (wt%) plotted against Zr (ppm) for selected stratigraphic groups and lavas. For key explanation see Figure 6.13.*

contain basic inclusions outcrop at some distance from the central magma chamber, it is proposed that they originate from separate magma chambers.

The variation diagrams in Figure 6.13 and 6.14 suggest that maximum abundances of TiO_2 and Fe_2O_3T are variable for different batches of magma. This in turn suggests that each magmatic lineage evolved under different oxygen fugacities. The high Fe lavas were presumably produced from a parental magma of especially low fO_2. Extremely Fe enriched dykes were noted by Furman *et al.* (1992a) at Austurhorn, who also suggested that they were generated under conditions of low fO_2.

6.7 PETROGENESIS - CRUSTAL PROCESSES

6.7.1 FRACTIONAL CRYSTALLISATION

Petrological and geochemical evidence suggests that the fractional crystallisation of olivine, clinopyroxene, plagioclase and Ti-magnetite is of prime importance in the

differentiation of Eyjafjöll basalts. Despite abundant petrological evidence that open-system magma chamber processes occurred, the modelling of closed-system fractional crystallisation was attempted to see if it could, to a first approximation, explain the geochemical data. Where closed-system fractional crystallisation does not fit the data, processes such as magma mixing and assimilation are investigated.

6.7.1.1 MODELLING FRACTIONAL CRYSTALLISATION FROM BASALT TO HAWAIITE

Fractional crystallisation was modelled using the TRACE3 program developed by Nielsen (1988). This program combines major element phase equilibria with trace element partitioning to model differentiation processes at 1 atmosphere pressure. A suitable primitive starting composition is chosen, this should be a liquid composition, preferably a melt which has been subjected to minimal differentiation. The oxygen fugacity of the starting composition can be set prior to modelling. TRACE3 then calculates the proportions and compositions of crystallising minerals and the incremental liquid compositions. The TRACE3 program does not model the fractionation of apatite or alkali feldspar. Since apatite appears on the liquidus at about 4 wt% MgO (Figure 6.2), the model is unlikely to fit observed whole rock compositions with less than 4 wt% MgO.

Despite the existence of several lavas containing magnesian olivine (Fo_{88-90}) there are no lava compositions at Eyjafjöll which represent primary melt from a peridotite source. This problem makes the selection of a starting composition rather difficult. Sample 43, an ankaramite, with olivine of Fo_{90}, shows a comparatively small range in phenocryst compositions. This sample was selected as a possible starting composition but modelling proved that it is not a suitable parental magma. Modelled trends matched other ankaramites but did not match the observed basalt trends very well. There are several reasons why this may be so. Firstly, TRACE3 only models differentiation at 1 atmosphere pressure, the petrology of the ankaramites suggests that they have undergone extensive differentiation at high pressures. Secondly, this sample is unlikely to be a liquid composition so does not make a suitable starting composition.

The most primitive, aphyric basalt is sample 206, from the Nupakotsdalur Group which contains 6.98 wt% MgO. Another possible starting composition is sample 8, a member of the Laugara Group which contains less than 10 vol% phenocrysts of olivine, clinopyroxene and plagioclase. Sample 8 is the oldest analysed lava and contains 6.9 wt% MgO. Clinopyroxene compositions are close to those calculated by TRACE3 to be in equilibrium with the bulk rock composition but some olivine phenocrysts have compositions of Fo_{90} compared to a predicted Fo_{80} by TRACE3. Plagioclase compositions are also poorly predicted, being generally more calcic (An_{80}; but see Figure 5.18) than the predicted composition (An_{64}). Sample 8 has clearly undergone a degree of differentiation and mixing prior to eruption.

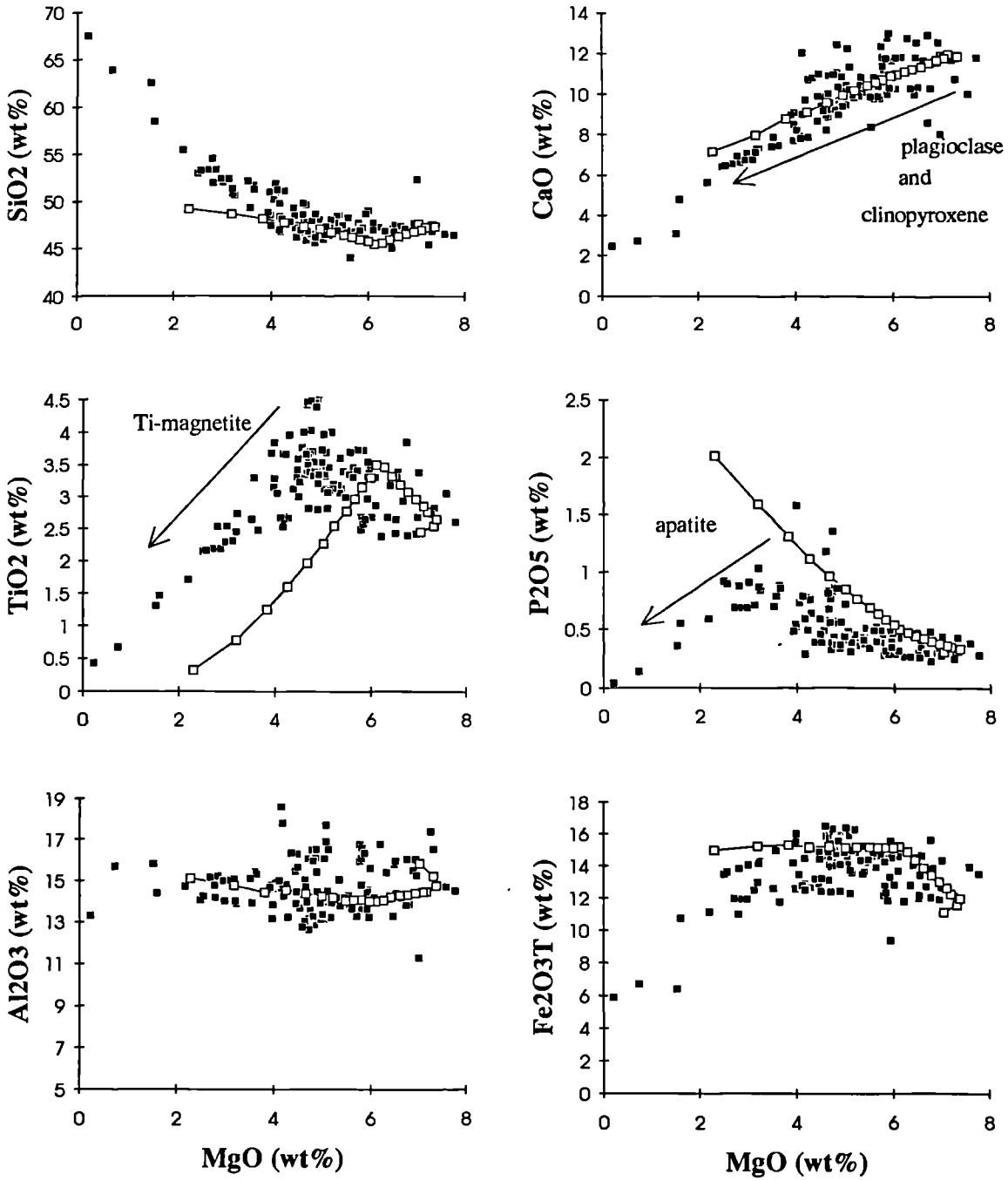

Figure 6.16 *Selected major and trace elements plotted against MgO (wt%) for the whole rock data (closed squares). Open squares represent the liquid trend calculated by TRACE3 (Nielson, 1988) for sample 8 as a starting composition. Each increment on the modelled trend represents 4% crystallisation.*

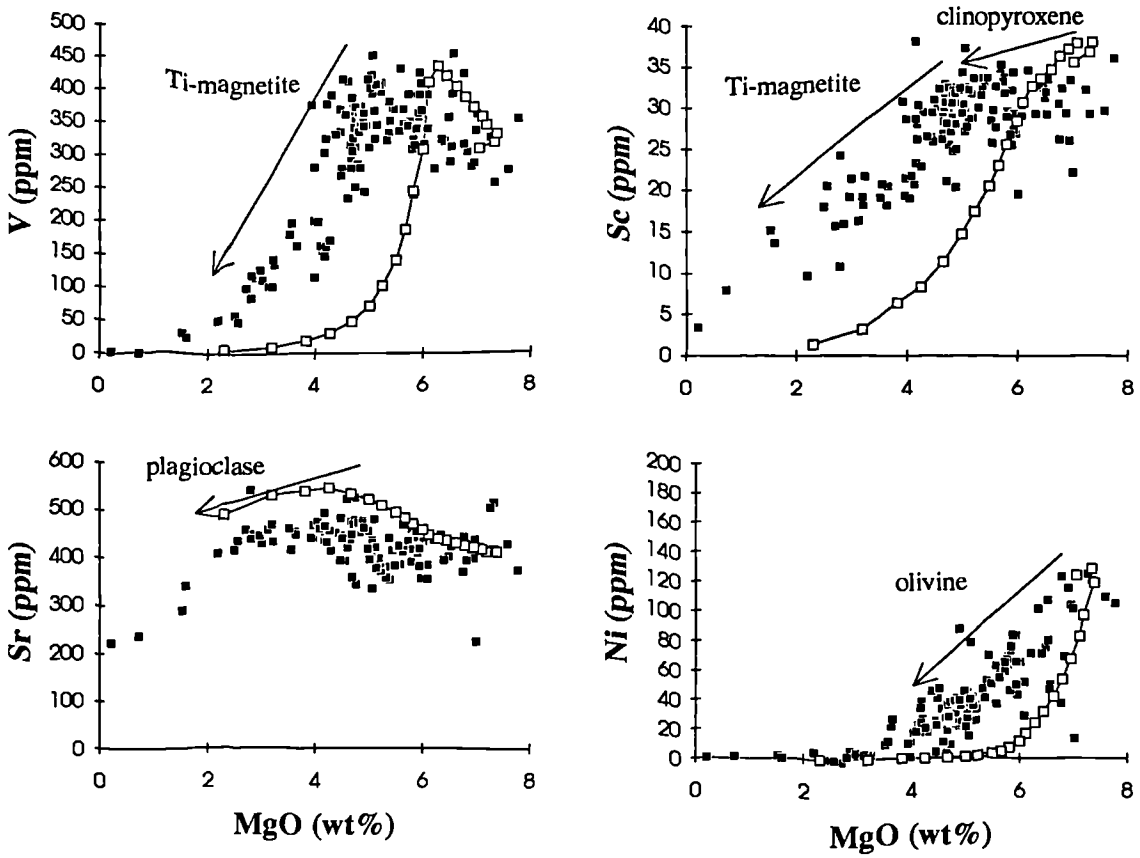

Figure 6.16 *(continued).*

When both starting compositions are modelled with the oxygen fugacity set at the QFM buffer, the fractionating trends are very similar. However, despite the poor predictions of mineral compositions by TRACE3, sample 8 matches the whole rock data better than sample 206. The order of appearance of minerals on the liquidus for sample 8 (as calculated by TRACE3) is as follows: Cr-spinel, plagioclase, olivine, clinopyroxene, Ti-magnetite. The order of appearance of minerals on the liquidus for sample 206 is: plagioclase, olivine, clinopyroxene, Ti-magnetite. This order of crystallisation reflects the evolved nature of the starting compositions.

Figure 6.16 shows calculated liquid compositions (using sample 8 as a parental liquid) and whole rock data plotted on variation diagrams. The diagrams show that for MgO>4, the modelled data fit some whole rock trends very well (SiO_2, CaO, Al_2O_3, Fe_2O_3T), but for others there is a marked discrepancy. Particularly poor correlations are obtained for TiO_2, V, Sc and Ni, possible reasons for this will be discussed below.

The liquid trends all show an initial enrichment in MgO because plagioclase has been calculated as the first mineral on the liquidus. This results in all the liquid compositions being slightly offset to more MgO-rich compositions.

When plotted versus TiO_2, the calculated liquid compositions increase as olivine and clinopyroxene join plagioclase on the liquidus. However TRACE3 predicts the arrival of Ti-magnetite on the liquidus too early, resulting in an inflection at 6.5% MgO rather than 5% MgO, Almost identical behaviour is shown by V. These discrepancies may partly be explained by oxygen fugacity. Vanadium occurs in three oxidation states, V^{4+} and V^{5+} which readily substitute for Ti^{4+} under oxidising conditions and V^{3+} which may substitute for Fe^{3+} and Cr^{3+} in more reducing conditions (Shervais, 1982). The behaviour of V is thus strongly affected by the oxidation state of the magma. In oxidising conditions, the partition coefficient for V in Ti-magnetite is high and the partition coefficient for clinopyroxene is low, the reverse is true in reducing conditions. The variation diagrams show that when Ti-magnetite begins to precipitate at ~ 5 wt% MgO, V abundance drops dramatically as predicted by TRACE3. It closely

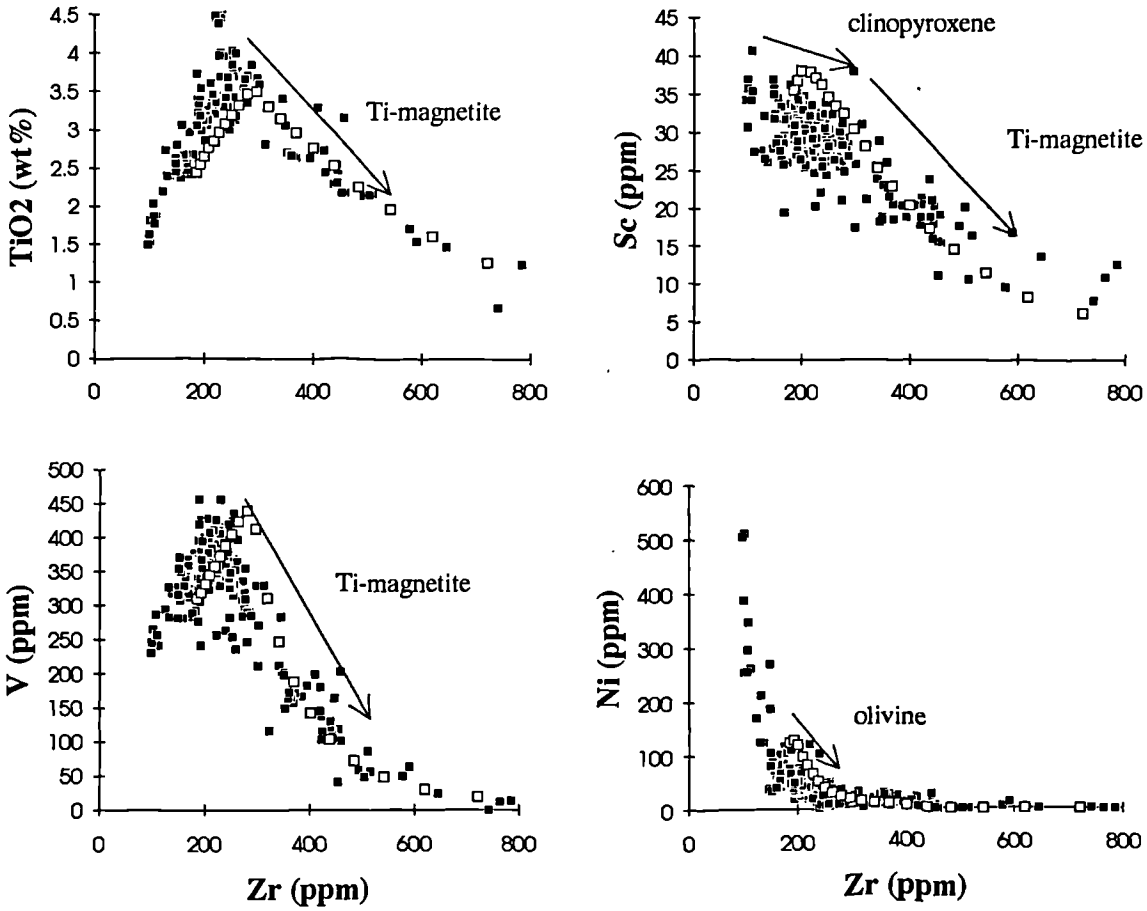

Figure 6.17 *Selected major and trace elements plotted against Zr (ppm) for the whole rock data. Open squares represent the liquid trend calculated by TRACE3 (Nielson, 1988) for sample 8 as a starting composition. Each increment on the modelled trend represents 4% crystallisation.*

mirrors the behaviour of TiO_2 suggesting that most V is in the oxidation states V^{4+} and V^{5+} in more oxidising conditions. TRACE3 predicts that before the onset of Ti-magnetite crystallisation, V will sharply increase. The whole rock data do not form a distinct trend, some samples appear to from a flatter trend suggesting that V has been buffered, perhaps by incorporation in clinopyroxene in more reducing conditions.

Whole rock data show an initial flat trend in Sc also corresponding to the removal of clinopyroxene. A steepening of this negative trend below 5wt% MgO coresponds to the removal of Ti-magnetite as well. Modelled liquid compositions match the whole rock data very well for CaO, showing a fall in CaO abundance throughout the range of compositions, reflecting the removal of both clinopyroxene and plagioclase.

The modelled trend for Ni shows a steeply curving trend which matches some of the whole rock data. Nevertheless, some of the whole rock data appear to lie along a straight line rather than a curved line suggesting that magma mixing may be involved in the petrogenesis of some of these rocks.

Using Zr as a differentiation index (Figure 6.17) avoids the initial increase in MgO, a problem inherent with having plagioclase modelled as the first crystallising mineral. The relatively good fit of modelled data to real data suggests that low pressure fractional crystallisation in a closed system can to a first approximation produce the *basalt* compositions observed at Eyjafjöll. Crystallising phases are olivine, clinopyroxene, plagioclase and Ti-magnetite. Minor discrepancies can be explained by variations in oxygen fugacity or crystallisation at pressures greater than 1 atmosphere.

Ankaramites are controlled by the high pressure crystallisation of olivine and clinopyroxene. This makes them unsuitable for modelling but does not discount the possibilty that they are parental compositions to the fractionating basalt sequence.

6.7.1.2 FRACTIONAL CRYSTALLISATION OF FELSIC ROCKS (MUGEARITE TO TRACHYTE).

Felsic rocks in Iceland have been described as either extreme differentiates (e.g. Carmichael, 1964; Wood, 1978; Sigurdsson and Sparks, 1981; Macdonald *et al.*, 1990; Furman *et al.*, 1992a) or as partial melts of hydrated, metamorphosed basaltic crust (O'Nions and Gronvold, 1973; Oskarsson *et al.*, 1982, 1985; Sigmarsson *et al.*, 1991). Extreme fractionates should show evidence of the removal of fractionating phases such as plagioclase, K-feldspar, apatite, Fe-oxides or zircon.

Highly incompatible element ratios should remain the same in felsic rocks as in basic rocks, any variation may be attributed to crustal contamination or extreme fractional crystallisation. Thy *et al.* (1990) discussed evidence that Iceland felsic rocks are formed by partially-melted, water-saturated, metamorphosed basalts. They concluded that the composition of experimentally-produced melts did not match the compositions of Icelandic felsic rocks. For example, experimental melts and liquids coexisting with hornblende tend to be peraluminous (e.g. Helz, 1978; Beard and

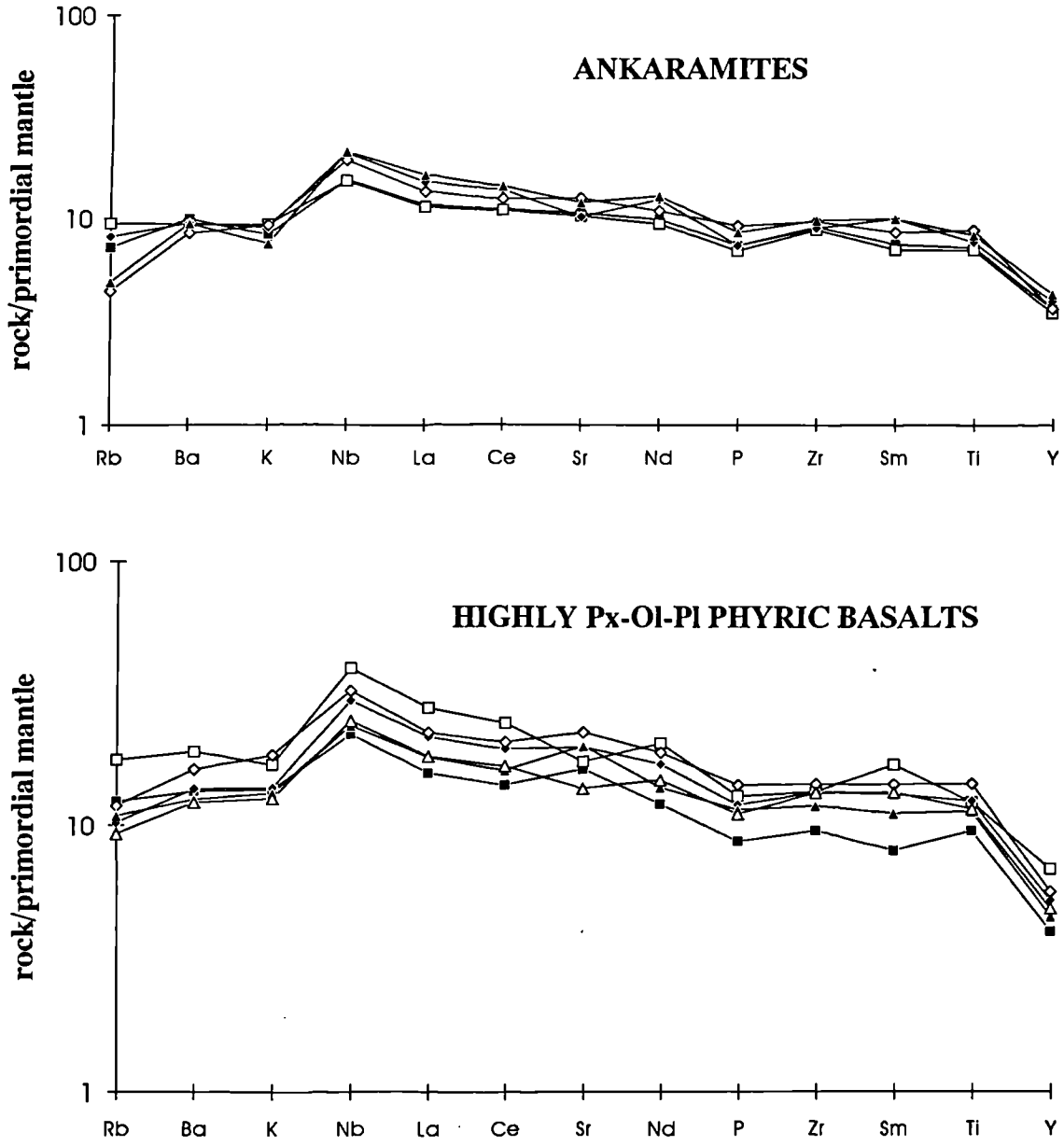

Figure 6.18 a) *Ankaramite data normalised to primordial mantle compositions (Sun & McDonough, 1989).* **b)** *Highly px-ol-pl phyric basalts normalised to primordial mantle compositions (Sun & McDonough, 1989) showing an increase in abundance of incompatible elements with degree of fractionation. Sr anomalies relate to a loss or addition of plagioclase.*

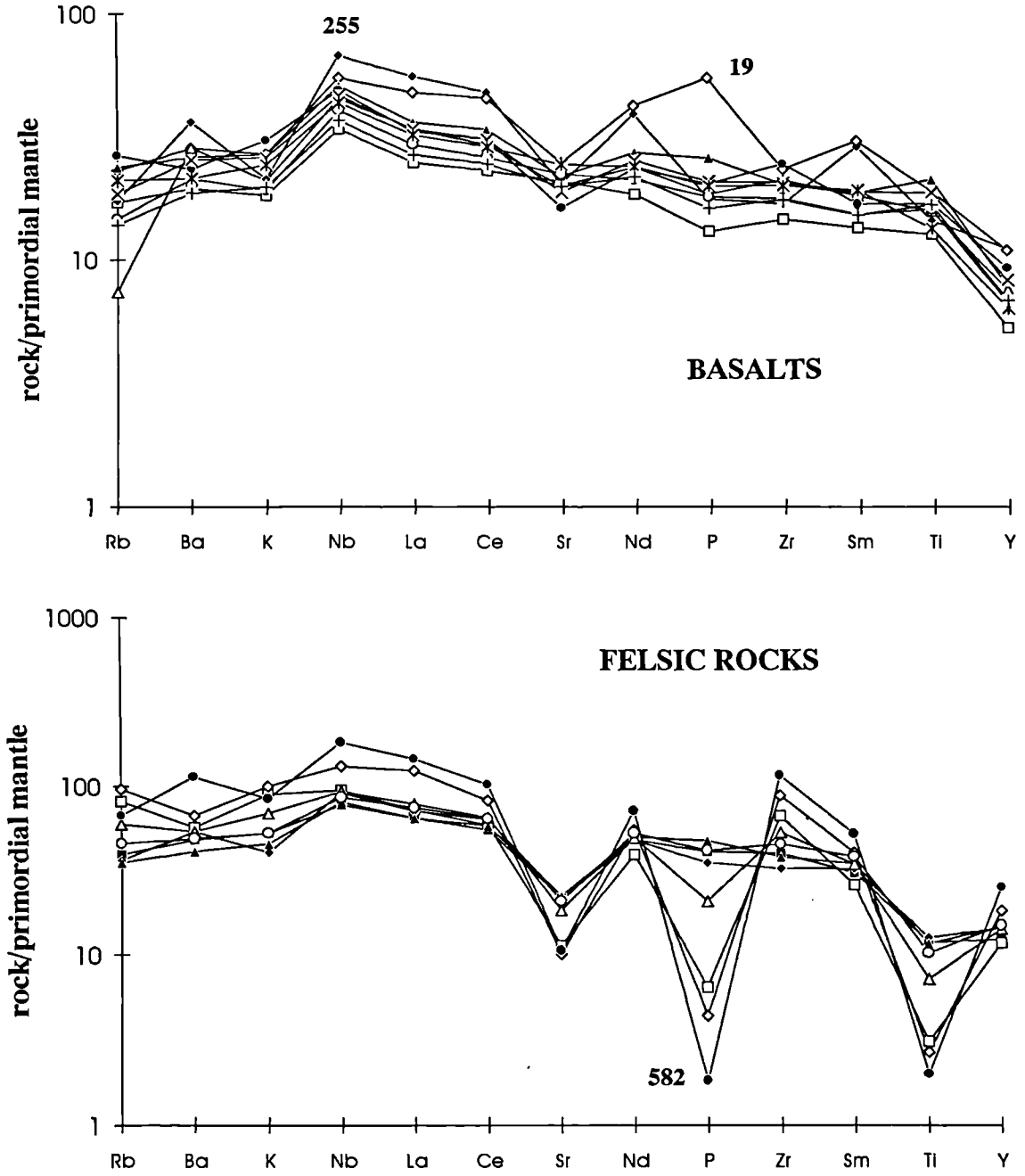

Figure 6.18 continued. **c)** *Basalts normalised to primordial mantle compositions (Sun & McDonough, 1989). Variation of Rb and Ba is caused by hydrothermal alteration. Sample 255 is a hawaiite, sample 19 is a hydrothermally altered dyke anomalously rich in* P_2O_5. **d)** *Felsic rocks (mugearites, benmoreite and trachytes) normalised to primordial mantle compositions (Sun & McDonough, 1989). All the felsic rocks show Sr troughs indicating the removal of plagioclase feldspar and Ti troughs indicating the removal of Ti-magnetite, the benmoreite and trachytes show P troughs indicating the removal of apatite.*

Lofgren, 1991; Holloway and Burnham, 1972) whereas many Icelandic felsic rocks are metaluminous. Another problem is the high K_2O of Iceland felsic rocks, which is not consistent with derivation from an amphibole-bearing source (Thy *et al.*, 1990).

TRACE cannot be used to model fractional crystallisation of evolved magmas since it does not take into account the crystallisation of apatite, K-feldspar and other minerals common in evolved rocks. However, using a mantle normalised multi-element diagram, crystallising phases in evolved rocks may be identified using the peaks and troughs of compatible elements on the diagram (Figure 6.18a-d). The mugearites (Figure 6.18d) show shallow Ti troughs and substantial Sr troughs representing the crystallisation of FeTi oxides (Ti-magnetite and ilmenite) and feldspar respectively. These troughs increase in size for more evolved compositions showing that substantial crystallisation of these phases has occurred. A marked P trough for benmoreite and trachyte compositions signifyies the crystallisation of apatite (Figure 6.18d). Zr remains incompatible throughout, showing that zircon is not a crystallising phase in any of the rocks.

This supplements previous evidence from REE patterns that fractional crystallisation is the main process in the formation of felsic rocks at Eyjafjöll. Crystallising phases include those observed in evolved rocks i.e. Ti-magnetite, ilmenite, apatite, plagioclase and K-feldspar.

6.7.2 MAGMA CHAMBER PROCESSES - MAGMA MIXING

Modelling suggests that closed-system fractional crystallisation under variable oxygen fugacity can explain much of the whole rock data. However, petrological and geochemical evidence suggests that replenishment of magma chambers has occurred, albeit infrequently.

6.7.2.1 REPLENISHMENT

Ankaramite lavas have been found above basalts in the stratigraphic sequence suggesting that primitive melts, from depth, were still being supplied to crustal levels until at least 600Ka (age of the Hvammsmuli ankaramite; Wiese, 1992). The Nupakotsdalur Group shows petrological evidence for replenishment of an evolving basaltic magma chamber by more primitive liquids e.g. the coexistence of skeletal primitive megacrysts and euhedral to resorbed, evolved phenocrysts (section 5.3.2.3).

Periodic replenishment may result in an increase in abundance of incompatible elements in the magma chamber (O'Hara and Mathews, 1981). Elements such as phosphorus which behave incompatibly prior to the crystallisation of, in this case, apatite may also be concentrated in the magma chamber, depending on the periodicity of replenishment. It is proposed that replenishment at Eyjafjöll was infrequent, evidence for this assumption includes the coexistence of skeletal, primitive megacrysts of clinopyroxene and euhedral to resorbed phenocrysts of clinopyroxene of more evolved

composition in basalts of the Nupakotsdalur Group. As described in section 5.3.2.3, the skeletal phenocrysts form during undercooling of the replenishing magma (Figure 6.20). The presence of evolved euhedral phenocrysts of plagioclase and pyroxene suggests that the magma chamber had fractionated to some degree prior to replenishment. In addition, the occurrence of lavas which have undergone extreme fractional crystallisation to acid compositions indicates prolonged periods when no replenishment occurred.

Replenishment may have included both primitive magmas from the base of the crust and more evolved magmas from interconnected crustal reservoirs. Furman *et al.* (1992a, 1992b) found abundant evidence at Austurhorn that rhyolite had intruded into basic magma chambers from below, indicating that there are evolving magma chambers at depth in the crust. Although there are no rhyolites at Eyjafjöll, the crustal structure may be similar to that at Austurhorn. In addition, to replenishment from below, high FeTi magmas from the Katla system may be fed laterally into the Eyjafjoll system. There is no evidence that the two systems are connected at depth, but they are certainly connected by surface fissures. The 1821-1823 eruption of Eyjafjoll was rapidly followed by an eruption of Katla suggesting that the magmatic systems are connected.

6.7.2.2 ZONED MAGMA CHAMBERS

There is abundant evidence in ultrabasic, basic and felsic rocks that magma mixing has occurred at Eyjafjöll. In particular, the occurrence of basic and intermediate inclusions in some trachytes suggests that basic, intermediate and felsic liquids were in close proximity prior to eruption. The simplest explanation for the close proximity of such magmas at Eyjafjöll is that they coexisted in a stable, density-stratified magma chamber, similar to that envisaged by Sigurdsson and Sparks (1980) for the Askja eruption of 1875.

Askja is not the only Icelandic central volcano which has been proposed to have a zoned magma chamber. Macdonald *et al.* (1990) proposed that a zoned magma chamber exists beneath the Torfajökull complex, in which rhyolite overlies parental transitional basalts. Einarsson (1950) described the products of the 1947-1948 eruption of Hekla, in which lavas and tephra become more mafic throughout an eruption, reflecting the compositional zoning in the magma chamber. Such compositional and thermal layering, in which cooler more evolved magmas overlie hotter, denser magmas may be achieved by various processes which are outlined below:

Experimental studies have shown that sidewall crystallisation may lead to the formation of a low density liquid which accumulates at the top of a magma chamber (Chen and Turner, 1980; McBirney, 1980). The liquid is depleted in heavy elements and forms a low density boundary layer which moves upwards to accumulate at the top of the chamber (Marshall and Sparks, 1984). As this layer grows, it develops compositional and thermal layering; convecting, double-diffusive layers may develop within it as heat from the hotter, deeper parts of the chamber is transported upwards

(Turner and Gustafson, 1981; Huppert *et al.*, 1982). This process can produce localised mixing and the formation of discrete, compositionally homogeous layers (Marshall and Sparks, 1984). Sparks *et al.*, (1984) proposed that convective separation of liquid from crystals is the dominant process of fractionation in magmas ('convective fractionation'), this process allows thermal and compositional layering to develop in both closed-system *and* replenished magma chambers. Heat loss from the sidewalls of a magma chamber is enhanced by hydrothermal systems and convection within the chamber.

If extensive plagioclase fractionation precedes Ti-magnetite fractionation, iron enrichment of the residual liquids occurs (Cattell, 1989). FeTi basaltic liquids are dense (Stolper and Walker, 1980) and collect at the base of a magma chamber. If the chamber is replenished by a primitive melt (>5% MgO), the primitive basalt may actually be less dense than the FeTi basalt and the two magmas will mix. Heating of the lower parts of the chamber may alter the overall stratification of the magma chamber by producing further double diffusive layers (Huppert *et al.*, 1982). Replenishment of the magma chamber from below by a denser, more primitive melt causes temporary layering as the primitive basalt cools and undergoes fractional crystallisation (Huppert and Sparks, 1980). As the magma approaches the same density as the overlying magma, mixing can occur.

6.7.2.3 MIXING ACID AND BASIC MAGMAS

Kouchi and Sunagawa (1983) showed that when a basalt and a dacite liquid were mixed by forced convection at constant temperatures, blobs of basalt magma were incorporated in the dacite and also, a small amount of hybrid andesite was formed. Incorporation of mafic inclusions in evolved host magmas during convective mixing was also proposed by Huppert *et al.* (1982, 1984). Thermal equilibration between an acid host and mafic inclusion is rapid (Sparks *et al.*, 1977), this is indicated by the groundmass of inclusions which may be glassy, or dominated by acicular and skeletal crystals (e.g vesicular inclusions in the Kolbeinsskard trachyte - section 5.3.4.2).

Evolved magmas such as trachytes and rhyolites may be erupted during a build up of silicic, volatile-rich magma at the top of a magma chamber. Inclusion-free trachyte lavas near the summit of Eyjafjöll may have formed this way. Trachytes which contain inclusions occur at some distance from the centre of the volcano. These lavas may have erupted as a result of a decrease in viscosity caused by mixing with basic magma. Such a process may be occurring at Torfajökull (Macdonald *et al.*, 1990) where tholeiitic injections trigger rhyolite eruptions.

Figure 6.19 shows all the Eyjafjöll whole rock data plotted on a silca versus total iron diagram. Samples 578B and 578M are mixed samples from the Laugara trachyte. These plot on a mixing line that connects the trachyte with the high Fe intermediate rocks of the Seljavellir Group. This suggests that liquids of these compositions may have co-existed in a magma chamber.

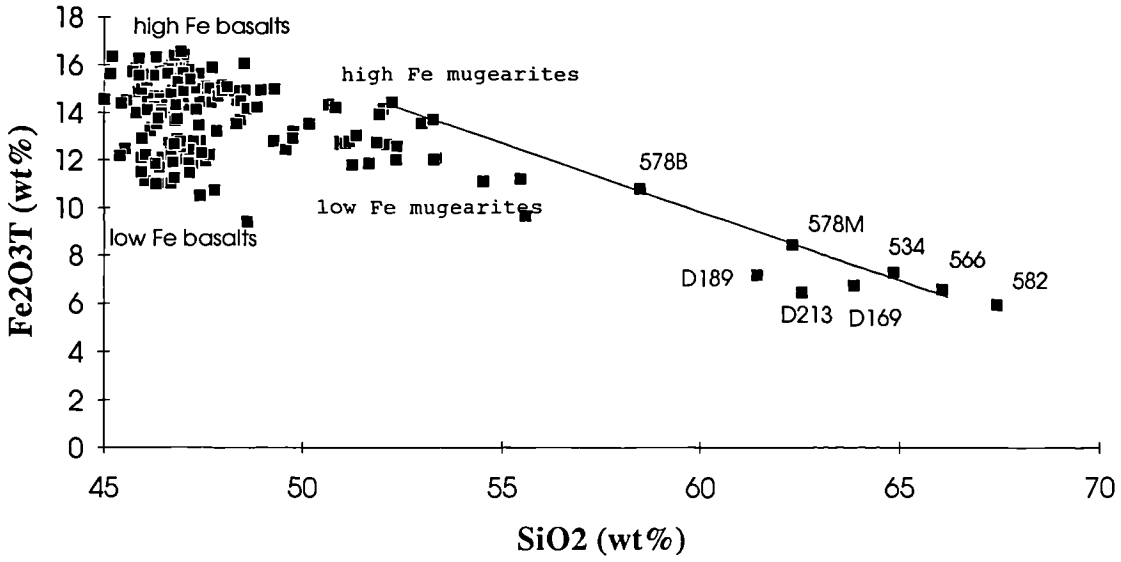

Figure 6.19 *Plot of Fe_2O_3T versus SiO_2 for all the whole rock compositions. A mixing line joining 578M and 578B, mixed samples from the Laugara trachyte, appears to extend towards the high Fe mugearites.*

6.7.2.4 MIXING BETWEEN BASALTS, HAWAIITES AND MUGEARITES

Low Fe hawaiites and mugearites of the Seljavellir Group contain abundant zoned calcic plagioclase and resorbed sodic plagioclase phenocrysts (section 5.3.3). They also contain a substantial range of forsteritic olivine compositions and heterogeneous groundmass textures. In contrast, the high Fe hawaiites and mugearites contain small, euhedral microphenocrysts of plagioclase with only sparse zoned microphenocrysts (other members of the high Fe_2O_3 series are likewise poor in phenocrysts). This suggests that the low Fe hawaiites have undergone mixing with primitive, low Fe basalts which contain such primitive plagioclase and olivine phenocrysts (Figure 6.19).

6.7.2.5 MIXING INVOLVING ANKARAMITES OR OTHER PRIMITIVE MAGMAS

The compositions of these lavas are controlled by a combination of accumulation of phenocrysts, fractional crystallisation and mixing. These processes occur at depth and the magma may escape straight to the surface, undergoing minimal further

differentiation, or may become trapped in crustal magma chambers. The dense primitive replenishing magma would collect at the base of the chamber until it had cooled and differentiated sufficiently to mix with overlying basalts. This is the process by which the Nupakotsdalur Group and other highly px-ol-pl phyric lavas probably formed (Figure 6.20). The occurrence of rare, resorbed alkali feldspar in some of these lavas suggests that they formed in compositionally zoned magma chambers.

The lack of ankaramite in the upper parts of the stratigraphic sequence may be a result of decreasing magma supply from the base of the crust, or they may be blocked by cooling, crystallising magma chambers.

The close association of some ankaramites and px-ol-pl phyric basalts (e.g. Nupakotsdalur Group) may be explained by partial mixing in the magma chamber (Figure 6.20). An evolving, crystallising magma chamber is replenished by ankaramitic magma. This causes convection and ultimately some mixing, however some of the dense ankaramite may remain at the bottom of the magma chamber. An eruption may begin with porphyritic basalts containing evolved xenoliths from the magma chamber walls; later stages or more distal parts of a fissure system may be characterised by ankaramites from the base of the magma chamber (e.g. the Nupakotsdalur Group). Convection must be sufficient to keep the phenocrysts suspended in the magma prior to eruption.

6.7.2.6 DENSITY MAXIMA

If extensive crystallisation of plagioclase takes place before the onset of FeTi oxide crystallisation i.e. under conditions of low fO_2, low density components are removed from the magma (Cattell, 1989). The residual iron-rich magma is then so dense that it tends to remain ponded at the base of magma chambers (Sparks and Huppert, 1984). Compositional gaps in basalt-hawaiite series often correspond to the composition of these dense liquids. Iron enrichment caused by extensive early crystallisation of plagioclase has been invoked to explain compositional gaps in the basalt-hawaiite fractionation series at Skye and elsewhere (Cattell, 1989).

Cumulate assemblages in magma chambers where FeTi oxide crystallisation is important might be expected to contain great abundances of FeTi oxides. Most gabbroic xenoliths found at Eyjafjöll are plagioclase and clinopyroxene dominated and are assumed to be from the upper parts of magma chambers. However, sample N2, a laminated cumulate xenolith from Nupakotsdalur may be an exception. It contains a particularly large abundance of Fe oxides, suggesting that it may have formed at lower levels in a magma chamber. Highly porphyritic basalts from the upper flanks of the volcano have been found to contain large, subhedral FeTi oxides intergrown with skeletal clinopyroxene megacrysts. Such aggregates of dense minerals would normally sink to the base of a magma providing an effective means of crystal - liquid separation but the viscosity of highly phyric magmas may keep them in suspension.

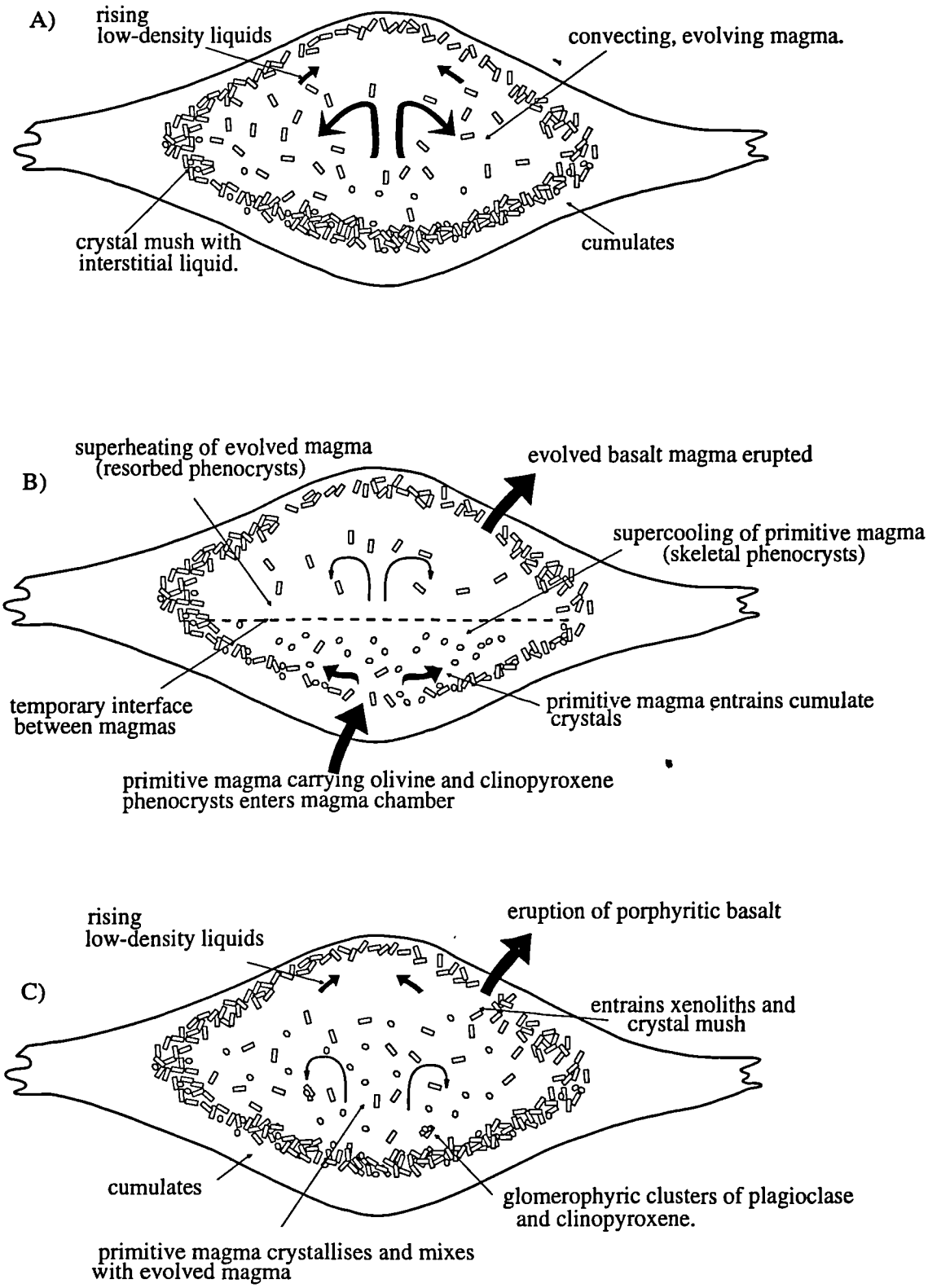

Figure 6.20. *A magma chamber model representing three stages in the evolution of the highly porphyritic basalts of the Nupakotsdalur Group.*

A) An evolving basaltic magma chamber undergoing differentiation.

B) Chamber is replenished by ankaramitic magma which fractionates at base of chamber.

C)Mixing of the two magmas occurs prior to eruption.

6.8 CRUSTAL ASSIMILATION

Fractional crystallisation combined with magma mixing in open-system magma chambers of variable oxygen fugacity generally explains most of the data acquired from Eyjafjöll. There are however a small number of exceptions. These include samples with anomalously high P_2O_5 (404. 406 and 19) and samples with high abundances of incompatible elements in general (e.g 82, 27, 255, 307).

There may be several explanations for the high abundance of P_2O_5 in samples 404, 406 and 19 (e.g. Figure 6.21). None of the samples contain apatite phenocrysts, but all contain apatite needles (<0.15mm) in the groundmass and intersertal glass. The heavily altered nature of sample 19 means it will not be discussed further.

The Drangshlid basalts (404 and 406) do not appear to have accumulated apatite, and yet the abundance of P_2O_5 is exceptionally high (1.18-1.35 wt%). Green and Watson (1982) found that the solubility of apatite depends on temperature and SiO_2 content. These lavas contain 47 wt% SiO_2, which is higher than the range that Watson (1979) found to be typical of lavas with high P_2O_5 (SiO_2 = 40-45 wt%). The Drangshlid basalts contain particularly high concentrations of TiO_2 (~4.0 wt%) and unusually high Zr (~255 ppm). Another distinctive feature of the Drangshlid basalts is that they are slightly MREE enriched (Figure 6.8). Mineral phases which have high partition coefficients for HREE include apatite (Watson and Green, 1981) and hornblende (Rollinson, 1992). Hornblende has not been identified in the basalts. It is possible that repeated replenishment of a magma chamber enriched the residual liquid in Ti-magnetite and apatite compatible elements, this process would also increase the concentration of Zr and other incompatible elements.

An alternative explanation is that these basalts incorporated a small degree of crustal melt on its way to the surface as envisaged by Oskarsson *et al.* (1981). They propose that after an initial fractionation event in which hydrated amphibolite loses a silicic melt, a second fractionation event melts kaersutitic amphibole and apatite leaving residual olivine and clinopyroxene. The resulting magma is rich in titanium, iron, phosphorus, zirconium and fluorine. LREE enrichment is also expected due to the retention of HREE in clinopyroxene. Addition of such a melt to a transitional alkali basalt magma could explain all the chemical characteristics of the Drangshlid basalts.

Lambafell basalts and the Seljavellir mugearites also fall away from the fractionation trend on Figure 6.22, but no apatite is evident in these samples. Their overall abundance of P_2O_5 is much less than basalts at Drangshlid.

Lambafell is a monogenetic eruption site, yet P_2O_5 and La contents of the samples show a positive correlation over a substantial range (La 36-45ppm) and K_2O abundance is also high (0.92 - 1.06).

There are three processes which may generate such a geochemical signature:

1) Low SiO_2 caused by Fe_2O_3T enrichment has increased the solubility of apatite. The solubility of apatite is dependent on SiO_2 content (Watson, 1979). The Lambafell basalts evolved under low fO_2 so SiO_2 has remained roughly constant during differentiation. This *relatively* low SiO_2 may have increased the solubility of apatite. However, this does not explain the high K_2O.

2) Contamination by hydrothermal fluids, assimilation of crustal melts or diffusion of K from an acid magma, has increased the solubility of apatite. Green and Watson (1982) found that K-rich basalts begin to crystallise apatite at higher P_2O_5 concentrations than low-K basalts of similar SiO_2 and MgO. An alternative scenario is that the Lambafell magmas assimilated some K at depth and that this affected the crystallisation history of the magmas. Experiments have shown that when liquid basalt and rhyolite come into contact, K diffuses rapidly into the basalt (Watson, 1982; Watson and Jurewicz, 1984). Hydrothermal fluids rich in K may provide another means of contaminating a crustal magma. Furman *et al.* (1992) concluded that melting of a hydrated transitional tholeiitic basalt might produce positively correlated abundances of La, Zr and P_2O_5 since apatite

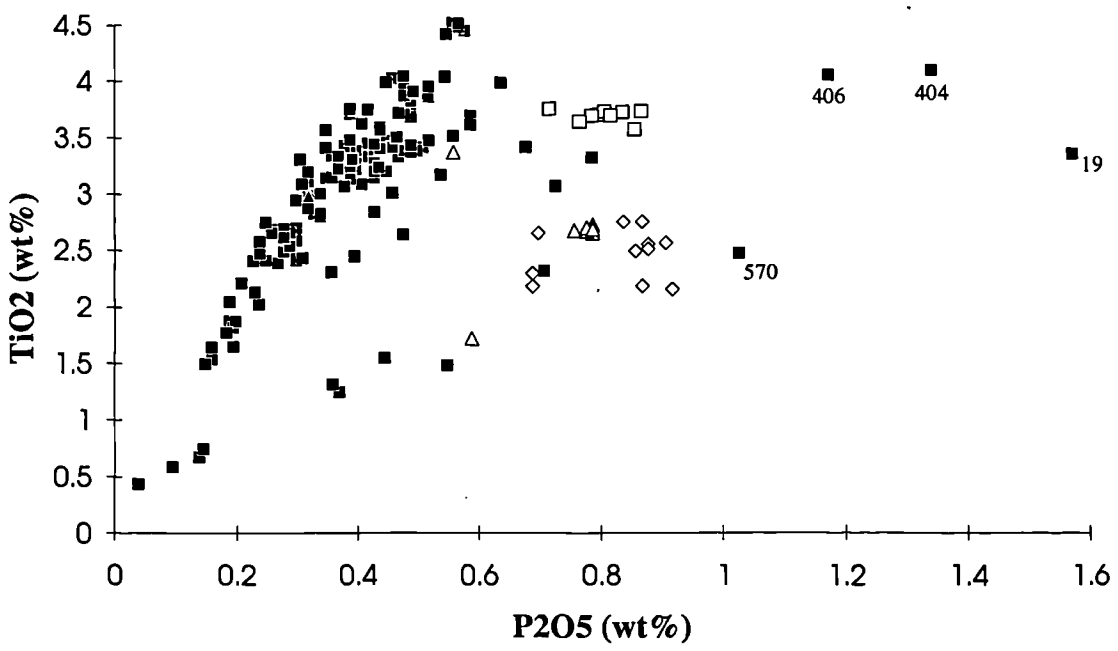

Figure 6.21 *TiO_2 plotted versus P_2O_5 for all the whole rock data. The open squares represent the Lambafell basalts (including sample 82), the open triangles represent basalts, hawaiites and mugearites from the western slopes of Eyjafjoll, the open diamonds represent members of the Seljavellir Group. Sample 570 is a hawaiite from Fimmvorduhals Pass, samples 404 and 406 are from Drangshlid and sample 19 is a dyke from the Laugara gorge.*

and zircon are not reported in any Tertiary basalts. It seems possible that the Lambafell basalts may have incorporated some partial melt which was high in K_2O, La, P_2O_5. However, since the Lambafell basalts evolved under low fO_2 conditions and such conditions can be initiated by contamination by fluids or partial melts, this seems to be a likely scenario.

3) Repeated replenishment of the magma chamber increases the abundances of incompatible elements such as K, Zr, La and P.

This process is also possible, the only factor against it being that all the lavas might be expected to be enriched in these elements when in fact these elements show variation and positive correlation with eachother, even in the small Lambafell eruption ($1km^3$).

6.9 PETROGENESIS - MANTLE MELTING PROCESSES

6.9.1 MODELLING MANTLE MELTING

Interpreting the mantle melting history of highly fractionated basalts such as those at Eyjafjöll is fraught with problems. None of the samples represents a primitive mantle melt therefore there is a very real danger that geochemical signatures reflect fractional crystallisation processes rather than partial melting processes. Nevertheless, some modelling was attempted to see if any source characteristics could be deduced. The equation for equilibrium (batch) melting (Cox *et al.*, 1979) was used:

$$C_l/C_0 = 1/(D_0 + F(1-P))$$

where:

C_l = concentration of element in melt

C_0 = concentration of element in source

D_0 = bulk partition coefficient for element with respect to source

P = bulk partition coefficient for phase proportions entering melt

F = degree of partial melting

Using the source and distribution coefficients of Kostopoulos and James (1992), (Appendix 3) the compositions of partial melts from a depleted source (DMM) and an enriched source (BSE) were calculated. Melting was calculated in the garnet and spinel lherzolite stability fields, a 50:50 mixture of garnet and spinel lherzolite was also calculated. Figure 6.22 shows the REE patterns expected from melting an enriched source at different depths and to different degrees. The flattest trends are produced by high degrees of melting of a spinel lherzolite, whereas the steepest patterns are produced by small degrees of melting of a garnet lherzolite. Figure 6.23 shows the incremental melting paths of the two source compositions under such conditions. The Eyjafjoll ankaramites and basalts are plotted onto this diagram.

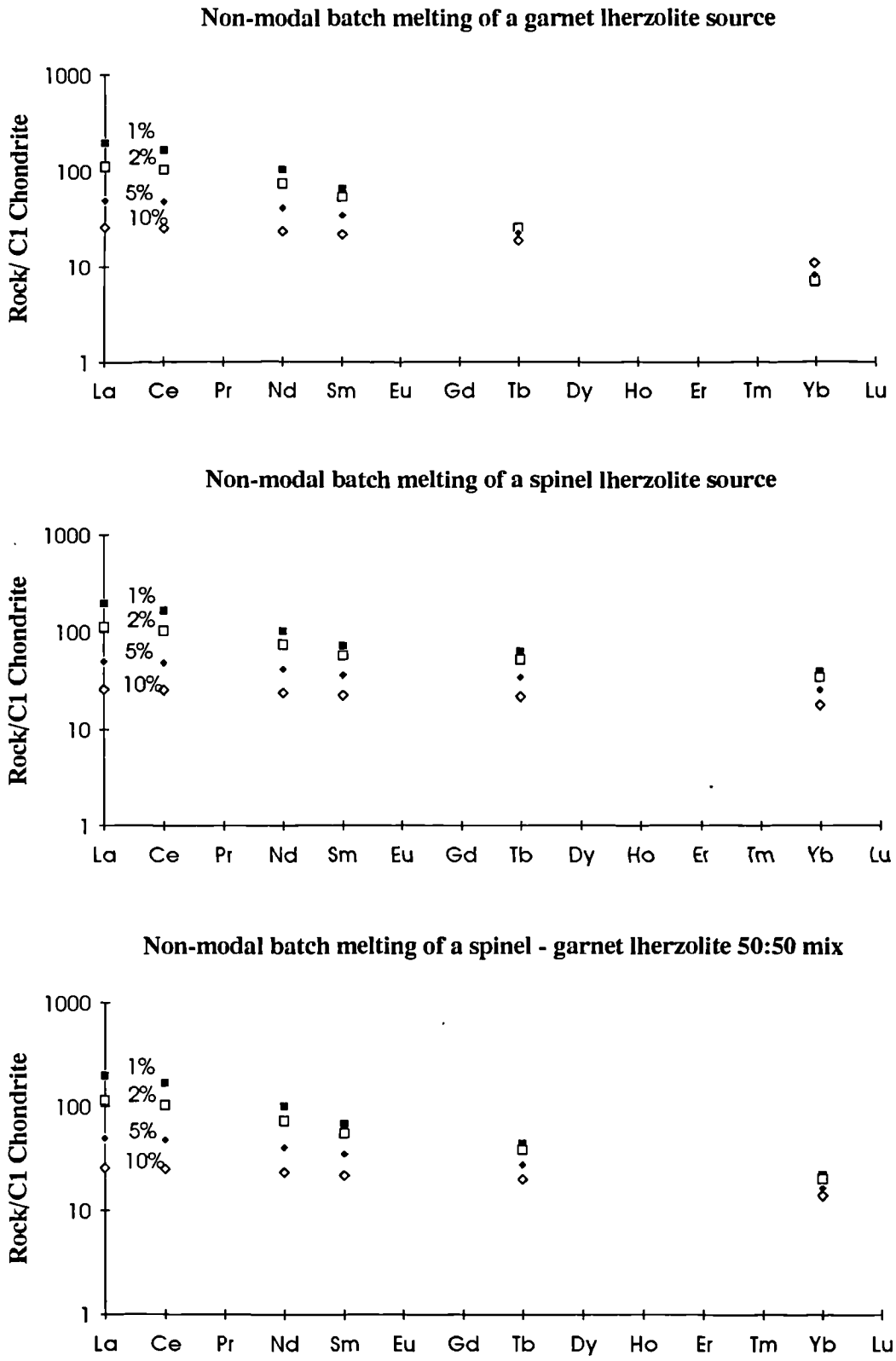

Figure 6.22 a) *Modelling the non-modal batch melting of an enriched garnet lherzolite source (BSE, James and Kostopoulos, 1992), small degrees of melting produce steep REE patterns with Yb retained in the source.* **b)** *Modelling the non-modal batch melting of an enriched spinel lherzolite source producing relatively flat REE patterns.* **c)** *Modelling a 50:50 mix of a spinel and garnet lherzolite source produces moderately LREE enriched trends.*

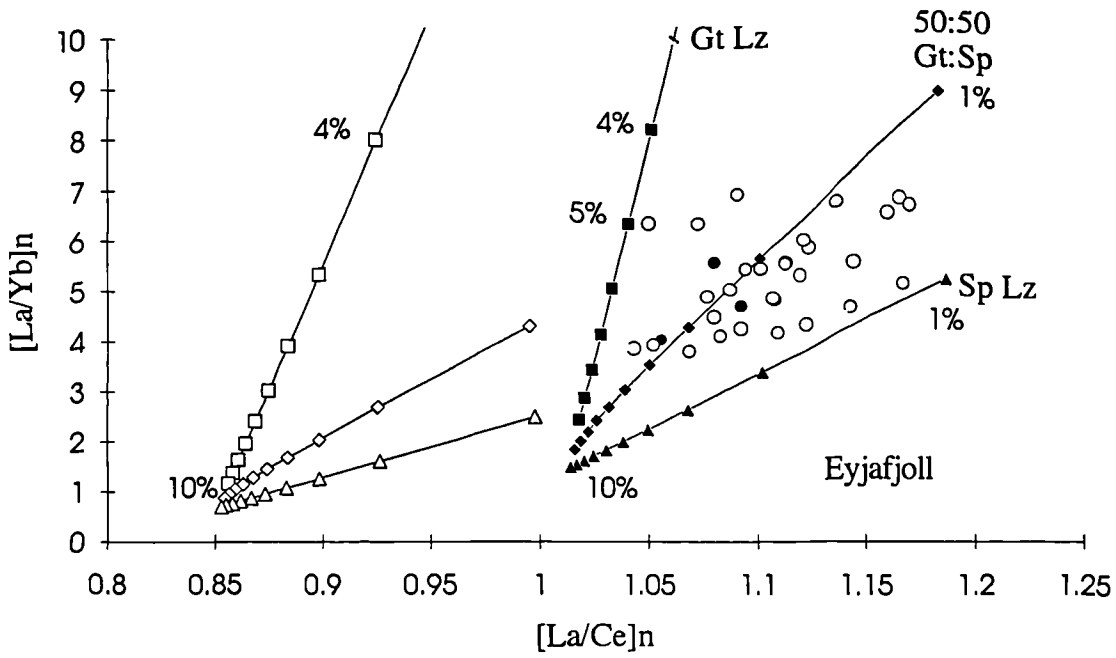

Figure 6.23 *La/Yb plotted versus La/Ce. Open symbols represent the partial melting of a depleted mantle source (DMM, James and Kostopoulos, 1992) and filled symbols represent melting of an enriched mantle source (BSE, James and Kostopoulos, 1992). Each increment on the modelled melting trends represents 1% melting. Most of the Eyjafjoll data (open circles) plot between 1 and 4% melting of an enriched mantle source near the garnet-spinel transition zone.*

The majority of samples plot on or just below the melting path of an enriched source near the spinel-garnet transition zone. The degree of melting is less than 4%. Meyer *et al.* (1985) predicted that melting in this area would be less than the 6% (as they calculated for the Vestmannaeyjar) and that it would occur near the spinel-garnet lherzolite transition. The degree of melting represents a point depth average so the real depths may extend to slightly higher degrees. Those samples which plot closer to a garnet lherzolite stability field include 82 (Lambafell) and 406 (Drangshlid). As predicted in section 6.5.1 these lavas were generated from small degree melts at depth. They have since undergone high degrees of fractional crystallisation in crustal magma chambers.

6.10 DISCUSSION - MAGMATIC EVOLUTION OF THE EYJAFJOLL VOLCANIC SYSTEM

Fractional crystallisation at variable depths and under different oxygen fugacities is the dominant differentiation process of Eyjafjöll magmas. The fractionating minerals are observed as phenocrysts in the lavas and in gabbroic xenoliths and crystal aggregates.

6.10.1 ANKARAMITES- PARENTAL MAGMAS?

There are no primitive aphyric basalts at Eyjafjöll with above 6.9 wt% MgO, suggesting that basalts are subjected to high degrees of differentiation before their eruption. Ankaramites provide the only possible parental material and yet trace element data suggests that they may have been generated in different mantle melting events to most of the basalts.

Ankaramites contain phenocrysts of olivine and clinopyroxene, the chemistry of which shows evidence for crystallisation at some depth (~10kbars). Plagioclase and Ti-magnetite crystallisation were inhibited and are generally only groundmass phases indicating that the ankaramites travelled rapidly to the surface. Ankaramites appear to be a feature of the older successions (>400,000 years), more recent successions contain highly px-ol-pl phyric basalts, but no true ankaramites. The ankaramites often occur in close association with porphyritic basalts (e.g. the Nupakotsdalur Group). The true ankaramites of the Nupakotsdalur Group outcrop at the furthest point from the centre of the volcano whereas the porphyritic basalts occur in abundance right into the volcano's core. The Hvammsmuli ankaramite and Arnarklettur ankaramite also occur at the periphery of the volcano. There is some suggestion that ankaramites ponded at the base of magma chambers in Hawaii are erupted at the distal end of fissures whilst overlying basalts are erupted along the main part of the fissure (Garcia pers. comm.). This does not appear to be the case at Eyjafjöll since outcrops such as the ankaramite of the Grettishaf Group, could not be described as peripheral, although they do occur at some distance from the centre of the volcano. There may be ankaramites buried in the lava pile that erupted close to the centre of the volcano.

The ankaramites do not contain ultramafic olivine-rich xenoliths as might be expected during rapid ascent from deep magma chambers. However, strain-banded olivines are all subhedral and have a very consistent composition of Fo_{84} suggesting that perhaps they equilibrated in a cumulate pile. They may be cumulate crystals entrained by the ankaramite from a magma chamber near, or at, the base of the crust. Euhedral olivines include the most primitive and the most evolved phenocrysts in the Eyjafjöll ankaramites (Fo_{81-90}). The most primitive olivines reflect crystallisation from a primitive mantle melt. They are not strain-zoned suggesting that their crystallisation history is different to that of the subhedral olivines. Ankaramite is by definition highly porphyritic with high modal olivine, it is therefore relatively viscous (Murase and

McBirney, 1973). Such a magma might be expected to retain phenocrysts and perhaps some xenoliths (Rudek *et al.*, 1992).

There is no great heterogeneity of incompatible trace element ratios in the Eyjafjoll data as a whole, suggesting that the mantle source composition is broadly similar for all the samples. However, degree and depth of melting appear to be the factors causing small degrees of variation, particularly in $[Ce/Yb]_n$.

Trace element ratios for ankaramites are consistently slightly different than those in most of the basalts (e.g. Figure 6.24). They have lower $[Ce/Yb]_n$, Zr/Y and Rb/Th and high Ba/La. This may reflect a relatively shallow mantle source for the ankaramites, or slightly higher degrees of melting. The ankaramites may then represent instantaneous shallow level melts, as envisaged by Elliot *et al.* (1991). The Asolfsskalaegg Group (erupted 129±20Ka, Wiese, 1992), which consists of highly px-ol-pl phyric basalts, may represent ankaramites which have fractionated under low pressures at low fO_2, since they have high Fe_2O_3T and high Zr (Figures 6.10 and 6.24). They are anomalous and may represent a rare occurrence of such high Fe magma reaching the surface. This suggests that ankaramites have become trapped within the crust and fractionated to some degree; samples 503 and 490 may also represent the fractionates of ankaramite.

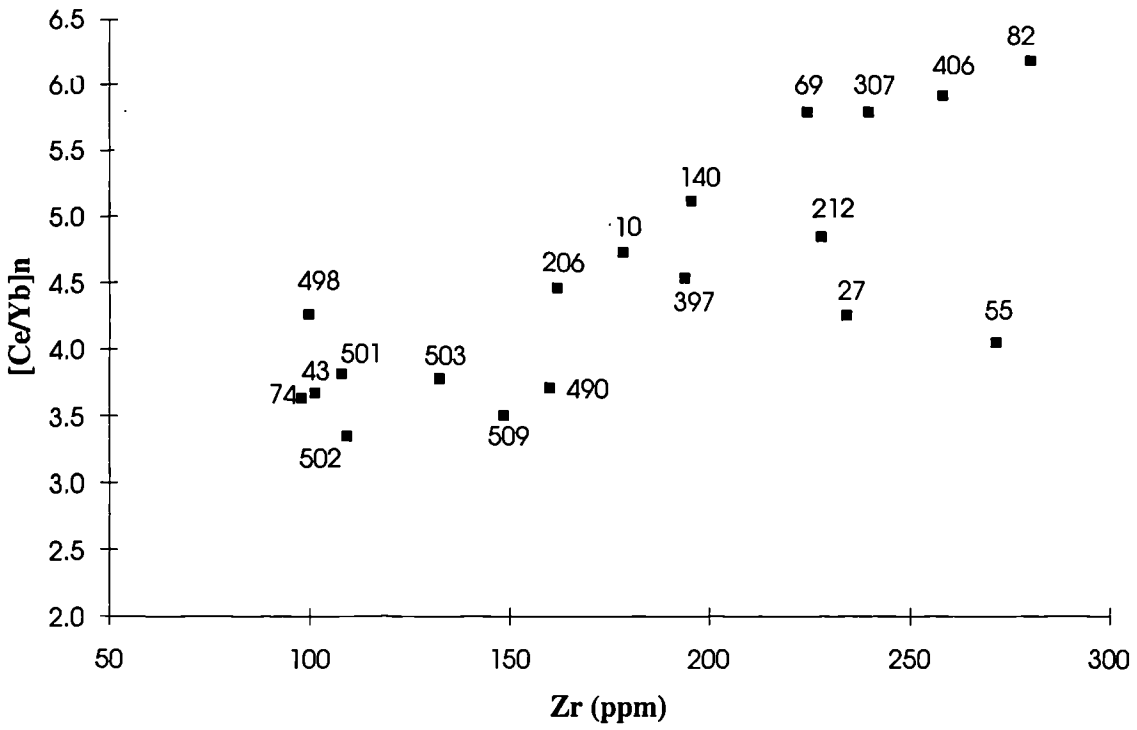

Figure 6.24 *Plot of Ce/Yb normalised to chondrite C1 (Sun and McDonough, 1989) versus Zr, showing the high degree of differentiation of the high FeTi, high Ce/Yb basalts.*

Primitive melts supplied to crust/mantle boundary have a variety of geochemical signatures reflecting melting at different depths and to different degrees. The ankaramites sampled at the surface may have characteristics which mean they are preferentially sampled from the crust-mantle boundary (e.g. low Fe). Elliot *et al.* (1991) proposed that mantle melts of higher Fe content (melts from deeper in the melting column) may become ponded below low Fe mantle melts in subcrustal magma chambers. The two would only mix when the high Fe melt had undergone a substantial degree of olivine fractionation (Sparks *et al.*, 1980). Therefore, Fe-rich parental magmas from deeper in the melting column must undergo more olivine fractionation than low Fe-melts from higher in the melting column before they are erupted. A similar process may have occurred beneath Eyjafjoll.

It is proposed that the ankaramites represent primitive, relatively low Fe magmas which segregate from shallow parts of the melting column. Such magmas crystallise olivine and clinopyroxene until they are buoyant enough to rise. Ankaramites represent a low Fe endmember in a spectrum of parental melts which contribute to the Eyjafjoll system (Figure 6.24).

Ankaramites may reach the surface directly, or they may be trapped in crustal magma chambers where they may to fractionate towards Fe-rich compositions in magma chambers of low oxygen fugacity. Such dense liquids are rarely erupted, the Asolfsskalaegg Group being an exception.

Most of the Eyjafjöll basalts have fractionated from mantle melts which have mixed throughout the melting column. The high FeTi, high $[Ce/Yb]_n$ basalts to the south and east of the volcano may have fractionated from relatively high Fe mantle melts. This may explain why they are so highly evolved (Figure 6.24).

6.10.2 MAGMATIC PLUMBING

Using seismic methods, magma chambers have been detected beneath the central volcanoes of Krafla, Askja and Katla (Brandsdottir *et al.*, 1994; Gudmundsson *et al.*, 1994). Each chamber appears to reside at the level for buoyant equilibrium of basaltic melt in a basaltic crust i.e. 1.5km below sea level (Brandsdottir, 1994: Gudmundsson *et al.*, 1994). The chambers were found to be circular in plan view, correlating closely with observed seismic activity. The Katla magma chamber is up to 5km across and roughly 1km thick, it therefore contains at least $5km^2$ of melt. Eyjafjöll has a small collapse caldera with a diameter just over 3km signifying the presence of a shallow crustal magma chamber. The central magma chamber at Eyjafjöll is probably smaller than the chamber beneath Katla, a closer analogue may be the Austurhorn intrusion in southeast Iceland (Furman et al., 1992a, 1992b). The gabbro body exposed at Austurhorn shows modal layering of plagioclase and clinopyroxene which is apparently rhythmic and varies from sub-horizontal to subvertical.

Furman *et al.* (1992b) and Walker (1963) have proposed that central volcanoes are fed by a central magma chamber and a series of smaller, deeper magma chambers (cedar tree model - Walker, 1963). At Austurhorn, in particular, there is abundant field evidence that evolved felsic magmas were intruded into the central solidifying magma chamber *from below*. This suggests that the felsic magmas evolved at depth.

The presence of a large, shallow central magma chamber at Eyjafjöll is beyond doubt. The acid eruption of 1821 to 1823 at the crater rim provides evidence that this chamber has evolved to acid compositions. Radial dykes have erupted porphyritic basalts, hawaiites and mugearites over the upper flanks of the volcano. This reflects the radial magmatic stress in the upper parts of the shallow crust which is sufficient to exceed the regional stress.

The existence of several liquid lines of descent and the concurrent eruption of lavas of distinctly different compositions suggests that batches of magma are evolving in different magma chambers. Evidence of mixing suggests that these chambers are connected. Magma chambers have different oxygen fugacities, resulting in differing degrees of Fe enrichment in the basalts.

In summary, the Eyjafjöll volcano has a large, shallow central magma chamber which has evolved to trachyte compositions. There may also be deeper magma chambers which have evolved to trachyte composition and lie at moderate depths, especially beneath the south side of the volcano. There may be numerous smaller pockets of magma in the crust as envisaged by Walker, 1963 and Furman *et al.*, 1992b). Ankaramites reached the surface direct from the base of the crust during the early stages of the volcano's growth.

6.10.3 TEMPORAL EVOLUTION

Early stages in the evolution of the volcano were characterised by relatively primitive basalts and ankaramites, FeTi rich basalts and low FeTi evolved basalts. The high FeTi basalts and the low FeTi basalts were produced contemporaneously from different magma chambers. The earliest lavas may have been produced from an early fissure system which developed prior to the development of the central volcano, as suggested by Walker, (1963). The earliest basalts (Laugara Group) contain gabbroic xenoliths which suggest they were derived from a well-established magma chamber.

Throughout the evolution of Eyjafjöll, the lavas have always been porphyritic, reflecting long time periods between magma chamber replenishment, even during the initial stages of the volcano's evolution. This enables magma to fractionate to more evolved compositions between replenishments and allows magma chambers to develop stable density and compositional stratification. The lavas of Eyjafjoll generally became more evolved as a result of this irregular and apparently waning replenishment.

The rhythmic layering described by Furman *et al.* (1992b) in the Austurhorn gabbro may have formed by sedimentation in a convecting magma chamber as described

by Sparks *et al.* (1993). They propose that as a magma chamber cools, the concentration of crystals increases, when it reaches a critical value an interface develops between a convecting crystal-free upper layer and a crystal-rich lower layer. A discrete sedimentation event occurs from the lower layer, the upper layer convects, cools and begins to crystallise, so the process begins again. Each mineral reaches its critical value at a different time so the proportions of different minerals in the convecting liquid changes throughout the process. This process may have occurred at Eyjafjöll, it can explain the widely varying phenocryst proportions and phenocryst abundancies found in the lavas throughout the evolution of the volcano.

6.11 SUMMARY

- Differentiation of basalts to hawaiites at the Eyjafjöll volcanic system was controlled by the fractional crystallisation of olivine, clinopyroxene, plagioclase, Ti-magnetite and ilmenite. Benmoreite and trachyte are generated from parental transitional alkali to mildly alkali basalt by the fractional crystallisation of plagioclase, clinopyroxene, olivine, Ti-magnetite, apatite and K-feldspar.

- Fractional crystallisation occured at pressures above 1 atmosphere. Recent evidence suggests that a major magma chamber may lie at a depth of 1.5km below sealevel (Gudmundsson, 1994). However, some samples lie close to 3.5kbars on the normative plot, suggesting depths of up to 10km. Ankaramites underwent fractional crystallisation of chrome spinel, olivine and clinopyroxene at about 10kbars.

- Magma is supplied in discrete batches of several lavas of very similar chemistry. However, each consecutive batch may lie on different liquid lines of descent, suggesting that magma is supplied from discrete pockets of magma or magma chambers in the crust.

- Each magma batch may have a evolved under different oxygen fugacities causing differing degrees of Fe enrichment at similar stages of differentiation.

- Mixing has occurred between basalts at different stages in the differentition process. This was probably triggered by replenishment events and suggests that crustal magma chambers and pockets of magma were interconnected.

- Variations in incompatible trace element ratios are small, suggesting that all the rock types sampled at Eyjafjoll are generated from a similar parental composition.

- REE patterns and modelling suggest that most melting occured in the spinel lherzolite stability field, with small amounts of garnet present. The degree of mantle melting appears to only reach 4%. This is a point and depth average so may be slightly higher. Lambafell, Drangshlid and the Skogaheidi high FeTi lavas appear to have generated at greater depths closer to the garnet lherzolite stability field.

- The depth and overall small degree of melting is primarily caused by the thickness of the crust beneath the EVZ.

- Ankaramites have low $[Ce/Yb]_n$ and other trace element ratios suggesting that they are generated from different mantle melting events to most of the basalts, perhaps at shallower depths and to higher degrees.

- Some of the high FeTi, high $[Ce/Yb]_n$ basalts outcropping at the periphery of the volcano show evidence of enrichment in incompatible elements. They may have assimilated partial melts from the crust. Such basalts are highly differentiated, possibly because they were generated from Fe-rich parental melts, so they may have spent extensive periods of time fractionating in lower crustal magma chambers.

- Most basalts appear to have fractionated from parental basalts with moderate $[Ce/Yb]_n$ which may represent mixing of the parental magmas of the ankaramites and the high FeTi basalts in the melting column and subcrustal magma chambers.

CHAPTER 7
CONCLUSIONS

7.1 INTRODUCTION

In this chapter, the overall conclusions documented in the thesis will be summarised. Possible future work will also be reviewed.

7.2 VOLCANOLOGICAL EVOLUTION

The Eyjafjallajökull volcano is composed of complex, intercalated deposits of diamictite, lava, hyaloclastite and reworked volcaniclastics. After detailed succession and lithofacies analysis, it has been shown that these diverse deposits often occur in distinctive assemblages, here referred to as lithofacies associations. The constituent lava and volcaniclastic lithofacies which make up these associations are genetically related and are emplaced almost contemporaneously. Vertical successions commonly reveal stacked lithofacies associations, deposited rapidly during a single eruption event. Such a succession may previously have been interpreted as representing several alternations between periods of subaerial and subaqueous deposition. The form of each lithofacies association depends on the topography, the thickness of ice cover, the volume and rate of eruption, the viscosity of the lava and the deposition environment.

Most of the lithofacies observed and described at Eyjafjöll are made up of materials that were redeposited by meltwater, they therefore formed during eruptions under thin temperate ice (<200m). The only exception is lithofacies association J which formed by ponding in an englacial lake beneath thick, valley-confined ice sheets (<400m). Apart from the valley-confined nature of such deposits, they formed in the same way as tuyas and tindas, although ponding may have been aided by the topography as well as the ice thickness. Such deposits will be rare on polygenetic volcanoes, since sufficient thicknesses of ice are unlikely to build up. The examples at Eyjafjöll formed in broad, flat-based glacial valleys carved into the flanks of the volcano in the mid to late stages of its growth.

Prior to an eruption beneath temperate ice, meltwater may begin to collect in a subglacial vault or may escape immediately through subglacial conduits. The initial phreatomagmatic stage of an eruption creates abundant volcaniclastics which are carried away by meltwater which may have laminar to turbulent flow. The volcaniclastics are deposited on level ground which may be within subglacial sheets and tunnels or in the glacio-fluvial environment. Early phreatomagmatic activity is replaced by more effusive activity as meltwater around the vent is dissipated. During the effusive part of an eruption, lava follows the path of the meltwater. Lava may intrude as sheets between piles of early phreatomagmatic deposits and the subglacial topography or it may flow

over the early cogenetic sediments. The former is more likely to occur when lava has a high eruption rate and sheet flow is the most effective means of transport (lithofacies association C). Such deposits also require a degree of ponding of both volcaniclastics and lava and so will occur beneath ice in flat-based glacial valleys, not on slopes. Eruptions under similar conditions but on slopes, or perhaps of lower eruption rate, may form tunnel flows (lithofacies association D). Lavas flowing in glacial tunnels are rapidly frozen and block subglacial conduits, forcing subsequent lavas and volcaniclastics to follow newly created tunnels. Such processes often create stacked deposits. Sheet and tunnel lavas must have relatively low viscosity, they tend to have pillowy or sharp margins with the cogenetic sediments.

When lava is relatively viscous, or the eruption rate is not high, lava may preferably flow over cogenetic phreatomagmatic deposits. The upper surface of such lavas continuously interacts with meltwater and ice forming hyaloclastite breccias which flow contemporaneously with the underlying lava (lithofacies associations A and B). These lavas tend to have blocky rather than pillowy margins. Such deposits are also deposited on relatively flat topography and are often vertically stacked, suggesting rapid deposition in distinct pulses.

On steep slopes, lavas are likely to form autoclastic debris flows or block and ash flows; fine-grained sediments are rare since they are trnsported away in meltwater. Either sheet flows or channelled/valley-confined flows may form, depending essentially on the subglacial topography. Channels or valleys in the subglacial topography are preferentially utilised (lithofacies associations E and F).

Where substantial thicknesses of subglacial deposits occur, it has been inferred that they were deposited during a glacial period. Subglacial successions deposited between 600 and 800Ka formed stacked, laterally extensive, flat-lying successions, however, as the volcano grew in size, valley-confined glaciers became more common and deposits were laterally confined. Such valley-confined deposits are commonly eroded at their margins following their deposition and this can ultimately lead to topographic inversion. Topographic inversion is diagnostic of subglacial valley-confined volcanism and can lead to problems in correlating the stratigraphy.

By identifying subglacial periods in vertical successions and then correlating sections it has been found that the Eyjafjöll volcanic system has been constructed through up to six glacial and six interglacial periods over the last 800Ka. This is in contrast to Tjörnes in north Iceland where evidence of only four glacial periods since 700Ka has been found (Einarsson and Albertsson, 1988). Glaciations at Eyjafjöll are between 70 and 120Ka in length with corresponding interglacials of similar length. The periodicity of glaciations at Eyajfjöll appears to correlate well with that predicted using stable isotopes of deep sea sediments (Shackleton, 1973; Johnson, 1985).

7.3 STRUCTURAL EVOLUTION

The Eyjafjöll volcanic system is anomalous due to its E-W orientation. This feature is maintained by an E-W stress field which has been superimposed on a magmatic, radial stress regime (Nakamura, 1977). The lavas and volcaniclastics which comprise the western part of the volcano, most of which were erupted from E-W and radial sheets, were only deposited in the last 600Ka (since the eruption of the Hvammsmuli Group). Early activity at the volcano (prior to 600Ka) appears to have been concentrated in a central area and not along an E-W trend. This central area (comprising the core and southern section of the volcano), is dominated by abundant NE-SW orientated sheets some of which extend to the summit of Steinafjall and were erupted towards the end of the last glacial period. Therefore, although the volcano appears to be dominated by an E-W stress regime, a concurrent NE-SW stress regime has, for a long period of time, been dominant in the volcano's core.

Since the radial fissures are shallow crustal features, it is proposed that the E-W stress regime affecting them is also a shallow crustal phenomenon. In contrast, the regional NE-SW stress regime is more pervasive and affects the whole crust. The close proximity of the Katla volcano may partly account for the E-W orientation of the Eyjafjöll volcanic system.

The zone of NE-SW orientated sheets in the core of the volcano is 8km wide at the most. The confined nature of this zone may be related to the thickness of the crust.

7.4 MAGMATIC EVOLUTION

The observed mineral phases in basalts to hawaiites and in gabbroic xenoliths represent the fractionating mineral assemblage: olivine, clinopyroxene, plagioclase, Ti-magnetite and ilmenite. Further fractionation of plagioclase, clinopyroxene and Ti-magnetite produces mugearite compositions and the addition of apatite to the fractionating assemblage allows fractionation to trachyte compositions. The fractionation of Ti-magnetite at high oxygen fugacity causes residual liquids to become enriched in SiO_2. At low oxygen fugacity, Ti-magnetite precipitation is inhibited and the residual liquid becomes Fe enriched. The variable abundance of Fe in basalts at a similar stage in the differentiation process, suggests that magma has fractionated in conditions of slightly differing oxygen fugacity.

Magma has been supplied to the surface at Eyjafjöll in discrete batches usually consisting of several lava flows. No individual batch shows evidence for a zoned magma chamber, since compositions are very similar. Each batch has a distinct chemistry and petrography suggesting that magma is not supplied from a homogenous well-mixed magma chamber. In general, each batch within a sequence is successively more evolved, although occasional ankaramites or highly px-pl-ol phyric basalts

interupt a sequence. This also suggests that magma chambers are only infrequently replenished. Hawaiite, mugearite and trachyte compositions are only observed in the upper levels of the stratigraphy suggesting that although replenishment was infrequent it was sufficient during the early stages of the volcano's growth to prevent fractionation to evolved compositions.

All postglacial activity at the Eyjafjöll volcanic system has been from the shallow central magma chamber, which has erupted acid tephra from the crater rim (1821-1823) and basalts to mugearites from radial fissures. The chamber is clearly not solidified and appears to be zoned from basalt to trachyte compositions. The lavas and volcaniclastics which comprise the sequences to the west of the volcano and were erupted from radial and E-W fissures include sparsely phyric to very highly phyric (<60%) lavas. This suggests that the magma chamber cooled and crystallised to high degrees between replenishments and on occasions may have almost clogged up, alternatively it may reflect crystallisation and separation of crystals in discrete cycles as envisaged by Sparks *et al.* (1990). The volcano is clearly still active and in time, the magma chamber may evolve to rhyolite compositions.

Ankaramites have not been erupted since at least 600Ka although magmatic supply has clearly continued since that time. It is proposed that crustal magma chambers and shallow level intrusions have blocked their route to the surface. Some highly porphyritic basalts may represent residual liquids of ankaramites forced to fractionate at crustal levels. Other ankaramites may have replenished magma chambers although this process may be retarded due to the relatively dense nature of ankaramites, causing them to pond at the base of magma chambers, alternatively crystal cumulates may block the incoming magmas altogether (Campbell, 1978), (Figure 7.1). The Nupakotsdalur Group, which is at least 700Ka in age, contains the only lavas which show evidence of mixing between an ankaramite composition and a more evolved basalt. This suggests that during later stages of the evolution of the volcano, magma has had to undergo greater degrees of differentiation in order to reach shallow crustal levels.

The diversity of lava and intrusive sheet compositions, the abundance of vertical NE-SW sheets in the core of the volcano and the supply of batches of magma suggests that magma is fractionating in several crustal magma chambers at different depths and under different oxygen fugacities. These chambers are fractionating concurrently towards trachyte compositions. Such a crustal structure is proposed for Icelandic Tertiary central volcanoes by Furman *et al.* (1992a, 1992b) and Walker (1963) based on the hypabyssal remains of such centres. It seems very likely that the Eyajfjöll volcanic system has a similar crustal structure (Figure 7.1).

The abundant evidence for mixing at Eyjafjöll suggests that these crustal magma chambers are connected. Many basalts contain bimodal compositions of phenocryst and most contain phenocrysts which are clearly not in equilibrium with the whole rock

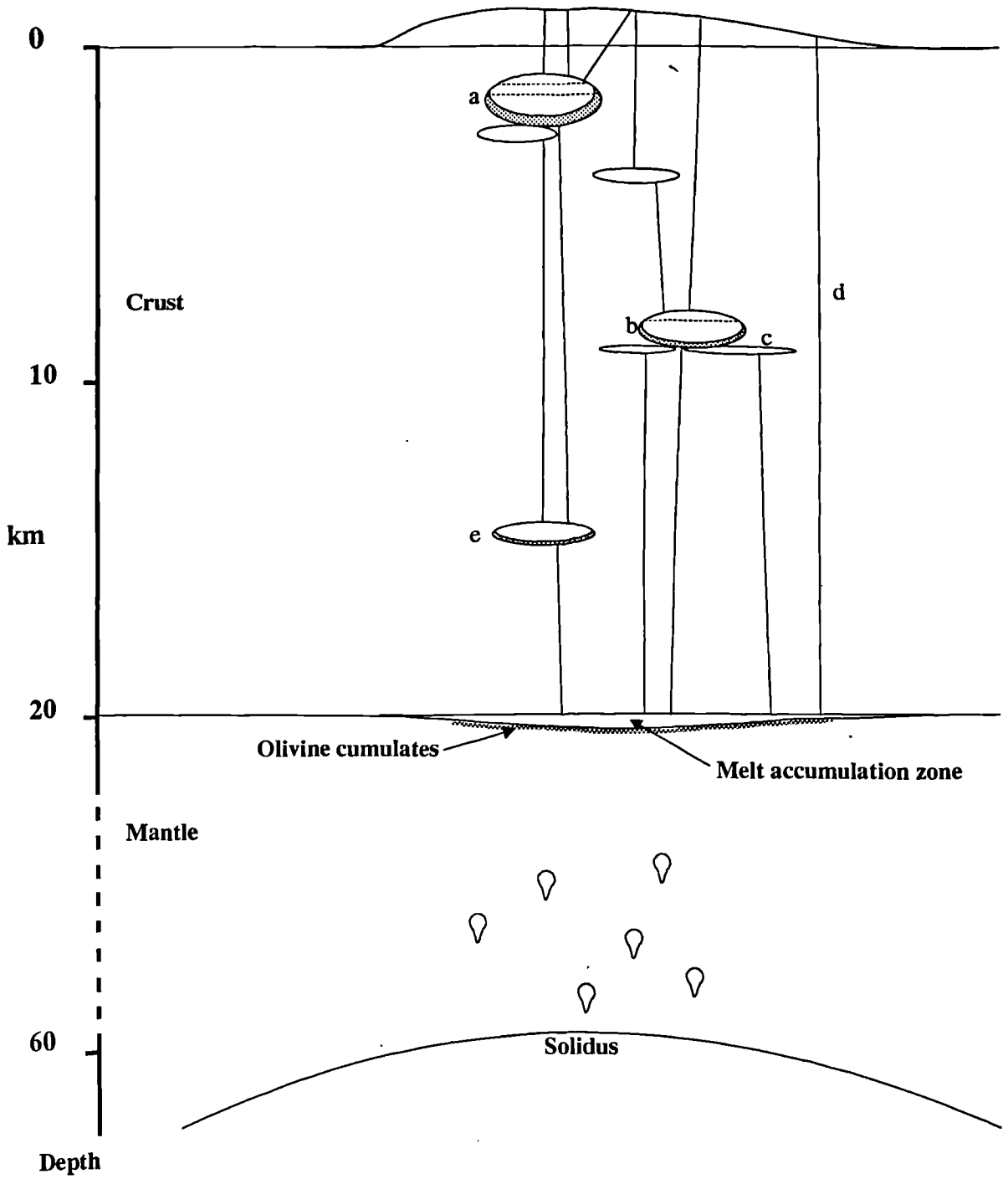

Figure 7.1 *Schematic diagram showing the proposed magmatic plumbing system beneath the Eyjafjallajökull volcano.*

- *Stratified crustal magma chambers such as (a) and (b) evolve towards trachyte compositions.*
- *Cumulates may block primitive replenishing magmas which form pockets in the crust, such as (c).*
- *Ankaramitic magmas penetrated the entire crust prior to ~600Ka (d) but have since been blocked by crustal magma chambers.*
- *Isolated pockets of primitive magma (eg. e) fractionate at depth and may assimilate some crustal material.*

composition. There is also evidence for mixing between basalt and trachyte, presumably during forced mixing (convective overturn?) in stratified magma chambers or during replenishment.

Lavas are all LREE-enriched and there is no great variation in incompatible trace element ratios. This suggests that all basalts have generated from a similar parental material. Although isotope studies were not carried out, this investigation suggests that a heterogeneous source is not required in the generation of Eyjafjöll basalts. There is a small degree of variation for some incompatible trace element ratios which may be explained in terms of depth or degree of melting. In particular, Ce/Yb and La/Ce are quite varied, suggesting that basalts are produced from different mantle melting events. Modelling suggests that melting occurred in a melting column extending down to the spinel-garnet transition zone. Small amounts of melting of such a source give the LREE-enriched trends. Modelling suggests that the degree of melting was up to 4%, since this is a point depth average, actual degrees of melting may have exceeded this value.

There appears to be a positive correlation between Fe content and Ce/Yb. Since Fe abundance increases in a basalt melt with increasing pressure, this may suggest that the basalts of high Ce/Yb, included melts separated from substantial depths in the melting column. Conversely, ankaramites have very low Ce/Yb and Fe, but high MgO, these may be melts segregated from shallower depths in the mantle. Mantle melts of high Fe content are too dense to rise through the crust so they must fractionate to high degrees first. This may explain why there are no examples of high Ce/Yb primitive basalt at the surface. These basalts also have unusual trace element signatures which may indicate a degree of crustal assimilation. This is not surprising if such basalts have to fractionate to such high degrees prior to eruption, especially if much of the fractionation occurs at substantial depths. The high Ce/Yb basalts have similarities to basalts from the Katla volcanic system and are all erupted to the south and east of Eyjafjöll. It seems likely that the melting column beneath Katla extends to greater depths than the column beneath Eyjafjöll and that some mixing of melts from the two systems has occurred.

7.5 FURTHER WORK

- The proximal deposits of subglacial eruptions are poorly documented and not well understood. Work in Antarctica (Smellie *et al.*, 1993) and work presented in this thesis, suggests that the products of such eruptions are very distinctive. Further detailed study of these unusual deposits will undoubtably tell us much more about the processes which occur during subglacial volcanism. Specifically, the spatial variation of such deposits requires further work.

- Further K-Ar dating of specific lavas would be useful now that a stratigraphy has been established. In particular, the age of deposits which comprise Raufarfell is not known and dating of all the ankaramites might reveal if they are temporally related or not. In addition, dating of glacial deposits described in this thesis may fill in the apparent time gaps described by Wiese (1992).

- This study has revealed the existence of several petrographically interesting lavas, especially the trachytes and mixed magmas, unfortunately a detailed study of these lavas was not possible here because of time restrictions. A detailed study of the mixed magmas may reveal a complex story involving several phases of magma mixing and mingling between several different compositions.

- The Eyjaföll volcanic system is clearly linked to the Katla volcanic system in some way. The Katla system is also poorly known, making comparison between the two systems rather difficult. Detailed geochemical, petrological and structural studies of Katla would enable the relationship between the two systems to be elucidated. Geophysical work may also help to constrain the crustal structure in this area and may reveal whether or not the magmatic plumbing systems are connected.

- The origin of ankaramites, which are common in flank zones, is not well understood. The presence at Eyjafjöll of several ankaramites may make this a particularly good area for the study of these rocks. Microprobe trace element data of the phenocrysts of these lavas may be particularly useful in further understanding the processes involved in their generation.

REFERENCES

Allen, C. C., 1980. Icelandic subglacial volcanism; thermal and physical studies. *J. Geol.*, **88,** 108-117.

Anderson, E. M., 1935. The dynamics of the formation of cone sheets, ring dykes and cauldron subsidences. *Proc. R. Soc. Edin.*, **56,** 128-157.

Angenheister, G. et al., 1980. Reykjanes Ridge Iceland seismic experiment (RRISP 77) *Journal of Geophysics,* **47,** 228-238.

Arney, B. H., 1978. Geochemistry of Eyjafjöll, a volcano in southern Iceland. Unpubl. MSc Thesis. M.I.T.

Bacon, C. R., 1986. Magmatic inclusions in silicic and intermediate volcanic rocks. *J. Geophys. Res.*, **91,** 6091-6112.

Baldridge, W. S., McGetchin, T. R. & Frey, F. A., 1973. Magmatic evolution of Hekla, Iceland. *Contr. Miner. Petrol.*, **42,** 245-258.

Ballard, R. D., Holcomb, R. D. & van Andel, Tj. H., 1979. The Galapagos at 86 W: Sheet flows, collapse pits and lava lakes of the rift valley. *J. Geophys. Res.*, **84,** 5407-5422.

Bannerjee, I. and McDonald, B. C., 1975. Nature of esker sedimentation. In: A. V. Jopling and B. C. McDonald (Eds), Glaciofluvial and Glaciolacustrine Sedimentation. Soc. Econ. Paleontol. Mineral., Spec. Publ., **23,** 132-154.

Beard, J. S., and Lofgren, G. E., 1991. Dehydration melting and water-saturated melting of basaltic and andesitic greenstones and amphibolites at 1, 3 and 6.9kb. *J. Petrology*, **32,** 365-402.

Beblo, M & Björnsson, H., 1980. A new model of electrical resistivity beneath NE Iceland: correlation with temperature. *Journal of Geophysics,* **47,** 184-190.

Bender, J. F., Hodges, F. N. and Bence, A. E., 1978. Petrogenesis of basalts from the project Famous area: experimental study from 0 to 15 Kbars. *Earth Planet. Sci. Lett.* **41,** 277-302.

Bergh, S. G. & Sigvaldason, G. E., 1991. Pleistocene mass-flow deposits of basaltic hyaloclastite on a shallow submarine shelf, South Iceland. *Bull. Volcanol*, **53,** 597-611.

Beverage, J. P. and Culbertson, J. K., 1964. Experiments on a gravity-free dispersion of large solid spheres in a Newtonian fluid under shear: *Proc. Roy. Soc. Lond.*, **A225,** 49-63.

Björnsson, H., 1975. Subglacial water reservoirs, jokulhlaups and volcanic eruptions. *Jökull*, **25,** 1-26.

Björnsson, H., 1988. Hydrology of ice caps in volcanic regions. Societas Scientarium Islandica Rit XLV. University of Iceland.

Boulton, G. S., 1972. Modern Arctic Glaciers as depositional models for former ice sheets. *J. Geol. Soc. Lond.*, **128**, 361-394.

Brink, U., 1991. Volcano spacing and plate rigidity. *Geology,* **19**, 397-400.

Budkewitsch, P. & Robin, P-Y., 1994. Modelling the evolution of columnar joints. *J. Volcanol. Geotherm. Res.,* **59**, 219-239.

Carlisle, D., 1963. Pillow breccias and their aquagene tuffs, Quadra Island, British Columbia. *J. Geol.* **71**, 48-71.

Carmichael, I .S. E., 1964. The petrology of Thingmuli, a Tertiary volcano in eastern Iceland. *J. Petrology,* **5,** 435-460.

Carmichael, I .S. E., 1967. The mineralogy of Thingmuli, a Tertiary volcano in eastern Iceland. *Am.Mineral.,* **52,** 1815-1841.

Carswell, D, A., 1983. The volcanic rocks of the Solheimajokull area, southern Iceland. *Jokull,* **33**, 61-71.

Cas, R. A. F. & Wright, J. V., 1988. *Volcanic successions modern and ancient.* Unwin Hyman, London, 487pp.

Cattell, A. C., 1989. The Skye Main Lava Series: liquid density and the absence of basaltic hawaiites. *Geol. Mag.*, **126** (6), 681-684.

Chen, C. F. and Turner, J. S., 1980. Crystallisation in a double diffusive system. *J. Geophys. Res.*, **85**, 2573-2593.

Crowell, J. C., 1957. Origin of pebbly mudstones. *Bull. Geol. Soc. Am.***68** , 993- 1010.

DeGraff, J. M. and Aydin, A., 1987. Surface morphology of columnar joints and its significance to mechanics and direction of of joint growth. *Geol. Soc. Am. Bull.*, **99**, 605-617.

Dreimanis, A. & Schluchter, C., 1985. Field criteria for the recognition of till or tillite. *Palaeogeog. Palaeoclim. Palaeoecol.*, **51**, 7-14.

Druitt, T. H. & Sparks, R. S. J., 1984. On the formation of calderas during ignimbrite eruptions. *Nature*, **310**, 679-681.

Einarsson, T., 1950. The eruption of Hekla 1947-1948. *Visindafelag Islendinga*, **4(4)**, 1-34.

Einarsson, T., 1991. Earthquakes and present-day tectonism in Iceland. *Tectonophysics*, **189,** 261-279.

Einarsson, T. & Albertsson, K. J., 1988. The glacial history of Iceland during the past three million years. *Phil. Trans. R. Soc. Lond.*, **B318**, 637-644.

Elliot, T. R., Hawkesworth, C. J. & Gronvold, K., 1991. Dynamic melting of the Iceland Plume. *Nature,* **351,** 201-206.

Emeleus, C. H., 1985. The Tertiary lavas and sediments of northwest Rhum, Inner Hebrides. *Geol. Mag.* **5**, 419-437.

Eyles, C. H., Eyles, N. & Miall, A. D., 1983. Lithofacies types and vertical profile models; an alternative approach to the description and environmental interpretation of glacial diamict and diamictite sequences. *Sedimentology*, **30**, 393-410.

Eyles, C. H., Eyles, N. & Miall, A. D., 1985. Models of glaciomarine sedimentation and their application to the interpretation of ancient glacial sequences. *Palaeogeog, Palaeoclim. Palaeoecol.*, **51**, 15-84.

Eysteinsson, H. & Hermance, J. F.,1985. Magnetotelluric measurements across the eastern neovolcanic zone in southern Iceland. *J. Geophys. Res.*, **90** No.B12, 10,043-10,072.

Fisher, R. V. and Schmincke, H.-U., 1984. *Pyroclastic rocks.* Berlin: Springer-Verlag.

Foder, R. V. & Vandermeyden H. J., 1988. Petrology of gabbroic xenoliths from Mauna Kea volcano, Hawaii. *J. Geophys. Res.*, **93**, 4435-4452.

Foder, R. V., Rudek, E. A. & Bauer, G. R. 1993. Hawaiian magma-resevoir processes *Bull. Volcanol.*, **55**,204-218.

Foulger, G. R., Beutler, R., Bilham, R., Einarsson, P., Fankhauser, S.,, Gurtner, U., Hugentobler, W. J., Morgan, M., Rochacher, G., Thorbergsson, G. and Wild, U., 1993. The Iceland 1986 GPS geodetic survey: Tectonic goals and data processing results, *Bull. Geodetica.*

Frey, F. A., Garcia, M. O. Wise, W. S. Kennedy, A., Gurriet, P. and Albarede, F., 1991. The evolution of Mauna Kea volcano, Hawaii: petrogenesis of tholeiitic and alkalic basalts. *J. Geophys. Res.* **96**, 14347-14375.

Frey, F. A., Wise, W. S., Garcia, M. O., West, H., Kwon, S-T. and Kennedy, A., 1990. Evolution of Mauna Kea volcano, Hawaii: Petrological and Geochemical Constraints on Postshield Volcanism. *J. Geophys. Res.* **95**, 1271-1300.

Furman, T., Frey, F. A. and Meyer, P. S., 1992a. Petrogenesis of Evolved Basalts and Rhyolites at Austurhorn, Southern Iceland: the Role of Fractional Crystallisation. *J. Petrol.* **33** (6), 1405-1445.

Furman, T., 1992b. Evolution of Icelandic central volcanoes: evidence from the Austurhorn intrusion, southern Iceland. *Bull. Volcanol.* **55**, 45-62.

Furnes, H., Fridleifsson, I. B. & Atkins, F. B., 1980. Subglacial volcanics - on the formation of acid hyaloclastites. *J. Volcanol. Geotherm. Res.*, **8**, 95-110.

Gautneb, H., Gudmundsson, A. & Oskarsson, N., 1989. Structure, petrochemistry and evolution of a sheet swarm in an Icelandic central volcano. *Geol. Mag.*, **126,** 659-673.

Gebrande, H., Miller, H., & Einarsson, P., 1980. Seismic structure of Iceland along RRISP. *J. Geophys.*, **47**, 239-249.

Geirsdottir, A. 1991. Diamictites of late Pliocene age in western Iceland. *Jökull*, **40**, 3-24.

Gibson, I. L., Kirkpatrick, R. J., Emmerman, R., Schmincke, H-U., Pritchard, G., Oakley, P. J., Thorpe, R. S. and Marriner, G. F., 1982. The trace element composition of the lavas and dykes from a 3km vetical section of the lava pile of Eastern Iceland. *J. Geophys. Res.*, **87 (B8)**, 6532-6546.

Goldthwait, R.P., 1974. Till deposition versus glacial erosion. In: *Research in Polar and Alpine Geomorphology* (Eds B. H. Fahey and R. D. Thompson), 159-166.

Green, T. H. and Watson, E.B., 1982. Crystallisation of apatite in natural magmas under high pressure, hydrous conditions, with particular reference to 'orogenic' rock series. *Contr. Miner. Petrol.* **79.** 96-105.

Grove, T. L. and Bryan, W. B., 1983. Fractionation of pyroxene-phyric MORB at low pressure: an experimental study. *Contrib. Mineral. Petrol.* **84**, 293-309.

Gudmundsson, A., 1984. Formation of dykes, feeder dykes and the intrusion of dykes from magma chambers. *Bull. Volcanol.* **47**, 537-550.

Gudmundsson, A., 1988. Formation of collapse calderas. *Geology.* **16**, 808-810.

Gudmundsson, A., 1990. Emplacement of dikes, sills and crustal magma chambers at divergent plate boundaries. *Tectonophysics.* **176**, 257-275.

Gudmundsson, A., 1995. Infrastructure and mechanics of volcanic systems in Iceland. *J. Volcanol. Geotherm. Res.*, **64**, 1-22.

Gudmundsson, O., Brandsdottir, B., Menke, W. and Sigvaldason, G. E., 1994. The crustal magma chamber of the Katla volcano in south Iceland revealed by 2-D seismic undershooting. *Geophys. J. Int.* **119,** 277-296.

Hanson, G. N. and Langmuir, C. H., 1978. Modelling of major elements in mantle-melt systems using trace element approaches. *Geochim. Cosmochim. Acta* **42**, 725-741.

Hardardottir, V., 1986. The Petrology of the Maelifell Picrite Basalt, Southern Iceland. *Jokull,* **36,** 31-40.

Hardarson, B. S. & Fitton, J. G., 1991. Increased mantle meltig beneath Snaefellsjõkull volcano during late Pleistocene deglaciatiation. *Nature,* **353,** 62-64.

Hards, V., 1995. Geochemistry of the Snaefell volcano, eastern Iceland. Unpubl. Ph. D. thesis, Univ. of Durham.

Helgason, J., 1984. Frequent shifts of the volcanic zone in Iceland. *Geology*, **12**, 212-216.

Helgason, J., 1985. Shifts of the plate boundary in Iceland: some aspects of tertiary volcanism. *J. Geophys. Res.*, **90** No. B12, 10084-10092.

Helz, R.T., 1978. Phase relations of basalts in their melting ranges at Ph2o-5kb. Part II. Melt compositions. *J. Petrology.*, **17**, 139-193.

Helz, R. T., 1980. Crystallisation history of Kilauea Iki lava lake, as seen in drill core recovered in 1967-1979. *Bull. Volcanol.*, **43-4**, 675-701.

Helz, R. T., 1987. Differentiation behaviour of Kilauea IIki lava lake, Kilauea volcano, Hawaii: an overview of past and current work. In: Mysen, B. O. (ed) Magmatic processes:physicochemical principles. Geochem. Soc. Spec. Pub. **1**, 241-258.

Helz, R. T., Kirschenbaum, H. and Marinenko, J. W. 1989. Diapiric transfer of melt in Kilauea Iki lava lake, Hawaii: A quick, efficient process of igneous differentiation. *Geol. Soc. Am. Bull.* **101**, 578-594.

Herzberg, C. T. and Chapman, N. A., 1976. Clinopyroxene geothermometry of spinel-lherzolite. *Amer. Miner.*, **61**, 626-637.

Hill, R. I., 1991. Starting plumes and continental break-up. *Earth Plane. Sci. Lett.*, **104**, 398-416.

Hjartarson, A. and Ingolfsson, O., 1988. Preboreal Glaciation of Southern Iceland. *Jökull*, **38**, 1-13.

Honnorez, J., 1961. Sur l'origine des hyaloclastites. *Bull. Soc. Belge. Geol.*, **70**, 407-412.

Honnorez, J. & Kirst, P., 1975. Submarine basaltic volcanism: morphometric parameters for discriminating hyaloclastites from hyalo-tuffs. *Bull. Volcanol.*, **39**, 1-25.

Humphris, S. E. and Thompson, G., 1978. Trace element mobility during hydrothermal alteration of oceanic basalts. *Geochim. Cosmochim. Act.*, **42**, 127-136.

Humphris, S. E., Morrison, M. A. and Thompson, R. N., 1978. Influence of rock crystallisation history upon subsequent lanthanide mobility during hydrothermal alteration of basalts. *Chem. Geol.*, **23**, 125-137.

Huppert, H. E. and Sparks, R. S. J., 1980. The fluid dynamics of a basaltic magma chamber replenished by influx of hot, dense, ultrabasic magam. *Contr. Mineral. Petrol.*, **75**, 279-289.

Huppert, H. E., Turner, J. S. and Sparks, R. S. J., 1082. Replenished magma chambers: effects of compositional zonation and input rates. *Earth Planet. Sci. Lett.*, **57**, 345-357.

Iddings, J. P., 1909. Igneous rocks, I. New York.

IOC,IHO & BODC., 1994. GEBCO digital atlas (CD-ROM) published on behalf of the Intergovernment Oceanographic Commission (of Unesco) and the International

Hydrographic Organisation as part of the general bathymetric chart of the oceans (GEBCO); British Oceanographic data centre, Birkenhead.

Irvine, T. N. and Barager, W. R. A., 1972. A guide to the chemical classification of the common volcanic rocks. *Can. J. Earth Sci.*, **8**, 523-548.

Jaeger, J. C., 1961. The cooling of irregularly shaped igneous bodies. *Am. J. Science,* **259**, 721-734.

Jones, J. G., 1969a. Intraglacial volcanoes of the Laugarvatn region, SW Iceland, I. *J. Geol. Soc. London*, **124**, 197-211

Jones, J. G., 1969b. Pillow lavas as depth indicators. *Amer. J. Sci.*, **267**, 181-195.

Jones, J. G., 1970. Intraglacial volcanoes of the Laugarvatn region, SW Iceland, II. *J. Geol.*, **78**, 127-140.

Jakobsson, S. P., 1978. Environmental factors controlling the palagonitization of the Surtsey tephra, Iceland. *Bulletin of the Geological Society of Denmark,* **27,** Special Issue, 91-105.

Jakobsson, S. P., 1979a. Outline of the petrology of Iceland. *Jokull*, **29**, 57-73.

Jakobsson, S. P., 1979b. Petrology of Recent basalts of the Eastern Volcanic Zone, Iceland. *Acta Naturalia Islandica,* **26**, 103.

Jakobsson, S. P. and Moore, J. G., 1980. Unique hole shows how volcano grew. Geotimes, **25**,14-16.

Jakobsson, S, P., Pedersen, A. K., Rõnsbo, J. G. & Larsen, L. M., 1973. Petrology of mugearite-hawaiite: Early extrusives in the 1973 Heimaey eruption, Iceland. *Lithos,* **6,** 203-214.

Johannesson, H., 1985 . On the ages of two recent lava flows in Eyjafjoll and the late glacial terminal moraines in south Iceland. *Jökull*, **35**,

Johnson, R. G., 1982. Brunhes-Matuyama magnetic reversal dated at 790, 000 yr BP. by marine-astronomical correlations. *Quat. Res.*, **17**, 135-147.

Jonsson, J., 1982. Notes on the Katla volcanoglacial Debris Flows. *Jokull*, **32**, 61-68.

Jonsson, J., 1990. Geological Map of Eyjafjoll. Research Institute Nedri As, Hveragerdi.

Jorgensen, K. A., 1980. The eruption of the Thorsmork ignimbrite, south Iceland: the structure of the magma chamber deduced from the eruption products. *Nordic Volcanic Institute Report,* **8103.**

Kjartansson, G., 1958. Endaslepp hraun undir Eyjafjollum. (Lava flows deprived of their distal ends in Eyjafjoll, South Iceland). Natt. fraed., **28**, 127-140.

Kokelaar, P., 1986. Magma-water interactions in subaqueous and emergent basaltic volcanism. *Bull. Volcanol.*, **48**, 275-289.

Komuro, H., 1987. Experiments on cauldron formation: a polygonal cauldron and ring fractures. *J.Volcanol. Geotherm. Res.* **31**, 139-149.

Kostopoulos, D. K. and James, S. D., 1992. Parameterisation of the Melting Regime of the Shallow Upper Mantle and the Effects of Variable Lithospheic Stretching on Mantle Modal Stratification and Trace-Element Concentrations in Magmas. *J. Petrol.*, **33** (3), 665-691.

Kristjansson, L., Johannesson, H., Eiriksson, J. & Gudmundsson, A.I., 1988. Brunhes-Matuyama paleomagnetism in three lava sections in Iceland. *Can. J. Earth Sci.*, **25**, 215-225.

Kuo, L. C. and Kirkpatrick, R. J., 1982. Pre-eruption history of phyric basalts from DSDP legs 45 and 46: evidence from morphology and zoning patterns in plagioclase. *Contr. Mineral. Petrol.*, **79**, 13-27.

Kurz, M. D., Meyer, P. S. & Sigurdsson, H., 1985. Helium isotope systematics within the neovolcanic zones of Iceland. *Earth and Planetary Science Letters,* **74,** 291-305.

La Breque, J. L., Kent, D. V. and Cande, S. C., 1977. Revised magnetic polarity time scale for late Cretaceous and Cenozoic time. *Geology*, **5-6**, 330-335.

Lapin, I. V., Lukanin, O. A. and Kadik, A. A., 1985. Effects of redox conditions on near-surface Icelandic basalt crystallisation and differentiation. *Geokhimiya*, **6**, 747-760.

Larsen, J. G., 1979. Glass bearing inclusions in hyaloclastites from Tindfjallajokull, Iceland. *Lithos,* **12,** 289-302.

Larsen, L. M., Watt, W. S. and Watt, M., 1989. Geology and petrology of the Lower Teriary plateau basalts of the Scoresby Sund region, East Greenland. Bull. Gronlands geol. Unders. **157**, pp164.

Lawver, L. A. and Muller, R. D., 1994. Iceland hotspot track. *Geology*, **22,** 311-314.

LeBas, M. J., LeMaitre, R. W., Streckeisen, A. and Zanettin, B., 1986. A chemical classification of volcanic rocks based on the total alkali silica diagram. *J. Petrol.*, **27**, 745-750.

LeBas, M. J. and Streckeisen, A., 1991. A chemical classification of volcanic rocks. J. Geol. Soc. Lond. **148**, 825-833.

Leeder, M. R., 1982. Sedimentology: process and product. Unwin Hyman Ltd.

Le Maitre R. W., Bateman, P., Dudek, A., Keller, J., Le Bas M. J., Sabine, P. A., Schmid, R., Sorensen, H., Streckeisen, A., Woollley, A. R. and Zanettin, B., 1989. A classification of igneous rocks and glossary of terms. Blackwell, Oxford.

Long, P. E. & Wood, B. J., 1986. Structures, textures and cooling histories of Columbia River basalt flows. *Geol. Soc. Am. Bull.*, **97**, 1144-1155.

Lowe, D. R., 1976. Grain flow and grain flow deposits. *J. Sed. Petrol.*, **46**, 188-199/.

Lowe, D. R., 1982. Sediment gravity flows: II. Depositional models with special reference to the deposits of high-density turbidity currents. *J. Sedim. Petrol.*, **52**, 279-297.

Luyendyk, B. P. *et al.*, 1979. Leg 49, site 409, Deep Sea Drilling Project. *In* Initial Reports of the Deep Sea Drilling Project, **49**, 161-225.

Maaloe, S., Sorensen, I. B. and Hertogen, J., 1986. The Trachybasalt Suite of Jan Mayen, *J. Petrology*, **27** (2), 439-466.

Macdonald, G. A., 1972. *Volcanoes.* Englewood Cliffs, New Jersey: Prentiice-Hall.

Macdonald, G. A. and Katsura, T., 1964. Chemical composition of Hawaiian lavas. *J. Petrol.*, **5**, 82-133.

Marsh, B. D., 1982. On the mechanics of igneous diapirisim, stoping, and zone melting. *Am. J. Sci.*, **282,** 808-855.

Marshall, L. A. & Sparks, R. S. J., 1984. Origin of some mixed-magma and net-veined ring intrusions. *J. Geol. Soc. Lond.*, **141,** 171-182.

Macdonald, G. A., Sparks, R. S. J., Sigurdsson, H., Mattey, D. P., McGarvie, D. W. and Smith, R. L., 1987. The 1875 eruption of Askja volcano Iceland: combined fractional crystallisation and elective contamination in the generation of rhyolitic magma. *Miner. Mag.*, **51**, 183-202.

Macdonald, R., McGarvie, D. W., Pinkerton, H., Smith, R. L. and Palacz, Z. A., 1990. Petrogenetic evolution of the Torfajokull volcanic complex, Iceland I. Relationship between the magma types. *J. Petrol.*, **31,** 429-459.

Mackenzie, D. P., 1984. The generation and composition of molten rock. *J. Petrol.*, **25**, 713-765.

Maizels, J., 1993. Lithofacies variations within sandur deposits; the role of runoff regime, flow dynamics and sediment supply characteristics. *Sedim. Geol.*, **85**,299-325.

Maizels, J., 1989. Sedimentology, palaeoflow dynamics and flood history of jokulhlaup deposits; paleohydrology of Holocene sediment sequences in southern Iceland sandur deposits. *J. Sedim. Petrol.***59**, 204-223.

Marshall, L. A. and Sparks, R. S. J., 1984. Origin of some mixed-magma and net-veined ring intrusions. *J. Geol. Soc. Lond.*, **141**, 171-182.

Mathews, W. H., 1947. "Tuyas", flat topped volcanoes in northern British Columbia. *Am. Jour. Sci.*, **245**, 560-570.

McBirney, A. R., 1980. Mixing and unmixing of magmas. *J. Geotherm.Res.*, **7**, 357-371.

McBirney, A. R., 1993. Igneous petrology, Jones and Bartlett, pp 106.

McBirney, A. R. and Williams, H., 1969. Geology and petrology of the Galapagos Islands. *Mem. Geol. Soc. Am.*, **118**, 197pp.

McGarvie, D. W., 1984. Torfajökull: A volcano dominated by magma mixing. *Geology,* **12,** 685-688.

McGarvie, D. W., Macdonald, R., Pinkerton, H. & Smith, R. L., 1990. Petrogenic evolution of the Torfajõkull volcano complex, Iceland II. The role of magma mixing. *J. Petrol.*, **31,** 461-481.

Melson, W. G., Vallier, T. L., Wright, T. L., Byerly, C., Nelen, J., 1976. Geochemical diversity of volcanic glass erupted along Pacific, Atlantic and Indian Ocean sea floor spreading centres, from *The Geophysics of the Pacific Ocean Basin and its Margins.* (eds) Sutton, G., Manghani, M. H., Moberly, R., Am. Geophys. Union, Geophys. Monogram 4, pp351.

Meyer, P. S., Sigurdsson, H. & Schilling, J. G., 1985 Petrological and geochemical variations along Iceland's neovolcanic zones. *J. Geophys. Res.*, **90**, 10043-10072.

Miall, A. D., 1977. A review of the braided-river depositional environment. *Earth Sci. Rev.*, **13**, 1-62.

Miyashiro, A., 1978. Natureof alkalic volcanic rock series. *Contributions to Mineralology and Petrology.*, **66**, pp 91-104.

Moore, J. G., 1985. Structure and eruptive mechanisms at Surtsey Volcano, Iceland. *Geol. Mag.*, **122**, 649-661.

Moore, J. G. and Evans, B. E., 1967. The role of olivine in the crystallisation of the prehistoric Makaopuhi tholeiitic lava lake, Hawaii. *Contr. Miner. Petrol.*, **15**, 202-223

Moore, J. G. & Fiske, R. S., 1969. Volcanic substructure inferred from dredge samples and ocean bottom photographs, *Hawaii. Geol. Soc. Amer. Bull.*, **80**, 1191-1202.

Moore, J. G. & Schilling, J-G., 1973. Vesicles, water and sulfur in Reykjanes Ridge basalts. *Contr. Mineral. Petrol.*, **41**, 105-118.

Mori, J. & McKee, C., 1987. Outward-dipping ring fault structure at Rabaul Caldera as shown by earthquake localities. *Science*, **235**, 193-195.

Morse, S. A., 1980. Basalts and phase diagrams. Springer-Verlag, pp 493.

Mottl, M. J. and Holland, H. D. 1978. Chemical exchange during hydrothermal alteration of basalt by seawater-I Experimental results for major and minor components of seawater. *Geochim. Cosmochim. Act.*, **42**, 1103-1115.

Murase, T. and McBirney, A. R., 1973. Properties of some common igneous rocks and their melts at high temperatures. *Geol. Soc. Am. Bull.*, **84**, 3563-3592.

O'Hara, M. J. and Matthews, R. E., 1981. Geochemical evolution in an advancing, periodically replenished, periodically tapped, continuously fractionated magma chamber. *J. Geol. Soc. Lond.*, **138**, 237-277.

Nakamura, K., 1977. Volcanoes as posssible indicators of tectonic stress orientation - principal and proposal. *J. Volcanol. Geotherm. Res.*, **2**, 1-16.

Nayadu, Y. R., 1962. A new hypothesis of origin of guyots and seamount terraces. In; *The crust of the Pacific basin.* Amer. Geophys. Un. Monog. **6**, 171-180.

Nayadu, Y. R., 1964a. Palagonite tuffs (hyaloclastites) and the prodocts of post eruptive processes. *Bull. Volcanol.*, 27, 391-410.

Nicholson, H. & Latin, D., 1992. Olivene tholeites from Krafta, Iceland: evidence for variations in melt fraction within a plume. *J. Petrol.*, **33,** 1105-1124.

Nicholson, H., Condomines, M., Fitton, G. J., Fallick, A. E., Grõnvold, K. & Rogers, G., 1991. Geochemical and isotopic evidence for crustal assimilation beneath Krafta Iceland. *J. Petrol.*, **32 - 5,** 1005-1020.

Nielson, N., 1936. A volcano under an ice cap, Vatnajökull, Iceland. *Geog. J.*, **40**, 6-23.

Nielsen, R. L.,1988.A model for the simulation of combined major and trace element liquid line of descent. *Geochimica et Cosmochimica Acta.*, **52,** 27-38.

Noe-Nygaard, A., 1940. Sub-glacial volcanic activity in ancient and recent times. *Fol. Geogr. Dan.* 1, **2**, 5-67.

Nye, J. F., 1976. Water flow in glaciers; jokulhlaups, tunnels and veins. *J. Glaciol.*, **76**, 181-207.

O'Hara, M. J. & Mathews, R. E., 1981. Geochemical evolution in an advancing, periodically replenished, periodically tapped, continuously fractionating magma chamber. *J. Geol. Soc. London,* **138, 237-277.**

Oskarsson, N., Sigvaldason, G. E. and Steinthorsson, S., 1982. A dynamic model of rift zone petrogenesis and the regional petrology of Iceland. *J. Petrology.* **23**, 28-74.

Oskarsson, N., Steinthorsson, S. & Sigvaldason, G. E., 1985. Iceland geochemical anomoly: origin, volcanotectonics, chemical fractionation and isotope evolution of the crust. *J. Geophys. Res.*, **90,** 10011-10025.

Pálmason, G., 1971. Crustal Structure of Iceland from explosion seismology. *Society Science Islandica Rit*, **40**, 187.

Pálmason, G., 1973. Kinematics and heat flow in a volcanic rift zone, with application to Iceland. *Geophys. J. Royal Astron. Soc.* **33**, 451-481.

Pálmason, G. & Saemundsson, K., 1974. Iceland in relation to the Mid-Atlantic Ridge. *Ann. Review: Earth Planet. Sci. Lett.*, **2**, 25-50.

Pálmason, G., Árnorsson, S., Feiðleifsson, I. B. Kristmansdóttir, H., Sæmundsson, K., Stefansson, V., Steingrimsson, B., Tomasson, J. Kristjansson, L., 1979. The Iceland crust; evidence from drill hole data on structure and processes. *In*: TALWANI, M., HAY, W. & RYAN, W. B. F. (eds) *Deep Sea Drilling Results in the Atlantic Ocean: Oceanic Crust.* Maurice Ewing series, **2**. American Geophysical Union, Washington, 43-65.

Peacock, M. A. and Fuller, R. R., 1928. Chlororphaeite, sideromelane and palagonite from the Columbia River Plateau. *Am. Miineral.*, **13**, 360-383.

Phillips, 1974. The dynamic emplacement of cone sheets. *Tectonophysics*, **24**, 69-84.

Poldervaart, A. and Hess, H. H., 1951. Pyroxenes in the crystallisation of basaltic magma. *J. Geol.*, **59**, 472-489.

Richey, J. E., 1932a. The Tertiary ring complex of Slieve Gullion (Ireland). *Q. J. Geol. Soc.*, **88**, 776.

Rittman, A., 1962. *Volcanoes and their activity.* John Wiley and Sons, New York, 1-305.

Robson, G. R., 1957. The volcanic geology of Vestur-Skaftafellsysla, Iceland. Unpubl. Ph. D. thesis, Univ. of Durham, 259 p.

Robson & Barr., 1964. The effect of stress on faulting and minor intrusions in the vicinity of the magma body. *Bull. Volcanol.*, **27**, 315-330.

Roeder, P. L. and Emslie, R. F., 1970. Olivine-liquid equilibrium. *Contrib. Mineral. Petrol.*, **29**, 275-291.

Rothlisberger, H., 1972. Water pressure in intra- and subglacial channels. *J. Glaciol.*, **11**, 177-203.

Rudek, E. A., Fodor, R. V. and Bauer, G. R., 1992. Petrology of Ultramafic and Mafic Xenoliths in Picrite of Kahoolawe Island, Hawaii. *Bull. Volcanol.*, **55**, 74-84.

Ryan, M. P. & Sammis, C. G., 1978. Cyclic fracture mechanism of cooling basalt. *Geol. Soc. Am. Bull.* **89**. 1295-1308.

Sæmundsson, K., 1970. Interglacial lava flows in the lowlands of southern Iceland and the problem of two-tiered columnar jointing. *Jökull*, **20**, 62-76.

Saemundsson, K., 1974. Evolution of the axial rifting zone in northern Iceland and the Tjornes Fracture Zone. *Geological Society of America Bulletin,* **85,** 495-504.

Sæmundsson, K., 1978. Fissure swarms and central volcanoes of the neovolcanic zones in Iceland. *Geological Journal Special Issue*, **10,** 415-432.

Saemundsson, K., 1979. Outline of the geology of Iceland. *Jokull*, **29**, 7-28.

Sæmundsson, K., 1986. Subaerial volcanism in the western North Atlantic; in Vogt, P. P., and Tucholke, B. E., eds., The Geology of North America, Volume M, The Western North Atlantic Region: The Geological Society of America.

Schilling, J-G., Meyer, P. S. & Kingsley, R. H., 1982. Evolution of the Iceland hotspot. *Nature*, **296**, 313-320.

Schmincke, H.-U., 1967. Graded lahars in the type sections of the Ellensburg Formation, south-central Washington. *J. Sed. Petrol.*, **37**, 438-448.

Schultz, A.W., 1983. Subaerial debris-flow deposition in the upper Palaeozoic Cutler Formation, Western Colorado. *J. Sedim. Petrol.,* **54**, 0759-0772.

Self, S. and Sparks, R. S. J. (eds), 1981. *Tephra studies*, Dordrecht: D. Reidel.

Shackleton, N. J., and Opdyke, N. D., 1973. Oxygen isotope and palaeomagnetic stratigraphy of equatorial core V28-238: Oxygen isotope temperatures and ice volumes on a 105 and 106 year scale. *Quat. Res.*, **3,** 39-55.

Shaw, J., 1987. Glacial sedimentary processes and environmental reconstruction based on lithofacies. *Sedimentology*, **34**, 103-116.

Shervais, J. W., 1981. Ti-V plots and the petrogenesis of modern and ophiolitic lavas. *Earth Planet. Sci. Lett.*, **59**, 101-118.

Shoemaker, E. M., 1992. Subglacial floods and the origin of low relief ice sheet lobes. *J. Glaciol.*, **38**(128), 105-112.

Shreve, R. L., 1972. Movement of water in glaciers. *J. Glaciol.*, **11**, 205-214.

Sigmarsson, O., Hemond, C., Condomines, M., Fourcade, S. and Oskarsson, N., 1991. Origin of silicic magma in Iceland revealed by Th isotopes. *Geology*, **19**, 621-624.

Sigurdsson, H., 1970a. *Petrology of the Setberg volcanic region and acid rocks of Iceland.* Unpubl. PhD Thesis. University of Durham.

Sigurdsson, H., 1970b. Structural origin and plate tectonics of the Snaefellsnes volcanic zone, western Iceland. *Earth Planet. Sci. Lett.*, **10**, 129-135.

Sigurdsson, H. and Sparks, R. S. J., 1981. Petrology of rhyolitic and mixed magma ejecta from the 1875 eruption of Askja, Iceland. *J. Petrology.* **22**, 41-84.

Sigvaldasson, G. E., 1968. Structure and products of subaquatic volcanoes in Iceland. *Contr. Mineral. Petrol.*, **18**, 1-16.

Simkin, T. and Smith, J.V.,1970. Minor element distribution in olivine. *J. Geol.* **78**, 304-325.

Skilling, I.P., 1994. Evolution of an englacial volcano: Brown Bluff Antarctica. *Bull. Volcanol.*, **56**, 573-591.

Sleep, N. H., 1990. Hotspots and mantle plumes: some phenomenology. *J. Geophys. Res.*, **95**, 6715-6736.

Smellie, J. L. and Skilling, I. P., 1994. Products of subglacial volcanic eruptions under different ice thicknesses: two examples from Antarctica. *Sediment. Geol.*, **91**, 115-129.

Smellie, J. L., Hole, M. J. & Nell, P. A. R., 1993. Late Miocene valley-confined subglacial volcanism in northern Alexander Island, Antarctic Peninsula. *Bull. Volcanol.*, **55**, 273-288.

Smith, G. A., 1986. Course-grained nonmarine volcaniclastic sediment: terminology and depositional process. *Geological Society of America Bulletin,* **97,** 1-10.

Sparks, R. S. J., 1976. Grain size variations in ignimbrites and implications for the transport of pyroclastic flows. *Sedimentology*, **23**, 147-188.

Sparks, R. S. J., Huppert, H. E., Koyaguchi, T. and Hallworth, M. a., 1993. Origin of modal and rhythmic igneous layering by sedimentation in a convecting magma chamber., *Nature*, **361**, 246-249.

Spry, A., 1962. The origin of columnar jointing, particularly in basalt flows. *Geol. Soc. Aust. Jour.*, **8 no.2**. 191-216.

Steinthorsson, S., 1964. The ankaramites of Hvammsmuli Eyjafjoll, southern Iceland. *Acta Naturalia Islandica,* Vol.2 No.4.

Steinthorsson, S., Okarsson, N. K. & Sigvaldason, G. E., 1985. Origin of alkali basalts in Iceland: A plate tectonic model. *J. Geophys. Res.*, **90,** 10027-10042.

Stolper, E. and Walker, D., 1980. Melt density and the average composition of basalt. *Contr. Mineral. Petrol.*, **74**, 7-12.

Sun, S-S. and McDonough, W. F., 1989. Chemical and isotopic systematics of oceanic basalts: implications for mantle composition and processes. In: Saunders, A. D. and Norry, M. J. (eds.) *Magmatism in the Ocean Basins. Geol. Soc. Spec. Publ.* **42**, 313-345.

Takada, A., 1988. Subvolcanic structure of the central dike swarm associated with the ring complexes in the Shitara district, central Japan. *Bull. Volcanol.*, **50**, 106-118.

Takada, A., 1994. Development of a subvolcanic structure by the interaction of liquid-filled cracks. *J. Volcanol. Geotherm. Res.*, **62**, 207-224.

Thorarinsson, S., 1965. Changes of the water-firn level in the Grimsvotn caldera 1954-1965. *Jokull*, **15**, 109-119.

Thorarinsson, S., 1969. Ignimbrit i Thorsmork. *Natt. fraed*, **39**, 139-155.

Thordarson, Th. and Self, S., 1993. The Laki (Skaftar Fires) and Grimsvotn eruptions in 1783-1785. *Bull. Volcanol.*, **55**, 233-263.

Thy, P., 1991a. High and low pressure phase equilibria of a mildly alkalic lava from the 1965 Surtsey eruption: Experimental results. *Lithos.*, **26,** 223-243.

Thy, P., 1991b. High and low pressure phase equilibria of a mildly alkalic lava from the 1965 Surtsey eruption : Implications for the evolution of mildly alkalic and transitional basalts in the south eastern propagating rift zone of Iceland. *Lithos.*, **26,** 253-269.

Thy, P., Beard, J. S. and Lofgren, G. E., 1990. Experimental constraints on the origin of Icelandic rhyolites. *J. Geol.*, **98,** 417-421.

Tilley, C. E., 1950. Some aspects of magmatic evolution. *Q. Jl. Geol. Soc. Lond.*, **106,** 37-61.

Tomkeieff, S. I., 1940. The basalt lavas of the Giant's Causeway district of northern Ireland. *Bull. Volcanol.*, **11 (6).** 89-143.

Turner, J. S. and Gustafson, L. B., 1981. Fluid motions and compositional gradients produced by crystallisation or melting at vertical boundaries. *J. Volcanol. Geotherm. Res.*, **11**, 93-125.

Wager, L. R. and Brown, G. M., 1967. *Layered Igneous Rocks*. London: Oliver & Boyd, 588pp.

Walker, C. L. 1992. The volcanic history and geochemical evolution of the Hveragerdi region, SW Iceland. Unpubl. PhD Thesis, University of Durham.

Walker, G. P. L., 1963. The Breiddalur central volcano eastern Iceland. *Quart. J. geol. Soc. Lond.* **119,** 29-63.

Walker, G. P. L., 1971. Compound and Simple Lava Flows and Flood Basalts. *Bull. Volcanol.*, **35**, 579-590.

Walker, G. P. L., 1978. Major and trace element variations in the Tertiary lavas of eastern Iceland and their significance with respect to the Iceland geochemical anomaly. *J. Petrology*. **19**, 392-436.

Walker, G. P. L. & Blake, D. H., 1966. The formation of a palagonite breccia mass beneath a valley glacier in Iceland. *Q Jl Geol Soc Lond,* **122**, 45-61.

Watson, E. B., 1979. Apatite saturation in basic to intermediate magmas. *Geophys. Res. Lett.* **6**, 937-940.

Watson, E. B., 1982. Basalt contamination by continental crust. some experiments and models. *Contr. Mineral. Petrol.*, **80**, 83-87.

Watson, E. B. and Green, T. H., 1981. Apatite/liquid partition coefficients for the rare earth elements and strontium. *Earth Planet. Sci. Lett.* **56**, 405-421.

Watson, E. B. and Jurewicz, S. R., 1984. Behaviour of alkalis during diffusive interaction of granitic xenoliths with basaltic magma. *J. Geol.*, **92**, 121-131.

Weertman, J. and Birchfield, G. E. 1983. Stability of sheet water flow under a glacier. *J. Glaciol.*, **29**, 374-384.

Wessel, P. and Smith, W. H. F., 1991. Free software helps map and display data. EOS *Trans. Am. Geophys. Un.* **72**, 441, 445-446.

White, R.S., Spence, G. D., Fowler, S. R.,McKenzie, D. P., Westbrook, G. K. & Bowen, A. N., 1987. Magmatism at rifted continental margins. *Nature*, **330**, 439-444.

Wiese, P. K., 1992. Geochemistry and geochronology of the Eyjafjoll Volcanic System. Unpubl. MSc Thesis, University of Oregon.

Wilkinson, J. F. G. and Hensel, H. D., 1988. The petrology of some picrites from Mauna Loa and Kilauea volcanoes, Hawaii. *Contrib. Mineral. Petrol.* **98**, 326-345.

Wood, D. A., 1978. Major and trace element variations in the Tertiary lavas of Eastern Iceland and their significance with respect to the Iceland geochemical anomaly. *J. Petrology.* **19**, 392-436.

Wood, D. A., 1981. Partial Melting models for the petrogenesis of Reykjanes Penisula basalts, Iceland: implications for the use of trace elements and strontium and neodynium isotope ratios to record inhomogeneities in the upper mantle, *Earth and Planetary Science Letters,* **52,** 183-190.

Wood, D. A., Gibson, I. L. and Thompson, R. N., 1976. Elemental mobility during zeolite-facies metamorphism of the Tertiary basalts of Eastern Iceland. *Contr. Mineral. Petrol.*, **55**, 241-253.

Wood, D. A., Joron, J. L., Treuil, M. Norry, M. and Tarney, J., 1979. Elemental and Sr isotope variations in basic lavas from Iceland and the surrounding ocean floor. *Contr. Miner. Petrol.* **70**, 319-339.

Zverev, S. M., Litvinenko, L. V., Palmason, G., Yaroshevskaya, G. A. & Osokin, N. M., 1980. A seismic crustal study of the axial rift zone in SW Iceland. *Journal of Geophys.* **47**, 202-210.

APPENDIX A

In this appendix, all the microprobe data obtained from the Manchester and Durham University electron microprobes will be presented.

Appendix A1 - Feldspar compositions.
Appendix A2 - Clinopyroxene compositions.
Appendix A3 - Olivine compositions.
Appendix A4 - FeTi oxide compositions.

APPENDIX A1 - FELDSPAR COMPOSITIONS

Sample no.
Feldspar compositions are arranged in order of sample number. Prefix 'L' to the sample signifies the sample is a lava; prefix 'D' indicates that the sample is an intrusive sheet; prefix 'H' indicates that the sample is a hyaloclastite glass. Grid references for each sample are given in Appendix B.

Strat. Gp.
Where appropriate, the stratigraphic Group (as defined in Chapter 4) to which the sample belongs is recorded.

Spot Ref.
This is the recorded reference number of each analysed point.

Phenocryst no.
Each analysed phenocryst was numbered. Microphenocrysts are described as 'mp'.

Position
The position of the analysed spot in relation to the crystal is recorded as:

IC - core of the phenocryst;
IM - mantle of the phenocryst;
IR - rim of the phenocryst; and
QG - quench groundmass crystals.

Sample No.	L8	L8	L8	L8	L8	L8	L8	L8	L8	L8	L8	L8	L8	D19	D19
Strat. Gp.	La	La	La	La	La	La	La	La	La	La	La	La	La		
Spot Ref.	3	4	5	8	9	10	11	24	25	26	27	28	32	8	3
Phenocryst No.	1	1	mp1	mp2	2	2	2	3	3	3	mp3	mp3		mp1	mp2
Position	IM	IC	IC	IC	IM	IC	IR	IC	IC	IM	IR	IC	QG	IC	IC
SiO2	47.74	47.73	47.09	46.75	46.71	47.81	47.18	46.80	45.91	45.87	46.87	47.30	46.64	59.35	56.30
Al2O3	32.97	32.89	33.94	33.64	33.54	33.01	33.16	32.16	32.37	32.87	31.16	33.20	32.14	26.32	25.87
FeO	0.67	0.79	0.59	0.64	0.63	0.56	0.70	0.56	0.61	0.61	0.65	0.81	0.70	0.57	0.66
MgO	0.28	0.38	0.41	0.35	0.42	0.43	0.38	0.29	0.34	0.33	0.32	0.48	0.32		
CaO	16.82	16.66	17.50	17.10	17.36	16.45	17.02	16.65	16.62	16.76	15.36	16.91	16.29	8.26	8.67
Na2O	1.98	2.18	1.78	1.72	1.58	2.28	1.93	2.00	1.81	1.70	2.45	1.94	2.03	7.06	6.25
K2O	0.00	0.00	0.00	0.00	0.00	0.00	0.00	0.00	0.00	0.00	0.00	0.00	0.00	0.27	0.17
TOTAL	100.44	100.63	101.32	100.19	100.24	100.54	100.39	98.47	97.64	98.13	96.80	100.64	98.12	101.82	97.91
O=8															
Si	2.19	2.18	2.14	2.15	2.15	2.19	2.17	2.19	2.17	2.15	2.22	2.17	2.19	2.62	2.58
Al	1.78	1.77	1.82	1.82	1.82	1.78	1.79	1.77	1.80	1.82	1.74	1.79	1.78	1.37	1.40
Fe	0.03	0.03	0.02	0.02	0.02	0.02	0.03	0.02	0.02	0.02	0.03	0.03	0.03	0.02	0.03
Ca	0.83	0.82	0.85	0.84	0.86	0.81	0.84	0.83	0.84	0.84	0.78	0.83	0.82	0.39	0.43
Na	0.18	0.19	0.16	0.15	0.14	0.20	0.17	0.18	0.17	0.16	0.23	0.17	0.18	0.60	0.56
K	0.00	0.00	0.00	0.00	0.00	0.00	0.00	0.00	0.00	0.00	0.00	0.00	0.00	0.02	0.01
Total	4.993	4.999	4.995	4.992	4.985	4.996	4.997	4.997	4.994	4.993	4.996	4.991	4.994	5.011	5.000
Or%	0.000	0.000	0.000	0.000	0.000	0.000	0.000	0.000	0.000	0.000	0.000	0.000	0.000	1.488	1.008
Ab%	17.604	19.169	15.567	15.400	14.094	20.086	17.068	17.859	16.451	15.531	22.406	17.199	18.351	59.854	56.015
An%	82.40	80.83	84.43	84.60	85.91	79.91	82.93	82.14	83.55	84.47	77.59	82.80	81.65	38.66	42.98

Sample No.	L25	L25	L25	L25	L33	L33	L33	L33	L33	L33	L33	L33	L33	L33	L58
Strat. Gp.	La	La	La	La	Se	Se	Se	Se	Se	Se	Se	Se	Se	Se	
Spot Ref.	25	26	29	30	36	37	44	50	51	52	55	56	57	60	1
Phenocryst No.	1	1	2	2	1	1		2	2	2	3	3	3		1
Position	IM	IM	IC	IM	IC	IR	QG	IR	IM	IC	IR	IM	IC	QG	IR
SiO2	47.57	47.04	47.31	46.38	50.08	48.74	51.76	47.41	47.31	47.49	53.93	49.67	49.33	54.76	54.67
Al2O3	32.30	32.90	33.49	33.71	31.07	32.40	29.72	31.99	32.20	32.25	27.31	30.93	30.60	26.40	28.60
FeO	0.81	0.61	0.82	0.60	0.70	0.62	0.68	0.68	0.69	0.64	0.82	0.62	0.69	0.82	0.82
MgO	0.55	0.31	0.44	0.35	0.29	0.35	0.28	0.25	0.41	0.31		0.25	0.33		
CaO	16.24	16.92	16.93	17.13	14.48	15.78	13.17	15.72	16.05	15.70	10.43	14.39	14.00	9.64	11.71
Na2O	2.26	1.88	1.78	1.83	3.10	2.46	4.04	2.19	2.31	2.44	5.45	3.27	3.30	5.40	5.06
K2O		0.00	0.00	0.00	0.11	0.00	0.11	0.00	0.00	0.00	0.17	0.00	0.10	0.19	0.15
TOTAL	99.74	99.66	100.77	99.99	99.82	100.33	99.76	98.24	98.97	98.99	98.31	99.13	98.54	97.38	101.18
O=8															
Si	2.20	2.17	2.16	2.14	2.29	2.23	2.36	2.21	2.20	2.20	2.48	2.29	2.29	2.54	2.45
Al	1.76	1.79	1.80	1.83	1.68	1.75	1.60	1.76	1.76	1.76	1.48	1.68	1.67	1.44	1.51
Fe	0.03	0.02	0.03	0.02	0.03	0.02	0.03	0.03	0.03	0.02	0.03	0.02	0.03	0.03	0.03
Ca	0.80	0.84	0.83	0.85	0.71	0.77	0.64	0.79	0.80	0.78	0.51	0.71	0.70	0.48	0.56
Na	0.20	0.17	0.16	0.16	0.28	0.22	0.36	0.20	0.21	0.22	0.49	0.29	0.30	0.49	0.44
K	0.00	0.00	0.00	0.00	0.01	0.00	0.01	0.00	0.00	0.00	0.01	0.00	0.01	0.01	0.01
Total	4.990	4.994	4.985	5.003	4.989	4.985	4.998	4.987	4.995	4.992	5.009	4.998	4.989	4.982	5.006
Or%	0.000	0.000	0.000	0.000	0.605	0.000	0.661	0.000	0.000	0.000	0.988	0.000	0.601	1.163	0.857
Ab%	20.119	16.766	16.008	16.205	27.755	21.960	35.459	20.108	20.655	21.907	48.138	29.122	29.706	49.778	43.507
An%	79.88	83.23	83.99	83.80	71.64	78.04	63.88	79.89	79.34	78.09	50.87	70.88	69.69	49.06	55.64

Sample No.	L58	L58	L58	L58	L58	L58	L58	L58	L58	L58	L68	L68	L68	L74	L74
Strat. Gp.														Hv	Hv
Spot Ref.	2	8	9	13	16	18	19	20	21	24	28	32	33	64	70
Phenocryst No.	1	2	2	3	mp1	mp2	mp3	mp4				mp1	mp1		
Position	IC	IM	IC	IR	IC	IC	IC	IC	QG	QG	QG	IR	IC	QG	QG
SIO2	48.06	47.46	46.79	49.46	48.96	48.06	46.85	47.38	50.67	53.75	50.68	52.70	50.92	50.18	52.95
AI2O3	33.76	32.41	32.63	31.60	31.96	32.64	31.61	32.73	30.28	27.87	28.60	27.10	29.23	30.58	28.91
FeO	0.76	0.78	0.66	0.59	0.77	0.64	0.89	0.68	0.85	0.75	0.98	1.19	0.91	1.13	0.83
MgO	0.53	0.37	0.50	0.46	0.37	0.39	0.44	0.40	0.35	0.27	0.25		0.38	0.54	0.27
CaO	17.15	16.64	16.62	15.19	15.60	16.21	15.89	16.60	13.82	11.51	12.84	10.85	13.10	13.56	12.20
Na2O	2.05	2.08	1.96	2.90	2.58	2.27	2.20	2.20	3.55	4.89	4.05	4.79	3.76	3.39	4.12
K2O	0.00	0.00	0.00	0.00	0.00	0.00	0.00	0.00	0.10	0.24	0.13	0.28	0.00	0.26	0.37
TOTAL	**102.30**	**99.74**	**99.17**	**100.20**	**100.23**	**100.21**	**98.01**	**99.98**	**99.63**	**99.28**	**97.70**	**97.17**	**98.48**	**100.16**	**99.65**
O=8															
SI	2.17	2.19	2.17	2.26	2.24	2.20	2.20	2.18	2.32	2.46	2.37	2.46	2.36	2.29	2.41
Al	1.79	1.76	1.79	1.70	1.72	1.76	1.75	1.78	1.64	1.50	1.58	1.49	1.60	1.65	1.55
Fe	0.03	0.03	0.03	0.02	0.03	0.02	0.04	0.03	0.03	0.03	0.04	0.05	0.04	0.04	0.03
Ca	0.83	0.82	0.83	0.74	0.77	0.80	0.80	0.82	0.68	0.56	0.64	0.54	0.65	0.66	0.60
Na	0.18	0.19	0.18	0.26	0.23	0.20	0.20	0.20	0.32	0.43	0.37	0.43	0.34	0.30	0.36
K	0.00	0.00	0.00	0.00	0.00	0.00	0.01	0.00	0.01	0.01	0.01	0.02	0.00	0.02	0.02
Total	4.992	4.995	4.988	4.986	4.987	4.990	4.997	5.000	4.994	4.998	5.002	4.997	4.976	4.966	4.983
Or%	**0.000**	**0.000**	**0.000**	**0.000**	**0.000**	**0.000**	**0.760**	**0.000**	**0.599**	**1.385**	**0.786**	**1.676**	**0.000**	**1.564**	**2.172**
Ab%	**17.754**	**18.428**	**17.629**	**25.683**	**23.012**	**20.207**	**19.921**	**19.363**	**31.558**	**42.862**	**36.039**	**43.681**	**34.211**	**30.670**	**37.122**
An%	**82.25**	**81.57**	**82.37**	**74.32**	**76.99**	**79.79**	**79.32**	**80.64**	**67.84**	**55.75**	**63.18**	**54.64**	**65.79**	**67.77**	**60.71**

Sample No.	L74	L74	L74	L74B	L74B	L74B	L74B	L74B	L74B	L74B	L74B	L74B	L81	L81	L81
Strat. Gp.	Hv	Hv	Hv	Hv	Hv	Hv	Hv	Hv	Hv	Hv	Hv	Hv			
Spot Ref.	85	86	87	43	44	45	46	47	48	50	51	55	3	4	5
Phenocryst No.		1	1	6	6	6	6	6	6	6	6	gmv	1	1	2
Position	QG	IR	IC	IC	IC	IM	IM	IM	IM	IR	IR	QG	IC	IM	IC
SIO2	54.21	46.70	47.01	45.81	46.58	45.12	44.87	49.37	51.33	50.33	53.04	49.37	47.15	47.26	55.61
Al2O3	28.30	33.89	33.81	32.89	32.23	32.77	33.51	29.67	29.40	29.20	26.63	29.28	32.04	32.59	26.58
FeO	0.67	0.60	0.61	0.68	0.85	0.73	0.53	0.67	0.41	0.77	0.74	0.93	0.60	0.78	0.54
MgO		0.37	0.29	0.11	0.13		0.16	0.00	0.06	0.00	0.06	0.08	0.31	0.48	0.00
CaO	11.09	17.36	17.60	17.30	16.58	17.01	17.44	13.66	13.19	12.84	10.16	13.32	16.11	16.49	9.52
Na2O	4.60	1.56	1.59	1.70	1.89	1.35	1.47	3.53	3.79	3.67	5.14	3.45	2.30	2.09	5.56
K2O	0.86	0.00	0.00	0.08	0.02	0.03	0.00	0.20	0.16	0.24	0.54	0.17	0.00	0.00	0.37
TOTAL	99.72	100.47	100.91	98.72	98.31	97.15	98.06	97.44	98.65	97.15	96.56	96.88	98.51	99.69	98.17
O=8															
Si	2.47	2.14	2.15	2.14	2.18	2.14	2.11	2.32	2.37	2.36	2.49	2.33	2.20	2.18	2.55
Al	1.52	1.83	1.82	1.81	1.78	1.83	1.86	1.64	1.60	1.61	1.47	1.63	1.76	1.77	1.44
Fe	0.03	0.02	0.02	0.03	0.03	0.03	0.02	0.03	0.02	0.03	0.03	0.04	0.02	0.03	0.02
Ca	0.54	0.85	0.86	0.87	0.83	0.87	0.88	0.69	0.65	0.65	0.51	0.67	0.81	0.82	0.47
Na	0.41	0.14	0.14	0.15	0.17	0.12	0.13	0.32	0.34	0.33	0.47	0.32	0.21	0.19	0.49
K	0.05	0.00	0.00	0.00	0.00	0.00	0.00	0.01	0.01	0.01	0.03	0.01	0.00	0.00	0.02
Total	5.004	4.987	4.993	5.013	5.001	4.997	5.008	5.01	4.984	4.999	5.002	4.996	5.000	4.991	4.991
Or%	4.988	0.000	0.000	0.455	0.100	0.168	0.000	1.208	0.933	1.409	3.199	1.034	0.000	0.000	2.202
Ab%	40.710	13.959	14.005	15.032	17.054	12.538	13.215	31.495	33.877	33.624	46.240	31.554	20.520	18.671	50.237
An%	54.30	86.04	85.99	84.51	82.85	87.29	86.79	67.30	65.19	64.97	50.56	67.41	79.48	81.33	47.56

Sample No.	L81	L81	L81	L81	L81	L98	L98	L98	L98	L98	L121	L121	L121	L121	L121
Strat. Gp.						La2	La2	La2	La2	La2	LI	LI	LI	LI	LI
Spot Ref.	6	7	8	9	15	4	5	10	12	13	3	4	5	6	7
Phenocryst No.	2	2	mp1	mp2	mp3	1	1	2		3	1	1	1	mp1	mp1
Position	IR	IM	IR	IR	IC	IM	IC	IR	QG	IC	IR	IM	IC	IC	IC
SiO2	53.28	56.39	52.89	53.03	54.42	47.67	47.32	51.54	51.68	48.61	56.15	49.27	50.79	47.89	47.75
Al2O3	27.71	26.26	27.90	27.71	28.28	32.95	32.71	29.85	29.75	32.57	26.93	31.86	30.35	32.47	32.69
FeO	0.74	0.52	0.73	0.85	0.90	0.82	0.71	0.91	1.07	0.72	0.88	0.64	0.74	0.68	0.76
MgO	0.35	0.00	0.27	0.24	0.00	0.29	0.26	0.33	0.40	0.39	0.36	0.26	0.00	0.00	0.00
CaO	11.11	9.09	11.43	11.24	11.51	16.69	16.50	13.42	13.09	16.09	9.73	15.42	13.82	0.36	0.26
Na2O	4.77	5.88	4.57	4.69	4.87	2.11	2.11	3.95	3.86	2.49	6.01	2.86	3.56	16.16	16.40
K2O	0.19	0.29	0.18	0.18	0.20	0.00	0.00	0.12	0.19	0.00	0.32	0.00	0.13	2.53	2.22
TOTAL	98.39	98.63	97.97	98.09	100.27	100.53	98.79	100.30	100.04	100.88	100.55	100.30	99.40	100.09	100.08
O=8															
Si	2.45	2.57	2.45	2.45	2.46	2.18	2.18	2.35	2.36	2.21	2.52	2.25	2.33	2.20	2.19
Al	1.50	1.41	1.52	1.51	1.51	1.78	1.78	1.60	1.60	1.75	1.43	1.72	1.64	1.76	1.77
Fe	0.03	0.02	0.03	0.03	0.03	0.03	0.03	0.03	0.04	0.03	0.03	0.02	0.03	0.03	0.03
Ca	0.55	0.44	0.57	0.56	0.56	0.82	0.82	0.66	0.64	0.79	0.47	0.76	0.68	0.80	0.81
Na	0.43	0.52	0.41	0.42	0.43	0.19	0.19	0.35	0.34	0.22	0.52	0.25	0.32	0.23	0.20
K	0.01	0.02	0.01	0.01	0.01	0.00	0.00	0.00	0.01	0.00	0.02	0.00	0.01	0.00	0.00
Total	4.973	4.979	4.984	4.981	5.001	5.000	4.994	4.987	4.991	4.995	4.996	5.000	5.009	5.008	5.001
Or%	1.149	1.701	1.114	1.047	1.172	0.000	0.000	0.000	1.108	0.000	1.813	0.000	0.763	0.000	0.000
Ab%	43.258	53.027	41.492	42.539	42.852	18.582	18.812	34.718	34.419	21.883	51.846	25.124	31.575	22.070	19.715
An%	55.59	45.27	57.39	56.41	55.98	81.42	81.19	65.28	64.47	78.12	46.34	74.88	67.66	77.93	80.28

Sample No.	L121	L121	L121	L121	L121	L121	L121	L121	L121	L121	L121	L121	D131	D131	D131
LI	LI	LI	LI	LI	LI	LI	LI	LI	LI	LI	LI	LI	Sv	Sv	Sv
Spot Ref.	8	9	12	13	14	15	19	20	21	22	25	27	22	25	26
Phenocryst No.	mp1	mp1	mp2	mp2	2	2	mp3	mp3	mp4	3			mp1	1	1
Position	IC	IC	IR	IC	IR	IC	IR	IR	IR	IR	QG	QG	IC	IR	IC
SIO2	47.09	48.11	49.94	47.20	49.59	48.84	50.67	51.83	51.70	47.37	54.86	54.45	48.74	51.39	48.05
Al2O3	32.73	32.08	31.28	32.18	30.44	31.98	30.93	29.49	29.46	32.43	26.94	27.38	31.86	30.05	32.32
FeO	0.72	0.60	0.76	0.84	0.72	0.72	0.72	0.64	0.74	0.52	1.09	0.68	0.64	0.83	0.68
MgO	0.00	0.21	0.35	0.30	0.00	0.29	0.31	0.33	0.24	0.31	0.33	0.32	0.33	0.30	0.29
CaO	16.69	15.84	14.60	16.14	14.24	15.57	13.91	12.88	12.82	16.09	9.83	10.35	15.37	13.24	15.98
Na2O	2.01	2.44	3.18	2.30	3.09	2.81	3.47	4.02	3.92	2.13	5.52	5.34	2.70	3.88	2.37
K2O	0.00	0.00	0.00	0.00	0.00	0.00	0.12	0.10	0.17	0.00	0.27	0.31	0.00	0.09	0.00
TOTAL	99.39	99.43	100.11	98.95	98.07	100.21	100.12	99.29	99.29	98.84	99.10	99.03	99.63	100.01	99.69
O=8															
Si	2.18	2.22	2.28	2.20	2.31	2.24	2.31	2.38	2.37	2.20	2.51	2.49	2.24	2.34	2.21
Al	1.79	1.75	1.68	1.76	1.67	1.73	1.66	1.59	1.59	1.78	1.45	1.47	1.73	1.62	1.75
Fe	0.03	0.02	0.03	0.03	0.03	0.03	0.03	0.02	0.03	0.02	0.04	0.03	0.02	0.03	0.03
Ca	0.83	0.78	0.72	0.80	0.71	0.76	0.68	0.63	0.63	0.80	0.48	0.51	0.76	0.65	0.79
Na	0.18	0.22	0.28	0.21	0.28	0.25	0.31	0.36	0.35	0.19	0.49	0.47	0.24	0.34	0.21
K	0.00	0.00	0.00	0.00	0.00	0.00	0.01	0.01	0.01	0.00	0.02	0.02	0.00	0.01	0.00
Total	5.004	4.991	4.992	5.005	4.995	5.005	4.994	4.987	4.979	4.987	4.982	4.986	4.993	4.987	4.995
Or%	0.000	0.000	0.000	0.000	0.000	0.000	0.671	0.603	1.012	0.000	1.589	1.837	0.000	0.536	0.000
Ab%	17.851	21.823	28.237	20.487	28.186	24.622	30.883	35.867	35.256	19.281	49.611	47.395	24.166	34.461	21.186
An%	82.15	78.18	71.76	79.51	71.81	75.38	68.45	63.53	63.73	80.72	48.80	50.77	75.83	65.00	78.81

Sample No.	D131	D131	D131	D131	D131	D131	L134	L134	L134	L134	L134	L134	L134	L134	L134
Strat. Gp.	Sv	Sv	Sv	Sv	Sv	Sv	Sv	Sv	Sv	Sv	Sv	Sv	Sv	Sv	Sv
Spot Ref.	29	30	31	32	33	34	92	93	94	96	97	98	100	101	102
Phenocryst No.	2	2	3	4	4	mp	1	1	1	2	2	2		3	3
Position	IR	IC	IC	IR	IC	IC	IM	IM	IC	IR	IM	IC	QG	IR	IR
SIO2	52.57	50.78	49.36	50.06	49.02	49.95	47.64	48.47	48.57	49.20	49.35	47.59	51.18	52.18	49.38
Al2O3	30.48	32.62	32.54	31.89	33.34	32.54	33.51	32.74	32.86	32.20	31.79	33.43	30.95	30.34	32.20
FeO	0.83	0.77	0.81	0.81	0.49	0.72	0.74	0.59	0.87	0.68	0.59	0.67	0.63	0.83	0.89
MgO	0.41	0.44	0.26	0.32	0.42	0.37	0.25	0.39	0.46	0.31	0.40	0.29	0.38	0.42	0.38
CaO	13.75	15.48	16.15	15.38	16.32	15.53	16.84	16.22	16.26	15.78	15.48	17.13	14.39	13.44	15.65
Na2O	3.94	2.88	2.68	2.87	2.35	2.69	2.13	2.32	2.38	2.55	2.93	1.97	3.40	3.98	2.78
K2O	0.00	0.00	0.00	0.10	0.00	0.00	0.00	0.00	0.00	0.00	0.00	0.00	0.10	0.00	0.00
TOTAL	101.98	102.97	101.79	101.43	102.11	101.80	101.11	100.73	101.39	101.09	100.53	101.08	101.04	101.18	101.28
O=8															
Si	2.35	2.26	2.23	2.26	2.20	2.25	2.17	2.21	2.20	2.23	2.25	2.17	2.31	2.35	2.24
Al	1.61	1.71	1.73	1.70	1.77	1.73	1.80	1.76	1.76	1.72	1.71	1.80	1.65	1.61	1.72
Fe	0.03	0.03	0.03	0.03	0.02	0.03	0.03	0.02	0.03	0.03	0.02	0.03	0.02	0.03	0.03
Ca	0.66	0.74	0.78	0.75	0.79	0.75	0.82	0.79	0.79	0.77	0.76	0.84	0.70	0.65	0.76
Na	0.34	0.25	0.23	0.25	0.21	0.23	0.19	0.21	0.21	0.22	0.26	0.17	0.30	0.35	0.24
K	0.00	0.00	0.00	0.01	0.00	0.00	0.00	0.00	0.00	0.00	0.00	0.00	0.01	0.00	0.00
Total	4.989	4.982	5.006	4.995	4.978	4.983	5.007	4.988	4.993	4.976	4.997	5.000	4.988	4.989	4.998
Or%	0.000	0.000	0.000	0.566	0.000	0.000	0.000	0.000	0.000	0.000	0.000	0.000	0.566	0.000	0.000
Ab%	34.122	25.194	23.079	25.083	20.693	23.872	18.614	20.555	20.967	22.633	25.484	17.195	29.770	34.873	24.328
An%	65.88	74.81	76.92	74.35	79.31	76.13	81.39	79.45	79.03	77.37	74.52	82.81	69.66	65.13	75.67

Sample No.	D169	D169	D169	D169	D169	D169	D169	D189	D189	D189	D189	D189	L190	L190	L190
Strat. Gp.													Nd	Nd	Nd
Spot Ref.	1	4	5	6	7	8	9	1	2	3	6	8	1	2	3
Phenocryst No.	mp1	mp2	1	1	2	3	3	1	1	mp1	2	mp2	1	1	1
Position	IR	IC	IR	IC	IC	IR	IC	IC	IR	IC	IC	IC	IR	Im	IM
SIO2	62.59	60.54	61.54	61.46	58.83	62.52	63.15	62.37	61.83	60.92		61.00	49.68	52.48	52.58
Al2O3	24.22	24.77	24.36	24.71	26.57	24.22	24.30	23.66	23.61	24.08		24.94	31.00	29.83	29.79
FeO	0.29	0.43	0.31	0.39	0.37	0.43	0.31	0.37	0.43	0.39		0.45	0.80	0.84	0.56
MgO	0.00	0.00	0.00	0.00	0.00	0.00	0.00	0.00	0.00	0.00	0.00	0.00	0.22	0.21	0.28
CaO	5.25	6.68	6.18	6.15	8.60	5.59	5.42	5.45	5.53	5.98		6.73	14.76	12.90	12.81
Na2O	8.33	7.78	7.80	7.89	6.67	8.11	8.03	8.32	8.07	7.99		7.63	3.17	4.07	4.16
K2O	0.49	0.29	0.37	0.45	0.26	0.45	0.50	0.59	0.51	0.50		0.42	0.00	0.11	0.13
TOTAL	101.27	100.49	100.55	101.05	101.30	101.31	101.71	100.75	99.98	99.85		101.19	99.63	100.60	100.31
O=8															
Si	2.75	2.69	2.72	2.71	2.60	2.74	2.75	2.75	2.75	2.72	2.73	2.69	2.28	2.37	2.38
Al	1.25	1.30	1.27	1.28	1.39	1.25	1.25	1.23	1.24	1.27	1.25	1.30	1.68	1.59	1.59
Fe	0.01	0.02	0.01	0.01	0.01	0.02	0.01	0.01	0.02	0.01	0.02	0.02	0.03	0.03	0.02
Ca	0.25	0.32	0.29	0.29	0.41	0.26	0.25	0.26	0.26	0.29	0.28	0.32	0.73	0.63	0.62
Na	0.71	0.67	0.67	0.67	0.57	0.69	0.68	0.71	0.70	0.69	0.71	0.65	0.28	0.36	0.37
K	0.03	0.02	0.02	0.03	0.02	0.03	0.03	0.03	0.03	0.03	0.03	0.02	0.00	0.01	0.01
Total	4.996	5.006	4.987	4.998	4.998	4.989	4.975	5.002	4.993	5.007	5.014	5.000	5.003	4.986	4.990
Or%	2.768	1.627	2.103	2.525	1.508	2.557	2.883	3.291	2.934	2.817	2.722	2.411	0.000	0.607	0.737
Ab%	71.742	66.722	68.114	68.114	57.487	70.576	70.754	71.011	70.388	68.744	69.367	65.606	28.005	36.131	36.784
An%	25.49	31.65	29.78	29.36	41.01	26.87	26.36	25.70	26.68	28.44	27.91	31.98	71.99	63.26	62.48

Sample No.	L190	L190	L190	L190	L190	L190	L190	L205	L205	L205	L215	L215	L215	L215	L215
Strat. Gp.	Nd	Nd	Nd	Nd	Nd	Nd	Nd	Nd	Nd	Nd	w.slopes	w.slopes	w.slopes	w.slopes	w.slopes
Spot Ref.	4	5	6	7	12	13	15	2	7	17	6	7	8	9	10
Phenocryst No.	1	1	1	1	2	2	3	1	1	1		1	2	2	3
Position	IM	IC	IC	IC	IR	IC	IC	IC	IC	IC	QG	IR	IC	IM	IR
SiO2	52.58	47.32	47.83	47.44	47.51	46.93	58.47	53.29	48.62	51.77	57.33	55.57	56.32	55.05	57.70
Al2O3	28.90	32.56	33.00	32.79	32.30	32.07	25.71	29.80	33.57	30.20	26.06	26.90	27.14	27.31	25.68
FeO	0.72	0.68	0.54	0.46	0.68	0.67	0.42	0.96	0.72	0.65	0.58	0.33	0.44	0.47	0.52
MgO	0.20	0.21	0.33	0.24	0.26	0.20	0.00	0.00	0.34	0.00	0.00	0.00	0.00	0.00	0.00
CaO	12.29	16.41	16.40	16.34	16.24	16.19	7.64	12.56	17.12	13.52	8.75	9.60	9.60	10.10	8.05
Na2O	4.45	2.11	2.26	2.19	2.27	2.20	6.97	4.34	2.18	3.81	6.35	5.68	5.87	5.48	6.53
K2O	0.09	0.00	0.00	0.00	0.00	0.09	0.35	0.32	0.00	0.23	0.20	0.19	0.19	0.16	0.26
TOTAL	**99.39**	**99.30**	**100.36**	**99.47**	**99.26**	**98.34**	**99.56**	**101.28**	**102.54**	**100.38**	**99.26**	**98.42**	**99.71**	**98.56**	**98.74**
O=8															
Si	2.40	2.19	2.19	2.19	2.20	2.20	2.63	2.40	2.18	2.35	2.59	2.54	2.54	2.52	2.62
Al	1.56	1.78	1.78	1.79	1.76	1.77	1.36	1.58	1.78	1.62	1.39	1.45	1.44	1.47	1.37
Fe	0.03	0.03	0.02	0.02	0.03	0.03	0.02	0.04	0.03	0.02	0.02	0.01	0.02	0.02	0.02
Ca	0.60	0.81	0.80	0.81	0.81	0.81	0.37	0.61	0.82	0.66	0.42	0.47	0.46	0.49	0.39
Na	0.39	0.19	0.20	0.19	0.20	0.20	0.61	0.38	0.19	0.34	0.56	0.50	0.51	0.49	0.57
K	0.01	0.00	0.00	0.00	0.00	0.01	0.02	0.02	0.00	0.01	0.01	0.01	0.01	0.01	0.02
Total	4.991	4.999	4.997	4.996	5.001	5.007	5.003	5.013	5.001	5.001	4.996	4.984	4.990	4.995	4.991
Or%	0.532	0.000	0.000	0.000	0.000	0.525	2.009	1.864	0.000	1.323	1.142	1.084	1.113	0.943	1.564
Ab%	39.368	18.864	19.934	19.295	20.172	19.613	60.998	37.737	18.690	33.344	56.097	51.135	51.955	49.057	58.566
An%	60.10	81.14	80.07	80.71	79.83	79.86	36.99	60.40	81.31	65.33	42.76	47.78	46.93	50.00	39.87

Sample No.	L215	L215	L221	L221	L221	L221	L221	L221	L221	L221	L221	L221	L221	L221	L221
Strat. Gp.	w.slopes	w.slopes													
Spot Ref.	11	12	1	2	5	9	10	11	12	13	14	15	16	17	18
Phenocryst No.	3	3	1	1	2	3	3	3	4	4	mp1	4	4	4	4
Position	IC	IM	IR	IM	IC	IR	IM	IM	IR	IM	IC	IR	IM	IM	IC
SIO2	50.41	49.86	54.29	47.18	48.96	52.41	53.87	53.27	52.77	47.73	48.41	52.74	47.15	48.32	47.78
AI2O3	31.16	30.87	28.35	32.78	31.53	29.07	28.37	28.34	28.52	31.67	32.46	28.58	32.79	31.49	32.44
FeO	0.53	0.58	0.85	0.46	0.64	0.81	0.53	0.66	0.72	0.78	0.92	0.57	0.83	0.72	0.78
MgO	0.24	0.00	0.00	0.21	0.35	0.26	0.38	0.00	0.00	0.22	0.35	0.00	0.24	0.00	0.37
CaO	14.10	14.15	11.39	16.71	15.19	12.11	10.96	11.13	11.66	15.79	15.99	11.80	16.49	15.45	15.92
Na2O	3.29	3.49	4.86	1.98	3.10	4.33	4.98	4.89	4.59	2.47	2.49	4.56	2.10	2.62	2.44
K2O	0.09	0.00	0.17	0.00	0.00	0.18	0.11	0.19	0.20	0.00	0.00	0.11	0.00	0.00	0.00
TOTAL	**99.83**	**98.96**	**99.91**	**99.33**	**99.80**	**99.17**	**99.20**	**98.48**	**98.45**	**98.65**	**100.62**	**98.36**	**99.60**	**98.59**	**99.73**
O=8															
SI	2.30	2.30	2.46	2.18	2.25	2.40	2.46	2.45	2.43	2.22	2.21	2.43	2.18	2.25	2.20
AI	1.68	1.68	1.52	1.79	1.71	1.57	1.52	1.54	1.55	1.74	1.75	1.55	1.79	1.73	1.76
Fe	0.02	0.02	0.03	0.02	0.02	0.03	0.02	0.03	0.03	0.03	0.04	0.02	0.03	0.03	0.03
Ca	0.69	0.70	0.55	0.83	0.75	0.59	0.54	0.55	0.58	0.79	0.78	0.58	0.82	0.77	0.79
Na	0.29	0.31	0.43	0.18	0.28	0.38	0.44	0.44	0.41	0.22	0.22	0.41	0.19	0.24	0.22
K	0.01	0.00	0.01	0.00	0.00	0.01	0.01	0.01	0.01	0.00	0.00	0.01	0.00	0.00	0.00
Total	4.990	5.015	4.999	4.997	5.009	4.992	4.981	5.006	5.005	5.004	4.999	5.000	5.005	5.007	5.000
Or%	**0.540**	**0.000**	**0.976**	**0.000**	**0.000**	**1.044**	**0.679**	**1.105**	**1.170**	**0.000**	**0.000**	**0.669**	**0.000**	**0.000**	**0.000**
Ab%	**29.541**	**30.840**	**43.170**	**17.676**	**26.977**	**38.848**	**44.822**	**43.804**	**41.090**	**22.024**	**21.960**	**40.863**	**18.787**	**23.459**	**21.732**
An%	**69.92**	**69.16**	**55.85**	**82.32**	**73.02**	**60.11**	**54.50**	**55.09**	**57.74**	**77.98**	**78.04**	**58.47**	**81.21**	**76.54**	**78.27**

Sample No.	L251	L251	L255	L255	L255	L255	L255	L255	L255	L255	L255	L255	L255	L255	L255
Strat. Gp.	Nd	Nd													
Spot Ref.	10	14	4	5	6	7	8	9	10	11	12	13	18	19	20
Phenocryst No.	mp1	mp2	1	1	1	1	1	1	1	1	1	1	2	2	2
Position	GM	QG	IM	IM	IR	IM	IM	IM	IM	IM	IC	IC	IR	IR	IM
SIO2	54.82	65.40	47.98	48.74	53.37	49.80	48.59	51.23	48.09	48.03	48.86	47.61	50.88	51.96	48.72
Al2O3	27.98	19.61	32.98	33.02	29.70	31.69	32.95	31.97	33.52	33.80	33.43	33.50	30.74	29.67	32.48
FeO	0.78	0.39	0.51	1.21	0.95	0.56	0.61	0.72	0.60	0.57	0.46	0.66	0.75	0.68	0.57
MgO	0.20	0.00	0.00	0.36	0.33	0.26	0.38	0.45	0.28	0.21	0.32	0.31	0.27	0.00	0.35
CaO	10.84	1.14	16.47	15.91	12.67	15.39	16.19	14.71	16.79	17.35	16.69	17.10	14.39	12.88	15.77
Na2O	5.35	6.45	2.11	2.51	4.33	2.94	2.31	3.37	2.12	1.86	2.44	2.00	3.42	4.00	2.61
K2O	0.26	6.42	0.00	0.00	0.20	0.00	0.00	0.00	0.00	0.00	0.00	0.00	0.00	0.00	0.11
TOTAL	100.23	99.62	100.04	102.00	101.76	100.63	101.04	102.62	101.39	101.82	102.20	101.18	100.62	99.19	100.62
O=8															
Si	2.48	2.94	2.20	2.20	2.39	2.27	2.21	2.28	2.18	2.17	2.20	2.17	2.31	2.38	2.22
Al	1.49	1.04	1.78	1.76	1.57	1.70	1.76	1.68	1.79	1.80	1.77	1.80	1.65	1.60	1.75
Fe	0.03	0.01	0.02	0.05	0.04	0.02	0.02	0.03	0.02	0.02	0.02	0.03	0.03	0.03	0.02
Ca	0.53	0.06	0.81	0.77	0.61	0.75	0.79	0.70	0.82	0.84	0.80	0.83	0.70	0.63	0.77
Na	0.47	0.56	0.19	0.22	0.38	0.26	0.20	0.29	0.19	0.16	0.21	0.18	0.30	0.36	0.23
K	0.02	0.37	0.00	0.00	0.01	0.00	0.00	0.00	0.00	0.00	0.00	0.00	0.00	0.00	0.01
Total	5.006	4.987	5.001	4.991	4.986	4.997	4.986	4.983	4.997	4.997	5.003	5.001	4.988	4.996	4.999
Or%	1.488	37.365	0.000	0.000	1.172	0.000	0.000	0.000	0.000	0.000	0.000	0.000	0.000	0.000	0.628
Ab%	46.446	57.061	18.817	22.211	37.776	25.677	20.511	29.319	18.596	16.274	20.944	17.502	30.050	35.955	22.917
An%	52.07	5.57	81.18	77.79	61.05	74.32	79.49	70.68	81.40	83.73	79.06	82.50	69.95	64.04	76.46

Sample No.	L255	L255	L255	L255	L255	L255	L256	L256	L256	L256	L256	L256	L256	L256	L270
Strat. Gp.															
Spot Ref.	21	22	23	29	32	34	4	7	12	14	15	16	18	21	1
Phenocryst No.	2	2	2	3	4		1	mp	mp	2	3	3	4		mpl
Position	IM	IC	IC	IC	IC	QG	IC	IC	IR	IR	IC	IM	IC	QG	IC
SiO2	49.47	48.63	48.62	47.45	53.22	52.49	51.80	51.06	51.02	50.97	49.50	49.78	50.48	50.61	55.01
Al2O3	32.21	33.41	33.21	32.34	29.33	29.87	30.17	30.04	30.29	29.72	31.12	30.80	29.81	29.17	27.50
FeO	0.75	0.72	0.77	0.52	0.72	0.83	0.71	0.65	0.83	0.71	0.64	0.65	0.78	0.81	0.88
MgO	0.22	0.33	0.24	0.22	0.36	0.30	0.22	0.26	0.00	0.00	0.00	0.25	0.28	0.00	0.00
CaO	15.60	16.66	16.79	16.03	12.08	12.89	13.33	13.57	13.66	13.29	14.63	14.48	13.38	12.82	10.59
Na2O	2.79	2.31	2.27	2.22	4.62	4.20	3.78	3.77	3.61	3.77	3.18	3.26	3.60	4.00	5.43
K2O	0.00	0.00	0.00	0.00	0.21	0.17	0.20	0.13	0.14	0.00	0.00	0.00	0.15	0.22	0.27
TOTAL	101.04	102.05	101.91	98.77	100.54	100.96	100.20	99.49	99.56	98.67	99.07	99.23	98.48	97.63	99.87
O=8															
Si	2.25	2.19	2.20	2.21	2.41	2.37	2.36	2.34	2.34	2.35	2.29	2.29	2.34	2.36	2.49
Al	1.72	1.78	1.77	1.77	1.56	1.59	1.62	1.62	1.64	1.62	1.69	1.67	1.63	1.61	1.47
Fe	0.03	0.03	0.03	0.02	0.03	0.03	0.03	0.03	0.03	0.03	0.02	0.03	0.03	0.03	0.03
Ca	0.76	0.80	0.81	0.80	0.58	0.62	0.65	0.67	0.67	0.66	0.72	0.72	0.66	0.64	0.51
Na	0.25	0.20	0.20	0.20	0.40	0.37	0.33	0.34	0.32	0.34	0.29	0.29	0.32	0.36	0.48
K	0.00	0.00	0.00	0.00	0.01	0.01	0.01	0.01	0.01	0.00	0.00	0.00	0.01	0.01	0.02
Total	5.001	5.000	5.004	4.995	4.996	4.990	4.994	5.000	5.007	4.993	5.011	4.998	4.994	5.020	5.005
Or%	0.000	0.000	0.000	0.000	1.166	0.967	1.174	0.759	0.833	0.000	0.000	0.000	0.903	1.310	1.555
Ab%	24.436	20.040	19.677	20.040	40.406	36.700	33.501	33.179	32.089	33.936	28.255	28.950	32.441	35.604	47.403
An%	75.56	79.96	80.32	79.96	58.43	62.33	65.33	66.06	67.08	66.06	71.74	71.05	66.66	63.09	51.04

Sample No.	L270	L270	L270	L270	L270	L270	L270	L270	L270	L270	L270	L270	L270	L296	L296
Strat. Gp.														St	St
Spot Ref.	2	6	7	8	9	10	11	12	13	14	15	18	19	2	3
Phenocryst No.	mp1	mp2	1	2	2	3	3	3	3	3	3	4	4	1	1
Position	IR	IR	IR	IM	IC	IR	IC	IC	IC	IM	IR	IC	IR	IC	IC
SiO2	59.28	55.09	52.18	53.23	51.19	55.66	62.84	60.78	62.81	57.55	54.42	58.36	55.45	46.49	46.89
Al2O3	25.82	27.93	29.65	28.92	30.33	27.34	23.62	24.62	23.32	26.26	28.06	25.90	27.35	32.72	33.19
FeO	0.50	0.85	0.93	0.71	0.65	0.77	0.27	0.47	0.35	0.76	0.90	0.43	0.80	0.62	0.56
MgO	0.00	0.25	0.23	0.00	0.00	0.00	0.00	0.00	0.00	0.00	0.00	0.00	0.00	0.00	0.43
CaO	7.79	10.77	12.72	11.88	13.62	9.92	5.27	6.35	4.59	8.71	11.00	8.18	10.21	16.84	16.86
Na2O	6.78	5.51	4.43	4.68	3.75	5.77	7.94	7.44	8.23	6.37	4.94	6.68	5.58	1.83	1.92
K2O	0.40	0.25	0.19	0.12		0.31	0.56	0.79	0.60	0.55	0.31	0.28	0.32	0.00	0.00
TOTAL	100.57	100.86	100.32	99.54	99.54	99.78	100.49	100.45	99.89	100.19	99.63	99.84	99.87	98.49	99.85
O=8															
Si	2.64	2.48	2.37	2.43	2.34	2.52	2.77	2.70	2.79	2.59	2.47	2.62	2.51	2.17	2.16
Al	1.35	1.48	1.59	1.55	1.64	1.46	1.23	1.29	1.22	1.39	1.50	1.37	1.46	1.80	1.80
Fe	0.02	0.03	0.04	0.03	0.02	0.03	0.01	0.02	0.01	0.03	0.03	0.02	0.03	0.02	0.02
Ca	0.37	0.52	0.62	0.58	0.67	0.48	0.25	0.30	0.22	0.42	0.54	0.39	0.50	0.84	0.83
Na	0.59	0.48	0.39	0.41	0.33	0.51	0.68	0.64	0.71	0.56	0.44	0.58	0.49	0.17	0.17
K	0.02	0.01	0.01	0.01	0.00	0.02	0.03	0.05	0.03	0.03	0.02	0.02	0.02	0.00	0.00
Total	4.989	5.000	5.018	5.007	5.005	5.014	4.970	4.997	4.976	5.012	5.001	4.995	5.003	5.009	4.993
Or%	2.315	1.383	1.077	0.700	0.000	1.789	3.299	4.552	3.544	3.148	1.819	1.615	1.827	0.000	0.000
Ab%	59.755	47.415	38.251	41.306	33.245	50.364	70.729	64.869	73.732	55.169	44.022	58.681	48.837	16.446	17.114
An%	37.93	51.20	60.67	57.99	66.76	47.85	25.97	30.58	22.72	41.68	54.16	39.70	49.34	83.55	82.89

Sample No.	L296	L296	L296	L296	L296	L315	L315	L315	L315	L315	L315	L315	L315	L315	L315
Strat. Gp.	St	St	St	St	St	St	St	St	St	St	St	St	St	St	St
Spot Ref.	4	13	19	20	21	5	8	9	12	14	15	16	17	18	19
Phenocryst No.	2	3		4	4	mp1	1	mp2	1	2	2	2	2	2	mp3
Position	IR	IC	QG	IM	IC	IC	IR	IR	IC	IM	IM	IC	IM	IC	IR
SiO2	47.31	55.45	50.58	46.72	47.04	47.98	47.54	50.92	47.35	47.27	46.98	47.05	47.43	46.60	51.25
Al2O3	32.35	27.56	30.17	33.04	32.59	32.18	32.77	30.46	32.82	32.41	32.39	32.90	32.38	32.23	30.50
FeO	0.69	0.37	0.60	0.67	0.49	0.58	0.54	0.67	0.56	0.56	0.38	0.63	0.60	0.32	0.67
MgO	0.27	0.00	0.31	0.25	0.00	0.28	0.27	0.00	0.00	0.26	0.00	0.24	0.00	0.00	0.35
CaO	16.06	9.82	13.61	16.63	16.51	16.08	15.95	13.62	16.57	16.21	16.43	16.31	16.18	16.32	13.88
Na2O	2.25	5.68	3.59	1.86	2.19	2.44	2.25	3.63	1.91	2.19	1.94	2.03	2.14	1.90	3.84
K2O	0.00	0.27	0.16	0.00	0.00	0.00	0.00	0.13	0.13	0.00	0.00	0.00	0.00	0.00	0.16
TOTAL	98.92	99.15	99.16	99.16	98.82	99.53	99.32	99.58	99.34	98.91	98.12	99.15	98.72	97.37	100.65
O=8															
Si	2.20	2.52	2.33	2.17	2.19	2.21	2.20	2.33	2.19	2.20	2.20	2.18	2.21	2.20	2.33
Al	1.77	1.48	1.64	1.81	1.79	1.75	1.78	1.64	1.79	1.77	1.79	1.80	1.77	1.79	1.63
Fe	0.03	0.01	0.02	0.03	0.02	0.02	0.02	0.03	0.02	0.02	0.02	0.02	0.02	0.01	0.03
Ca	0.80	0.48	0.67	0.83	0.82	0.80	0.79	0.67	0.82	0.81	0.82	0.81	0.81	0.82	0.68
Na	0.20	0.50	0.32	0.17	0.20	0.22	0.20	0.32	0.17	0.20	0.18	0.18	0.19	0.17	0.34
K	0.00	0.02	0.01	0.00	0.00	0.00	0.00	0.01	0.01	0.00	0.00	0.00	0.00	0.00	0.01
Total	4.998	5.002	4.988	4.996	5.016	5.000	4.994	5.000	5.003	4.997	4.998	4.995	5.003	4.996	5.007
Or%	0.000	1.577	0.966	0.000	0.000	0.000	0.000	0.768	0.733	0.000	0.000	0.000	0.000	0.000	0.913
Ab%	20.200	50.352	32.001	16.862	19.334	21.546	20.343	32.287	17.128	19.668	17.584	18.374	19.340	17.435	33.051
An%	79.80	48.07	67.03	83.14	80.67	78.45	79.66	66.94	82.14	80.33	82.42	81.63	80.66	82.57	66.04

Sample No.	L345	L345	L345	L345	L345	L345	L345	L345	L345	L345	L345	L345	L345	L345	L345
Strat. Gp															
Spot Ref.	1	2	3	5	6	7	13	14	15	18	19	20	21	22	24
Phenocryst No.	1	2	2	3	4	4	5	5		6	6	mpl		7	7
Position	IM	IR	IC	IC	IM	IC	IR	IC	QG	IR	IC	IC	QG	IR	IM
SIO2	47.62	48.28	48.31	48.48	48.29	47.53	51.24	47.97	51.45	55.44	48.94	47.58	47.62	54.01	47.06
Al2O3	33.06	33.05	32.76	33.31	32.89	33.28	30.14	32.48	29.65	27.19	32.01	32.91	24.62	28.63	33.37
FeO	0.50	0.80	0.82	0.69	0.73	0.70	0.82	0.52	0.81	0.56	0.67	0.80	12.14	1.00	0.68
MgO	0.25	0.34	0.00	0.31	0.20	0.24	0.00	0.23	0.00	0.00	0.24	0.27	0.23	0.25	0.42
CaO	16.86	16.50	16.33	16.61	16.47	16.74	13.49	16.14	13.17	10.05	15.36	16.57	9.17	11.39	16.94
Na2O	2.18	2.35	2.22	2.22	2.17	2.11	3.82	2.35	4.01	5.68	2.66	2.15	5.05	4.94	1.96
K2O	0.00	0.00	0.00	0.00	0.09	0.00	0.16	0.00	0.11	0.32	0.08	0.00	0.22	0.26	0.00
TOTAL	100.46	101.32	100.44	101.61	100.84	100.60	99.66	99.70	99.42	99.52	99.96	100.27	99.25	100.49	100.43
O=8															
Si	2.18	2.19	2.21	2.19	2.20	2.17	2.35	2.21	2.36	2.52	2.24	2.18	2.32	2.44	2.16
Al	1.78	1.77	1.77	1.78	1.77	1.80	1.63	1.76	1.60	1.45	1.73	1.78	1.41	1.53	1.80
Fe	0.02	0.03	0.03	0.03	0.03	0.03	0.03	0.02	0.03	0.02	0.03	0.03	0.49	0.04	0.03
Ca	0.83	0.80	0.80	0.81	0.80	0.82	0.66	0.80	0.65	0.49	0.75	0.82	0.48	0.55	0.83
Na	0.19	0.21	0.20	0.19	0.19	0.19	0.34	0.21	0.36	0.50	0.24	0.19	0.48	0.43	0.17
K	0.00	0.00	0.00	0.00	0.01	0.00	0.01	0.00	0.01	0.02	0.00	0.00	0.01	0.02	0.00
Total	5.006	5.003	5.005	4.995	4.999	5.004	5.015	4.998	5.004	4.998	4.995	5.003	5.191	5.004	4.997
Or%	0.000	0.000	0.000	0.000	0.499	0.000	0.924	0.000	0.627	1.821	0.469	0.000	1.412	1.533	0.000
Ab%	18.942	20.469	19.753	19.446	19.168	18.552	33.564	20.835	35.302	49.652	23.762	19.007	49.190	43.300	17.285
An%	81.06	79.53	80.25	80.55	80.33	81.45	65.51	79.17	64.07	48.53	75.77	80.99	49.40	55.17	82.72

Sample No.	L345	H514c	H514c	H514c	H514c	H514c	H514c	H514c	H514c	H514c	H517a	L534	L534	L534	L534
Strat. Gp		glass	glass	glass	glass	glass	glass	glass	glass	glass	glass				
Spot Ref.	26	1	1	2	3	4	5	6	7	8	9	1	2	4	5
Phenocryst No.	7	mp	mp	mp	mp	mp	mp	mp	mp	mp	mp	1	1	2	3
Position	IC											IC	IR	IC	IC
SIO2	47.03	47.64	49.83	50.55	49.91	49.87	49.52	50.08	49.23	49.19	51.38	62.52	61.69	62.47	63.02
AI2O3	32.86	32.23	25.76	29.28	31.56	31.93	31.29	31.58	31.74	32.11	26.79	23.44	23.32	23.32	22.18
FeO	0.60	0.70	5.00	2.54	1.22	1.32	1.12	1.08	1.15	1.00	2.99	0.35	0.28	0.48	0.59
MgO	0.29	0.00	1.11	0.36	0.00	0.08	0.00	0.00	0.00	0.15	0.66	0.00	0.00	0.00	0.00
CaO	16.41	16.67	13.66	13.91	15.12	15.56	15.74	15.37	15.91	16.03	12.15	5.01	5.06	5.05	4.18
Na2O	2.21	1.75	2.79	2.71	2.71	2.72	2.75	2.84	2.47	2.39	3.56	8.63	8.33	8.09	8.34
K2O	0.00	0.15	0.35	0.35	0.12	0.11	0.19	0.10	0.13	0.21	0.34	0.70	0.71	0.86	1.14
TOTAL	99.41	99.29	99.90	100.35	100.80	101.86	100.73	101.35	100.76	101.33	98.94	100.65	99.39	100.27	99.45
O=8															
Si	2.18	2.21	2.34	2.32	2.27	2.25	2.26	2.27	2.25	2.23	2.39	2.76	2.76	2.77	2.82
Al	1.79	1.76	1.42	1.58	1.69	1.70	1.69	1.69	1.71	1.72	1.47	1.22	1.23	1.22	1.17
Fe	0.02	0.03	0.20	0.10	0.05	0.05	0.04	0.04	0.04	0.04	0.12	0.01	0.01	0.02	0.02
Ca	0.81	0.83	0.69	0.68	0.74	0.75	0.77	0.75	0.78	0.78	0.61	0.24	0.24	0.24	0.20
Na	0.20	0.16	0.25	0.24	0.24	0.24	0.24	0.25	0.22	0.21	0.32	0.74	0.72	0.69	0.72
K	0.00	0.01	0.02	0.02	0.01	0.01	0.01	0.01	0.01	0.01	0.02	0.04	0.04	0.05	0.07
Total	5.006	4.99	4.919	4.948	4.995	4.999	5.016	5.001	5.005	4.993	4.928	5.015	5.006	4.989	4.994
Or%	0.000	0.940	2.183	2.220	0.712	0.701	1.073	0.598	0.796	1.198	2.110	3.870	4.042	4.956	6.579
Ab%	19.618	15.839	26.403	25.476	24.313	23.848	23.707	24.925	21.692	20.958	33.966	72.811	71.836	70.604	73.144
An%	80.38	83.22	71.41	72.30	74.97	75.45	75.22	74.48	77.51	77.84	63.92	23.32	24.12	24.44	20.28

APPENDIX A2 - CLINOPYROXENE COMPOSITIONS

Sample no.
Clinopyroxene compositions are arranged in order of sample number. Prefix 'L' to the sample signifies the sample is a lava; prefix 'D' indicates that the sample is an intrusive sheet; prefix 'H' indicates that the sample is a hyaloclastite glass. Grid references for each sample are given in Appendix B.

Strat. Gp.
Where appropriate, the stratigraphic Group (as defined in Chapter 4) to which the sample belongs is recorded.

Spot Ref.
This is the recorded reference number of each analysed point.

Phenocryst no.
Each analysed phenocryst was numbered. Microphenocrysts are described as 'mp'.

Position
The position of the analysed spot in relation to the crystal is recorded as:

IC - core of the phenocryst;
IM - mantle of the phenocryst;
IR - rim of the phenocryst; and
QG - quench groundmass crystals.

Sample No.	L8	L8	L8	L8	L8	L8	L8	L8	L25	L25	L25	L25	L33	L33	L33	L33
Strat. Gp.	La	La	La	La	La	La	La	La	La	La	La	La	Se	Se	Se	Se
Spot Ref.	1	2	6	7	12	13	33	34	24	27	28	31	38	39	46	47
Phenocryst No.	1	1	2	2	mp	mp	3	3	mp1	mp2	mp3	mp4	1	1	1	1
Position	IR	IM	IR	IC	IC	IC	IC	IR	IC	IC	IR	IR	IR	IC	IR	IR
SiO2	51.64	51.94	50.58	49.94	51.52	50.35	49.05	49.46	52.21	47.92	51.10	46.93	48.36	48.79	47.93	48.42
TiO2	1.14	1.03	1.27	1.45	1.07	1.32	1.50	1.07	0.91	0.87	1.02	2.05	2.00	1.87	1.97	2.01
Cr2O3		0.21	0.30			0.19	0.25	0.18	0.00	0.00	0.27	0.45	0.24	0.26		0.25
Al2O3	3.33	2.81	4.29	4.40	2.87	3.92	4.01	3.63	17.21	22.50	3.48	5.76	6.11	5.48	5.78	5.91
FeO	6.42	6.56	6.17	6.92	6.30	6.53	7.36	6.50	5.49	3.78	6.58	8.03	7.90	7.91	8.18	7.89
Mn	0.00	0.00	0.00	0.00	0.00	0.00	0.00	0.00	0.00	0.00	0.00	0.00	0.00	0.00	0.00	0.00
MgO	15.69	15.76	15.43	14.85	15.58	15.17	14.25	14.82	6.87	4.90	15.51	13.50	14.03	14.00	13.89	14.07
CaO	22.05	21.82	22.27	22.02	21.98	22.20	21.15	21.58	14.33	16.53	21.62	20.42	20.92	20.80	20.78	20.81
NaO	0.61	0.56	0.50	0.73	0.62	0.49	0.78	0.73	3.16	2.07	0.76	0.67	0.80	0.62	0.82	0.92
TOTAL	**100.87**	**100.67**	**100.81**	**100.31**	**99.95**	**100.17**	**98.36**	**97.97**	**100.18**	**98.57**	**100.32**	**97.82**	**100.36**	**99.72**	**99.34**	**100.27**
0=6																
Si	1.89	1.91	1.86	1.85	1.90	1.86	1.86	1.87	1.85	1.72	1.88	1.79	1.80	1.82	1.80	1.80
Al	0.14	0.12	0.19	0.19	0.13	0.17	0.18	0.16	0.72	0.95	0.15	0.26	0.27	0.24	0.26	0.26
Ti	0.03	0.03	0.04	0.04	0.03	0.04	0.04	0.03	0.02	0.02	0.03	0.06	0.06	0.05	0.06	0.06
Cr	0.00	0.01	0.01	0.00	0.00	0.01	0.01	0.01	0.00	0.00	0.01	0.01	0.01	0.01	0.00	0.01
Fe	0.20	0.20	0.19	0.21	0.19	0.20	0.23	0.21	0.16	0.11	0.20	0.26	0.25	0.25	0.26	0.25
Mn	0.00	0.00	0.00	0.00	0.00	0.00	0.00	0.00	0.00	0.00	0.00	0.00	0.00	0.00	0.00	0.00
Mg	0.86	0.86	0.84	0.82	0.86	0.84	0.80	0.84	0.36	0.26	0.85	0.77	0.78	0.78	0.78	0.78
Ca	0.87	0.84	0.88	0.87	0.87	0.88	0.86	0.88	0.54	0.64	0.85	0.84	0.83	0.83	0.84	0.83
Na	0.04	0.04	0.04	0.05	0.04	0.04	0.06	0.05	0.22	0.14	0.05	0.05	0.06	0.04	0.06	0.07
Total	4.028	4.000	4.029	4.041	4.026	4.030	4.037	4.041	3.876	3.852	4.035	4.036	4.039	4.024	4.045	4.043
Wo	**45.09**	**44.00**	**45.86**	**45.81**	**45.25**	**45.87**	**45.27**	**45.64**	**50.85**	**62.87**	**44.73**	**44.91**	**44.88**	**44.79**	**44.71**	**44.71**
En	**44.65**	**45.40**	**44.21**	**42.96**	**44.62**	**43.59**	**42.43**	**43.62**	**33.94**	**25.91**	**44.65**	**41.31**	**41.88**	**41.93**	**41.56**	**42.06**
Fs	**10.26**	**10.60**	**9.93**	**11.23**	**10.13**	**10.54**	**12.30**	**10.73**	**15.20**	**11.22**	**10.62**	**13.78**	**13.24**	**13.28**	**13.73**	**13.23**

Sample No.	L33	L33	L43	L43	L43	L43	L43	L43	L43	L43	L43	L43	L43	L43	L43	L43
Strat. Gp.	Se	Se	Hv	Hv	Hv	Hv	Hv	Hv	Hv	Hv	Hv	Hv	Hv	Hv	Hv	Hv
Spot Ref.	48	49	2	3	4	5	6	7	37	38	39	40	41	42	43	44
Phenocryst No.	1	1	1	1	1	1	1	1	2	3	2	2	4	4	4	4
Position	IM	IM	IM	IR	IR	IC	IC	IC	IR	IR	IM	IC	IC	IR	IR	IC
SiO2	48.52	48.66	50.92	50.19	50.31	50.57	50.40	50.54	51.30	51.60	50.73	51.01	51.13	51.61	51.69	51.74
TiO2	1.80	1.83	0.89	1.05	1.06	0.99	1.08	1.01	1.07	1.07	0.98	1.00	0.87	0.69	0.69	0.75
Cr2O3	0.19	0.24	0.47	0.25	0.42	0.32		0.22	0.36	0.35	0.24	0.30	0.67	0.97	0.54	0.91
Al2O3	5.58	5.49	3.52	3.82	3.76	3.66	3.49	3.78	4.02	3.62	3.96	3.49	4.45	3.82	3.42	3.76
FeO	7.83	7.97	6.38	6.21	6.78	6.82	7.36	6.72	6.03	5.92	6.20	5.87	4.75	4.67	4.71	4.97
Mn	0.00	0.00	0.00	0.00	0.00	0.00	0.00	0.00	0.00	0.00	0.00	0.00	0.00	0.00	0.00	0.00
MgO	13.98	13.94	15.87	15.26	15.43	15.21	15.05	15.20	15.94	15.85	15.72	15.91	16.36	16.89	16.97	17.08
CaO	20.41	20.87	21.21	21.14	21.27	21.54	21.31	21.20	21.78	21.62	21.59	21.81	21.51	21.31	21.18	21.09
NaO	0.67	0.77	0.73	0.53	0.52	0.70	0.58	0.56	0.62	0.65	0.64	0.56	0.59	0.58	0.70	0.63
TOTAL	**98.97**	**99.76**	**99.98**	**98.45**	**99.55**	**99.81**	**99.28**	**99.23**	**101.12**	**100.67**	**100.05**	**99.95**	**100.33**	**100.53**	**99.89**	**100.94**
O=6																
Si	1.82	1.82	1.88	1.88	1.87	1.88	1.88	1.88	1.87	1.89	1.87	1.88	1.87	1.88	1.89	1.88
Al	0.25	0.24	0.15	0.17	0.17	0.16	0.15	0.17	0.17	0.16	0.17	0.15	0.19	0.16	0.15	0.16
Ti	0.05	0.05	0.02	0.03	0.03	0.03	0.03	0.03	0.03	0.03	0.03	0.03	0.02	0.02	0.02	0.02
Cr	0.01	0.01	0.01	0.01	0.01	0.01	0.00	0.01	0.01	0.01	0.01	0.01	0.02	0.03	0.02	0.03
Fe	0.25	0.25	0.20	0.19	0.21	0.21	0.23	0.21	0.18	0.18	0.19	0.18	0.15	0.14	0.14	0.15
Mn	0.00	0.00	0.00	0.00	0.00	0.00	0.00	0.00	0.00	0.00	0.00	0.00	0.00	0.00	0.00	0.00
Mg	0.78	0.78	0.87	0.85	0.86	0.84	0.84	0.84	0.87	0.86	0.86	0.88	0.89	0.92	0.93	0.93
Ca	0.82	0.84	0.84	0.85	0.85	0.86	0.85	0.85	0.85	0.85	0.85	0.86	0.84	0.83	0.83	0.82
Na	0.05	0.06	0.05	0.04	0.04	0.05	0.04	0.04	0.04	0.05	0.05	0.04	0.04	0.04	0.05	0.04
Total	4.025	4.034	4.036	4.021	4.030	4.035	4.031	4.023	4.030	4.022	4.034	4.030	4.024	4.025	4.030	4.029
Wo	**44.39**	**44.89**	**43.94**	**44.77**	**44.28**	**44.85**	**44.41**	**44.55**	**44.76**	**44.78**	**44.72**	**44.95**	**44.84**	**43.99**	**43.71**	**43.28**
En	**42.31**	**41.73**	**45.74**	**44.96**	**44.70**	**44.06**	**43.63**	**44.43**	**45.57**	**45.66**	**45.27**	**45.61**	**47.43**	**48.49**	**48.71**	**48.76**
Fs	**13.30**	**13.38**	**10.32**	**10.27**	**11.02**	**11.08**	**11.96**	**11.02**	**9.67**	**9.56**	**10.01**	**9.45**	**7.73**	**7.52**	**7.58**	**7.96**

Sample No.	L43	L58	L58	L58	L58	L58	L58	L58	L74	L74	L74	L74	L74	L74	L74	L74
Strat. Gp.	Hv								Hv	Hv	Hv	Hv	Hv	Hv	Hv	Hv
Spot Ref.	50	10	11	12	14	15	17	30	63	68	69	71	74	77	78	79
Phenocryst No.	mp	1	2	2	mp 1	mp2	mp3	mp	1	2	2			3	3	3
Position	IC	IC	IR	IC	IC	IC	IC	IC	IM	IM	IM	mp	mp	IR	IM	IC
SiO2	51.11	49.65	50.70	50.18	50.31	51.12	51.83	48.38	51.51	51.27	51.02	50.94	50.67	53.52	51.66	51.92
TiO2	1.16	1.27	1.04	1.18	1.23	0.97	0.85	2.14	1.08	0.98	1.03	1.34	1.43	0.58	0.74	0.83
Cr2O3	0.29	0.00	0.36	0.32	0.00	0.00	0.24		0.25	0.44	0.48	0.62	0.58	1.20	0.89	0.39
Al2O3	3.71	3.07	4.62	3.96	3.94	4.03	3.01	3.35	3.76	4.01	3.95	3.25	3.89	2.42	3.67	3.11
FeO	6.11	8.79	5.75	6.78	8.17	6.60	6.50	10.99	6.40	5.99	5.44	6.79	7.78	4.01	4.95	5.87
Mn	0.00	0.00	0.00	0.00	0.00	0.00	0.00	0.00	0.00	0.00	0.00	0.00	0.00	0.00	0.00	0.00
MgO	15.72	14.42	15.72	15.29	15.01	15.66	15.97	13.17	15.65	15.79	15.74	15.88	14.80	18.27	16.47	16.60
CaO	21.96	20.35	21.24	21.17	20.90	21.50	21.25	19.43	21.74	21.82	21.92	21.28	21.24	20.55	21.25	20.88
NaO	0.55	0.64	0.49	0.47	0.79	0.64	0.51	0.70	0.53	0.63	0.61	0.57	0.50	0.64	0.41	0.65
TOTAL	100.60	98.18	99.92	99.35	100.34	100.51	100.16	98.17	100.93	100.92	100.18	100.65	100.87	101.20	100.02	100.25
0=6																
Si	1.88	1.89	1.87	1.87	1.87	1.88	1.91	1.86	1.88	1.87	1.88	1.87	1.87	1.92	1.89	1.90
Al	0.16	0.14	0.20	0.17	0.17	0.17	0.13	0.15	0.16	0.17	0.17	0.14	0.17	0.10	0.16	0.13
Ti	0.03	0.04	0.03	0.03	0.03	0.03	0.02	0.06	0.03	0.03	0.03	0.04	0.04	0.02	0.02	0.02
Cr	0.01	0.00	0.01	0.01	0.00	0.00	0.01	0.00	0.01	0.01	0.01	0.02	0.02	0.03	0.03	0.01
Fe	0.19	0.28	0.18	0.21	0.25	0.20	0.20	0.35	0.20	0.18	0.17	0.21	0.24	0.12	0.15	0.18
Mn	0.00	0.00	0.00	0.00	0.00	0.00	0.00	0.00	0.00	0.00	0.00	0.00	0.00	0.00	0.00	0.00
Mg	0.86	0.82	0.86	0.85	0.83	0.86	0.88	0.75	0.85	0.86	0.86	0.87	0.81	0.98	0.90	0.91
Ca	0.86	0.83	0.84	0.84	0.83	0.85	0.84	0.80	0.85	0.85	0.86	0.84	0.84	0.79	0.83	0.82
Na	0.04	0.05	0.04	0.03	0.06	0.05	0.04	0.05	0.04	0.04	0.04	0.04	0.04	0.05	0.03	0.05
Total	4.027	4.032	4.018	4.024	4.042	4.031	4.019	4.031	4.021	4.029	4.026	4.030	4.018	4.014	4.010	4.024
Wo	45.20	43.04	44.63	44.35	43.39	44.38	43.79	41.93	44.80	45.02	45.62	43.73	44.33	41.85	44.25	43.01
En	44.99	42.45	45.94	44.57	43.37	44.98	45.76	39.56	44.90	45.33	45.56	45.39	42.99	51.76	47.71	47.57
Fs	9.81	14.51	9.43	11.08	13.24	10.63	10.45	18.51	10.30	9.65	8.82	10.88	12.68	6.38	8.04	9.43

Sample No.	L74	L74	L74	74B	74B	L82	L82	L82	L82	L82	L82	L82	L82	L98	L98	L98
Strat. Gp.	Hv	Hv	Hv			Lf	Lf	Lf	Lf	Lf	Lf	Lf	Lf	La2	La2	La2
Spot Ref.	80	84	90			1	2	10	11	13	17	18	19	1	2	3
Phenocryst No.	4	mp				1	1	mp1	mp2	mp3	2	2		mp1	1	1
Position	IC	IC	QG			IR	IC	IC	IC	IC	IC	IR	QG	IC	IR	IC
SiO2	52.47	51.56	50.99	49.73	48.78	49.03	48.30	47.00	48.12	47.39	51.29	48.91	48.92	47.43	47.57	47.72
TiO2	0.57	1.09	1.23	0.92	1.73	2.34	2.17	2.37	2.58	2.80	1.36	2.16	2.18	2.26	2.58	2.31
Cr2O3	0.78	0.49	0.48	0.18	0.28	0.00	0.00	0.00	0.00	0.00	0.00	0.00	0.00	0.27	0.21	0.21
Al2O3	3.38	3.08	3.22	3.55	3.21	4.91	4.18	4.82	5.08	5.84	2.72	3.93	4.12	5.33	5.71	5.59
FeO	4.93	6.17	6.53	5.70	7.65	10.79	10.56	10.17	11.37	11.34	10.11	9.95	10.48	9.41	9.47	9.13
Mn	0.00	0.00	0.00	0.16	0.15	0.00	0.00	0.00	0.00	0.00	0.00	0.00	0.00	0.00	0.00	0.00
MgO	16.88	15.90	15.71	15.02	13.91	14.31	13.96	13.36	13.40	13.78	15.34	14.11	14.03	13.32	13.37	13.27
CaO	21.21	21.43	21.42	21.73	21.26	18.85	19.44	19.15	19.81	18.40	19.01	20.02	19.69	21.08	20.80	21.11
NaO	0.48	0.63	0.65	0.42	0.52	0.70	0.65	0.77	0.78	0.74	0.68	0.65	0.64	0.63	0.66	0.58
TOTAL	100.69	100.36	100.22	97.45	97.61	100.94	99.27	97.63	101.14	100.28	100.51	99.72	100.05	99.72	100.38	99.92
0=6																
Si	1.91	1.90	1.88	1.88	1.87	1.82	1.83	1.81	1.80	1.78	1.90	1.84	1.84	1.79	1.78	1.79
Al	0.14	0.13	0.14	0.01	0.01	0.22	0.19	0.22	0.22	0.26	0.12	0.17	0.18	0.24	0.25	0.25
Ti	0.02	0.03	0.03	0.03	0.05	0.07	0.06	0.07	0.07	0.08	0.04	0.06	0.06	0.06	0.07	0.07
Cr	0.02	0.01	0.01	0.00	0.00	0.00	0.00	0.00	0.00	0.00	0.00	0.00	0.00	0.01	0.01	0.01
Fe	0.15	0.19	0.20	0.16	0.14	0.34	0.33	0.33	0.36	0.36	0.31	0.31	0.33	0.30	0.30	0.29
Mn	0.00	0.00	0.00	0.00	0.00	0.00	0.00	0.00	0.00	0.00	0.00	0.00	0.00	0.00	0.00	0.00
Mg	0.91	0.87	0.86	0.88	0.87	0.79	0.79	0.77	0.75	0.77	0.85	0.79	0.79	0.75	0.75	0.74
Ca	0.83	0.84	0.85	0.85	0.79	0.75	0.79	0.79	0.79	0.74	0.76	0.81	0.79	0.85	0.84	0.85
Na	0.03	0.05	0.05	0.18	0.24	0.05	0.05	0.06	0.06	0.05	0.05	0.05	0.05	0.05	0.05	0.04
Total	4.012	4.023	4.030	3.99	3.98	4.031	4.039	4.040	4.045	4.039	4.025	4.032	4.034	4.046	4.040	4.036
Wo	43.69	44.31	44.29	44.91	43.83	39.96	41.27	41.93	41.87	39.64	39.40	42.31	41.54	44.89	44.46	45.21
En	48.38	45.73	45.18	46.69	48.17	42.19	41.24	40.70	39.39	41.30	44.25	41.27	41.19	39.48	39.74	39.53
Fs	7.93	9.96	10.53	8.40	8.00	17.85	17.49	17.37	18.75	19.07	16.35	16.42	17.27	15.64	15.80	15.26

Sample No.	L98	L98	L98	L98	L98	L121	L121	D131	D189	L190	L190	L190	L190	L190	L190	L190
Strat. Gp.	La2	La2	La2	La2	La2	LI	LI	Sv		Nd	Nd	Nd	Nd	Nd	Nd	Nd
Spot Ref.	6	7	8	9	11	10	11	21	7	10	11	14	16	17	18	19
Phenocryst No.	mp2	mp3	mp3	mp3	mp4	1	1	mp	1	1	1	2		3	3	3
Position	IR	IC	IC	IR	IR	IR	IM	IC	IC	IR	IC	IC	QG	IR	IM	IM
SIO2	50.89	51.34	46.78	45.71	48.55	48.51	48.73	49.48	51.21	50.01	49.13	49.38	50.14	50.66	50.47	50.67
TIO2	1.10	1.22	2.66	3.20	1.97	1.86	1.65	1.95	0.53	1.40	1.81	1.51	1.06	0.80	0.79	0.99
Cr2O3	0.00	0.00	0.00	0.24	0.00	0.34	0.44	0.00	0.00	0.21	0.29	0.28	0.54	1.34	1.18	0.42
Al2O3	2.58	2.58	6.10	6.70	3.99	5.43	5.39	3.53	0.81	3.96	4.72	4.99	5.14	4.05	4.04	4.27
FeO	9.23	9.02	10.51	10.40	10.05	7.98	6.96	9.49	18.27	7.10	7.90	6.76	5.21	4.63	4.42	4.95
Mn	0.00	0.00	0.00	0.00	0.00	0.00	0.00	0.00	0.50	0.00	0.00	0.00	0.00	0.00	0.00	0.00
MgO	15.58	15.35	12.90	12.33	14.48	13.95	14.34	13.88	9.32	14.87	13.98	14.92	15.58	16.12	16.01	15.69
CaO	19.93	20.39	20.71	20.79	19.86	20.61	20.95	20.51	19.67	21.26	21.43	21.34	21.79	21.56	21.59	22.05
NaO	0.45	0.56	0.66	0.66	0.45	0.75	0.78	0.77	0.49	0.60	0.59	0.63	0.64	0.59	0.67	0.56
TOTAL	99.76	100.46	100.33	100.03	99.34	99.42	99.25	99.61	100.80	99.40	99.83	99.81	100.09	99.75	99.17	99.60
0=6																
SI	1.90	1.90	1.76	1.73	1.83	1.82	1.82	1.86	1.97	1.87	1.84	1.83	1.84	1.87	1.87	1.87
Al	0.11	0.11	0.27	0.30	0.18	0.24	0.24	0.16	0.04	0.17	0.21	0.22	0.22	0.18	0.18	0.19
Ti	0.03	0.03	0.08	0.09	0.06	0.05	0.05	0.06	0.02	0.04	0.05	0.04	0.03	0.02	0.02	0.03
Cr	0.00	0.00	0.00	0.01	0.00	0.01	0.01	0.00	0.00	0.01	0.01	0.01	0.02	0.04	0.03	0.01
Fe	0.29	0.28	0.33	0.33	0.32	0.25	0.22	0.30	0.59	0.22	0.25	0.21	0.16	0.14	0.14	0.15
Mn	0.00	0.00	0.00	0.00	0.00	0.00	0.00	0.00	0.02	0.00	0.00	0.00	0.00	0.00	0.00	0.00
Mg	0.87	0.85	0.73	0.70	0.82	0.78	0.80	0.78	0.54	0.83	0.78	0.83	0.85	0.89	0.88	0.86
Ca	0.80	0.81	0.84	0.84	0.80	0.83	0.84	0.83	0.81	0.85	0.86	0.85	0.86	0.85	0.86	0.87
Na	0.03	0.04	0.05	0.05	0.03	0.05	0.06	0.06	0.04	0.04	0.04	0.05	0.05	0.04	0.05	0.04
Total	4.029	4.027	4.050	4.048	4.038	4.031	4.034	4.033	4.012	4.027	4.027	4.034	4.030	4.025	4.027	4.024
Wo	40.84	41.80	44.19	45.14	41.50	44.57	45.21	43.42	41.94	44.76	45.54	45.05	45.84	45.30	45.63	46.18
En	44.41	43.77	38.30	37.24	42.11	41.97	43.07	40.89	27.65	43.57	41.36	43.81	45.59	47.12	47.07	45.72
Fs	14.75	14.43	17.50	17.62	16.39	13.46	11.73	15.69	30.41	11.67	13.10	11.14	8.57	7.58	7.30	8.10

Sample No.	L190	L190	L205	205	L205	L205	L205	L205	L205	L205	L205	L205	L215	L215	L215	L215
Strat. Gp.	Nd	Nd	Nd	Nd	Nd	Nd	Nd	Nd	Nd	Nd	Nd	Nd	w.slopes	w.slopes	w.slopes	w.slopes
Spot Ref.	20	21	1	4	5	6	8	9	12	13	15	16	1	2	3	4
Phenocryst No.	3	3	1	2	2	3	mpl	mpl	4				1	1	1	1
Position	IC	IC	IC	IR	IC	IC	IC	IC	IC	QG	QG	QG	IC	IM	IR	IR
SIO2	49.59	50.81	51.20	49.71	51.55	51.46	52.06	51.02	50.48	48.29	51.11	48.34	48.62	50.67	51.48	51.43
TIO2	1.28	0.65	1.29	1.86	1.29	1.16	1.13	1.20	1.41	2.29	1.48	2.09	1.77	1.27	0.73	0.78
Cr2O3	0.23	0.93	0.38	0.37	0.38	0.40	0.31	0.39	0.49	0.39	0.00	0.65	0.30	0.18	0.00	0.00
Al2O3	5.11	3.79	4.15	5.64	4.27	4.06	3.76	4.20	4.55	5.52	1.86	6.11	5.44	4.36	1.67	1.80
FeO	5.52	4.44	6.95	7.51	7.02	6.77	6.95	6.92	7.16	8.43	12.52	8.06	8.24	7.94	12.90	12.74
Mn	0.00	0.00	0.00	0.00	0.00	0.00	0.00	0.00	0.00	0.00	0.00	0.00	0.00	0.00	0.32	0.36
MgO	15.26	16.04	15.23	14.14	15.32	15.59	15.90	15.40	14.94	13.55	12.77	13.59	14.46	15.21	13.05	13.53
CaO	21.99	21.67	22.20	21.92	22.27	21.66	21.81	22.05	21.99	21.56	21.09	21.47	20.40	20.56	19.45	19.00
NaO	0.52	0.48	0.53	0.57	0.69	0.70	0.60	0.59	0.60	0.56	0.74	0.61	0.71	0.75	0.60	0.62
TOTAL	99.52	98.80	101.92	101.72	102.79	101.79	102.52	101.78	101.63	100.58	101.57	100.93	99.93	100.94	100.21	100.26
O=6																
Si	1.84	1.89	1.86	1.82	1.86	1.87	1.88	1.86	1.85	1.80	1.91	1.79	1.81	1.86	1.94	1.94
Al	0.22	0.17	0.18	0.24	0.18	0.17	0.16	0.18	0.20	0.24	0.08	0.27	0.24	0.19	0.07	0.08
Ti	0.04	0.02	0.04	0.05	0.04	0.03	0.03	0.03	0.04	0.06	0.04	0.06	0.05	0.04	0.02	0.02
Cr	0.01	0.03	0.01	0.01	0.01	0.01	0.01	0.01	0.01	0.01	0.00	0.02	0.01	0.01	0.00	0.00
Fe	0.17	0.14	0.21	0.23	0.21	0.21	0.21	0.21	0.22	0.26	0.39	0.25	0.26	0.24	0.41	0.40
Mn	0.00	0.00	0.00	0.00	0.00	0.00	0.00	0.00	0.00	0.00	0.00	0.00	0.00	0.00	0.01	0.01
Mg	0.84	0.89	0.83	0.77	0.82	0.84	0.86	0.84	0.81	0.75	0.71	0.75	0.80	0.83	0.73	0.76
Ca	0.87	0.86	0.87	0.86	0.86	0.84	0.84	0.86	0.86	0.86	0.84	0.85	0.82	0.81	0.79	0.77
Na	0.04	0.03	0.04	0.04	0.05	0.05	0.04	0.04	0.04	0.04	0.05	0.04	0.05	0.05	0.04	0.05
Total	4.030	4.018	4.027	4.023	4.033	4.030	4.028	4.033	4.032	4.031	4.035	4.031	4.038	4.032	4.021	4.024
Wo	46.27	45.65	45.47	46.20	45.38	44.54	44.20	45.11	45.46	45.89	43.37	46.00	43.44	42.91	40.81	39.77
En	44.66	47.03	43.41	41.46	43.46	44.59	44.82	43.83	42.98	40.11	36.54	40.51	42.86	44.16	38.07	39.41
Fs	9.07	7.31	11.12	12.34	11.16	10.86	10.98	11.06	11.56	14.00	20.09	13.49	13.70	12.93	21.12	20.81

Sample No.	L215	L221	L221	L221	L221	L221	L251	L251	L251	L251	L251	L255	L255	L255	L255	L255
Strat. Gp.	w.slopes															
Spot Ref.	5	3	4	6	7	8	7	8	9	11	13	1	2	3	30	31
Phenocryst No.		1	1	1	2	2	1	1	1	2	2	1	1		2	3
Position	QG	IR	IM	IC	IR	IC	IC	IC	IM	IC	IR	IC	IR	QG	IM	IR
SiO2	51.37	49.04	49.38	48.69	49.46	50.88	50.16	50.75	48.73	51.33	52.30	50.53	50.33	50.05	48.82	49.73
TiO2	0.86	1.56	1.40	1.41	1.71	0.86	1.20	1.23	1.84	1.12	0.53	1.04	1.32	2.03	1.52	1.23
Cr2O3	0.00	0.79	0.58	0.70	0.00	0.00	0.38	0.21	0.24		1.18	0.59	0.75	0.00	0.51	0.62
Al2O3	1.78	5.42	5.16	5.36	3.70	2.28	4.17	3.39	5.15	1.72	2.45	4.55	4.87	3.48	5.75	5.09
FeO	12.73	7.34	7.19	7.48	9.84	10.50	5.93	7.37	8.03	10.10	4.16	6.72	6.62	8.84	6.84	6.92
Mn	0.00	0.00	0.00	0.00	0.20	0.24	0.00	0.00	0.00	0.00	0.00	0.00	0.00	0.00	0.00	0.00
MgO	13.18	14.75	14.37	14.57	14.01	13.82	15.23	15.19	14.09	14.15	16.86	15.55	15.35	13.91	14.57	14.79
CaO	19.54	20.86	20.71	20.46	20.05	20.34	21.25	21.23	21.56	20.55	22.26	20.74	21.08	20.92	20.99	20.97
NaO	0.71	0.74	0.81	0.77	0.78	0.69	0.59	0.70	0.57	0.62	0.42	0.60	0.74	0.75	0.70	0.55
TOTAL	100.16	100.49	99.59	99.43	99.75	99.60	98.92	100.07	100.21	99.59	100.16	100.31	101.05	99.97	99.69	99.90
O=6																
Si	1.94	1.81	1.84	1.82	1.86	1.92	1.87	1.88	1.82	1.93	1.91	1.86	1.84	1.87	1.82	1.84
Al	0.08	0.24	0.23	0.24	0.16	0.10	0.18	0.15	0.23	0.08	0.11	0.20	0.21	0.15	0.25	0.22
Ti	0.02	0.04	0.04	0.04	0.05	0.02	0.03	0.03	0.05	0.03	0.01	0.03	0.04	0.06	0.04	0.03
Cr	0.00	0.02	0.02	0.02	0.00	0.00	0.01	0.01	0.01	0.00	0.03	0.02	0.02	0.00	0.01	0.02
Fe	0.40	0.23	0.22	0.23	0.31	0.33	0.19	0.23	0.25	0.32	0.13	0.21	0.20	0.28	0.21	0.21
Mn	0.00	0.00	0.00	0.00	0.01	0.01	0.00	0.00	0.00	0.00	0.00	0.00	0.00	0.00	0.00	0.00
Mg	0.74	0.81	0.80	0.81	0.79	0.78	0.85	0.84	0.78	0.79	0.92	0.85	0.84	0.77	0.81	0.82
Ca	0.79	0.83	0.83	0.82	0.81	0.82	0.85	0.84	0.86	0.83	0.87	0.82	0.83	0.84	0.84	0.83
Na	0.05	0.05	0.06	0.06	0.06	0.05	0.04	0.05	0.04	0.05	0.03	0.04	0.05	0.05	0.05	0.04
Total	4.024	4.039	4.029	4.039	4.038	4.031	4.021	4.032	4.036	4.023	4.017	4.025	4.031	4.023	4.033	4.022
Wo	40.87	44.29	44.72	43.95	42.46	42.59	45.14	44.13	45.45	42.72	45.47	43.55	44.28	44.35	45.05	44.68
En	38.35	43.56	43.16	43.52	41.27	40.25	45.02	43.91	41.34	40.90	47.90	45.43	44.86	41.02	43.50	43.83
Fs	20.78	12.15	12.12	12.53	16.27	17.16	9.84	11.95	13.21	16.39	6.63	11.02	10.86	14.63	11.46	11.49

Sample No.	L255	L255	L256	L256	L256	L270	L270	L270	L270	L270	L270	L270	L296	L296	L296	L296
Strat. Gp.													St	St	St	St
Spot Ref.	37	38	6	17	20	3	4	20	21	22	23	24	10	11	12	16
Phenocryst No.	4	4		1	1			mpl	mpl	1	1	1	1	1	1	2
Position	IR	IC	QG	IC	IM	QG	QG	IC	IR	IR	IM	IC	IR	IM	IC	IR
SiO2	49.06	51.26	52.25	49.01	49.45	50.34	50.35	49.06	47.53	50.64	50.86	50.68	48.70	49.98	49.59	52.22
TiO2	1.98	0.76	1.18	1.60	1.74	1.52	1.38	1.78	2.68	1.20	1.10	1.11	2.04	1.45	1.59	0.64
Cr2O3	0.00	0.89	0.00	0.52	0.43	0.00	0.18	0.00	0.00	0.00	0.44	0.58	0.18	0.55	0.31	0.00
Al2O3	3.50	3.57	10.93	4.71	3.61	3.24	2.88	3.79	4.52	2.70	3.95	4.05	3.98	4.49	4.39	2.06
FeO	8.70	6.41	7.14	7.91	10.09	10.71	10.22	11.92	11.65	11.23	6.77	6.59	9.00	7.74	8.06	9.74
Mn	0.00	0.00	0.00	0.00	0.00	0.26	0.23	0.00	0.00	0.00	0.00	0.00	0.00	0.00	0.00	0.27
MgO	13.78	16.87	9.99	14.39	13.90	13.77	13.47	12.91	12.24	13.49	15.64	15.70	13.77	14.13	14.37	14.58
CaO	20.78	19.21	17.77	20.66	19.71	19.95	20.60	18.79	19.78	19.87	21.23	21.10	20.84	21.35	21.11	20.08
NaO	0.62	0.77	2.18	0.63	0.73	0.71	0.76	0.73	0.77	0.80	0.75	0.42	0.69	0.53	0.71	0.68
TOTAL	98.43	99.75	101.54	99.43	99.65	100.50	100.06	98.98	99.16	99.93	100.75	100.23	99.19	100.22	100.12	100.28
0=6																
Si	1.86	1.89	0.00	1.84	1.86	1.88	1.89	1.87	1.82	1.91	1.87	1.87	1.84	1.86	1.85	1.94
Al	0.16	0.15	0.46	0.21	0.16	0.14	0.13	0.17	0.20	0.12	0.17	0.18	0.18	0.20	0.19	0.09
Ti	0.06	0.02	0.03	0.05	0.05	0.04	0.04	0.05	0.08	0.03	0.03	0.03	0.06	0.04	0.04	0.02
Cr	0.00	0.03	0.00	0.02	0.01	0.00	0.01	0.00	0.00	0.00	0.01	0.02	0.01	0.02	0.01	0.00
Fe	0.28	0.20	0.21	0.25	0.32	0.33	0.32	0.38	0.37	0.35	0.21	0.20	0.28	0.24	0.25	0.30
Mn	0.00	0.00	0.00	0.00	0.00	0.01	0.01	0.00	0.00	0.00	0.00	0.00	0.00	0.00	0.00	0.01
Mg	0.78	0.93	0.53	0.80	0.78	0.77	0.75	0.73	0.70	0.76	0.86	0.86	0.78	0.78	0.80	0.81
Ca	0.85	0.76	0.68	0.83	0.80	0.80	0.83	0.77	0.81	0.80	0.84	0.83	0.84	0.85	0.84	0.80
Na	0.05	0.06	0.15	0.05	0.05	0.05	0.06	0.05	0.06	0.06	0.05	0.03	0.05	0.04	0.05	0.05
Total	4.025	4.028	2.076	4.030	4.030	4.029	4.031	4.023	4.034	4.030	4.036	4.020	4.035	4.017	4.034	4.019
Wo	44.45	40.28	47.71	44.09	42.02	42.04	43.54	40.81	43.11	41.92	43.98	43.89	44.32	45.38	44.55	41.86
En	41.02	49.22	37.33	42.74	41.20	40.36	39.60	39.00	37.08	39.59	45.07	45.42	40.74	41.77	42.17	42.28
Fs	14.52	10.49	14.95	13.17	16.79	17.60	16.85	20.20	19.81	18.49	10.95	10.69	14.94	12.84	13.28	15.86

Sample No.	L296	L296	L296	L315	L315	L315	L315	L315	L315	L345	L345	L345	L345	L345	L534	L534
Strat. Gp.	St	St	St	St	St	St	St	St	St							
Spot Ref.	17	22	23	3	4	6	7	13	22	4	8	29	32	33	6	7
Phenocryst No.	2	3	4	1	1	1				1	1	2	3	3	1	1
Position	IC	IR	IR	IR	IM	IC	QG	QG	QG	IC	IC	IC	IM	IR	IC	IR
SiO2	50.70	48.19	47.98	48.65	48.75	49.35	51.54	48.17	51.71	49.78	49.14	49.15	48.19	49.15	48.52	48.53
TiO2	1.26	1.83	2.22	2.34	2.04	1.84	1.34	2.06	1.09	1.84	2.13	1.28	2.13	1.73	0.59	0.58
Cr2O3	0.00	0.33	0.00	0.44	0.36	0.20	0.38	0.47	0.48	0.26	0.18	0.62	0.32	0.26	0.00	0.00
Al2O3	3.11	5.70	5.50	4.95	4.76	4.63	2.50	5.21	3.14	4.81	5.12	4.76	4.09	4.87	0.73	0.92
FeO	8.87	6.86	8.03	8.08	7.85	7.41	7.94	7.49	6.66	8.42	8.02	6.15	8.43	7.80	23.04	23.24
Mn	0.00	0.00	0.00	0.00	0.00	0.00	0.00	0.00	0.00	0.00	0.00	0.00	0.00	0.00	0.49	0.55
MgO	14.57	14.33	13.58	13.89	14.14	14.30	15.76	13.87	15.84	14.41	14.13	14.96	13.59	14.43	5.51	5.60
CaO	20.76	21.46	20.94	21.36	21.66	21.66	20.66	21.39	21.29	21.51	21.51	21.11	20.88	21.11	19.11	19.21
NaO	0.77	0.57	0.78	0.69	0.73	0.61	0.64	0.66	0.64	0.63	0.70	0.68	0.62	0.73	0.41	0.67
TOTAL	100.03	99.26	99.03	100.40	100.28	99.99	100.75	99.33	100.85	101.65	100.92	98.71	98.24	100.08	98.40	99.30
0=6																
Si	1.89	1.80	1.81	1.81	1.82	1.84	1.90	1.81	1.89	1.83	1.82	1.84	1.84	1.83	1.97	1.95
Al	0.14	0.25	0.24	0.22	0.21	0.20	0.11	0.23	0.14	0.21	0.22	0.21	0.18	0.21	0.03	0.04
Ti	0.04	0.05	0.06	0.07	0.06	0.05	0.04	0.06	0.03	0.05	0.06	0.04	0.06	0.05	0.02	0.02
Cr	0.00	0.01	0.00	0.01	0.01	0.01	0.01	0.01	0.01	0.01	0.01	0.02	0.01	0.01	0.00	0.00
Fe	0.28	0.21	0.25	0.25	0.24	0.23	0.24	0.24	0.20	0.26	0.25	0.19	0.27	0.24	0.78	0.78
Mn	0.00	0.00	0.00	0.00	0.00	0.00	0.00	0.00	0.00	0.00	0.00	0.00	0.00	0.00	0.02	0.02
Mg	0.81	0.80	0.76	0.77	0.79	0.79	0.87	0.78	0.87	0.79	0.78	0.84	0.77	0.80	0.33	0.34
Ca	0.83	0.86	0.85	0.85	0.87	0.86	0.82	0.86	0.84	0.85	0.85	0.85	0.85	0.84	0.83	0.83
Na	0.06	0.04	0.06	0.05	0.05	0.04	0.05	0.05	0.05	0.05	0.05	0.05	0.05	0.05	0.03	0.05
Total	4.033	4.034	4.035	4.032	4.042	4.029	4.027	4.034	4.024	4.035	4.035	4.032	4.029	4.038	4.014	4.033
Wo	43.29	45.91	45.43	45.46	45.64	45.77	42.36	45.96	43.87	44.70	45.36	45.18	45.03	44.66	42.69	42.55
En	42.27	42.64	40.99	41.11	41.45	42.02	44.94	41.48	45.42	41.65	41.44	44.54	40.78	42.47	17.14	17.27
Fs	14.43	11.45	13.59	13.42	12.91	12.21	12.70	12.56	10.71	13.65	13.20	10.27	14.18	12.87	40.17	40.18

Sample No.	L534	L534	L534	L534	L534	L534	L567	L567	L576	L576	L576	L576	L576	L579	L579
Strat. Gp.															
Spot Ref.	14	15	21	22	26	28			10	11	14	15	21	5	6
Phenocryst No.	2	2	3	3			1	2		mp	1	1	2	1	1
Position	IC	IR	IR	IC	QG	QG	IC	IC	QG	IC	IC	IR	IR	IC	IC
SiO2	49.33	49.44	49.27	49.54	49.24	48.39	45.76	46.61	50.09	49.77	48.71	49.32	50.29	48.91	48.74
TiO2	0.53	0.57	0.44	0.60	0.53	0.64	2.45	2.42	0.44	0.40	0.71	0.75	0.42	0.32	0.56
Cr2O3	0.00	0.00	0.00	0.00	0.00	0.00	0.15	0.12	0.00	0.00	0.00	0.00	0.00	0.00	0.00
Al2O3	1.11	0.88	0.99	0.89	0.86	1.32	5.67	4.99	0.90	1.05	1.46	1.28	0.91	0.97	0.92
FeO	23.08	23.17	22.65	22.23	23.46	24.38	10.17	11.31	22.61	22.85	23.67	22.35	21.99	21.55	23.10
Mn	0.47	0.47	0.44	0.65	0.73	0.48	0.14	0.19	0.51	0.42	0.27	0.46	0.40	0.50	0.43
MgO	5.54	5.58	5.95	6.28	5.43	5.06	11.63	11.76	5.80	5.79	4.79	5.69	6.50	5.96	5.14
CaO	19.45	19.32	19.59	19.50	18.80	18.12	19.38	19.83	19.80	19.59	19.51	19.70	19.82	18.87	19.66
NaO	0.72	0.48	0.59	0.66	0.52	0.64	0.64	0.41	0.76	0.62	0.61	0.63	0.62	0.62	0.57
TOTAL	100.21	99.92	99.92	100.34	99.58	99.02	96.09	97.70	100.89	100.49	99.73	100.19	100.95	97.71	99.12
0=6															
Si	1.96	1.97	1.96	1.96	1.97	1.96	1.80	1.81	1.97	1.97	1.95	1.96	1.97	1.98	1.96
Al	0.05	0.04	0.05	0.04	0.04	0.06	0.26	0.23	0.04	0.05	0.07	0.06	0.04	0.05	0.04
Ti	0.02	0.02	0.01	0.02	0.02	0.02	0.07	0.07	0.01	0.01	0.02	0.02	0.01	0.01	0.02
Cr	0.00	0.00	0.00	0.00	0.00	0.00	0.00	0.00	0.00	0.00	0.00	0.00	0.00	0.00	0.00
Fe	0.77	0.77	0.75	0.74	0.79	0.82	0.33	0.37	0.74	0.76	0.79	0.74	0.72	0.73	0.78
Mn	0.02	0.02	0.01	0.02	0.02	0.02	0.00	0.00	0.02	0.01	0.01	0.02	0.01	0.02	0.01
Mg	0.33	0.33	0.35	0.37	0.32	0.31	0.68	0.68	0.34	0.34	0.29	0.34	0.38	0.36	0.31
Ca	0.83	0.83	0.84	0.83	0.81	0.78	0.82	0.82	0.84	0.83	0.84	0.84	0.83	0.82	0.85
Na	0.06	0.04	0.05	0.05	0.04	0.05	0.05	0.03	0.06	0.05	0.05	0.05	0.05	0.05	0.04
Total	4.025	4.011	4.025	4.026	4.011	4.019	4.01	4.01	4.023	4.019	4.016	4.017	4.019	4.012	4.020
Wo	43.07	42.78	43.01	42.77	42.10	41.00	44.57	44.06	43.50	43.07	43.70	43.71	43.06	42.90	43.86
En	17.05	17.19	18.17	19.16	16.91	15.94	37.19	36.33	17.73	17.72	14.93	17.57	19.66	18.85	15.94
Fs	39.88	40.03	38.82	38.07	40.99	43.06	18.24	19.61	38.77	39.21	41.37	38.71	37.28	38.25	40.20

Sample No.	L579	L579	L579	L579	L579	L582	L582	L582	L582	L582	L582	L582	S2	S2	S2	S2
Strat. Gp.													G.X.	G.X.	G.X.	G.X.
Spot Ref.	7	8	9	11	14	3	6	13	16	20	21	22	17	41	42	43
Phenocryst No.	mp		2	2	3	mp1	1	2	3	mp2	mp3	4	1	2	2	2
Position	IC	QG	IR	IC	IC	IC	IM	IC	IC			IC	IM	IR	IM	IC
SiO2	49.02	49.17	49.60	49.21	49.07	48.06	47.58	48.08	47.72	48.06	47.81	47.965	49.06	49.39	49.35	50.36
TiO2	0.46	0.38	0.50	0.61	0.60	0.57	0.67	0.57	0.56	0.62	0.72	0.621	1.62	1.72	1.88	1.58
Cr2O3	0.00	0.00	0.00	0.00	0.00	0.00	0.00	0.00	0.00	0.00	0.00	0.00	0.00	0.00	0.00	0.00
Al2O3	0.91	0.95	1.12	0.97	0.80	0.52	0.63	0.69	0.59	0.68	0.70	0.564	3.84	4.07	4.18	3.41
FeO	21.53	21.66	19.96	23.44	23.85	28.48	27.99	26.55	27.83	27.81	28.70	27.762	9.25	9.70	9.23	9.30
Mn	0.26	0.43	0.38	0.44	0.47	0.91	0.95	0.75	0.71	0.68	0.84	0.843	0.00	0.00	0.00	0.00
MgO	6.72	6.09	7.37	4.99	4.88	1.57	1.55	2.85	2.23	2.02	1.57	1.771	13.55	13.68	13.49	14.06
CaO	19.27	19.46	19.43	19.82	19.56	19.20	19.04	19.50	19.36	19.26	19.22	19.386	20.40	20.40	20.60	20.39
NaO	0.57	0.57	0.44	0.61	0.61	0.65	0.68	0.52	0.58	0.74	0.79	0.691	0.67	0.77	0.59	0.79
TOTAL	98.73	98.71	98.80	100.08	99.85	99.96	99.10	99.51	99.58	99.86	100.35	99.60	98.39	99.73	99.30	99.88
0=6																
Si	1.96	1.97	1.97	1.96	1.97	1.97	1.97	1.97	1.96	1.97	1.96	7.891	1.87	1.86	1.86	1.88
Al	0.04	0.05	0.05	0.05	0.04	0.03	0.03	0.03	0.03	0.03	0.03	0.109	0.17	0.18	0.19	0.15
Ti	0.01	0.01	0.02	0.02	0.02	0.02	0.02	0.02	0.02	0.02	0.02	0.077	0.05	0.05	0.05	0.04
Cr	0.00	0.00	0.00	0.00	0.00	0.00	0.00	0.00	0.00	0.00	0.00	0.00	0.00	0.00	0.00	.0.00
Fe	0.72	0.73	0.66	0.78	0.80	0.98	0.97	0.91	0.96	0.95	0.98	3.82	0.29	0.30	0.29	0.29
Mn	0.01	0.01	0.01	0.02	0.02	0.03	0.03	0.03	0.02	0.02	0.03	0.117	0.00	0.00	0.00	0.00
Mg	0.40	0.36	0.44	0.30	0.29	0.10	0.10	0.17	0.14	0.12	0.10	0.434	0.77	0.77	0.76	0.78
Ca	0.83	0.84	0.83	0.85	0.84	0.85	0.85	0.85	0.85	0.85	0.84	3.418	0.83	0.82	0.83	0.82
Na	0.04	0.04	0.03	0.05	0.05	0.05	0.05	0.04	0.05	0.06	0.06	0.22	0.05	0.06	0.04	0.06
Total	4.023	4.016	4.007	4.018	4.020	4.02	4.02	4.02	4.03	4.03	4.03	4.022	4.027	4.033	4.018	4.026
Wo	42.42	43.40	42.93	43.98	43.50	44.02	44.24	44.12	43.81	44.00	43.87	44.55	43.89	43.40	44.23	43.19
En	20.59	18.89	22.65	15.41	15.10	5.00	5.01	8.97	7.02	6.42	5.00	5.66	40.57	40.49	40.31	41.44
Fs	36.99	37.71	34.42	40.61	41.40	50.98	50.75	46.90	49.17	49.58	51.13	49.79	15.54	16.11	15.46	15.37

Sample No.	S2	N2	N2	N2	N2
Strat. Gp.	G.X.	G.X.	G.X.	G.X.	G.X.
Spot Ref.	44	18	19	26	27
Phenocryst No.	2	1	1	2	3
Position	IC	IR	IC	IR	IR
SIO2	50.23	49.13	48.77	49.24	49.37
TIO2	1.63	0.19	1.61	1.25	1.60
Cr2O3	0.00	0.00	0.00	0.00	0.00
Al2O3	3.51	0.72	4.13	4.20	3.94
FeO	9.40	1.15	9.62	9.07	9.55
Mn	0.00	0.00	0.00	0.00	0.00
MgO	13.98	3.16	13.72	13.71	13.93
CaO	20.50	3.22	19.54	20.12	20.29
NaO	0.76	0.19	0.68	0.70	0.86
TOTAL	100.01	98.29	98.06	98.28	99.53
0=6					
Si	1.88	1.86	1.86	1.87	1.86
Al	0.15	0.18	0.19	0.19	0.18
Ti	0.05	0.05	0.05	0.04	0.05
Cr	0.00	0.00	0.00	0.00	0.00
Fe	0.29	0.29	0.31	0.29	0.30
Mn	0.00	0.00	0.00	0.00	0.00
Mg	0.78	0.79	0.78	0.78	0.78
Ca	0.82	0.81	0.80	0.82	0.82
Na	0.06	0.05	0.05	0.05	0.06
Total	4.027	4.022	4.026	4.027	4.041
Wo	43.35	42.83	42.35	43.49	43.06
En	41.13	41.91	41.37	41.23	41.12
Fs	15.52	15.26	16.28	15.29	15.82

APPENDIX A3 - OLIVINE COMPOSITIONS

Sample no.
Olivine compositions are arranged in order of sample number. Prefix 'L' to the sample signifies the sample is a lava; prefix 'D' indicates that the sample is an intrusive sheet; prefix 'H' indicates that the sample is a hyaloclastite glass. Grid references for each sample are given in Appendix B.

Strat. Gp.
Where appropriate, the stratigraphic Group (as defined in Chapter 4) to which the sample belongs is recorded.

Spot Ref.
This is the recorded reference number of each analysed point.

Phenocryst no.
Each analysed phenocryst was numbered. Microphenocrysts are described as 'mp'.

Position
The position of the analysed spot in relation to the crystal is recorded as:

IC - core of the phenocryst;
IM - mantle of the phenocryst;
IR - rim of the phenocryst; and
QG - quench groundmass crystals.

Sample No.	L8	L8	L8	L8	L8	L8	L8	L8	L33	L33	L33	L33	L33	L33	L43
Strat. Gp.	La	La	La	La	La	La	La	La	Se	Se	Se	Se	Se	Se	Hv
Spot Ref.	14	15	16	17	18	21	28	30	40	41	42	43	58	59	1
Phenocryst no.	1	1	1	1	1	2	mp1	2	1	1	1	2	3	3	1
Position	IR	IM	IC	IM	IM	IM	IC	IM	IR	IM	IC	IC	IM	IR	IC
SIO2	41.07	40.92	41.04	40.54	40.69	39.19	38.74	38.43	38.57	38.47	38.69	38.90	38.27	37.79	39.51
FeO	10.14	10.53	10.47	10.30	10.73	17.62	23.31	22.85	23.38	23.48	23.52	23.11	22.67	22.76	13.02
MgO	48.38	47.91	48.32	47.56	48.26	41.76	38.14	38.49	38.33	38.48	38.26	38.61	38.15	37.92	45.46
Na2O	0.53	0.32	0.52	0.32	0.40	0.65	0.47	0.80	0.53	0.67	0.70	0.66	0.73	0.66	0.53
TOTAL	100.53	100.07	100.72	99.14	100.46	99.60	101.00	100.91	101.08	101.36	101.41	101.80	100.12	99.37	98.92
Si	1.00	1.01	1.00	1.01	1.00	1.00	1.00	1.00	1.00	0.99	1.00	1.00	1.00	0.99	1.00
Fe	0.21	0.22	0.21	0.21	0.22	0.38	0.50	0.49	0.51	0.51	0.51	0.50	0.49	0.50	0.27
Mg	1.76	1.76	1.76	1.76	1.76	1.59	1.47	1.49	1.48	1.48	1.47	1.48	1.48	1.49	1.71
Na	0.03	0.02	0.02	0.02	0.02	0.03	0.02	0.04	0.03	0.03	0.04	0.03	0.04	0.03	0.03
Total	3.01	3.00	3.01	3.00	3.01	3.01	3.01	3.02	3.02	3.02	3.02	3.01	3.02	3.02	3.02
Fo%	89.47	89.03	89.16	89.17	88.91	80.86	74.47	75.01	74.51	74.50	74.36	74.86	75.00	74.81	86.16

Sample No.	L43	L43	L43	L43	L43	L43	L43	L43	L43	L43	L43	L43	L43	L58	L58
Strat. Gp.	Hv	Hv	Hv	Hv	Hv	Hv	Hv	Hv	Hv	Hv	Hv	Hv	Hv		
Spot Ref.	22	29	30	31	33	34	35	36	47	48	49	51	52	4	5
Phenocryst no.	2	3	3	3	4	4	4	mp	5	5	5	6	6	1	1
Position	IC	IC	IC	IC	IM	IC	IM	IC	IR	IR	IC	IR	IC	IR	IR
SIO2	39.11	40.40	40.22	40.97	39.99	40.24	40.36	40.19	40.20	40.05	39.77	40.09	40.60	39.66	38.85
FeO	16.75	12.79	12.58	12.81	10.16	9.52	9.18	13.96	14.59	14.79	13.78	14.86	14.42	21.06	20.94
MgO	42.45	46.42	46.13	47.24	47.48	48.42	47.86	45.36	45.01	44.82	44.72	45.21	45.79	40.67	39.29
Na2O	0.47	0.43	0.37	0.49	0.36	0.49	0.40	0.36	0.53	0.37	0.46	0.57	0.44	0.54	0.49
TOTAL	99.09	100.42	99.72	101.81	98.29	99.10	98.00	100.30	100.73	100.34	98.99	101.07	101.54	102.23	99.87
Si	1.00	1.00	1.00	1.00	1.00	1.00	1.01	1.00	1.00	1.00	1.00	1.00	1.00	1.00	1.01
Fe	0.36	0.27	0.26	0.26	0.21	0.20	0.19	0.29	0.30	0.31	0.29	0.31	0.30	0.44	0.45
Mg	1.62	1.71	1.71	1.72	1.77	1.79	1.78	1.69	1.67	1.67	1.68	1.68	1.68	1.53	1.52
Na	0.02	0.02	0.02	0.02	0.02	0.02	0.02	0.02	0.03	0.02	0.02	0.03	0.02	0.03	0.02
Total	3.01	3.01	3.01	3.01	3.01	3.01	3.00	3.01	3.01	3.01	3.01	3.02	3.01	3.01	3.01
Fo%	81.88	86.61	86.73	86.80	89.28	90.07	90.29	85.28	84.61	84.38	85.26	84.43	84.98	77.49	76.98

Sample No.	L58	L58	L69	L69	L69	L74	L74	L74	L74	L74	L74	L74	L74	L74	L74
Strat. Gp.			Sk	Sk	Sk	Hv	Hv	Hv	Hv	Hv	Hv	Hv	Hv	Hv	Hv
Spot Ref.	7	23	29	31	34	55	56	57	59	60	61	62	65	66	88
Phenocryst no.	1					1	1	2	2	2	2	mp1	3	3	
Position	IC					IC	IM	IR	IM	IM	IM	IR	IR	IC	QG
SIO2	39.45	37.59	34.67	34.62	33.52	39.25	38.55	38.58	40.26	40.11	39.21	38.43	39.03	38.95	37.94
FeO	16.79	27.94	38.73	39.44	43.06	20.11	22.97	24.59	14.90	15.45	19.90	24.29	22.50	21.44	27.01
MgO	42.96	32.12	24.22	23.23	19.53	41.18	38.40	37.26	45.48	45.07	41.24	37.39	39.51	40.08	35.03
Na2O	0.43	0.77	0.68	0.55	0.72	0.37	0.57	0.62	0.37	0.53	0.47	0.52	0.58	0.50	0.55
TOTAL	99.91	99.89	98.65	98.20	97.16	101.24	101.04	101.28	101.34	101.50	101.12	100.91	101.95	101.28	100.72
Si	1.00	1.01	1.00	1.01	1.01	1.00	1.00	1.00	1.00	1.00	1.00	1.00	1.00	1.00	1.00
Fe	0.36	0.63	0.93	0.96	1.08	0.43	0.50	0.53	0.31	0.32	0.42	0.53	0.48	0.46	0.60
Mg	1.62	1.28	1.04	1.01	0.87	1.56	1.48	1.44	1.68	1.67	1.56	1.45	1.50	1.53	1.38
Na	0.02	0.04	0.04	0.03	0.04	0.02	0.03	0.03	0.02	0.03	0.02	0.03	0.03	0.02	0.03
Total	3.01	2.98	3.02	3.01	3.01	3.01	3.02	3.01	3.01	3.02	3.01	3.01	3.02	3.02	3.01
Fo%	82.02	67.21	52.71	51.21	44.70	78.50	74.88	72.98	84.47	83.87	78.69	73.28	75.79	76.92	69.80

Sample No.	L74	L82	L121	L121	L121	L121	L121	D130	D130	D130	D130	D130	D130	D131	D131
Strat. Gp.	Hv	Lf	Ll	Ll	Ll	Ll	Ll	Sv	Sv	Sv	Sv	Sv	Sv	Sv	Sv
Spot Ref.	89	14	1	2	23	24	26	134	135	136	137	143	147	23	24
Phenocryst no.			1	1	2	2		mp1	mp1	mp2	mp3		4	1	1
Position	QG	QG	IR	IC	IR	IC	QG	IR	IC	IC	IC	QG	IM	IM	IC
SIO2	38.11	36.06	37.08	39.74	39.06	39.29	35.26	38.80	38.92	38.65	38.47	37.28	38.72	38.63	38.67
FeO	27.55	35.50	31.48	18.65	19.78	19.17	37.89	24.01	24.07	23.86	23.79	26.55	23.81	23.80	23.97
MgO	35.22	27.71	31.00	42.19	40.38	41.13	24.60	37.65	37.63	37.55	37.55	34.01	37.72	37.74	37.92
Na2O	0.81	0.56	0.60	0.65	0.52	0.46	0.73	0.45	0.64	0.63	0.65	0.75	0.58	0.40	0.61
TOTAL	101.87	100.30	100.54	101.48	99.99	100.39	99.15	101.73	101.59	101.10	100.84	99.13	101.20	100.91	101.45
Si	1.00	1.00	1.00	1.00	1.00	1.00	1.01	1.00	1.00	1.00	1.00	1.00	1.00	1.00	1.00
Fe	0.60	0.82	0.71	0.39	0.43	0.41	0.90	0.52	0.52	0.52	0.52	0.60	0.52	0.52	0.52
Mg	1.37	1.15	1.25	1.58	1.55	1.56	1.05	1.45	1.45	1.45	1.46	1.36	1.46	1.46	1.46
Na	0.04	0.03	0.03	0.03	0.03	0.02	0.04	0.02	0.03	0.03	0.03	0.04	0.03	0.02	0.03
Total	3.02	3.01	3.01	3.02	3.01	3.01	3.01	3.00	3.01	3.01	3.02	3.02	3.01	3.01	3.02
Fo%	69.50	58.18	63.71	80.13	78.45	79.27	53.65	73.65	73.59	73.72	73.77	69.53	73.85	73.87	73.82

Sample no.	D131	D131	L134	L134	L134	L134	L134	L134	L134	L134	L190	L190	L205	L205	L221
Strat. Gp.	Sv	Sv	Sv	Sv	Sv	Sv	Sv	Sv	Sv	Sv	Nd	Nd	Nd	Nd	
Spot Ref.	27	28	99	106	109	110	111	112	113	115	8	9	10	11	19
Phenocryst no.		2	mp1	mp2		1	1	1	2	3					
Position	QG	IC	IC	IC	QG	IR	IC	IM	IC	IR	IR	IC			QM
SiO2	32.45	36.08	38.72	38.82	38.87	38.69	40.03	40.04	38.85	38.78	38.95	38.91	40.95	41.13	38.53
FeO	47.71	30.81	24.54	24.52	24.32	24.27	18.61	18.43	24.11	23.99	19.03	20.34	15.24	15.33	20.81
MgO	15.24	30.68	37.64	37.76	37.56	38.12	42.98	42.74	37.77	37.45	41.08	40.11	45.72	46.03	39.47
Na2O	0.80	0.54	0.54	0.57	0.44	0.58	0.55	0.64	0.40	0.59	0.49	0.41	0.45	0.33	0.58
TOTAL	**96.90**	**98.93**	**101.70**	**101.97**	**101.51**	**101.99**	**102.48**	**102.11**	**101.43**	**101.15**	**99.87**	**100.08**	**102.76**	**103.15**	**99.59**
Si	1.01	0.99	1.00	1.00	1.00	1.00	1.00	1.00	1.00	1.00	1.00	1.00	1.00	1.00	1.00
Fe	1.24	0.71	0.53	0.53	0.53	0.52	0.39	0.39	0.52	0.52	0.41	0.44	0.31	0.31	0.45
Mg	0.70	1.26	1.45	1.45	1.45	1.46	1.60	1.59	1.45	1.45	1.57	1.54	1.67	1.67	1.53
Na	0.05	0.03	0.03	0.03	0.02	0.03	0.03	0.03	0.02	0.03	0.02	0.02	0.02	0.02	0.03
Total	3.02	3.00	3.01	3.01	3.01	3.02	3.02	3.02	3.01	3.01	3.01	3.01	3.01	3.01	3.01
Fo%	**36.27**	**63.97**	**73.22**	**73.30**	**73.36**	**73.68**	**80.46**	**80.52**	**73.63**	**73.56**	**79.37**	**77.86**	**84.25**	**84.26**	**77.17**

Sample No.	L221	L251	L251	L251	L251	L251	L255	L255	L255	L255	L255	L255	L255	L255	L255
Strat. Gp.															
Spot Ref.	20	1	2	3	4	5	14	15	16	17	24	25	26	28	33
Phenocryst no.		1	1	1	1	1	1	1	1	1	2	2	2		
Position	QM	IR	IM	IM	IC	IC	IR	IM	IM	IC	IR	IC	IM	QG	QG
SiO2	38.81	38.82	40.21	40.07	40.10	39.97	39.63	40.09	39.95	40.12	38.24	39.67	39.58	37.46	37.86
FeO	20.27	20.44	13.07	12.84	12.52	12.23	20.22	19.06	19.04	19.60	25.96	18.99	19.13	30.71	28.27
MgO	40.16	40.06	46.48	46.32	46.12	46.23	41.04	42.76	42.55	42.33	36.07	41.70	41.49	32.74	34.30
Na2O	0.51	0.57	0.28	0.48	0.49	0.36	0.40	0.69	0.56	0.58	0.33	0.49	0.38	0.60	0.61
TOTAL	**100.03**	**100.26**	**100.45**	**100.16**	**99.62**	**99.19**	**101.59**	**102.84**	**102.32**	**102.89**	**100.82**	**101.11**	**100.89**	**101.86**	**101.30**
Si	1.00	1.00	1.00	1.00	1.00	1.00	1.00	1.00	1.00	1.00	1.00	1.00	1.00	1.00	1.00
Fe	0.44	0.44	0.27	0.27	0.26	0.26	0.43	0.40	0.40	0.41	0.57	0.40	0.41	0.68	0.62
Mg	1.54	1.54	1.72	1.72	1.72	1.72	1.55	1.59	1.59	1.57	1.41	1.57	1.57	1.30	1.35
Na	0.03	0.03	0.01	0.02	0.02	0.02	0.02	0.03	0.03	0.03	0.02	0.02	0.02	0.03	0.03
Total	3.01	3.01	3.01	3.02	3.01	3.01	3.01	3.02	3.01	3.01	3.01	3.01	3.01	3.02	3.02
Fo%	**77.94**	**77.74**	**86.38**	**86.54**	**86.79**	**87.07**	**78.35**	**80.00**	**79.93**	**79.38**	**71.23**	**79.64**	**79.45**	**65.52**	**68.38**

Sample No.	L255	L255	L256	L256	L256	L256	L256	L256	L256	L256	L256	L256	L270	L270	L270
Strat. Gp.															
Spot Ref.	35	36	1	2	3	5	8	9	10	11	13	18	16	17	25
Phenocryst no.			1	1	1	mp	2	3	mp		mp	mp	1	1	2
Position	QG	QG	IM	IR	IC	IC	IR	IR	IC	QG	IC	IC	IC	IR	IC
SiO2	37.32	36.17	37.66	39.50	37.62	37.67	39.67	37.59	35.85	35.67	37.51	35.83	40.03	35.97	39.12
FeO	29.79	34.05	30.79	20.10	32.23	30.81	21.66	30.36	38.06	38.19	27.94	34.22	17.67	35.19	20.47
MgO	32.31	28.44	32.99	41.44	31.31	32.43	40.30	32.87	26.23	25.40	34.60	28.25	43.34	27.52	40.73
Na2O	0.49	0.40	0.61	0.38	0.53	0.51	0.57	0.64	0.66	0.65	0.55	0.60	0.52	0.46	0.44
TOTAL	100.30	99.47	102.31	101.73	101.98	101.69	102.48	101.72	101.14	100.29	100.88	99.28	101.80	99.32	101.08
Si	1.00	1.00	1.00	1.00	1.01	1.00	1.00	1.00	1.00	1.00	0.99	1.00	1.00	1.01	1.00
Fe	0.67	0.79	0.68	0.42	0.72	0.69	0.46	0.68	0.89	0.90	0.62	0.80	0.37	0.82	0.44
Mg	1.30	1.18	1.30	1.56	1.25	1.29	1.52	1.30	1.09	1.07	1.37	1.17	1.61	1.15	1.55
Na	0.03	0.02	0.03	0.02	0.03	0.03	0.03	0.03	0.04	0.04	0.03	0.03	0.03	0.02	0.02
Total	3.01	3.01	3.02	3.01	3.01	3.01	3.01	3.02	3.02	3.01	3.02	3.02	3.01	3.01	3.01
Fo%	65.91	59.81	65.64	78.62	63.39	65.23	76.83	65.87	55.13	54.24	68.82	59.54	81.38	58.22	78.01

Sample No.	L270	L270	L270	L270	L296	L296	L296	L296	L296	L296	L296	L296	L296	L345	L345
Strat. Gp.					St	St	St	St	St	St	St	St	St		
Spot Ref.	26	27	28	29	1	5	6	7	8	9	14	15	18	12	16
Phenocryst no.	2	2	3	3	1	2	3	4	4	4	5	5	6	1	1
Position	IC	IC	IR	IC	IR	IR	IC	IC	IC	IR	IC	IR	IM	IR	IC
SiO2	38.92	38.95	38.67	39.47	39.95	37.41	40.21	39.19	39.36	39.11	36.73	36.89	36.49	39.56	38.52
FeO	19.98	21.22	23.40	16.58	14.56	28.12	14.50	19.13	19.31	19.39	33.36	30.68	33.06	19.26	23.14
MgO	39.75	39.90	38.41	43.68	44.89	33.66	45.19	41.58	41.84	41.01	29.90	32.09	30.01	41.82	38.34
Na2O	0.35	0.47	0.54	0.49	0.51	0.51	0.40	0.39	0.67	0.36	0.66	0.50	0.61	0.56	0.46
TOTAL	99.34	100.74	101.29	100.48	100.25	100.12	100.56	100.55	101.43	100.13	100.81	100.30	100.52	101.50	100.81
Si	1.01	1.00	1.00	1.00	1.00	1.00	1.00	1.00	1.00	1.00	1.00	1.00	1.00	1.00	1.00
Fe	0.43	0.46	0.51	0.35	0.30	0.63	0.30	0.41	0.41	0.42	0.76	0.69	0.76	0.41	0.50
Mg	1.53	1.53	1.48	1.64	1.67	1.34	1.68	1.58	1.58	1.57	1.22	1.29	1.22	1.57	1.48
Na	0.02	0.02	0.03	0.02	0.02	0.03	0.02	0.02	0.03	0.02	0.03	0.03	0.03	0.03	0.02
Total	3.00	3.01	3.02	3.02	3.01	3.01	3.01	3.01	3.02	3.01	3.02	3.02	3.02	3.02	3.01
Fo%	78.00	77.02	74.53	82.44	84.61	68.09	84.75	79.49	79.43	79.03	61.51	65.09	61.81	79.47	74.71

Sample no.	L345	L345	L345	L534	L534	L534	L534	L534	L582
Strat. Gp.									
Spot Ref.	17	30	34	3	17	18	19	20	17
Phenocryst no.	2	3	4	1	2	2	3	3	1
Position	IR	IM	IM	IC	IC	IR	IC	IM	IC
SIO2	38.77	39.21	38.85	**30.21**	30.74	30.07	30.53	30.45	29.70
FeO	22.26	19.46	22.36	**64.10**	62.54	63.79	62.14	61.55	66.34
MgO	38.80	40.91	39.24	**3.21**	4.28	2.95	4.90	4.84	1.29
Na2O	0.55	0.55	0.63	**0.44**	0.63	0.50	0.48	0.57	0.48
TOTAL	**100.66**	**100.37**	**101.40**	**100.23**	**100.36**	**99.41**	**100.14**	**99.60**	**100.81**
Si	1.00	1.00	1.00	1.00	1.00	1.00	1.00	1.00	0.99
Fe	0.48	0.42	0.48	1.77	1.70	1.77	1.69	1.69	1.85
Mg	1.49	1.56	1.50	0.16	0.21	0.15	0.24	0.24	0.06
Na	0.03	0.03	0.03	0.03	0.04	0.03	0.03	0.04	0.03
Total	3.01	3.01	3.02	3.02	3.02	3.02	3.02	3.02	3.02
Fo%	**75.65**	**78.94**	**75.78**	**8.19**	**10.87**	**7.62**	**12.32**	**12.29**	**3.35**

APPENDIX A4 - Fe Ti- OXIDE COMPOSITIONS

Sample no.

Fe-oxide compositions are arranged in order of sample number. Prefix 'L' to the sample signifies the sample is a lava; prefix 'D' indicates that the sample is an intrusive sheet; prefix 'H' indicates that the sample is a hyaloclastite glass. Grid references for each sample are given in Appendix B.

Strat. Gp.

Where appropriate, the stratigraphic Group (as defined in Chapter 4) to which the sample belongs is recorded.

Sample	L8	D19	D19	D19	D19	L33	L33	L205	L251	L270	L345	L345	L345	L190	L190
Strat. Gp.	La					Se	Se							Nd	Nd
SiO2	34.69	33.54	31.76	3.99	8.21	1.10	0.71	1.36	0.57	0.34	0.34	0.29	0.23	0.25	0.99
TiO2	11.07	20.25	20.37	42.76	18.96	21.96	22.49	25.72	22.38	22.74	19.61	17.09	30.04	14.67	14.22
Cr2O3						0.25	0.25	0.19		0.49	1.91	1.90		8.97	5.79
Al2O3	6.03	9.09	6.64	0.72	4.17	2.15	2.28	2.51	1.03	1.91	5.67	5.77	2.10	3.17	3.77
Fe2O3	19.35	14.65	15.33	31.95	37.71	43.53	44.67	41.63	45.71	45.66	41.72	43.38	38.45	42.56	43.21
FeO	29.03	21.98	22.99	47.93	56.57	65.30	67.00	62.45	68.57	68.48	62.59	65.07	57.67	63.84	64.81
Mno			0.38												
MgO	5.42	1.16	1.27	0.96	2.45	1.64	1.80	2.58	2.35	2.12	6.00	5.55	1.59	4.18	4.02
CaO	7.73	1.62	3.09	1.20	0.40	0.54	0.21			0.13		0.60	0.16		0.49
Na2O	2.23	4.44	2.36	0.33	0.75	0.53	0.47	0.72	0.45	0.44	0.45		0.35	0.27	0.38
K2O	1.92	1.03	1.62	0.19	1.09	0.13		0.15							
Total	98.11	93.09	90.48	98.08	92.59	93.59	95.21	95.68	95.34	96.65	96.56	96.26	92.14	95.34	94.47

APPENDIX - B

APPENDIX B1 -GEOCHEMISTRY DATA COLLECTION

B1.1 Preparation of rock powders

Hand specimens collected in the field were between 0.5-1.0kg. Weathered surfaces were removed and samples were cut down to cubes roughly 4cm in diameter using a stainless steel hand splitter. The samples were then washed using water and a bristle brush to remove traces of dust and soil. The clean, dry rock pieces were crushed to a fine gravel in a 'Fritsch Pulverisette' jaw crusher (type 01-704). All the crushing equipment was thoroughly cleaned before use and between samples, first using water, then wire brushes and absolute alcohol. Rock dust was kept to a minimum by using a vacuum cleaner. During crushing, fragments of altered rock, amygdales and zeolites were hand picked from the sample to improve the final results.

Each gravel sample was then put in a Fritsch agate ball mill for 25 to 30 minutes and ground down to a fine powder. The agate pots were carefully cleaned and dried between samples using water and absolute alcohol. Pots which contained altered samples required thorough cleaning with quartz sand between successive samples. Quartz sand was also used to clean the agate pots at the beginning and end of a session to prevent contamination.

B1.2 XRF Analysis

B1.2.1 POWDER PELLETS

Approximately 5g of fine powder was added to 8 to 12 drops of Mowiol binding agent and mixed thoroughly for at least one minute. The mixture was transferred to a mould and subjected to 10 bars pressure for at least 20 seconds. The analytical surface was then chosen and kept isolated, the pellet was labelled and dried overnight in an oven. Eachpellet was kept in an airtoght plastic bag and was dried overnight prior to analysis.

Several pellets were made of highly porphyritic samples and the results averaged to get a more accurate whole rock composition.

B1.2.2 FUSION DISCS

The loss on ignition (LOI) of each sample is first calculated by heating approximately 5g of each powder in a furnace at 900°C for 2 hours. The powder was then cooled

before reweighing. Some samples gain in weight during this process, these usually are the freshest samples, so this may reflect the oxidation of FeO to Fe_2O_3.

The powder was mixed thoroughly with dried lithium tetraborate flux (Spectroflux 100B) in the proportion 1:5 (0.25g powdered sample: 2.25g flux) using an agate mortar and pestle. The mixture was then placed in platinum crucibles and heated to 1050°C for 20 minutes. The molten glass was then poured into moulds standing on a hotplate and immediately flattened with a stainless steel plunger. Heated glass beakers were quickly placed over the moulds to prevent quench shattering.
The discs were left to cool slowly, then they were labelled and bagged, care being taken not to touch the chosen analytical surface. The fusion discs were stored in a desicator prior to analysis. The platinum crucibles were cleaned by boiling them in a solution of dilute hydrochloric acid for about 10 minutes between samples. All other equipment and was thoroughly cleaned using water and absolute alcohol between successive samples.

B1.2.3 XRF DATA ACQUISITION

Major element oxides and trace element concentrations of whole rock samples were determined using a Philips PW1500 spectrometer with a rhodium anode tube. The machine was calibrated using a range of International standards, the calibration programme calculates the best fit straight line of composition versus counts for every element. The operator may reduce the root mean square (RMS) error of the regression line by removing standards that plot away from the line.

The calibration was tested by analysing several standards that were not used in the calibration as unknowns.

Powder pellets were were analysed for major and trace element data over a four day period. The repeated analysis of International standards W2, BOB1 and QUBS3 during data collection gave an estimate of machine accuracy. These standards were treated as unknowns not used in the calibration of the machine. Internal standards 43, 279, 582, were chosen to cover the whole range of sample compositions. These were analysed between every 5 to 10 unknown samples and gave an estimate of machine precision.

RGM1, GSP1 and NBS688 were chosen as internal samples for REE dtermined using powder pellets, they were also analysed between every 5 to 10 unknown samples.

The same method was used for fusion discs.

B1.3 ICP-AES analysis

A subgroup of 40 samples which reflected the full compositional variety of the data set was prepared for analysis at Durham University. Rock powders were dissolved in nitric and hydrofluoric acid and made into solutions. Analysis took place at Royal Holloway and Bedford College, Egham, courtesy of Dr. K. Jarvis. The results from this analysis show minimal error for the REEs, Th and U. Results for other trace elements (Ba, Nb, Y) are not included in the data set in appendix B2 since they show a high degree of error (p289).

B1.4 Electron microprobe analysis

Microprobe analyses of rock samples were performed at Manchester University and glasses and glassy rocks were analysed at Durham University. The Manchester machine had an operating beam current of 5nA and an accelerating voltage of 15kv. A cobalt standard was used as a calibration and a long-term drift monitor. Standards may be referred to on the computer hard disc. A cobalt standard was also used at Durham University and standards held on the hard disc were referred to between each sample. Polished thin sections were carbon-coated and stored in a desicator prior to analysis.

B1.5 Analytical Error

Errors were recorded as 2 sigma form and are displayed on pages 287 and 288. Major oxides analysed using powder pellets were mostly acceptable, however, MgO was rejected because $2\sigma > 1$ for the international standards. Precision and accuracy for SiO_2 and Al_2O_3 were not especially good either and this was considered during study of the geochemical results. Trace element data is good for most elements and may be compared to the guide proposed by Harvey and Atkin (1988). Errors on La, Ce and Nd determined using powder pellets is significant, however when this data is plotted versus REE concentrations determined by ICP-AES the correlation is good (p290). Correlation coefficients are between 0.9 and 1.0. The higher concentrations of La and Ce seem to cause the most problem.

FUSION DISCS

International standards run as unknowns outside the calibration.

	G2 rec.	av	STDEV	2 s.d.
SiO2	69.08	69.19	0.08	0.16
Al2O3	15.38	15.31	0.05	0.10
Fe2O3	2.53	2.76	0.16	0.33
MgO	0.75	0.76	0.01	0.01
CaO	1.96	1.92	0.03	0.06
Na2O	4.08	4.03	0.04	0.07
K2O	4.48	4.45	0.02	0.04
TiO2	0.48	0.48	0.00	0.00
MnO	0.03	0.03	0.00	0.00
P2O5	0.14	0.13	0.01	0.01
Total		99.25		

	BHVO1			
		av	STDEV	2 s.d
SiO2	49.94	50.09	0.11	0.21
Al2O3	13.8	13.72	0.06	0.11
Fe2O3	10.4	12.4	1.41	2.83
MgO	7.23	7.22	0.01	0.01
CaO	11.4	11.41	0.01	0.01
Na2O	2.26	2.33	0.05	0.10
K2O	0.52	0.53	0.01	0.01
TiO2	2.71	2.73	0.01	0.03
MnO	0.168	0.17	0.00	0.00
P2O5	0.273	0.27	0.00	0.00
Total		100.88		

	BIR1 rec.	av	STDEV	2 s.d
SiO2	47.77	47.64	0.09	0.18
Al2O3	15.35	15.56	0.15	0.30
Fe2O3	10.46	11.37	0.64	1.29
MgO	9.68	9.71	0.02	0.04
CaO	13.24	13.34	0.07	0.14
Na2O	1.75	1.77	0.01	0.03
K2O	0.027	0.03	0.00	0.00
TiO2	0.96	0.95	0.01	0.01
MnO	0.171	0.17	0.00	0.00
P2O5	0.046	0.03	0.01	0.02
Total		100.57		

	AGV1 rec.	av	STDEV	2 s.d.
SiO2	59.25	60.21	0.68	1.36
Al2O3	17.15	17.54	0.28	0.55
Fe2O3	6.53	6.8	0.19	0.38
MgO	1.53	1.63	0.07	0.14
CaO	4.94	4.99	0.04	0.07
Na2O	4.25	4.45	0.14	0.28
K2O	2.9	2.97	0.05	0.10
TiO2	1.06	1.06	0.00	0.00
MnO	0.096	0.1	0.00	0.01
P2O5	0.48	0.52	0.03	0.06
Total		100.4		

POWDER PELLETS

International standards run as unknowns outside the calibration

	W2			BOB1			QUBS3		
	rec.	n=3 av	2 s.d	rec.	n=3	2 s.d	rec.	n=3 av	2 s.d
SiO2	52.44	52.45	0.01	50.20	50.74	0.76	44.73	45.20	0.66
Al2O3	15.35	15.24	0.16	16.50	16.30	0.28	14.30	14.67	0.53
Fe2O3T	10.74	10.72	0.03	8.61	8.87	0.37	13.89	13.59	0.42
MgO	6.37	6.19	0.25	7.57	7.35	0.31	11.35	13.12	2.50
CaO	10.87	10.73	0.20	11.21	10.97	0.34	9.75	9.37	0.54
Na2O	2.14	2.20	0.09	3.15	2.91	0.34	2.52	2.64	0.17
K2O	0.63	0.62	0.00	0.35	0.37	0.03	0.35	0.41	0.08
TiO2	1.06	1.03	0.05	1.28	1.30	0.02	2.09	1.96	0.18
MnO	0.16	0.17	0.01	0.14	0.15	0.01	0.19	0.17	0.02
P2O5	0.13	0.14	0.02	0.17	0.15	0.03	0.26	0.29	0.04
	rec.	n=4	2 s.d	rec.	n=4	2 s.d	rec.	n=4	2 s.d
Ba	182.00	166.15	22.42	48.90	41.15	10.96	145.00	149.87	6.88
Rb	20.00	21.13	1.59	5.30	5.60	0.42	5.00	4.17	1.18
Nb	7.90	7.03	1.24	5.60	7.00	1.98	5.00	5.30	0.42
Zr	94.00	92.50	2.12	102.00	113.20	15.84	162.00	165.57	5.04
Y	24.00	21.48	3.57	26.30	28.08	2.51	23.00	25.60	3.68
Sr	194.00	193.95	0.07	199.50	203.35	5.44	430.00	411.97	25.50
Ga	20.00	16.80	4.53	16.70	16.13	0.81	20.00	22.07	2.92
Ni	70.00	68.88	1.59	113.00	118.38	7.60	300.00	318.80	26.59
Cr	93.00	97.18	5.90	265.00	296.18	44.09	509.00	562.97	76.32
V	262.00	255.53	9.16	241.00	236.63	6.19	302.00	307.93	8.39
Sc	35.00	36.30	1.84	33.00	33.60	0.85			
	rec.	n=2	2 s.d	rec.	n=5	2 s.d	rec.	n=3	2 s.d
La	11.40	9.93	2.08	4.90	4.75	0.21	10.00	9.05	1.34
Ce	24.00	25.00	1.41	14.00	15.69	2.39	27.00	25.90	1.56
Nd	14.00	12.83	1.66	10.30	10.90	0.85	20.00	19.10	1.27

TABLE 2

Internal standards run as unknowns outside the calibration

	279		43		582	
	n=10 av	2 s.d	n=10 av	2 s.d	n=10 av	2 s.d
SiO2	46.21	0.11	45.62	0.26	68.71	0.12
Al2O3	14.87	0.11	10.52	0.21	12.28	0.10
Fe2O3T	13.44	0.04	11.66	0.12	5.90	0.02
MgO	7.15	0.10	15.28	0.21	0.21	0.05
CaO	11.43	0.03	11.54	0.05	2.43	0.02
Na2O	2.50	0.04	1.75	0.04	4.88	0.07
K2O	0.50	0.00	0.24	0.00	2.28	0.02
TiO2	2.60	0.01	1.57	0.01	0.43	0.00
MnO	0.19	0.00	0.16	0.00	0.18	0.00
P2O5	0.30	0.01	0.16	0.01	0.04	0.00
	n=12 av	2 s.d	n=11 av	2 s.d	n=10 av	2 s.d
Nb	21.04	0.99	9.54	0.65	129.72	2.86
Zr	144.43	5.52	99.10	1.27	1346.03	20.73
Y	27.23	1.50	17.60	0.70	124.81	1.94
Sr	365.73	2.04	220.55	1.60	219.77	1.73
Ga	21.53	4.40	15.24	2.50	31.74	4.00
Zn	98.39	4.14	79.21	3.41	213.34	4.37
Cu	91.03	5.70	75.57	4.78	-0.58	3.40
Ni	106.55	2.51	510.29	7.34	2.52	1.04
Co	52.06	2.99	69.85	2.25	5.46	2.15
Cr	195.33	5.03	1053.71	44.95	33.19	5.28
V	357.57	12.52	240.30	9.29	3.14	1.91
Rb	9.19	0.88	4.75	1.11	63.68	2.05
Ba	140.15	22.12	77.93	11.21	885.01	16.77
Sc	33.17	3.88	37.23	2.52	3.20	1.29
	RGM-1		GSP 1		NBS688	
	n=6 av	2 s.d	n=6 av	2 s.d	n=3 av	2 s.d
La	21.97	1.72	184.30	2.27	5.12	1.10
Ce	45.72	1.59	396.06	3.57	13.06	1.34
Nd	20.04	1.63	194.51	1.52	9.18	1.20

ICP-AES standards run as unknowns outside the calibration

Sample	BHVO-1				G-2			
	rec	average	STDEV	2 s.d	rec	average	STDEV	2 s.d
Y	27.60	22.80	0.10	0.20	11.40	7.65	0.28	0.57
Nb	19.00	17.70	0.10	0.20	13.00	11.47	0.31	0.61
Ba	139.00	124.33	1.15	2.31	1880.00	1843.33	30.66	61.33
La	15.80	14.30	0.10	0.20	86.00	76.97	1.62	3.24
Ce	39.00	34.87	0.90	1.79	159.00	144.67	2.08	4.16
Pr	5.70	5.04	0.10	0.19	19.00	14.40	0.96	1.93
Nd	25.20	23.10	0.95	1.91	53.00	47.50	2.52	5.03
Sm	6.20	5.39	0.58	1.16	7.20	5.99	0.75	1.51
Eu	2.06	2.06	0.08	0.17	1.41	1.49	0.12	0.23
Gd	6.40	5.47	0.17	0.33	4.10	4.96	0.38	0.76
Tb	0.96	0.92	0.09	0.18	0.48	0.44	0.02	0.05
Dy	5.20	5.01	0.52	1.04	2.50	1.84	0.02	0.04
Ho	0.99	1.07	0.15	0.31	0.37	0.35	0.07	0.13
Er	2.40	2.47	0.18	0.36	1.20	0.78	0.10	0.19
Tm	0.33	0.41	0.08	0.17	0.17	0.08	0.04	0.07
Yb	2.02	1.82	0.28	0.55	0.78	0.36	0.10	0.20
Lu	0.29	0.34	0.05	0.09	0.11	0.09	0.02	0.03
Th	1.08	1.29	0.08	0.15	24.60	20.87	0.40	0.81
U	0.42	0.48	0.05	0.10	2.04	1.61	0.09	0.17

	BIR-1				AGV-1			
	rec	average	STDEV	2 s.d	rec	average	STDEV	2 s.d
Y	16.00	14.03	0.40	0.81	21.00	16.73	0.32	0.64
Nb	2.00	1.53	0.52	1.05	15.00	13.00	0.26	0.53
Ba	7.70	5.73	0.56	1.12	1221.00	1174.00	4.36	8.72
La	0.88	0.36	0.04	0.07	38.00	34.30	0.70	1.40
Ce	2.50	1.68	0.13	0.26	66.00	60.93	0.60	1.21
Pr	0.50	0.11	0.06	0.12	6.50	7.46	0.22	0.45
Nd	2.50	2.03	0.11	0.22	34.00	28.40	0.44	0.87
Sm	1.08	0.59	0.42	0.84	5.90	5.96	0.90	1.81
Eu	0.54	0.47	0.05	0.11	1.66	1.78	0.51	1.03
Gd	1.90	1.38	0.19	0.38	5.20	5.61	0.78	1.56
Tb	0.41	0.34	0.10	0.20	0.71	0.71	0.07	0.14
Dy	2.40	2.42	0.25	0.50	3.80	3.51	0.33	0.66
Ho	0.50	0.53	0.05	0.11	0.73	0.71	0.07	0.14
Er	1.80	1.55	0.02	0.04	1.61	2.11	0.18	0.36
Tm	0.27	0.21	0.03	0.05	0.32	0.33	0.10	0.20
Yb	1.70	1.26	0.16	0.32	1.67	1.93	0.13	0.26
Lu	0.26	0.22	0.03	0.06	0.28	0.29	0.07	0.13
Th	0.03	0.12	0.08	0.15	6.50	5.68	0.15	0.30
U	0.01	-0.01	0.02	0.03	1.89	1.83	0.05	0.09

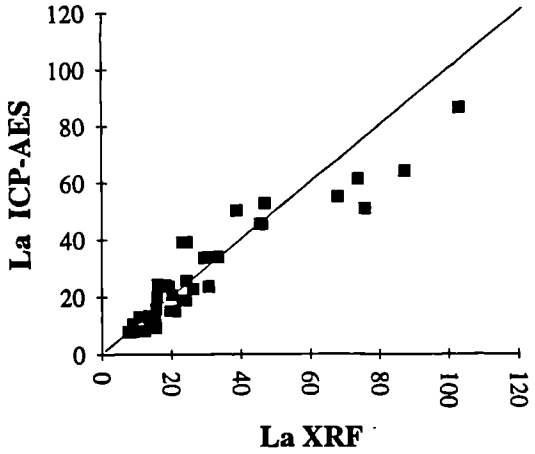
La ICP-AES
La XRF
0
20
40
60
80
100
120

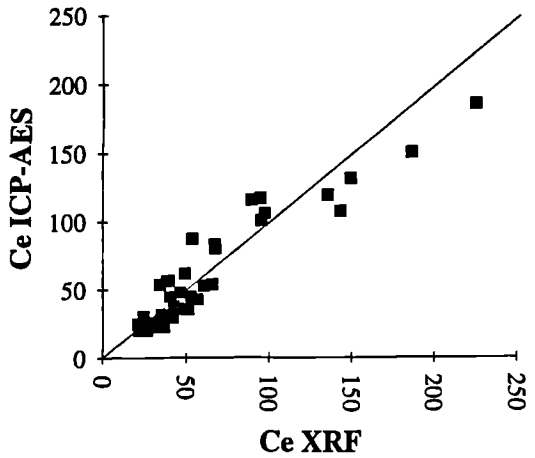
Ce ICP-AES
Ce XRF
0
50
100
150
200
250

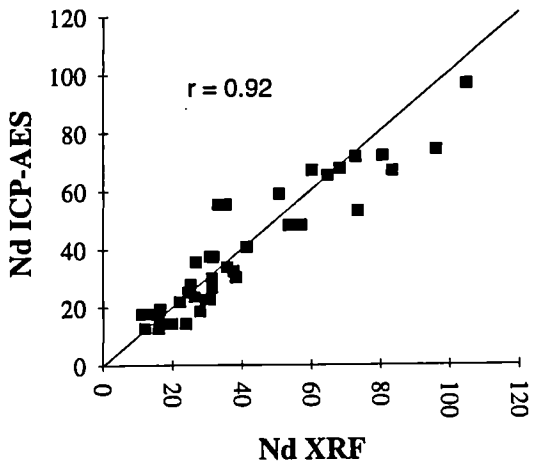
r = 0.92
Nd ICP-AES
Nd XRF
0
20
40
60
80
100
120

APPENDIX B2 - WHOLE-ROCK GEOCHEMICAL DATA

Sample no.

Whole rock data are arranged in order of increasing sample number. Prefix 'L' to the sample number signifies that the sample is a lava. Prefix 'D' indicates that the sample is an inclined sheet. Two stars following the sample number indicates that the major elements were determined using powder pellets.

Strat. Loc.

Where appropriate, the stratigraphic Group (as defined in Chapter 4) to which the sample belongs is recorded.

Grid Ref.

A grid reference is given for each sample. Grid references are taken from the 1:50,000 topographic map of 'Eyjafjallajökull', published by the Defense Mapping Agency Hydrographic/Topographic Center, Washington, D.C. in cooperation with the Iceland Geodetic Survey, 1990.

Structure

The structure of inclined sheets is presented.

Sample no.	D1	L2	L3	D4	S5	D6	L7	L8	L9	P10
Type	dyke	hawaiite	hawaiite	dyke	sill	dyke	mugearite	basalt	basalt	basalt
Strat. Loc.		Se	Se				Se	La	La	La
GRID REF.	6890 4950	6905 4935	6905 4935	6910 4970	6910 4970	6895 4955	6915 4985	6910 5000	6910 5005	6905 5000
Structure	274/30S			220/90	240/18S	040/90				
SiO2	46.23	51.71	51.28	46.51	47.42	50.98	54.57	46.56	47.08	47.32
Al2O3	14.40	15.41	15.34	16.07	13.87	14.80	14.78	15.54	15.82	15.94
Fe2O3T	13.35	11.81	11.76	14.12	15.60	12.60	11.04	11.98	12.01	12.33
MgO	5.92	3.63	3.65	5.06	3.99	3.97	2.79	6.90	6.51	5.79
CaO	12.80	7.41	7.46	9.47	9.09	7.71	6.67	11.67	11.84	12.38
Na2O	2.35	4.79	4.74	3.25	3.83	4.12	4.59	2.69	2.51	2.33
K2O	0.50	1.53	1.52	0.75	1.10	1.18	1.11	0.70	0.74	0.46
TiO2	2.97	2.49	2.47	3.32	3.84	3.15	2.17	2.40	2.43	2.68
Mn	0.20	0.21	0.21	0.24	0.25	0.24	0.24	0.17	0.18	0.24
P2O5	0.32	0.88	0.86	0.36	0.52	0.54	0.87	0.30	0.30	0.30
Total	99.04	99.87	99.29	99.15	99.51	99.29	98.83	98.91	99.42	99.77
LOI	1.19	0.00	0.00	0.57	0.25	0.86	0.38	0.22	0.34	0.34
Mg#	48.4	39.4	39.7	43.1	35.1	40.0	34.9	54.9	53.4	49.9
XRF										
Nb	19.5	49.1	52.7	26.7	38.1	55.6	63.4	24.4	24.3	23.6
Zr	172.5	445.2	445.6	194.4	287.7	456.7	510.2	175.8	181.2	178.5
Y	30.1	63.7	64.7	34.0	45.8	57.1	70.2	28.9	28.2	28.3
Sr	375.4	451.3	445.6	434.3	440.7	437.7	539.4	413.4	435.6	455.9
Zn	92.0	122.0	122.5	91.3	116.4	127.5	145.1	79.2	80.3	92.5
Ni	83.8	21.9	26.7	19.1	11.1	1.7	0.6	115.6	107.5	69.4
V	360.5	162.7	164.7	395.4	284.6	203.8	85.6	284.1	292.6	324.5
Cr	98.3	32.1	32.1	-2.8	1.2	0.5	4.5	187.8	123.6	60.3
Ga	21.6	48.9	27.0	25.9	24.9	25.7	23.8	21.2	20.3	23.2
Sc	32.1	18.1	20.4	27.2	28.6	19.3	10.7	29.4	31.2	33.8
Cu	130.3	38.9	39.7	88.3	42.7	12.4	6.4	112.7	122.6	138.1
Co	60.9	32.2	29.4	54.1	55.9	36.6	22.3	55.7	56.5	56.3
Rb	5.9	24.9	28.6	7.4	19.8	6.0	21.7	12.9	14.1	4.7
Ba	119.7	329.6	320.8	174.6	235.6	344.2	424.5	143.5	174.2	132.4
ICP-AES										
La	16.8	45.7	60.9	26.6	36.0	57.8	72.4	20.8	22.6	19.0
Ce	50.3	100.9	132.8	57.6	84.0	116.8	141.6	53.7	60.5	42.9
Pr		13.6								5.6
Nd	32.6	58.9	79.1	40.2	51.9	69.5	77.7	32.9	31.9	25.1
Sm		12.8								6.0
Eu		4.3								2.0
Gd		13.2								6.1
Dy		11.3								5.5
Ho		2.0								0.9
Er		5.9								2.7
Yb		5.0								2.5
Lu		0.7								0.3
Th		4.3								1.9
U		1.2								0.6
Tb		1.9								0.9
Tm		0.8								0.4
Nb		55.3								25.2
Y										24.5
Ba		338.0								147.0

Sample no.	L11	L12	L13	L16	D17	D18	D19	D20	D21	D22
Type	basalt	basalt	basalt	basalt	dyke	dyke	dyke	dyke	dyke	dyke
Strat. Loc.	La	La	La	La						
GRID REF.	6905 5000	6905 4995	6905 5000	6910 5010	6910 5000	6910 5005	6910 5000	6910 5000	6910 5005	6910 5005
Structure					275/48S	220/61S	008/90	050/85S	220/80S	095/50N
SiO2	46.84	47.59	47.45	47.26	47.56	45.88	48.57	46.52	49.31	47.66
Al2O3	15.63	16.05	16.08	16.80	13.26	14.00	13.20	14.39	15.44	14.05
Fe2O3T	12.87	11.96	12.77	11.85	15.07	14.83	16.03	14.66	12.76	14.64
MgO	6.01	6.95	5.82	6.21	4.30	5.07	3.98	6.57	4.46	6.09
CaO	11.67	11.57	11.87	11.85	10.72	12.22	8.50	10.43	9.91	10.31
Na2O	2.47	2.50	2.55	2.43	2.66	2.66	3.57	2.81	3.03	2.65
K2O	0.68	0.70	0.64	0.59	0.72	0.58	0.89	0.64	0.61	0.52
TiO2	2.68	2.42	2.63	2.38	3.96	3.45	3.29	3.39	3.31	3.30
Mn	0.19	0.17	0.18	0.17	0.21	0.23	0.26	0.23	0.20	0.23
P2O5	0.29	0.31	0.30	0.27	0.64	0.45	1.58	0.35	0.40	0.43
Total	99.33	100.22	100.29	99.81	99.10	99.37	99.87	99.99	99.43	99.88
LOI	0.27	0.26	0.42	0.27	0.95	1.02	0.95	2.05	0.83	1.16
Mg#	49.7	55.2	49.1	52.6	37.7	42.0	34.5	48.7	42.5	46.8
XRF										
Nb	22.3	25.4	23.1	19.9	30.5	29.6	38.7	24.5	29.1	29.0
Zr	167.4	174.6	160.7	157.3	248.9	224.5	321.5	187.6	205.8	243.5
Y	27.8	28.9	28.0	26.6	46.4	37.2	75.1	30.9	35.6	39.7
Sr	430.6	394.4	430.6	433.5	412.7	428.7	464.8	432.6	443.0	380.9
Zn	89.0	80.7	88.7	72.8	106.5	96.7	135.7	85.1	86.4	103.8
Ni	65.9	103.9	62.8	71.7	17.9	30.8	0.7	49.9	25.2	29.0
V	319.4	288.9	326.7	281.6	394.5	415.7	116.7	455.9	372.6	394.6
Cr	65.7	125.0	56.7	86.1	0.7	8.0	1.3	29.8	12.0	6.3
Ga	25.7	19.1	20.6	23.1	25.1	19.4	24.3	19.5	22.3	23.4
Sc	19.5	26.1	29.4	34.6	29.5	29.7	21.4	33.5	26.5	30.3
Cu	121.4	121.0	138.3	89.9	47.8	57.1	4.7	106.1	51.5	38.1
Co	54.1	63.8	59.9	52.9	54.9	59.3	35.3	71.4	51.3	57.0
Rb	11.3	11.4	7.4	7.6	5.3	6.3	7.9	3.6	6.0	6.8
Ba	146.1	154.1	151.6	133.2	169.8	160.5	199.7	153.4	176.9	141.2
ICP-AES										
	19.0	22.5	21.2	17.5	31.6	27.0	57.0	23.5	28.0	29.7
	49.9	51.3	54.6	42.8	75.7	67.8	115.0	52.0	63.5	63.8
	28.0	31.6	32.1	29.0	53.1	41.3	79.0	36.6	41.4	42.7
Sm										
Eu										
Gd										
Dy										
Ho										
Er										
Yb										
Lu										
Th										
U										
Tb										
Tm										
Nb										
Y										
Ba										

Sample no.	D23	L25	L26	L27	D28	D29	L30	L31	L32	L35
Type	dyke	basalt	basalt	basalt	basalt	dyke	basalt	mugearite	mugearite	mugearite
Strat. Loc.		La	La	Mo				Se	Se	Se
GRID REF.	6910 5005	6910 5010	6905 5015	6905 5015	6905 5015	6905 5015	6905 5020	6905 5020	6905 5035	6890 5045
Structure	040/40N				205/62S	220/55S				
SiO2	47.41	47.68	47.22	47.75	46.78	47.28	48.38	53.38		53.34
Al2O3	14.38	16.75	16.60	14.35	13.17	14.20	14.58	15.18		15.22
Fe2O3T	13.45	12.19	12.39	15.87	15.90	12.78	14.48	12.02		11.99
MgO	6.55	5.79	5.84	4.61	5.07	6.67	4.17	2.71		2.86
CaO	10.37	11.35	11.26	9.88	10.45	11.69	9.01	6.55		6.63
Na2O	2.59	3.06	2.74	3.25	2.95	2.32	4.05	5.05		4.99
K2O	0.61	0.53	0.68	0.61	0.69	0.50	1.04	1.57		1.53
TiO2	3.31	2.48	2.57	3.34	3.69	2.93	3.67	2.18		2.18
Mn	0.22	0.18	0.17	0.23	0.23	0.22	0.22	0.23		0.22
P2O5	0.41	0.28	0.30	0.40	0.39	0.30	0.59	0.69		0.69
Total	99.30	100.29	99.77	100.29	99.32	98.89	100.19	99.56		99.65
LOI	1.11	0.69	0.50	0.31	0.99	1.53	0.00	0.04		0.07
Mg#	50.8	50.1	50.0	38.1	40.3	52.5	37.9	32.3		33.6
XRF										
Nb	31.4	21.5	23.5	29.4	26.8		38.7	49.5	56.3	51.6
Zr	221.4	167.3	167.5	234.2	229.5		297.6	458.1	515.9	453.2
Y	35.6	25.2	28.4	37.0	41.2		46.4	64.6	69.7	62.0
Sr	418.4	388.7	435.6	418.5	333.4		435.6	456.2	435.6	446.7
Zn	93.9	84.5	81.6	123.4	103.7		129.2	145.0	153.8	142.4
Ni	46.9	63.6	70.5	24.7	15.3		17.3	-1.6	0.8	5.9
V	394.5	312.4	318.4	415.7	456.3		329.5	101.6	56.3	117.8
Cr	8.1	56.8	67.1	2.0	0.7		1.4	8.6	10.1	98.5
Ga	24.0	20.4	18.6	28.1	26.7		24.2	25.8	30.5	23.8
Sc	29.2	31.8	29.6	30.5	37.3		38.1	15.5	16.5	15.7
Cu	101.5	100.7	112.2	79.0	77.3		60.5	11.1	8.2	15.5
Co	57.0	54.9	55.5	65.9	53.1		48.9	27.4	22.4	27.8
Rb	6.9	7.5	11.2	4.7	11.3		18.2	29.7	34.6	37.8
Ba	150.8	128.6	143.7	168.6	136.8		228.1	322.2	367.3	330.1
ICP-AES										
La	31.1	17.9	20.7	24.3	23.9		41.0	59.4	65.0	57.0
Ce	70.0	49.7	54.0	53.7	62.5		89.0	113.5	121.6	106.7
Pr				7.4						
Nd	46.5	30.7	35.3	32.4	44.0		61.3	70.9	78.4	64.8
Sm				7.9						
Eu				2.7						
Gd				8.5						
Dy				7.8						
Ho				1.4						
Er				4.0						
Yb				3.5						
Lu				0.5						
Th				2.3						
U				0.7						
Tb				1.2						
Tm				0.6						
Nb				32.2						
Y				34.0						
Ba				201.0						

Sample no.	L37	L38	L39	L40	L41	L42	L43	L44	L45	L46
Type	hawaiite	hawaiite	FeTi bas	FeTi bas	FeTi bas	FeTi bas	ankaramite	basalt	basalt	basalt
Strat. Loc.	Se	Se	Sk	Sk	Sk	Sk	Hv	Hv	Hv	Hv
GRID REF.	6890 5045	6875 5060					5590 5025	5590 5025	5590 5025	5590 5025
Structure										
SiO2	52.07	51.97	46.85	47.03	47.17	46.92	46.38	45.01	46.75	47.05
Al2O3	14.03	14.19	13.08	12.97	12.85	12.82	9.87	13.31	14.13	14.26
Fe2O3T	14.10	13.87	15.75	15.90	15.77	15.84	11.01	14.53	14.58	14.27
MgO	3.00	2.80	4.71	4.67	4.68	4.75	16.84	6.48	5.91	5.43
CaO	7.07	6.92	9.34	9.24	9.35	9.34	11.19	9.99	10.03	10.06
Na2O	4.60	4.46	3.30	3.29	3.32	3.28	1.54	2.98	3.03	3.08
K2O	1.38	1.34	0.81	0.81	0.79	0.80	0.24	0.61	0.70	0.72
TiO2	2.54	2.53	4.43	4.42	4.46	4.47	1.53	3.31	3.36	3.39
Mn	0.25	0.26	0.23	0.23	0.23	0.23	0.16	0.21	0.20	0.18
P2O5	0.91	0.88	0.57	0.58	0.56	0.57	0.16	0.47	0.48	0.51
Total	99.95	99.24	99.08	99.15	99.19	99.00	98.93	96.90	99.16	98.95
LOI	0.08	0.00	0.00	0.00	0.00	0.00	0.01	0.00	0.19	0.14
Mg#	31.1	29.9	38.8	38.3	38.6	38.8	76.4	48.6	46.2	44.6
XRF										
Nb	48.5	50.1	31.6	32.2	31.4	32.5	10.5	25.8	26.5	27.2
Zr	442.4	437.9	228.4	225.6	219.9	228.7	101.4	199.5	206.5	213.5
Y	67.8	68.4	37.9	39.6	38.4	40.0	18.6	37.5	36.7	39.6
Sr	426.8	435.8	458.9	473.6	472.6	475.6	225.0	398.5	406.5	412.2
Zn	153.4	148.6	136.0	132.7	133.4	126.6	77.6	112.3	109.3	107.1
Ni	3.0	1.9	27.1	17.8	19.1	24.1	510.8	75.7	67.1	69.1
V	114.5	120.8	374.4	367.7	390.5	356.7	241.4	359.5	365.9	374.6
Cr	5.5	4.6	5.8	7.7	6.4	8.9	1054.3	95.8	88.6	85.7
Ga	22.9	28.5	21.2	23.2	25.4	21.6	12.0	21.7	22.1	22.3
Sc	21.2	24.0	32.9	26.9	31.4	28.6	36.9	32.4	25.5	33.1
Cu	20.9	23.3	32.7	33.9	37.0	33.2	79.1	60.2	48.1	55.9
Co	38.7	30.7	60.0	55.8	55.3	54.2	74.2	62.9	60.9	59.8
Rb	26.5	22.7	14.6	16.1	14.1	14.1	4.6	9.1	13.3	12.5
Ba	294.9	282.1	173.2	176.9	154.9	176.5	73.4	156.7	157.0	168.2
ICP-AES										
La	57.2	57.3	27.6	29.4	29.7	33.8	8.3	27.5	27.8	31.2
Ce	108.2	115.2	75.8	76.8	72.0	79.9	20.3	64.9	68.0	70.4
Pr							2.8			
Nd	69.9	70.0	49.3	55.0	55.0	58.2	13.6	44.7	45.7	49.6
Sm							3.3			
Eu							1.2			
Gd							4.0			
Dy							3.4			
Ho							0.7			
Er							1.8			
Yb							1.5			
Lu							0.2			
Th							0.8			
U							0.3			
Tb							0.6			
Tm							0.3			
Nb							11.1			
Y							16.6			
Ba							69.6			

Sample no.	L47	L48	L49	L50	D51	L52	L53	L54	L55	L56
Type	basalt	basalt	basalt	basalt	dyke	basalt	basalt	basalt	basalt	basalt
Strat. Loc.	Hv	Hv	Hv	Hv		Hv	Hv	Hv	Hvamm	Hvamm
GRID REF.	5600 5025	5600 5025	5600 5025	5600 5025	5610 5030	5615 5040	5615 5040	5615 5040	5615 5050	5615 5050
Structure					275/90	~				
SiO2	46.97	46.85	46.75	46.86	47.44	46.70	46.85	46.59	47.93	48.47
Al2O3	14.21	14.02	13.96	14.32	14.70	14.14	13.89	14.14	13.58	13.81
Fe2O3T	14.74	14.71	14.89	14.64	10.49	14.71	13.88	14.09	14.93	13.65
MgO	5.54	5.76	5.63	5.56	8.40	5.72	6.82	6.40	4.77	5.39
CaO	9.85	9.81	9.82	9.88	13.42	9.91	10.30	10.31	9.23	10.12
Na2O	3.19	3.08	3.17	3.13	2.16	3.23	2.84	3.06	3.58	3.14
K2O	0.71	0.69	0.72	0.71	0.22	0.70	0.60	0.67	0.89	0.76
TiO2	3.36	3.39	3.45	3.35	2.20	3.41	3.07	3.18	3.57	3.13
Mn	0.21	0.20	0.22	0.21	0.16	0.21	0.21	0.20	0.24	0.21
P2O5	0.50	0.46	0.52	0.49	0.21	0.49	0.41	0.45	0.44	0.43
Total	99.29	98.97	99.12	99.15	99.40	99.22	98.88	99.10	99.15	99.11
LOI	0.06	0.23	0.03	0.09	0.71	0.04	0.02	0.00	0.00	0.32
Mg#	44.3	45.3	44.5	44.6	62.9	45.2	51.0	49.0	40.4	45.5
XRF										
Nb	26.8	25.5	27.3	27.3	15.6	25.6	25.7	27.7	32.0	30.0
Zr	211.4	204.5	219.4	208.8	124.1	205.2	190.1	207.4	271.6	258.5
Y	37.2	36.3	38.6	39.6	23.0	36.7	36.7	36.7	44.9	42.9
Sr	418.7	416.8	409.3	420.9	371.5	421.9	390.3	392.6	340.8	350.4
Zn	113.4	120.1	126.7	118.7	95.8	109.4	102.7	97.5	121.5	121.7
Ni	63.4	67.1	60.6	62.5	169.2	59.0	69.5	71.4	24.8	51.9
V	372.4	354.6	350.1	339.5	294.3	347.3	306.4	324.1	336.5	355.3
Cr	74.7	87.2	73.9	92.8	394.1	100.1	140.8	145.1	9.6	53.3
Ga	22.3	23.2	19.8	19.0	20.0	21.2	25.3	24.8	26.5	26.1
Sc	28.5	33.2	27.7	25.8	27.7	34.8	32.4	32.8	25.6	32.3
Cu	52.7	46.5	51.1	50.8	115.9	38.5	51.9	60.7	67.7	90.8
Co	59.1	61.7	62.5	57.9	64.3	60.4	57.5	55.1	61.2	60.2
Rb	13.0	12.0	11.8	11.9	3.4	12.3	9.5	9.4	17.0	14.3
Ba	165.1	162.7	160.4	168.2	90.3	165.6	165.9	170.6	157.5	152.7
ICP-AES										
La	28.2	25.7	28.4	27.8	15.1	28.2	25.5	27.4	23.6	25.5
Ce	65.5	55.4	64.9	67.8	35.2	66.5	64.0	69.2	56.5	66.5
Pr									8.1	
Nd	45.3	37.5	45.9	44.2	25.3	43.4	42.1	45.7	34.2	43.3
Sm									8.3	
Eu									2.8	
Gd									9.0	
Dy									8.4	
Ho									1.6	
Er									4.5	
Yb									3.9	
Lu									0.6	
Th									2.3	
U									0.8	
Tb									1.4	
Tm									0.6	
Nb									34.7	
Y									41.6	
Ba									164.0	

Sample no.	L57	L58	D59	P60	L61	L62	L63	L64	D65	L66
Type	basalt	basalt	dyke	basalt	basalt	basalt	FeTi bas	FeTi bas	dyke	FeTi bas
Strat. Loc.	Hvamm	Hvamm		Hvamm	Hvamm		Sk	Sk		Sk
GRID REF.	LOOSE	5615 5050	5625 5060	5620 5055	5620 5055	5620 5055	7710 5060	7705 5040	7715 5020	7715 5015
Structure			042/80E			–			267/90	
SiO2	46.72	48.99		47.54	48.36	47.71	46.85	46.83	46.88	46.75
Al2O3	13.43	13.24		13.68	14.26	14.19	12.95	12.89	13.63	12.95
Fe2O3T	11.02	14.93		14.61	13.50	14.39	15.86	15.68	14.50	15.80
MgO	11.64	5.98		4.56	5.36	5.32	4.93	4.90	5.84	4.90
CaO	11.44	10.43		9.42	10.48	9.93	9.42	9.37	10.62	9.39
Na2O	0.35	2.49		3.77	3.06	3.18	3.34	3.36	2.95	3.68
K2O	0.35	0.52		0.96	0.62	0.70	0.78	0.81	0.59	0.81
TiO2	1.87	3.43		3.76	3.06	3.18	4.49	4.44	3.72	4.46
Mn	0.16	0.23		0.22	0.19	0.22	0.23	0.22	0.20	0.23
P2O5	0.19	0.42		0.49	0.38	0.43	0.56	0.57	0.39	0.57
Total	99.18			99.01	99.27	47.71	99.42	99.06	99.31	99.53
LOI	0.00	0.27		0.10	0.07	0.00	0.00	0.04	0.00	0.00
Mg#	69.1	45.9		39.8	45.7	43.9	39.7	39.8	46.0	39.6
XRF										
Nb	14.8	29.2	23.4	35.5	25.6	30.2	31.2	31.2	26.1	31.3
Zr	112.2	254.1	191.2	261.7	205.7	258.9	232.2	225.8	184.1	224.9
Y	20.6	39.8	33.3	43.7	39.6	43.9	40.1	39.7	31.8	40.4
Sr	329.9	354.3	423.3	390.3	376.5	354.9	471.2	467.6	438.9	458.3
Zn	79.5	118.7	110.4	125.2	111.7	110.5	127.5	132.4	116.7	125.7
Ni	262.4	50.7	40.1	33.6	43.9	46.6	22.5	22.6	75.9	25.2
V	241.2	369.8	426.1	365.4	336.8	325.4	349.6	368.8	394.5	348.4
Cr	663.7	63.1	18.6	18.2	26.6	60.1	8.6	6.5	58.8	9.5
Ga	18.7	20.9	29.9	32.4	23.0	25.5	21.8	29.2	25.0	29.0
Sc	27.5	26.9	36.4	30.1	33.7	30.1	32.1	20.4	29.1	32.1
Cu	96.1	93.6	55.7	64.2	73.4	75.6	33.3	41.3	117.3	37.0
Co	68.0	56.2	63.9	55.5	52.1	52.5	56.7	54.3	58.4	55.0
Rb	8.4	14.4	9.4	10.2	7.9	10.8	12.8	12.0	8.3	15.8
Ba	93.2	149.3	156.0	219.5	134.1	173.9	197.1	175.3	140.7	185.6
ICP-AES										
La	10.9	26.2	23.0	35.3	22.2	30.5	32.4	33.1	20.9	33.3
Ce	32.0	59.7	65.1	85.0	60.0	73.7	80.5	83.7	55.0	79.2
Pr										
Nd	19.5	40.7	44.5	59.6	40.3	50.2	58.1	62.5	36.7	62.1
Sm										
Eu										
Gd										
Dy										
Ho										
Er										
Yb										
Lu										
Th										
U										
Tb										
Tm										
Nb										
Y										
Ba										

Sample no.	L67	L68	L69	F70	P71	F72	D73	L74	L75	P76
Type	FeTi bas	basalt	FeTi bas	FeTi bas	FeTi bas	FeTi bas	FeTi bas	ankaramite	basalt	basalt
Strat. Loc.	Sk	Sk	Sk	Sk	Sk	Sk		Hv	Lambafeli	Lambafeli
GRID REF.	7715 5015	7715 5015	7715 5015	7710 5025	7710 5025	7710 5025	7710 5025	5590 5025	6765 4735	6765 4735
Structure							010/64W			
SiO2	46.73	46.27	46.65	46.43	46.53	46.90	46.63	46.07	48.00	48.20
Al2O3	12.95	13.31	12.99	12.97	12.89	13.01	12.85	9.47	13.14	13.05
Fe2O3T	15.93	14.65	15.82	15.69	15.59	15.40	15.60	11.13	15.12	14.94
MgO	4.89	5.73	4.85	4.81	4.84	4.75	4.86	17.44	4.99	4.66
CaO	9.31	10.42	9.41	9.41	9.51	9.53	9.32	11.07	9.40	9.01
Na2O	3.25	3.00	3.31	3.30	3.29	3.26	3.26	1.61	3.25	3.39
K2O	0.79	0.63	0.78	0.83	0.82	0.82	0.80	0.27	0.92	1.06
TiO2	4.49	3.73	4.49	4.45	4.45	4.48	4.39	1.49	3.73	3.69
Mn	0.23	0.20	0.23	0.23	0.23	0.23	0.23	0.16	0.21	0.22
P2O5	0.56	0.39	0.56	0.57	0.57	0.57	0.55	0.15	0.72	0.84
Total	99.14	98.33	99.08	98.70	98.72	98.97	98.50	98.86	99.48	99.05
LOI	0.00	0.00	0.00	0.18	0.39	0.44	0.10	0.00	0.00	0.00
Mg#	39.4	45.3	39.4	39.4	39.7	39.5	39.7	76.8	41.1	39.8
XRF										
Nb	30.5	25.6	32.5	31.6	31.5	31.4	31.5	9.5	35.3	38.6
Zr	225.6	186.7	224.5	227.8	229.8	220.1	226.8	98.0	253.7	274.5
Y	40.7	33.1	40.7	38.0	38.2	38.3	38.7	17.8	44.3	47.1
Sr	473.6	431.8	456.7	459.8	459.9	467.2	459.5	217.3	453.2	440.6
Zn	124.5	108.7	124.7	140.9	138.2	138.3	132.4	76.4	138.7	142.9
Ni	21.7	65.4	23.4	27.2	23.2	25.0	25.6	505.0	37.6	28.7
V	353.5	395.6	354.6	367.8	378.9	376.5	367.9	231.2	315.6	299.7
Cr	8.4	52.9	9.9	3.7	4.9	19.2	6.6	1029.2	20.1	14.0
Ga	26.7	25.9	24.6	25.3	26.7	27.8	26.9	16.0	27.7	26.8
Sc	32.1	35.3	24.8	29.6	32.6	32.5	32.1	34.3	32.6	28.5
Cu	28.5	86.6	39.1	38.4	33.2	38.1	47.3	121.6	69.1	58.6
Co	52.0	55.9	56.4	61.7	62.8	58.8	51.7	77.6	59.2	51.1
Rb	10.8	10.0	15.2	15.4	15.6	14.7	14.8	6.0	17.8	19.7
Ba	210.4	153.4	172.8	167.8	162.5	169.3	175.8	85.2	195.8	199.5
ICP-AES										
La	34.8	24.7	25.7	29.0	29.3	29.2	30.1	8.0	35.8	40.0
Ce	79.8	64.6	61.9	80.2	72.6	80.5	83.6	19.9	79.1	85.4
Pr			8.3					2.6		
Nd	59.8	45.0	37.2	57.3	51.6	53.9	54.2	12.9	53.8	59.2
Sm			8.2					3.1		
Eu			3.0					1.1		
Gd			9.0					3.7		
Dy			7.7					3.3		
Ho			1.4					0.7		
Er			3.6					1.7		
Yb			3.0					1.5		
Lu			0.4					0.2		
Th			2.3					0.7		
U			0.7					0.2		
Tb			1.4					0.6		
Tm			0.5					0.2		
Nb			36.2					10.9		
Y			35.0					15.8		
Ba			183.7					65.6		

Sample no.	L77	L78	L81	L82	L83	F84	L85	L86	D87	D88
Type	basalt	basalt		basalt	basalt	basalt	basalt	basalt	basalt	basalt
Strat. Loc.	Lambafell	Lambafell	Lambafell	Lambafell	Lambafell	Lambafell	Lambafell	Lambafell		
GRID REF.	6770 4735	6770 4735	6785 4740	6770 4750	6750 4750	6790 4760	6745 4785	6745 4790	6890 4950	6910 4970
Structure						-			236/85S	235/20S
SiO2	47.99	47.70		47.98	47.99	46.41	48.59	47.90	46.11	49.61
Al2O3	13.12	13.05		13.21	13.16	12.86	13.02	13.28	14.57	13.94
Fe2O3T	14.91	14.97		15.02	14.90	14.55	14.90	14.68	14.57	12.40
MgO	4.67	4.73		4.78	4.73	4.69	4.65	4.83	5.96	4.70
CaO	9.09	9.07		9.11	9.11	8.87	8.98	9.22	10.33	10.03
Na2O	3.62	3.59		3.42	3.57	3.32	3.50	3.37	2.89	3.15
K2O	0.99	1.02		0.96	0.98	1.01	1.03	0.93	0.28	0.91
TiO2	3.67	3.70		3.70	3.66	3.61	3.66	3.54	3.37	2.81
Mn	0.23	0.22		0.22	0.21	0.21	0.21	0.21	0.18	0.19
P2O5	0.80	0.81		0.87	0.79	0.77	0.82	0.86	0.43	0.33
Total	99.09	98.86		99.27	99.09	96.30	99.36	98.83	98.69	98.08
LOI	0.00	0.00		0.00	0.00	0.00	0.00	0.00	2.20	1.46
Mg#	39.9	40.1		40.3	40.2	40.6	39.8	41.1	46.4	44.5
XRF										
Nb	38.7	36.7	38.5	36.7	36.6	37.5	37.8	36.0	29.5	35.5
Zr	274.6	275.6	284.1	280.1	270.8	271.6	274.9	272.9	230.7	312.4
Y	47.8	46.3	48.2	48.4	47.1	45.2	50.2	48.2	34.6	42.5
Sr	450.4	438.9	445.4	456.7	446.5	440.5	447.5	449.5	420.5	356.7
Zn	137.8	140.9	144.8	144.1	139.5	139.4	138.9	131.8	103.4	107.8
Ni	31.1	28.7	25.8	25.8	25.7	26.7	27.3	30.7	43.3	27.9
V	313.4	316.8	292.1	290.9	317.4	308.9	318.9	284.9	411.2	329.9
Cr	8.3	8.5	8.7	8.4	11.3	10.2	6.9	20.2	18.1	10.4
Ga	29.0	21.3	28.6	23.4	26.4	23.0	29.1	25.1	18.5	22.8
Sc	26.9	21.2	27.8	29.4	28.4	30.1	26.3	28.9	29.3	31.2
Cu	59.9	62.1	57.0	53.7	64.1	56.4	59.9	65.5	93.4	58.2
Co	58.8	58.1	54.1	50.6	57.8	61.9	59.2	55.4	66.6	62.7
Rb	17.8	18.4	20.1	18.7	12.7	22.6	20.7	12.8	1.2	10.2
Ba	214.6	200.9	207.5	211.5	210.6	196.9	198.9	226.4	137.4	185.6
ICP-AES										
La	40.0	39.0	34.1	40.7	37.8	40.7	43.8	45.0	27.3	33.3
Ce	85.4	83.9	80.6	100.2	91.8	91.6	92.4	99.9	58.7	80.2
Pr			10.4							
Nd	57.4	57.3	46.7	63.4	58.1	62.1	62.2	67.2	39.8	46.1
Sm			10.7							
Eu			3.6							
Gd			11.5							
Dy			9.4							
Ho			1.7							
Er			4.5							
Yb			3.6							
Lu			0.4							
Th			2.9							
U			0.9							
Tb			1.6							
Tm			0.6							
Nb			41.7							
Y			42.2							
Ba			224.0							

Sample no.	D90	D91	D92	D93	D94	D95	L96	L97	L98	L99
Type	dyke	dyke	dyke	dyke	dyke	dyke	basalt	basalt	basalt	basalt
Strat. Loc.							La2	La2	La2	La2
GRID REF.	6915 4985	6915 4985	6915 4985	6910 5000	6910 5000	6910 5000	6625 4735	6625 4735	6625 4735	6625 4735
Structure	213/78S	206/40S	045/42S	210/45E	010/15W	168/72W				
SiO2	45.86	48.21	48.64	47.01	52.29	49.81	48.00	47.16	47.43	46.71
Al2O3	13.99	13.89	14.48	13.83	11.31	15.02	14.14	16.35	14.20	14.12
Fe2O3T	15.86	14.85	9.40	15.64	14.37	13.13	14.90	11.86	14.42	14.76
MgO	2.78	5.58	5.94	6.76	7.01	4.66	5.23	5.88	5.48	5.03
CaO	11.37	8.39	13.01	8.62	8.05	8.23	9.84	11.79	10.43	10.07
Na2O	3.51	3.42	2.98	2.37	1.59	3.89	3.35	2.82	3.15	3.33
K2O	1.07	0.95	0.69	0.53	0.08	0.58	0.76	0.62	0.71	0.66
TiO2	3.58	3.69	3.31	3.85	3.38	3.40	3.20	2.64	2.99	3.12
Mn	0.47	0.23	0.25	0.22	0.31	0.18	0.22	0.17	0.20	0.19
P2O5	0.45	0.49	0.40	0.48	0.44	0.68	0.40	0.29	0.34	0.35
Total	98.95	99.70	99.10	99.33	98.83	99.56	100.02	99.58	99.35	98.34
LOI	1.77	1.58	2.50	2.21	2.58	1.56	0.55	0.58	0.42	0.49
Mg#	27.1	44.3	57.2	47.8	50.8	42.9	42.6	51.2	44.6	41.9
XRF										
Nb	30.1	31.6	32.1	27.4	27.6	47.7	28.5	22.8	25.5	26.0
Zr	231.9	254.3	205.6	251.7	235.3	344.1	219.8	163.4	194.8	198.0
Y	38.4	40.3	37.0	41.0	35.4	53.4	37.0	27.3	33.3	35.6
Sr	383.2	382.9	377.8	367.0	224.5	435.1	369.5	452.0	380.2	397.1
Zn	111.9	103.7	98.6	95.4	105.8	134.0	110.4	85.5	103.2	109.8
Ni	32.1	36.8	65.8	37.7	13.4	3.4	35.6	83.4	49.8	30.8
V	426.4	435.6	427.6	424.8	363.6	283.6	412.7	342.8	373.4	400.4
Cr	12.6	27.9	121.4	9.8	17.2	-0.6	13.6	98.0	21.7	7.3
Ga	25.6	25.8	22.4	23.5	21.9	26.4	20.2	24.0	17.7	20.0
Sc	25.6	29.8	27.3	30.5	22.2	29.0	33.6	26.8	33.7	34.3
Cu	104.6	95.0	121.2	76.4	23.6	30.2	104.8	85.4	132.7	80.1
Co	57.9	60.9	67.6	60.5	62.4	42.5	60.8	49.1	60.3	58.0
Rb	14.9	10.5	2.1	2.8	0.2	1.3	9.2	6.1	10.4	5.2
Ba	210.2	182.8	183.7	119.9	357.2	253.1	160.7	134.2	159.4	148.4
ICP-AES										
La	26.4	31.8	24.0	31.2	28.9	55.2	29.2	19.4	21.5	24.5
Ce	68.3	67.9	72.6	71.9	62.6	109.2	61.4	49.5	53.7	56.8
Pr										
Nd	45.4	49.8	43.8	46.1	40.5	70.3	43.7	29.9	33.9	38.4
Sm										
Eu										
Gd										
Dy										
Ho										
Er										
Yb										
Lu										
Th										
U										
Tb										
Tm										
Nb										
Y										
Ba										

Sample no.	L100	L101	D102	L103	L104	L105	L106	L107	L108	L121
Type	basalt	basalt	basalt	basalt	hawaiite	hawaiite	mugearite	hawaiite	hawaiite	basalt
Strat. Loc.	La2	La2		La2	Se	Se	Se	Se	Se	Li
GRID REF.	6625 4735	6625 4735	6625 4735	6625 4740	6880 5070	6875 5075	6880 5070	6900 5060	6895 5015	6780 4915
Structure			168/90			–				
SiO2	47.22	48.31	43.97	47.04	50.70	50.86	53.03	52.39	52.16	47.35
Al2O3	13.95	13.88	13.66	14.20	13.92	14.03	14.05	15.00	15.12	14.70
Fe2O3T	14.89	14.88	13.95	14.62	14.26	14.16	13.50	11.99	12.60	14.10
MgO	5.21	4.47	5.63	5.04	3.24	3.21	2.50	2.97	3.52	4.68
CaO	10.00	8.62	10.87	10.06	7.32	7.29	6.39	6.73	7.41	9.23
Na2O	3.42	3.83	3.16	3.39	4.49	4.47	4.88	5.30	4.77	3.78
K2O	0.78	0.92	0.53	0.82	1.36	1.39	1.54	1.51	1.42	0.96
TiO2	3.13	3.42	3.30	3.36	2.73	2.73	2.14	2.29	2.64	3.49
Mn	0.22	0.22	0.21	0.21	0.25	0.25	0.26	0.22	0.23	0.21
P2O5	0.36	0.43	0.40	0.40	0.84	0.87	0.92	0.69	0.70	0.56
Total	99.17	98.99	95.67	99.14	99.12	99.25	99.21	99.09	100.55	99.11
LOI	0.47	0.58	0.16	0.42	0.00	0.01	0.00	0.13	0.00	
Mg#	42.6	38.9	46.1	42.2	32.5	32.4	28.2	34.4	37.2	41.3
XRF										
Nb	26.4	32.4	33.7	29.8	48.6	48.1	53.5	51.8	46.7	36.7
Zr	206.7	240.2	236.7	221.3	422.0	419.6	492.9	438.5	394.5	276.8
Y	34.5	40.6	35.8	36.1	65.8	64.4	72.5	62.1	59.4	46.0
Sr	384.4	392.1	465.1	405.4	430.9	430.2	413.6	442.8	457.8	445.6
Zn	108.9	120.2	114.7	118.5	154.0	154.0	160.7	138.3	130.9	124.2
Ni	33.0	4.2	54.5	44.5	2.7	2.6	0.0	5.0	9.3	36.2
V	399.2	338.5	373.4	425.8	137.8	145.6	58.7	130.3	182.6	309.8
Cr	7.8	-0.5	7.5	10.6	5.0	6.0	2.4	9.8	12.8	25.3
Ga	22.5	24.1	25.7	25.3	26.3	27.0	23.3	25.7	27.6	23.3
Sc	28.8	29.5	32.7	30.4	21.5	18.0	17.8	19.0	19.0	28.4
Cu	75.8	21.4	128.4	109.9	27.8	22.2	17.7	18.5	27.6	63.5
Co	62.1	59.2	59.6	62.9	38.1	42.3	29.1	33.3	30.7	48.0
Rb	12.1	12.8	6.0	11.6	22.9	25.5	26.9	26.7	23.9	17.1
Ba	157.7	175.2	171.8	176.7	276.1	281.2	320.7	313.4	278.6	217.8
ICP-AES										
La	22.2	29.1	30.7	26.3	56.6	54.3	64.8	55.8	51.4	34.0
Ce	59.6	62.0	77.2	63.0	104.6	107.7	111.1	111.3	109.7	73.8
Pr										
Nd	35.4	44.6	43.7	40.2	71.6	66.9	69.9	69.0	68.6	55.9
Sm										
Eu										
Gd										
Dy										
Ho										
Er										
Yb										
Lu										
Th										
U										
Tb										
Tm										
Nb										
Y										
Ba										

Sample no.	L122	L124	L125	L126	L127	L128	L129	D130	D131	L132
Type	basalt	basalt	hawaiite	basalt	basalt	basalt	basalt	basalt	dyke	basalt
Strat. Loc.	Ll	Ll	Se	Se	Se	Ll	Sv			Sv
GRID REF.	6790 4910	6780 4930	6815 4940	6845 4990	6820 5020	6790 4935	6805 5050	6805 5050	6810 5075	6785 5140
Structure								008/90	060/90	
SiO2	47.18		52.40					46.88		
Al2O3	16.28		15.02					15.06		
Fe2O3T	12.43		12.52					15.26		
MgO	4.49		3.12					5.37		
CaO	9.88		6.76					10.86		
Na2O	3.59		4.71					2.91		
K2O	0.84		1.53					0.53		
TiO2	3.00		2.31					3.61		
Mn	0.18		0.23					0.21		
P2O5	0.46		0.71					0.41		
Total	98.39		99.38					101.15		
LOI										
Mg#	43.3		34.5					42.7		
XRF										
Nb	33.8	34.1	51.5	42.8	43.2	34.3	26.7	26.7	25.8	26.2
Zr	247.1	254.3	443.7	346.5	340.5	248.9	193.6	212.3	179.5	185.7
Y	40.3	42.7	62.9	53.2	54.0	41.4	34.9	36.0	34.9	34.5
Sr	480.3	456.5	455.3	463.6	479.5	468.9	456.7	437.6	441.8	454.3
Zn	105.3	113.2	144.0	134.6	130.5	111.8	119.3	119.7	104.3	104.2
Ni	40.5	40.4	3.5	16.0	16.0	40.0	43.1	40.3	42.0	37.7
V	282.3	331.7	104.2	203.2	212.1	338.5	350.7	384.5	376.9	340.4
Cr	58.2	35.1	8.6	21.5	19.1	42.7	51.5	48.9	55.3	51.3
Ga	24.6	25.2	23.4	26.0	26.6	27.9	27.5	25.6	23.9	28.1
Sc	26.2	27.4	16.1	18.4	24.1	26.2	31.7	31.6	36.3	31.8
Cu	60.2	71.1	16.5	29.8	30.1	69.6	112.6	113.6	73.6	74.7
Co	42.4	48.2	33.1	40.2	38.5	45.1	57.6	59.2	50.8	53.8
Rb	12.7	18.0	30.3	21.6	19.6	11.0	9.0	8.2	7.7	10.1
Ba	217.2	200.7	332.7	274.7	275.3	208.9	140.1	151.9	144.3	136.0
ICP-AES										
La	34.3	35.1	54.3		46.4	30.7	23.6	22.0		23.3
Ce	78.8	80.3	108.4		96.1	70.4	54.4	50.6		55.4
Pr										
Nd	54.8	58.8	75.5		69.9	51.0	40.7	40.6		38.0
Sm										
Eu										
Gd										
Dy										
Ho										
Er										
Yb										
Lu										
Th										
U										
Tb										
Tm										
Nb										
Y										
Ba										

Sample no.	L133	L134	L135	L136	L137	L138	L139	L140	L141	L142
Type	basalt	basalt	basalt	basalt	basalt	hawaiite	basalt	basalt	basalt	basalt
Strat. Loc.	Sv	Sv	Se	Se	Se	Se		Sv	Sv	U
GRID REF.	6790 5180	6810 5215	6850 5110	6830 5070	6830 5070	6750 4920	6745 4920	6720 4950	6695 4950	6790 4995
Structure										
SiO2				50.20				45.84		
Al2O3				14.93				16.07		
Fe2O3T				13.48				13.97		
MgO				4.05				4.72		
CaO				8.22				10.91		
Na2O				4.23				3.07		
K2O				1.17				0.56		
TiO2				3.06				3.38		
Mn				0.23				0.19		
P2O5				0.73				0.39		
Total				100.37				99.17		
LOI										
Mg#				38.9				41.7		
XRF										
Nb	26.5	27.0	48.7	45.3	45.4	53.7	41.4	27.8	27.4	35.0
Zr	193.0	192.7	422.7	349.5	350.2	418.7	300.3	195.7	195.5	249.5
Y	34.3	34.2	66.7	52.5	53.1	58.6	45.6	33.6	33.1	39.9
Sr	451.9	451.7	450.8	471.7	471.6	490.8	534.8	466.7	465.7	468.4
Zn	110.4	115.6	144.5	134.8	137.8	123.3	110.9	118.7	113.8	115.3
Ni	37.0	38.9	5.0	16.9	15.9	18.7	15.7	37.8	36.1	40.5
V	356.6	348.6	115.6	201.8	198.7	180.7	212.3	345.3	342.9	324.6
Cr	50.3	47.4	7.3	13.9	13.4	17.0	5.5	35.9	33.1	29.8
Ga	28.6	26.1	27.8	29.1	29.8	25.5	29.4	28.3	25.9	31.6
Sc	31.1	29.2	20.7	19.0	18.7	19.1	17.5	30.7	26.9	26.9
Cu	98.7	100.8	31.4	35.6	36.5	27.9	28.5	103.2	106.1	63.5
Co	52.3	54.1	39.0	42.4	38.6	32.9	38.4	50.8	50.5	50.6
Rb	9.0	8.9	24.1	20.4	21.6	25.6	13.8	9.3	13.1	15.4
Ba	140.3	132.0	291.2	260.5	250.9	305.1	257.4	149.9	152.1	197.8
ICP-AES										
La	25.0		53.1	47.1	46.9	58.3	44.0	20.8	24.5	29.3
Ce	56.7		105.0	96.5	102.4	121.9	105.5	47.8	61.1	65.2
Pr					76.2			6.2		
Nd	40.2		79.2	71.2		83.7	70.8	28.9	43.9	48.0
Sm								6.7		
Eu								2.6		
Gd								7.5		
Dy								6.6		
Ho								1.2		
Er								3.1		
Yb								2.6		
Lu								0.4		
Th								1.7		
U								0.5		
Tb								1.0		
Tm								0.5		
Nb								28.9		
Y								30.1		
Ba								150.0		

Sample no.	L143	L144	L146	L147	L148	L149	L150	L151	L152	L153
Type	basalt	basalt	basalt	basalt	basalt	basalt	basalt	basalt	basalt	basalt
Strat. Loc.	LI		Sv	Sv	Sv	Sv	Sv	Sv	Sv	Sv
GRID REF.	6790 5000	6805 5010	6775 5195	6710 5170	6710 5170	6675 5150	6675 5150	6720 5140	6720 5140	6720 5140
Structure						–				
SIO2										46.49
Al2O3										16.06
Fe2O3T										14.30
MgO										4.85
CaO										11.06
Na2O										2.99
K2O										0.54
TIO2										3.38
Mn										0.20
P2O5										0.38
Total										100.31
LOI										
Mg#										41.8
XRF										
Nb	34.5	45.7	27.0	26.0	26.1	26.1	27.4	26.9	27.8	26.6
Zr	246.9	383.5	190.4	186.7	191.1	186.1	189.0	192.0	189.8	195.2
Y	42.4	60.5	33.8	33.2	33.5	34.2	34.8	34.8	33.2	33.2
Sr	459.1	468.4	458.7	468.4	462.6	459.0	479.6	452.9	450.8	463.4
Zn	111.8	135.6	103.6	103.5	109.1	112.2	113.2	100.2	117.3	112.3
NI	43.1	19.3	42.1	35.7	34.1	37.5	35.3	40.4	40.6	40.6
V	327.0	167.3	338.2	328.9	378.3	369.4	364.3	360.4	334.1	350.6
Cr	43.3	17.0	45.5	47.4	43.5	47.8	44.5	49.8	52.7	42.3
Ga	32.8	29.4	25.1	25.4	30.1	26.0	26.6	26.3	22.6	25.0
Sc	24.5	20.5	29.3	29.2	33.2	33.5	29.6	31.9	34.5	31.5
Cu	75.1	28.1	93.4	95.7	89.2	95.9	114.0	96.1	103.7	113.8
Co	48.7	37.0	54.3	47.8	45.3	53.3	56.3	52.9	53.0	52.9
Rb	15.3	20.5	11.0	9.9	10.3	12.0	6.4	8.8	10.2	5.7
Ba	200.4	280.5	145.6	157.0	143.4	138.1	150.1	152.3	135.1	132.4
ICP-AES										
La	34.1	51.8	24.7	26.5	24.7	23.1	23.1	22.8	21.8	23.3
Ce	75.8	106.1	57.0	68.4	60.3	54.5	54.9	54.1	50.9	52.5
Pr										
Nd	56.8	77.0	37.1	44.8	41.1	36.8	38.2	37.8	35.1	38.1
Sm										
Eu										
Gd										
Dy										
Ho										
Er										
Yb										
Lu										
Th										
U										
Tb										
Tm										
Nb										
Y										
Ba										

Sample no.	L154	L155	L156	L157	L158	L160	L161	L162	L165	D168
Type	basalt	basalt	basalt	basalt	basalt	basalt	basalt	basalt	basalt	basalt
Strat. Loc	Sv	Sv	Sv	Sv	Sv	Sv	Sv	Sv	Sv	
GRID REF.	6715 5110	6700 5070	6700 5070	6690 5060	6675 5050	6675 5050	6690 5000	6690 5000	6690 5000	6610 5020
Structure						–				010/30S
SiO2						46.28	46.28		46.46	
Al2O3						16.08	15.95		16.47	
Fe2O3T						14.25	14.22		14.07	
MgO						4.88	4.83		4.81	
CaO						11.05	10.98		10.96	
Na2O						2.96	3.00		2.94	
K2O						0.54	0.57		0.53	
TiO2						3.40	3.39		3.32	
Mn						0.19	0.19		0.19	
P2O5						0.38	0.38		0.37	
Total						100.08	99.86		100.18	
LOI										
Mg#						42.0	41.8		42.0	
XRF										
Nb	26.8	26.9	28.2	28.7	27.7	26.8	28.2	26.8	25.6	34.5
Zr	196.3	191.6	197.9	202.5	194.6	192.5	192.5	194.0	190.0	257.8
Y	34.1	34.2	34.2	36.1	35.3	35.1	34.0	34.1	34.9	47.0
Sr	458.1	461.7	463.9	455.5	467.8	469.3	465.5	464.0	469.9	367.8
Zn	110.4	117.1	118.2	119.8	107.0	111.5	114.3	113.5	116.7	134.2
Ni	34.7	33.5	35.1	35.6	38.5	36.0	37.8	35.0	38.9	17.8
V	365.5	354.7	354.7	360.2	352.3	354.0	347.9	356.4	339.4	353.5
Cr	45.3	45.7	43.8	44.6	39.6	40.4	41.3	43.6	42.5	-1.4
Ga	27.9	25.6	28.7	27.9	24.9	25.1	28.7	30.1	21.3	25.4
Sc	29.3	35.3	33.8	33.0	31.2	30.6	30.6	27.4	27.2	28.7
Cu	109.5	96.5	112.3	109.4	94.6	85.6	95.7	101.4	97.6	41.7
Co	53.6	51.8	51.4	52.6	52.9	55.0	53.2	54.8	54.2	55.2
Rb	8.9	8.9	9.4	10.0	5.6	7.5	7.3	11.1	4.9	10.3
Ba	142.6	155.9	148.9	128.4	143.3	142.7	143.3	139.9	149.9	174.6
ICP-AES										
La	27.4	26.0	26.6	22.9	23.6	20.7	24.7	22.9	22.5	28.0
Ce	66.1	59.5	62.0	52.6	52.7	49.2	56.8	53.3	56.5	54.5
Pr										
Nd	47.4	42.8	44.2	38.8	35.8	34.2	39.7	37.7	41.9	56.4
Sm										
Eu										
Gd										
Dy										
Ho										
Er										
Yb										
Lu										
Th										
U										
Tb										
Tm										
Nb										
Y										
Ba										

Sample no.	D169	L170	D171	D173	L174	F175	D176	L179**	L182	L183
Type	trachyte	basalt	basalt	basalt	basalt	basalt	dyke	p.basalt	basalt	basalt
Strat. Loc		Nu			Nu	Nu		Nd	U	U
GRID REF.	6610 5020	6610 5035	6615 4995	6600 5020	6605 5040	6605 5040	6605 5040	6600 5035	6685 4880	6685 4890
Structure	045/90		043/90	178/90			182/20W			
SiO2	63.90							46.33	48.49	
Al2O3	15.66							12.76	14.45	
Fe2O3T	6.73							11.00	14.46	
MgO	0.73								4.48	
CaO	2.68							12.44	8.67	
Na2O	5.95							1.80	3.94	
K2O	2.60							0.34	1.01	
TiO2	0.67							1.81	3.59	
Mn	0.20							0.15	0.22	
P2O5	0.14							0.20	0.59	
Total	99.32							99.02	99.96	
LOI										
Mg#	18.7							0.0	39.6	
XRF										
Nb	80.6	29.0	37.8	33.8	25.7	23.9	28.7	13.9	40.5	39.2
Zr	741.2	206.1	276.8	241.2	164.5	166.8	245.4	101.4	301.7	288.2
Y	72.7	36.5	44.3	40.0	30.0	30.1	43.9	19.4	49.0	47.0
Sr	237.1	415.2	406.0	435.7	505.9	465.3	356.4	315.2	445.1	451.9
Zn	120.7	110.0	125.0	125.6	92.2	97.6	126.4	72.6	120.9	125.3
Ni	1.0	51.8	8.6	39.1	51.2	49.9	34.3	254.6	22.2	20.1
V	-0.3	377.3	355.4	386.3	358.2	367.6	399.7	265.2	272.3	286.0
Cr	2.8	38.8	47.3	1.9	48.8	50.9	12.0	603.4	16.8	14.7
Ga	25.7	25.3	31.1	25.8	27.8	21.8	22.0	14.9	27.7	27.0
Sc	7.9	30.6	31.3	31.1	29.3	25.9	27.6	35.8	26.0	27.0
Cu	8.2	99.1	23.6	72.0	75.4	91.7	74.6	77.4	35.8	33.5
Co	6.6	54.3	52.8	47.6	52.7	53.9	54.9	65.9	44.3	45.1
Rb	51.6	10.6	5.5	1.8	13.3	8.4	9.3	6.5	17.7	19.4
Ba	543.7	174.1	210.5	183.9	444.8	148.2	182.3	90.3	223.6	220.6
ICP-AES										
La	51.1	25.3		30.1	23.5	20.4	24.6	11.4	38.3	37.7
Ce	107.6	55.0		63.2	54.7	50.3	52.5	31.4	81.6	81.1
Pr	12.7									
Nd	52.2	38.1		45.6	34.4	34.2	52.5	18.5	65.5	62.7
Sm	10.6									
Eu	3.1									
Gd	11.6									
Dy	10.2									
Ho	2.1									
Er	5.8									
Yb	5.2									
Lu	0.8									
Th	6.2									
U	2.2									
Tb	1.7									
Tm	0.9									
Nb	67.5									
Y	52.9									
Ba	398.7									

Sample no.	L184	D189**	L190	D191	D192	L193	L194	D195	D196	P199
Type	basalt	benmoreite	p.basalt	dyke	dyke	p.basalt	p.basalt	dyke	dyke	basalt
Strat. Loc.	Se		Nd			Nd	Nd			
GRID REF.	6690 4890	6595 5040	6595 5040	6595 5040	6590 5040	6580 5040	6580 5040	6580 5040	6575 5040	6570 5040
Structure		044/88NW		043/85NW	040/45NW	–		115/30S	080/55N	
SiO2	49.33	61.46	45.96			46.86	46.48			
Al2O3	13.94	13.76	13.23			15.43	16.07			
Fe2O3T	14.95	7.14	11.47			12.85	12.08			
MgO	3.56		10.35			6.34	6.77			
CaO	7.87	2.73	13.37			12.81	12.95			
Na2O	4.37	5.03	2.01			2.49	2.32			
K2O	1.34	2.45	0.40			0.52	0.48			
TiO2	3.29	1.24	2.04			2.68	2.40			
Mn	0.24	0.18	0.16			0.13	0.15			
P2O5	0.79	0.37	0.19			0.27	0.23			
Total		97.41	99.23			100.43	100.43			
LOI										
Mg#	33.5	0.0	65.6			51.1	54.3			
XRF										
Nb	50.9	93.4	14.2	50.1	35.4	20.3	18.9	32.0	56.2	28.9
Zr	408.8	784.5	106.8	370.6	262.1	157.4	136.7	228.7	453.1	247.6
Y	62.9	85.7	20.0	56.5	41.8	24.8	23.1	35.4	67.6	39.2
Sr	414.5	317.8	345.4	412.9	415.7	444.3	440.6	436.3	390.6	387.7
Zn	144.0	142.6	75.4	122.7	114.2	90.4	80.4	114.3	128.7	122.1
Ni	11.5	-0.3	255.8	2.0	37.4	101.4	123.2	61.2	-0.6	37.6
V	199.8	13.3	286.4	172.3	397.6	326.7	318.2	330.1	40.9	338.7
Cr	2.6	3.3	468.1	0.0	4.6	150.8	192.5	73.8	2.9	20.4
Ga	23.8	28.3	19.0	26.2	22.1	22.0	21.3	24.8	28.7	25.4
Sc	20.6	12.7	34.4	18.7	26.5	29.2	26.2	28.7	11.2	27.8
Cu	44.5	1.3	50.7	12.8	99.2	100.4	95.6	111.8	8.6	58.0
Co	40.1	7.8	57.7	34.8	54.6	62.5	58.7	51.7	21.3	57.1
Rb	24.7	47.9	7.8	21.1	2.0	7.1	9.0	5.7	25.8	12.9
Ba	286.8	526.4	108.6	292.7	198.0	138.7	127.9	151.4	361.2	201.3
ICP-AES										
La	50.5	91.6	11.2	50.5	30.8	21.4	15.2	31.2	62.1	24.1
Ce	100.4	173.4	26.0	98.4	59.6	54.5	40.3	68.8	118.2	53.6
Pr			3.3							
Nd	82.1	96.3	16.5	71.4	49.5	32.7	24.4	44.9	72.7	39.6
Sm			3.6							
Eu			1.4							
Gd			4.2							
Dy			4.1							
Ho			0.8							
Er			2.0							
Yb			1.5							
Lu			0.3							
Th			1.1							
U			0.3							
Tb			0.7							
Tm			0.3							
Nb			15.8							
Y			18.1							
Ba			94.1							

Sample no.	D200	L201	L202	L203	L203B	L206	L207	L208	L209	S210
Type	dyke	basalt	basalt	basalt	p.basalt	basalt	basalt	basalt	FeTi basalt	sill
Strat. Loc.		N.dalur	N.dalur	N.dalur	Nd	N.dalur	N.dalur	N.dalur	N.dalur	
GRID REF.	6570 5040	6565 5040	6560 5040	6565 5040	6605 5035	6580 5040	6580 5030	6580 5030	6575 5030	6575 5030
Structure	085/23N					-				
SiO2				46.82		46.66	45.55	46.70	46.34	47.86
Al2O3				16.50		15.28	16.50	16.91	13.25	16.33
Fe2O3T				13.62		12.68	12.45	12.29	16.30	13.19
MgO				5.14		6.98	4.89	5.09	5.19	4.38
CaO				11.35		12.57	12.48	12.32	9.98	10.81
Na2O				2.92		2.41	2.81	2.87	3.16	3.22
K2O				0.64		0.53	0.57	0.57	0.77	0.71
TiO2				3.09		2.68	2.79	2.81	4.00	3.12
Mn				0.19		0.17	0.15	0.21	0.23	0.19
P2O5				0.32		0.28	0.34	0.34	0.46	0.39
Total				100.66		100.29	98.59	100.15	99.74	100.26
LOI										
Mg#				44.4		53.8	45.4	46.7	40.3	41.3
XRF										
Nb	28.5	29.3	28.0	28.7	24.6	21.3	25.7	25.6	28.4	29.1
Zr	239.8	245.2	245.4	248.8	167.2	162.0	153.5	150.6	229.6	198.9
Y	41.4	39.3	39.5	38.3	29.5	25.3	28.2	28.9	40.8	35.4
Sr	389.7	379.2	366.4	376.2	466.7	435.6	469.8	476.3	394.4	450.6
Zn	112.5	112.8	116.7	118.0	100.0	94.0	93.5	87.8	121.2	102.2
Ni	47.5	35.1	33.7	35.5	53.8	101.4	87.8	78.9	25.2	45.6
V	357.7	349.7	341.3	349.0	358.9	338.1	348.9	370.9	410.3	335.0
Cr	29.9	18.5	15.7	26.1	51.0	143.4	112.7	113.8	0.3	34.2
Ga	24.7	25.8	25.0	25.2	18.9	20.3	20.9	22.9	23.6	21.7
Sc	26.3	31.3	34.0	28.7	28.7	33.4	31.8	32.5	31.7	26.6
Cu	115.4	57.8	62.6	58.7	85.1	103.4	85.5	73.6	74.3	83.3
Co	55.8	60.8	43.2	60.3	45.6	47.7	40.5	39.5	45.5	48.6
Rb	3.6	16.1	14.4	12.9	14.9	10.9	10.5	9.7	12.4	11.9
Ba	175.6	184.5	178.5	190.2	266.1	137.3	161.5	160.2	184.6	179.9
ICP-AES										
La	28.3	26.9	27.6	24.0	23.1	17.6	23.9	21.2	25.1	29.6
Ce	66.0	57.1	62.5	52.1	51.9	42.1	57.6	49.6	56.2	66.8
Pr						5.8				
Nd	50.2	41.9	47.4	39.4	33.2	25.1	35.1	30.4	51.5	42.8
Sm						5.9				
Eu						2.0				
Gd						6.2				
Dy						5.6				
Ho						1.0				
Er						2.7				
Yb						2.6				
Lu						0.4				
Th						1.7				
U						0.5				
Tb						0.9				
Tm						0.4				
Nb						24.4				
Y						23.9				
Ba						136.7				

Sample no.	L211	L212	D213	L214	S215	S216	S217	S218	L219	S220
Type	FeTi basalt	FeTi basalt	dyke	basalt	mugearite	hawaiite	basalt	hawaiite	hawaiite	hawaiite
Strat. Loc.	N.dalur	N.dalur		N.dalur	W.slopes	W.slopes	W.slopes	W.slopes	W.slopes	W.slopes
GRID REF.	6550 5015	6550 5015	6550 5020	6550 5015	5520 5675	5530 5725	5530 5720	5530 5725	5540 5730	5620 5715
Structure						–				
SiO2	47.04	47.03	62.60	48.13	55.51	51.14	49.79	51.90	50.98	51.12
Al2O3	13.33	13.39	15.81	14.28	14.72	14.97	14.68	14.96	14.87	14.83
Fe2O3T	16.41	16.42	6.41	15.02	11.16	12.73	12.87	12.68	12.73	12.66
MgO	5.05	5.02	1.53	4.22	2.19	4.13	4.17	4.09	4.19	4.27
CaO	10.09	10.16	3.05	9.73	5.64	7.70	7.75	7.81	7.92	7.86
Na2O	3.14	3.21	5.20	3.49	4.98	4.23	4.13	4.19	4.23	4.19
K2O	0.76	0.76	3.20	0.79	1.77	1.16	1.12	1.17	1.18	1.18
TiO2	3.96	3.97	1.31	3.66	1.71	2.64	2.71	2.66	2.68	2.66
Mn	0.23	0.23	0.12	0.22	0.24	0.22	0.22	0.22	0.22	0.22
P2O5	0.48	0.45	0.36	0.49	0.59	0.79	0.79	0.78	0.78	0.76
Total	100.54	100.69	99.68	100.08	98.59	99.78	98.31	100.52	99.85	99.82
LOI										
Mg#	39.5	39.3	33.6	37.3	29.4	40.7	40.7	40.6	41.1	41.7
XRF										
Nb	30.1	30.1	93.8	36.7	56.5	47.9	46.5	43.5	42.0	42.1
Zr	236.1	228.0	991.6	246.7	578.0	368.9	352.7	363.5	358.2	360.2
Y	42.4	38.0	80.1	45.3	74.3	56.7	55.0	55.7	57.3	56.7
Sr	399.7	393.6	289.1	430.4	405.8	455.1	453.1	458.7	464.6	453.7
Zn	126.5	125.0	126.9	135.0	149.4	130.5	136.2	133.2	132.3	133.5
Ni	26.7	21.3	1.5	26.7	4.8	22.3	21.0	17.6	24.1	20.4
V	397.6	406.6	29.8	380.4	49.7	157.5	149.8	165.3	164.1	172.9
Cr	3.1	-1.8	-1.0	-1.7	7.6	29.5	33.6	31.5	35.6	40.3
Ga	25.9	23.5	25.2	23.7	29.0	29.9	32.5	28.5	27.9	25.8
Sc	32.1	29.4	15.2	30.3	9.6	20.7	23.3	21.7	26.2	22.9
Cu	73.4	73.1	5.8	71.2	17.6	29.6	27.2	29.2	35.6	31.4
Co	60.4	62.8	13.7	36.3	12.3	29.4	23.7	26.9	20.9	21.9
Rb	12.4	11.8	66.8	11.9	35.3	22.2	23.2	21.5	24.3	23.1
Ba	168.3	156.9	589.0	187.6	401.9	273.2	268.6	270.1	287.3	268.5
ICP-AES										
La	29.5	24.0	94.0	29.7	68.0	51.4	48.3	45.7	51.6	50.4
Ce	62.5	56.7	185.5	60.5	136.4	110.4	97.9	95.1	105.6	116.0
Pr		7.8								15.4
Nd	53.3	34.7	100.4	48.6	82.6	78.7	67.7	67.9	70.6	65.1
Sm		8.2								14.1
Eu		2.9								4.6
Gd		8.9								15.7
Dy		8.2								14.0
Ho		1.6								2.6
Er		4.3								7.1
Yb		3.2								6.1
Lu		0.5								1.0
Th		2.2								5.5
U		0.8								1.8
Tb		1.4								2.1
Tm		0.6								1.1
Nb		33.0								65.3
Y		37.1								64.4
Ba		178.7								377.7

Sample no.	S221	L222	L234	L235	L236	L237	D238	L239	P240	D241
Type	hawaiite	basalt	basalt	basalt	basalt	basalt	dyke	basalt	basalt	dyke
Strat. Loc.	W.slopes	W.slopes	La2	La2	La2	La2		La2	La2	
GRID REF.	5635 5670	5630 5630	6625 4740	6625 4740	6625 4740	6615 4740	6605 4740	6605 4740	6605 4740	6605 4740
Structure							046/88E			020/85S
SiO2	51.20	48.63	46.78	48.88	46.97	47.31	47.03	46.11	46.18	
Al2O3	15.02	14.47	17.81	14.70	18.63	14.50	13.92	15.41	15.64	
Fe2O3T	12.75	14.14	12.55	14.20	12.53	14.99	14.87	14.11	13.22	
MgO	4.12	4.91	4.19	3.93	4.17	5.13	4.98	4.90	4.51	
CaO	7.82	8.99	12.03	8.99	12.06	10.25	10.87	10.36	10.99	
Na2O	4.18	3.73	2.85	3.83	2.65	3.28	3.04	3.51	3.09	
K2O	1.16	0.94	0.65	0.96	0.54	0.83	0.97	0.81	0.75	
TiO2	2.67	3.35	2.58	3.68	2.52	3.46	3.55	3.20	3.22	
Mn	0.22	0.22	0.18	0.27	0.17	0.20	0.21	0.20	0.22	
P2O5	0.79	0.56	0.28	0.48	0.29	0.39	0.44	0.37	0.39	
Total	100.00	100.00	99.96	99.98	100.59	100.40	99.94	99.07	98.27	
LOI										
Mg#	40.6	42.4	41.4	37.0	41.3	42.0	41.5	42.4	41.9	
XRF										
Nb		36.7	21.8	36.5	20.6	30.2	33.1	27.9	29.0	26.4
Zr		280.1	146.6	244.0	152.5	215.7	244.6	193.0	188.1	207.6
Y		46.6	27.1	42.2	28.5	35.7	37.3	33.2	33.2	34.7
Sr		460.4	463.4	439.5	491.1	418.8	415.1	876.4	438.2	411.8
Zn		117.8	92.6	127.5	92.8	112.7	117.2	97.7	107.7	113.5
Ni		35.8	38.5	9.5	33.7	41.5	45.6	39.3	47.2	44.2
V		247.5	328.2	379.6	307.3	411.3	420.2	367.7	418.7	406.7
Cr		48.5	19.1	-1.7	21.2	13.2	11.7	28.0	33.7	12.0
Ga		28.5	25.3	27.8	23.1	22.8	25.8	26.1	23.5	23.1
Sc		25.0	28.0	30.7	28.7	32.2	32.5	28.1	31.0	29.9
Cu		42.5	75.2	20.4	66.7	108.3	104.7	78.3	78.3	135.9
Co		37.1	38.6	39.6	36.5	58.7	50.3	47.9	55.8	38.5
Rb		15.5	9.8	15.9	6.4	15.0	16.5	15.6	10.9	14.9
Ba		234.1	139.7	221.7	157.6	187.6	187.5	179.2	173.5	180.0
ICP-AES										
La		40.1	20.2	30.3	21.1	27.1	28.5	26.4	24.0	23.7
Ce		85.8	45.8	65.9	48.2	58.0	57.7	63.7	53.9	47.1
Pr										
Nd		61.4	28.4	54.5	28.8	45.5	43.6	43.2	37.1	37.1
Sm										
Eu										
Gd										
Dy										
Ho										
Er										
Yb										
Lu										
Th										
U										
Tb										
Tm										
Nb										
Y										
Ba										

Sample no.	L255	L278**	L279	L292**	L294	S296	L307	L323**	L324**	D326
Type	p.basalt	p.basalt	p.basalt	p.basalt	p.basalt	p.basalt	basalt	basalt	basalt	dyke
Strat. Loc.	Fimmvord.	Nd	Nd	Nr		S.S	S.S	Nr	Nr	
GRID REF.	7715 5530	6610 4800	6620 4760	6610 4780	6565 4780	6475 4970	6515 4935	6570 4835	6670 4835	6605 4790
Structure						–				124/90
SiO2	46.46	45.17	46.35	45.59	46.71	46.77		47.20	45.96	46.87
Al2O3	14.72	14.39	14.54	14.72	15.98	16.56		14.32	15.64	14.21
Fe2O3T	13.96	15.60	13.50	14.47	12.18	11.91		15.37	14.94	13.72
MgO	7.59		7.78		6.53	7.33				6.09
CaO	10.04	9.44	11.84	10.57	12.57	10.78		9.02	9.84	11.82
Na2O	3.20	3.63	2.45	3.09	2.49	2.99		3.60	3.92	2.82
K2O	0.62	0.89	0.49	0.66	0.40	0.71		0.86	0.83	0.60
TiO2	3.06	3.89	2.60	3.29	2.64	2.82		3.70	3.48	2.86
Mn	0.19	0.23	0.19	0.20	0.17	0.16		0.21	0.21	0.20
P2O5	0.38	0.50	0.28	0.39	0.26	0.43		0.47	0.47	0.32
Total	100.27	98.83	100.08	99.36	99.99	100.52		98.56	99.49	99.56
LOI										
Mg#	53.5	0.0	55.0	0.0	53.2	56.6		0.0	0.0	48.5
XRF										
Nb	25.5		20.0		19.6	26.9	28.6			23.4
Zr	186.8		149.7		149.0	221.5	239.8			201.2
Y	35.8		29.1		26.1	31.0	30.4			34.6
Sr	425.7		370.2		420.8	512.2	486.1			351.9
Zn	99.0		101.6		94.2	90.7	93.1			115.8
Ni	109.6		105.0		80.2	120.9	104.0			52.0
V	276.8		354.2		314.9	257.3	263.9			342.8
Cr	194.4		196.5		166.9	222.0	234.6			40.2
Ga	23.8		19.8		22.6	25.1	23.3			28.7
Sc	29.7		36.1		31.9	29.3	25.6			29.0
Cu	57.5		92.9		105.6	63.5	56.3			113.6
Co	53.6		58.2		40.5	38.3	34.7			50.9
Rb	11.1		11.3		6.5	13.4	13.3			8.3
Ba	152.7		136.0		119.0	173.4	194.6			145.8
ICP-AES										
La	39.2		19.8		15.3	22.9	23.7			23.6
Ce	87.3		44.8		35.8	52.7	53.8			54.5
Pr	12.0		6.0		4.7	7.0	7.1			
Nd	53.3		28.0		23.3	32.7	32.2			36.1
Sm	12.7		7.5		5.8	8.4	7.4			
Eu	3.8		2.4		2.1	2.5	2.4			
Gd	12.3		7.9		6.3	8.3	7.8			
Dy	10.8		7.1		5.3	6.7	6.4			
Ho	2.0		1.3		1.0	1.3	1.3			
Er	5.1		3.6		2.9	3.7	3.1			
Yb	4.4		3.1		2.3	3.1	3.1			
Lu	0.7		0.5		0.3	0.5	0.4			
Th	3.7		1.7		1.5	2.2	2.3			
U	1.2		0.5		0.4	0.8	0.9			
Tb	1.8		1.2		0.9	1.2	1.2			
Tm	0.8		0.6		0.4	0.5	0.5			
Nb	48.2		28.2		21.2	31.1	32.0			
Y	49.9		31.1		23.8	28.6	28.7			
Ba	257.0		133.2		96.1	150.7	159.0			

Sample no.	D344	L345	L390**	L391**	L392**	L397	S404	S406	L490	L498
Type	dyke	p.basalt	ankaramite	basalt	basalt	basalt	FeTi basalt	FeTi basalt	basalt	p.basalt
Strat. Loc.		Halsar	Ira	Ira	Ira	Ira	Drangshlid	Drangshlid	La	Gr
GRID REF.	5860 5320	5860 5320	5835 5050	5835 5050	5835 5050	5900 5140	7345 4495	7345 4495	6985 4735	6050 4960
Structure						-				
SiO2	46.84	45.42	45.97	46.10	46.27	46.00	46.80	46.97	46.39	46.41
Al2O3	14.82	17.43	12.24	14.94	14.54	13.65	12.65	12.76	17.71	9.41
Fe2O3T	14.29	12.16	12.09	15.31	15.54	15.58	16.35	16.51	13.75	11.67
MgO	5.82	7.26				5.94	4.74	4.60	5.10	16.42
CaO	11.41	11.73	11.74	10.58	10.76	10.99	9.60	9.18	12.28	12.48
Na2O	2.68	2.55	1.81	3.04	2.84	2.90	3.33	3.38	2.92	1.47
K2O	0.52	0.42	0.26	0.60	0.60	0.57	0.75	0.78	0.54	0.26
TiO2	3.18	2.74	1.64	3.22	3.29	3.54	4.03	4.00	3.07	1.63
Mn	0.19	0.15	0.18	0.23	0.24	0.21	0.27	0.27	0.18	0.17
P2O5	0.32	0.25	0.20	0.44	0.31	0.35	1.35	1.18	0.31	0.16
Total	100.11	100.17	101.12	99.22	99.17	99.78	99.93	99.70	102.28	99.98
LOI										
Mg#	46.3	55.8	0.0	0.0	0.0	44.7	38.0	37.1	44.0	74.9
XRF										
Nb	23.2	17.3				22.1	35.5	35.6	17.2	11.3
Zr	192.1	130.8				194.1	252.5	258.3	160.1	99.9
Y	32.9	23.3				32.2	50.3	52.4	27.7	17.2
Sr	414.9	501.5				416.0	523.3	521.1	478.3	216.6
Zn	110.9	85.9				108.6	147.0	140.6	96.9	75.8
Ni	46.2	124.9				50.1	9.2	11.0	40.2	387.5
V	241.6	326.9				394.2	254.6	236.7	329.2	247.0
Cr	49.1	222.2				42.2	2.2	0.8	40.8	825.8
Ga	20.6	23.8				24.6	32.8	24.6	25.4	16.1
Sc	28.9	32.2				34.3	28.2	32.4	27.7	30.8
Cu	66.3	77.6				96.1	35.8	39.7	71.2	125.2
Co	53.8	52.8				44.5	26.7	36.7	33.2	63.2
Rb	9.4	8.9				8.8	14.8	14.7	7.5	5.2
Ba	142.1	114.2				154.7	190.6	211.6	135.0	70.8
ICP-AES										
La	24.9	17.8				19.0	38.3	33.7	15.9	10.8
Ce	53.7	40.6				45.0	85.2	83.0	38.0	25.1
Pr						6.4		12.0	5.2	3.4
Nd	34.5	23.0				29.7	73.8	57.7	25.8	17.1
Sm						6.7		13.3	6.3	4.4
Eu						2.4		4.7	2.2	1.4
Gd						7.8		14.8	6.8	4.5
Dy						6.9		11.4	5.7	4.2
Ho						1.3		2.0	1.1	0.8
Er						3.4		4.9	3.0	2.3
Yb						2.8		3.9	2.8	1.6
Lu						0.4		0.6	0.5	0.3
Th						1.6		2.4	1.5	1.0
U						0.6		0.8	0.5	0.3
Tb						1.1		1.9	1.1	0.7
Tm						0.4		0.7	0.5	0.3
Nb						26.5		39.1	23.1	14.9
Y						30.8		49.3	25.5	18.0
Ba						131.3		200.7	114.3	66.6

Sample no.	L500**	L501	L502	L503	L507**	L509	L523**	L524**	L525**	L530**
Type	basalt	ankaramite	ankaramite	p.basalt	FeTi basalt	p.basalt	ankaramite	ankaramite	basalt	p.basalt
Strat. Loc.	Mo	Gr	Gr	Gr		As	Raufarfell	Raufarfell	Raufarfell	
GRID REF.	6040 4960	6180 5030	6180 5030	6190 5035	6135 4970	6125 5125	6940 4895	6940 4895	6940 4895	5685 5540
Structure						–				
SiO2	45.84	47.18	46.80	46.06	45.22	45.44	46.94	46.80	47.81	45.99
Al2O3	13.45	11.19	10.50	15.35	13.25	11.28	12.95	13.05	17.49	15.96
Fe2O3T	15.84	11.44	11.24	12.20	16.34	14.38	12.76	12.63	10.71	12.88
MgO		12.71	14.32	9.89		13.27				
CaO	9.34	13.01	13.12	11.31	10.15	10.84	11.48	11.37	12.11	10.84
Na2O	3.38	1.69	1.58	2.38	3.13	1.93	2.16	2.08	3.00	3.01
K2O	0.80	0.27	0.22	0.38	0.61	0.37	0.46	0.45	0.73	0.47
TiO2	3.86	1.86	1.76	2.41	3.93	2.46	2.02	2.12	2.43	2.30
Mn	0.23	0.16	0.17	0.16	0.26	0.19	0.17	0.17	0.17	0.18
P2O5	0.52	0.20	0.19	0.25	0.52	0.24	0.24	0.23	0.40	0.36
Total	98.22	99.76	100.12	100.43	98.42	100.43	100.27	101.25	99.07	99.52
LOI										
Mg#	0.0	70.2	73.0	63.2	0.0	66.1	0.0	0.0	0.0	0.0
XRF										
Nb		13.4	15.9	14.7		13.7				
Zr		108.0	109.3	132.5		148.6				
Y		21.3	21.5	21.8		23.4				
Sr		266.2	254.3	423.6		292.4				
Zn		82.4	77.5	85.1		102.4				
Ni		295.7	347.9	211.6		270.2				
V		257.7	257.7	282.6		281.8				
Cr		872.1	1143.8	354.2		452.5				
Ga		16.8	19.9	23.1		19.8				
Sc		40.7	35.4	26.7		37.0				
Cu		107.2	111.9	88.2		82.9				
Co		52.4	78.0	46.9		63.9				
Rb		2.8	3.1	6.9		5.9				
Ba		97.5	78.3	125.7		101.9				
ICP-AES										
La		9.6	11.6	12.9		12.9				
Ce		22.7	26.1	29.6		30.8				
Pr		3.3	3.6	3.9		4.2				
Nd		15.0	17.8	19.0		19.0				
Sm		3.8	4.4	4.9		5.6				
Eu		1.3	1.7	1.8		1.8				
Gd		3.8	4.8	5.4		5.4				
Dy		3.8	4.3	4.3		4.7				
Ho		0.7	0.8	0.9		1.0				
Er		1.9	2.1	2.2		2.4				
Yb		1.5	2.2	2.2		2.3				
Lu		0.3	0.3	0.3		0.4				
Th		0.9	1.1	1.1		1.2				
U		0.3	0.3	0.3		0.5				
Tb		0.6	0.7	0.7		0.9				
Tm		0.3	0.3	0.3		0.4				
Nb		13.7	15.1	17.0		17.8				
Y		16.6	19.5	20.6		22.1				
Ba		59.2	66.1	87.8		85.5				

Sample no.	L534**	L564**	L566**	L570	L571**	L575**	L576	L578B	L578M	L578F
Type	trachyte	basalt	trachyte	hawaiite	basalt	basalt	basalt	trachyte	trachyte	trachyte
Strat. Loc.	Gigjokull							Laugara	Laugara	Laugara
GRID REF.	6770 5970	6495 5080	6490 5100	6225 5925	6235 5915	6815 5220	6825 5225	6830 5225	6830 5225	6830 5225
Structure						–				
SiO2	64.88	45.75	66.10	51.38	46.31	55.63	47.48	58.52	62.35	
Al2O3	14.22	14.04	13.83	15.08	16.46	15.44	13.90	14.40	14.05	
Fe2O3T	7.25	15.69	6.54	12.99	11.85	9.62	12.29	10.78	8.41	
MgO				3.19			9.05	1.60	0.82	
CaO	12.31	10.02	2.20	7.11	10.49	5.09	12.37	4.77	3.43	
Na2O	6.03	3.40	5.41	4.90	3.37	5.43	2.13	5.04	5.30	
K2O	2.90	0.82	2.78	1.32	0.62	2.01	0.26	2.12	2.65	
TiO2	0.58	3.73	0.74	2.45	2.62	1.53	2.57	1.47	0.91	
Mn	0.20	0.23	0.12	0.25	0.17	0.19	0.17	0.22	0.19	
P2O5	0.10	0.42	0.15	1.03	0.48	0.45	0.24	0.55	0.26	
Total	98.56	98.41	98.41	99.77	99.33	97.09	100.50	99.54	98.44	
LOI										
Mg#	0.0	0.0	0.0	34.2	0.0	0.0	60.9	23.9	17.1	
XRF										
Nb	89.1		98.9	46.9		58.5	16.5	62.5	72.0	73.7
Zr	978.6		1068.1	421.8		590.4	149.1	644.4	735.0	763.9
Y	101.9		101.1	68.7		72.5	24.6	85.4	85.2	86.7
Sr	211.9		214.8	466.5		382.5	359.6	339.3	283.5	271.1
Zn	153.6		158.0	132.1		131.7	96.4	148.0	124.9	129.3
Ni	1.1		1.2	1.1		12.7	186.8	0.2	0.8	0.2
V	0.9		-0.5	103.1		63.6	316.4	24.0	15.4	11.5
Cr	0.3		0.8	1.0		20.4	367.8	0.6	1.2	3.6
Ga	30.6		29.1	30.6		28.4	16.7	28.4	27.0	29.0
Sc	7.7		4.2	19.0		16.9	35.1	13.7	5.8	10.9
Cu	3.7		-0.7	12.0		20.3	124.6	12.0	9.8	8.8
Co	0.9		3.2	12.2		11.9	42.2	8.8	4.7	0.2
Rb	61.2		64.3	22.3		37.8	3.0	43.1	54.3	58.2
Ba	596.4		620.2	316.2		446.6	99.9	453.2	525.7	528.2
ICP-AES										
La	64.3		88.4	45.8		55.5	13.5	66.8	61.7	75.6
Ce	150.7		190.3	106.3		119.3	31.5	136.4	131.3	153.6
Pr	18.6			15.0		15.4	4.5		16.9	
Nd	70.9		93.9	61.6		62.6	19.9	84.3	67.4	79.5
Sm	16.2			15.1		13.7	5.8		15.5	
Eu	4.2			4.7		4.3	1.8		4.0	
Gd	17.0			16.8		14.5	5.9		16.6	
Dy	15.7			13.9		12.9	5.4		13.8	
Ho	3.1			2.5		2.5	0.9		2.8	
Er	8.7			6.9		7.3	2.4		7.4	
Yb	8.6			6.0		6.3	2.4		7.9	
Lu	1.3			0.9		0.8	0.3		1.1	
Th	8.7			3.7		6.0	1.2		9.3	
U	2.6			1.2		1.9	0.4		2.8	
Tb	2.8			2.3		2.2	0.9		2.4	
Tm	1.3			1.0		1.0	0.4		1.2	
Nb	93.6			57.8		66.3	18.3		80.5	
Y	81.7			65.8		63.8	22.4		72.3	
Ba	468.0			288.0		379.0	81.4		473.3	

Sample no.	D581**	L582	L583	L585**
Type	dyke	trachyte	mugearite	FeTi bas
Strat. Loc.	Fjell	Fjell	La?	Fjell
GRID REF.	6690 5280	6690 5275	6830 5225	6690 5280
Structure				
SiO2	45.89	67.46	53.33	45.90
Al2O3	11.65	13.32	14.24	14.41
Fe2O3T	16.25	5.90	13.67	15.53
MgO		0.21	2.56	
CaO	9.90	2.43	6.45	9.02
Na2O	2.22	5.13	4.52	3.93
K2O	0.80	2.45	1.53	0.85
TiO2	4.02	0.43	2.16	4.01
Mn	0.25	0.18	0.26	0.24
P2O5	0.48	0.04	0.90	0.55
Total	97.48	97.65	99.69	98.38
LOI				
Mg#	0.0	7.0	28.4	0.0
XRF				
Nb		122.8	49.2	
Zr		1282.0	504.2	
Y		134.0	72.5	
Sr		222.0	431.7	
Zn		203.5	170.9	
Ni		0.4	-0.6	
V		3.2	48.2	
Cr		-0.5	-0.3	
Ga		26.2	27.8	
Sc		3.4	20.3	
Cu		0.9	18.2	
Co		-0.5	17.8	
Rb		42.7	29.0	
Ba		882.5	350.8	
ICP-AES				
La		86.7	53.0	
Ce		186.0	117.3	
Pr		24.1	15.8	
Nd		95.7	71.8	
Sm		22.0	16.9	
Eu		4.7	4.7	
Gd		23.6	18.0	
Dy		22.1	14.2	
Ho		4.4	2.5	
Er		12.4	6.7	
Yb		11.7	5.7	
Lu		1.7	0.9	
Th		10.2	5.0	
U		3.3	1.6	
Tb		3.6	2.5	
Tm		1.9	1.0	
Nb		130.7	61.4	
Y		113.3	67.0	
Ba		794.0	342.7	

APPENDIX - B3 GLASS DATA

Glass samples taken from hyaloclastite samples, pillow margins and interstitial glass.
Grid references are as Appendix B2.

Sample No.	447	447	447	447	447	447	447	514b	514b	514b	514c	514c	514c	517a	517b	517a
Grid Ref.	704478	704478	704478	704478	704478	704478	704478	717484	717484	717484	717484	717484	717484	715491	715491	715491
Spot Ref.	1	2	3	8	9	11	12	1	2	3	2	3	4	1	1	3
SiO2	49.29	48.41	48.62	48.65	49.13	47.76	48.83	48.88	48.59	49.08	48.52	48.51	49.36	50.34	49.02	50.01
Al2O3	13.88	13.73	13.50	14.16	14.00	14.21	13.94	13.29	13.46	13.33	11.81	12.37	13.67	13.55	13.65	13.75
K2O	0.97	0.83	0.88	0.89	0.84	0.90	0.85	0.95	0.91	0.88	0.97	0.96	0.94	1.03	0.77	0.79
Na2O	3.65	3.52	3.71	3.52	3.69	3.01	3.53	3.06	3.17	3.11	2.73	3.19	2.96	2.74	2.83	2.98
FeO	12.90	12.86	12.76	12.62	13.01	12.45	13.04	14.00	13.28	13.58	15.22	14.72	14.23	14.35	13.54	14.08
TiO2	3.65	3.59	3.47	3.78	3.70	3.55	3.68	3.78	3.78	3.76	4.07	3.92	4.25	3.82	3.82	3.90
MgO	5.14	5.00	4.87	4.97	4.99	4.29	5.27	4.60	4.17	4.42	4.70	4.52	3.63	4.74	4.39	4.99
CaO	9.99	9.69	9.83	9.81	9.85	9.53	10.13	9.95	10.00	10.17	9.49	9.88	9.45	9.89	9.82	9.84
MnO	0.20	0.14	0.17	0.26	0.37	0.15	0.15	0.17	0.15	0.10	0.17	0.16	0.06	0.12	0.27	0.10
Cr2O3	0.07		0.10	0.07		0.09	0.05	0.04		0.20	0.06	0.06		0.04		0.04
Total	99.86	97.77	97.91	98.82	99.59	96.21	99.67	98.97	97.84	98.62	97.74	98.34	98.71	100.61	98.13	100.50

Sample No.	517a	517a	517a	517a	517b	517b	517a	561	561	561	561	566b	566b	566b	566c	566c
Grid Ref.	715491	715491	715491	715491	715491	715491	715491	636502	636502	636502	636502	649510	649510	649510	649510	649510
Spot Ref.	4	5	6	8	3	4	2	2	3	9	10	2	3	9	2	7
SiO2	49.98	50.42	50.92	49.61	49.09	49.70	49.89	50.02	49.90	51.45	50.95	69.50	69.41	69.19	56.32	57.79
Al2O3	13.78	14.35	15.37	13.64	13.68	13.48	13.82	13.53	13.28	16.48	14.51	14.32	14.19	14.33	24.00	22.18
K2O	0.81	0.72	0.87	0.94	0.74	0.83	0.96	1.05	1.19	0.86	0.88	1.97	3.06	2.73	1.43	0.84
Na2O	2.65	3.46	3.18	2.37	2.65	2.54	2.78	1.11	0.81	2.20	1.64	6.39	6.00	6.30	5.65	6.93
FeO	14.19	12.79	12.64	13.41	13.89	13.71	13.50	14.66	15.36	11.68	13.13	4.80	5.68	4.99	1.32	2.16
TiO2	3.82	3.46	3.61	3.76	3.71	3.57	3.78	4.31	4.28	3.55	3.94	0.58	0.60	0.50	0.20	0.18
MgO	4.90	3.80	2.67	5.04	4.83	4.73	4.95	4.33	4.38	3.69	5.07	0.04	0.09	0.13		
CaO	10.02	10.09	9.24	9.98	9.74	9.31	9.70	10.31	10.31	10.65	11.36	1.76	1.90	1.56	7.93	5.75
MnO	0.24	0.28	0.13	0.27	0.11	0.10	0.47	0.40	0.28	0.26	0.31	0.22	0.21	0.15		
Cr2O3					0.11	0.09		0.02	0.09	0.15		0.01			0.05	
Total	100.59	99.60	98.66	99.02	98.63	98.05	99.83	99.74	100.12	101.04	101.77	99.60	101.14	100.02	7.98	5.75

Sample No.	567	567	567	567	574a	574a	574a	578	578	578	578	578	578	578	579	579
Grid Ref.	649510	649510	649510	649510				684525	684525	684525	684525	684525	684525	684525	LOOSE	LOOSE
Spot Ref.	16	17	18	21	1	2	3	1	2	3	4	5	6	12	5	6
SiO2	48.74	48.47	48.49	47.98	52.01	52.64	51.91	59.72	68.04	62.74	49.05	50.35	57.29	59.59	71.92	71.55
Al2O3	11.50	14.77	13.20	4.01	13.37	14.73	12.51	23.67	13.97	13.32	11.70	13.67	26.00	5.17	12.86	13.73
K2O	1.05	1.08	1.20	0.29	1.63	1.61	1.83	1.10	4.45	2.59	1.07	1.19	0.37	0.84	3.87	3.89
Na2O	2.85	3.57	3.47	0.54	3.58	4.39	3.79	7.08	5.37	4.60	4.58	5.15	6.30	2.40	5.14	5.24
FeO	13.30	12.81	14.38	10.51	12.25	11.94	13.13	1.25	4.00	7.13	16.94	13.94	0.50	25.47	3.33	2.86
TiO2	3.44	3.19	3.61	1.84	3.72	3.26	3.44	0.10	0.88	0.51	2.84	2.94		0.13	0.27	0.25
MgO	5.55	2.99	3.29	12.09	3.14	3.04	3.21			1.51	3.51	2.35		1.01		
CaO	10.87	8.80	8.86	18.04	8.03	8.47	7.71	6.78	0.81	6.11	8.82	7.00	8.69	0.85	0.95	1.02
MnO	0.19	0.18	0.30	0.24	0.20	0.17	0.11	0.07	0.17	0.25	0.08	0.21		1.01		0.08
Cr2O3	0.04			0.09		0.21		0.07	0.09	0.06		0.07	0.00		0.04	
Total	97.70	95.92	96.94	96.10	97.94	100.49	97.64	6.92	1.07	7.93	12.41	9.63	8.69	2.88	98.41	98.66

Sample No.	579	579	579	600	600	600	G2	G2	G2	G2	G2	G2	P1	P1	P1
Grid Ref.	LOOSE	LOOSE	LOOSE	515558	515558	515558	LOOSE	LOOSE	LOOSE	LOOSE	LOOSE	LOOSE	526524	526524	526524
Spot Ref.	4	5	6	1	3	1	1	2	4	6	7	8	2	3	4
SiO2	72.07	68.90	70.86	50.58	49.12	36.47	70.35	69.31	69.92	69.27	70.72	69.77	53.23	53.91	53.20
Al2O3	14.96	13.06	15.70	13.82	13.52	10.35	14.79	16.25	14.86	13.86	13.76	14.54	11.92	12.10	12.08
K2O	3.68	3.81	3.31	1.17	1.07	0.76	3.52	3.06	3.55	3.68	4.21	4.01	1.55	1.44	1.52
Na2O	5.96	4.78	6.07	3.62	3.50	3.16	5.72	6.40	6.07	5.51	5.17	5.05	3.43	3.60	3.38
FeO	2.91	4.25	3.97	12.24	12.62	20.64	2.73	2.46	3.21	3.08	2.92	2.56	14.22	13.87	14.16
TiO2	0.37	0.37	0.12	3.31	3.70	15.31	0.26	0.41	0.27	0.24	0.40	0.56	3.41	3.34	3.14
MgO	0.17	0.12	0.13	3.93	4.00	3.88				0.03		0.14	3.09	2.90	2.84
CaO	1.56	1.58	1.95	7.96	8.31	5.74	1.46	1.85	1.41	1.13	0.95	1.78	6.84	6.96	6.80
MnO	0.23	0.07	0.32	0.11	0.26	0.30	0.06		0.27	0.01	0.11	0.11	0.28	0.26	0.21
Cr2O3	0.02	0.03		0.03					0.03				0.09	0.07	0.09
Total	102.03	96.95	102.59	96.75	96.10	96.87	99.01	99.74	99.71	96.85	98.23	98.60	98.07	98.45	97.41

APPENDIX B-4 - SYSTEMATICS USED IN MODELLING

Normalising values from Sun and McDonough (1989).

Element	C1 chondrite	Primitive mantle
Cs	0.188	0.032
Tl	0.14	0.005
Rb	2.32	0.635
Ba	2.41	6.989
W	0.095	0.02
Th	0.029	0.085
U	0.008	0.021
Nb	0.246	0.713
Ta	0.014	0.041
K	545	250
La	0.237	0.687
Ce	0.612	1.775
Pb	2.47	0.185
Pr	0.095	0.276
Mo	0.92	0.063
Sr	7.26	21.1
P	11220	95
Nd	0.467	1.354
F	60.7	26
Sm	0.153	0.444
Zr	3.87	11.2
Hf	0.1066	0.309
Eu	0.058	0.168
Sn	1.72	0.17
Sb	0.16	0.005
Ti	445	1300
Gd	0.2055	0.596
Tb	0.0374	0.108
Dy	0.254	0.737
Li	1.57	1.6
Y	1.57	4.55
Ho	0.0566	0.164
Er	0.1655	0.48
Tm	0.0255	0.074
Yb	0.17	0.493
Lu	0.0254	0.074

Source compositions used for mantle melting models, Kostopoulos and James (1992)

	BSE	DMM
Sr	19.9	10.9
K	254	80.6
Rb	0.6	0.2
Ba	6.9	2.1
Th	0.078	0.025
Ta	0.037	0.021
Nb	0.62	0.35
La	0.62	0.29
Ce	1.6	0.89
P	78.6	59.4
Nd	1.2	0.87
Hf	0.3	0.27
Zr	10.8	9.7
Sm	0.39	0.32
Ti	1139	1049
Tb	0.095	0.089
Y	4.4	4.3
Yb	0.42	0.41

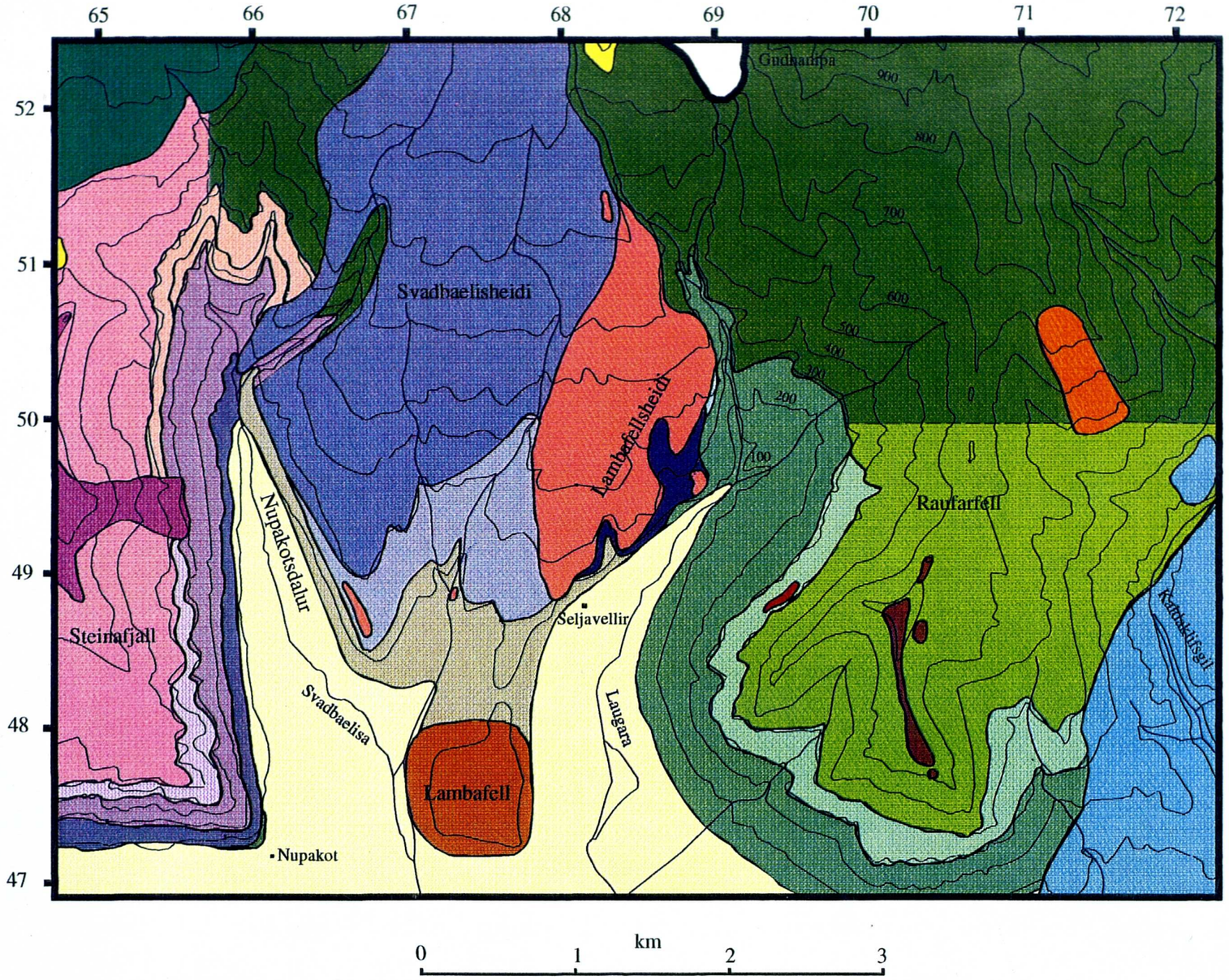

M1. Geological Map of The Eyjafjallajökull Volcano (South Section).

LEGEND.

ka

I
G
I
G
I
G
I
G
I
G
I
G
I
G

100
200
300
400
500
600
700
800

Glacial Rocks.

- Svadbaelisheidi Group.
- Lambafell.
- Seljavellir Group.
- Other Glacial and Intraglacial Lavas and Hyaloclastites.
- Skogaheidi Group.
- Faxi Group.
- Raudafell Group.
- Ankaramite.
- Raufarfell Group.
- Morleysur Group.
- Basalt.
- Nupakotsdalur Group.
- Laugara Group.

Interglacial Rocks.

- Lambafellsa Subgroup 2.
- Lambafellsa Group.
- Trachyte lavas.
- Steinafjall Summit Group.
- Nupur Group.
- Nupakot Group.

Sediments.

- Holocene sediments (sandur).
- Glacial Outwash.

Intrusives.

- Hawaiite.

- Unmapped, hydrothermally-altered rocks.
- Extinct crater ?

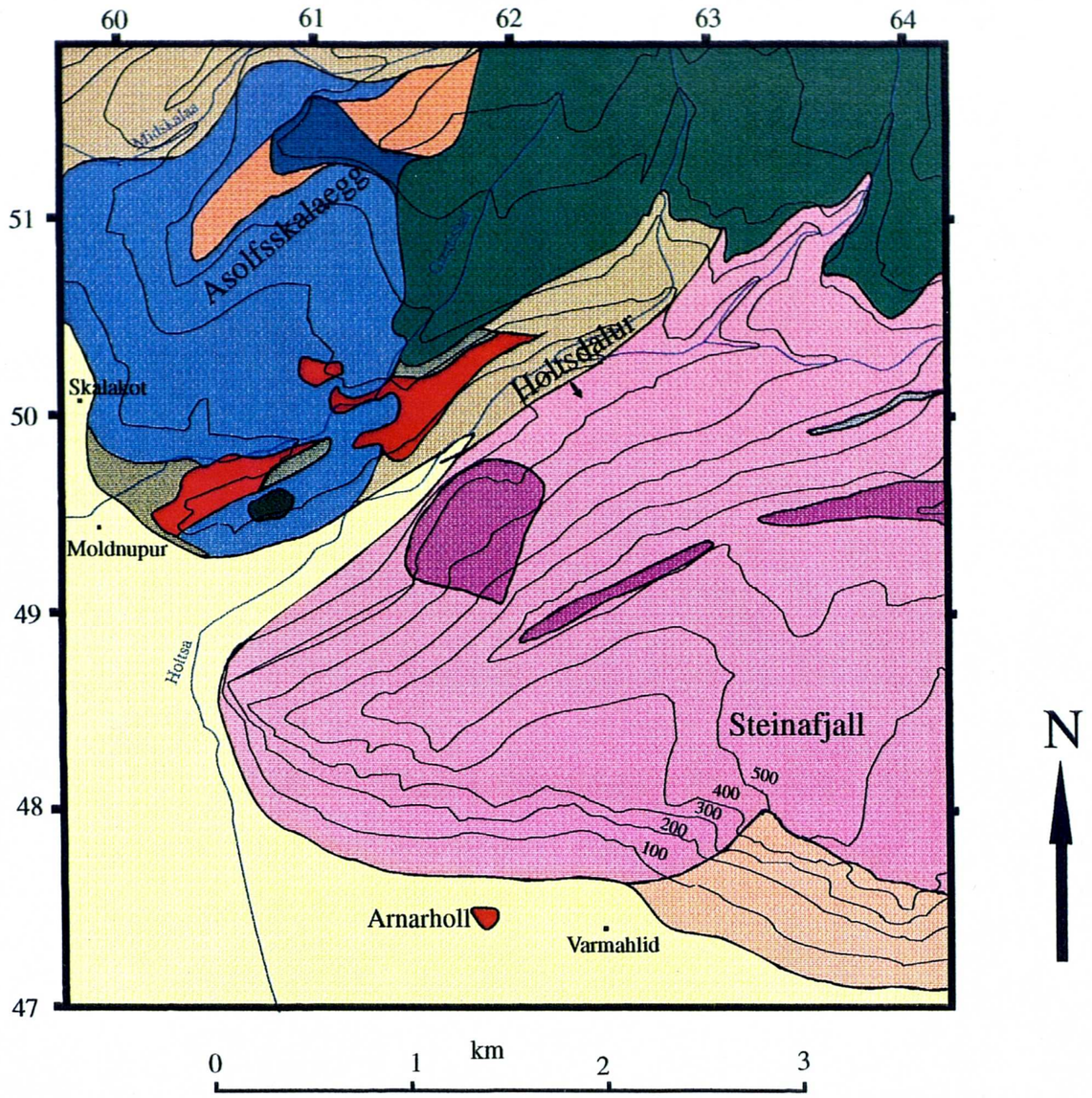

Arrow represents dip direction of a diamictite horizon defining a palaeovalley margin.

M2. Geological Map of the Eyafjallajökull Volcano (South West Section).

LEGEND.